

**Investigations on the biosynthesis of secondary
metabolites and biosynthetic enzymes from *Aspergillus*
species**

**Untersuchungen zur Biosynthese von
Sekundärmetaboliten und zu biosynthetischen Enzymen
aus *Aspergillus*-Arten**

Dissertation

zur Erlangung des Doktorgrades

der Naturwissenschaften

(Dr. rer. nat.)

dem Fachbereich Pharmazie

der Philipps-Universität Marburg

vorgelegt von

Liujuan Zheng

aus Shangrao, China

Marburg an der Lahn, 2021

Erstgutachter: **Prof. Dr. Shu-Ming Li**

Zweitgutachter: **Prof. Dr. Michael Keusgen**

Eingereicht am 23. März 2021

Tag der mündlichen Prüfung: 04. Mai 2021

Hochschulkennziffer: 1180

Dedicated to my family

(献给我的家人)

Table of Contents

Table of Contents	I
List of publications	III
Erklärung zum Eigenanteil	V
Academic activities	VII
Abbreviations	IX
Summary	1
Zusammenfassung	3
1. Introduction	5
1.1 Natural products as important source for drug discovery.	5
1.1.1 Polyketides	6
1.1.1.1 Clinically used polyketides from bacteria and fungi	6
1.1.1.2 Phenyethyl polyketides and their origins	7
1.1.2 Nonribosomal peptides	7
1.1.2.1 Clinically utilized bacterial and fungal nonribosomal peptides	7
1.1.2.2 Oxepinamides, a rare class of NRP derivatives in nature	8
1.2 Natural product producers	9
1.2.1. Fungi as important sources for natural products and their genetic potentials	9
1.2.2. <i>Aspergillus ustus</i> and its secondary metabolites	10
1.3 Biosynthesis of natural products	11
1.3.1 Polyketide synthases	11
1.3.1.1 Modular type I polyketide synthases	11
1.3.1.2 Iterative type I polyketide synthases	13
1.3.1.3 Type II polyketide synthases	14
1.3.2 Nonribosomal peptide synthetases	14
1.3.2.1 Assembly logics of nonribosomal peptide synthetases	14

TABLE OF CONTENTS

1.3.2.2 Biosynthesis of quinazolinone derivatives in fungi.....	17
1.3.3 Tailoring enzymes.....	18
1.3.3.1 Cytochrome P450 enzymes	19
1.3.3.2 Flavin-dependent oxygenases.....	20
1.3.3.3 Nonheme Fe ^{II} /2-oxoglutarate-dependent monooxygenases	22
1.3.3.4 Prenyltransferases	23
2. Aim of this thesis.....	25
3. Results and discussion.....	27
3.1 Biosynthesis of ustethylins in <i>Aspergillus ustus</i> and the shunted pathway after alcoholic feeding.....	27
3.2 Biosynthesis of oxepinamides D, E, and F in <i>Aspergillus ustus</i>	32
3.3 Switching a regular tryptophan C4-prenyltransferase to a reverse tryptophan-containing cyclopeptide C3-prenyltransferase by sequential site-directed mutagenesis.....	41
4. Publications	47
4.1 Ustethylin biosynthesis implies phenethyl derivative formation in <i>Aspergillus ustus</i>	47
4.2 Benzoyl ester formation in <i>Aspergillus ustus</i> by hijacking the polyketide acyl intermediates with alcohols.	115
4.3 Oxepinamide F biosynthesis involves enzymatic D-aminoacyl epimerization, 3H-oxepin formation, and hydroxylation induced double bond migration.	133
4.4 Oxepin formation in fungi implies specific and stereoselective ring expansion	177
4.5 Switching a regular tryptophan C4-prenyltransferase to a reverse tryptophan-containing cyclic dipeptide C3-prenyltransferase by sequential site-directed mutagenesis.....	219
5. Conclusions and future prospects	247
6. References	249
Statutory Declaration.....	257
Acknowledgements	259
Curriculum Vitae	261

List of publications

Liujuan Zheng,[#] Haowen Wang,[#] Aili Fan, and Shu-Ming Li. (2020). Oxepinamide F biosynthesis involves enzymatic D-aminoacyl epimerization, 3*H*-oxepin formation, and hydroxylation induced double bond migration. *Nature Communications* 11: 4914. doi: 10.1038/s41467-020-18713-0. ([#] equal contribution)

Liujuan Zheng,[#] Yiling Yang,[#] Haowen Wang, Aili Fan, Liping Zhang, and Shu-Ming Li. (2020) Ustethylin biosynthesis implies phenethyl derivative formation in *Aspergillus ustus*. *Organic Letters*. 22: 7837-7841. doi:10.1021/acs.orglett.0c02719. ([#] equal contribution)

Liujuan Zheng,[#] Haowen Wang,[#] Lena Ludwig-Radtke, and Shu-Ming Li. (2021). Oxepin formation in fungi implies specific and stereoselective ring expansion. *Organic Letters*. 23, 6, 2024–2028. doi.org/10.1021/acs.orglett.1c00166. ([#] equal contribution)

Liujuan Zheng,[#] Peter Mai,[#] Aili Fan, and Shu-Ming Li. (2018). Switching a regular tryptophan C4-prenyltransferase to a reverse tryptophan-containing cyclic dipeptide C3-prenyltransferase by sequential site-directed mutagenesis. *Organic & Biomolecular Chemistry* 16: 6688-94. doi: 10.1039/C8OB01735B. ([#] equal contribution)

Liujuan Zheng and Shu-Ming Li. (2021) Benzoyl ester formation in *Aspergillus ustus* by hijacking the polyketide acyl intermediates with alcohols. *Archives of Microbiology*. doi.org/10.1007/s00203-021-02182-0.

Elena Ostertag, **Liujuan Zheng**, Karina Broger, Thilo Stehle, Shu-Ming Li, and Georg Zocher. (2021). Reprogramming substrate and catalytic promiscuity of tryptophan prenyltransferases. *Journal of Molecular Biology*. 433: 166726. doi: 10.1016/j.jmb.2020.11.025.

ERKLÄRUNG ZUM EIGENANTEIL

Erklärung zum Eigenanteil

Titel der Publikation und Journal incl. Jahr, Heft, Seitzahl O: Originalarbeit Ü: Übersichtartikel/Review	Autoren	geschätzter Eigenanteil in %	Bitte angeben: angenommen /eingereicht
Oxepinamide F biosynthesis involves enzymatic D-aminoacyl epimerization, 3H-oxepin formation, and hydroxylation induced double bond migration. Nature Communications, 2020, 11: 4914 Originalarbeit	<u>Liujuan Zheng</u> , [#] Haowen Wang, [#] Aili Fan, and Shu-Ming Li.	35	angenommen
Ustethylin biosynthesis implies phenethyl derivative formation in <i>Aspergillus ustus</i> . Organic Letters, 2020, 22:7837-7841 . Originalarbeit	<u>Liujuan Zheng</u> , [#] Yiling Yang, [#] Haowen Wang, Aili Fan, Liping Zhang, and Shu-Ming Li.	32	angenommen
Oxepin formation in fungi implies specific and stereoselective ring expansion. Organic Letters, 2021, 23, 6, 2024–2028 Originalarbeit	<u>Liujuan Zheng</u> , [#] Haowen Wang, [#] Lena Ludwig- Radtke, and Shu-Ming Li	35	angenommen
Switching a regular tryptophan C4-prenyltransferase to a reverse tryptophan-containing cyclic dipeptide C3-prenyltransferase by sequential site-directed mutagenesis. Organic & Biomolecular Chemistry, 2018, 16: 6688-6694 . Originalarbeit	<u>Liujuan Zheng</u> , [#] Peter Mai, [#] Aili Fan, and Shu-Ming Li.	35	angenommen
Benzoyl ester formation in <i>Aspergillus ustus</i> by hijacking the polyketide acyl intermediates with alcohols. Archives of Microbiology, 2021, doi.org/10.1007/s00203-021-02182-0 Originalarbeit	<u>Liujuan Zheng</u> and Shu-Ming Li.	60	angenommen
Reprogramming substrate and catalytic promiscuity of tryptophan prenyltransferases. Journal of Molecular Biology, 2021, 433: 166726 . Originalarbeit	Elena Ostertag, <u>Liujuan Zheng</u> , Karina Broger; Thilo Stehle, Shu-Ming Li, and Georg Zocher.	20	angenommen

[#]: These authors contributed equally to this work.

Kandidat(in)

Unterschrift Betreuer(in)

Academic activities

Oral presentation, International PhD Students/Postdoc Meeting of the German Pharmaceutical Society (DPhG) 11.03.2021 – 12.03.2021 (video conference)

Liujuan Zheng, Haowen Wang, and Prof. Dr. Shu-Ming Li. Biosynthesis of the Liver X Receptor transcriptional activation reagent oxepinamide F from fungus *Aspergillus ustus*.

ABBREVIATIONS

Abbreviations

The international system of units and units derived thereof have been used

A domain	adenylation domain
<i>A. fumigatus</i>	<i>Aspergillus fumigatus</i>
<i>A. nidulans</i>	<i>Aspergillus nidulans</i>
<i>A. terreus</i>	<i>Aspergillus terreus</i>
aa	amino acid
ACP domain	acyl carrier protein domain
AT domain	acyltransferase domain
ATP	adenosine triphosphate
BGC	biosynthetic gene cluster
bp	base pair
br	broad (NMR)
C domain	condensation domain
CD ₃ OD	deuterated methanol
CDCl ₃	deuterated chloroform
cDNA	copy deoxyribonucleic acid
CoA	coenzyme A
COSY	correlation spectroscopy
C _T domain	condensation-like domain
<i>cyclo</i> -L-Trp-L-Ala	<i>cyclo</i> -L-tryptophanyl-L-alanyl
<i>cyclo</i> -L-Trp-Gly	<i>cyclo</i> -L-tryptophanyl-glycyl
<i>cyclo</i> -L-Trp-L-Phe	<i>cyclo</i> -L-tryptophanyl-L-phenylalanyl
<i>cyclo</i> -L-Trp-L-Pro	<i>cyclo</i> -L-tryptophanyl-L-prolyl
<i>cyclo</i> -L-Trp-L-Trp	<i>cyclo</i> -L-tryptophanyl-L-tryptophanyl
<i>cyclo</i> -L-Trp-L-Tyr	<i>cyclo</i> -L-tryptophanyl-L-tyrosyl
d	doublet
D ₂ O	deuterium oxide
Da	dalton
dd	double doublet
ddd	double doublet of doublet
DEBS	6-deoxyerythronolide B synthase
DH domain	dehydratase domain

ABBREVIATIONS

DMA	dimethylallyl
DMAPP	dimethylallyl diphosphate
DMATS	dimethylallyltryptophan synthase
DMSO- <i>d</i> 6	deuterated dimethyl sulfoxide
DNA	deoxyribonucleic acid
dq	double quartet
dt	double triplet
<i>E. coli</i>	<i>Escherichia coli</i>
<i>e.g.</i>	exempli gratia
EIC	extracted ion chromatogram
ER domain	enoyl reductase domain
ESI	electrospray ionization
FAD	flavin adenine dinucleotide
Fl _{C4a} [OOH]	flavin-C4a-hydroperoxide
Fl _{N5} [O]	flavin-N5-oxide
Fl _{ox}	oxidized flavin
Fl _{red}	reduced flavin
FMN	flavin mononucleotide
gDNA	genomic DNA
GMM	glucose minimal medium
GPP	geranyl diphosphate
GTP	guanosine triphosphate
HE	heterologous expression
His ₆	Hexahistidine six
HMBC	heteronuclear multiple bond correlation
HPLC	high performance liquid chromatography
<i>hph</i>	hygromycin B phosphotransferase gene
HRMS	high resolution mass spectrometry
HR-PKS	highly-reducing polyketide synthase
HSQC	heteronuclear single quantum coherence
<i>Hz</i>	<i>hertz</i>
<i>i.e.</i>	id est
<i>J</i>	coupling constant
kbp	kilo base pairs

ABBREVIATIONS

k_{cat}	turnover number
kDa	kilodaltons
K_M	Michaelis-Menten constant
KR domain	β -ketoreductase domain
KS domain	β -ketoacyl synthase domain
LC-MS	liquid chromatography–mass spectrometry
m/z	mass-to-charge ratio
MAT domain	malonyl-CoA-ACP transacylase
mAU	milli absorbance unit
Mb	mega base pairs
MHz	mega hertz
MOS	3-methylcrotonaldehyde synthase
mRNA	messenger ribonucleic acid
MeT	methyltransferase
MS	mass spectroscopy
multi	multiplicity
NADH	nicotinamide adenine dinucleotide
NADPH	nicotinamide adenine dinucleotide phosphate
<i>N. fischeri</i>	<i>Neosartorya fischeri</i>
NMR	nuclear magnetic resonance
NP	natural product
NR-PKS	non-reducing polyketide synthase
nonheme Fe ^{II} /2-OG	nonheme Fe ^{II} /2-oxoglutarate
Opa cluster	Oxepinamide cluster
NRPS	nonribosomal peptide synthetase
P450	cytochrome P450
<i>P. crustosum</i>	<i>Penicillium crustosum</i>
<i>P. citrinum</i>	<i>Penicillium citrinum</i>
PCP domain	peptidyl carrier protein domain
PCR	polymerase chain reaction
PD	potato dextrose
PDA	potato dextrose agar
PDB	potato dextrose broth
PEG	polyethylene glycol

ABBREVIATIONS

PKS	polyketide synthase
ppm	parts per million
PR-PKS	partially-reducing polyketide synthase
PT	prenyltransferase
PT domain	Product template domain
q	quartet
R domain	reductase domain
RNA	ribonucleic acid
rpm	revolutions per minute
s	singlet
<i>S. cerevisiae</i>	<i>Saccharomyces cerevisiae</i>
SAT domain	starter unit acyltransferase domain
SDS-PAGE	sodium dodecyl sulfate polyacrylamide gel electrophoresis
SM	secondary metabolite
t	Triplet
T domain	thiolation domain
TB	terrific broth
td	triple doublet
TE domain	thioesterase domain
Tris	tris(hydroxymethyl)aminomethane
UV	ultraviolet
<i>utt</i> cluster	<u>u</u> <i>st</i> <u>e</u> <i>th</i> ylin cluster
<i>v/v</i>	volume per volume
WT	wild type
α -KG	α -ketoglutarate
δ_C	chemical shift of ^{13}C
δ_H	chemical shift of ^1H

Summary

Secondary metabolites, especially those from microorganisms like bacteria and fungi, play an important role in defending the host against natural enemies, competitors or environmental pressure. These ecological functions provide the microbial natural products with a significant role in drug discovery, determination of new enzyme reaction mechanisms and interactions between species. Plentiful microbial secondary metabolites, including polyketides (PKs), nonribosomal peptides (NRPs), alkaloids and terpenes have been isolated and identified in the last decades. The progress in sequencing technologies and bioinformatics analysis provide a huge advantage of studying the biosynthesis of these metabolites. Polyketide synthases (PKSs) and nonribosomal peptide synthetases (NRPSs) follow logical assembly lines and are the most studied enzymes in the last years. Together with the versatile tailoring enzymes like prenyltransferases (PTs), flavin-dependent monooxygenases, nonheme Fe^{II}/2-oxoglutarate dependent monooxygenases, and cytochrome P450 enzymes, these enzymes are responsible for the formation of a large number of secondary metabolites.

The biosynthetic pathways of many fungal metabolites have special features. For example, nonreducing polyketide synthetases are merely found to assemble fungal polyketides and their multiple domains can be iteratively utilized. Compared to bacteria, less fungi were sequenced and the genetic manipulation in fungi is usually more complex and difficult. Thus, the biosynthesis of many intriguing fungal secondary metabolites still remains unclear.

In cooperation with Haowen Wang and Yiling Yang, biosynthetic pathways of three metabolites from *Aspergillus ustus* were elucidated in this thesis. Ustethylin A, a highly oxygenated aryl aldehyde containing a common phenethyl residue, was isolated and identified from this fungus. Isotopic labelling experiments proved that the backbone of ustethylin A is derived from malonyl-CoA, the methyl group in the phenethyl residue, the phenyl methyl group, and the O-methyl group from L-methionine. Transcriptome analysis, gene deletion and expression as well as isotopic labelling experiments confirmed that ustethylin A is biosynthesized via a PKS-related pathway. The PKS UttA as a key enzyme is responsible for the formation of the phenethyl backbone with methylation as essential steps. Consecutive and coordinated modifications by three different types of oxidoreductases and one O-MeT lead to the formation of ustethylin A. The Utt biosynthetic gene cluster (BGC) is the first reported cluster for a phenethyl-containing fungal metabolite.

30 years ago, two benzoyl esters were identified after feeding an *Aspergillus ustus* culture with EtOH and MeOH. The experiments were reproduced by this PhD candidate and proven to be shunt products of the

SUMMARY

ustethylin A biosynthetic pathway, with the UttA-bound thioesters as precursors for the methyl and ethyl ester formation. The fed alcohols hijack the polyketide acyl intermediates from the ustethylin A pathway.

Besides ustethylin A, oxepinamides D, E, and F were isolated and identified in *A. ustus*. Two similar NRPS-containing gene clusters, *opa* and *opa2*, were identified by bioinformatics analysis. Enzymes from the *opa* cluster are responsible for the biosynthesis of oxepinamides E and F and those from the *opa2* cluster are involved in the formation of oxepinamide D. In the biosynthetic pathway of oxepinamide F, the NRPS enzyme OpaA with a domain structure of A-T-C-A-T-E-C-A-T-C_T, activates Ant, L-Ile, and L-Phe, changes the configuration of L-Phe to D-Phe by an epimerase domain, and assembles the quinazolinone derivative protuboxepin K. Afterwards, the P450 enzyme OpaB catalyzes the expansion of the benzene to oxepin ring in the Ant residue of protuboxepin K. Subsequently, the flavin-dependent oxidase OpaC catalyzes the regio- and stereospecific hydroxylation accompanied by double bond migration, which leads to the conversion of a 1*H*-oxepin to a 3*H*-oxepin system. The epimerase OpaE catalyzes the D-Phe residue back to L-Phe, which is essential for the final 12-OH methylation by the O-MeT OpaF to produce oxepinamide F.

For the biosynthesis of oxepinamide D, a similar NRPS OpaA2 in the *opa2* cluster utilizes Ant, L-Phe, and L-Ala to assemble a fused quinazolinone core structure. In analogy to OpaB, the P450 enzyme OpaB2 is responsible for the oxepin formation via a specific and stereoselective manner to form the 1*H*-oxepin oxepinamide. Subsequently, OpaC2 installs a hydroxyl group at C-3 position to produce the final product oxepinamide D.

Prenylation is one of the most important enzymatic modifications of natural products. FgaPT2 from *Aspergillus fumigatus* had been identified as a regular C4-prenyltransferase of L-Trp. Previous studies showed that mutation on key residues Lys174 and Arg244 led to the enhanced acceptance of the cyclodipeptides (CDPs) for C4-prenylation. However, the FgaPT2_K174F mutant shows only low activity for reverse C3-prenylation of six cyclodipeptides. The combinational mutations on Lys174 and Arg244 was demonstrated to increase the catalytic activity of these cyclodipeptides. Except for *cyclo*-L-Trp-L-Trp, FgaPT2_K174F_R244X (X=L, N, Q, Y) show much better acceptance, with an increase of two- to six-fold activity, to the tested cyclodipeptides than that of FgaPT2. More importantly, compared to FgaPT2_K174F, even two- to ten-fold conversion yields were calculated for the double mutants. These results proved that site-directed mutagenesis is an effective method to modify the enzyme function, which increases the structural diversity of natural products.

Zusammenfassung

Sekundärmetabolite, insbesondere solche aus Bakterien und Pilzen, spielen eine wichtige Rolle bei der Verteidigung gegen natürliche Feinde, Konkurrenten oder Umweltbelastungen. Diese ökologischen Funktionen verleihen den mikrobiellen Naturstoffen eine wichtige Rolle bei der Wirkstoffentdeckung, Erforschung von Enzymen und Artenwechselwirkungen. Zahlreiche mikrobielle Sekundärmetabolite, einschließlich Polyketide, nichtribosomale Peptide, Alkaloide und Terpene wurden isoliert und identifiziert. Fortschritte bei Sequenzierungstechnologien und der Bioinformatik-Analyse ermöglichen es, die Biosynthese dieser Metabolite zu untersuchen und aufzuklären. Polyketidsyntasen und nichtribosomalen Peptidsyntasen folgen einer logischen Kettenverlängerungsstrategie und sind die am besten untersuchten Enzyme der letzten Jahrzehnte. Zusammen mit Modifikationsenzymen wie Prenyltransferasen, FAD-abhängigen Oxidoreduktasen, nicht-Häm-Fe^{II} / 2-Oxoglutarat-abhängigen Monooxygenasen und Cytochrom P450-Enzymen sind sie für die Entstehung einer großen Anzahl an Sekundärmetabolite verantwortlich.

Die Biosynthesewege vieler Pilzmetabolite weisen besondere Merkmale auf. Zum Beispiel wurden nichtreduzierende Polyketidsyntasen lediglich in Pilzen gefunden und ihre Domänen können wiederholt durchlaufen werden. Im Vergleich zu Bakterien wurden bisher weniger Pilze sequenziert und die genetische Manipulation bei Pilzen ist normalerweise komplexer und schwieriger. Daher bleibt die Biosynthese vieler faszinierender sekundärer Pilzmetabolite noch ungeklärt.

In Zusammenarbeit mit Haowen Wang und Yiling Yang wurden in dieser Arbeit Biosynthesewege von drei Metaboliten aus *Aspergillus ustus* aufgeklärt. Aus diesem Pilz wurde zuerst Ustethylin A, ein stark hydroxyliertes Arylaldehyd mit einem Phenethylrest isoliert und identifiziert. Isotopenmarkierungsexperimente zeigten, dass das Grundgerüst von Ustethylin A aus Malonyl-CoA und die Methylgruppen im Phenethylrest und Phenylmethyl sowie die O-Methylgruppe aus L-Methionin stammen. Transkriptomanalyse, Gendeletion und -expression sowie Isotopenmarkierungsexperimente bestätigten, dass Ustethylin A über einen PKS-Biosyntheseweg entsteht. Das PKS-Enzym UttA ist ein Schlüsselenzym für die Bildung des Phenethylgerüsts mit Methylierung als Schlüsselschritten. Aufeinanderfolgende und koordinierte Modifikationen durch drei verschiedene Arten von Oxidoreduktasen und eine O-MeT führen zur Bildung von Ustethylin A. Das Utt-Biosynthesegencluster ist das erste bekannte Cluster, das für einen Phenethyl-haltigen Pilzmetaboliten codiert.

Vor 30 Jahren wurden zwei Benzoyl ester nach EtOH- und MeOH-Fütterungen in einer *Aspergillus ustus*-Kultur identifiziert. Die Experimente wurden von diesem Doktoranden reproduziert und erwiesen sich als Nebenprodukte des Ustethylin A-Biosynthesewegs, bei dem die UttA-gebundenen Thioester als

ZUSAMMENFASSUNG

Vorläufer für die Methyl- und Ethylesterbildung dienen. Die zugeführten Alkohole entführen die Polyketidacyl-Zwischenprodukte aus dem Ustethylin A-Weg.

Neben Ustethylin A wurden Oxepinamide D, E und F aus *A. ustus* isoliert und identifiziert. Zwei ähnliche NRPS-haltige Gencluster, *opa* und *opa2*, wurden durch bioinformatische Analyse identifiziert. Enzyme aus dem *opa*-Cluster sind für die Biosynthese der Oxepinamide E und F und solche aus dem *opa2*-Cluster für die Bildung von Oxepinamid D verantwortlich. Im Biosyntheseweg von Oxepinamid F aktiviert das NRPS-Enzym OpaA mit einer Domänenstruktur von A-T-C-A-T-E-C-A-T-C_T Ant, L-Ile und L-Phe, ändert die Konfiguration von L-Phe zu D-Phe durch eine Epimerasedomäne und baut das Chinazolinonderivat Protuboxepin K zusammen. Das P450-Enzym OpaB katalysiert anschließend die Expansion des Benzolrings zum Oxepinring im Ant-Rest von Protuboxepin K. Anschließend katalysiert die flavin-abhängige Oxidase OpaC die regio- und stereospezifische Hydroxylierung, begleitet von einer Doppelbindungsmigration, die zur Umwandlung eines 1*H*-Oxepin in ein 3*H*-Oxepin-System führt. Die Epimerase OpaE verändert den D-Phe-Rest zurück zu L-Phe, was für die endgültige 12-OH-Methylierung durch das O-MeT-OpaF zur Herstellung von Oxepinamid F essentiell ist.

Für die Biosynthese von Oxepinamid D verwendet ein ähnliches NRPS OpaA2 im *opa2*-Cluster Ant, L-Phe und L-Ala, um eine kondensierte Chinazolinon-Kernstruktur aufzubauen. In Analogie zu OpaB ist das P450-Enzym OpaB2 auf spezifische und stereoselektive Weise für die Oxepinbildung verantwortlich, um das 1*H*-Oxepinoxepinamid zu bilden. Anschließend führt OpaC2 eine Hydroxylgruppe an der C3-Position ein, wodurch das Endprodukt Oxepinamid D herzustellen.

Die Prenylierung ist eine der wichtigsten enzymatischen Modifikationen von Naturstoffen. FgaPT2 aus *Aspergillus fumigatus* wurde als reguläre C4-Prenyltransferase von L-Trp identifiziert. Frühere Studien zeigten, dass die Mutation an den Schlüsselpositionen Lys174 und Arg244 zu einer erhöhten Akzeptanz der cyclischen Dipeptide für die C4-Prenylierung führt. Die FgaPT2_K174F-Mutante zeigt jedoch nur eine geringe Aktivität für die reverse C3-Prenylierung von sechs Cyclodipeptiden. Es wurde in dieser Arbeit gezeigt, dass die kombinierten Mutationen an Lys174 und Arg244 die katalytische Aktivität dieser cyclischen Dipeptide erhöhen. Mit Ausnahme von Cyclo-L-Trp-L-Trp zeigt FgaPT2_K174F_R244X (X = L, N, Q, Y) eine viel bessere Akzeptanz, mit einer zwei- bis sechsfachen Aktivität, für die getesteten Dipeptide als FgaPT2. Noch wichtiger ist, dass im Vergleich zu FgaPT2_K174F für die Doppelmutanten sogar zwei- bis zehnfache Umwandlungsausbeuten berechnet wurden. Diese Ergebnisse zeigen, dass ortsgerichtete Mutagenese eine wirksame Methode zur Modifizierung der Enzymfunktion ist, die die strukturelle Vielfalt von Naturstoffen erhöht.

1. Introduction

1.1 Natural products as important source for drug discovery.

2020 was a special year to all of us, because of the nightmare of Coronavirus (SARS-Covid19). Until now, just a few vaccines have been approved for improving the immune system and no drug is effective against this virus. New drugs to combat viruses or other multidrug-resistant pathogens are urgently needed, because we do not know when similar viruses or other “super bacteria” will be brought into our live suddenly.

Based on the statistics from 01/1981 to 09/2019, 1881 new drugs including vaccines, biologicals, and small molecules were approved by the FDA for clinical use.¹ 85 (4.5%) of them are unaltered natural products, 346 (18.4%) are biological macromolecules, 356 (18.9%) are natural product derivatives, and 272 (14.5%) are natural product pharmacophore or mimics of natural products (Figure 1). More than sixty percent of the approved drugs are natural product relevant, proving the essential role of natural products in drug discovery. Natural products offer the best choices for finding agents/active templates, which provide the potential to discover the leading agents in a variety of human diseases in conjunction with synthetic chemistry and biology.¹ Elucidation of the biosynthetic pathway largely extends our knowledge for understanding the assembly line and the structural diversity of natural products.

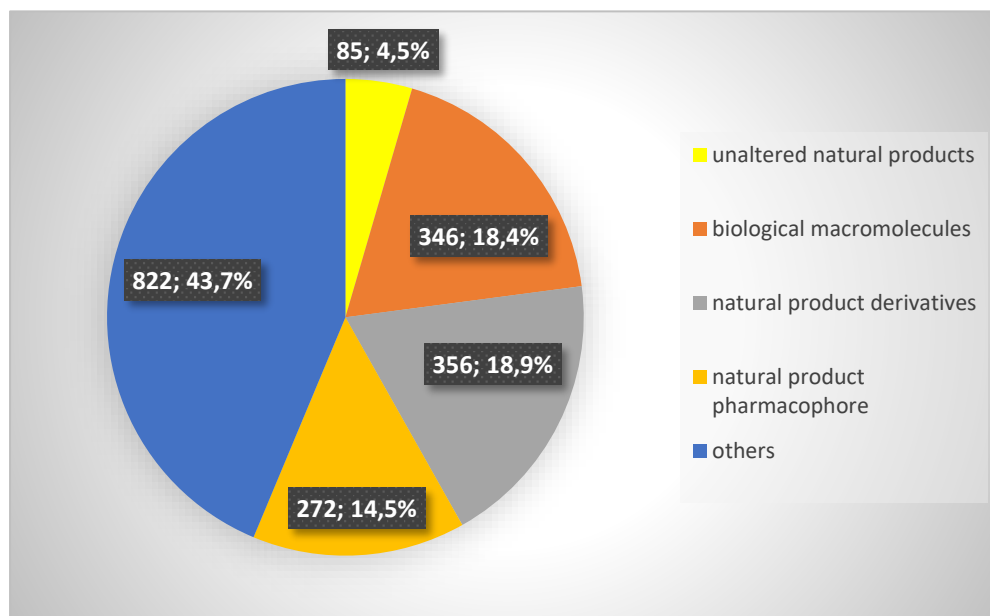


Figure 1. New approved drugs from 01/1981 to 09/2019 and their origins.

1.1.1 Polyketides

1.1.1.1 Clinically used polyketides from bacteria and fungi

Polyketides (PKs), which have been isolated and identified from plants, fungi, and bacteria, are a large group of natural products.² Some of them are important drugs for clinical use. Outstanding examples from bacteria are tetracyclines isolated from *Streptomyces aureofaciens* and erythromycins obtained from *Saccharopolyspora erythraea* for the treatment of a number of bacterial infections³ as well as ivermectin produced by *Streptomyces avermectinius* against parasite infestations.³ While α -zearalanol as an anabolic agent isolated from *Fusarium* sp, lovastatin produced by *Aspergillus terreus* is used as a blood cholesterol lowering agent. Griseofulvin as antifungal medication from *Penicillium* sp. is also an excellent fungal example (Figure 2).⁴ These market drugs are just small numbers of PKs or their derivatives. The versatile scaffolds and functional groups of PKs provide many active templates or leading agents for drug discovery.

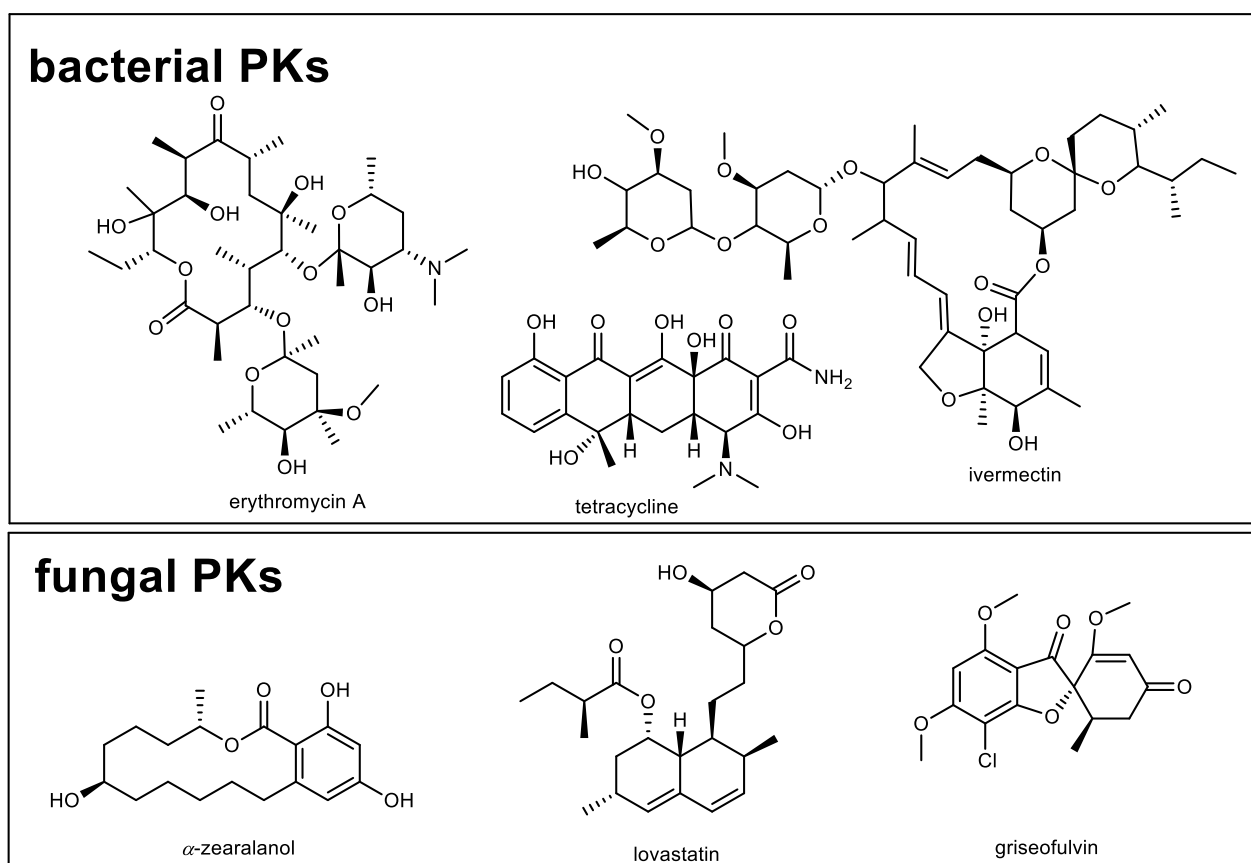


Figure 2. Examples of clinically used polyketides from bacteria and fungi

1. INTRODUCTION

1.1.1.2 Phenethyl polyketides and their origins

Phenethyl-containing PKs, with multiple biological activities, are frequently identified microbial SMs (Figure 3). Gilvocarcin E⁵ and tiacumicin B⁶ occur in *Streptomyces*, while barnol⁷ and marilone A⁸ are examples from fungi. Isotopic feeding experiments and genetic studies proved that the phenethyl units are products of PKS biosynthetic gene clusters (BGCs).^{5,6,9} The ethyl groups in the phenethyl residue of bacterial SMs are mostly originated from propionate as a starter unit of PKSs.^{5,6} In fungi, it can be derived from acetate as in the cases of LL-D253 α ¹⁰ and O-methylasparvenone,¹¹ which was confirmed by feeding with [1, 2-¹³C] acetate. However, most methyl groups of the phenethyl residue in fungal metabolites are derived from S-adenosyl methionine (SAM), which has been proven by feeding experiments with [methyl-¹³C]-L-methionine (Figure 3).^{8,12} Methyltransferases (MeTs) for the methylation and the biosynthetic pathways for such metabolites in fungi have not been described before.

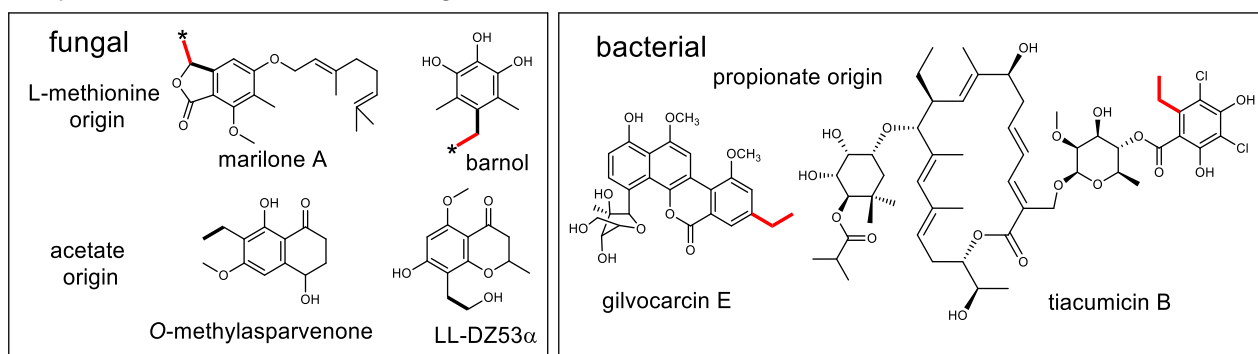


Figure 3. Phenethyl natural products from fungi and bacteria

1.1.2 Nonribosomal peptides

1.1.2.1 Clinically utilized bacterial and fungal nonribosomal peptides

Nonribosomal peptides (NRPs) belong to another important group of natural products, which are mainly found in bacteria and fungi. Similar to PKs, NRPs used as clinical drugs are evident. Around 30 NRP (core) structures are found in the marketed drugs currently, contributing to sales of billions Euros in the chemical and pharmaceutical industry.¹³ Examples of bacterial NRPs used clinically as antibiotics are vancomycins from *Amycolatopsis orientalis*, daptomycin from *Streptomyces roseosporus* and lincomycin from *Streptomyces lincolnensis*.¹³ Well-known cases in fungal NRPs are β -lactam antibiotics like penicillins from *Penicillium chrysogenum* and cephalosporins from *Acremonium chrysogenum*. Ergotamine from *Claviceps purpurea*, is used for treatment of migraine (Figure 4).¹³ The various core structures of peptides together with multiple tailoring enzymatic modifications extensively increase the structural diversity of NRPs, which have huge potential for drug discovery.

1. INTRODUCTION

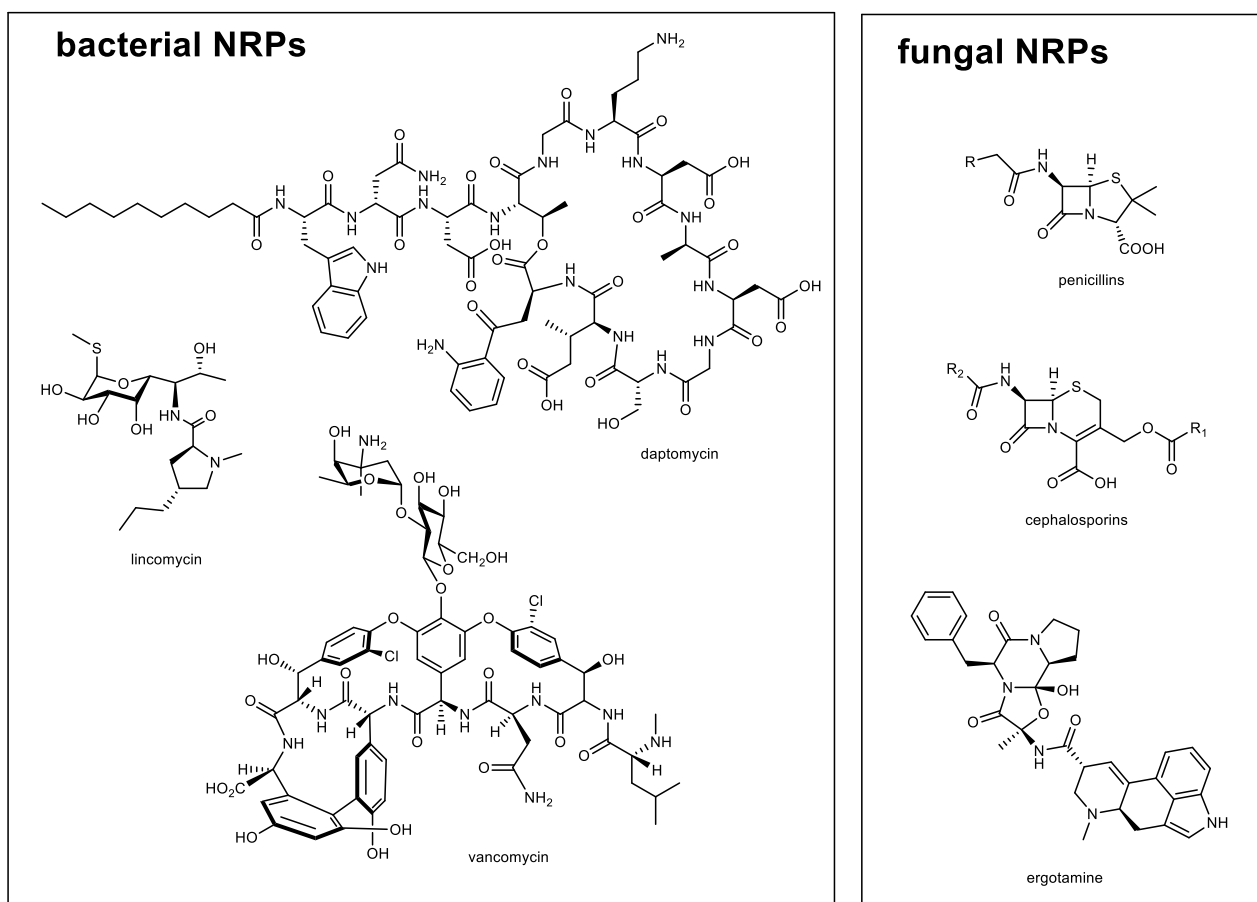


Figure 4. Examples of market drugs derived from nonribosomal peptides

1.1.2.2 Oxepinamides, a rare class of NRP derivatives in nature

Oxepinamides with an Oxepine-Pyrimidinone-Ketopiperazine (OPK) backbone are a rarely observed class of fungal NRP derivatives with a broad range of biological activities, which are mainly found in *Aspergillus* and *Penicillium* species. Since 1988, more than thirty seven OPK derivatives were isolated and identified (Figure 5).^{14,15} Some of them show high affinity to liver X receptors (LXRs) and are potential agents for the treatment of Alzheimer's disease, atherosclerosis, diabetes, and inflammation.^{16,17} Oxepinamides are usually derived from quinazolinones with anthranilyl (Ant) residue in common. They differ from each other by incorporation of two other varying amino acids and additional modifications. The natural oxepinamides can basically be divided into two classes: 1*H*-oxepins with three C=C in the oxepin ring including oxepinamide D, versicoloid A/B, circumdatin A/B and dihydrocineain and 3*H*-oxepin core structure with two C=C in the ring and one *exo* C=N bond, such as varioxepine A, varioloid A, oxepinamide F and oxepinamide G.^{16-19 20,21 22 23}

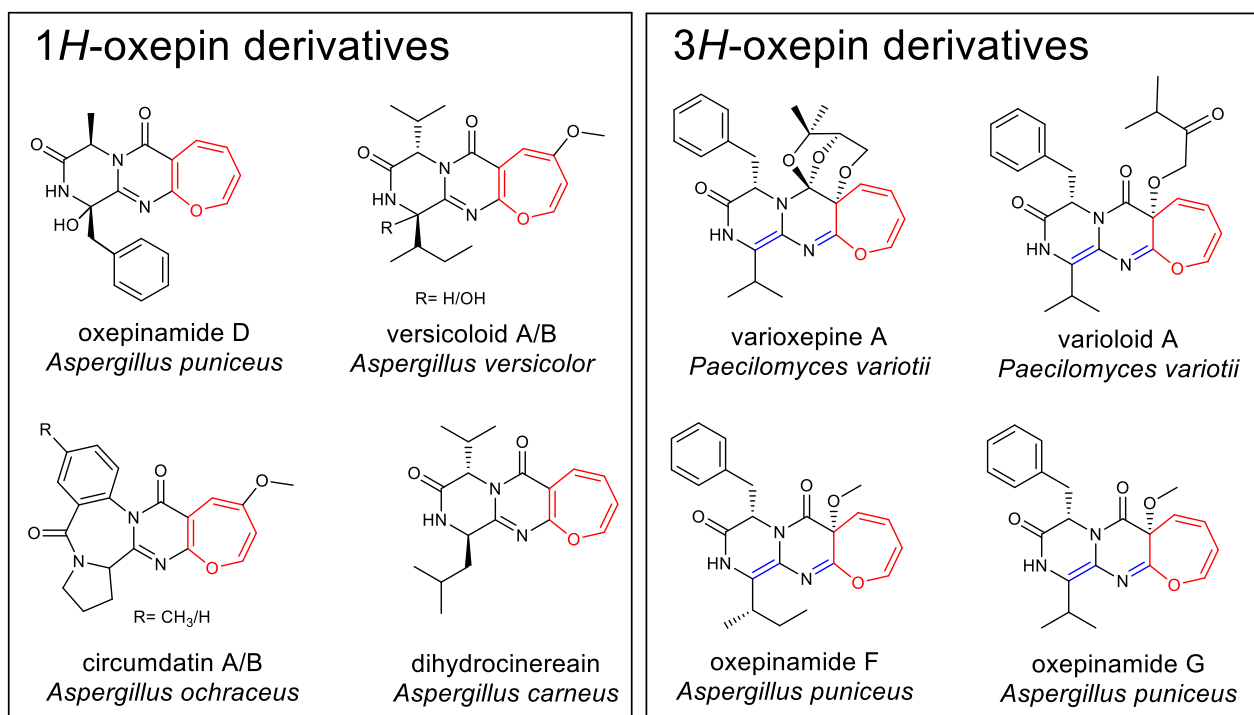


Figure 5. Examples of 1*H*- and 3*H*-oxepin oxepinamides from various fungi

1.2 Natural product producers

1.2.1. Fungi as important sources for natural products and their genetic potentials

Microorganisms including bacteria and fungi produce plentiful secondary metabolites and therefore are recognized as important natural product producers. Recently, a high-throughput sequencing analysis revealed that about 5.1 million fungal species live on earth, about 6 times of the number of all plant species.²⁴ Filamentous fungi are notable for producing huge numbers of secondary metabolites, which have ecological fitness roles for fungi.²⁵ Melanin, for example, protects hosts from UV damage, phenazine acts as a weapon for defense in *Aspergillus*,^{24,26-28} and several secondary metabolites are proven to protect host from toxic natural products.²⁵ More importantly, many fungal SMs including the aforementioned antibiotics, immunosuppressants, anti-osteoporosis agents, and cholesterol-lowering drugs, have benefitted human health.²⁹ These examples offer the confidence and motivation for a deeper understanding of fungal secondary metabolites.

Recent advances achieved in sequencing technologies and bioinformatics analysis revealed that fungal genomes are usually larger than those of bacteria. Genes for fungal SMs are usually clustered in a chromosome presented as BGCs.²⁹ However, under laboratory culture conditions, most BGCs are only lowly expressed or even not expressed. Therefore, only a small number of BGCs have been accurately assigned to the corresponding SMs.^{25,29} Since last decades, genetic tools like modification of regulators

1. INTRODUCTION

including pathway-specific transcription factors, global regulators, epigenetic regulators, and other regulators largely increased the diversity of fungal SMs.²⁹ PKs, NRPs, terpenes, indole alkaloids as well as ribosomally synthesized and post-translationally modified peptides are important classes of fungal SMs.⁴ In this thesis, polyketides synthases (PKSs) and nonribosomal peptides synthases (NRPSs) will be discussed in details.

1.2.2. *Aspergillus ustus* and its secondary metabolites

Aspergillus ustus, a member of the division Ascomycota, is usually found in indoor environments and soil.³⁰ Colonies of this species appear greyish brown or dark brown.³¹ Since more than 20 invasive aspergillosis cases have been reported for this species, *A. ustus* is considered as a rare human pathogen that can cause invasive infection in immunocompromised hosts.³¹ Molecular data, including random amplification of polymorphic DNA analysis, indicate that *A. ustus* is highly variable.³¹ Phylogenetic analysis shows that *A. ustus* is close to *Aspergillus puniceus* and *Aspergillus granulosis*.³¹

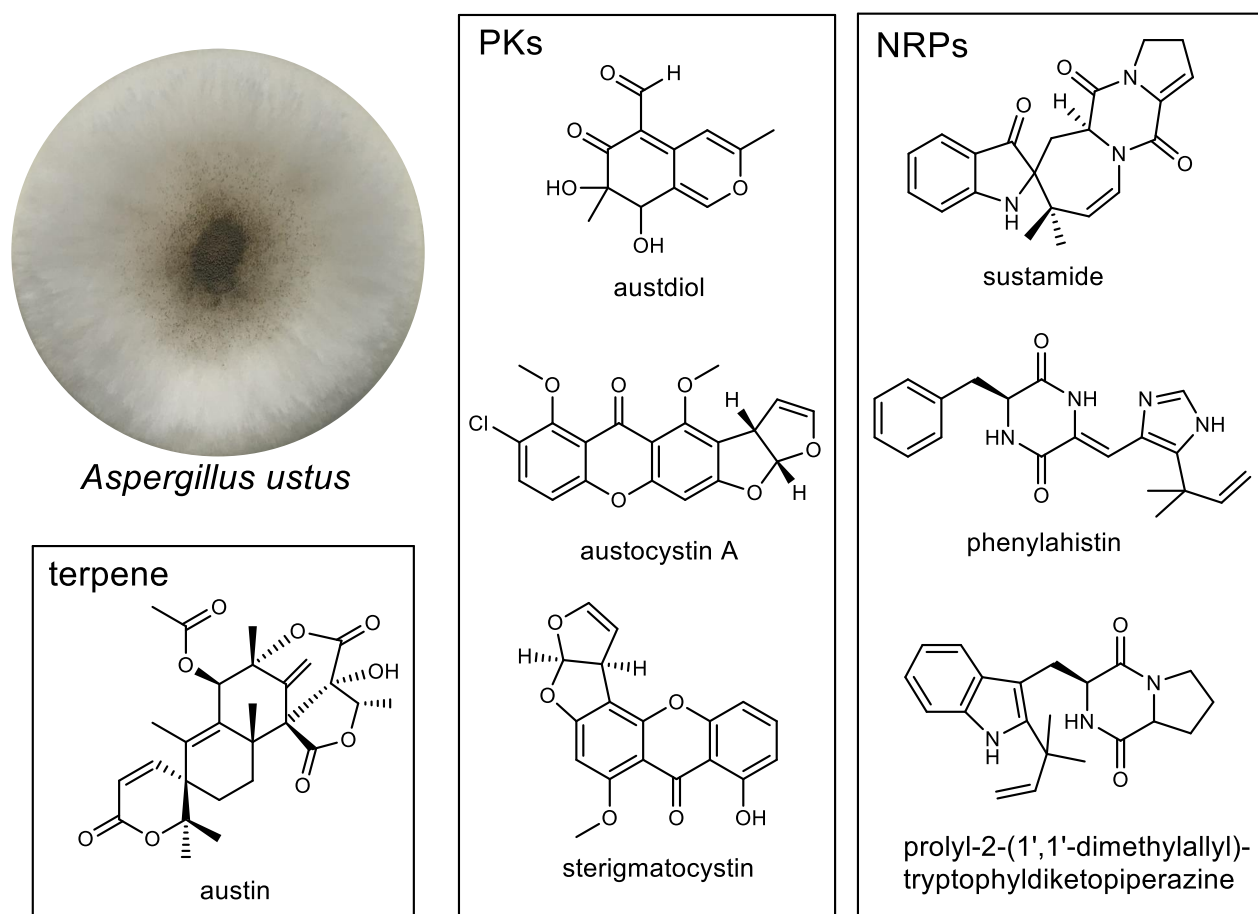


Figure 6. *Aspergillus ustus* and its known secondary metabolites

1. INTRODUCTION

Aspergillus ustus has been proven to be a good producer for SMs. Until now, versatile natural products (Figure 6) including PKs such as austdinol, austocystin A, and sterigmatocystin, NRPs like austamide, phenylahistin, and prolyl-2-(1',1'-dimethylallyl)-tryptophyldiketopiperazine (Figure 6) as well as terpenes e.g. austin, have been obtained from different isolates of this fungus.³²⁻³⁴ It is noteworthy that alcohol feeding into the culture of an *A. ustus* strain led to the accumulation of benzoic esters. The molecular mechanism for this phenomenon has not been elucidated prior to this thesis.

Aspergillus ustus 3.3904 was purchased from the China General Microbiological Culture Collection Center (Beijing, China) and used in this thesis. In 2015, this strain was sequenced and a total of 38.3 Mbp length scaffolds were assembled.³⁵ Bioinformatics analysis revealed the presence of more than 52 BGCs of secondary metabolites. 28 of these BGCs contain genes coding for PKSs and 18 for NRPSs or NRPS-like enzymes. Some of these BGCs show considerable similarity to those of known compounds such as sterigmatocystin and viridicatumtoxin.³⁵ However, neither genetic manipulation in *A. ustus* 3.3904, nor investigations on the biosynthesis of its metabolites has been reported, prior to our studies. In this thesis, this PhD candidate mainly focuses on the genetic manipulation in *A. ustus* 3.3904 to elucidate the biosynthetic pathways of several SMs.

1.3 Biosynthesis of natural products

1.3.1 Polyketide synthases

Polyketide synthase (PKS) is one of the most abundant enzyme class attributed in microorganisms for natural product biosynthesis. On the basis of their structural composition, PKSs can basically be divided into three classes. Type I PKSs are large multidomain megaenzymes with distinct modules. Type II PKSs, are enzyme complexes with mono functional proteins. Type III PKSs have no acyl carrier protein domain. The polyketide backbone is formed by condensation of starter units such as acetyl-CoA, propionyl-CoA, or benzoyl-CoA with extender units via Claisen condensation.^{2,36,37} The type I and type II PKSs will be discussed in this section.

1.3.1.1 Modular type I polyketide synthases

Type I PKSs have been discovered in both bacteria and fungi. Type I PKSs can be basically classified into two subdivisions, *i.e.* modular and iterative type I PKSs.³⁶ Modular type I PKSs are commonly found in bacteria³⁶ and are usually large enzymes containing multi-domains including β -ketoacyl synthase (KS), acyl transferase (AT), and acyl carrier protein (ACP), keto reductase (KR), dehydratase (DH), enoyl reductase (ER), and thioesterase (TE) domains. Each module is used only once. One example of the

1. INTRODUCTION

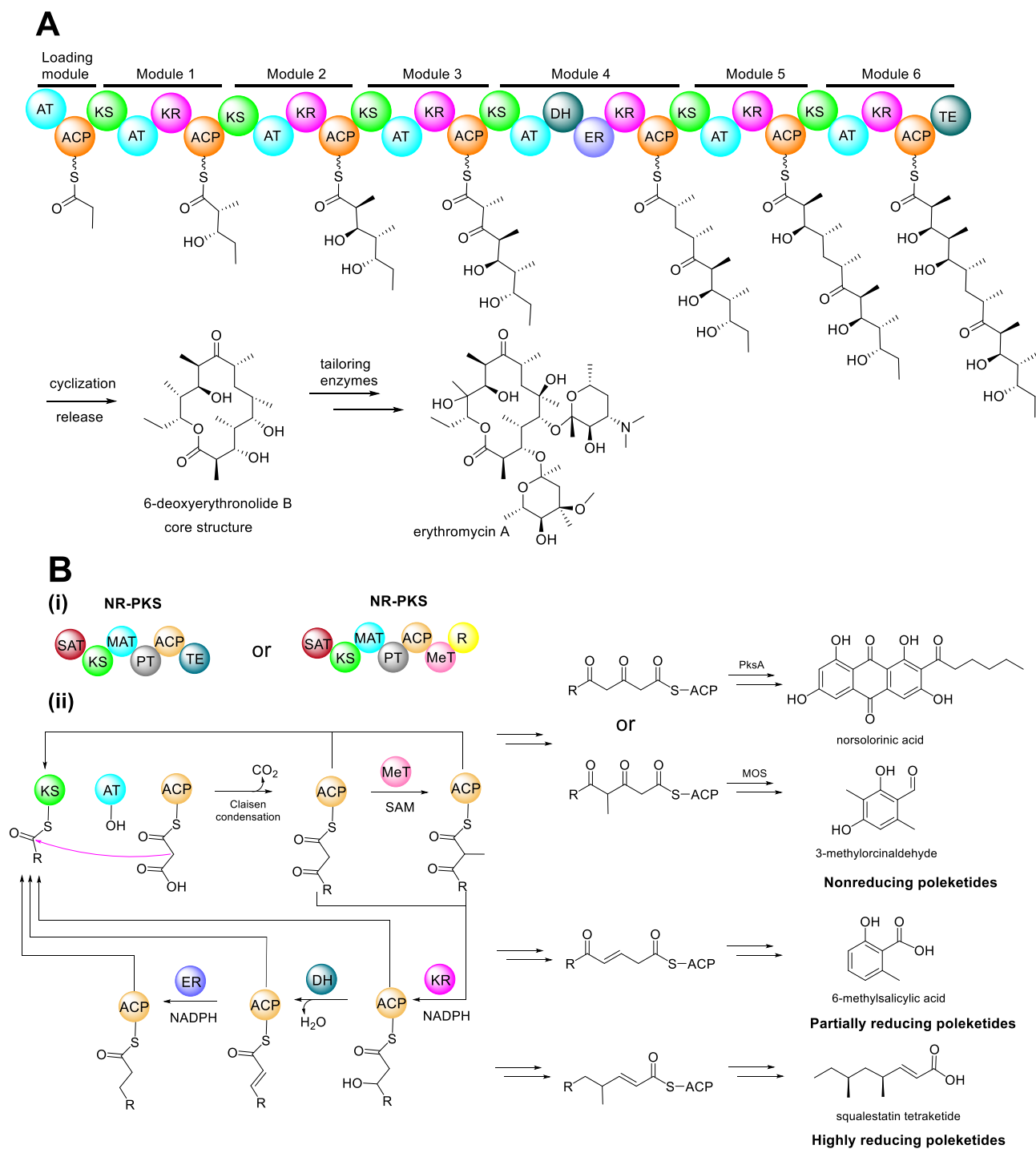


Figure 7. Assembly line for type I PKS. **A** example of modular type I PKSs. **B** iterative type I PKSs

typical modular type I PKS is the 6-deoxyerythronolide B synthase (DEBS) from *Saccharopolyspora erythraea*, assembling the core structure 6-deoxyerythronolide B. Subsequent modifications by tailoring enzymes lead to the production of erythromycin A (Figure 7A).³⁸

1.3.1.2 Iterative type I polyketide synthases

Iterative type I PKSs are usually found in fungi. The multiple domain enzymes can be basically divided into three classes by the reduction level of their products: nonreducing PKS (NR-PKS), partially reducing PKS (PR-PKS), and highly reducing PKS (HR-PKS). All of them contain the minimal PKS domains (KS, AT, and ACP), the NR-PKSs lack the β -keto processing domains including KR, DH, and ER domains present in the HR-PKSs or PR-PKS. On the other hand, there are additional functional domains that are unique to the NR-PKSs, including the starter unit acyl transferase (SAT) domain, product template domain (PT domain), and thioesterase–Claisen cyclase (TE–CLC) domain (Figure 7Bii).^{39,40}

The fungal NR-PKSs are usually responsible for the production of aromatic PKs. Norsolorinic acid, a precursor in the biosynthesis of aflatoxin, for example, is a typical NR-PKS product. The PksA utilizes hexanoyl-CoA as starter unit by SAT domain and elongates with 7 malonyl-CoA catalyzed by KS, MAT (malonyl-CoA-ACP transacylase), and ACP to form the polyketide chain. Cyclization of the intermediate is catalyzed by the product template domain and the aromatic intermediate is released by TE–CLC domain to form the end product norsolorinic acid.⁴¹ This is an example of the simplest NR-PKS systems (Figure 7Bi).

In some cases, NR-PKSs contain a reductive (R) domain at the C-terminal as release domain (Figure 7Bi). In addition, a methyltransferase (MeT) domain is usually located between the ACP and the R domain. The products of such NR-PKSs are usually found to be aldehydes. For example, the 3-methylorcinaldehyde synthase (MOS) with a SAT-KS-MAT-PT-ACP-MeT-R domain structure from *Acremonium strictum* is responsible for the production of 3-methylorcinaldehyde. Instead of releasing the intermediate by TE domain, the R domain was identified as a releasing domain.^{42,43}

Another significant difference between fungal and bacterial PKS systems is the mode of methylation (Figure 7Bii). Bacterial PKSs can utilize methyl-malonate as an extender unit. However, the fungal PKSs usually methylate growing chains at the β -dicarbonyl position by a C-methyltransferase (C-MeT) domain with SAM as cosubstrate.³⁶ Mutation of key residues in the C-MeT domain of a PKS led to complete abolishment of polyketide production, indicating the essential role of the C-MeT domain in PKS assembly line.⁴⁴ Recently, the crystal structure of the C-MeT in the biosynthesis of citrinin from *Monascus purpureus* was elucidated with a 1.5 Å resolution, which largely extended the knowledge of the catalytic mechanism.⁴⁵ The conserved motif GxGxGG (residues 1,992–1,997) and the key catalytic residue H2067 for enolization was verified in the structure. Biochemical investigation proved that the C-MeT domain can catalyze the multi methylation steps during the PKS assembly line.

1.3.1.3 Type II polyketide synthases

Type II PKSs are usually found in bacteria and responsible for the biosynthesis of aromatic core structure.² An outstanding example is the oxy BGC coding the enzymes in the biosynthesis of oxytetracycline, which has been identified in several *Streptomyces* strains (Figure 8).^{46,47} The minimal PKSs containing KS- α , KS- β , and ACP, employ malonamyl-CoA as starter unit to assemble eight malonyl-CoA extender units into a poly- β -carbonyl intermediate. The intermediate is then cyclized and modified to the core structure 1,6-methylpretetramid, which can be further converted to oxytetracycline by diverse tailoring enzymes.^{46,47}

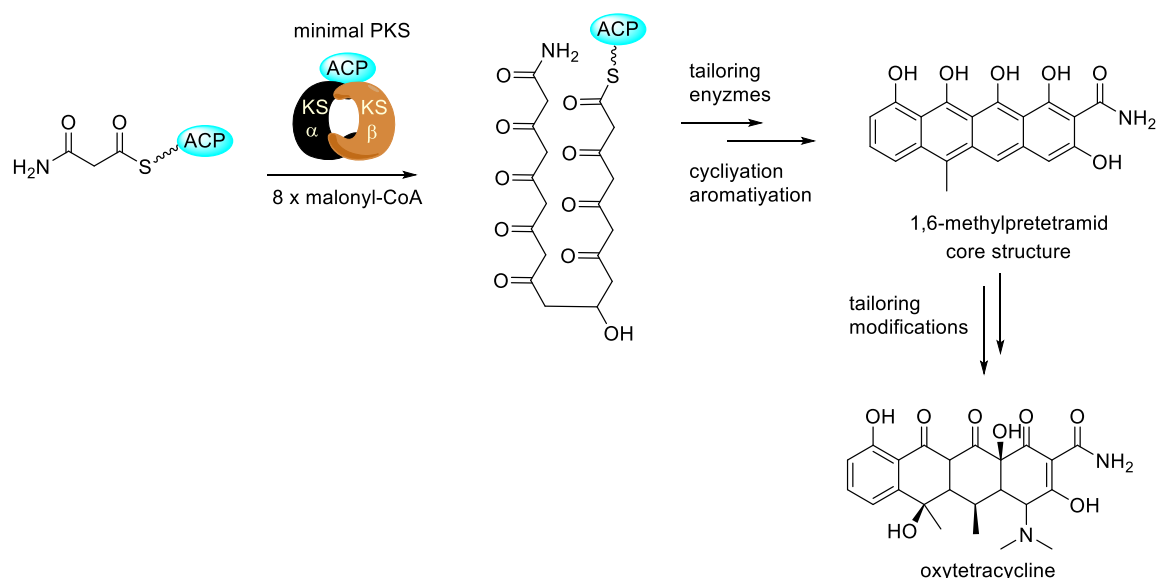


Figure 8. Assembly line for oxytetracycline by a typical type II PKS

1.3.2 Nonribosomal peptide synthetases

NRPSs are ribosomally independent enzymes that form modular templates to assemble specific peptide derivatives. Usually, the NRPSs are large modular complexes (Type I NRPS).⁴⁸ Recently, some standalone NRPSs or di-domains that coordinate to form unique amino acid derivatives were also reported (Type II NRPS).⁴⁸ In this part, the assembly line for the Type I NRPSs is discussed.

1.3.2.1 Assembly logics of nonribosomal peptide synthetases

As aforementioned, NRPs from microorganisms are important sources for drug discovery and many market drugs are from NRPs. Excellent examples are ergotamine for migraine (Figure 4), tyrothricin, vancomycin, capreomycin, lincomycin and daptomycin as antibiotics, and cyclosporine as an immunosuppressive drug.¹³ The backbones of NRPs are biosynthesized by the well-known NRPSs.

1. INTRODUCTION

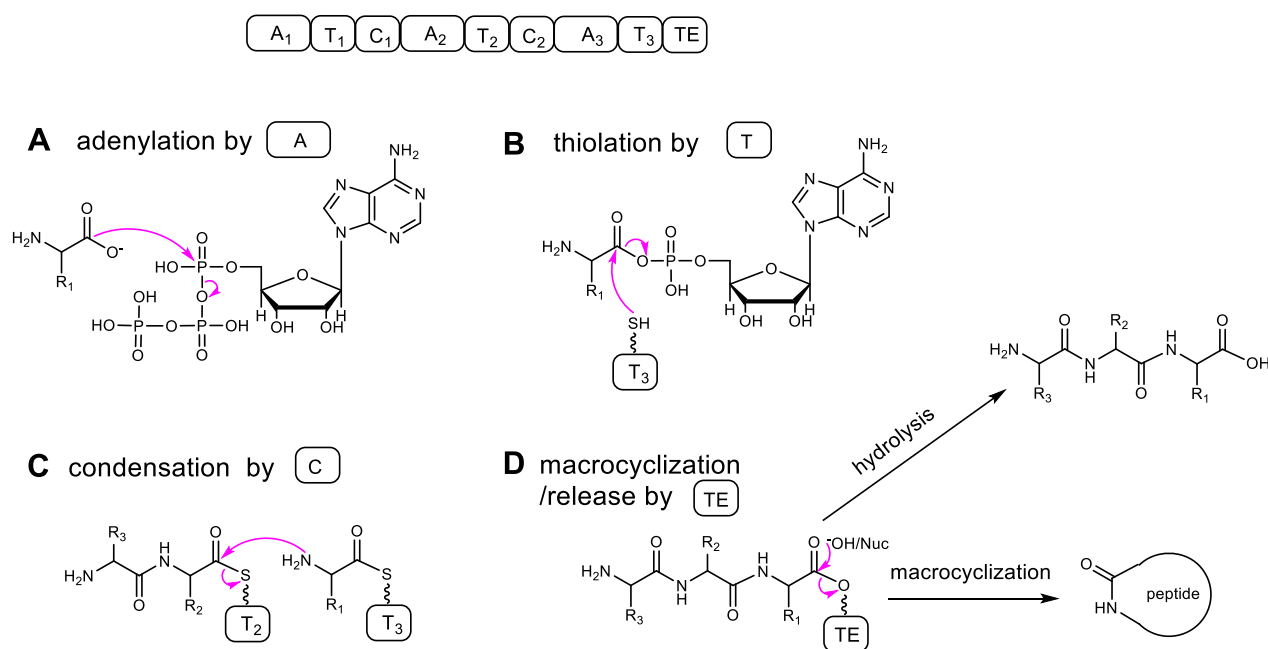


Figure 9. Core domains of NRPS and their catalyzed reactions

The core NRPS domains consist of adenylation (A) domain, thiolation or peptidyl carrier protein (T or PCP) domain, and condensation (C) domain (Figure 9). Firstly, A domains recognize and activate their cognate amino acids by selectively binding the amino acids and converting them to high-energy aminoacyl-AMPs at the expense of ATP molecules. Secondly, the A domain protects the high-energy intermediate from bulk water to subsequently catalyze its loading onto the Ppant arm of the holo-T domain. Then, the C domain catalyzes peptide bond formation between the activated amino acids or nascent peptide which is attached to the upstream T domain. After aforementioned three steps, the oligopeptidyl-enzyme intermediate is formed. Usually, a conserved serine residue in TE domain forms an ester bond with the C terminus of the oligopeptide. Hydrolysis or intramolecular attack of a nucleophilic moiety of the intermediate leads to the formation of a linear or macrocyclic product, respectively (Figure 9).^{13,49,50}

Additional domains of NRPSs

TE domain. After NRP assembly line is finalized, the T domain located in the termination module transfers the mature peptide to the TE domain for releasing the peptide from the NRPS. The TE domain contains a conserved catalytic triad of Ser residue that links the mature peptidyl intermediates. Product release from the TE domain follows either by hydrolysis (water as a nucleophile) or aminolysis (amine as a nucleophile), thereby liberating linear products. In addition, TE domains often acts as cyclases by constraining the substrate's conformation to form a lactone or lactam. Both head-to-tail, e.g. gramicidin S,⁵¹ and side-chain-to-tail, e.g. daptomycin,⁵² exist in numerous NRPs.

1. INTRODUCTION

Epimerization domain. Most of NRPs are equipped with D-amino acids which confer beneficial properties, e.g. predetermining bioactive conformations or protecting against peptidase and protease attacks.⁵³ The epimerization in NRPS is usually catalyzed by an epimerization (E) domains, embedded within the assembly line (Figure 10). It acts on T domain-bound aminoacyl substrates and plays an essential role in NRPS assembly line.⁵⁰ In tyrocidine biosynthesis in *Bacillus brevis*, the C₅ domain only utilizes D-Phe-L-Pro-L-Phe-D-Phe-PCP, a product of E₄ domain, as a substrate for condensation.⁵⁴ In the biosynthesis of acetylszonalenin from the fungus *Neosartorya fischeri*, compared with the amount of the cyclodipeptide with Ant and D-Trp produced by the wild-type, less than 1% of *cyclo*-Ant-L-Trp was detected as product after inactivation of the E domain.

Bioinformatics analysis indicated that E domain is descendant of the C domain. A common acid-base catalytic mechanism of E domains with exogenous cofactors was proposed.¹³ For example, in the TycA assembly line, the Glu882 residue abstracts the α -proton, while the His743 residue and the dipole moment of α -helix 4 possibly stabilize the transient enolated intermediates.⁵⁵

Methyltransferase domain. Most of methylations in NRP biosynthetic pathways are performed by MeT domains which are integrated into the A domain (Figure 10). A MeT domain transfers the methyl group from its co-substrate SAM to the growing peptide chain. Until now, *N*-methylation of the peptide backbone is the most abundant type. *O*-, *S*-, and *C*-methylations have also been reported.¹³

Reductase domain. The R domain catalyzes the reduction of the tethered peptidyl thioester to aldehyde or primary alcohol (Figure 10). It has been proven biochemically that the R domain acts as a NAD(P)H-dependent reductase and replaces the TE domain of a termination module.⁵⁶ Similar to TE domains, R domains do not essentially need tethered substrates to be provided by their upstream T domains.

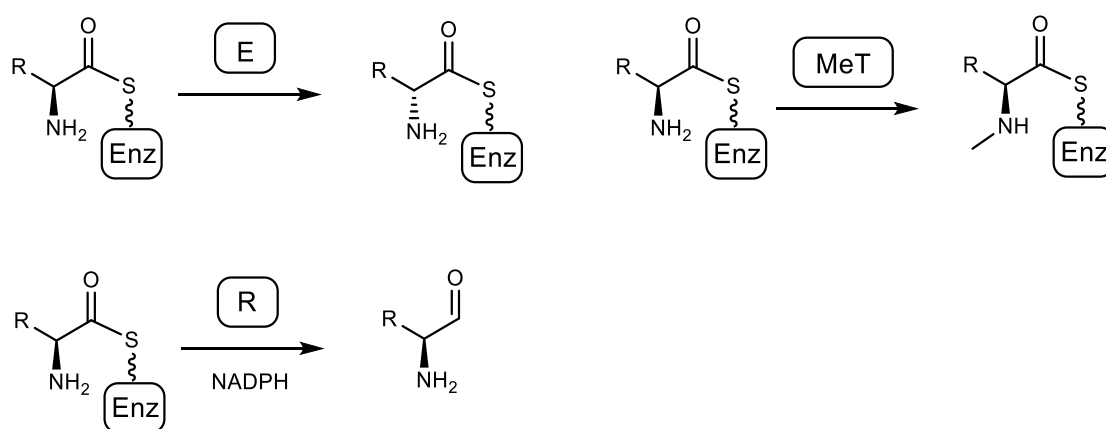


Figure 10. Tailoring enzymes in NRPS assembly line and their functions

1. INTRODUCTION

Other tailoring domains. Besides the aforementioned domains, other features like communication domains for the interactions between the C-terminal domain of the first modular and the N-terminal domain of the second modular, formylation domain for *N*-formylation, halogenase domain, cyclization domain and oxidation domain for the five-membered ring formation (thiazoline to thiazole), and monooxygenase domain have also been reported.¹³ Even the typical PKS domains KR and DH were found in NRPSs, which largely expand the NRPS diversity.¹³

1.3.2.2 Biosynthesis of quinazolinone derivatives in fungi

As described in sections 1.1.2, fungal peptidyl alkaloids, especially those biosynthesized by NRPSs are structurally diverse natural products with high affinity for various biological targets. Unlike bacterial NRPSs employing TE domains to perform cyclization, many fungal NRPSs use a terminal condensation-like domain (C_T domain) as the terminal domain to produce peptidyl products.⁵⁷ Bioinformatics analysis of the C_T domain from several fungi revealed the highly conserved HXXXDXXS motif in the active sites. Point mutation of the His residue led the inactivation of the C_T domain, proving its essential role for the NRP cyclization (Figure 11).⁵⁸

It has been proven that quinazolinone-related cyclic tripeptide derivatives are natural products assembled by a tri-modular NRPS containing three A-T-C modules, which use anthranilate as a common residue for the backbone formation.⁵⁹ Normally, the macrocycle of NRPs is formed via an ester bond catalyzed by a TE domain, which leads to the production of the most cyclized peptides.¹³ However, for the biosynthesis of the quinozalinone NRPs, a two-step cyclization mechanism was speculated.^{58,60} The first step is the formation of a ten-membered macro ring from the tripeptidyl thioester, followed by spontaneous intramolecular annulation as second step to form the quinazolinone core (Figure 11).

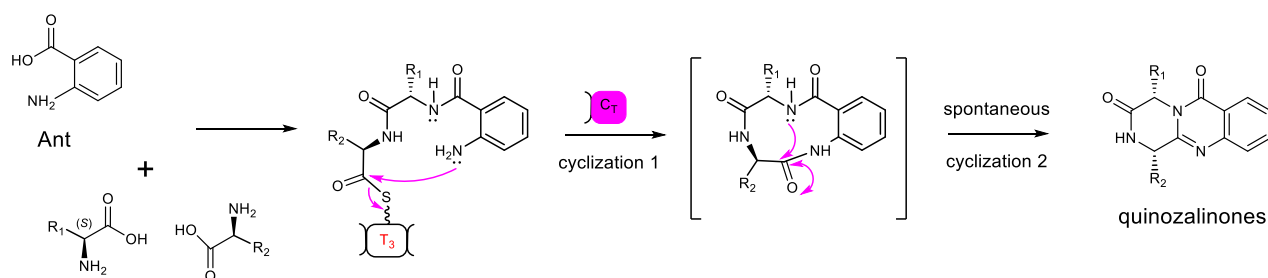


Figure 11. Quinazolinone backbone formation catalyzed by a terminal condensation-like domain in NRPS

1. INTRODUCTION

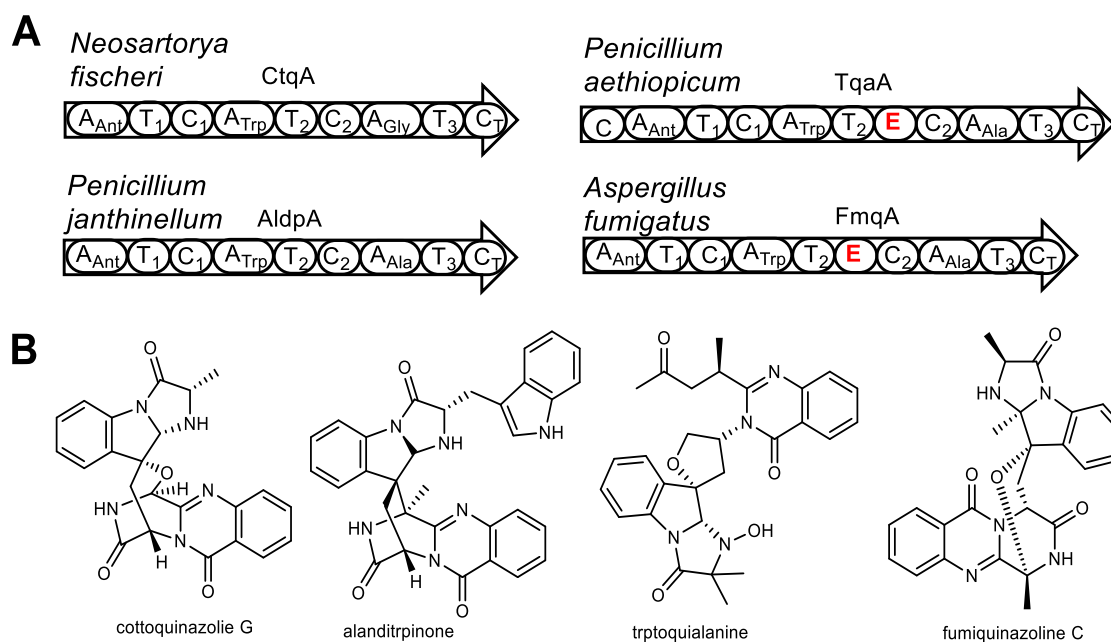


Figure 12. Known NRPS genes in different fungi (A) for quinazolinone derivatives (B)

Despite the structural diversity of quinazolinone peptidyl products, only a few NRPSs for quinazolinone tripeptides have been reported previously. These are FmqA from *Aspergillus fumigatus* for the fumiquinazoline C biosynthesis,⁶¹ TqaA from *Penicillium aethiopicum* for the tryptoquialanine formation,⁶² AldpA from *Penicillium janthinellum* for alanditrypinone, and CtqA from *Neosartorya fischeri* NRRL181 for the biosynthesis of cottoquinazolines.⁶³ The NRPS AspA from *Aspergillus alliaceus*, which coordinates Ant, Ant, and Trp to form asperlicins, shares similar domain structure with FmqA, TqaA, AldpA, and CtqA.⁶⁴ The NRPSs together with their tailing redox enzymes, mostly flavin-dependent- and nonheme Fe^{II}/2-oxoglutarate-dependent monooxygenases (Fe^{II}/2-OG-dependent oxygenases), increase the structural complexity in quinazolinone peptidyl products (Figure 12). Comparison of the structures of oxepinamides with that of the quinazolinone backbone revealed the only difference in the Ant residue. While quinazolinones contain a benzene ring in quinazolinone backbone, oxepinamides carry an oxepin ring. It can be speculated that the oxepinamides might also be trimodular NRPS derivatives.

1.3.3 Tailoring enzymes

As introduced in section 1.3.1 and 1.3.2, PKSs and NRPSs synthesize different backbones of numerous SMs. For the most natural products, they are further modified in an enzymatic or nonenzymatic manner. As the rapid development in studies on the natural product biosynthesis, plentiful enzymes for backbone modifications have been identified biochemically, e.g. oxidoreductases, transferases like. MeTs, glycosyltransferases, acyltransferases, and prenyltransferases.^{65,66} In this section, four important enzyme

Cytochrome P450 enzymes (P450s) are the most common biological biocatalysts in natural product biosynthesis. Generally, P450s function as monooxygenases catalyzing the hydroxylation and epoxidation steps. Recently, increased cases demonstrated other intriguing functions of P450s, *e.g.* intramolecular and intermolecular aromatic ring coupling, C–C bond cleavage, ring formation or expansion.⁶⁷ Here, the general catalytic mechanism of hydroxylation and epoxidation by P450s will be discussed.

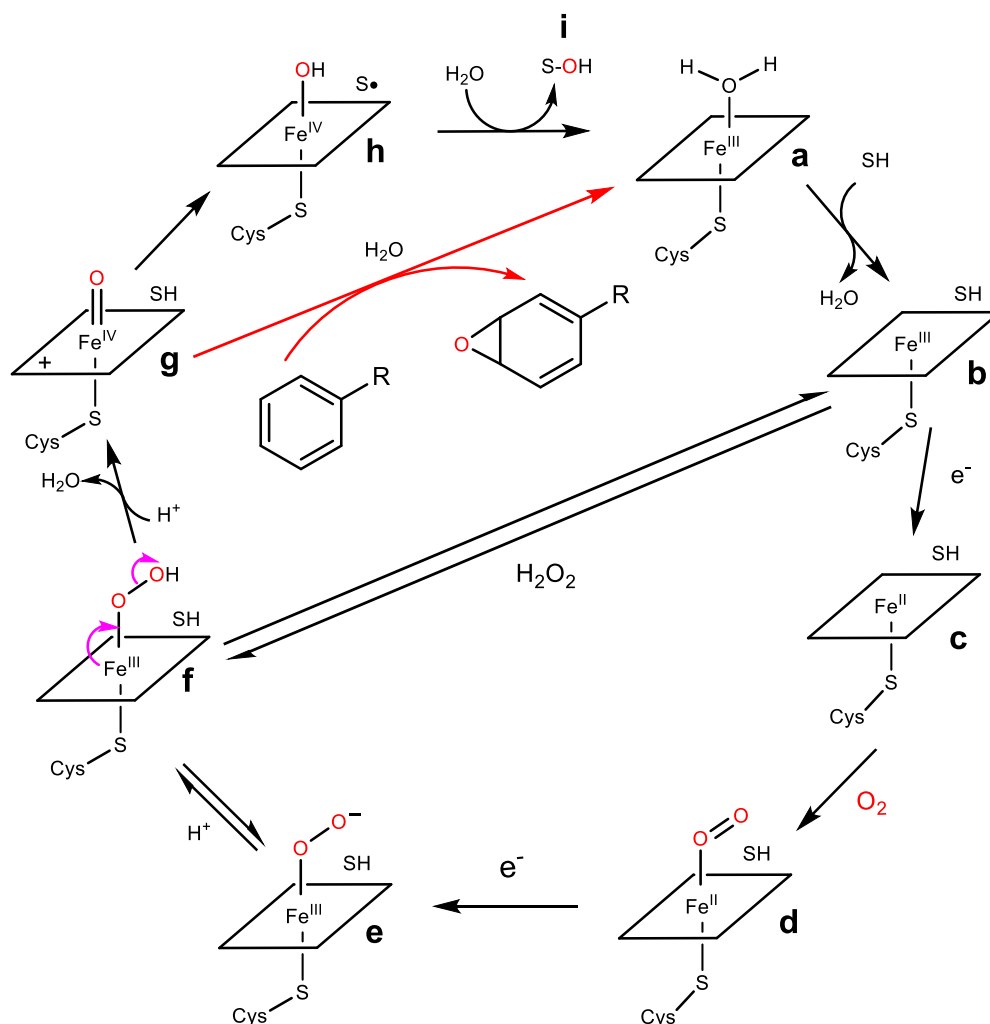


Figure 13. Catalytic cycle of a cytochrome P450 enzyme for hydroxylation and epoxidation in fungi

1. INTRODUCTION

Based on amino acid sequences, P450s can be basically divided into ten classes.⁶⁸ In fungi, the diversity of P450s is tremendous, and they are involved in the biosynthesis of a wide range of metabolites including primary and secondary metabolites as well as in the environmental pollutant degradation process.⁶⁹ The majority of the fungal P450s are membrane-bound proteins belonging to class II P450s and catalyze extremely diverse oxidations. Basically, fungal P450s perform the monooxygenase reaction by inserting one atom of oxygen molecular into the substrate, and reducing the second oxygen atom into water.⁷⁰

P450-catalyzed hydroxylation undergoes a general nine-stage catalytic mechanism (Figure 13): **(a)** the formation of the ferric heme-iron (Fe^{III}) complex with six ligands that contain four nitrogen atoms of the porphyrin (Por) ring, the absolutely conserved cysteine (Cys), and one water molecule. **(b)** The substrate (SH) enters the active site and binds to the Fe^{III} complex with the replacement of the water ligand, which is in the oxidized state. **(c)** Cytochrome P450 reductase (CPR) using FAD and FMN as cofactor transfers one electron to from NAD(P)H to Fe^{III} complex leading to the production of Fe^{II} complex as the 'first reduction step. **(d)** By binding of one molecular oxygen, the ferrous heme-iron (Fe^{II}) converts to the dioxygen adduct [$\text{Cys-Fe}^{\text{II}}\text{-O}_2$]. **(e)** The CPR (or cytochrome b5) transfers the second electron to [$\text{Cys-Fe}^{\text{II}}\text{-O}_2$] leading to the production of ferric peroxo intermediate [$\text{Cys-Fe}^{\text{III}}\text{-OO}^-$]. **(f)** The negatively charged intermediate can be quickly protonated to ferric hydroperoxo intermediate [$\text{Cys-Fe}^{\text{III}}\text{-OOH}$]. **(g)** Subsequently, the second protonation and heterolytic cleavage of the O–O bond gives the reactive ferryl-oxo intermediate [$\text{Cys-Fe}^{\text{IV}}\text{=O}]^+$ with concurrent loss of a water molecule (porphyrin π -cation radical). **(h)** This extremely reactive species abstracts a hydrogen atom from the substrate, yielding a substrate radical and the ferryl-hydroxo compound. **(i)** The radical rebound to the hydroxyl group of intermediate results in the insertion of an oxygen atom into the substrate leading to the formation of the hydroxylated product (SOH) or epoxidation products. The product is then released from the active site and rebounding a water molecule to the ferric heme-iron (Fe^{III}) complex restores the resting state **(a)**. An alternative route is binding of H_2O_2 to the ferric heme-iron (stage **b**), which leads to the peroxide stage **f**.^{67,70,71}

1.3.3.2 Flavin-dependent oxygenases

Flavin cofactors are mostly used as redox catalysts by enzymes and are originated from riboflavin (vitamin B2) that is converted to flavin mononucleotide (FMN) and flavin adenine dinucleotide (FAD) in the cells. The majority of flavin-dependent enzymes catalyzes oxidations. However, reactions such as halogenation by the brominase Bmp2,⁷² pyrrolizine ring reconstruction via intramolecular C–N bond formation catalyzed by Clz9,⁷³ and C–N bond formation⁷⁴ have also been reported.^{75,76} In this section,

1. INTRODUCTION

the catalytic mechanisms of flavin-dependent oxygenases using NAD(P)H as cofactor will be discussed briefly.

Based on protein sequence motifs, structural features, electron donors, and oxygenation types, flavin-dependent monooxygenases can be basically divided into eight classes. Most flavin-dependent monooxygenases, which utilize NAD(P)H as electron donor, belong to the classes A and B.⁷⁷ Despite of the fact that various flavin-dependent monooxygenases have been discovered, just two catalytic mechanisms with C4a-hydroperoxy and N5-oxide as reactive oxygenating species were reported (Figure 14).⁷⁸

Usually, the flavins including FAD and FMN exist commonly in their oxidized form Fl_{ox} under aerobic conditions. After transferring two electrons from the donor NAD(P)H, the Fl_{ox} intermediate is converted to its reduced form Fl_{red} . O_2 as electron acceptor reacts with Fl_{red} in two ways, which produces oxygenating species in form of flavin-C4a-hydroperoxide ($\text{Fl}_{\text{C4a[OOH]}}$) or flavin-N5-oxide ($\text{Fl}_{\text{N5[O]}}$). These two

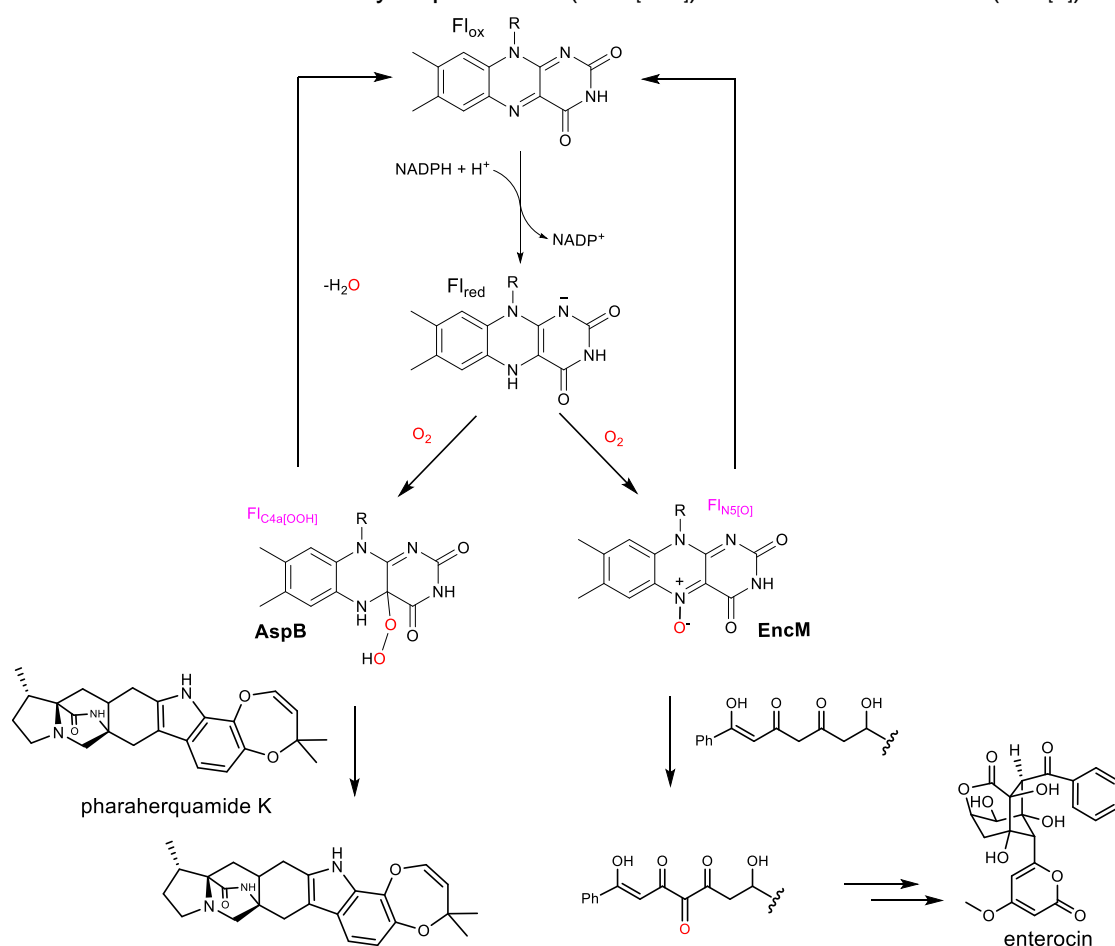


Figure 14. $\text{Fl}_{\text{C4a[OOH]}}$ and $\text{Fl}_{\text{N5[O]}}$ catalytic mechanisms of flavin-dependent enzymes with AspB and EncM as examples

1. INTRODUCTION

intermediates can serve as nucleophilic oxygenating agents for their substrates.⁷⁶ The produced C4a-hydroflavin will be dehydrated to Fl_{ox} for the next reaction cycle (Figure 14).

Most reactions catalyzed by flavin-dependent monooxygenases including hydroxylation, epoxidation, and Baeyer-Villiger oxidation follow the typical Fl_{C4a}[OOH] mechanism.⁷⁶ The fungus-derived flavin-dependent monooxygenase AspB converts an indole to a 2-keto indoline ring via a postulated arene oxide intermediate, which was proven to utilize Fl_{C4a}[OOH] as a key intermediate.⁷⁹ The typical Fl_{N5}[O] monooxygenase is EncM in the biosynthesis of enterocin from several *Streptomyces* strains.^{80,80-82} EncM harbors the Fl_{N5}[O] as oxygenating species and the poly- β -carbonyl intermediate acts as electrophilic substrate that triggers the Favorskii-like rearrangement of the polyketide carbon backbone and multiple cyclization reactions to form the final product enterocin (Figure 14).^{80,80-82}

1.3.3.3 Nonheme Fe^{II}/2-oxoglutarate-dependent monooxygenases

Nonheme Fe^{II}/2-oxoglutarate (Fe^{II}/2-OG)-dependent monooxygenases are widely distributed in microorganisms and catalyze numerous types of reactions. For example, CitB acts as a hydroxylase, AmbO5 as a halogenase, and CODM as an O-demethylase.⁸³ In this section, the general catalyzed mechanism of Fe^{II}/2-OG-dependent monooxygenases is briefly introduced.

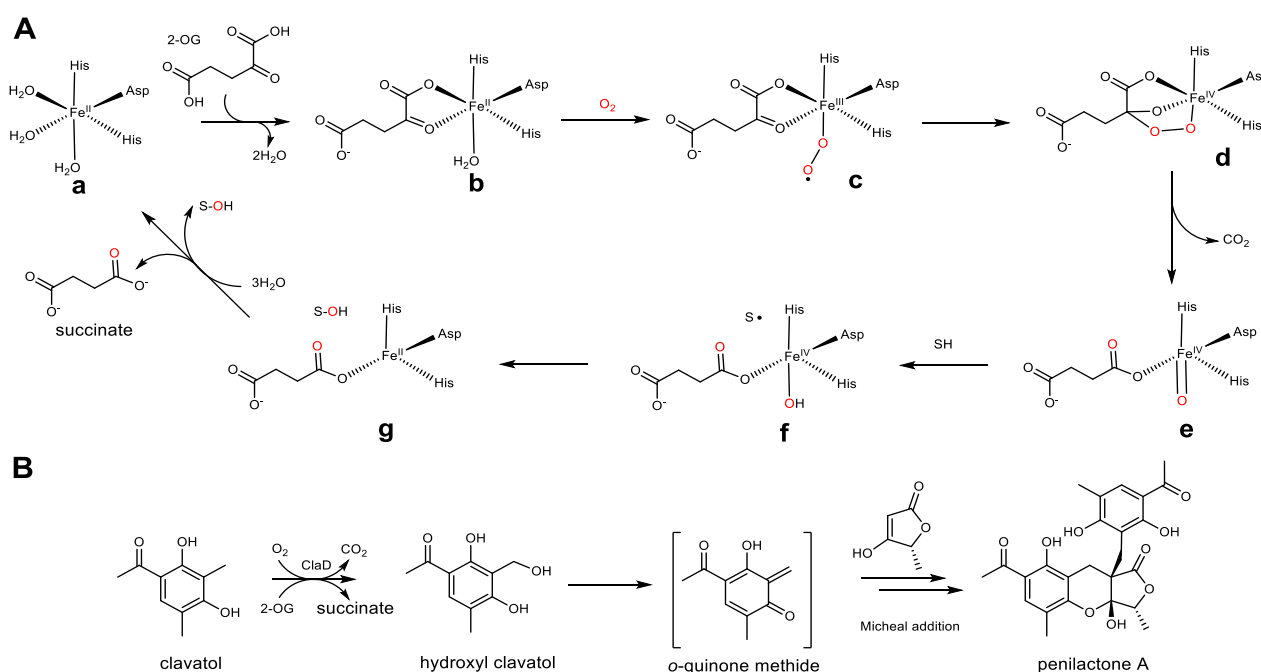


Figure 15. Catalytic mechanisms of Fe^{II}/2-OG-dependent enzymes. **A:** The catalytic cycle of hydroxylation by Fe^{II}/2-OG-dependent enzymes. **B:** Fe^{II}/2-OG-dependent enzyme ClaD in the biosynthesis phenylactone A

1. INTRODUCTION

For the most of previously reported Fe^{II}/2-OG-dependent monooxygenases, the catalysis is initiated by coordination of Fe^{II} to three water molecules and the conserved 2-His-1-Asp facial triad ligands (stage **a**) (Figure 15A).^{84,85} The intermediate of stage **b** is produced via the displacement of two water molecules with the keto and carboxyl groups of 2-oxoglutarate in the Fe^{II} center. The replacement of the third water molecule of the Fe^{II} center with one O₂ molecule leads to the production of the Fe^{III}-superoxo intermediate (stage **c**). A peroxohemiketal bicyclic intermediate (stage **d**) is generated after attacking the keto group in the 2-oxoglutarate by the distal oxygen atom of the Fe^{III}-superoxo species. A subsequently oxidative decarboxylation yields the high valence Fe^{IV}=O (ferryl) intermediate (stage **e**). Similar to that of P450s, this very reactive species abstracts a hydrogen atom from the substrate (SH) to reduce the iron to the Fe^{III}-OH form accompanied by the substrate radical (S•) formation (stage **f**). The rebounding of hydroxyl radical with the substrate radical leads to the production of the hydroxylated product (S-OH) as well as the Fe^{II} species binding with one succinate (stage **g**). The release of the succinate and the attachment of three water molecules regenerate the initial state **a** for the next catalytic cycle (Figure 15A).⁸⁶

An outstanding example of the fungal Fe^{II}/2-OG-dependent monooxygenase is ClaD in the biosynthetic pathway of peniphenones and penilactones in *Penicillium crustosum*. ClaD utilizes Fe^{II} and 2-oxoglutarate as cofactors to hydroxylate the methyl group of clavatul. After spontaneous dehydration to an *ortho*-quinone methide, the intermediate undergoes a nonenzymatic 1,4-Michael addition, which is essential for the backbone formation in the final products (Figure 15B).⁸⁷

1.3.3.4 Prenyltransferases

Prenyltransferases belong to one of the most important modifying enzymes of natural products and catalyze the transfer reactions of prenyl units ($n \times \text{C}_5$, $n=1, 2, 3, 4$ etc.) from prenyl diphosphates to different aliphatic and aromatic acceptors, which largely increases the diversity of natural products.⁸⁸ Members of the mostly biochemically and structurally investigated PT group share significant sequence identities with the dimethylallyltryptophan synthase in the biosynthesis of ergot alkaloids and are therefore termed DMATS enzymes.^{57,88-90} Most PTs of the DMATS superfamily use dimethylallyl diphosphate (DMAPP) as donor and L-tryptophan or tryptophan-containing cyclodipeptides as acceptors and are involved in the biosynthesis of diverse indole alkaloids.^{57,88} The dimethylallyl moieties are attached to N-1, C-2, C-3, C-4, C-5, C-6, or C-7 of the indole ring in a regular or reverse manner (Figure 16A). For the regular prenylation, DMAPP was proposed to form a dimethylallyl cation/pyrophosphate ion pair. The primary center of DMAPP is attacked by the electron-rich aromatic ring with a concerted displacement of pyrophosphate to form the arenium ion intermediate, which re-aromatizes by deprotonation to form the final product.⁹¹⁻⁹³ For the reverse prenylation, the nucleophilic attack takes place at the tertiary center instead of the primary center of the dimethylallyl carbocation. Reverse prenylation on the indole ring takes

1. INTRODUCTION

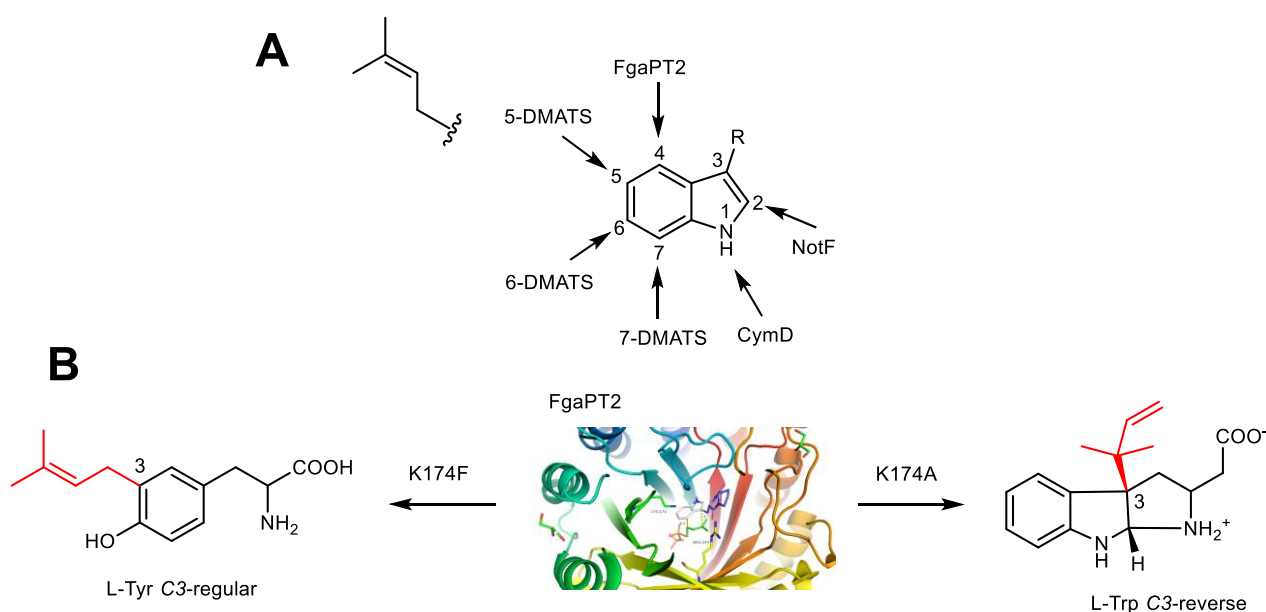


Figure 16. A Enzymatic N1, C2, C4, C5, C6 and C7 prenylation of indole ring. **B** multifunction of FgaPT2 after site-directed mutation

mainly place at C-2 and C-3 of the cyclodipeptides, like those of *cyclo*-L-Trp-L-Pro catalyzed by NotF and BrePT,^{94,95} *cyclo*-L-Trp-L-Ala by EchPT1,⁹⁶ *cyclo*-D-Trp-Ant by AnaPT,⁹⁷ and *cyclo*-L-Trp-L-Leu by CdpC3PT.⁹⁸ L-tryptophan is usually regularly prenylated at C-4, C-5, C-6, and C-7 positions, as demonstrated for FgaPT2,⁹⁹ 5-DMATS,¹⁰⁰ 6-DMATS,¹⁰¹ and 7-DMATS, respectively.¹⁰²

FgaPT2 from *Aspergillus fumigatus* was identified as a C4-DMATS, which initiates the biosynthesis of the ergot alkaloids fumigaclavines.⁹⁹ The crystal structure of FgaPT2 contains a rare β/α fold (PT barrel) and serves as a basis for understanding the prenylation mechanism and for enzyme design.^{92,93} Structure-based molecular modelling and site-directed mutagenesis revealed that Lys174 facilitates the entrance of substrates in the reactive center and Ile80, Leu81, Tyr191, and Arg244 anchor the polar side chain of L-tryptophan.⁹³ Mutation of Lys174 to Phe switches FgaPT2 to a tyrosine C3-prenyltransferase FgaPT2_K174F.¹⁰³ Arg244 mutants significantly enhance the catalytic ability of FgaPT2 towards tryptophan-containing CDPs and keep the prenylation position at C-4.¹⁰⁴ Luk *et al*¹⁰⁵ demonstrated that FgaPT2_K174A can prenylate L-tryptophan at both C-3 and C-4 position and proposed the C4-prenylated derivative to be the result of Cope rearrangement of a C3-prenylated derivative. Acceptance of tryptophan-containing CDPs by FgaPT2_K174A has not been tested before, while FgaPT2 was also demonstrated to prenylate these compounds at C-4, *i.e.* the same position as for the natural substrate L-tryptophan (Figure 16B). All these results proved FgaPT2 as an excellent model for enzyme design by site-directed mutagenesis.

2. Aim of this thesis

In this thesis, the following issues have been addressed:

(1). Biosynthesis of ustethylins and the formation of benzoyl esters

Despite the abundant secondary metabolites from *Aspergillus ustus*, biosynthesis of only few natural products were reported. Cultivation of the fungus *Aspergillus ustus* 3.3904 in PD media led to the detection of a dominant unknown product. Feeding alcohols to the three-day old culture led to significant decrease of this peak and the formation of benzoyl esters. The biosynthesis of these esters has not been reported before. The aim of this project is to identify the structure of the unknown dominant peak and to elucidate its biosynthetic pathway as well as the molecular basis for the ester formation after feeding with alcohols.

The following experiments were carried out:

- Isolation and structural identification of the dominant peak ustethylin A from *Aspergillus ustus* culture in PD media.
- Elucidation of the origin of ustethylin A by feeding with different isotopic precursors
- Identification of the putative *utt* BGC by bioinformatics analysis
- Verification of the gene function of *utt* BGC in the biosynthesis of ustethylin A by gene deletion, feeding experiments, and heterologous expression
- proving the relationship of ester formation to the ustethylin A biosynthesis

The designed experiments of this project have been successfully finished in cooperation with Yiling Yang. She isolated and identified the metabolites and also carried out isotopic feeding experiments.

(2). Elucidation of two oxepinamide biosynthetic pathways

Oxepinamides D, E, and F are rare bioactive fungal metabolites derived from Oxepine-Pyrimidinone-Ketopiperazine (OPK) backbone and were isolated from rice cultures of *Aspergillus ustus*. Based on their structures, it can be deduced that oxepinamides are products of NRPSs. The biosynthesis of the oxepinamides, especially the formation of the oxepin ring was still unclear before this study. Furthermore, elucidation of the tailoring enzymes will largely contribute to our understanding on the structural diversity of the oxepinamide family. The aim of this project is to identify the biosynthetic gene clusters of oxepinamides D, E, and F, to elucidate the formation of the oxepin ring, and the tailoring modifications afterward.

The following experiments were carried out:

2. AIM OF THIS THESIS

- Isolation and identification of oxepinamides D, E, and F from the rice culture of *Aspergillus ustus* 3.3904.
- Identification of the *opa* BGC for the biosynthesis of oxepinamides E and F and *opa2* BGC for oxepinamide D.
- Verification of the putative NRPSs OpaA and OpaA2 for assembling the quinazolinone core structures.
- Identification of OpaB and OpaB2 as oxepinases for the oxepin formation and proof of their substrate specificity.
- Biochemical characterization of the flavin-dependent oxegenases OpaC and OpaC2 for hydroxylation at different positions of OPK backbone.
- Biochemical investigation of the epimerase OpaE catalyzing the configuration change of Phe residue from D- back to L- form during the biosynthesis of oxepinamides E and F.

The designed experiments of this project have been successfully finished in cooperation with Haowen Wang. She isolated and identified the oxepinamides and the biosynthetic intermediates.

(3). Switch the catalytic activity of a tryptophan prenyltransferases by protein design.

PTs belong to one of the most important modification enzymes of cyclodipeptides (CDPs) and are key enzymes to increase the structural diversity and biological activity of secondary metabolites. FgaPT2 has been characterized as a regular C4-prenyltransferase of L-Trp. Mutation of Lys174 and Arg244 can change the function of the enzyme and enhance its acceptance for CDPs as substance. The aim of this project is to explore the additional function of FgaPT2 and its mutants towards L-Trp containing CDPs.

The following experiments were carried out:

- Construction of mutants FgaPT2_K174A, FgaPT2_K174F, and FgaPT2_K174F_R244X (X= L, N, Q, Y) via sequential site-directed mutagenesis.
- Overexpression of the obtained mutants in *E. coli* BL21 (DE3).
- Purification of the recombinant proteins
- Activity tests of the obtained variants toward L-tryptophan-containing CDPs.
- Isolation and structural elucidation of the products.
- Determination of the kinetic parameters.

The designed experiments of this project have been successfully finished in cooperation with Dr. Peter Mai. He constructed several mutants and verified by sequencing.

3. Results and discussion

3.1 Biosynthesis of ustethylins in *Aspergillus ustus* and the shunted pathway after alcoholic feeding

As described in section 1.1.1.2, phenethyl-containing natural products are common microbial metabolites. The ethyl groups in phenethyl residue of bacterial metabolites are mostly originated from propionate as starter unit of PKSs.^{5,6} In fungi, the methyl group of the phenethyl residue is generally derived from SAM.^{8,12} However, the responsible genes/enzymes for the methylation have not been reported previously.

HPLC analysis of the EtOAc extract of an *A. ustus* 3.3904 culture in PD media revealed that ustethylin A (**1**) was almost the only product peak in the chromatogram. During isolation, the amount of ustethylin A (**1**) decreased evidently. Dissolving the finally isolated 7 mg sample in DMSO-*d*₆ led to precipitation immediately. The ¹H NMR spectrum of the supernatant was very complex, so that an interpretation was impossible. To overcome the instability, **1** in the fungal extract was immediately converted with Ac₂O NaOAc at room temperature¹⁰⁶ by Haowen Wang to its triacetate **2** for structural elucidation (Figure 17).

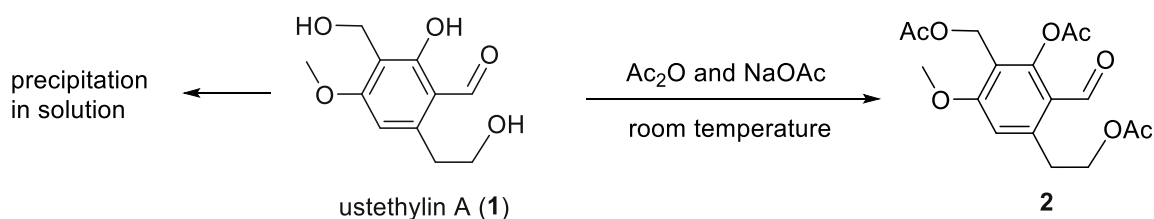


Figure 17. The structures of ustethylin A (**1**) and its triacetate (**2**)

To elucidate the origin of ustethylin A (**1**), we carried out feeding experiments with sodium [1,2-¹³C] acetate, sodium [1-¹³C] acetate, sodium [2-¹³C] acetate and [2-¹³C] malonic acid. The ¹³C NMR results proved that C-1/C-7, C-2/C-3, C-4/C-5, and C-6/C-9 are from four intact units originating from

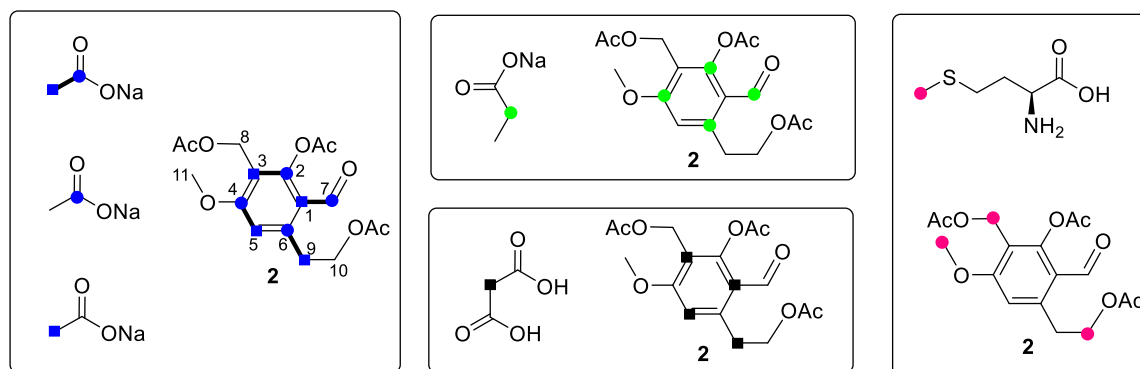


Figure 18. Labelling pattern of compound **2** after feeding different precursors.

3. RESULTS AND DISCUSSION

acetate/malonate (Figure 18). The ^{13}C NMR spectrum of **2** after feeding with [methyl- ^{13}C]-L-methionine showed enhanced signals for C-8, C-10 and C-11, proving that the methyl group of the phenethyl residue is also from SAM. To figure out whether *A. ustus* utilizes propionate as starter unit, sodium [2- ^{13}C] propionate was fed into the culture. To our surprise, the labelling pattern of **2** is very similar to that with [1- ^{13}C] acetate. No enrichment for C-9 at 31.5 ppm was observed. These results proved unequivocally that sodium [2- ^{13}C] propionate was not directly utilized for incorporation, but was degraded to acetyl-CoA likely via pyruvate by α -oxidation (Figure 18).¹⁰⁷

From the structure of **1**, it can be deduced that a NR-PKS would be responsible for the formation of its backbone.¹⁰⁸ Based on the bioinformatics and transcriptome analyses, the PKS gene *uttA* coding for KIA75596 (Figure 19) was one of the eighty best expressed genes under our culture conditions. HPLC analysis of the culture extract of a ΔuttA mutant showed complete loss of **1** production, proving its involvement in the biosynthesis of **1**. Heterologous expression of *uttA* in *A. nidulans* LO8030¹⁰⁹ leading to the production of three benzoic acid derivatives **3** – **5** (Figure 20). They differ from each other just in the methyl group at C-3 and the ethyl group at C-6 of the benzene ring, indicating multi-methylation steps during **5** formation.

Bioinformatics analysis revealed that UttA is a NR-PKS with a domain architecture of KS-MAT-PT-ACP-ACP-MeT-TE (Figure 20).³⁹ It can be speculated that the methyl groups in **3** are transferred by the MeT domain from SAM. Creation of the mutants at the key catalytic residues, UttA_G1778V and UttA_H1850A, and expression in *A. nidulans* LO8030 resulted in the abolishment of the PKS products **3** – **5**. Feeding propionate to the two mutants did not lead to any detectable product formation, confirming that UttA cannot directly utilize propionate as starter as described above. These results indicated that the methylation step is essential for the polyketide assembling by UttA. However, it cannot be excluded that mutation at G1778 and H1850 had influences on the transcription, translation process or protein stability. We proposed that malonyl-CoA is loaded onto the MAT domain and transferred to the ACP domain. The propionyl-ACP complex is formed by methylation *via* SAM and decarboxylation. After condensation with

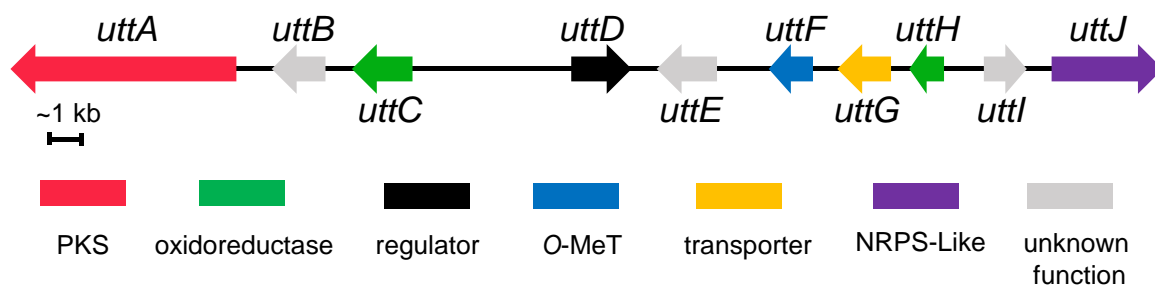


Figure 19. Putative BGC (*utt* BGC) for ustethylin A (**1**).

3. RESULTS AND DISCUSSION

two malonyl-CoA molecules, the MeT domain attaches the second methyl group. Condensation with another malonyl-CoA molecule leads to the production of a polyketide chain, which is subsequent cyclized by the PT domain and released by the TE domain, resulting in the formation of the predominant product **5** (Figure 20).

1 differs structurally from **5** in oxidation states of the functional groups at C-1, C-3 and C-6 as well as O-methylation at OH-4. The conversion of **5** to **1** would require three oxidoreductases and an O-MeT. Deletion of the NRPS_like gene *uttJ* abolished the formation of **1** and accumulation of **3** – **5** with almost the same product profile of the *A. nidulans* *uttA* expression strain. This proved unambiguously its role in the reduction of carboxyl group to aldehyde. Feeding **5** into the *A. nidulans* *uttJ* overexpression strain led to the detection of ustethylin D (**6**), confirming UttJ as an aryl acid reductase. Deletion of the putative nonheme Fe^{II}/2-oxoglutarate dependent oxygenase UttH led to the accumulation of UttJ product **6**, proving the reaction order of both enzymes. Deletion of *uttC* coding for a cytochrome P450 enzyme abolished the formation of **1** and the production of **7** (ustethylin B), which differs from **1** just in the oxidation state of the ethyl group. This proved that UttC catalyzed the last step in the biosynthesis of **1**. One predominant peak ustethylin C (**8**) was observed in the Δ *uttF* mutant. Similar to **1**, **8** was also found to be unstable and could not be obtained in pure form for structure elucidation. However, its structure could be elucidated after conversion to its diacetylated derivative. Deletion of *uttD* coding for a regulator completely abolished product formation, proving its role in the *utt* BGC. The biosynthetic pathway of ustethylin A is illustrated in Figure 20.

In 1987, a study reported the accumulation of 2,4-dihydroxy-3-methyl-6-ethyl benzoyl methyl and ethyl ester after feeding an *Aspergillus ustus* culture with MeOH and EtOH, respectively. Isotope incorporation was observed for both methyl groups of the aryl acid after feeding with [methyl-¹³C]-L-methionine, indicating their origin from SAM. Isotope labelling experiments also proved that other carbons are derived from acetate.¹² However, the biosynthetic process for these compounds was unclear. We repeated the feeding experiments with MeOH and EtOH into three-day-old cultures of *A. ustus* 3.3904. In the extracts of the cultures with externally fed MeOH and EtOH, three benzoyl esters each, **9** – **11** and **12** – **14**, were detected, respectively, with **11** and **14** as the major products. These results are in good consistence with those reported previously.¹² Compared the structures, the products of the PKS enzyme UttA **3** – **5** are the acyl moieties of **9** – **11** and **12** – **14**. Thus, we speculated that compounds **9** – **14** are also derived from the ustethylin pathway (Figure 20).

To prove this hypothesis, MeOH was fed into Δ *uttA* mutant, which did not lead to an accumulation of **9** – **11**. Similar results were also observed after feeding the Δ *uttA* mutant with EtOH. This clearly proved the

3. RESULTS AND DISCUSSION

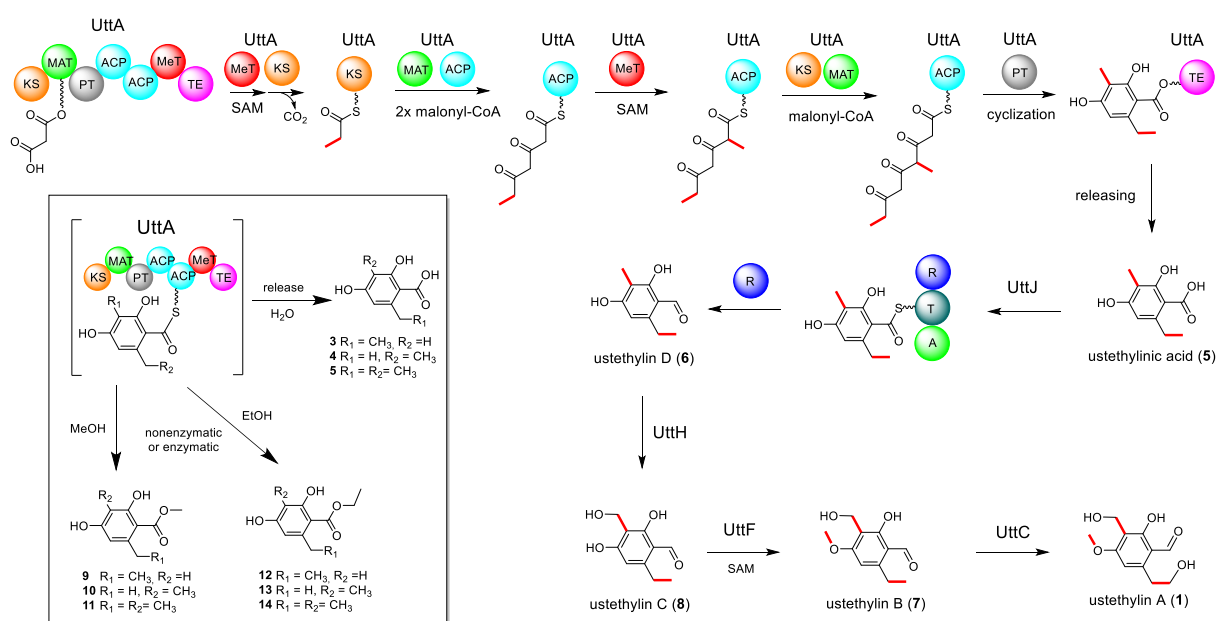


Figure 20. Proposed biosynthetic pathway of ustethylin A and the shunt products after feeding with MeOH and EtOH

involvement of Utta in the formation of compounds **9** – **14**. To figure out whether the ester formation utilizes free acids in *A. ustus*, **5** dissolved in MeOH was fed to the culture of Δ utta mutant. No trace of **11** was detected in the HPLC result. Alternatively, **5** was converted to the corresponding benzaldehyde **6** (ustethylin D). Additionally, **11** was not detected after incubation of **5** with MeOH at 37°C for 16 h. These results proved that the ester formation in **9** – **14** requires activation of the acidic precursors

As mentioned above, we proposed that malonyl-CoA is utilized as both the starter and extension units for the PKS Utta. Two methylation steps, at C-3 of the benzene ring and the C6-methyl group, are involved in the formation of the aryl acyl-ACP molecules (Figure 20), which are then released as free aryl acids and modified by tailoring enzymes. The Utta bound acyl component can also be hijacked by alcohols to form the esters (Figure 20). The production of the trace products **9**, **10**, **12**, and **13** after feeding with alcohols confirmed the incomplete methylation by Utta. The reduction of the acid **5** to the benzaldehyde **6** by the NRPS-like enzyme UttaJ is a prerequisite for further modification. Therefore, the esters **9** – **14** cannot be further metabolized by the tailoring enzymes in the Utt pathway and were accumulated as artificial products. Ester bonds are universally present in natural products and are usually formed during chain release in the PKS¹¹⁰ or NRPS and by Baeyer–Villiger monooxygenases.¹¹¹ However, spontaneous ester formation has also been reported for carboxylic acids by incubation in alcoholic solvents at room temperature.¹¹² Therefore, the enzymatic or nonenzymatic formation of **9** – **14** still needs further exploration (Figure 20).

3. RESULTS AND DISCUSSION

In conclusion, we verified the biosynthetic gene cluster of the highly oxygenated aryl-aldehyde derivative ustethylin A and elucidated its biosynthetic pathway by gene deletion and expression as well as isotopic labelling experiments. The PKS UttA as a key enzyme is responsible for the formation of the phenethyl core structure with methylation as key reactions. Consecutive and coordinated modifications by three different kinds of oxidoreductases and one O-MeT lead to the final product. Alternatively, this pathway can be shunted by feeding with MeOH and EtOH to produce benzoyl ester derivatives.

For details on these works, see please the publications (sections 4.1 and 4.2)

Liujuan Zheng,[#] Yiling Yang,[#] Haowen Wang, Aili Fan, Liping Zhang, and Shu-Ming Li (2020). Ustethylin biosynthesis implies phenethyl derivative formation in *Aspergillus ustus*. *Organic Letters*. 22:7837-7841 doi:10.1021/acs.orglett.0c02719. ([#] equal contribution)

Liujuan Zheng and Shu-Ming Li (2021). Benzoyl ester formation in *Aspergillus ustus* by hijacking the polyketide acyl intermediates with alcohols. *Archives of Microbiology*. doi.org/10.1007/s00203-021-02182-0

3.2 Biosynthesis of oxepinamides D, E, and F in *Aspergillus ustus*

Oxepinamides including 1*H*-oxepins with three C=C double bonds in the oxepin ring and 3*H*-oxepins with two C=C double bonds in the ring and one *exo* C=N bond are fungal natural products with a fused pyrimidinone ring system. Despite the intriguing structural features and biological activities, studies on the biosynthesis of oxepinamides, especially the formation of the oxepin ring, have not been reported before. Oxepinamide F (**15**) and E (**16**) were isolated from *A. ustus* 3.3904 after cultivation in rice media. The NMR signals at δ_H 6.7 (d, 7.3 Hz), δ_H 5.5 (t, 7.1 Hz), δ_H 6.2 (dd, 10.0, 7.0 Hz), and δ_H 5.8 ppm (d, 10.1 Hz) as well as δ_C 144, 104, 130, and 128 ppm were observed in their spectra and indicate the existence of 3*H*-oxepins. Their structures were identified by comparison with the reported data.^{16,17}

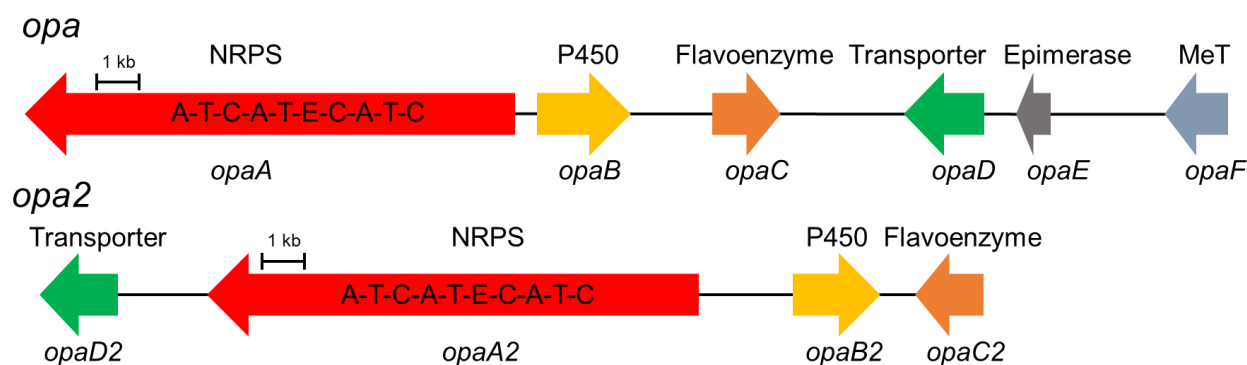


Figure 21. Putative biosynthetic gene clusters of oxepinamide F (*opa*) and oxepinamide D (*opa2*)

To investigate the biosynthesis of **15**, we sequenced the *A. ustus* 3.3904 genome with the help of Prof. Aili Fan in Beijing, predicted the putative BGCs by using AntiSMASH,¹¹³ and compared them with the published data.³⁵ The core structure of **15** is likely assembled from Ant, Phe, and Ile by a NRPS containing at least three A-T-C modules.¹¹⁴ **15** differs from **16** only in the methyl group at OH-12, indicating that an O-methyltransferase (O-MeT) should be involved in the biosynthesis. Bioinformatics analysis of the *A. ustus* genome revealed two NRPSs, KIA75458 and KIA75688, containing three A-T-C modules. In addition, a gene coding for a putative O-MeT (KIA75453) was only found neighboring to the gene for KIA75458. Thus, the KIA75458-related BGC was the best candidate for the biosynthesis of **15** and **16**. Inspecting the genomic neighborhood of *opaA*, coding for KIA75458, revealed the presence of a putative BGC comprising six genes *opaA* – *opaF* (Figure 21), coding for the putative proteins KIA75458 – KIA75453 in the NCBI database. Sequence analysis and comparison indicated their putative functions

3. RESULTS AND DISCUSSION

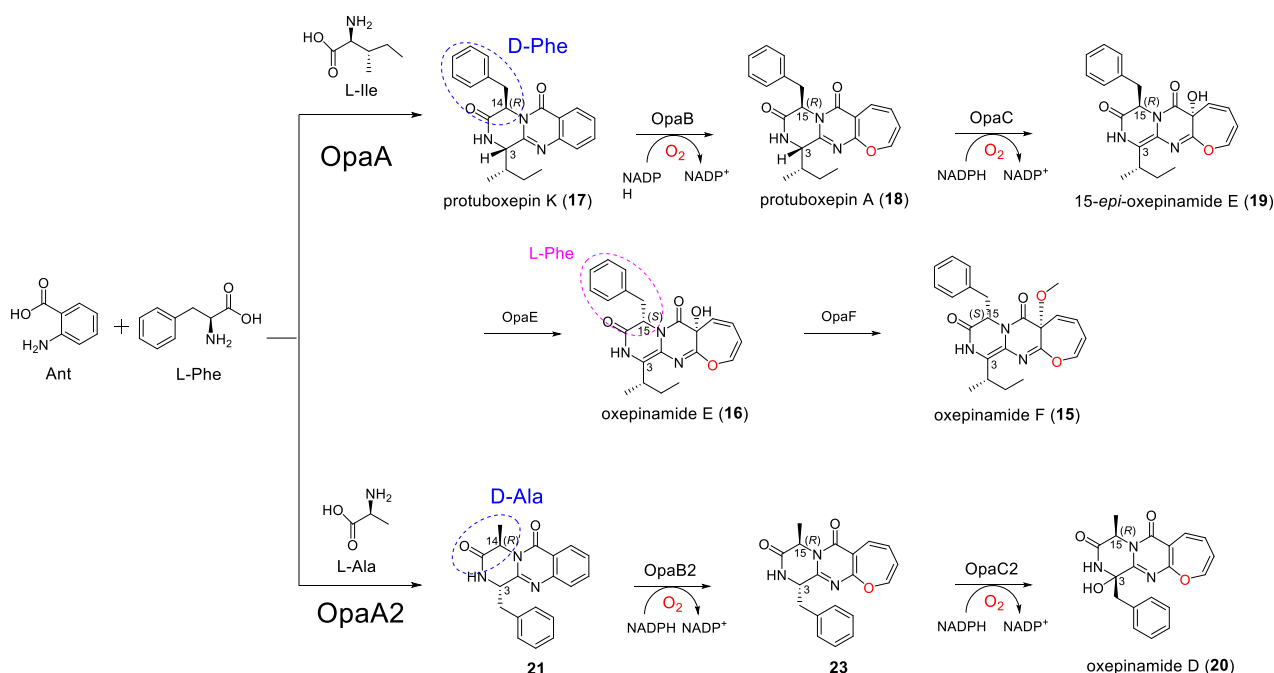


Figure 22. Comparative illustration of the biosynthetic pathways for oxepinamides D and F in *Aspergillus ustus*

as cytochrome P450 enzyme (OpaB, KIA75457), flavin-dependent oxygenase (OpaC, KIA75456), transporter (OpaD, KIA75455), epimerase (OpaE, KIA75454), and O-MeT (OpaF, KIA75453).

To prove their roles in the biosynthesis of **15**, we carried out gene deletion experiments with hygromycin as selection marker. HPLC analysis of a rice culture extract of the *opaA* deletion mutant revealed the abolishment of the production of both **15** and **16**, proving its involvement in their biosynthesis. Deletion

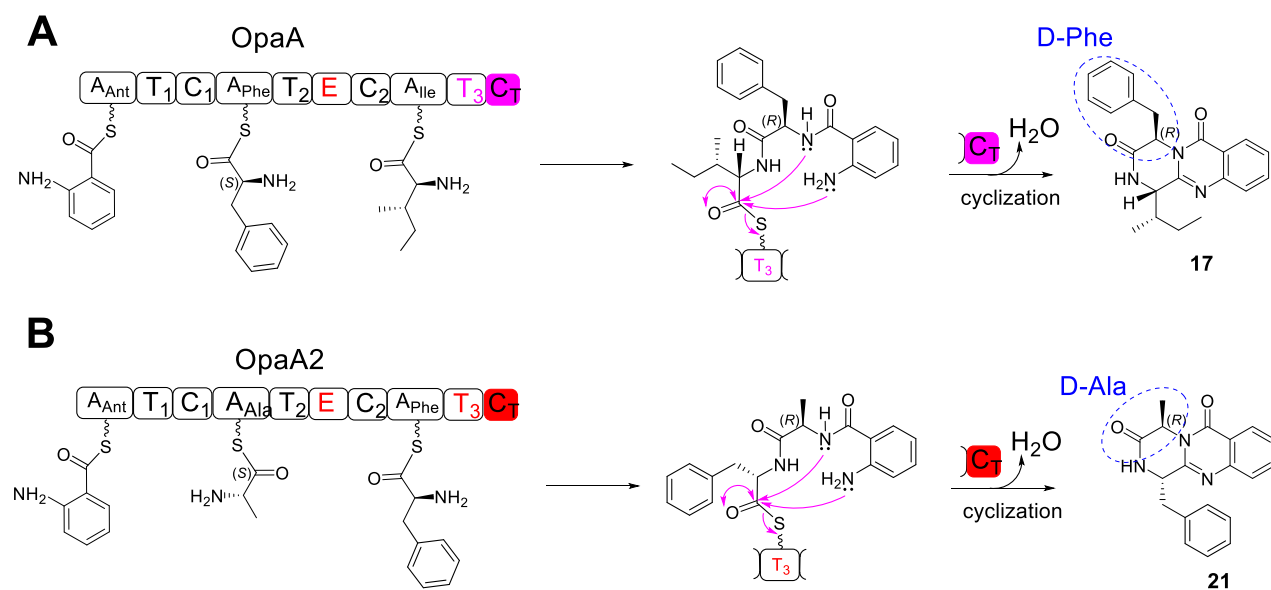


Figure 23. Quinoxalinone core formation by NRPSs OpaA (A) and OpaA2 (B)

3. RESULTS AND DISCUSSION

of *opaF* coding for a methyltransferase abolished the production of **15**, but not that of **16**, proving OpaF is responsible for the conversion of **16** to **15** (Figure 22). Heterologous expression of *opaA* in *A. nidulans* LO8030^{115,116 117} led to the production of the tripeptide protuboxepin K (**17**)^{118 119} proving its function for assembling the quinazolinone core (Figure 23). These results proved unequivocally that the *opaA*-related BGC is involved in the biosynthesis of **15** and **16**.

Deletion of *opaB* coding for a P450 enzyme abolished the production of **15** and **16**, accompanied by accumulation of compound **17**. Heterologous expression of *opaB* in *A. nidulans* LO8030^{115,116 117} was carried out to figure out its function. Protuboxepin A (**18**)¹²⁰ was detected as sole product after feeding **17** in the obtained overexpression strain. This proved that the P450 enzyme OpaB alone catalyzes the oxepin ring formation (Figure 24). Phylogenetic analysis of P450 enzymes indicated that OpaB is located near to the epoxidase AtaY, but far away from the oxepinase AtaF in *Aspergillus terreus*,¹²¹ providing additional evidence for identification of a new class of oxepinases. Sequence alignments revealed that the conserved P450 motif ExxR is present as ETMR in OpaB.¹²²⁻¹²⁴ Similar to the alkane hydroxylations and alkene epoxidations catalyzed by P450 enzyme,^{125,126} the electrophilic oxoferryliron ($\text{Fe}^{\text{IV}}=\text{O}$) is speculated to be the active oxygen intermediate in the OpaB reaction. An arene oxide was formed after attacking of the oxoferryliron species by the nucleophilic benzene double bond in **17**. Such arene oxide is in rapid spontaneous equilibrium with the oxepin **18** through 6π electrocyclic ring opening (Figure 24).^{127,128}

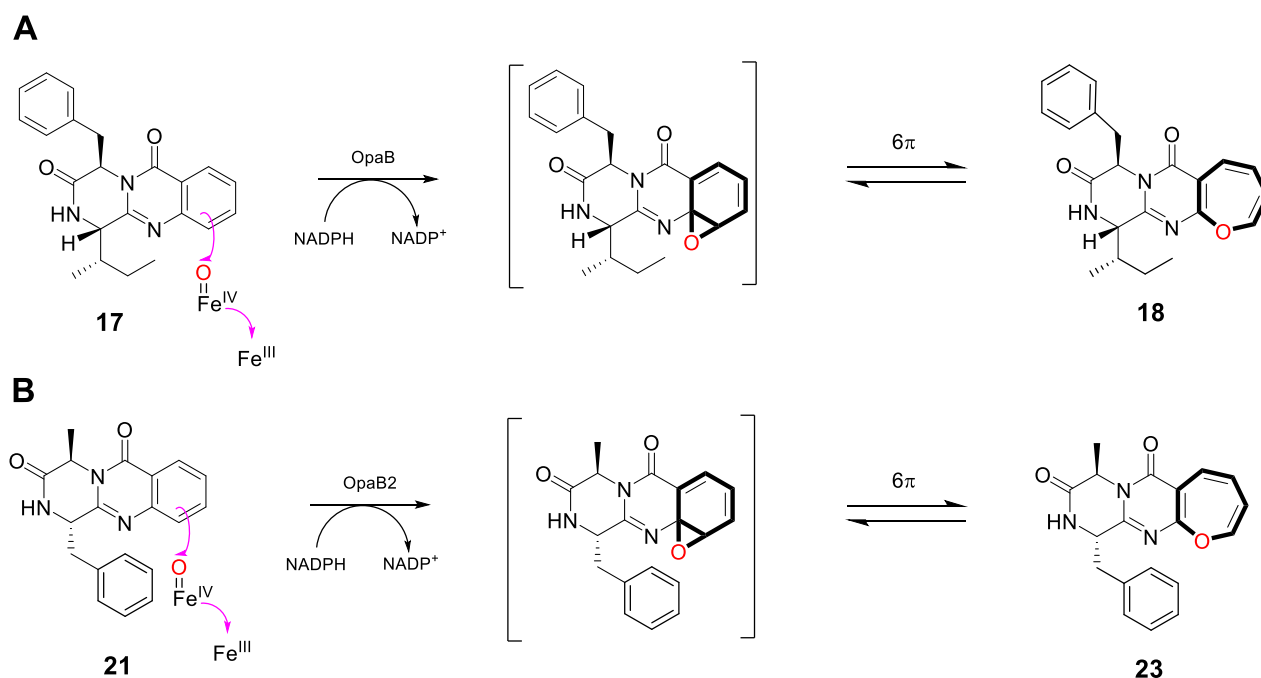


Figure 24. Oxepin ring formation catalyzed by oxepinases OpaB (**A**) and OpaB2 (**B**)

3. RESULTS AND DISCUSSION

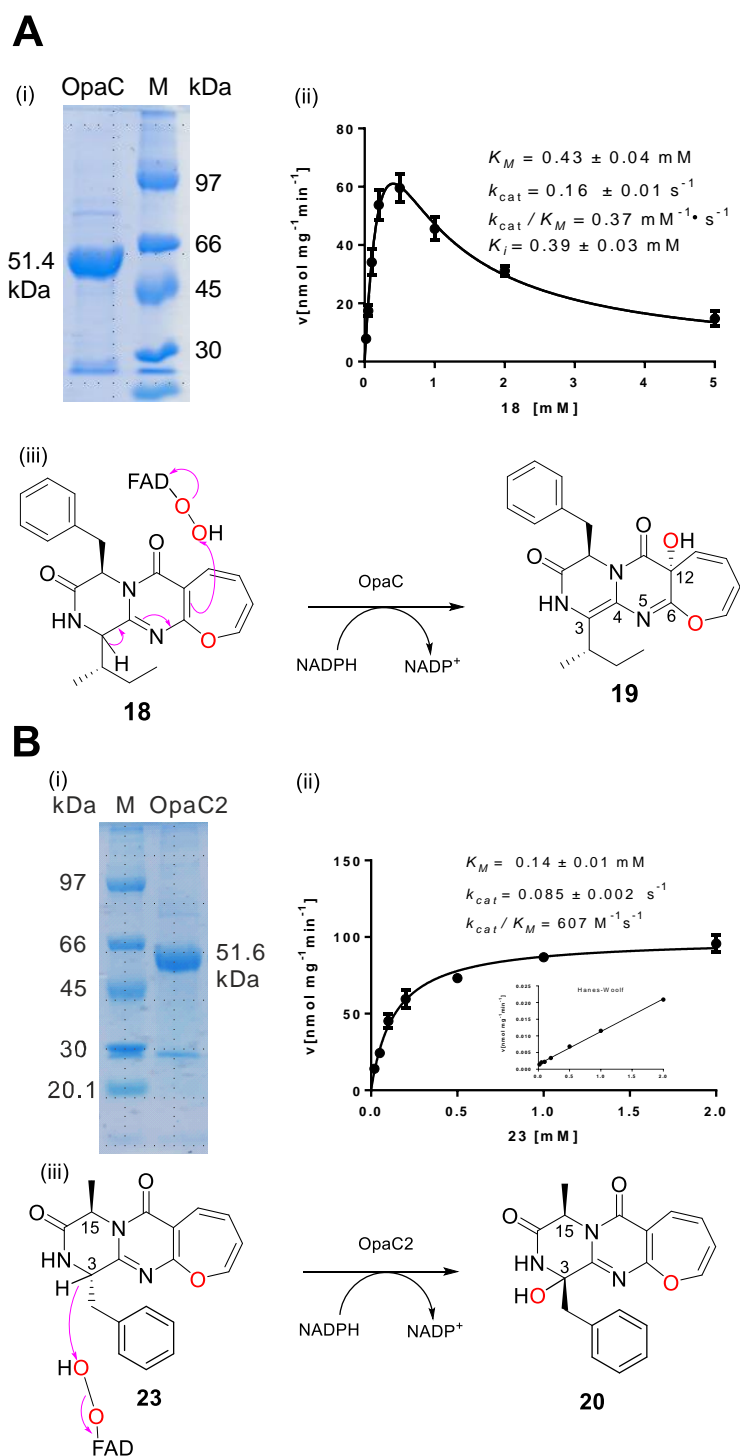


Figure 25. Hydroxylation catalyzed by the flavin-dependent enzymes OpaC (A) and OpaC2 (B)

Deletion of *opaC* from the *A. ustus* genome led to the accumulation of **19** (Figure 25). NMR and CD analyses revealed that **19** (termed 15-*epi*-oxepinamide E) and **16** are diastereomers and differ from each other merely in the configuration at C15. To figure out the catalytic role, *opaC* was amplified from cDNA

3. RESULTS AND DISCUSSION

and cloned into pET28a (+) for overexpression in *Escherichia coli*. The recombinant *N*-terminally His₆-tagged protein was purified to near homogeneity with a yield of 3.5 mg per liter culture [Figure 25A(i)]. As expected, one product peak **19** was detected in the incubation mixture of **18** with the purified OpaC in the presence of NADPH. In the incubation mixture of **17** and OpaC, no substrate consumption was observed, proving the prerequisite of the oxepin ring for an acceptance by OpaC. The reaction of OpaC with **18** in the presence of NADPH follows a typical substrate inhibition equation. An apparent K_M value at 0.15 ± 0.006 mM and a turnover number (k_{cat}) at 0.25 ± 0.003 s⁻¹ were calculated [Figure 25A(ii)]. Phylogenetic analysis revealed that OpaC belongs to the well-studied class A flavin-dependent monooxygenases.⁷⁷ Thus, a mechanism with a C4a-hydroperoxyflavin intermediate⁷⁵ was postulated for the OpaC reaction. The oxidized flavin Fl_{ox} is converted to Fl_{red} by external electron donor NADPH. The Fl_{red} then reacts with O₂, leading to the production of the electrophilic reagent C4a-hydroperoxyflavin.

Elimination of the proton at C3 in **18** results in the double bond migration and attack on the C4a-hydroperoxyflavin, leads to the formation of **19** and C4a-hydroxyflavin. The C4a-hydroxyflavin is then regenerated to Fl_{ox} by elimination of one water molecule for the next reaction cycle.

As aforementioned, **16** differs from **19** only in the configuration at C15. Conversion of **19** to **16** would need an epimerase like OpaE. Deletion of *opaE* indeed abolished the production of **15** and **16** and mainly accumulated **19** as well as a trace amount of a methylated product 15-*epi*-oxepinamide F. *opaE* was subsequently cloned and overexpressed as described for OpaC (Figure 26A). HPLC analysis of the reaction mixture of **19** with the recombinant OpaE revealed **16** as the mere product peak, proving unequivocally its function as an epimerase. Epimerization at C15 is essential for further methylation to the final product **15**, because only trace amounts of **19** were converted to its methylated product in the $\Delta opaE$ mutant. Incubation of OpaE and **19** in Tris-HCl buffer containing D₂O/H₂O (9:1) and subsequent analysis on LC-MS led to detection of the shifted [M + H]⁺ isotopic pattern of **16** (m/z 395.184), which is 1 Da larger than that in H₂O (m/z 394.177). Incubation of **16** in Tris-HCl buffer containing D₂O/H₂O (9:1) without OpaE did not change the isotopic pattern. These results confirmed the involvement of an enol intermediate in the OpaE-catalyzed epimerization (Figure 26C).¹²⁹ The kinetics of OpaE reaction with **19** followed the typical Michaelis-Menten equation and gave a K_M value of 0.46 ± 0.03 mM and a turnover number (k_{cat}) of 1.67 ± 0.09 s⁻¹ (Figure 26B).

Taken together, oxepinamide F has been proven to be the final product of the *opa* cluster. OpaA is responsible for assembling the quinazolinone **17**. The P450 enzyme OpaB catalyzes the ring expansion of the benzene ring in the Ant residue of **17** to form the oxepin ring in **18**. The regio- and stereospecific hydroxylation of **18** catalyzed by the flavin-dependent enzyme OpaC was accompanied by double bond migration from C4-N5 and C6-C12 in **18** to C3-C4 and N5-C6 in **19**, converting 1*H*-oxepin to 3*H*-oxepin

3. RESULTS AND DISCUSSION

system. The *R*-configuration in **19** was converted to *S*-configuration by the epimerase OpaE, which is essential for the final methylation of the OH-12 by the *O*-methyltransferase OpaF to form the end product **15** (Figure 22).

In addition to ustethylin A, oxepinamides E and F, HPLC analysis of the EtOAc extract of an *A. ustus* rice culture also revealed the presence of an additional peak **20**. The NMR data of the isolated compound **20** correspond well to those of oxepinamide D, which has been isolated from *Aspergillus puniceus*.¹⁷ Based on the structure, it can be speculated that **20** is derived from Ant, Ala, and Phe.

The aforementioned *opaA* deletion mutant did not produce **15** and **16**, but still **20**, proving the involvement of another biosynthetic pathway for **20**. As mentioned above, NRPS KIA75688 (termed OpaA2 in this study) also contained the domain architecture of A-T-C-A-T-E-C-A-T-C and shares a sequence identity of 48% with OpaA on the amino acid level. Bioinformatics analysis of *opaA2* indicated the presence of a putative BGC containing three additional genes *opaB2* – *opaD2*, corresponding to a putative cytochrome P450 enzyme (OpaB2, KIA75687), a flavin-dependent oxygenase (OpaC2, KIA75686), and a transporter (OpaD2, KIA75689) (Figure 21). HPLC-MS analysis of the cultural extract of $\Delta opaA2$ confirmed the abolishment of **20** production, but not that of **15** and **16**. Heterologous expression of *opaA2* in *Aspergillus*

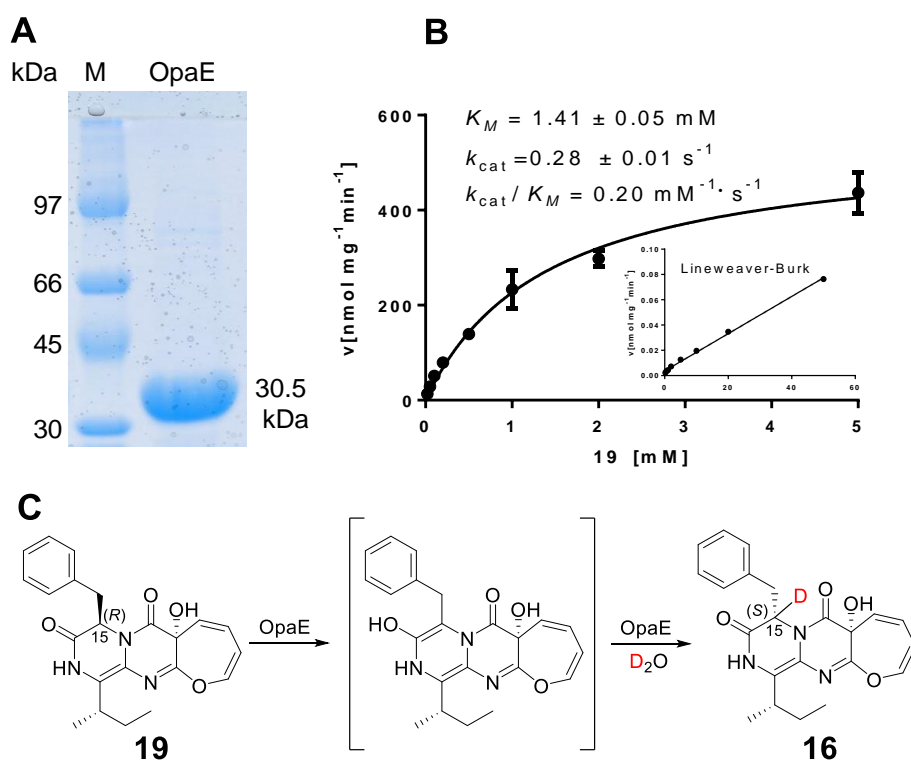


Figure 26. **A** SDS-PAGE analysis of OpaE, **B** kinetics of OpaE reacted with compound **19**. **C** Epimerization performed by the epimerase OpaE

3. RESULTS AND DISCUSSION

nidulans led to the production of compounds **21** and **22**. Detailed spectroscopic analysis proved that **21** and **22** are diastereomeric quinazolinones derived from Ant, Ala, and Phe. They just carry different configurations at C-3 position (Figure 27).

In parallel, *opaA* was also heterologously expressed in *A. nidulans*, leading to the accumulation of protuboxepin K (**18**) with a D-Phe residue and proving the function of E domain in the second module of OpaA for the epimerization of L-phenylalanine. The presence of D-Ala residue in **21** and **22** can be explained by the existence of the E domain in the second module in OpaA2. However, for the D-Phe residue in **22**, no redundant epimerization domain in OpaA2 was predicted. HPLC analysis of **21** and **22** after incubation at 37°C and different pH values showed that **22** is a nonenzymatic product of **21** via a keto-enol tautomeric event with involvement of a two double bond migration mechanism in the fused quinazolinone ring (Figure 27).

Deletion of *opaB2* from *A. ustus* genome abolished the production of **20** accompanied by the accumulation of two tripeptide derivatives **21** and **22**, the same products after heterologous expression of *opaA2* in *A. nidulans*. To figure out its catalytic role, *opaB2* was amplified from genomic DNA and expressed in *A. nidulans*. Feeding **21** in the *A. nidulans opaB2* transformant led to the production of compound **23**, which was not observed in a negative control. **23** was identified as an OPK derivative by intensive interpretation of NMR spectra including ^1H , ^{13}C , HMQC and HMBC. Feeding **22** into the *A. nidulans opaB2* culture did not lead to any conversion, indicating the stereochemistry at C-3 position of the quinazolinone core is essential for the OpaB2 reaction. As described before, the E domain of OpaA

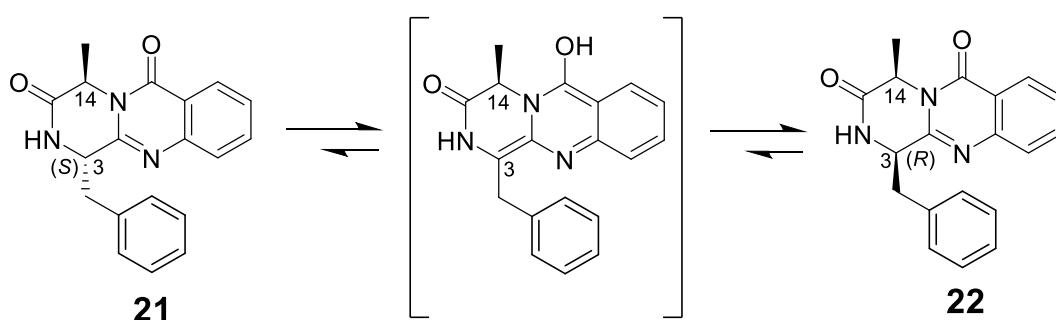


Figure 27. Nonenzymatic keto-enol tautomerization of compounds **21** and **22**

changes the configuration of Phe residue from L- to D-form during the formation of the quinazolinone derivative (14*R*) protuboxepin K (**17**), the substrate of another oxapinase OpaB. To figure out whether this configuration change is essential for the oxepin ring formation catalyzed by OpaB, (14*S*)-*epi*-protuboxepin K was chemically synthesized by Lena Ludwig-Radtke^{130,131} and fed into the culture of an *A. nidulans opaB* transformant. No product was detected by HPLC analysis. In contrast, almost complete

3. RESULTS AND DISCUSSION

conversion of the natural substrate protuboxepin K (**17**) to protuboxepin A (**18**) was observed after feeding into the *A. nidulans opaB* culture. Feeding **21** and **22** into the *A. nidulans opaB* transformant did not lead to any consumption. Similar results were also obtained after feeding of **17** and (14*S*)-*epi*-protuboxepin K into the *A. nidulans opaB2* transformant. These results proved the high substrate specificity and stereoselectivity of the ring expansion reactions catalyzed by the two oxepinases OpaB and OpaB2 and the necessity of the configuration change during the NRPS assembly line (Figure 24).

In comparison to **23**, **20** bears an additional hydroxyl group at C-3 position of the OPK backbone. Bioinformatics analysis results suggested OpaC2 to be a FAD-containing monooxygenase. OpaC2 shares a sequence identity of 61% with OpaC and might also function as a hydroxylase. Deletion of *opaC2* from the *A. ustus* genome led indeed to the abolishment of **20** production and the accumulation of **23**. *opaC2* was then amplified from cDNA of *A. ustus* and cloned into pET28a (+) for overexpression in *Escherichia coli* to characterize its catalytic role (Figure 25). The recombinant *N*-terminally His₆-tagged protein was purified to near homogeneity with a yield of 1.6 mg per liter culture. After incubation of **23** with the purified OpaC2 in the presence of NADPH, **20** was detected as the sole product. **23** and **20** show apparently different CD spectra, indicating the change of the orientation of the phenyl ring at C-3 position. These results proved that OpaC2 catalyzed the regio- and stereospecific C3-hydroxylation of **23** with retaining the 1*H*-oxpin system (Figure 25B). Similar to OpaC, OpaC2 also utilized NADH as a cofactor, but with an observably reduced activity. The kinetic data of the OpaC2 reaction with **23** in the presence of NADPH fits well to a velocity equation of Michaelis-Menten. An apparent K_M value at 0.14 ± 0.01 mM, a turnover number (k_{cat}) at 0.085 ± 0.002 s⁻¹ and the catalytic efficiency (k_{cat}/K_M) at 607 M⁻¹ s⁻¹ were calculated [Figure 25B(ii)]. To prove the substrate flexibility for the flavin-dependent enzymes, **23** and **18** were incubated with OpaC2 and OpaC, respectively. No product formation was detected on HPLC in both cases, which are consisted with the *in vivo* results of the $\Delta opaC$ and $\Delta opaC2$ mutants and demonstrating their high substrate specificity. Together with the abovementioned feeding results in the *opaB* and *opaB2* transformants, it can be concluded that there is no crosstalk between the two BGCs.

In conclusion, the second oxepinamide BGC *opa2* in *A. ustus* is responsible for the biosynthesis of the 1*H*-oxepin oxepinamide D carrying a C3-hydroxyl group. Both oxepinamide clusters share a NRPS (OpaA and OpaA2) for quinazolinone skeleton and P450 (OpaB and OpaB2) for the oxepin formation. The two flavin-dependent monooxygenases OpaC and OpaC2 install hydroxyl groups at different positions in OPK backbones. In the biosynthesis of oxepinamide F, two additional enzymes (an O-Met and an epimerase) are involved in the pathway. Additionally, the E domains in OpaA and OpaA2 are responsible for the epimerization of phenylalanine and alanine, respectively, which is a prerequisite for the ring expansion catalyzed by the oxepinases OpaB and OpaB2 (Figure 22).

3. RESULTS AND DISCUSSION

For details on this work, please see the publication (sections 4.3 and 4.4)

Liujuan Zheng,[#] Haowen Wang,[#] Aili Fan, and Shu-Ming Li (2020). Oxepinamide F biosynthesis involves enzymatic D-aminoacyl epimerization, 3*H*-oxepin formation, and hydroxylation induced double bond migration. *Nature Communications* 11: 4914 doi: 10.1038/s41467-020-18713-0. ([#] equal contribution)

Liujuan Zheng,[#] Haowen Wang,[#] Lena Ludwig-Radtke, and Shu-Ming Li (2021). Oxepin formation in fungi implies specific and stereoselective ring expansion. *Organic Letters*. 23, 6, 2024–2028. doi.org/10.1021/acs.orglett.1c00166. ([#] equal contribution)

3.3 Switching a regular tryptophan C4-prenyltransferase to a reverse tryptophan-containing cyclodipeptide C3-prenyltransferase by sequential site-directed mutagenesis

As mentioned in the introduction, enzymatic prenylation plays a significant role in structure modification of CDPs,^{57,132-134} and FgaPT2 from *Aspergillus fumigatus* has been proven to be an excellent example of a multiple functional enzyme, especially for regular C4-prenylation of tryptophan derivatives and CDPs as well as reverse C3-prenylation of tryptophan¹⁰³⁻¹⁰⁵. However, a reverse C3-prenylation of tryptophan-containing CDPs has not been reported before.

Based on the results with FgaPT2_R244 mutants, which significantly enhance the catalytic ability for C4-prenylation towards the tryptophan-containing CDPs¹⁰⁴, as well as FgaPT2_K174A, which can prenylate L-tryptophan at both C-3 and C-4 positions of the indole ring, we were inspired to test the two step-mutations on Lys174 and Arg244 of FgaPT2 to create a reverse C3-prenyltransferase of tryptophan-containing CDPs. The general working flow is illustrated in Figure 28.

To test the activity to tryptophan-containing CDPs, the plasmid pLZ1 for overproduction of FgaPT2_K174A was constructed. From the SDS-PAGE analysis, an apparent protein band at 53 kDa was detected for the purified FgaPT2_K174A (Figure 29). After incubation with L-tryptophan and DMAPP, two product peaks with the same $[M+H]^+$ ion were detected on LC-MS, which were identified as C4-prenylated (UV λ_{\max} 278nm) and C3-prenylated derivative (UV λ_{\max} at 240 and 294nm), respectively.¹⁰⁵

FgaPT2_K174A was incubated afterward with six L-tryptophan-containing CDPs, *i.e.* *cyclo*-L-Trp-L-Ala (**24**), *cyclo*-L-Trp-L-Trp (**25**), *cyclo*-L-Trp-Gly (**26**), *cyclo*-L-Trp-L-Phe (**27**), *cyclo*-L-Trp-L-Pro

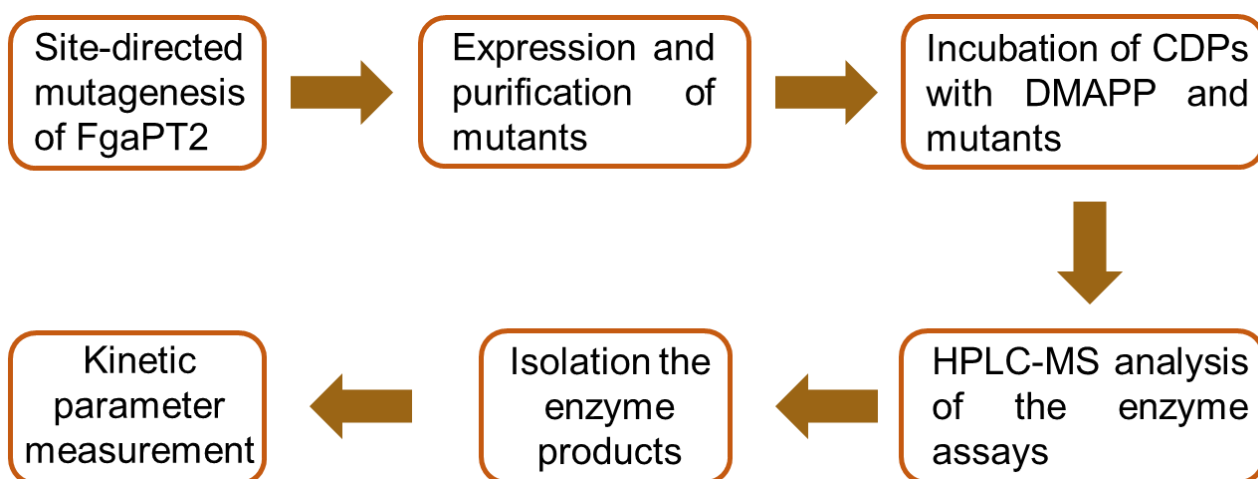


Figure 28. Working flow for switching FgaPT2 to a C3-prenyltransferase by sequential site-directed mutagenesis

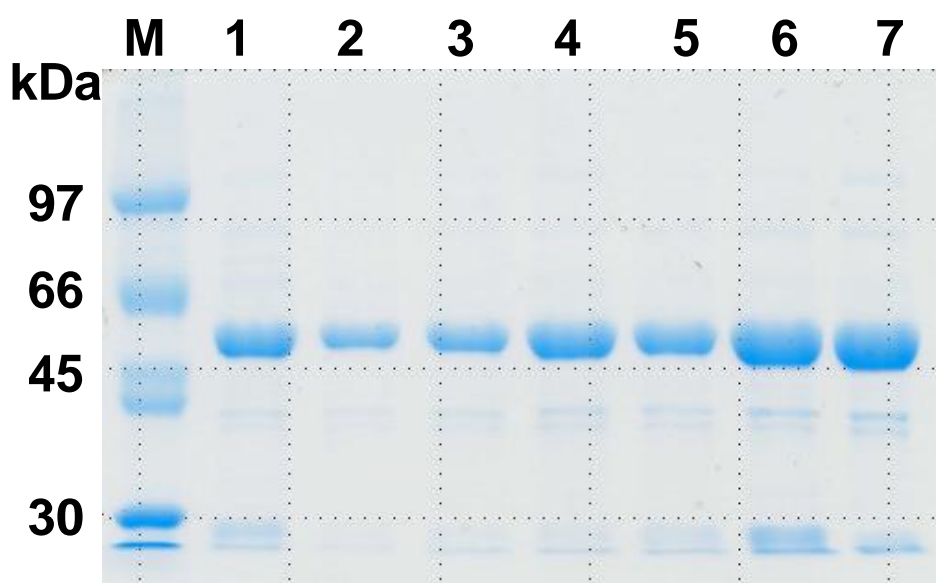


Figure 29. SDS-PAGE analysis of the purified FgaPT2 and its mutants. The proteins were separated on a 12% polyacrylamide gel and stained with Coomassie brilliant blue R-250. M-maeker, 1: FgaPT2, 2: FgaPT2_K174A, 3: FgaPT2_K174F, 4: FgaPT2_K174F_R244L, 5: FgaPT2_K174F_R244N, 6: FgaPT2_K174F_R244Q, 7: FgaPT2_K174F_R244Y.

(**28**), and *cyclo*-L-Trp-L-Tyr (**29**) in the presence of DMAPP at 37°C for 3 h. No product was detected on LC-MS in all enzyme assays under the tested conditions. For the wild type FgaPT2, the cyclodipeptides **24** – **29** showed product yields in the range from 6.6 to 29.5 %. With the exception for **25**, one product peak each (**24a** or **26a** – **29a**) was detected. The products show the typical UV λ_{max} at 278 nm for indole system and 68 daltons higher $[M + H]^+$ ion, indicating the presence of an indole chromophore and the prenylation of the cyclodipeptides by FgaPT2.¹³⁵ For compound **25**, two products **25a** and **25a*** were detected, with $[M+H]^+$ ions, which are 68 and 136 daltons larger than that of **25**, indicating a mono- and diprenylation, respectively.

As described above, the key residue Lys174 was proven to be essential for aromatic substrate selection. Compared with FgaPT2, the activity of FgaPT2_K174F to L-tryptophan decrease evidently.¹⁰³ Similarly, all six CDPs were accepted by FgaPT2_K174F, but with very low product yields, ranging from 2.5 to 6.5 %. The clearly different UV spectra (λ_{max} at 240 and 294nm) of the products indicated that **24b** - **29b** were C3-prenylated derivatives of **24** – **29**, respectively.^{105,136} For compound **25**, a diprenylated product **25b*** with the similar UV spectrum to that of **25b** was also detected by LC-MS analysis. The previous study proved that Arg244 mutants, especially R244N, R244Q, R244Y, and R244L, showed evidently increased activities to tryptophan-containing CDPs, which led to the production of regular C4-prenylated products compared with

3. RESULTS AND DISCUSSION

those of wild type FgaPT2.¹⁰⁴ In analogy, double mutants of Lys174 to Phe and Arg244 to Leu, Asn, Gln, and Tyr were constructed by site-directed mutagenesis and overexpressed in *E. coli*, creating the four double mutants FgaPT2_K174F_R244L, FgaPT2_K174F_R244N, FgaPT2_K174F_R244Q, and FgaPT2_K174F_R244Y (Figure 29).

HPLC analysis of the reaction mixtures of the obtained mutants showed that all double mutants exhibited increased activities towards the six CDPs. Total product yields of 20.3 to 41.4 % were calculated for the best mutant with a given substrate, *i.e.* FgaPT2_K174F_R244N for **24** – **27** and FgaPT2_K174F_R244L for **28** and **29**, which showed an activity increase of two to ten-fold compared to those of FgaPT2_K174F. The products showed same retention times and UV spectra as those of the FgaPT2_K174F for a given substrate (**24b** – **29b**) and the corresponding products also have the same $[M+H]^+$ ions with those of FgaPT2_K174F by LC-MS analysis. For compound **25**, the additional peak **25b*** with a $[M+H]^+$ ion for a diprenylated derivative was also detected. All these data proved the successful mutational combinations for acceptance of tryptophan-containing CDPs (Figure 30).

To get NMR spectra, the enzyme products of **25** – **27** were isolated from incubation mixtures with FgaPT2_K174F_R244N and those of **28** and **29** with FgaPT2_K174F_R244L in 10 mL scale. The typical signals for a reverse prenyl moiety each at δ_H 4.97-5.13 (dd, 1H), 5.05-5.09 (dd, 1H), 5.76-5.98 (dd, 1H), 0.93-1.11 (s, 3H), and 0.79-1.01 (s, 3H) ppm were clearly present in the ¹H NMR spectra of **24b** – **29b**. The signals of H-2 at the original indole rings are apparently shifted up-field to 5.32 – 5.55 ppm, indicating the disruption of the indole and formation of a hexahydropyrroloindole system caused by a C3-prenylation.^{98,136} The signals of H-11 appear as double doublets with coupling constants of approximate 11, 6.0, and 2.0 Hz, proving the 3 β -prenylation of L-configured tryptophanyl moiety, *i.e.* *syn-cis* configuration (3*R*, 2*S*, 11*S*).¹³⁶ For the product **25b***, the structure could not be confirmed by NMR analysis, due to the low quantity. Here, we speculated here C3-prenylation at both indole rings, as observed for other C3-prenyltransferases with *cyclo*-L-Trp-L-Trp.⁸⁸

Kinetic parameters including Michaelis-Menten constants (K_M) and turnover numbers (k_{cat}) were determined at pH 7.5 for the two best mutants in the presence of DMAPP, *i.e.* FgaPT2_K174F_R244N with **25** – **27** as well as FgaPT2_K174F_R244L with **28** and **29**. The reactions catalyzed by both mutants followed the typical Michaelis-Menten kinetics. With the exception for **27**, K_M values in the range of 0.15 to 0.79 mM were determined.

3. RESULTS AND DISCUSSION

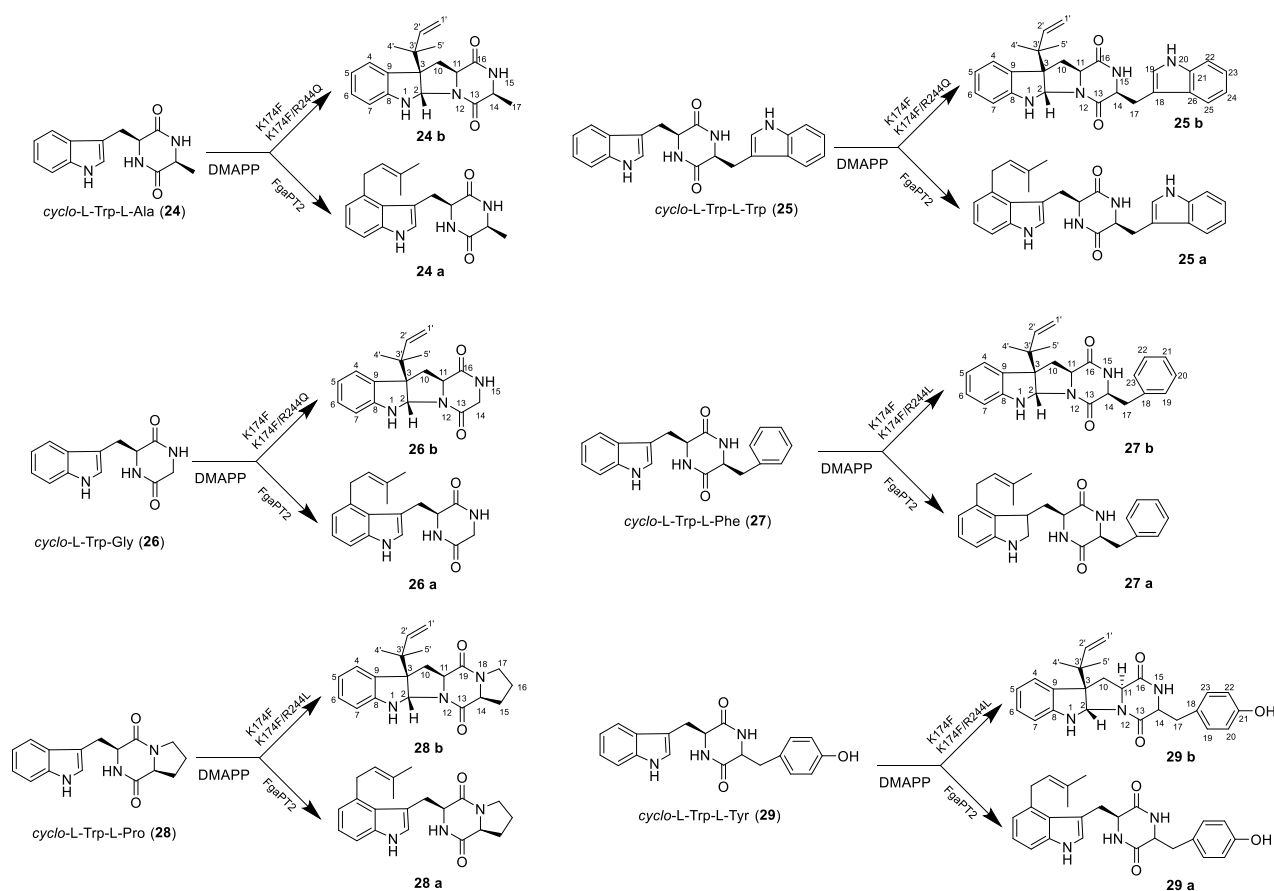


Figure 30. Prenylations of six tested CDPs catalyzed by FgaPT2 and its double mutants.

Taken together, the variant FgaPT2_K174F can utilize *cyclo*-L-Trp-L-Ala, *cyclo*-L-Trp-L-Trp, *cyclo*-L-Trp-L-Gly, *cyclo*-L-Trp-L-Phe, *cyclo*-L-Trp-L-Pro, and *cyclo*-L-Trp-L-Tyr as substrates for reverse C3-prenylation, but only with low activity. Compared with the wild-type FgaPT2, the combinational mutations on Lys174 and Arg244 significantly increases the catalytic activity for these cyclodipeptides. With the exception for *cyclo*-L-Trp-L-Trp, FgaPT2_K174F_R244X (X=L, N, Q, Y) show much better acceptance, with an increase of two- to six-fold activity, to the tested cyclodipeptides than that of FgaPT2. More importantly, compared to FgaPT2_K174F, even two- to ten-fold conversion yields were calculated for the double mutants (Figure 30).

3. RESULTS AND DISCUSSION

For details on this work, please see the publication (section 4.5)

Liujuan Zheng,[#] Peter Mai,[#] Aili Fan, and Shu-Ming Li (2018). Switching a regular tryptophan C4-prenyltransferase to a reverse tryptophan-containing cyclic dipeptide C3-prenyltransferase by sequential site-directed mutagenesis. *Organic & Biomolecular Chemistry* 16: 6688-94. doi: 10.1039/C8OB01735B. ([#] equal contribution)

4. Publications

4.1 Ustethylin biosynthesis implies phenethyl derivative formation in *Aspergillus ustus*.

Ustethylin Biosynthesis Implies Phenethyl Derivative Formation in *Aspergillus ustus*

Liujuan Zheng,[▽] Yiling Yang,[▽] Haowen Wang, Aili Fan, Liping Zhang, and Shu-Ming Li*

Cite This: *Org. Lett.* 2020, 22, 7837–7841

Read Online

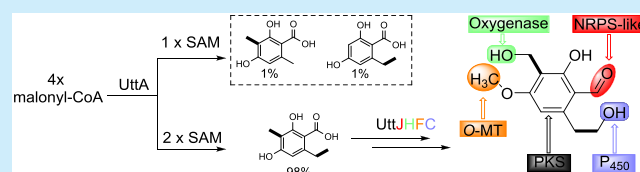
ACCESS |

Metrics & More

Article Recommendations

Supporting Information

ABSTRACT: A highly oxygenated phenethyl derivative ustethylin A was isolated from *Aspergillus ustus*. Gene deletion, isotope labeling, and heterologous expression proved that the phenethyl core structure is assembled from malonyl-CoA by a polyketide synthase harboring a methyltransferase domain. Propionate was converted via acetyl-CoA to malonyl-CoA and incorporated into the molecule. Modifications on the core structure by three different oxidoreductases and one *O*-methyltransferase lead to the final product, ustethylin A.



Phenethyl-containing natural products are common microbial metabolites. Barnol¹ and marilone A² are examples from fungi, while gilvocarcin E³ and tiacumicin B⁴ occur in *Streptomyces* (Figure 1). Feeding experiments and genetic

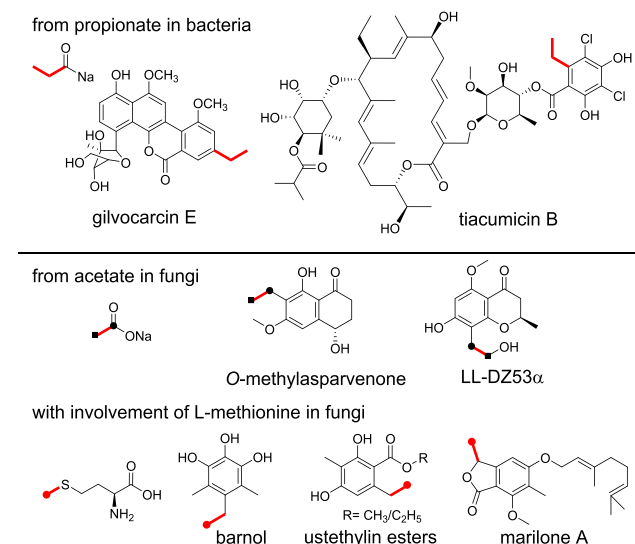


Figure 1. Origins of ethyl groups in phenethyl-containing natural products.

studies proved that the phenethyl units are products of polyketide synthases (PKSs).^{3–5} The ethyl groups in phenethyl residue of bacterial metabolites are mostly originated from propionate as starter unit of PKSs.^{3,4} In fungi, it can be derived from acetate, as in the cases of LL-DZ53α⁶ and *O*-methylasparvenone,⁷ which was confirmed by feeding with [1,2-¹³C] acetate. However, the most methyl groups of the phenethyl residue in fungal metabolites are derived from *S*-adenosyl *L*-methionine (SAM), which has been proven by

feeding experiments with [methyl-¹³C]-*L*-methionine.^{2,8} The responsible enzymes for the methylation and the biosynthetic pathways for such metabolites have not been reported prior to this study.

HPLC analysis of the EtOAc extract of an *A. ustus* culture in PD media revealed the presence of one predominant peak 1 (Figure 2B(i)) with a [M + Na]⁺ ion at *m/z* 249.0732 and a deduced molecular formula of C₁₁H₁₄O₅ (see Figure S7 in the Supporting Information). Attempts to get interpretable ¹H NMR spectrum for 1 from a large-scale fermentation failed, although it was almost the only product peak in the HPLC chromatogram. During isolation, the amount of 1 decreased evidently. Dissolving the finally isolated 7 mg sample in DMSO-*d*₆ led to precipitation immediately. The ¹H NMR spectrum of the supernatant was very complex, so that an interpretation was impossible (data not shown). To overcome the instability, 1 in the fungal extract was immediately converted to its triacetate 2 for structural elucidation (see Table S5, Figure S19, and Figures S21–S25 in the Supporting Information), which confirmed 1 to be 2-hydroxy-3-hydroxymethyl-4-methoxy-6-hydroxyethylbenzaldehyde, termed ustethylin A (Scheme 1).

To elucidate the origin of 1, we performed a feeding experiment with sodium [1,2-¹³C] acetate in *A. ustus*. In the ¹³C NMR spectrum of the acetylated product 2 (Figure 3), four signal pairs of coupling carbons, C-1/C-7, C-2/C-3, C-4/C-5, and C-6/C-9, were detected, proving unequivocally the incorporation of four intact acetate units. Feeding with sodium

Received: August 14, 2020

Published: October 2, 2020

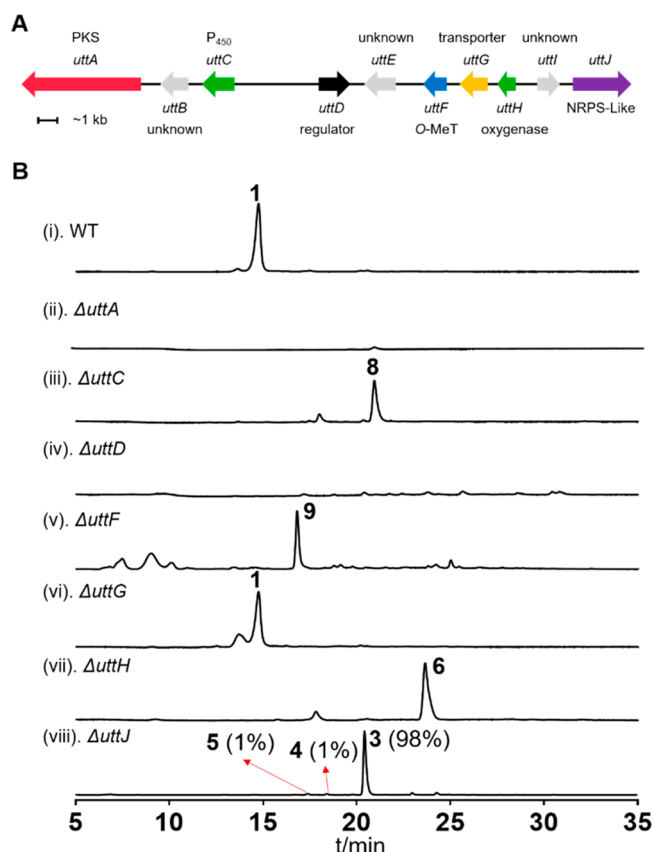


Figure 2. (A) Schematic representation of the *utt* cluster in *A. ustus* and (B) HPLC analysis of the fungal extracts.

[1-¹³C] acetate revealed that C-2 at δ_C 152.5, C-4 at 162.1, C-6 at 144.9, and C-7 at 189.0 ppm are from the carbonyl group of acetate, with 3.8–6.1-fold enrichments (see Table S11 in the Supporting Information). Correspondingly, significantly increased intensity was observed for the signals at δ_C 119.8 (C-1), 116.0 (C-3), 112.1 (C-5), and 31.5 ppm (C-9), with 4.9–8.9-fold of those of the unlabeled **2** after feeding with sodium [2-¹³C] acetate and [2-¹³C] malonic acid (see Table S11). This confirmed the methyl/methylene group of acetate/malonate as their origin.

To determine whether *A. ustus* utilizes propionate as a starter unit, sodium [2-¹³C] propionate was fed into the culture. To our surprise, the labeling pattern of **2** is very similar to that with [1-¹³C] acetate (Figure 3), with 3.6–6.1-fold

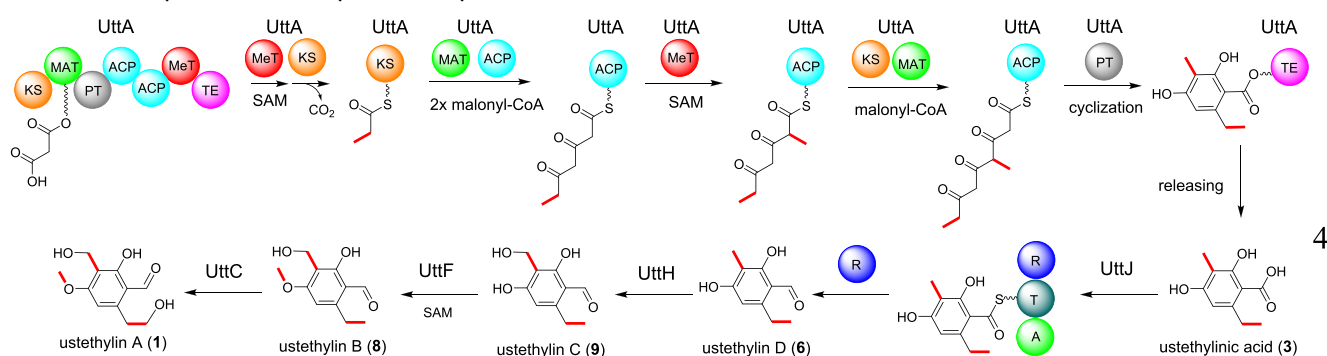
enrichments for C-2, C-4, C-6, and C-7 (see Table S11). No enrichment for C-9 at 31.5 ppm was observed. These results proved unequivocally that sodium [2-¹³C] propionate was not directly utilized for incorporation, but was degraded to acetyl-CoA likely via pyruvate by α -oxidation.⁹ Acetyl-CoA was converted to malonyl-CoA and incorporated in **1**.

In the ¹³C NMR spectrum of **2** after feeding with [methyl-¹³C]-L-methionine (Figure 3), the three signals at δ_C 54.1 (C-8), 63.9 (C-10), and 56.6 ppm (C-11) were enhanced to 13.1–15.9-fold of those of the unlabeled **2** (see Table S11), proving that the methyl group of the phenethyl residue is also from SAM.

The genome of *A. ustus* 3.3904 was sequenced and published in 2015.¹⁰ For our biosynthetic studies, we resequenced it and used both sequences for prediction of putative gene clusters by AntiSMASH.¹¹ Our sequence correlated very well with the published data, at least for the cluster described in this study. From the structure of **1**, it can be deduced that a PKS would be responsible for the formation of its backbone.¹² Genome mining indicated the presence of more than 20 putative PKS genes. Transcriptome analysis revealed that the PKS gene coding for KIA75596, termed *uttA* in this study (recall Figure 2A), was one of the 80 best expressed genes under our culture conditions (data not included).

To prove its function, *uttA* was replaced with a hygromycin B resistance cassette by using a split marker gene replacement protocol.¹³ The potential mutants were verified by PCR (Figure S1 in the Supporting Information) and cultivated in PD medium for secondary metabolite production. HPLC analysis of the culture extract of a $\Delta uttA$ mutant showed complete loss of **1** production (recall Figure 2B(ii)). Afterward, *uttA* was cloned into pYH-*gpdA*-*pyrG* via homologous recombination in yeast¹⁴ for heterologous expression.¹⁵ The obtained plasmid pLZ51 was linearized by *Sma*I and integrated into the genome of *A. nidulans* LO8030 (Figure S2 in the Supporting Information).¹⁶ In comparison to that of the negative control, three additional products **3**–**5** were detected in the *uttA* overexpression transformant with **3** as the predominant peak (98%) (see Figure 4B). The *UttA* products **3**–**5** were identified as benzoic acid derivatives by NMR analysis and comparison with published data^{17,18} (see Tables S6 and S7 in the Supporting Information, as well as Figure 4C and Figures S26–S31 in the Supporting Information). They differ from each other only in the methyl group at C-3 and the ethyl group at C-6 of the benzene ring (Figure 4C), indicating multimethylation steps during the formation of **3**.

Scheme 1. Biosynthetic Pathway of Ustethylins in *A. ustus*^a



^aThe red bonds indicate SAM-associated methylation.

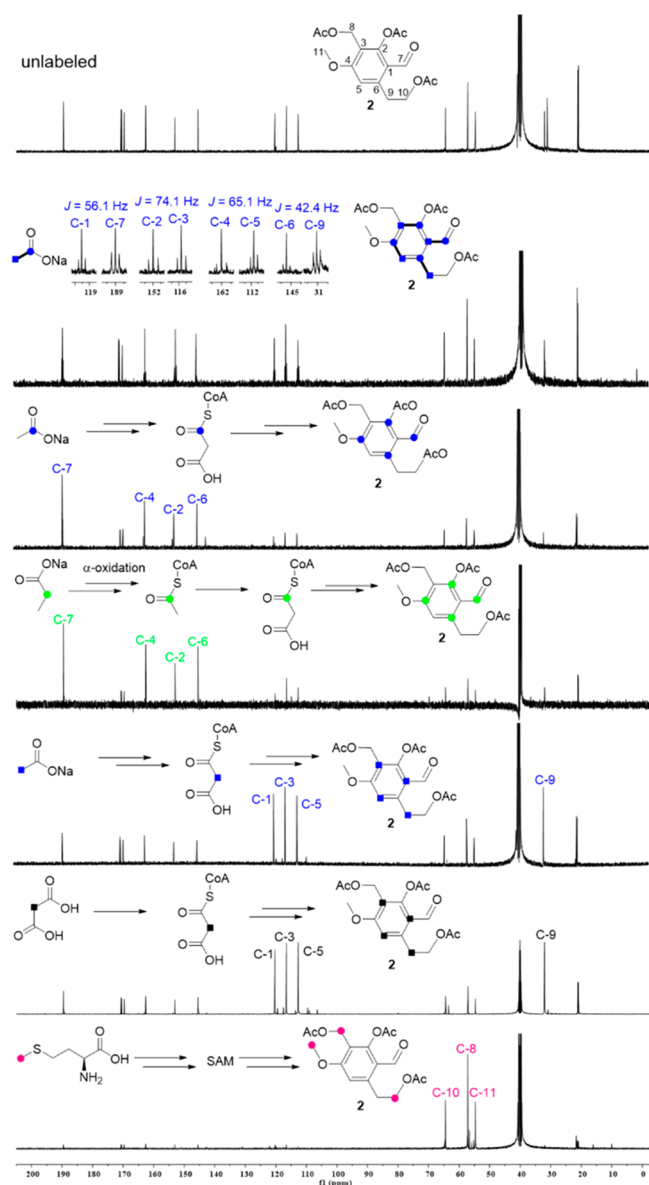


Figure 3. ^{13}C NMR spectra of the labeled and unlabeled **2**. [Legend: solid blue circles represent the labeled carbons after feeding with sodium $[1\text{-}^{13}\text{C}]$ acetate, solid green circles represent sodium $[2\text{-}^{13}\text{C}]$ propionate, solid blue squares represent sodium $[2\text{-}^{13}\text{C}]$ acetate, solid black squares represent $[2\text{-}^{13}\text{C}]$ malonic acid, bold bonds represent sodium $[1,2\text{-}^{13}\text{C}]$ acetate for the intact acetate unit, and solid pink circles represent $[methyl\text{-}^{13}\text{C}]\text{-L-methionine}$.]

Feeding **3** into the ΔuttA mutant led to detection of one additional major peak **6** and one minor peak **7** (see Figure 5A). Structure elucidation confirmed **6** to be the corresponding aldehyde of **3** (ustethylin D; see Scheme 1, as well as Table S7 and Figure S32 in the Supporting Information) and the minor peak **7** as a dimerization product (see Table S8 and Figures S33–S37 in the Supporting Information). Trace amounts of **1** were also detected in this culture (Figure 5A), proving **3** to be a precursor of **1**. It can be speculated that the metabolism of **6** is a limited step in the biosynthesis. Interestingly, **3** was not detected in the ΔuttA mutant after feeding with **4** (Figure S18 in the Supporting Information), excluding the direct methylation of the C6-methyl group in **4**.

Bioinformatics analysis revealed that UttA is a nonreducing PKS with a domain architecture of KS-MAT-PT-ACP-ACP-

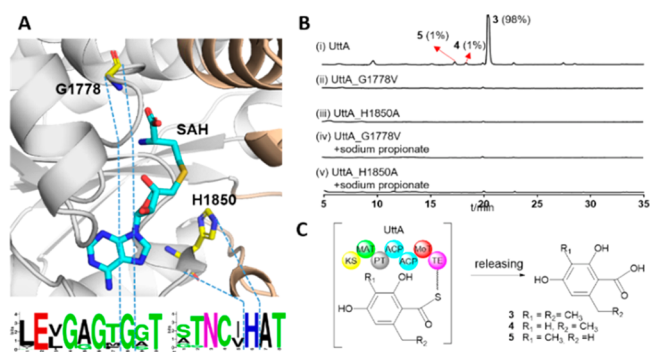


Figure 4. (A) Structural model of UttA-MeT with conserved motifs by alignments of 96 MeT domains in PKSs; (B) HPLC results of *A. nidulans* heterologous expression strains; and (C) the reactions catalyzed by UttA.

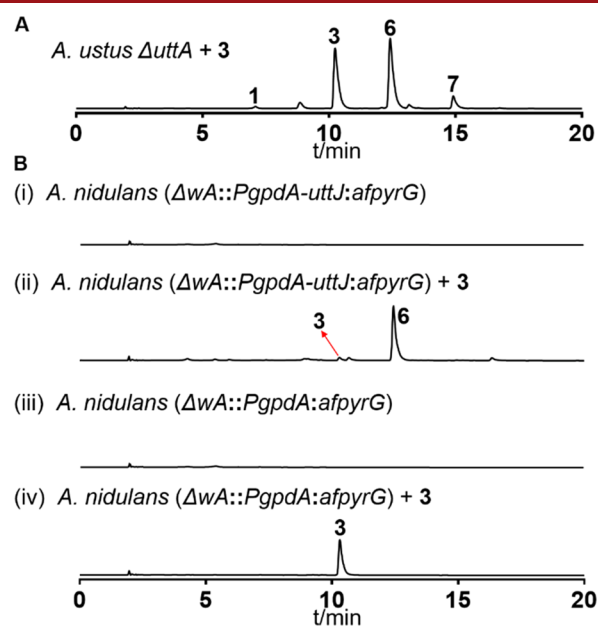


Figure 5. HPLC analysis of culture extracts of (A) *A. ustus* ΔuttA and (B) *A. nidulans* uttJ overexpression mutant after feeding with **3**.

MeT-TE (β -ketoacyl synthase, KS; malonyl-CoA-ACP transacylase, MAT; product template, PT; acyl carrier protein, ACP; methyltransferase, MeT; thioesterase, TE) (Figure 4C).¹⁹ The PT domain was deduced by phylogenetic analysis with 30 known PKS PTs (see Figure S3 in the Supporting Information).²⁰ It can be speculated that the methyl groups in **3** are transferred by the MeT domain from S-adenosyl L-methionine. UttA shares a sequence identity of 37.8% with the citrinin synthase PksCT from *Monascus purpureus*.²¹ The sequence identity of their MeT domains is found to be 39.7%. Therefore, a model of UttA-MeT was built, using PksCT-MeT as a template with SWISS-MODEL.²² Meanwhile, 96 MeT domains in PKSs were analyzed and presented with Weblogo (Figure 4A).^{23,24} The highly conserved residues of the SAM binding motif ExGxGxGx were identified at residues 1772–1779 in UttA. His1850 acting as a key catalytic residue for enolization is also highly conserved (see Figure S4 in the Supporting Information). To delete MeT activity from UttA, the UttA_G1778 V and UttA_H1850A mutants were constructed and expressed in *A. nidulans* LO8030. HPLC results showed the abolishment of the PKS products **3**–**5**

without accumulation of any other products, indicating the essential role of MeT domain for the functionality of UttA. Feeding propionate to the two mutants did not result in any detectable product formation, confirming that UttA cannot directly utilize propionate as starter as described above (Figure 4B(ii)–(v)). These results indicated that the methylation step is essential for the polyketide assembling by UttA. We propose that malonyl-CoA is loaded onto the MAT domain and transferred to the ACP domain. The propionyl-ACP complex is formed by methylation via SAM and decarboxylation. After condensation with two malonyl-CoA molecules, the MeT domain attaches the second methyl group. Condensation with another malonyl-CoA molecule led to the production of a polyketide chain, which is subsequent cyclized by the PT domain and released by the TE domain, resulting in the formation of the predominant product **3** (98%; see Figures 2B and 4B). However, it cannot be excluded that mutation at G1778 and H1850 had influence on the transcription, translation process, or protein stability. Attempts to get recombination protein of the MeT domain failed, so that no in vitro study was possible. The reaction catalyzed by UttA with involvement of two methylation steps is closely related to that of 3-methylorcinolaldehyde synthase MOS from *Acremonium strictum*. However, MOS contains a terminal reductase domain for direct release of an aldehyde,²⁵ while the UttA product, an aryl acid, is afterward reduced to an aldehyde.

1 differs structurally from **3** in oxidation states of the functional groups at C-1, C-3, and C-6, as well as O-methylation at OH-4. The conversion of **3** to **1** would require three oxidoreductases and an O-MeT. Inspection of the genomic neighborhood of *uttA* in *A. ustus* revealed the presence of a putative biosynthetic gene cluster (*uttA*–*uttJ*, coding for the putative proteins KIA75596–KIA75587 in the database; see Figure 2A) containing such genes as well as those coding for regulator and transporter (Table S1 in the Supporting Information). *UttJ* coding for an NRPS-like enzyme with an A-T-R domain architecture is 1 of the 10 highly expressed genes in *A. ustus* under our culture conditions (data not included). Given such enzymes from different fungal strains for aryl acid reduction to aldehydes,^{26,27} *UttJ* is likely involved in the conversion of **3** to **6**. Indeed, deletion of *uttJ* abolished the formation of **1** and accumulation of **3**–**5** with almost the same product profile of the *A. nidulans* *uttA* overexpression strain (see Figures 2B(viii) and 4B(i), as well as Figure S16 in the Supporting Information). This unambiguously proved its role in the reduction of the carboxyl group to an aldehyde. Feeding **3** into the *A. nidulans* *uttJ* overexpression strain led to the detection of **6** (see Figure 5B(ii)), proving *UttJ* as an aryl acid reductase (Scheme 1). Further sequence comparison and analysis revealed *UttH* to be a putative nonheme Fe^{II}/2-oxoglutarate dependent oxygenase and shares 58% and 52% sequence identities with CitB from *Monascus ruber*²⁸ and ClaD from *Penicillium crustosum*,²⁹ respectively (see Table S1 and Figure S5 in the Supporting Information). Both known enzymes catalyze hydroxylations of aryl methyl groups. Deletion of *uttH* led to the accumulation of *UttJ* product **6**, proving the reaction order of both enzymes (see Figure 2B(vii), as well as Figure S15 in the Supporting Information). Deletion of *uttC* coding for a cytochrome P₄₅₀ enzyme abolished the formation of **1** and production of **8** (ustethylin B; see Table S9 in the Supporting Information, Figure 2B(iii), and Figures S9 and S38–S41 in the Supporting Information), which differs from **1** just in the oxidation state of

the ethyl group. This proved that *UttC* catalyzed the last step in the biosynthesis of **1**. Bioinformatics analysis showed that *UttC* contains the conserved motifs ExxR (EAGR, 349–352) and CxG (CLG, 434–436) of P₄₅₀ enzymes (see Figure S6 in the Supporting Information).³⁰ Usually, the hydroxylation of phenethyl group occurs at the α -position (–CH₂–), e.g., in the biosynthesis of marilone A.³¹ Here, we present an unusual β -hydroxylation of the phenethyl group by the cytochrome P₄₅₀ *UttC*. Detection of **8** with a methoxy group in Δ *uttC* mutant indicates that the methylation of the C4-hydroxyl group occurs before *UttC* and after *UttH* reactions and could be catalyzed by the putative O-MeT *UttF*. Indeed, one predominant peak **9** (ustethylin C) with a [M + Na]⁺ ion at *m/z* 219.0626, which is 14 Da less than that of **8**, was observed in the Δ *uttF* mutant (see Figure 2B(v), as well as Figure S13 in the Supporting Information). Similar to **1**, **9** was also found to be unstable and could not be obtained in pure form for structure elucidation. However, its structure can be elucidated after conversion to its diacetylated derivative **10** (see Table S10 and Figures S42–S45 in the Supporting Information).

Gene deletion results revealed the reaction sequence of the tailoring enzymes for **3** conversion to **1**. Extracted ion chromatograms of the culture proved the presence of **1** as almost the only pathway product (see Figure S7 in the Supporting Information), indicating the high efficiency of the involved enzymes in wildtype *A. ustus*. The *utt* cluster is positively regulated by a DNA binding enzyme *UttD*. Deletion of *uttD* completely abolished product formation (see Figure 2B(iv), as well as Figure S11 in the Supporting Information). Even feeding **3** to the Δ *uttD* deletion mutant did not lead to any conversion (see Figure S17 in the Supporting Information). Deletion of *uttG* coding for an MFS transporter reduced **1** production to 30.8% of that of the wildtype *A. ustus* (see Figures 2B(vi), as well as Figure S14 in the Supporting Information). **1** was still detected in the deletion mutants of the two oxidoreductase genes *uttB* and *uttE* (see Figures S9 and S12 in the Supporting Information). They very likely are not involved in the formation of ustethylin A.

In summary, in this study, we have identified the biosynthetic gene cluster of the highly oxygenated aryl-aldehyde derivative ustethylin A and elucidated its biosynthetic pathway by transcriptome analysis, gene deletion, and expression, as well as isotopic labeling experiments. The PKS *UttA*, as a key enzyme, is responsible for the formation of the phenethyl core structure with methylation as key reactions. Consecutive and coordinated modifications by three different types of oxidoreductases and one O-MeT lead to the final product. To the best of our knowledge, this is the first report on the biosynthetic pathway of a phenethyl-containing fungal metabolite.

■ ASSOCIATED CONTENT

Supporting Information

The Supporting Information is available free of charge at <https://pubs.acs.org/doi/10.1021/acs.orglett.0c02719>.

Supplementary methods, tables, and figures (PDF)

■ AUTHOR INFORMATION

Corresponding Author

Shu-Ming Li – Institut für Pharmazeutische Biologie und Biotechnologie, Fachbereich Pharmazie, Philipps-Universität

Marburg, 35037 Marburg, Germany; orcid.org/0000-0003-4583-2655; Email: shuming.li@staff.uni-marburg.de

Authors

Liujuan Zheng – Institut für Pharmazeutische Biologie und Biotechnologie, Fachbereich Pharmazie, Philipps-Universität Marburg, 35037 Marburg, Germany

Yiling Yang – Institut für Pharmazeutische Biologie und Biotechnologie, Fachbereich Pharmazie, Philipps-Universität Marburg, 35037 Marburg, Germany

Haowen Wang – Institut für Pharmazeutische Biologie und Biotechnologie, Fachbereich Pharmazie, Philipps-Universität Marburg, 35037 Marburg, Germany

Aili Fan – College of Life Science and Technology, Beijing University of Chemical Technology, Chaoyang District 100029 Beijing, China

Liping Zhang – Key Laboratory of Tropical Marine Bio-resources, South China Sea Institute of Oceanology Chinese Academy of Sciences, Guangzhou 510301, China

Complete contact information is available at:
<https://pubs.acs.org/10.1021/acs.orglett.0c02719>

Author Contributions

[†]These authors contributed equally.

Notes

The authors declare no competing financial interest.

ACKNOWLEDGMENTS

We thank Rixa Kraut, Lena Ludwig-Radtke, and Stefan Newel (Fachbereich Pharmazie, Philipps-Universität Marburg) for taking MS and NMR spectra. This project was financially funded in part by the Deutsche Forschungsgemeinschaft (DFG) (No. INST 160/620-1). L.Z. (No. 201604910536) and Y.Y. (No. 201808530447) are scholarship recipients from the China Scholarship Council.

REFERENCES

- (1) Better, J.; Gatenbeck, S.; Hornfeldt, A.-B.; Thorstad, O.; Undheim, K.; Berg, J.-E.; Pilotti, A.-M. *Acta Chem. Scand.* **1977**, *31*, 391.
- (2) El Maddah, F.; Eguereva, E.; Kehraus, S.; König, G. M. *Org. Biomol. Chem.* **2019**, *17*, 2747.
- (3) Shepherd, M. D.; Kharel, M. K.; Zhu, L. L.; Van Lanen, S. G.; Rohr, J. A. *Org. Biomol. Chem.* **2010**, *8*, 3851.
- (4) Yu, Z.; Zhang, H.; Yuan, C.; Zhang, Q.; Khan, I.; Zhu, Y.; Zhang, C. *Org. Lett.* **2019**, *21*, 7679.
- (5) Yeh, H. H.; Chang, S. L.; Chiang, Y. M.; Bruno, K. S.; Oakley, B. R.; Wu, T. K.; Wang, C. C. *Org. Lett.* **2013**, *15*, 756.
- (6) McIntyre, C. R.; Simpson, T. J.; Trimble, L. A.; Vederas, J. C. *J. Chem. Soc., Chem. Commun.* **1984**, 706.
- (7) Simpson, T. J.; Stenzel, D. J. *J. Chem. Soc., Chem. Commun.* **1981**, 239.
- (8) De Jesus, A. E.; Horak, R. M.; Steyn, P. S.; Vleggaar, R. J. *Chem. Soc., Perkin Trans. 1* **1987**, 2253.
- (9) Brock, M.; Fischer, R.; Linder, D.; Buckel, W. *Mol. Microbiol.* **2000**, *35*, 961.
- (10) Pi, B.; Yu, D.; Dai, F.; Song, X.; Zhu, C.; Li, H.; Yu, Y. *PLoS One* **2015**, *10*, No. e0116089.
- (11) Blin, K.; Shaw, S.; Steinke, K.; Villebro, R.; Ziemert, N.; Lee, S. Y.; Medema, M. H.; Weber, T. *Nucleic Acids Res.* **2019**, *47*, W81.
- (12) Cox, R. J. *Org. Biomol. Chem.* **2007**, *5*, 2010.
- (13) Goswami, R. S. *Methods Mol. Biol.* **2012**, 835, 255.
- (14) Joska, T. M.; Mashruwala, A.; Boyd, J. M.; Belden, W. J. *J. Microbiol. Methods* **2014**, *100*, 46.

- (15) Zhang, P.; Wang, X.; Fan, A.; Zheng, Y.; Liu, X.; Wang, S.; Zou, H.; Oakley, B. R.; Keller, N. P.; Yin, W. B. *Mol. Microbiol.* **2017**, *105*, 469.
- (16) Chiang, Y. M.; Ahuja, M.; Oakley, C. E.; Entwistle, R.; Asokan, A.; Zutz, C.; Wang, C. C.; Oakley, B. R. *Angew. Chem., Int. Ed.* **2016**, *55*, 1662.
- (17) Durrani, A. A.; Tyman, J. H. P. *J. Chem. Soc., Perkin Trans. 1* **1980**, 1658.
- (18) Culberson, C. F.; Culberson, W. L. *Exp. Mycol.* **1978**, *2*, 245.
- (19) Chooi, Y. H.; Tang, Y. J. *Org. Chem.* **2012**, *77*, 9933.
- (20) Li, Y.; Xu, W.; Tang, Y. J. *Biol. Chem.* **2010**, *285*, 22764.
- (21) Storm, P. A.; Herbst, D. A.; Maier, T.; Townsend, C. A. *Cell Chem. Biol.* **2017**, *24*, 316.
- (22) Waterhouse, A.; Bertoni, M.; Bienert, S.; Studer, G.; Tauriello, G.; Gumieny, R.; Heer, F. T.; de Beer, T. A. P.; Rempfer, C.; Bordoli, L.; Lepore, R.; Schwede, T. *Nucleic Acids Res.* **2018**, *46*, W296.
- (23) Crooks, G. E.; Hon, G.; Chandonia, J. M.; Brenner, S. E. *Genome Res.* **2004**, *14*, 1188.
- (24) Schneider, T. D.; Stephens, R. M. *Nucleic Acids Res.* **1990**, *18*, 6097.
- (25) Bailey, A. M.; Cox, R. J.; Harley, K.; Lazarus, C. M.; Simpson, T. J.; Skellam, E. *Chem. Commun.* **2007**, 4053.
- (26) Li, C.; Matsuda, Y.; Gao, H.; Hu, D.; Yao, X. S.; Abe, I. *ChemBioChem* **2016**, *17*, 904.
- (27) Wang, M.; Beissner, M.; Zhao, H. *Chem. Biol.* **2014**, *21*, 257.
- (28) He, Y.; Cox, R. J. *Chem. Sci.* **2016**, *7*, 2119.
- (29) Fan, J.; Liao, G.; Kindinger, F.; Ludwig-Radtke, L.; Yin, W.-B.; Li, S.-M. *J. Am. Chem. Soc.* **2019**, *141*, 4225.
- (30) Syed, K.; Mashele, S. S. *PLoS One* **2014**, *9*, e95616–1.
- (31) Du, L.; Dong, S.; Zhang, X.; Jiang, C.; Chen, J.; Yao, L.; Wang, X.; Wan, X.; Liu, X.; Wang, X.; Huang, S.; Cui, Q.; Feng, Y.; Liu, S. J.; Li, S. *Proc. Natl. Acad. Sci. U. S. A* **2017**, *114*, No. E5129.

Supporting Information

Ustethylin biosynthesis implies phenethyl derivative formation in *Aspergillus ustus*

Liujuan Zheng,^{‡a} Yiling Yang,^{‡a} Haowen Wang,^a Aili Fan,^b Liping Zhang^c and Shu-Ming Li^{*a}

^a Institut für Pharmazeutische Biologie und Biotechnologie, Fachbereich Pharmazie, Philipps-Universität Marburg, Robert-Koch Straße 4, 35037 Marburg (Germany)

^b College of Life Science and Technology, Beijing University of Chemical Technology, North Third Ring Road 15, Chaoyang District, 100029 Beijing (China)

^c Key Laboratory of Tropical Marine Bio-resources, South China Sea Institute of Oceanology Chinese Academy of Sciences 164 West Xingang Road, Guangzhou 510301 (China)

Table of Contents

Experimental Procedures	5
1. Chemicals	5
2. Strains, media, and growth conditions	5
3. Genomic DNA isolation	5
4. Genome sequencing and sequence analysis	5
5. PCR amplification, gene cloning and plasmid construction	6
6. Molecular modeling for UttA_MeT	6
7. Genetic manipulation in <i>A. ustus</i> 3.3904 and cultivation of deletion mutants	6
8. Heterologous expression in <i>A. nidulans</i>	7
9. Site-directed mutagenesis of UttA	7
10. HPLC equipment for analysis and metabolite isolation	7
11. Large-scale fermentation, extraction and isolation of secondary metabolites	7
12. Feeding experiments	9
13. LC-MS analysis	10
14. NMR analysis	10
15. Physiochemical properties of the compounds described in this study	10
16. Structural elucidation	11
Table S1. Putative functions of the genes from the ustethylin (<i>utt</i>) gene cluster	13
Table S2. Strains used in this study	14
Table S3. Plasmids used and constructed in this study	15
Table S4. Primers used in this study	16
Table S5. NMR data of compound 2 in DMSO- <i>d</i> ₆ (500 MHz, δ in ppm, <i>J</i> in Hz)	20
Table S6. NMR data of compound 3 in DMSO- <i>d</i> ₆ (500 MHz, δ in ppm, <i>J</i> in Hz)	21
Table S7. ¹ H NMR data of compounds 4 – 6 in DMSO- <i>d</i> ₆ (500 MHz, δ in ppm, <i>J</i> in Hz)	22
Table S8. NMR data of compound 7 in DMSO- <i>d</i> ₆ (500 MHz, δ in ppm, <i>J</i> in Hz)	23
Table S9. NMR data of compound 8 in CDCl ₃ (500 MHz, δ in ppm, <i>J</i> in Hz)	24
Table S10. NMR data of compound 10 in DMSO- <i>d</i> ₆ (500 MHz, δ in ppm, <i>J</i> in Hz)	25
Table S11. Enrichments in 2 after feeding with ¹³ C labeled precursors	26
Figure S1. PCR verification of deletion mutants of <i>A. ustus</i> 3.3904	27

SUPPORTING INFORMATION

Figure S2. PCR verification of heterologous expression transformants.	28
Figure S3. Phylogenetic analysis of UttA_PT domain with 30 known PT domains from fungi. ...	29
Figure S4. Point mutation in UttA and analysis of the obtained mutants.	30
Figure S5. Sequence alignments of 2-OG-dependent oxygenases.	31
Figure S6. Weblogo illustration for the conserved ExxR and CxG motifs in UttC by using 96 P ₄₅₀ enzyme in fungi.	32
Figure S7. LC-MS analysis of the metabolite profile of the <i>A. ustus</i> wild type.	33
Figure S8. LC-MS analysis of the metabolite profile of the <i>A. ustus</i> Δ uttA mutant	34
Figure S9. LC-MS analysis of the metabolite profile of the <i>A. ustus</i> Δ uttB mutant	35
Figure S10. LC-MS analysis of the metabolite profile of the <i>A. ustus</i> Δ uttC mutant	36
Figure S11. LC-MS analysis of the metabolite profile of the <i>A. ustus</i> Δ uttD mutant	37
Figure S12. LC-MS analysis of the metabolite profile of the <i>A. ustus</i> Δ uttE mutant	38
Figure S13. LC-MS analysis of the metabolite profile of the <i>A. ustus</i> Δ uttF mutant	39
Figure S14. LC-MS analysis of the metabolite profile of the <i>A. ustus</i> Δ uttG mutant	40
Figure S15. LC-MS analysis of the metabolite profile of the <i>A. ustus</i> Δ uttH mutant	41
Figure S16. LC-MS analysis of the metabolite profile of the <i>A. ustus</i> Δ uttJ mutant	42
Figure S17. LC-MS analysis of the metabolite profile of the <i>A. ustus</i> Δ uttD after feeding with 3 . ..	43
Figure S18. LC-MS analysis of the metabolite profile of the <i>A. ustus</i> Δ uttA after feeding with 4 . ..	44
Figure S19. LC-MS analysis of the acetylated EtOAc extract from <i>A. ustus</i>	45
Figure S20. LC-MS analysis of the acetylated EtOAc extract from Δ uttF of <i>A. ustus</i>	45
Figure S21. UV spectra of the compounds identified in this study	46
Figure S22. ¹ H NMR spectrum of compound 2 in DMSO- <i>d</i> ₆ (500 MHz)	47
Figure S23. ¹³ C{ ¹ H} NMR spectrum of compound 2 in DMSO- <i>d</i> ₆ (125 MHz)	47
Figure S24. HSQC spectrum of compound 2 in DMSO- <i>d</i> ₆	48
Figure S25. HMBC spectrum of compound 2 in DMSO- <i>d</i> ₆	48
Figure S26. ¹ H NMR spectrum of compound 3 in DMSO- <i>d</i> ₆ (500 MHz)	49
Figure S27. ¹³ C{ ¹ H} NMR spectrum of compound 3 in DMSO- <i>d</i> ₆ (125 MHz)	49
Figure S28. HSQC spectrum of compound 3 in DMSO- <i>d</i> ₆	50
Figure S29. HMBC spectrum of compound 3 in DMSO- <i>d</i> ₆	50
Figure S30. ¹ H NMR spectrum of compound 4 in DMSO- <i>d</i> ₆ (500 MHz)	51
Figure S31. ¹ H NMR spectrum of compound 5 in DMSO- <i>d</i> ₆ (500 MHz)	51

SUPPORTING INFORMATION

Figure S32. ^1H NMR spectrum of compound 6 in $\text{DMSO}-d_6$ (500 MHz).....	52
Figure S33. ^1H NMR spectrum of compound 7 in $\text{DMSO}-d_6$ (500 MHz).....	52
Figure S34. $^{13}\text{C}\{^1\text{H}\}$ NMR spectrum of compound 7 in $\text{DMSO}-d_6$ (125 MHz).....	53
Figure S35. HSQC spectrum of compound 7 in $\text{DMSO}-d_6$	53
Figure S36. ^1H - ^1H COSY spectrum of compound 7 in $\text{DMSO}-d_6$	54
Figure S37. HMBC spectrum of compound 7 in $\text{DMSO}-d_6$	54
Figure S38. ^1H NMR spectrum of compound 8 in CDCl_3 (500 MHz)	55
Figure S39. $^{13}\text{C}\{^1\text{H}\}$ NMR spectrum of compound 8 in CDCl_3 (125 MHz)	55
Figure S40. HSQC spectrum of compound 8 in CDCl_3	56
Figure S41. HMBC spectrum of compound 8 in CDCl_3	56
Figure S42. ^1H NMR spectrum of compound 10 in $\text{DMSO}-d_6$ (500 MHz).....	57
Figure S43. $^{13}\text{C}\{^1\text{H}\}$ NMR spectrum of compound 10 in $\text{DMSO}-d_6$ (125 MHz).....	57
Figure S44. HSQC spectrum of compound 10 in $\text{DMSO}-d_6$	58
Figure S45. HMBC spectrum of compound 10 in $\text{DMSO}-d_6$	58
References	59

Experimental Procedures

1. Chemicals

Sodium [1-¹³C] acetate, sodium [2-¹³C] acetate, and sodium [2-¹³C] propionate were purchased from Cambridge Isotope Laboratories. Sodium [1,2-¹³C] acetate, [2-¹³C] malonic acid, and [methyl-¹³C]-L-methionine were obtained from Sigma-Aldrich. Other reagents were from Fisher scientific, VWR or Sigma-Aldrich.

2. Strains, media, and growth conditions

Escherichia coli DH5 α cells were grown in LB medium (1% NaCl, 1% tryptone, and 0.5% yeast extract). 50 mg/mL ampicillin were supplemented for cultivation of recombinant *E. coli* strains.

Saccharomyces cerevisiae HOD114-2B cells were grown in YPD medium (1% yeast extract, 2% peptone and 2% glucose). 1.5% agarose was used for plates. The SC-uracil medium (6.7 g/L yeast nitrogen base with ammonium sulfate, 650 mg/L CSM-His-Leu-Ura (MP Biomedicals), 20 mg/L His and 60 mg/L Leu, 2% glucose, pH 6.2 – 6.3, 1.5% agarose was used for plates) was used for selection.

Fungal strains used in this study are summarized in Table S2. *Aspergillus ustus* (*A. ustus*) 3.3904 was purchased from China General Microbiological Culture Collection Center (Beijing, China) and cultivated in PD (potato dextrose broth, Sigma) or ISP3 (6% oat) medium at 230 rpm and 30 °C for secondary metabolite (SM) production.

Aspergillus nidulans strains were grown at 37 °C on GMM medium (1.0% glucose, 50 mL/L salt solution, 1 mL/L trace element solution, 1.6% agar) for sporulation and transformation with appropriate nutrition as required. The salt solution comprises (w/v) 12% NaNO₃, 1.04% KCl, 1.04% MgSO₄·7H₂O, and 3.04% KH₂PO₄. The trace element solution contains (w/v) 2.2% ZnSO₄·7H₂O, 1.1% H₃BO₃, 0.5% MnCl₂·4H₂O, 0.16% FeSO₄·7H₂O, 0.16% CoCl₂·5H₂O, 0.16% CuSO₄·5H₂O, 0.11% (NH₄)₆Mo₇O₂₄·4H₂O, and 5% Na₄EDTA.

3. Genomic DNA isolation

The mycelia of *A. ustus* 3.3904 and *A. nidulans* were dried on filter paper and collected in 2 mL Eppendorf tubes. Four glass beads (2.85 mm in diameter) and 400 μ L of LETS buffer (10 mM Tris-HCl pH 8.0, 20 mM EDTA pH 8.0, 0.5% SDS, and 0.1 M LiCl) were added to the tubes. After vigorous mixing for 4 min, 300 μ L LETS buffer were added. The solution was then treated with 700 μ L phenol: chloroform: isoamyl alcohol (25: 24: 1). Genomic DNA was precipitated by addition of 900 μ L of absolute EtOH. After centrifugation at 13,000 rpm for 30 min and washing with 70% EtOH, the obtained DNA was dissolved in 50 – 100 μ L distilled H₂O.

4. Genome sequencing and sequence analysis

The genome of *A. ustus* 3.3904 was sequenced by Genewiz (Suzhou, China) using Nova-seq6000/X-ten (Illumina). Initial prediction and analysis of biosynthetic gene clusters were carried out by using AntiSMASH.¹

Prediction of the enzyme function was performed with the online BLAST tools (<http://blast.ncbi.nlm.nih.gov>). The genes *uttA-J* in the *utt* cluster are summarized in Table S1. The genomic DNA sequence of the *utt* cluster reported in this study corresponds to that depicted at GenBank under accession numbers JOMC01000079.1.

5. PCR amplification, gene cloning and plasmid construction

Plasmids and primers used in this study are listed in Table S3 and Table S4, respectively. Primers were synthesized by SeqLab GmbH (Göttingen, Germany). PCR amplification was carried out by using Phusion® High-Fidelity DNA polymerase from New England Biolabs (NEB) on a T100™ Thermal cycler from Bio-Rad. PCR thermal profiles were set as recommended by the manufacturer's instruction. The plasmids for gene deletion and heterologous expression were constructed *via* homologous recombination in *Escherichia coli* DH5α or *Saccharomyces cerevisiae* HOD114-2B by using primers listed Table S4.

6. Molecular modeling for UttA_MeT

Homolog modelling for 300 amino acids of UttA_MeT was carried out by using SWISS-MODEL.² S-Adenosyl-L-homocysteine (SAH) was manually positioned by using Coot.³ The illustration was created with Pymol (DeLano Scientific LLC, Version 1.3.x.).

7. Genetic manipulation in *A. ustus* 3.3904 and cultivation of deletion mutants

Fresh spores of *A. ustus* 3.3904 were inoculated into 50 mL LMM medium in 250 mL flask and incubated at 230 rpm and 30 °C for germination. The germlings were harvested after 11 h by centrifugation at 5,000 rpm and 4 °C for 10 min and washed with distilled H₂O. The mycelia were then transferred into a 25 mL flask with 10 mL of osmotic buffer (1.2 M MgSO₄ in 10 mM sodium phosphate, pH 5.8) containing 40 mg lysing enzyme from *Trichoderma harzianum* (Sigma) and 30 mg yatalase from *Corynebacterium sp.* OZ-21 (OZEKI Co., Ltd.). After shaking at 100 rpm and 30 °C for 10 h, the mixture was transferred into a 50 mL falcon tube and overlaid gently with 10 mL of trapping buffer (0.6 M sorbitol in 0.1 M Tris-HCl, pH 7.0). After centrifugation at 5,000 rpm and 4 °C for 10 min, the protoplasts were collected from the interface of the two buffer systems. The collected protoplasts were then transferred to a sterile 15 mL falcon tube and resuspended in 100 μL of STC buffer (1.2 M sorbitol, 10 mM CaCl₂ in 10 mM Tris-HCl, pH 7.5) for transformation.

The DNA fragments (2 – 3 μg in 8 – 10 μL) were mixed with 100 μL of the protoplasts and incubated for 50 min on ice. 1.25 mL of PEG solution (60% polyethylene glycol 4000, 50 mM CaCl₂, 50 mM Tris-HCl, pH 7.5) was then added and gently mixed. After incubation at room temperature for 30 min, 5 mL STC buffer was added into the mixture and spread on plates with SMM bottom medium (1.0% glucose, 50 mL/L salt solution, 1 mL/L trace element solution, 1.2 M sorbitol, and 1.6% agar) containing 100 μg/mL hygromycin B. SMM top medium (1.0% glucose, 50 mL/L salt solution, 1 mL/L trace element solution, 1.2 M sorbitol, and 0.8% agar) containing 50 μg/mL hygromycin B was overlaid softly on the plates. 3 – 4 days later, the transformants were transferred onto fresh PDA

plates (PD medium with 3% agar) containing 100 $\mu\text{g/mL}$ hygromycin B for selection. The obtained transformants were inoculated in PD medium for isolation of genomic DNA to verify the integrity *via* PCR amplification (Figure S2). After cultivation in PD liquid medium at 230 rpm and 30 °C for 7 days, the cultures were extracted with EtOAc, dissolved in DMSO and subjected to HPLC and LC-MS for analysis.

8. Heterologous expression in *A. nidulans*

A. nidulans LO8030⁴ was used as the recipient host. The protoplast preparation and transformation were performed as described previously.⁵ PLZ51 – 54 containing the PKS gene *uttA*, *uttA-G1778V* and *uttA-H1850A* as well as the NRPS-like gene *uttJ* were transformed into *A. nidulans* LO8030 to create expression strain LZ51, LZ52, LZ53 and LZ54, respectively. The transformants were verified by PCR (Figures S2 and S4).

9. Site-directed mutagenesis of UttA

The fragments containing the point mutation were constructed *via* fusion PCR. The mutated and non-mutated fragments of *uttA* were then integrated into pYH-*gpdA-pyrG* following the same procedure for pLZ51 to produce pLZ53 (UttA_G1778V) and pLZ54 (UttA_H1850A). The primers used for plasmids constructing were listed in Table S3 – S4.

10. HPLC equipment for analysis and metabolite isolation

EtOAc extracts of fungal strains were analyzed on an Agilent HPLC series 1200 (Agilent Technologies) equipped with an Agilent Eclipse XDB-C18 column (5 μm , 4.6 \times 150 mm). A linear gradient from 10 to 90% ACN in H₂O in 20 min was used. The column was then washed with 100% ACN for 5 min and equilibrated with 10% ACN in H₂O for another 5 min. Detection was carried out with a photodiode array detector from 190 to 400 nm.

The same HPLC system was also used for product isolation with a Multospher 120 RP-18 column (5 μm , 10 \times 250 mm). The products were eluted with different solvent gradients of ACN in H₂O, with or without HCOOH, at a flow rate of 2 mL/min.

11. Large-scale fermentation, extraction and isolation of secondary metabolites

For metabolite extraction after large-scale fermentation, the supernatant was separated from mycelia by filtration and extracted with equal volume of EtOAc for three times. The mycelia were extracted with acetone and concentrated under reduced pressure to afford an aqueous solution and then extracted with EtOAc for three times. Both EtOAc extracts were evaporated under reduced pressure to afford the crude extracts for further purification.

To isolate compound **1**, *A. ustus* spores were cultivated in 10 x 250 mL flasks containing 50 mL PDB liquid medium for 2 days, then transferred to 10 x 2 L flasks containing 500 mL PDB liquid medium each. The cultures were maintained on a rotary shaker at 230 rpm and 30 °C for 9 days. The cultures were harvested and extracted as

SUPPORTING INFORMATION

mentioned above to give 0.4 g crude extract. The crude extract was subjected to silica gel column chromatography by using stepwise gradient elution with mixtures of petroleum ether/EtOAc (20:1 to 0:1, v/v) to give five fractions (1 – 5). Fraction 2 was further purified on the HPLC system mentioned above by using ACN/H₂O (40:60) as elution solvents, resulting in 7.0mg of **1**.

To identify the structure of **1**, we used the previously published acetylation method.⁶ *A. ustus* spores were inoculated into 40 x 250 mL flasks containing 50 mL PDB liquid medium each and incubated on a rotary shaker at 230 rpm and 30 °C for 6 days. 400 mg of the obtained crude extracts were immediately acetylated with acetic anhydride (21.24 mmol) and NaOAc·3H₂O (0.3 mmol) at room temperature for 16 h. The mixture was extracted with 15 mL EtOAc and washed with 15 mL saturated solution of NaHCO₃ for three times. After evaporation of the solvent, 11.4 mg of **2** were isolated by isocratic elution with ACN/H₂O (55:45) on the aforementioned HPLC system for MS and NMR analyses.

To isolate compounds **3** – **5** from the *A. nidulans*-pYH-*gpdA-uttA-pryG* transformant, the strain was cultivated in ISP3 medium at 30 °C for 8 days. After extraction, 4.7 g crude extract was obtained from 5 L culture and subjected to silica gel column chromatography. Petroleum ether/EtOAc (50:1 to 0:1, v/v) were used as elution solvents to give 17 fractions (1 – 17). Fraction 6 was purified on the HPLC by isocratic elution with ACN/H₂O (40:60, 0.1% HCOOH) to get **3** (26.0 mg). **4** (14.6 mg) was obtained from fraction 8, which was purified on the HPLC system by isocratic elution with ACN/H₂O (25:75) containing 0.1% HCOOH. **5** (10.6 mg) was obtained from fraction 9 under the same conditions as for **4**. **3** – **5** were also isolated from the *A. ustus* *ΔuttJ* mutant in a similar procedure.

To isolate compound **6**, the *ΔuttH* mutant was cultivated in PDB medium at 30 °C for 7 days. After extraction, 0.1 g crude extract was obtained from 5 L culture and subjected to silica gel column chromatography by using petroleum ether/EtOAc (50:1 to 0:1, v/v) as elution solvents to give 11 fractions (1 – 11). **6** (1.0 mg) was obtained from fraction 2 after purification on HPLC using isocratic elution with ACN/H₂O (53:47) containing 0.1% HCOOH).

To isolate compound **8** from *ΔuttC* mutant, the mutant was cultivated in ISP3 medium at 30 °C for 8 days. After extraction, 8.2 g crude extract was obtained from 5 L culture and subjected to silica gel column chromatography by using petroleum ether/EtOAc (50:1 to 0:1, v/v) as elution solvents to give 13 fractions (1 – 13). Fraction 5 was purified on the HPLC with a linear gradient from 10 to 100% ACN containing 0.1% HCOOH in H₂O containing 0.1% HCOOH in 22 min. The column was then washed with 100% ACN containing 0.1% HCOOH for 5 min, followed by 5 min equilibration with 10% ACN containing 0.1% HCOOH. 9.3 mg of **8** were obtained for MS and NMR analyses.

To identify compound **9**, spores of *ΔuttF* mutant were inoculated into 40 x 250 mL flasks containing 50 mL PDB medium each and incubated on a rotary shaker at 230 rpm and 30 °C for 6 days. After extraction, the crude extract (175.0 mg) was also immediately acetylated *via* the same procedure described for compound **1**. Finally, 5.9 mg of

10 was obtained after purification on the HPLC by isocratic elution with ACN/H₂O (46:54) for MS and NMR analyses.

12. Feeding experiments

Feeding with ¹³C-labeled precursors

For labeling experiments, appropriate amounts of *A. ustus* spores were transferred from plates into 250 mL flasks containing 50 mL PDB medium and cultivated on a rotary shaker at 230 rpm and 30 °C. Aqueous stock solution of the respective precursor was fed after 30 h cultivation, followed by a second feeding 24 h later. After cultivation for another 60 h, the fungal cultures were extracted with EtOAc for three times. The EtOAc extracts were evaporated at 30 °C to dryness and acetylated as mentioned above. The acetylated product was further purified on the HPLC system and subjected to NMR analysis. The culture size, precursor amounts and product yields are given below.

250 and 125 mg of sodium [1-¹³C] acetate were used for the first and second feeding of the cultures in 25 flasks, leading to 0.5 mg of **2**. The feeding experiments with sodium [2-¹³C] acetate and sodium [1,2-¹³C] acetate followed the same procedure, resulting in 1.5 and 1.0 mg of **2**, respectively.

293 and 147 mg of [2-¹³C] malonic acid were used for the first and second feeding of the cultures in 22 flasks, yielding 2.5 mg of **2**.

200 and 100 mg of sodium [2-¹³C] propionate were used for the first and second feeding of the cultures in 12 flasks, giving 0.6 mg of **2**.

180 and 120 mg of [methyl-¹³C]-L-methionin were used for the first and second feeding of the cultures in 40 flasks, leading to 6.0 mg of **2**.

Feeding experiments in *A. nidulans* expression mutants with UttA_G1778V and UttA_H1850A

A. nidulans with empty vector, UttA_G1778V or UttA_H1850A mutant was cultivated as duplicate in 250 mL flask containing 50 mL PDB medium at 230 rpm and 30 °C. 3 mL propionic acid (3 g) were diluted with NaOH solution to 6 ml stock solution (pH 7). 650 µL (0.325 g propionic acid) of this solution were added into each of the two days-old cultures. Another 350 µL (0.175 g propionic acid) solution were added one day later. After cultivation in PD liquid medium at 230 rpm and 30 °C for 4 days, the cultures were extracted with EtOAc, dissolved in ACN and subjected to LC-MS analysis.

Precursor feeding in Δ uttA, Δ uttD and uttJ overproduction mutants

SUPPORTING INFORMATION

Compound **3** was dissolved in DMSO to a concentration of 18 mg/mL. 277 μ L (5 mg) of this solution was added into *A. ustus* Δ uttA cultures in 250 mL flasks containing 50 mL PDB medium each after fermentation at 230 rpm and 30 °C for three days. 2 L total culture in 40 flasks were used for this experiment and harvested after 7 days. 1.0 mg of **7** and 1.0 mg of **8** were obtained and subjected to NMR and MS analyses. Feeding compound **3** into *A. nidulans*-pYH-gpdA-uttJ-pyrG transformant led to the isolation of 12.4 mg of **6** for NMR and MS analyses. Compound **3** was also fed to *A. ustus* Δ uttD mutant.

1.0 mg (100 μ L) of **4** was administered to a 100 mL flask containing 10 mL *A. ustus* Δ uttA culture after 3 days fermentation at 230 rpm and 30 °C. 1 mL culture was extracted for LC-MS analysis.

13. LC-MS analysis

LC-MS analysis was carried out on an Agilent HPLC 1260 series system equipped with a Bruker microTOF QIII mass spectrometer by using an Agilent Eclipse XDB C18 column (5 μ m, 4.6 \times 150 mm). Separation was performed at a flow rate of 0.25 mL/min with a 40 min linear gradient from 5 to 100% ACN in H₂O, both containing 0.1% (v/v) HCOOH. The column was then washed with 100% ACN for 5 min and equilibrated for 5 min. The parameters of the spectrometer were set as the following: electrospray positive ion mode for ionization, capillary voltage with 4.5 kV, collision energy with 8.0 eV. Sodium formate was used in each run for mass calibration. The masses were scanned in the range of m/z 100 – 1500. Data were evaluated with the Compass DataAnalysis 4.2 software (Bruker Daltonik, Bremen, Germany).

14. NMR analysis

NMR spectra of the isolated products were recorded at room temperature on a JEOL ECA-500 spectrometer (JEOL, Akishima, Tokyo, Japan). The samples were dissolved in DMSO- d_6 or CDCl₃. All spectra were processed with MestReNov.9.0.0 (Mestrelab Research, Santiago de Compostella, Spain).

The ¹³C enrichments were calculated by comparison of the integrals of the ¹³C signals in the ¹³C NMR spectra of **2**. The integrals of the C-12 signal at δ_C 169.1 ppm in both labeled and unlabeled samples were chosen as reference and set as 1.0. The integrals of other signals were normalized and expressed as relative values to this signal. For a given carbon, the enrichment is the ratio of the normalized value of the labeled to unlabeled sample.

15. Physiochemical properties of the compounds described in this study

2: yellow powder; ¹H and ¹³C NMR data given in Table S5; UV spectrum in Figure S21; HRMS (ESI) m/z : [M + Na]⁺ calcd. for C₁₇H₂₀NaO₈ 375.1050; found 375.1057.

3: white powder; ¹H and ¹³C NMR data given in Table S6; UV spectrum in Figure S21; HRMS (ESI) m/z : [M + H]⁺ calcd. for C₁₀H₁₃O₄ 197.0808; found 197.0810.

4: white power; ^1H NMR data given in Table S7; UV spectrum in Figure S21; HRMS (ESI) m/z : $[\text{M} + \text{H}]^+$ calcd. for $\text{C}_9\text{H}_{11}\text{O}_4$ 183.0652; found 183.0652.

5: white power; ^1H NMR data given in Table S7; UV spectrum in Figure S21; HRMS (ESI) m/z : $[\text{M} + \text{H}]^+$ calcd. for $\text{C}_9\text{H}_{11}\text{O}_4$ 183.0652; found 183.0656.

6: white power; ^1H NMR data given in Table S7; UV spectrum in Figure S21; HRMS (ESI) m/z : $[\text{M} + \text{H}]^+$ calcd. for $\text{C}_{10}\text{H}_{13}\text{O}_3$ 181.0859; found 181.0862.

7: yellow power; ^1H and ^{13}C NMR data given in Table S8; UV spectrum in Figure S21; HRMS (ESI) m/z : $[\text{M} + \text{H}]^+$ calcd. for $\text{C}_{19}\text{H}_{23}\text{O}_5$ 331.1540; found 331.1544.

8: yellow power; ^1H and ^{13}C NMR data given in Table S9; UV spectrum in Figure S21; HRMS (ESI) m/z : $[\text{M} + \text{Na}]^+$ calcd. for $\text{C}_{11}\text{H}_{14}\text{NaO}_4$ 233.0784; found 233.0784.

10: yellow oil; ^1H and ^{13}C NMR data given in Table S10; UV spectrum in Figure S21; HRMS (ESI) m/z : $[\text{M} + \text{Na}]^+$ calcd. for $\text{C}_{14}\text{H}_{16}\text{NaO}_6$ 303.0839; found 303.0845.

16. Structural elucidation

The structures of the isolated products were elucidated by comprehensive interpretation of their MS and NMR data (Figures S21 – S45). By comparison with the literature data, **4**,⁷ **5**⁸ and **6**⁹ were identified as known compounds.

The molecular formula of **2** was deduced from its HRMS as $\text{C}_{17}\text{H}_{20}\text{O}_8$. **2** was obtained as a triacetylated derivative of **1** after acetylation of the crude extract from the wild type, which was confirmed by detection of the difference of their $[\text{M} + \text{Na}]^+$ ions and by the presence of the corresponding signals for three acetyl groups in the NMR spectra of **2** (δ_{C} 169.1 ppm, C-12, δ_{H} 2.32 and δ_{C} 20.4 ppm, CH_3 -13; δ_{C} 170.1 ppm, C-14, δ_{H} 1.96 and δ_{C} 20.6 ppm, CH_3 -15; δ_{C} 170.0 ppm, C-16, δ_{H} 1.96 and δ_{C} 20.4 ppm, CH_3 -17, Table S5). The ^1H NMR data of **2** suggested also the presence of an aldehyde group (δ_{H} 10.10 ppm), a five-substituted benzene ring (δ_{H} 7.05 ppm), an aromatic methoxy group (δ_{H} 3.94 ppm), and three methylene groups (δ_{H} 5.02, 3.33 and 4.22 ppm). This was also proven by interpretation of its ^{13}C NMR data. HMBC correlations revealed that two of the methylene groups are connected to each other (Table S5 and Figure S25). Elucidation of the structure of **2** proved **1** to be 2-hydroxy-6-(2-hydroxyethyl)-3-(hydroxymethyl)-4-methoxybenzaldehyde.

The molecular formula of **3** was deduced from its HRMS data to be $\text{C}_{10}\text{H}_{12}\text{O}_4$. Interpretation of its NMR spectra including ^1H , ^{13}C , HSQC, and HMBC (Table S6 and Figures S26 – S29) revealed its structure to be 6-ethyl-2,4-dihydroxy-3-methylbenzoic acid.

SUPPORTING INFORMATION

The molecular formula of **8** was deduced from the HRMS data to be $C_{11}H_{14}O_4$ with five degrees of unsaturation. Comparison of its NMR data with those of **2** revealed the presence of signals for two instead of three methylene groups. One of them couples with a methyl group, *i.e.* as an ethyl group as observed in **3** and **5**. The signals of an aromatic methoxy group are still detectable (δ_H 3.93 and δ_C 56.1 ppm). This proved the structure of **8** to be 6-ethyl-2-hydroxy-3-(hydroxymethyl)-4-methoxybenzaldehyde.

9 was unstable and its structure was elucidated after acetylation. The molecular formula of the diacetylated derivative **10** was deduced from the HRMS data to be $C_{14}H_{16}O_6$, one oxygen more than that of **6**. The existence of OH at C-2 was verified by the signal at δ_H 12.62 ppm. Comparison of the 1H NMR spectrum of **10** with that of **6** indicated the hydroxylation of the methyl group at C-3. Differing from those in **2** and **8**, no signal for an aromatic methoxy group was detected in the spectra of **6** and **10**. This proved **9** as the hydroxylation product of C3-methyl group in **6**.

SUPPORTING INFORMATION

Table S1. Putative functions of the genes from the *ustethylin* (*utt*) gene cluster

Protein	No.	Size (aa)	cover/identity, homologous protein, organism	Putative function			
UttA	KIA75596	2318	99/46, polyketide synthase PkbA, AN6448.4, <i>Aspergillus nidulans</i> FGSC A4	Ustethylinic acid synthase			
UttB	KIA75595	486	95/43, oxidoreductase Azal, G3XMD0.2, <i>Aspergillus niger</i> ATCC 1015	FAD-dependent oxidase			
UttC	KIA75594	506	93/48, cytochrome P ₄₅₀ Cich, AN6449.2, <i>Aspergillus nidulans</i> FGSC A4	P ₄₅₀ , ethyl hydroxylase			
UttD	KIA75593	490	100/55, myb-related protein B, KFX41786.1, <i>Talaromyces marneffei</i> PM1	DNA-binding protein, positive regulator			
UttE	KIA75592	503	95/33, bifunctional solanapyrone synthase Sol5, CEL54807.1, <i>Rhizoctonia solani</i> AG-1 IB	FAD-dependent oxidase			
UttF	KIA75591	417	100/83, O-methyltransferase FimD, KFX41536.1, <i>Talaromyces marneffei</i> PM1	O-methyltransferase			
UttG	KIA75590	532	95/49, MFS drug efflux transporter, PLN86962.1, <i>Aspergillus taichungensis</i>	MFS transporter			
UttH	KIA75589	344	92/58, 2-oxoglutarate-dependent dioxygenase CitB, A0A159BP93.1, <i>Monascus ruber</i> 92/52, clavariol oxidase Clad, QBK15042.1, <i>Penicillium crustosum</i>	Phenylmethyl oxidase			
UttI	KIA75588	340	100/82, putative oxidoreductase, CEN59745.1, <i>Aspergillus calidoustus</i>	Oxidoreductase			
UttJ	KIA75587	1120	97/42, NRPS-like CidB, AN6444.4, <i>Aspergillus nidulans</i> FGSC A4	aryl acid reductase			

SUPPORTING INFORMATION

Table S2. Strains used in this study

Stains	Genotype
Wild type	<i>A. ustus</i> 3.3904
$\Delta uttA$	$\Delta uttA::hph$ in <i>A. ustus</i> 3.3904
$\Delta uttB$	$\Delta uttB::hph$ in <i>A. ustus</i> 3.3904
$\Delta uttC$	$\Delta uttC::hph$ in <i>A. ustus</i> 3.3904
$\Delta uttD$	$\Delta uttD::hph$ in <i>A. ustus</i> 3.3904
$\Delta uttE$	$\Delta uttE::hph$ in <i>A. ustus</i> 3.3904
$\Delta uttF$	$\Delta uttF::hph$ in <i>A. ustus</i> 3.3904
$\Delta uttG$	$\Delta uttG::hph$ in <i>A. ustus</i> 3.3904
$\Delta uttH$	$\Delta uttH::hph$ in <i>A. ustus</i> 3.3904
$\Delta uttJ$	$\Delta uttJ::hph$ in <i>A. ustus</i> 3.3904
<i>A. nidulans</i> LO8030	<i>pyrA4</i> , <i>riboB2</i> , <i>pyrG89</i> , <i>nkuA::argB</i> sterigmatocystin cluster (<i>AN7804-AN7825</i>) Δ , emerellamide cluster (<i>AN2545-AN2549</i>) Δ , asperfuranone cluster (<i>AN1039-AN1029</i>) Δ , monodictyphenone cluster (<i>AN10023-AN10021</i>) Δ , terrequinone cluster (<i>AN8512-AN8520</i>) Δ , austinol cluster part 1 (<i>AN8379-AN8384</i>) Δ , austinol cluster part 2 (<i>AN9246-AN9259</i>) Δ , F9775 cluster (<i>AN7906-AN7915</i>) Δ , asperthecin cluster (<i>AN6000-AN6002</i>) Δ
LZ51	<i>gpdA::uttA::AfpYrG</i> in <i>A. nidulans</i> LO8030
LZ52	<i>gpdA:: uttJ::AfpYrG</i> in <i>A. nidulans</i> LO8030
LZ53	<i>gpdA:: uttA_G1778V::AfpYrG</i> in <i>A. nidulans</i> LO8030
LZ54	<i>gpdA:: uttA_H1850A::AfpYrG</i> in <i>A. nidulans</i> LO8030

SUPPORTING INFORMATION

Table S3. Plasmids used and constructed in this study

Plasmids	Description
p5HY	Two-third of the <i>hph</i> resistance gene at the 5'-end, originated from the pUChph and inserted into pESC-URA. For gene replacement using <i>hph</i> as selection marker.
p3YG	Two-third of the <i>hph</i> resistance gene at the 3'-end, originated from the pUChph and inserted into pESC-URA. For gene replacement using <i>hph</i> as selection marker.
pLZ101(p5HY- <i>uttA</i>)	a 1171 bp US PCR fragment of <i>uttA</i> from genomic DNA of <i>A. ustus</i> 3.3904 inserted in p5HY.
pLZ102(p3YG- <i>uttA</i>)	a 1170 bp DS PCR fragment of <i>uttA</i> from genomic DNA of <i>A. ustus</i> 3.3904 inserted in p3YG.
pLZ103(p5HY- <i>uttB</i>)	a 1535 bp US PCR fragment of <i>uttB</i> from genomic DNA of <i>A. ustus</i> 3.3904 inserted in p5HY.
pLZ104(p3YG- <i>uttB</i>)	a 1486 bp DS PCR fragment of <i>uttB</i> from genomic DNA of <i>A. ustus</i> 3.3904 inserted in p3YG.
pLZ105(p5HY- <i>uttC</i>)	a 1476 bp US PCR fragment of <i>uttC</i> from genomic DNA of <i>A. ustus</i> 3.3904 inserted in p5HY.
pLZ106(p3YG- <i>uttC</i>)	a 1463 bp DS PCR fragment of <i>uttC</i> from genomic DNA of <i>A. ustus</i> 3.3904 inserted in p3YG.
pLZ107(p5HY- <i>uttD</i>)	a 1477 bp US PCR fragment of <i>uttD</i> from genomic DNA of <i>A. ustus</i> 3.3904 inserted in p5HY.
pLZ108(p3YG- <i>uttD</i>)	a 1492 bp DS PCR fragment of <i>uttD</i> from genomic DNA of <i>A. ustus</i> 3.3904 inserted in p3YG.
pLZ109(p5HY- <i>uttE</i>)	a 1527 bp US PCR fragment of <i>uttE</i> from genomic DNA of <i>A. ustus</i> 3.3904 inserted in p5HY.
pLZ110(p3YG- <i>uttE</i>)	a 1410 bp DS PCR fragment of <i>uttE</i> from genomic DNA of <i>A. ustus</i> 3.3904 inserted in p3YG.
pLZ111(p5HY- <i>uttF</i>)	a 1580 bp US PCR fragment of <i>uttF</i> from genomic DNA of <i>A. ustus</i> 3.3904 inserted in p5HY.
pLZ112(p3YG- <i>uttF</i>)	a 1523 bp DS PCR fragment of <i>uttF</i> from genomic DNA of <i>A. ustus</i> 3.3904 inserted in p3YG.
pLZ113(p5HY- <i>uttG</i>)	a 1480 bp US PCR fragment of <i>uttG</i> from genomic DNA of <i>A. ustus</i> 3.3904 inserted in p5HY.
pLZ114(p3YG- <i>uttG</i>)	a 1449 bp DS PCR fragment of <i>uttG</i> from genomic DNA of <i>A. ustus</i> 3.3904 inserted in p3YG.
pLZ115(p5HY- <i>uttH</i>)	a 1479 bp US PCR fragment of <i>uttH</i> from genomic DNA of <i>A. ustus</i> 3.3904 inserted in p5HY.
pLZ116(p3YG- <i>uttH</i>)	a 1426 bp DS PCR fragment of <i>uttH</i> from genomic DNA of <i>A. ustus</i> 3.3904 inserted in p3YG.
pLZ117(p5HY- <i>uttJ</i>)	a 1416 bp US PCR fragment of <i>uttJ</i> from genomic DNA of <i>A. ustus</i> 3.3904 inserted in p5HY.
pLZ118(p3YG- <i>uttJ</i>)	a 1505 bp DS PCR fragment of <i>uttJ</i> from genomic DNA of <i>A. ustus</i> 3.3904 inserted in p3YG.
pYH-gpdA-pyrG	<i>URA3</i> , <i>wa</i> flanking, <i>gpdA</i> , <i>Afp</i> yrG, <i>Amp</i>
pLZ51	<i>pYH-gpdA-uttA-pyrG</i> ; a 7836 bp fragment of <i>uttA</i> with its terminator from genomic DNA of <i>A. ustus</i> 3.3904 inserted in <i>pYH-gpdA-pyrG</i>
pLZ52	<i>pYH-gpdA-uttJ-dMeT-pyrG</i> ; a 177 bp fragment of <i>uttA</i> was removed in <i>pYH-gpdA-pyrG</i> .
pLZ53	<i>pYH-gpdA-uttA_G1778V-pyrG</i> ; mutation at Gly1778 to Val in pLZ51.
pLZ54	<i>pYH-gpdA-uttA_H1850A-pyrG</i> ; mutation at His1778 to Ala in pLZ51.

US: upstream; DS: downstream

Table S4. Primers used in this study

Primers	Sequence 5'-3'	Targeted amplification
P5HY	CAAGACCAATGCGGAGCATATAC	2/3 of the <i>hph</i> resistance gene at the 5'-end from pUChph to construct p5HY
P3YG	GAATTGATTCCGGAAGTGCTTGAC	
p5HY-R	GCTGAAGTCGATTGGATCCAC	2/3 of the <i>hph</i> resistance gene at the 3'-end from pUChph to construct p3YG
p3YG-F	GCATTAAATGCATTGGACCTCGC	US of <i>hph</i> to verify 5F of <i>A. ustus</i> 3.3904 mutant
utIA-U-F	AAGAAATTGTTAATTAAAGAGCTCAGATCAAGAAGTGGGATCCGAAGGG	DS of <i>hph</i> to verify 3F of <i>A. ustus</i> 3.3904 mutant
utIA-U-R	ACCCTCACTAAAGGGCGCGCCGACCTAGGTTGAAGCGTGCAGGAAAAG	1171bp US fragment of <i>utIA</i> to construct pLZ101
utIA-D-F	ACTCACTATAGGGCCCGGGCGTCGAGATGGATGGATGAGCTGGAT	1170 bp DS fragment of <i>utIA</i> to construct pLZ102
utIA-D-R	TAGCCGCGGTACCAAGCTTACTCGACTATATCTGCGTACTGGTGCG	
utIA-F	CTTGAATCCTTCGGGAGCAAC	1594 bp partial fragment of <i>utIA</i>
utIA-R	GTTGAACACCTTGACACGAGC	
utIA-5F-F	CCCCTGCAATTTTGATCGAC	US of <i>hph</i> to verify Δ <i>utIA</i> mutant
utIA-3F-R	CTTGAATCCTTCGGGAGCAAC	DS of <i>hph</i> to verify Δ <i>utIA</i> mutant
utIB-U-F	AAGAAATTGTTAATTAAAGAGCTCAGATCAACGTAACAGCAGGAAAGCGA	1535 bp US fragment of <i>utIB</i> to construct pLZ103
utIB-U-R	ACCCTCACTAAAGGGCGCGCCGACCTAGTCCACCGAACCAGGAAAAGA	
utIB-D-F	ACTCACTATAGGGCCCGGGCGTCGAGTACTTCGCAATGAGGGGA	1486 bp DS fragment of <i>utIB</i> to construct pLZ104
utIB-D-R	TAGCCGCGGTACCAAGCTTACTCGAACGACACAAACACCGACATAG	
utIB-F	GCAAGCTTGTGACGAGAGCTCGAATTCCTAAACAACCGGCAACCCATT	1754 bp partial fragment of <i>utIB</i>
utIB-R	GGACAGCAAAATGGGTGCGCGGATCCATGTTTCGTTCTTCGATTACACAC	
utIB-5F-F	CAACGAAAAGACTCGAAGAGCTG	US of <i>hph</i> to verify Δ <i>utIB</i> mutant
utIB-3F-R	GCTAGAATTGCAATTGCAGGCTG	DS of <i>hph</i> to verify Δ <i>utIB</i> mutant
utIC-U-F	AAGAAATTGTTAATTAAAGAGCTCAGATCAGCTAGCTAGCTAGCAAGGT	1476 bp US fragment of <i>utIC</i> to construct pLZ105
utIC-U-R	ACCCTCACTAAAGGGCGCGCCGACCTAGTCGGTGGTTCTTCGTTTCG	

Table S4. (continued)

utIC-D-F	ACTCACTATAGGGCCCCGGCGTCGAATTTGCACCCCATCCAGCTAG	1463 bp DS fragment of <i>utIC</i> to construct pLZ106
utIC-D-R	TAGCCCGCGGTACCAAGCTTACTCGATGGAGACGGTGATCAGGTTT	
utIC-F	TCTACACAAAGCATCGCACTGAC	1555 bp partial fragment of <i>utIC</i>
utIC-R	AGTAAGAAAGTGCCCTCCCCA	
utIC-5F-F	TATCTGCTGAAACGGCTCCT	US of <i>hph</i> to verify Δ <i>utIC</i> mutant
utIC-3F-R	CATTGAACGAAGCCAGCGTC	DS of <i>hph</i> to verify Δ <i>utIC</i> mutant
utID-U-F	AAGAAATTGTTAATTAAAGAGCTCAGATCAGCGGATCGTATCGAGAAAG	1477 bp US fragment of <i>utID</i> to construct pLZ107
utID-U-R	ACCCTCACTAAAGGGCGGCCGACACTAGTGAAGAAATGTTGCGGGGAT	
utID-D-F	ACTCAGTAAGGGCCCCGGCGTCGATACCTTCAAGGGTATCTGGCG	1456 bp DS fragment of <i>utID</i> to construct pLZ108
utID-D-R	TAGCCGCGGTACCAAGCTTACTCGAGAACAGGGCAGTGAATCTTC	
utID-F	CATCAATGGGCGTATTCACG	
utID-R	CGGTGATCAAGCTGGATAGT	1492 bp partial fragment of <i>utID</i>
utID-5F-F	CACACCACTGCACAAGTACTAG	US of <i>hph</i> to verify Δ <i>utID</i> mutant
utID-3F-R	GTCGATGATGTCTCACCCAT	DS of <i>hph</i> to verify Δ <i>utID</i> mutant
utIE-U-F	AAGAAATTGTTAATTAAAGAGCTCAGATCTGCTTGGGCCACTAGATACAG	1527 bp US fragment of <i>utIE</i> to construct pLZ109
utIE-U-R	ACCCTCACTAAAGGGCGGCCGACACTAGAGATACCTCACCATCTTGCCC	
utIE-D-F	ACTCAGTAAGGGCCCCGGCGTCGAGAGACACAAGGAGCACATGTTTG	1410 bp DS fragment of <i>utIE</i> to construct pLZ110
utIE-D-R	TAGCCGCGGTACCAAGCTTACTCGACACACCAATCTCCACTTCGG	
utIE-F	CCGCAAGCTTGTGACGAGAGCTCGAATTTCTACCGCCGAGGAGGACTTTT	1909 bp partial fragment of <i>utIE</i>
utIE-R	GGTGACAGCAAAATGGGTCGCGGATCCATGCCGCCAACAACTGCTTCAA	US of <i>hph</i> to verify Δ <i>utIE</i> mutant
utIE-5F-F	TCGGACTGGAAGTCGCTCTTT	
utIE-3F-R	GAAGAATGACGGCTACAAACAGC	DS of <i>hph</i> to verify Δ <i>utIE</i> mutant

Table S4. (continued)

utIF-U-F	MAGAAATTGTTAATTAAAGAGCTCAGATCTGCTTGGGCCACTAGATACAG	1580 bp US fragment of <i>utIF</i> to construct pLZ111
utIF-U-R	ACCCCTACTAAAGGGCGCCGCGCACTAGAGATACCTCACCATCTTGCCC	
utIF-D-F	ACTCACTATAGGGCCCCGGCGTCGAGGACACAAGGAGCAGCATGTTG	1523 bp DS fragment of <i>utIF</i> to construct pLZ112
utIF-D-R	TAGCCCGCGGTACCAAGCTTACTCGACACACCATCTCCACTTCCG	
utIF-F	TTGCTGATCGCAGTCTTGACTG	1223 bp partial fragment of <i>utIF</i>
utIF-R	TGGACTTTAATTGTGCGGGGTG	
utIF-5F-F	TCGGACTGGAAGTCGCTCTTT	US of <i>hph</i> to verify Δ <i>utIF</i> mutant
utIF-3F-R	GAAGAATGACGGGTACAACAGC	DS of <i>hph</i> to verify Δ <i>utIF</i> mutant
utIG-U-F	MAGAAATTGTTAATTAAAGAGCTCAGATCTCCACAGTGGACATATCCG	1480 bp US fragment of <i>utIG</i> to construct pLZ113
utIG-U-R	ACCCCTACTAAAGGGCGCCGCGCACTAGCCCTAACACGTAACAACCTCGC	
utIG-D-F	ACTCACTATAGGGCCCCGGCGTCGAGGGGGAAGGAATGGGTTA	1449 bp DS fragment of <i>utIG</i> to construct pLZ114
utIG-D-R	TAGCCCGCGGTACCAAGCTTACTCGAGATCTGCGGGTAGAACGAGT	
utIG-F	TGCTGGCCATCCTCACTTCAA	1451 bp partial fragment of <i>utIG</i>
utIG-R	CAGACTATCCGCAATCGTGCT	
utIG-5F-F	GCCTGACTTCAAGAGTGAGACT	US of <i>hph</i> to verify Δ <i>utIG</i> mutant
utIG-3F-R	TGCGCCGTGAAGAAGTCATG	DS of <i>hph</i> to verify Δ <i>utIG</i> mutant
utIH-U-F	MAGAAATTGTTAATTAAAGAGCTCAGATCCATACCAACCATCAGCAGAAACC	1479 bp US fragment of <i>utIH</i> to construct pLZ115
utIH-U-R	ACCCCTACTAAAGGGCGCCGCGCACTAGGATGAAGGTGGTGATGATCGTG	
utIH-D-F	ACTCACTATAGGGCCCCGGCGTCGATTGGTTAACCGGATGCGGTTG	1426 bp DS fragment of <i>utIH</i> to construct pLZ116
utIH-D-R	TAGCCCGCGGTACCAAGCTTACTCGAAGAGCGGATTGTTAGTACGCC	
utIH-F	GCAAAAACCGCACCGACTCAA	
utIH-R	ATAACTCTCCGCAACCCCTCC	975 bp partial fragment of <i>utIH</i>

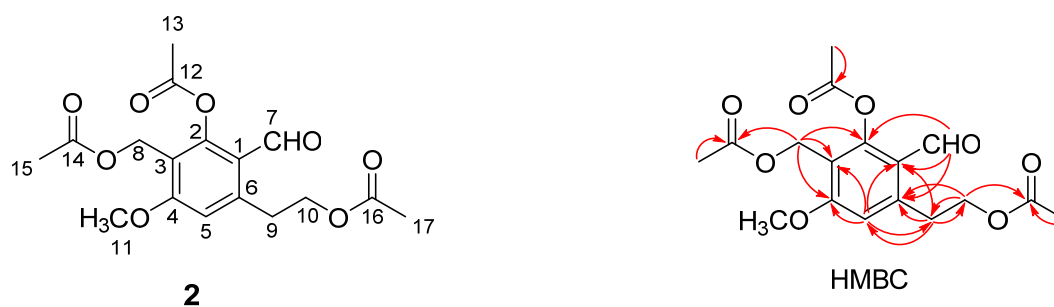
Table S4. (continued)

utH-5F-F	ATGTCACGACCACTCGCTTGA	US of <i>hph</i> to verify Δ <i>utH</i> mutant
utH-3F-R	CGATTGTGACGACGAGAAACAC	DS of <i>hph</i> to verify Δ <i>utH</i> mutant
utJ-U-F	AAGAATTGTTAATTAAAGAGCTCAGATCGTCTTCGCTGTAAGTCCACAG	1416 bp US fragment of <i>utJ</i> to construct pLZ119
utJ-U-R	ACCCTCACTAAAGGGCGGCCGACACTAGTCGGGTAAAGACACTAGATGG	
utJ-D-F	ACTCACATAAGGGCCCCGGGCGTCGAATGGAGTTCCAGGGGTCTCTCT	1505 bp DS fragment of <i>utJ</i> to construct pLZ120
utJ-D-R	TAGCCGGCGGTACCAAGCTTACTCGAGCCTCATCTTCACATCATCCA	
utJ-F	ACGAATATCCGGAAGATACCCC	1529 bp partial fragment of <i>utJ</i>
utJ-R	ACGATCTGATCCGCTAGCGA	US of <i>hph</i> to verify Δ <i>utJ</i> mutant
utJ-5F-F	CGCGATCCTCGACTTTTCTAGG	DS of <i>hph</i> to verify Δ <i>utJ</i> mutant
utJ-3F-R	AGCACTGCTGTTCAAGGCATAC	4014 bp partial fragment of <i>utA</i> from <i>A. ustus</i> 3,3904 to construct pLZ51
HE-utA-P1-F	TCATCTTCCCATCCAAGAACCCTTAATCATGTTGTCGTAAGGGTATCCA	4095 bp partial fragment of <i>utA</i> with its 624 bp terminator from <i>A. ustus</i> 3,3904 to construct pLZ51
HE-utA-P1-R	CGAGAGTCTTTTTCGATCCCT	4229 bp of <i>utJ</i> with its 651 bp terminator from <i>A. ustus</i> 3,3904 to construct pLZ52
HE-utA-P2-F	GTTTAGTCGGGTGCTCATCTCC	
HE-utA-P2-R	CGTCAGACACAGAATACTCTCGCTAGGCTTCTTCCCGCTTCTGAAGT	Containing a mutation for G1778 to Val to construct pLZ53
HE-utJ-F	CTTCCCATCCAAAGAACCTTTAATCATGTGCGTGATTAATGATCTGAAG	Containing a mutation for H1850 to Ala to construct pLZ54
HE-utJ-R	CATATTTGTCAGACACAGAATACTCTCAGCAACTGAGCCCTCAAAA	1203 bp of <i>utA</i> fragment including the mutated points to construct pLZ53 and pLZ54
UtA-G1778V-F	GGGACAGTCTCGACGACGAATGGGTTGTCGATGCGCT	
UtA-G1778V-R	CGTCGTCGAGACTGTCCCGCGCCGAGTTCAGGGATGC	
UtA-H1850A-F	TGCATC GG CGCCACGACGAATCTGCCCAACTCGCTCAC	
UtA-H1850A-R	GCTCGTGGCG GG CGATGCAGTTGGTCGAGAGGATGGTAT	
UtA-mutA-F	TCTGGAAGAACGTGTACCCAC	
UtA-mutA-R	TTGGTGAGGATATCCCGCTG	

US: upstream; DS: downstream

SUPPORTING INFORMATION

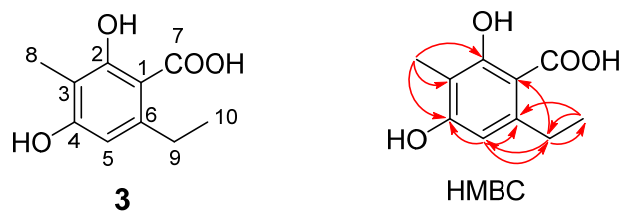
Table S5. NMR data of compound **2** in DMSO-*d*₆ (500 MHz, δ in ppm, *J* in Hz)



Position	δ_C	δ_H (multi. <i>J</i>)	HMBC
1	119.8 (C)	—	—
2	152.5 (C)	—	—
3	116.0 (C)	—	—
4	162.1 (C)	—	—
5	112.1 (CH)	7.05 (s)	C-1, C-3, C-4, C-9
6	144.9 (C)	—	—
7	189.0 (CH)	10.10 (s)	C-1, C-2, C-6
8	54.1 (CH ₂)	5.02 (s)	C-2, C-3, C-4, C-14
9	31.5 (CH ₂)	3.33 (t, <i>J</i> = 6.6 Hz)	C-1, C-5, C-6, C-10
10	63.9 (CH ₂)	4.22 (t, <i>J</i> = 6.6 Hz)	C-1, C-9, C-16
11	56.6 (OCH ₃)	3.94 (s)	C-4
12	169.1 (C)	—	—
13	20.4 (CH ₃)	2.32 (s)	C-12
14	170.1 (C)	—	—
15	20.6 (CH ₃)	1.96 (s)	C-14
16	170.0 (C)	—	—
17	20.4 (CH ₃)	1.96 (s)	C-16

SUPPORTING INFORMATION

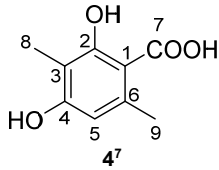
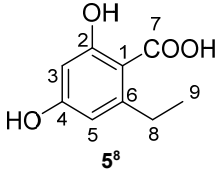
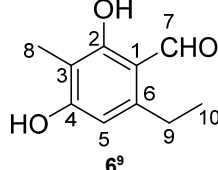
Table S6. NMR data of compound **3** in DMSO-*d*₆ (500 MHz, δ in ppm, *J* in Hz)



Position	δ_c	δ_H (multi. <i>J</i>)	HMBC
1	103.0 (C)	—	—
2	162.1 (C)	—	—
3	108.0 (C)	—	—
4	160.1 (C)	—	—
5	108.9 (CH)	6.28 (s)	C-1, C-4, C-6, C-9
6	145.8 (C)	—	—
7	173.8 (COOH)	9.97 (s)	—
8	8.0 (CH ₃)	1.93 (s)	C-2, C-3, C-4
9	28.8 (CH ₂)	2.81 (q, <i>J</i> = 7.4 Hz)	C-5, C-6, C-10
10	16.1 (CH ₃)	1.10 (t, <i>J</i> = 7.4 Hz)	C-6, C-9
4-OH	—	13.33 (s)	—
2-OH	—	12.65 (s)	—

SUPPORTING INFORMATION

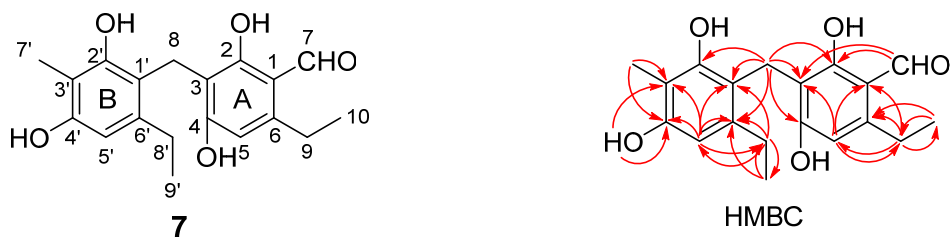
Table S7. ^1H NMR data of compounds **4** – **6** in $\text{DMSO}-d_6$ (500 MHz, δ in ppm, J in Hz)

Compounds			
Position	δ_{H} (multi., J)	δ_{H} (multi., J)	δ_{H} (multi., J)
3	—	6.13 (d, $J = 2.4$ Hz)	—
5	6.25 (s)	6.18 (d, $J = 2.4$ Hz)	6.33 (s)
7	—	—	10.63 (s)
8	1.93 (s)	2.78 (q, $J = 7.4$ Hz)	1.92 (s)
9	2.39 (s)	1.11 (t, $J = 7.4$ Hz)	2.83 (q, $J = 7.5$ Hz)
10	—	—	1.17 (t, $J = 7.5$ Hz)
2-OH	12.94 (s)	12.42 (s)	12.77 (s)
4-OH	12.94 (s)	12.42 (s)	10.02 (s)
7-OH	9.99 (s)	10.02 (s)	—

The NMR data of **3**, **4** and **5** correspond very well to those reported previously.⁷⁻⁹

SUPPORTING INFORMATION

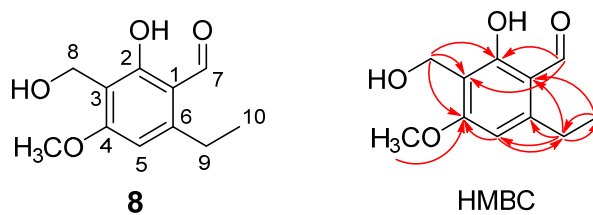
Table S8. NMR data of compound **7** in DMSO-*d*₆ (500 MHz, δ in ppm, *J* in Hz)



Position	δ_C	δ_H (multi., <i>J</i>)	HMBC
1	111.5 (C)	—	—
2	163.8 (C)	—	—
3	112.7 (C)	—	—
4	154.3 (C)	—	—
5	109.4 (CH)	6.28 (s)	C-1, C-3, C-9
6	148.8 (C)	—	—
7	194.1 (CH)	10.00 (s)	C-2, C-3
8	18.9 (CH ₂)	3.71 (s)	C-2, C-3, C-4, C-1', C-2', C-6'
9	24.3 (CH ₂)	2.82 (q, <i>J</i> = 7.5 Hz)	C-5, C-6, C-10
10	17.0 (CH ₃)	1.15 (t, <i>J</i> = 7.5 Hz)	C-6, C-9
1'	115.6 (C)	—	—
2'	163.8 (C)	—	—
3'	108.7 (C)	—	—
4'	154.4 (C)	—	—
5'	107.5 (CH)	6.16 (s)	C-1', C-3', C-4', C-8'
6'	141.2 (C)	—	—
7'	9.6 (CH ₃)	1.92 (s)	C-3', C-4'
8'	25.9 (CH ₂)	2.63 (q, <i>J</i> = 7.5 Hz)	C-1', C-5', C-6', C-9'
9'	16.1 (CH ₃)	0.98 (t, <i>J</i> = 7.5 Hz)	C-6', C-8'
4'-OH	—	8.72 (s)	C-3', C-4'
2-OH	—	13.15 (s)	—

SUPPORTING INFORMATION

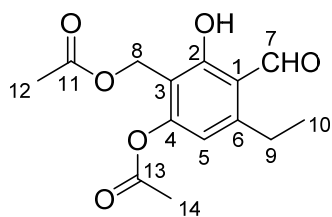
Table S9. NMR data of compound **8** in CDCl₃ (500 MHz, δ in ppm, *J* in Hz)



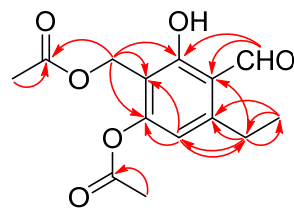
Position	δ_C	δ_H (multi., <i>J</i>)	HMBC
1	151.2 (C)	—	—
2	163.5 (C)	—	—
3	114.2 (C)	—	—
4	164.3 (C)	—	—
5	104.0 (CH)	6.34 (s)	C-3, C-4, C-6, C-9
6	112.7 (C)	—	—
7	193.3 (CH)	10.14 (s)	C-2, C-3
8	53.9 (CH ₂)	4.76 (s)	C-2, C-3, C-4
9	25.7 (CH ₂)	2.93 (q, <i>J</i> = 7.6 Hz)	C-5, C-6, C-10
10	17.3 (CH ₃)	1.31 (t, <i>J</i> = 7.6 Hz)	C-1, C-9
4-OCH ₃	56.1 (OCH ₃)	3.93 (s)	C-4
2-OH	—	12.62 (s)	—

SUPPORTING INFORMATION

Table S10. NMR data of compound **10** in DMSO-*d*₆ (500 MHz, δ in ppm, *J* in Hz)



10

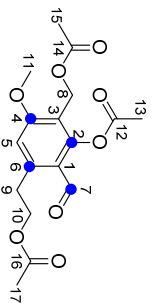
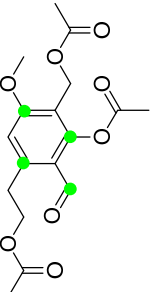
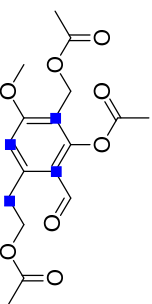
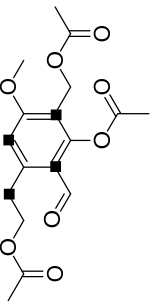
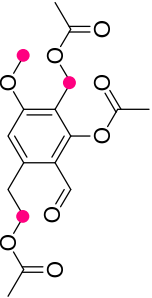


HMBC

Position	δ_C	δ_H (multi., <i>J</i>)	HMBC
1	114.3 (C)		
2	162.6 (C)		
3	115.6 (C)		
4	155.9 (C)		
5	115.0 (CH)	6.72 (s)	C-4, C-6, C-9
6	150.9 (C)		
7	196.1 (CH)	10.28 (s)	C-1, C-2
8	53.9 (CH ₂)	5.02 (s)	C-2, C-3, C-4, C-12
9	24.0 (CH ₂)	2.99 (q, <i>J</i> = 7.6 Hz)	C-5, C-6, C-1, C-10
10	16.2 (CH ₂)	1.21 (t, <i>J</i> = 7.6 Hz)	C-6, C-9
11	170.0 (C)		
12	20.4 (CH ₃)	1.96 (s)	C-11
13	168.4 (C)		
14	20.6 (CH ₃)	2.29 (s)	C-13
2-OH		12.58 (brs)	

SUPPORTING INFORMATION

Table S11. Enrichments in **2** after feeding with ^{13}C labeled precursors

		<div>sodium [1-¹³C] acetate</div> <div></div>	<div>sodium [2-¹³C] propionate</div> <div></div>	<div>sodium [2-¹³C] acetate</div> <div></div>	<div>[2-¹³C] malonic acid</div> <div></div>	<div>[methyl-¹³C]-L-methionine</div> <div></div>
Position	δ _c					
1	119.8 (C)	1.0	0.8	4.9	6.7	1.0
2	152.5 (C)	4.5	3.7	1.1	1.2	1.1
3	116.0 (C)	0.9	1.3	5.8	7.4	0.9
4	162.1 (C)	3.8	3.6	1.2	1.0	1.1
5	112.1 (CH)	1.0	1.4	7.9	8.5	1.2
6	144.9 (C)	4.4	4.0	1.1	1.2	1.2
7	189.0 (CH)	6.1	6.1	1.3	1.3	1.2
8	54.1 (CH ₂)	0.9	1.0	0.9	1.0	13.1
9	31.5 (CH ₂)	0.9	1.2	6.6	8.9	0.8
10	63.9 (CH ₂)	0.9	1.0	1.0	1.1	15.0
11	56.6 (OCH ₃)	0.8	0.8	1.1	1.0	15.9
12	169.1 (C)	1.0	1.0	1.0	1.0	1.0
13	20.4 (CH ₃)	0.9	1.1	1.1	1.0	1.1
14	170.1 (C)	0.9	0.8	0.9	1.0	1.0
15	20.6 (CH ₃)	0.9	1.0	1.0	1.0	1.0
16	170.0 (C)	1.0	0.9	1.0	1.0	1.0
17	20.4 (CH ₃)	0.9	1.1	1.1	1.2	1.2

SUPPORTING INFORMATION

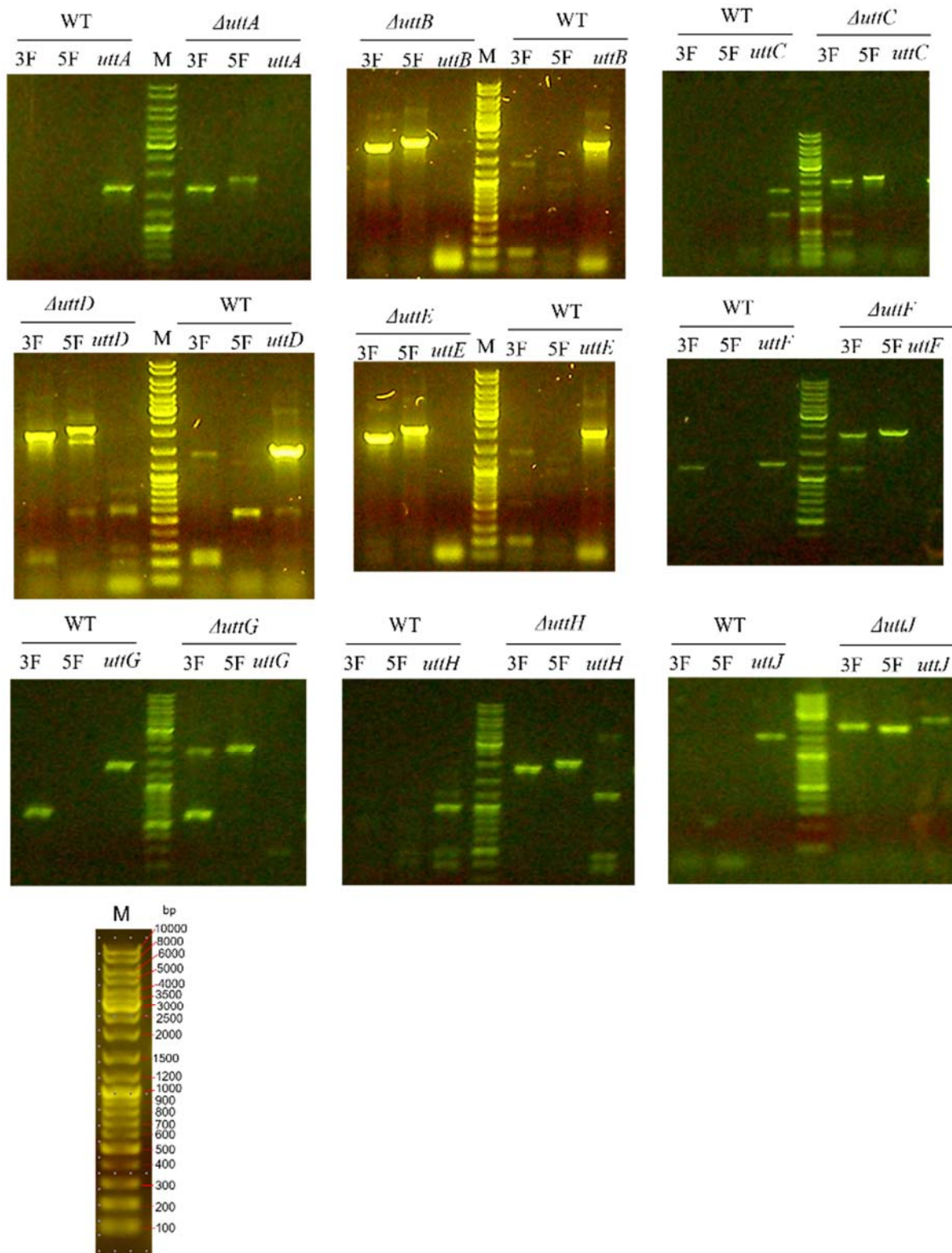


Figure S1. PCR verification of deletion mutants of *A. ustus* 3.3904.

PCR amplification for three different fragments from genomic DNA of WT and deletion mutants was used to prove the presence/absence of the target gene and the integration site of the selection marker with up- and downstream regions. The PCR primers are given in Table S4.

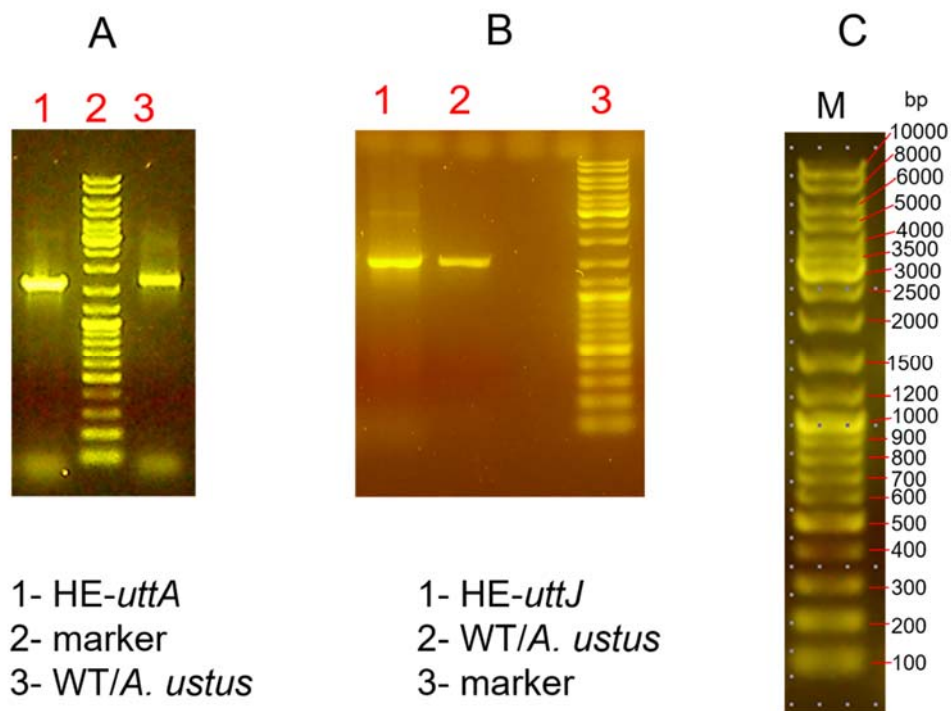


Figure S2. PCR verification of heterologous expression transformants.

A. nidulans-pYH-*gpdA-uttA-pyrG* (HE-*uttA*) (A), *A. nidulans*-pYH-*gpdA-uttJ-pyrG* (HE-*uttJ*) (B), and marker reference (C). A fragment of 1.5 kb within the target gene was amplified from the primers listed in Table S4.

SUPPORTING INFORMATION

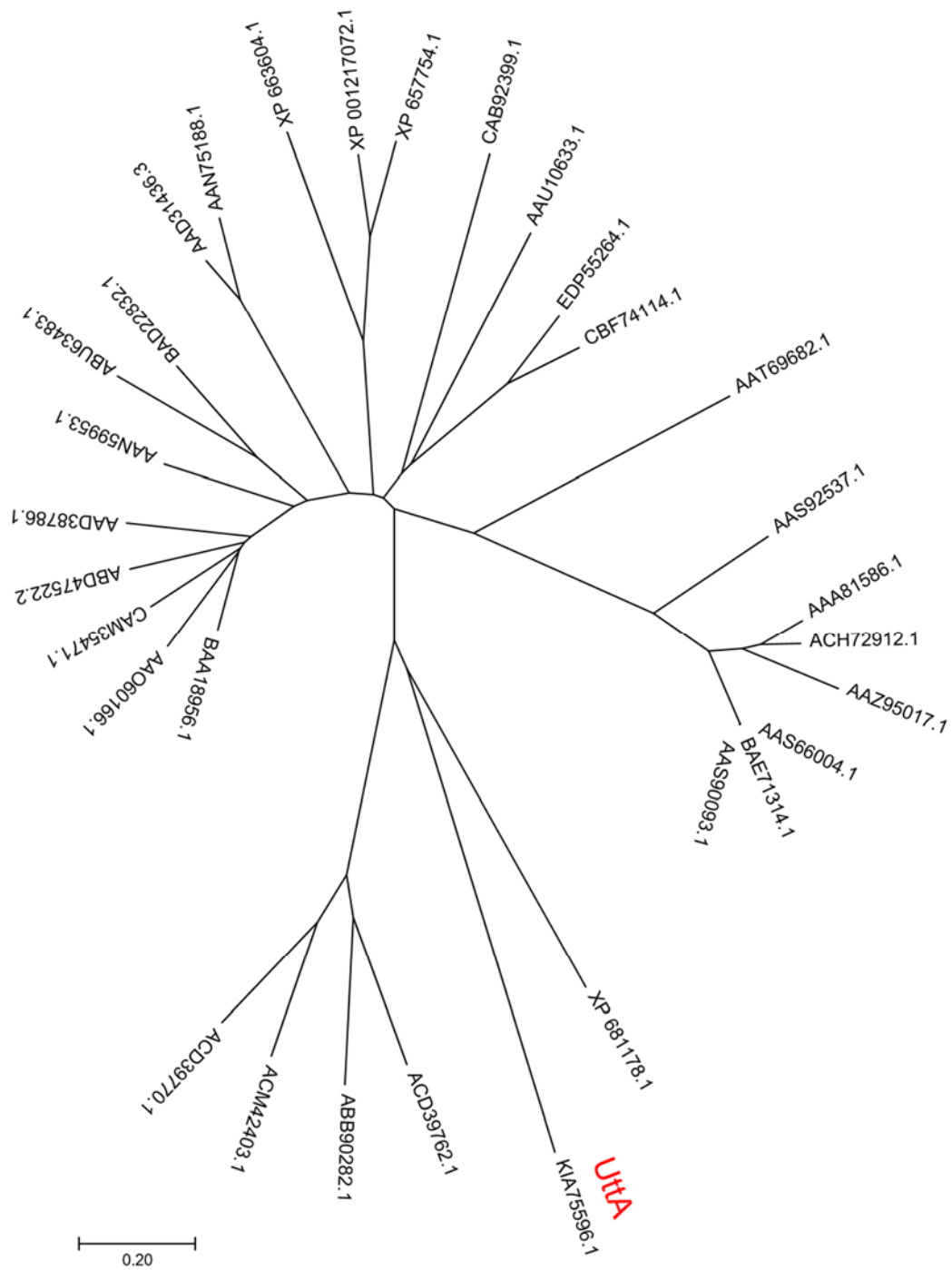


Figure S3. Phylogenetic analysis of UtaA_PT domain with 30 known PT domains from fungi.

SUPPORTING INFORMATION

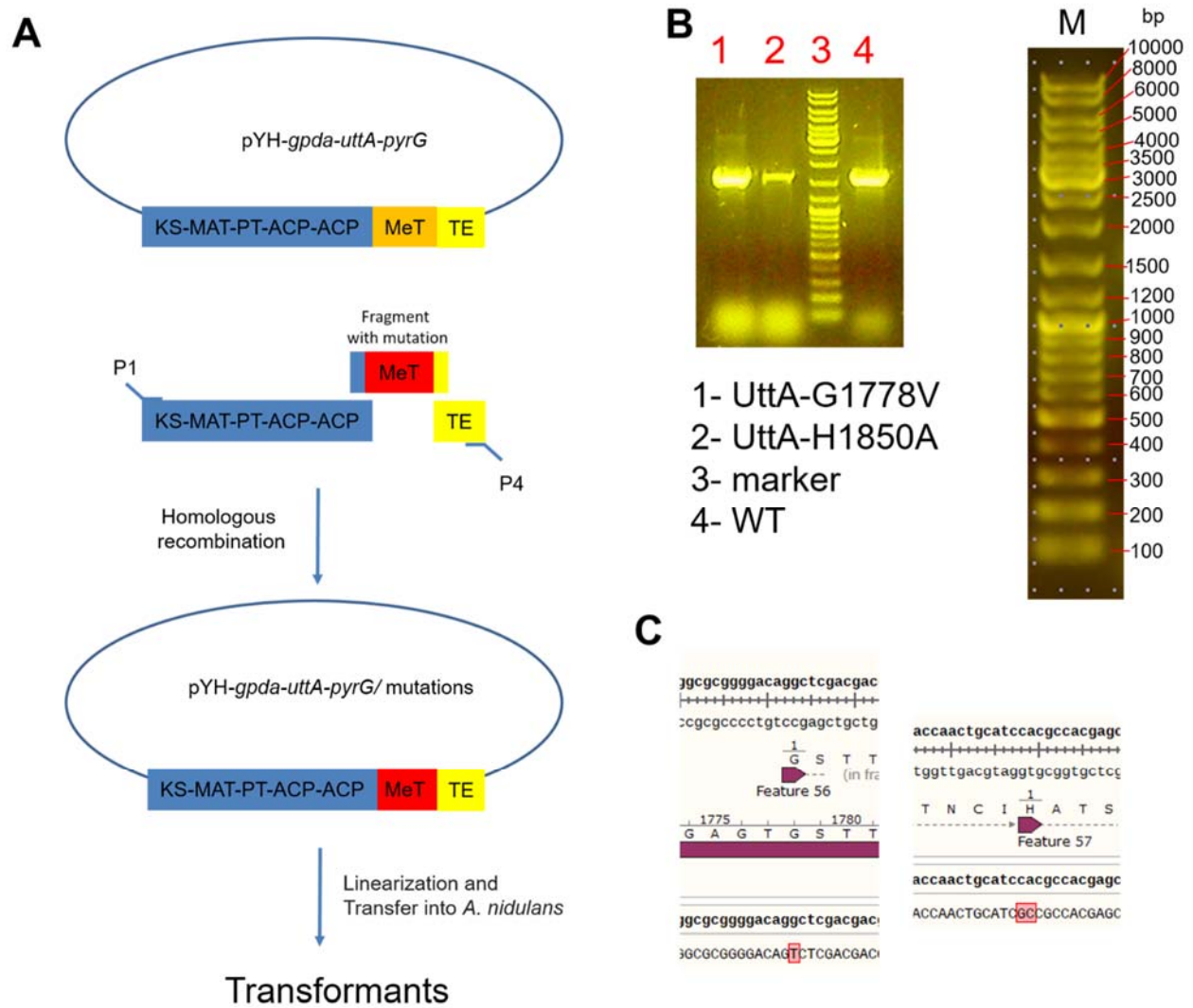


Figure S4. Point mutation in UttA and analysis of the obtained mutants.

(A) Schematic representation for the point mutation in UttA. (B) PCR verification of the mutants. (C) Sequence analysis of the UttA mutants

SUPPORTING INFORMATION

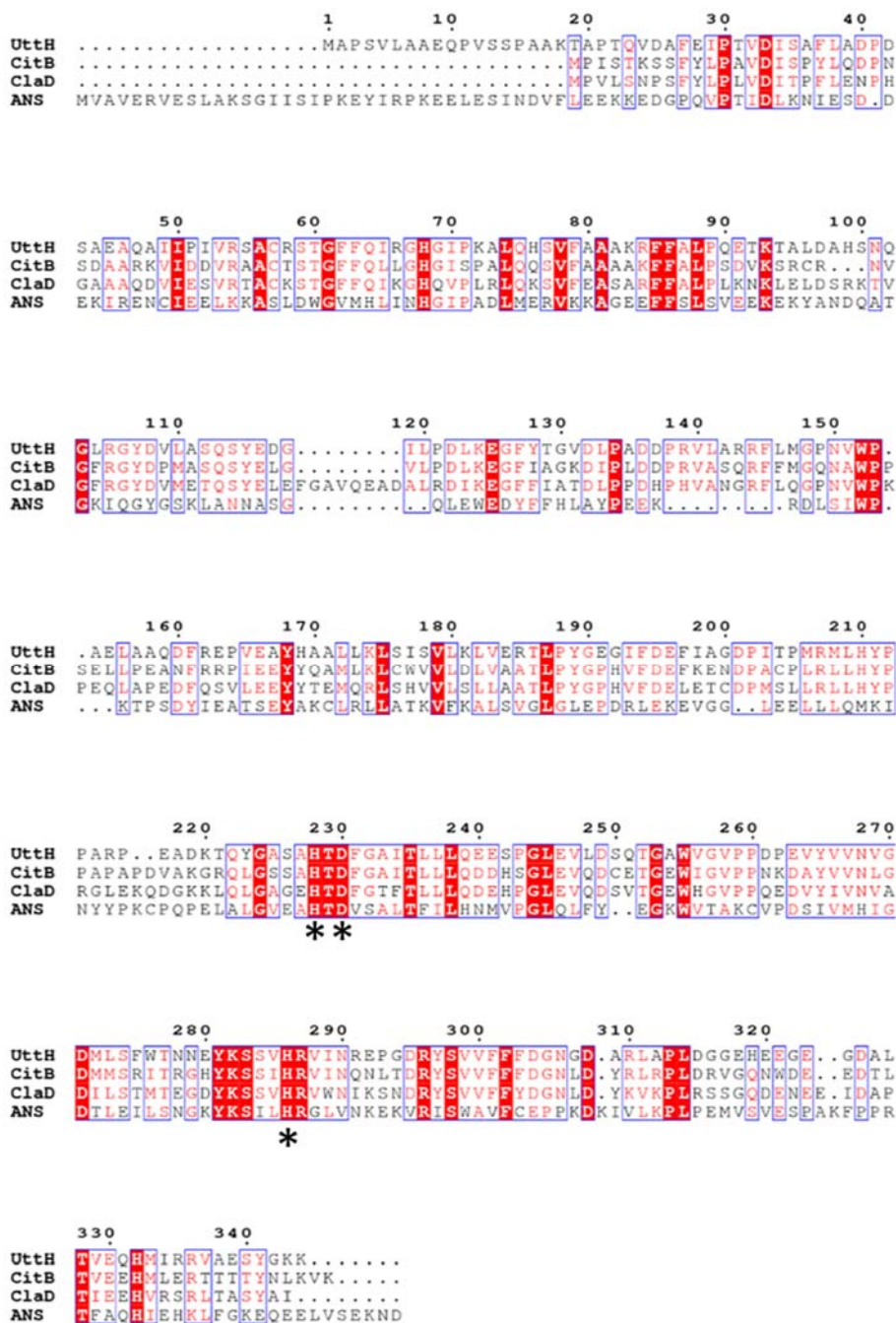


Figure S5. Sequence alignments of 2-OG-dependent oxygenases.

CitB (A192653)¹⁰, ClaD (QBK15042), and ANS (Q96323) are from *Monascus ruber* M7, *Penicillium crustosum* and *Arabidopsis thaliana*, respectively. UttH contains the typical conserved 2-His-1-Asp ion-binding triad of non-heme Fe^{II}/2-oxoglutarate-dependent oxygenases (His228, His296 and Asp296) (marked with *) compared with the crystal structure of ANS¹¹. Protein sequence alignments were carried out by using the sequence alignment function of Multiple Sequence Alignment by CLUSTALW (<https://www.genome.jp/tools-bin/clustalw>) and visualized with ESPript 3.0 (<http://esprict.ibcp.fr/ESPript/ESPript/>).

SUPPORTING INFORMATION

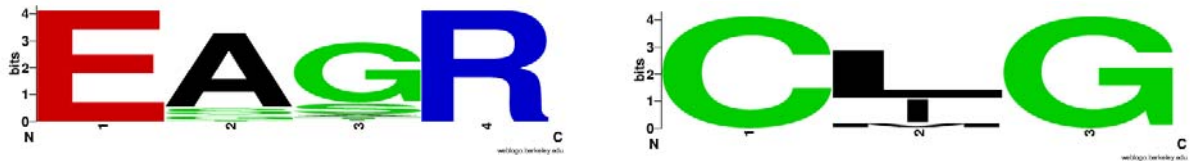


Figure S6. Weblogo illustration for the conserved ExxR and CxG motifs in UttC by using 96 P₄₅₀ enzyme in fungi. EAGR (349-352) in UttC (A); CLG (434-436) in UttC (B)

The amino acids in the following enzymes (accession number are listed) were used for analysis. **UttC (KIA75594)** is highlighted in red.

XP_664053.1_10-490, XP_033674816.1_17-507, XP_033595470.1_20-516, XP_033430050.1_21-509, XP_033391313.1_19-508, XP_026608368.1_1-495, XP_025573321.1_5-496, XP_025464315.1_5-498, XP_024692041.1_6-487, XP_016600678.1_16-516, XP_016589218.1_27-507, XP_016221951.1_24-495, XP_007806251.1_26-498, XP_007805323.1_1-429, XP_003234761.1_17-497, XP_003170503.1_31-508, XP_003071602.1_35-507, XP_002848393.1_22-522, XP_002145722.1_1-497, XP_001911463.1_5-497, XP_001905657.1_14-503, XP_001245240.2_35-507, XP_001228060.1_35-520, VBB75775.1_5-497, TVY58386.1_20-510, SLM38802.1_31-474, RYP92946.1_1-423, RYP43872.1_19-502, RVX74072.1_1-443, RMZ76241.1_762-1242, RMD39760.1_78-530, RAO64728.1_1-365, QGA14808.1_1-497, Q0CRQ3.2_13-480, PVH96859.1_19-500, POS74238.1_21-516, PLN86963.1_21-508, PCG99300.1_13-489, OXV11655.1_4-509, OTB02447.1_24-516, OTA92375.1_13-516, OTA64244.1_13-516, OSS44053.1_30-509, OJJ68595.1_1-492, OCK75412.1_40-531, KUL85074.1_3-484, KMP04844.1_28-510, KMM70176.1_35-510, KKY30492.1_16-525, KIH90520.1_27-527, **KIA75594.1_1-506**, KGO38587.1_16-495, KFY99026.1_1-431, KFY63720.1_19-514, KFH44065.1_16-507, KFA68360.1_26-512, KFA60546.1_25-483, KEY71920.1_31-483, KEY71720.1_26-512, KAF4779182.1_34-507, KAF4310737.1_17-496, KAF4228494.1_6-502, KAF3895032.1_17-525, KAF3406269.1_34-522, KAF3023069.1_9-517, KAF3012828.1_17-494, KAF2994041.1_1-422, KAF2847821.1_21-515, KAF2678715.1_16-511, KAF2258967.1_9-501, KAF2205452.1_8-503, KAF2189392.1_14-523, KAF2004773.1_15-520, KAE8553912.1_1-497, KAB8343000.1_743-1215, KAB5575480.1_31-514, KAA6412416.1_75-547, GFF93090.1_21-527, GFF54863.1_21-527, GFF23783.1_21-510, GES61355.1_13-512, GAW17174.1_5-514, GAO84805.1_21-527, GAM43297.1_34-522, EZF36180.1_17-525, EZF23312.1_17-525, ERS97303.1_27-525, EPE10457.1_18-502, EKG19934.1_1-426, EGE04287.1_17-525, EGD97508.1_17-525, EFW13271.1_28-510, CEN59739.1_4-442, CEJ60330.1_15-521, CBF69449.1_10-497

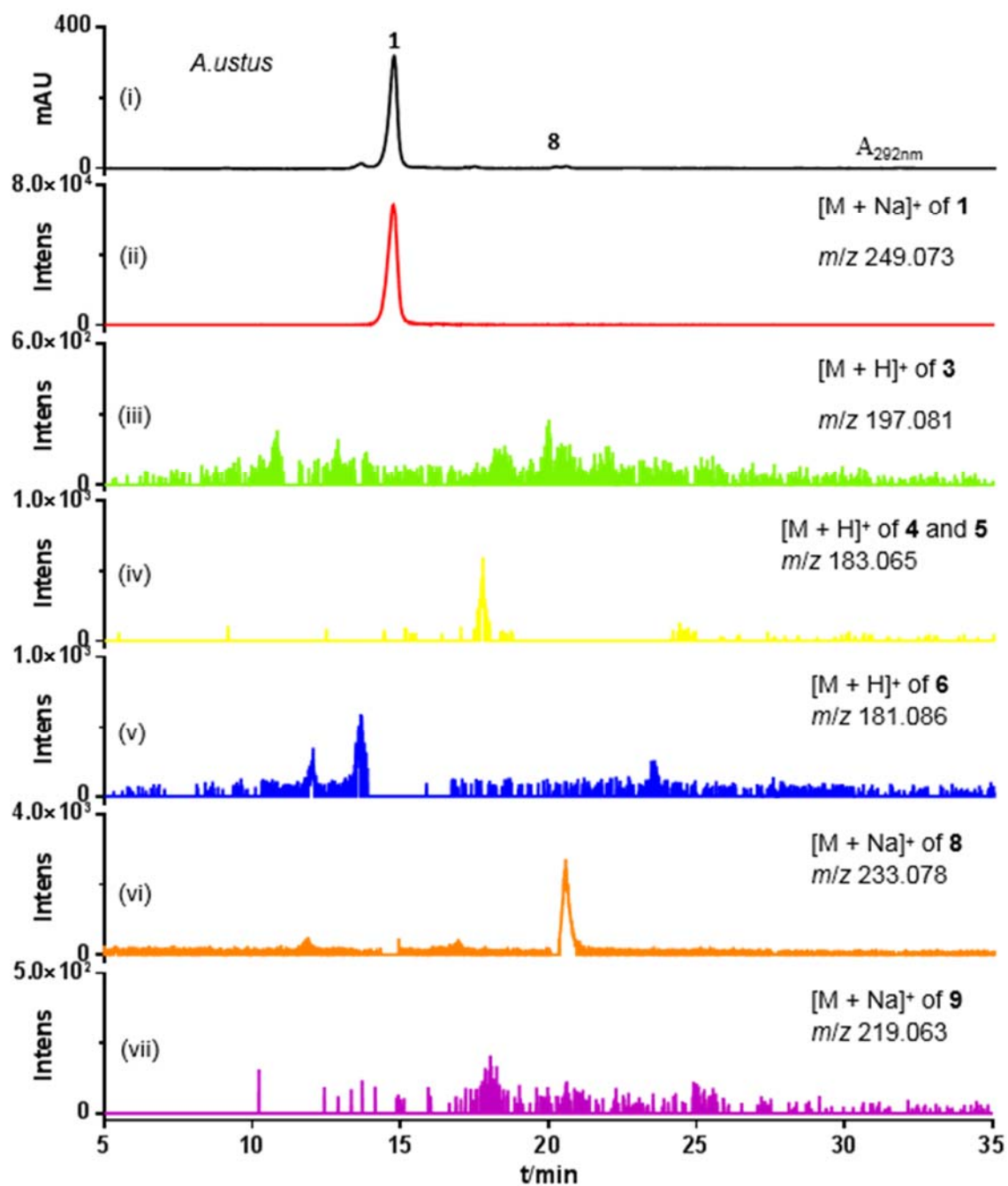


Figure S7. LC-MS analysis of the metabolite profile of the *A. ustus* wild type

UV detection was carried out on a diode array detector and absorptions at 292 nm are illustrated (i). EICs with a tolerance range of ± 0.005 refer to $[M + H]^+$ or $[M + Na]^+$ ions of 1, 3 – 6, 8 and 9 (ii – vii).

SUPPORTING INFORMATION

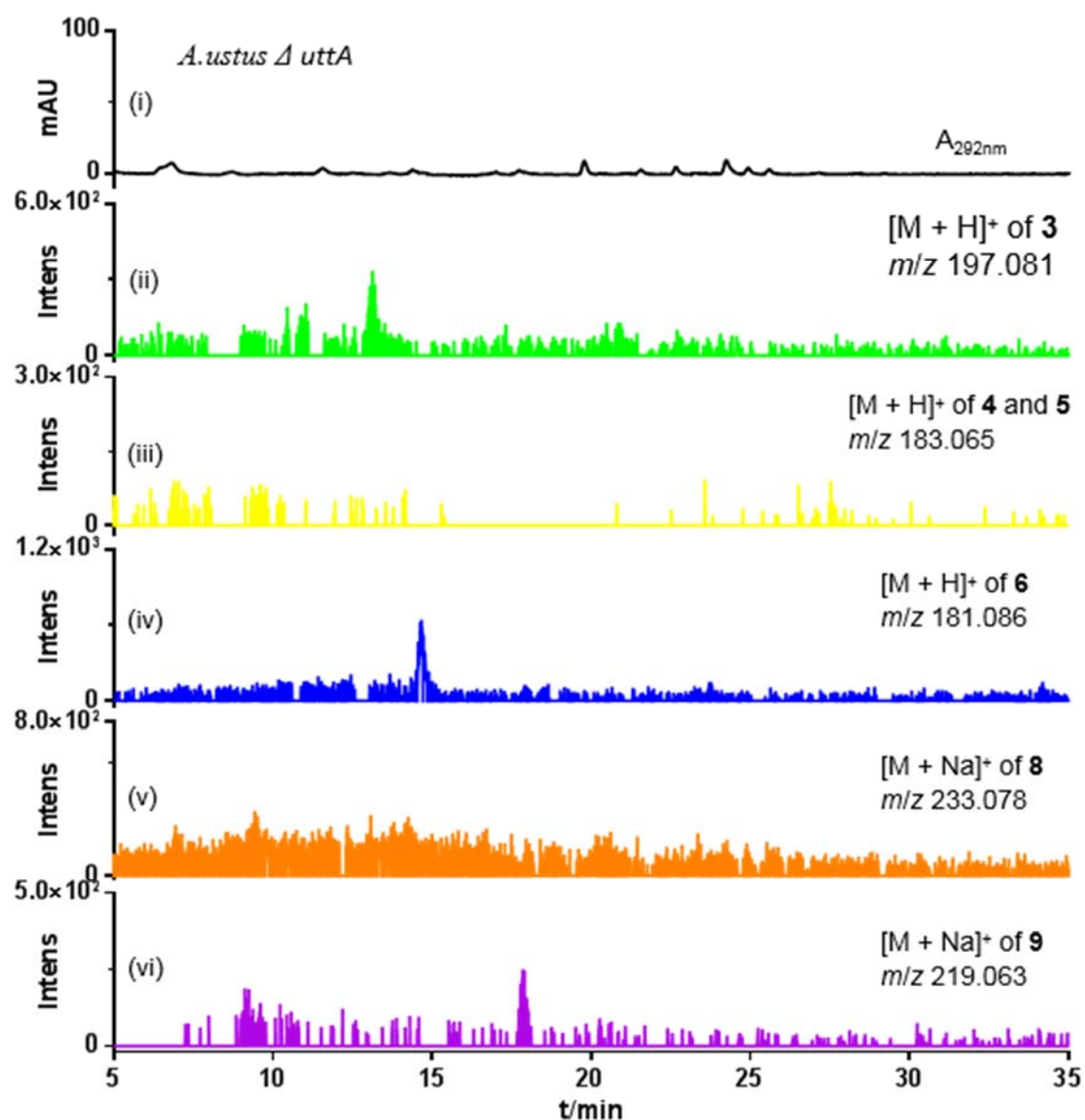


Figure S8. LC-MS analysis of the metabolite profile of the *A. ustus* Δ uttA mutant

UV detection was carried out on a diode array detector and absorptions at 292 nm are illustrated (i). EICs with a tolerance range of ± 0.005 refer to $[M + H]^+$ or $[M + Na]^+$ ions of **3 – 6**, **8** and **9** (ii – vi).

SUPPORTING INFORMATION

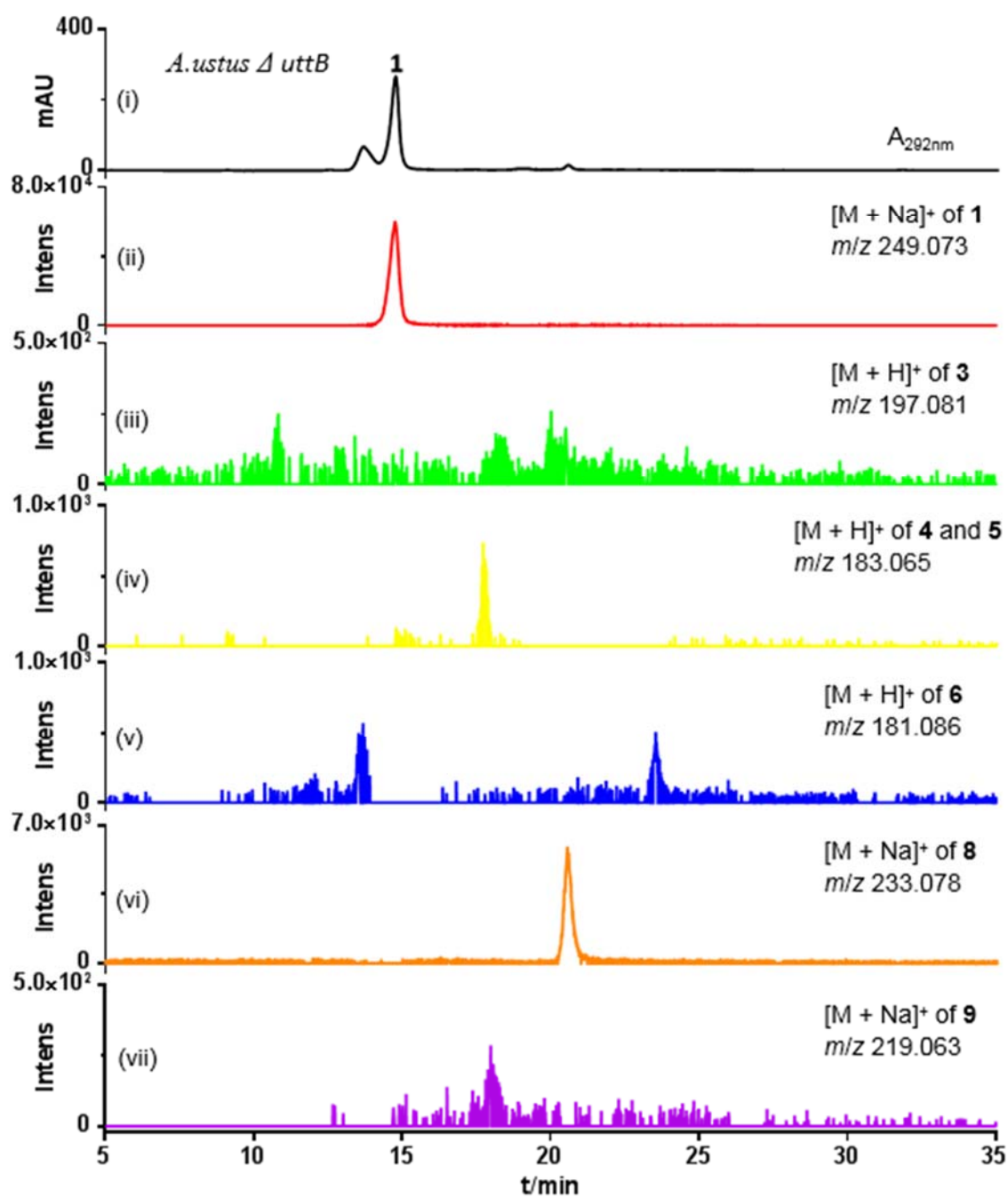


Figure S9. LC-MS analysis of the metabolite profile of the *A. ustus* Δ *uttB* mutant

UV detection was carried out on a diode array detector and absorptions at 292 nm are illustrated (i). EICs with a tolerance range of ± 0.005 refer to $[M + H]^+$ or $[M + Na]^+$ ions of **1**, **3 – 6**, **8** and **9** (ii – vii).

SUPPORTING INFORMATION

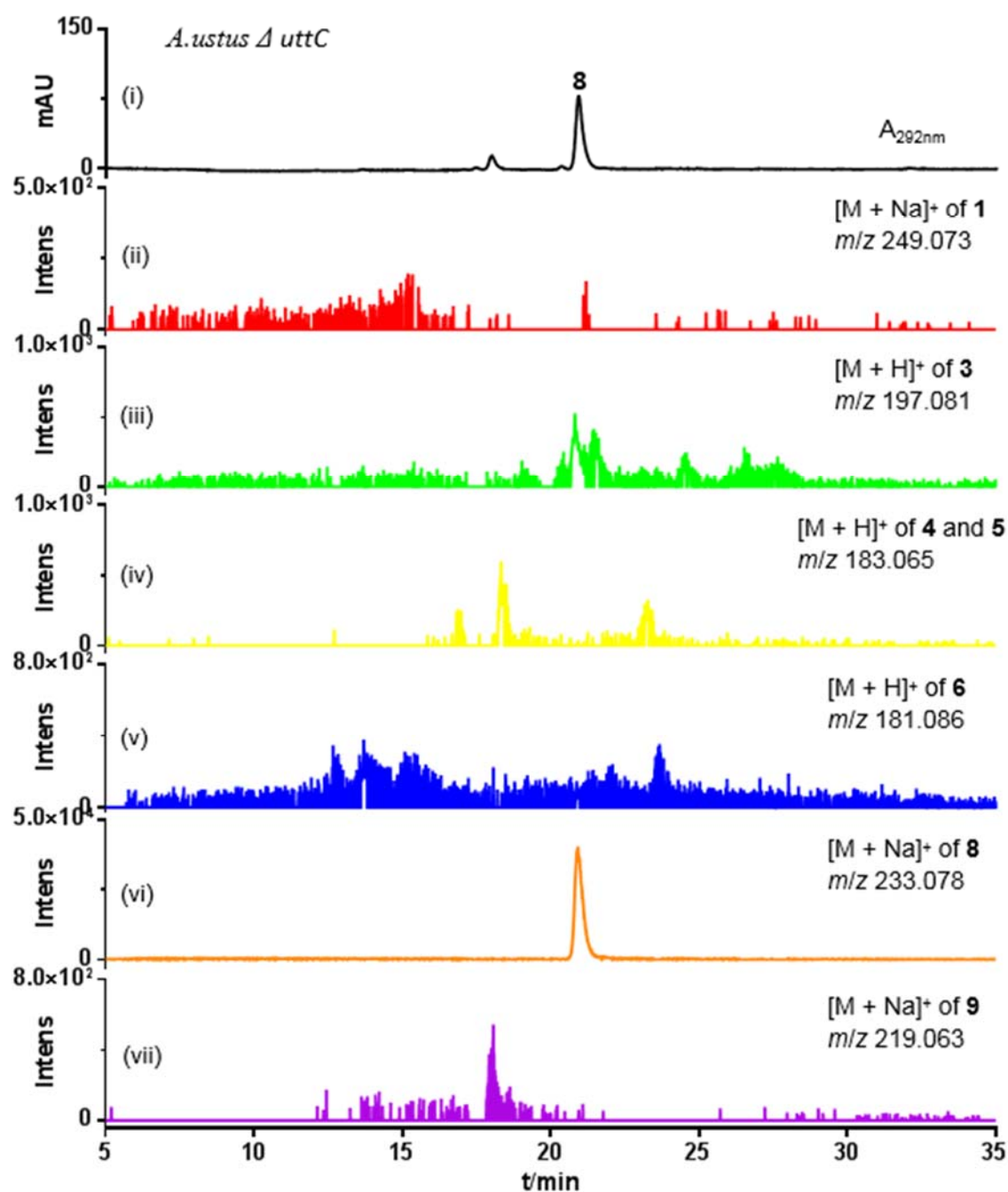


Figure S10. LC-MS analysis of the metabolite profile of the *A. ustus* Δ *uttC* mutant

UV detection was carried out on a diode array detector and absorptions at 292 nm are illustrated (i). EICs with a tolerance range of ± 0.005 refer to $[M + H]^+$ or $[M + Na]^+$ ions of **1**, **3 – 6**, **8** and **9** (ii – vii).

SUPPORTING INFORMATION

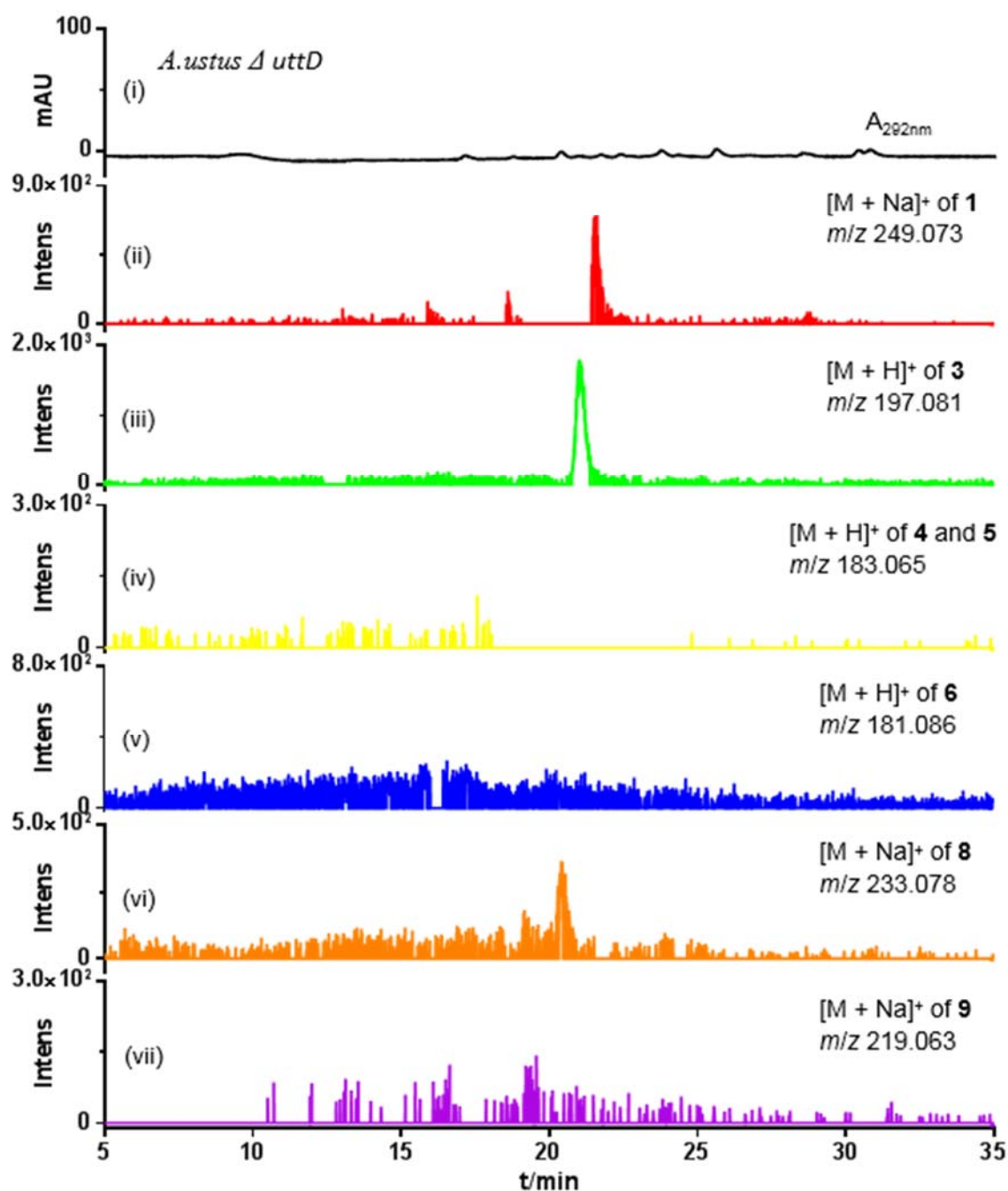


Figure S11. LC-MS analysis of the metabolite profile of the *A. ustus* Δ uttD mutant

UV detection was carried out on a diode array detector and absorptions at 292 nm are illustrated. (i). EICs with a tolerance range of ± 0.005 refer to $[M + H]^+$ or $[M + Na]^+$ ions of **1**, **3 – 6**, **8** and **9** (ii – vii).

SUPPORTING INFORMATION

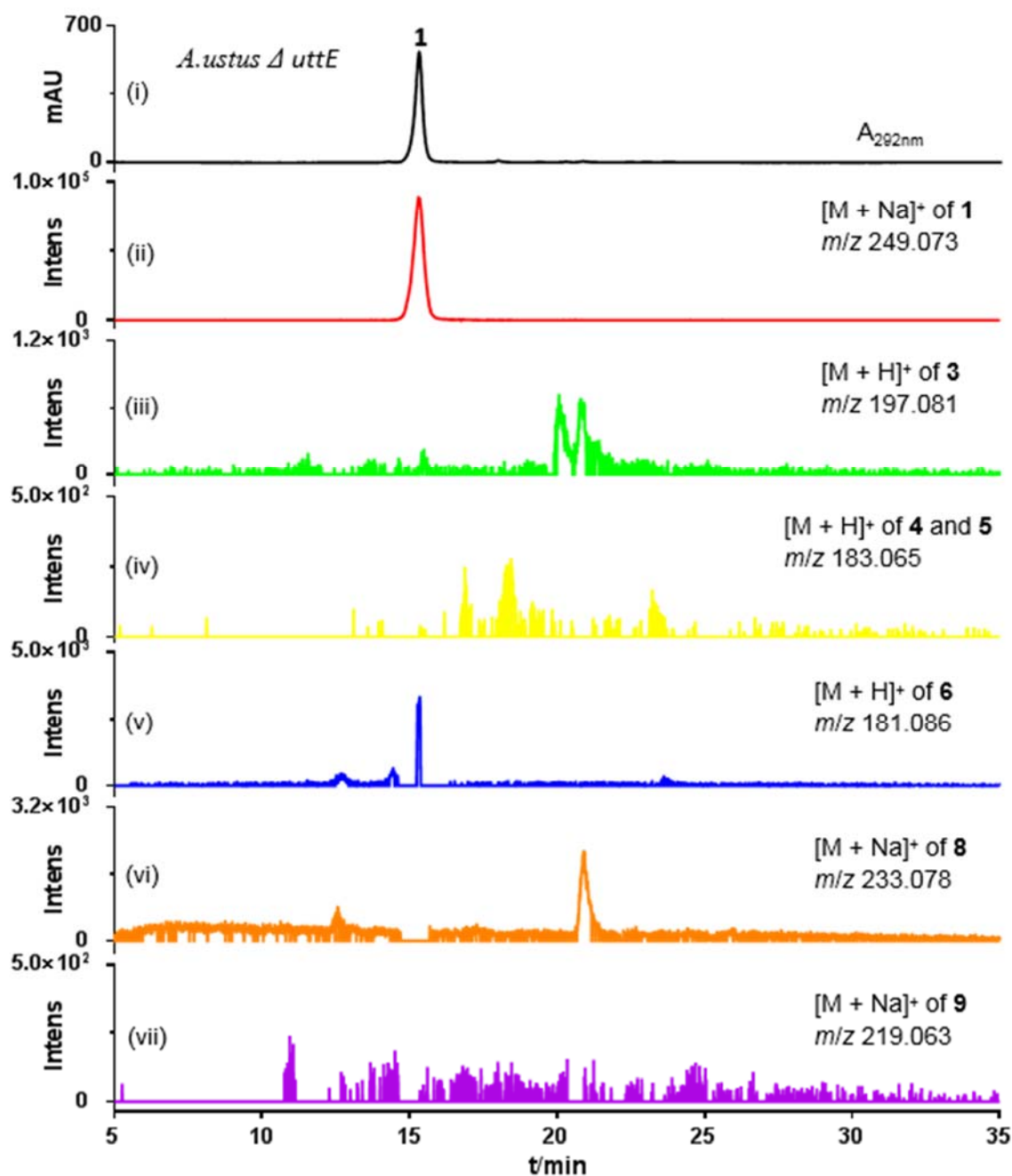


Figure S12. LC-MS analysis of the metabolite profile of the *A. ustus* Δ uttE mutant

UV detection was carried out on a diode array detector and absorptions at 292 nm are illustrated. (i). EICs with a tolerance range of ± 0.005 refer to $[M + H]^+$ or $[M + Na]^+$ ions of 1, 3 – 6, 8 and 9 (ii – vii).

SUPPORTING INFORMATION

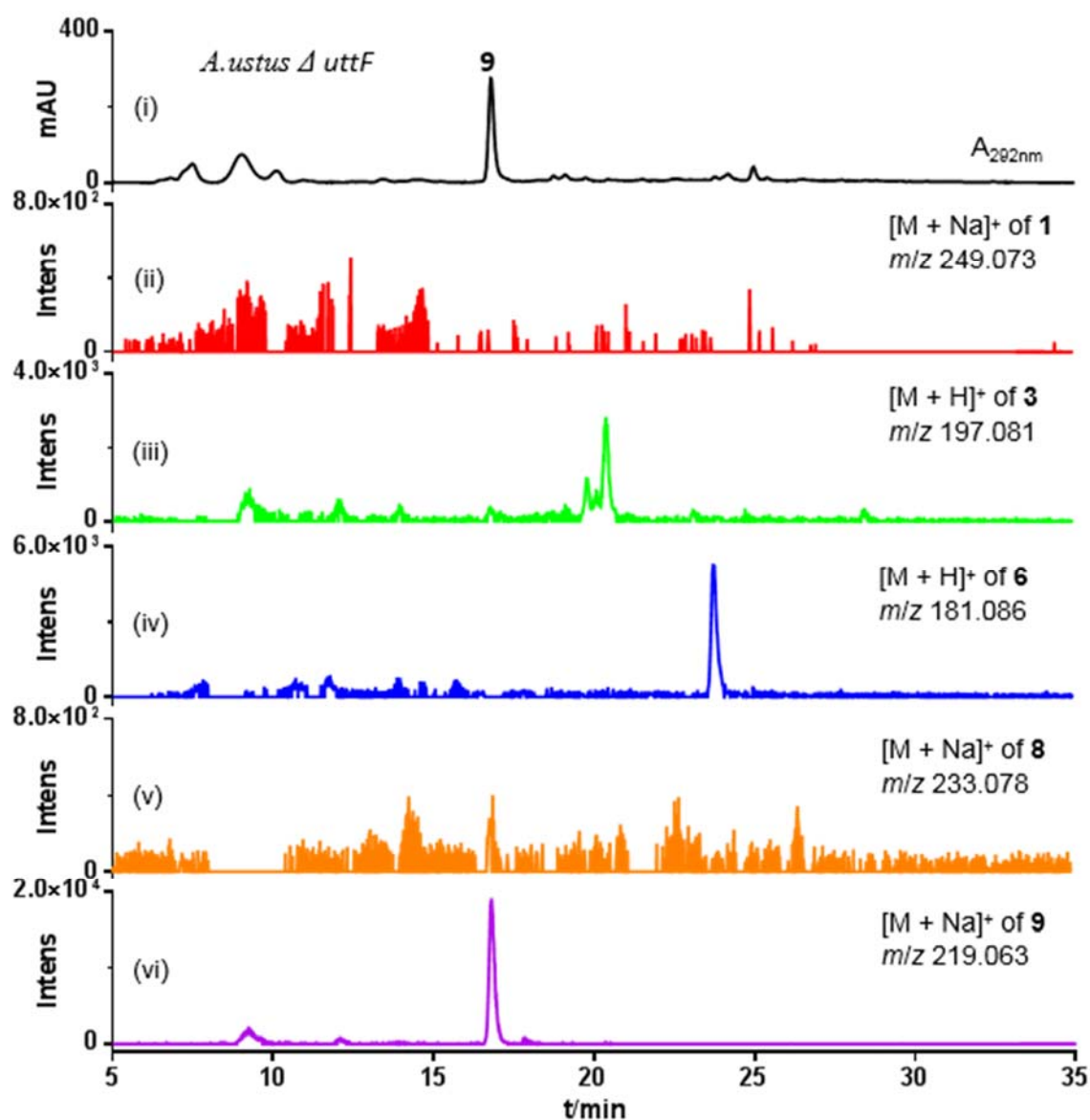


Figure S13. LC-MS analysis of the metabolite profile of the *A. ustus* Δ uttF mutant

UV detection was carried out on a diode array detector and absorptions at 292 nm are illustrated. (i). EICs with a tolerance range of ± 0.005 refer to $[M + H]^+$ or $[M + Na]^+$ ions of **1**, **3**, **6**, **8**, and **9** (ii – vi).

SUPPORTING INFORMATION

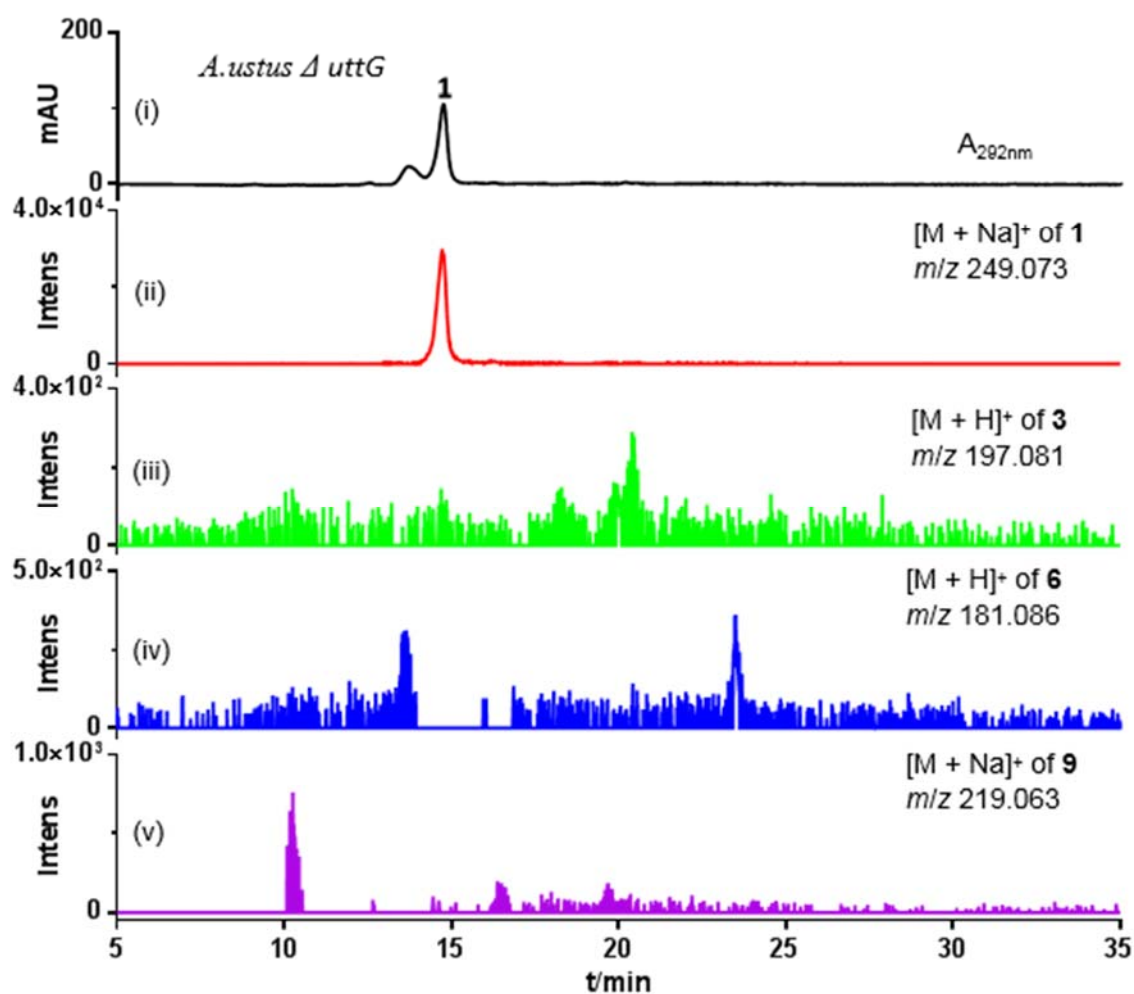


Figure S14. LC-MS analysis of the metabolite profile of the *A. ustus* Δ uttG mutant

UV detection was carried out on a diode array detector and absorptions at 292 nm are illustrated. (i). EICs with a tolerance range of ± 0.005 refer to $[M + H]^+$ or $[M + Na]^+$ ions of **1**, **3**, **6**, and **9** (ii – v).

SUPPORTING INFORMATION

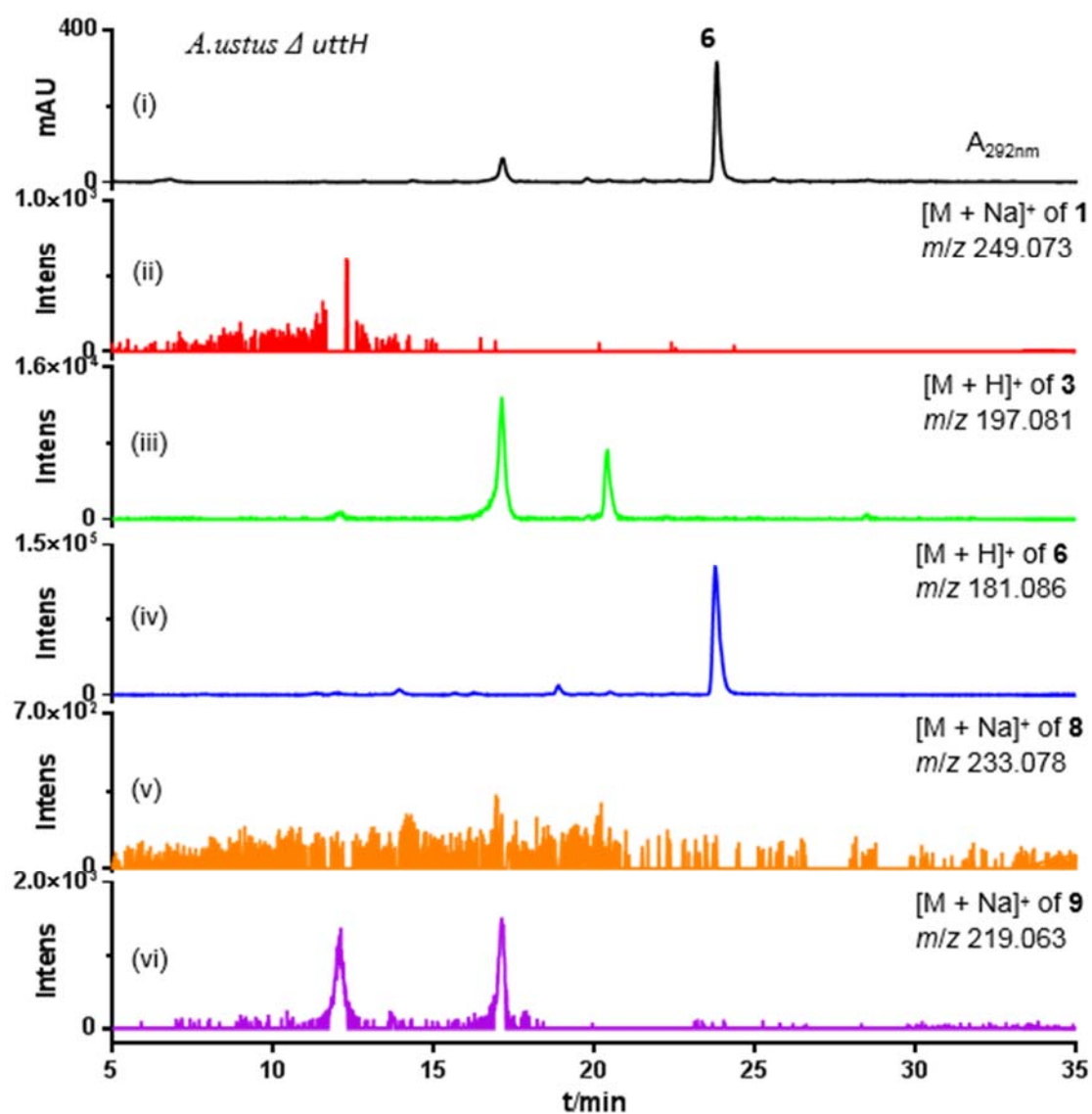


Figure S15. LC-MS analysis of the metabolite profile of the *A. ustus* Δ *uttH* mutant

UV detection was carried out on a diode array detector and absorptions at 292 nm are illustrated. (i). EICs with a tolerance range of ± 0.005 refer to $[M + H]^+$ or $[M + Na]^+$ ions of **1**, **3**, **6**, **8**, and **9** (ii – vi).

SUPPORTING INFORMATION

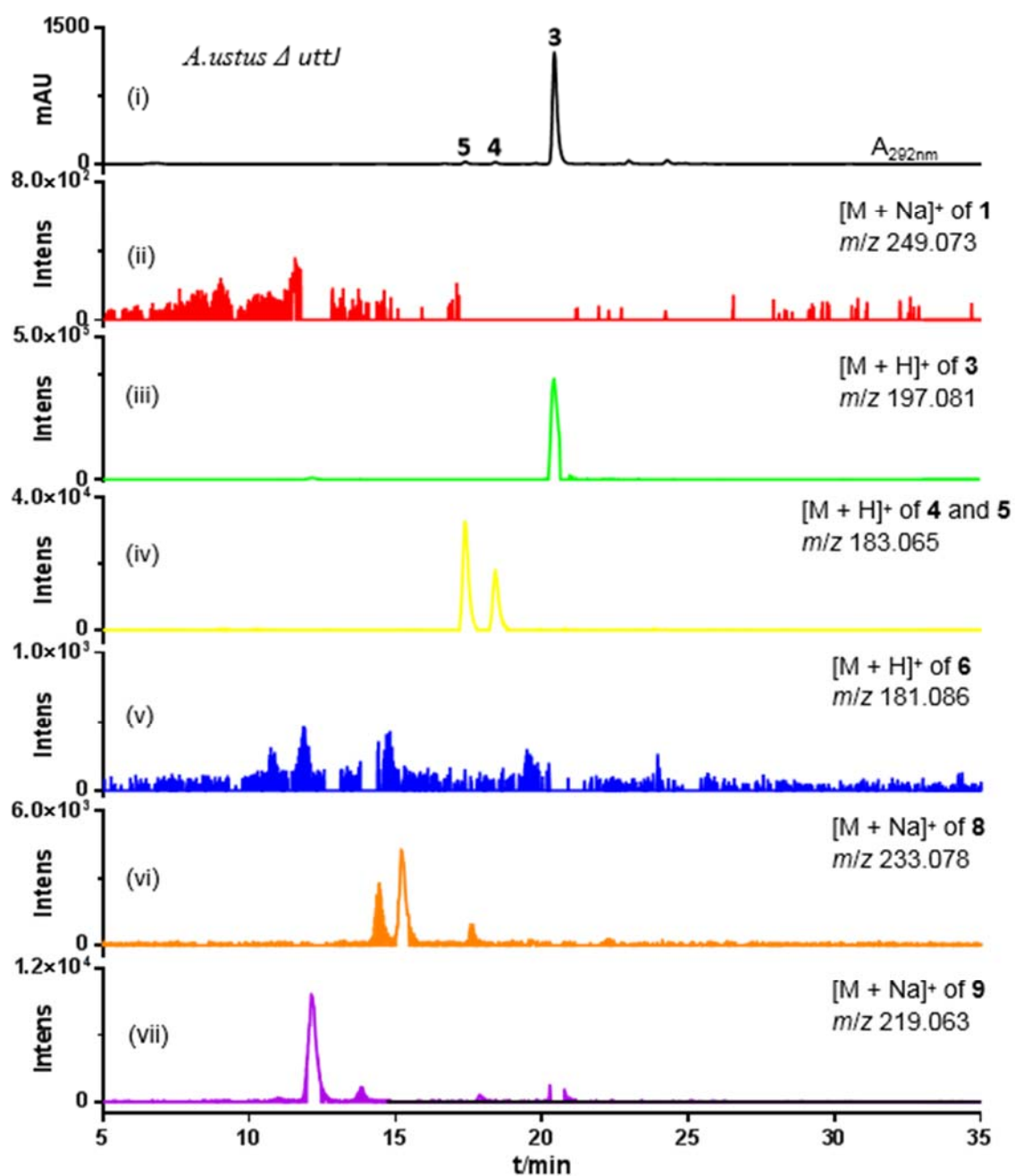


Figure S16. LC-MS analysis of the metabolite profile of the *A. ustus* Δ *uttJ* mutant

UV detection was carried out on a diode array detector and absorptions at 292 nm are illustrated. (i). EICs with a tolerance range of ± 0.005 refer to $[M + H]^+$ or $[M + Na]^+$ ions of **1**, **3** – **6**, **8** and **9** (ii – vii).

SUPPORTING INFORMATION

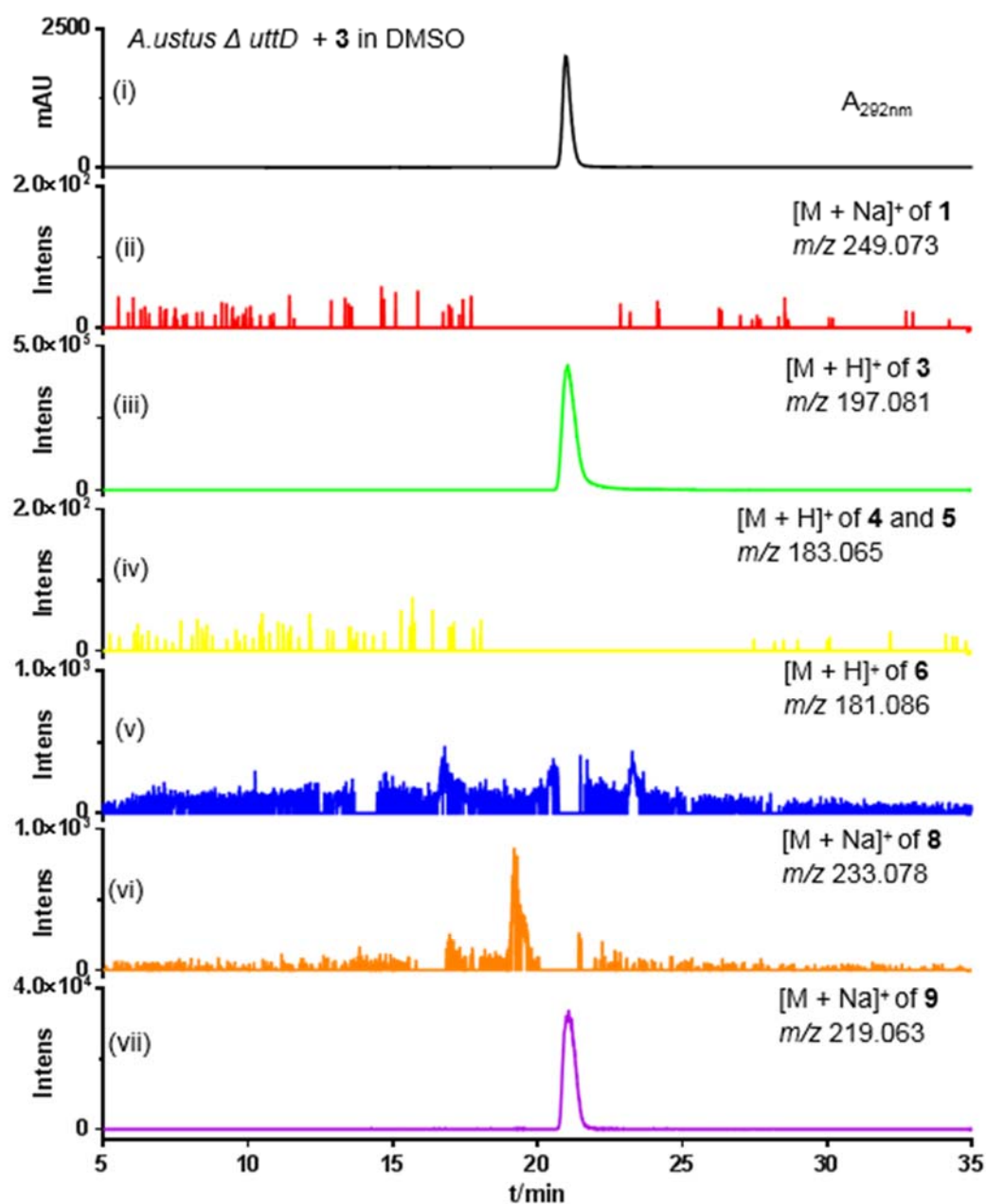


Figure S17. LC-MS analysis of the metabolite profile of the *A.ustus* Δ uttD after feeding with **3**. UV detection was carried out on a diode array detector and absorptions at 292 nm are illustrated (i). EICs with a tolerance range of ± 0.005 refer to $[M + H]^+$ or $[M + Na]^+$ ions of **1**, **3** – **6**, **8** and **9** (ii – vii).

SUPPORTING INFORMATION

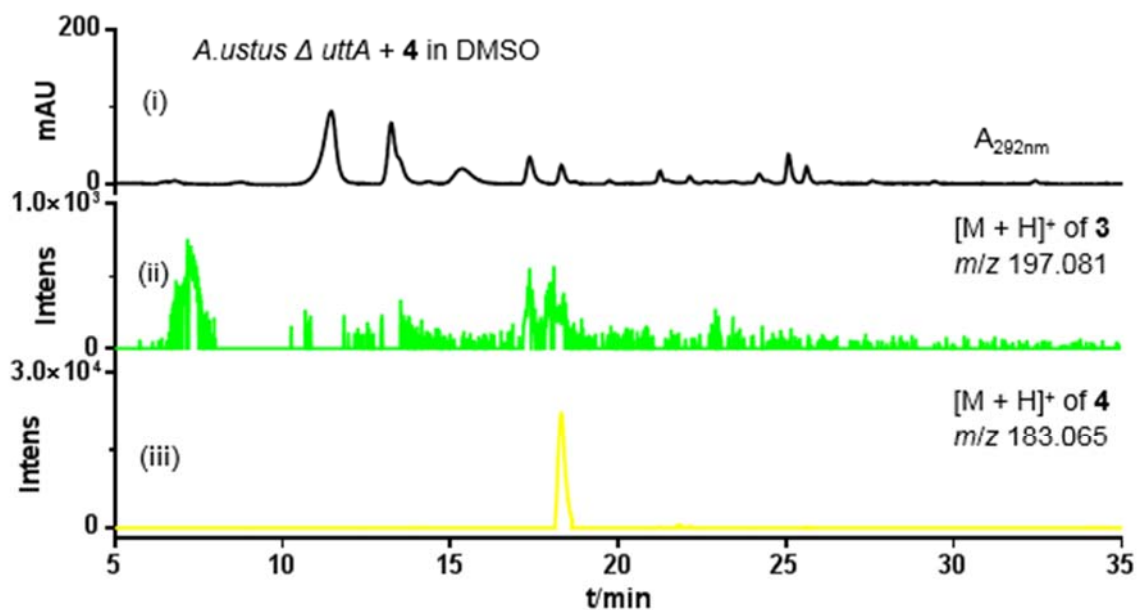


Figure S18. LC-MS analysis of the metabolite profile of the *A. ustus* Δ *uttA* after feeding with **4**.

UV detection was carried out on a diode array detector and absorptions at 292 nm are illustrated (i). EICs with a tolerance range of ± 0.005 refer to $[M + H]^+$ of **3** and **4** (ii – iii).

SUPPORTING INFORMATION

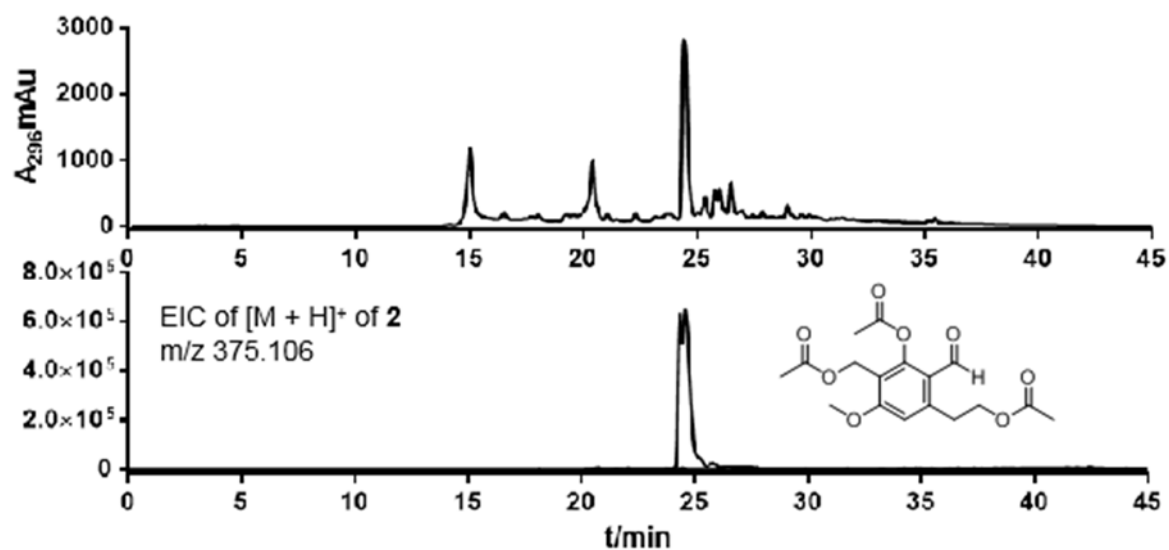


Figure S19. LC-MS analysis of the acetylated EtOAc extract from *A. ustus*.

EIC of **2** is selected with a tolerance range of ± 0.005 .

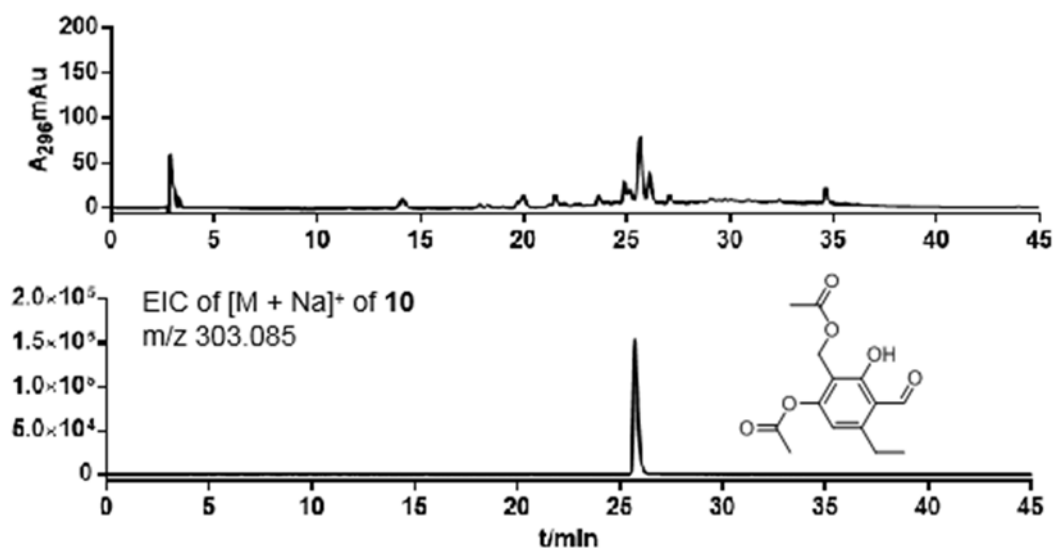


Figure S20. LC-MS analysis of the acetylated EtOAc extract from $\Delta uttf$ of *A. ustus*.

EIC of **10** is selected with a tolerance range of ± 0.005 .

SUPPORTING INFORMATION

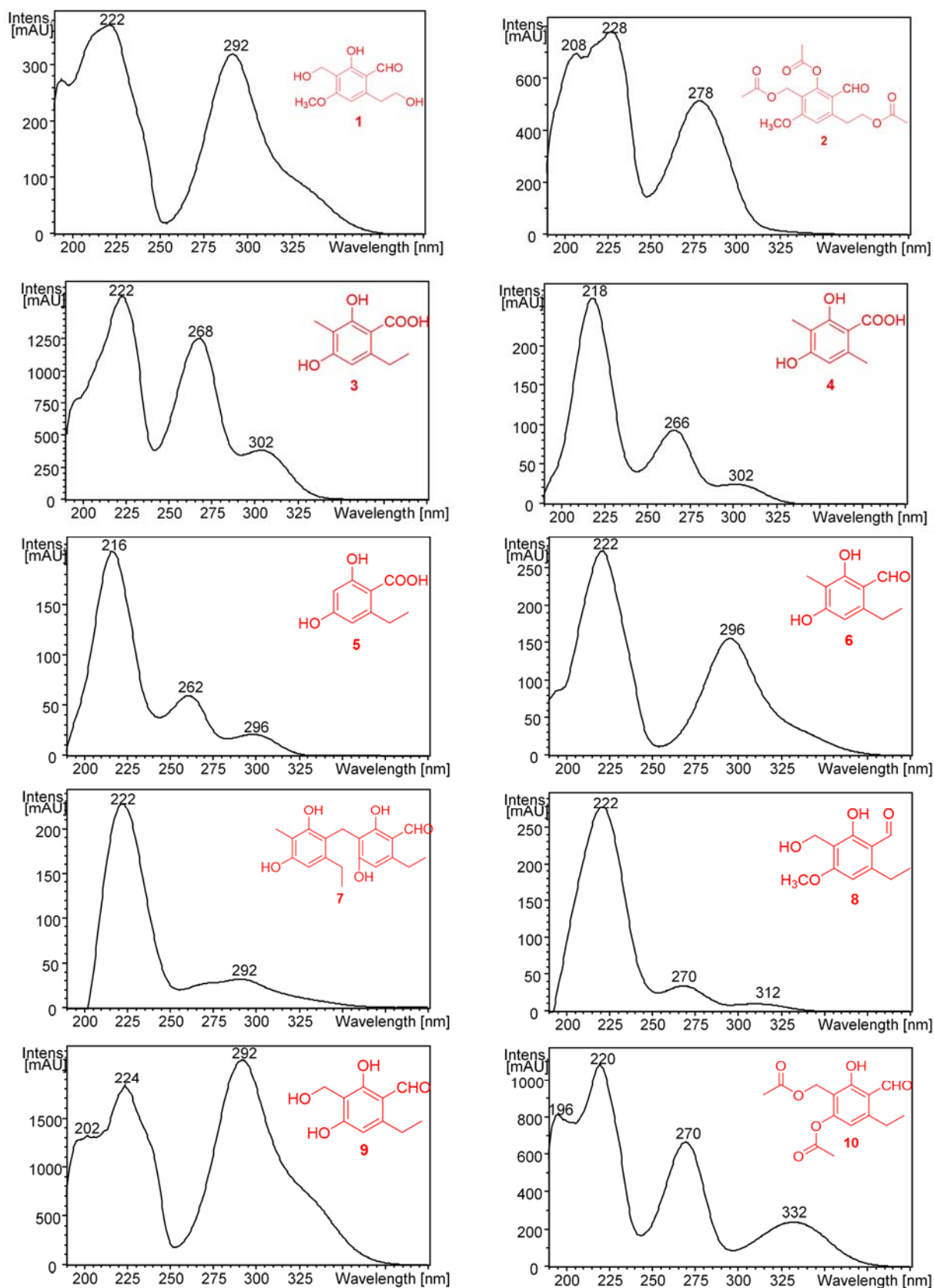


Figure S21. UV spectra of the compounds identified in this study

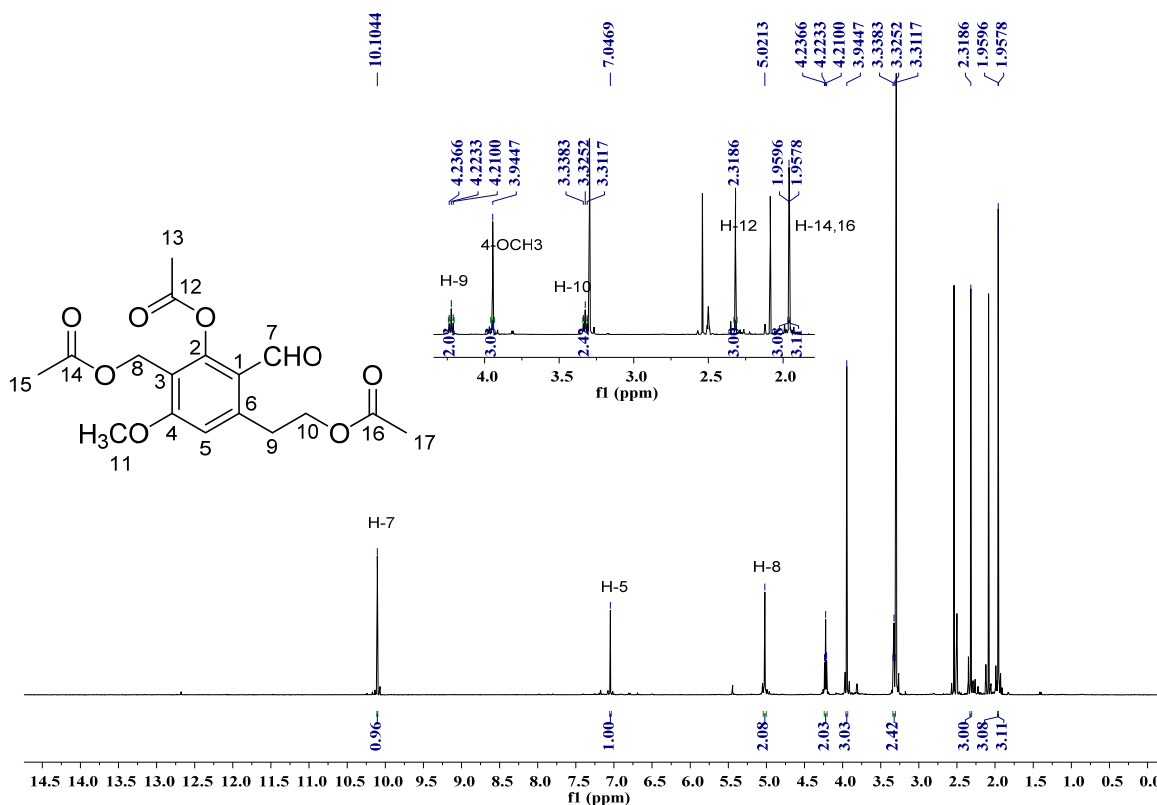


Figure S22. ^1H NMR spectrum of compound **2** in $\text{DMSO}-d_6$ (500 MHz)

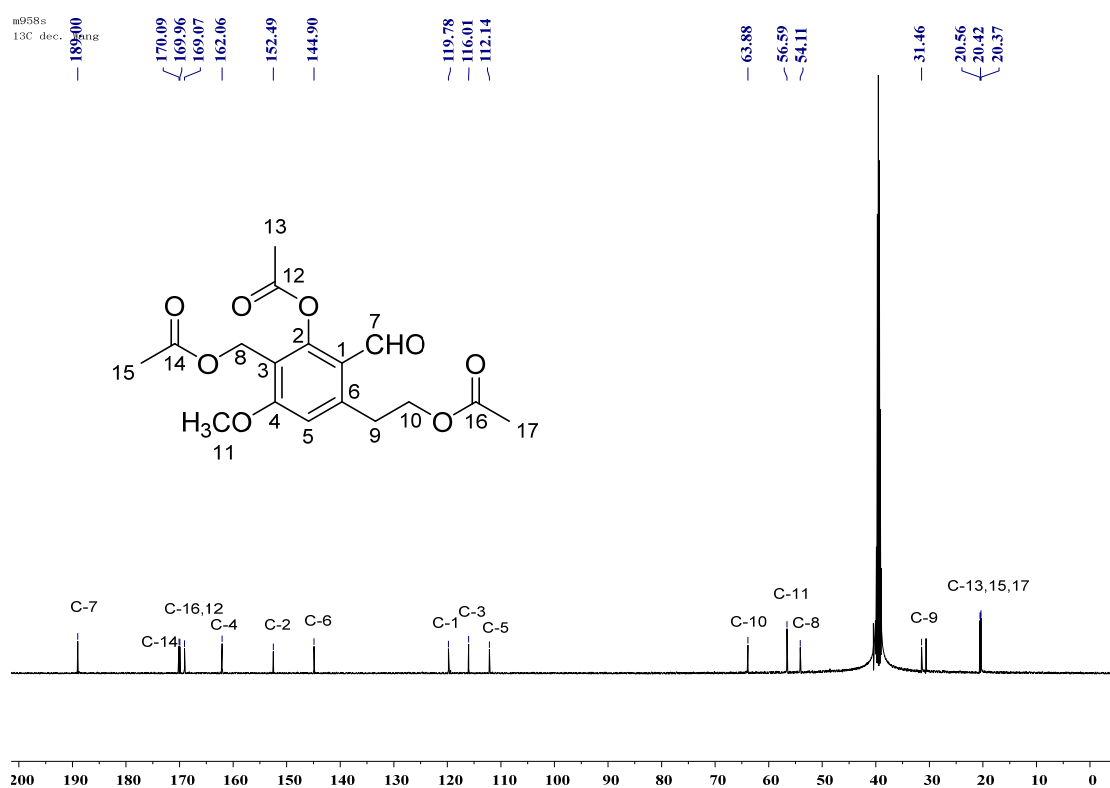


Figure S23. $^{13}\text{C}\{^1\text{H}\}$ NMR spectrum of compound **2** in $\text{DMSO}-d_6$ (125 MHz)

SUPPORTING INFORMATION

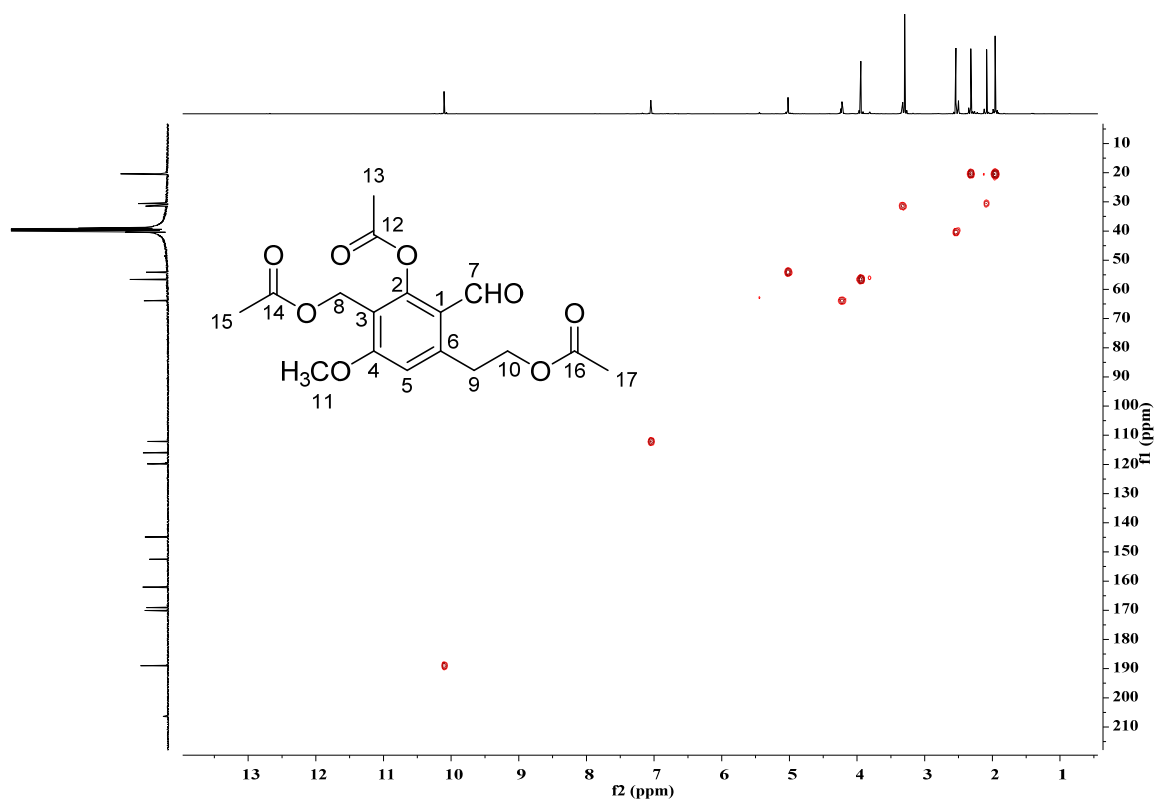


Figure S24. HSQC spectrum of compound **2** in DMSO- d_6

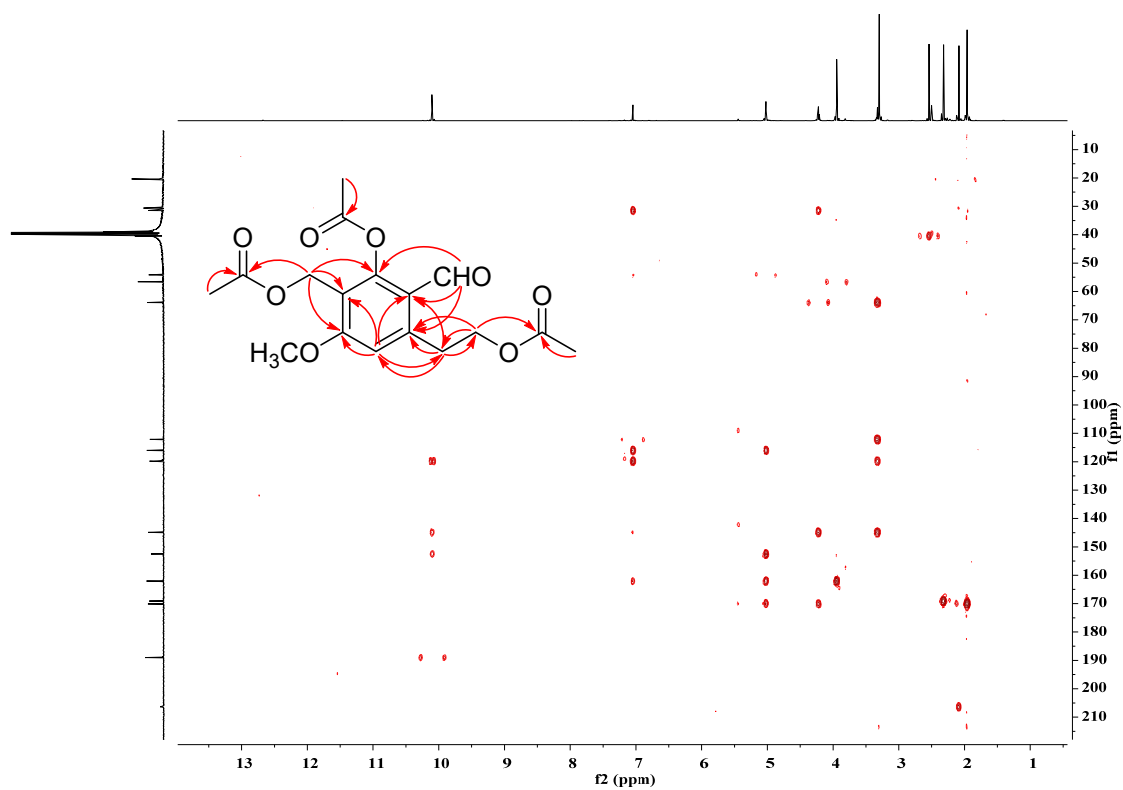


Figure S25. HMBC spectrum of compound **2** in DMSO- d_6

SUPPORTING INFORMATION

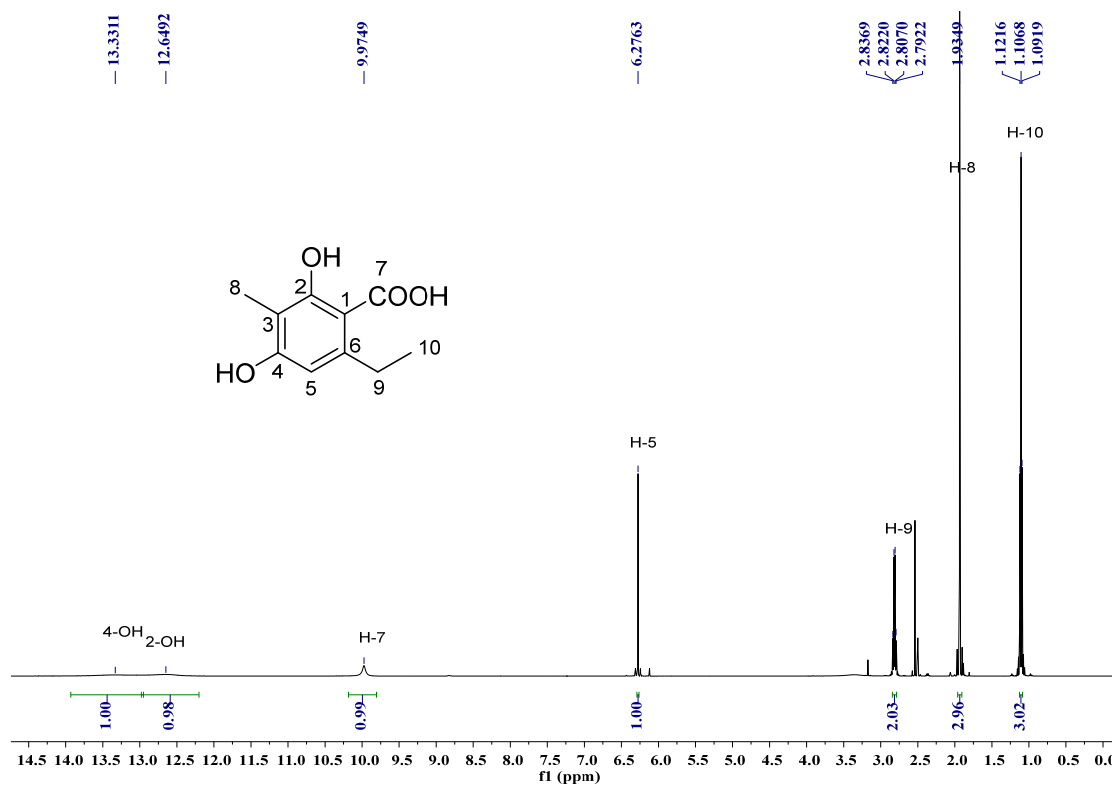


Figure S26. ¹H NMR spectrum of compound **3** in DMSO-*d*₆ (500 MHz)

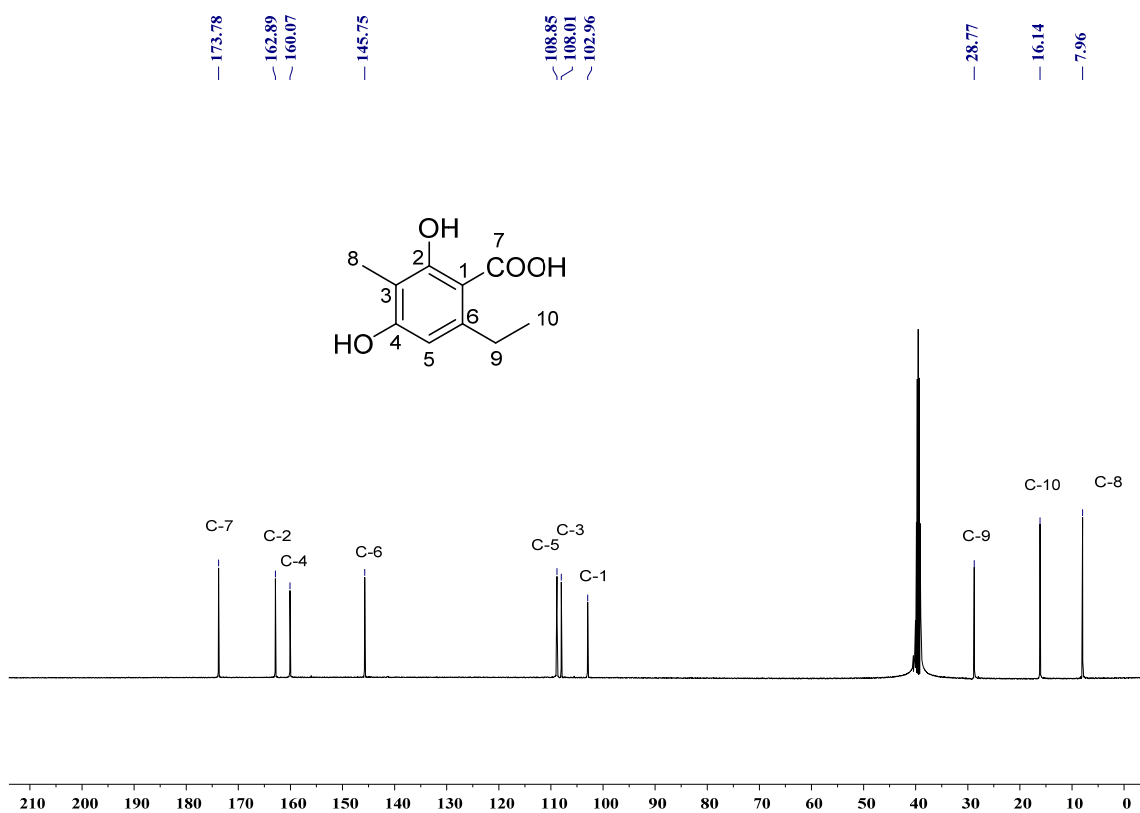


Figure S27. ¹³C{¹H} NMR spectrum of compound **3** in DMSO-*d*₆ (125 MHz)

SUPPORTING INFORMATION

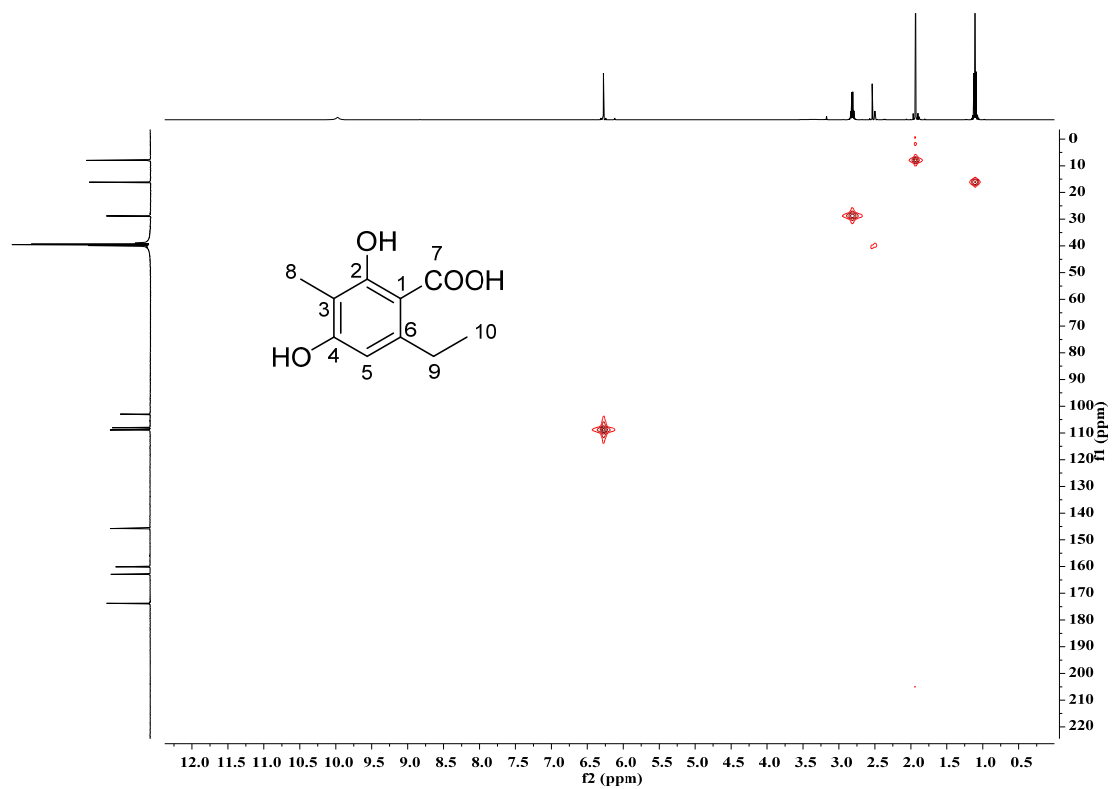


Figure S28. HSQC spectrum of compound **3** in $\text{DMSO}-d_6$

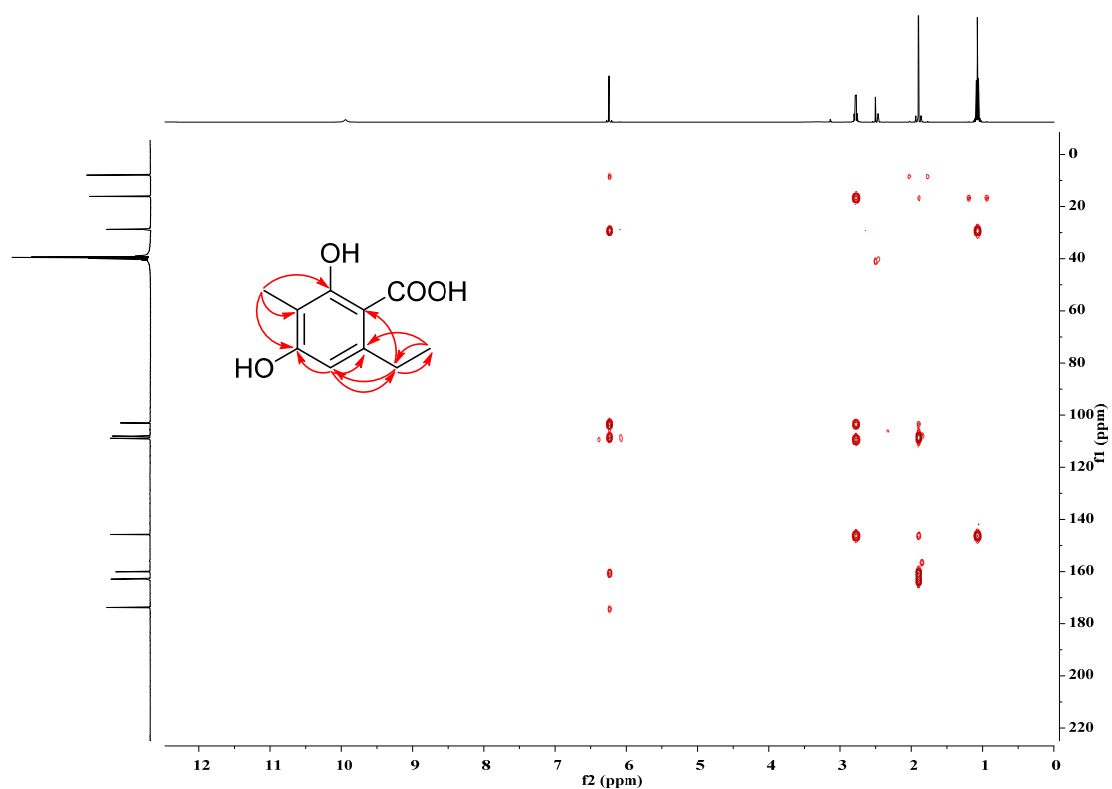


Figure S29. HMBC spectrum of compound **3** in $\text{DMSO}-d_6$

SUPPORTING INFORMATION

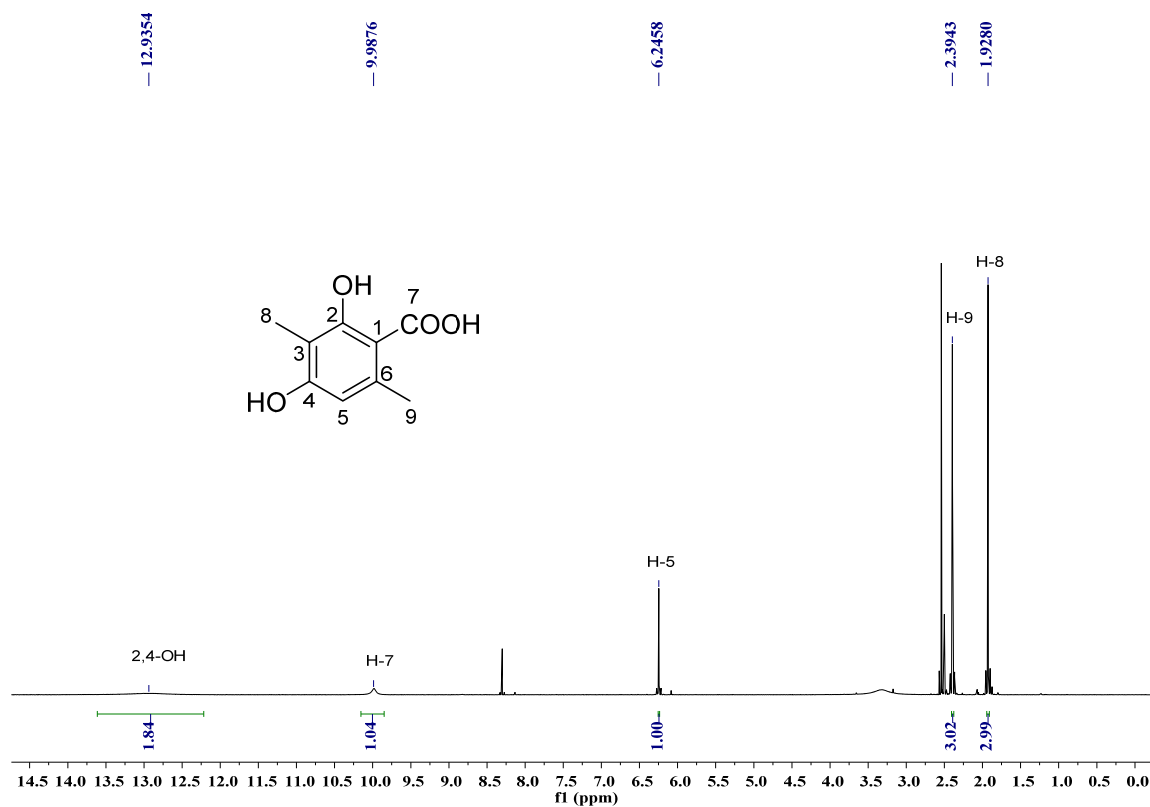


Figure S30. ¹H NMR spectrum of compound **4** in DMSO-*d*₆ (500 MHz)

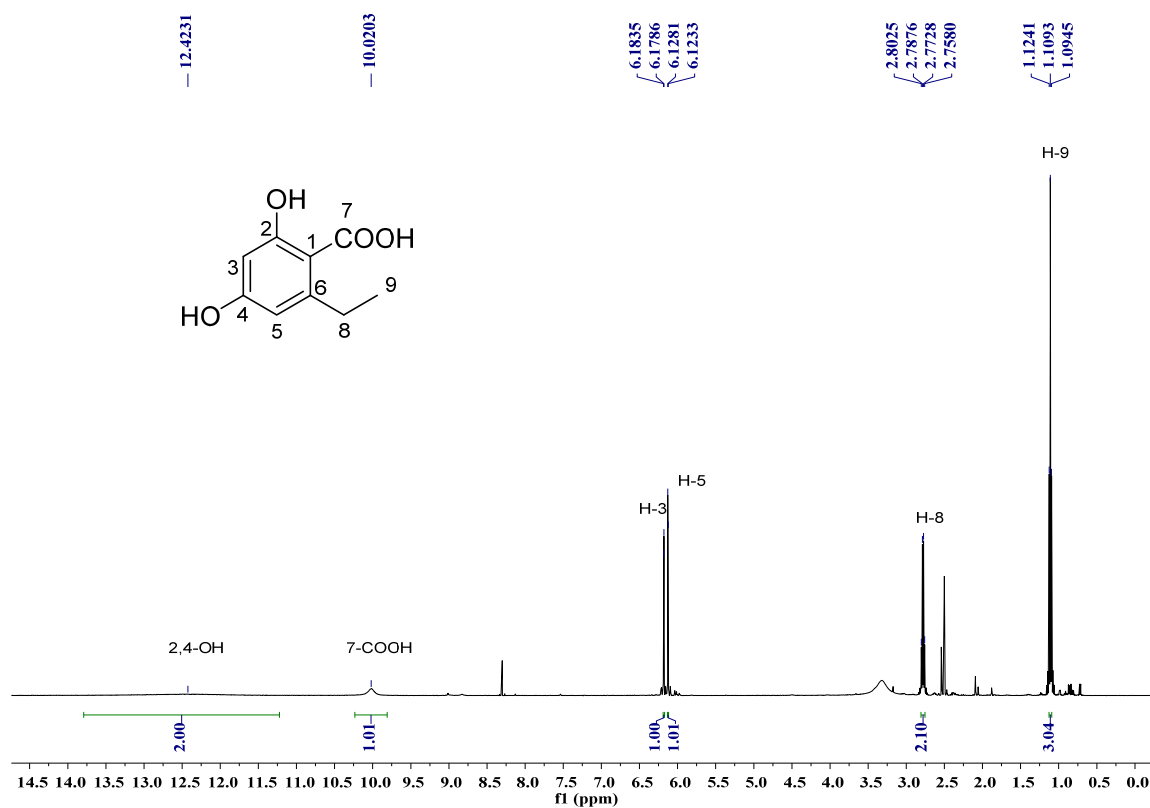


Figure S31. ¹H NMR spectrum of compound **5** in DMSO-*d*₆ (500 MHz)

SUPPORTING INFORMATION

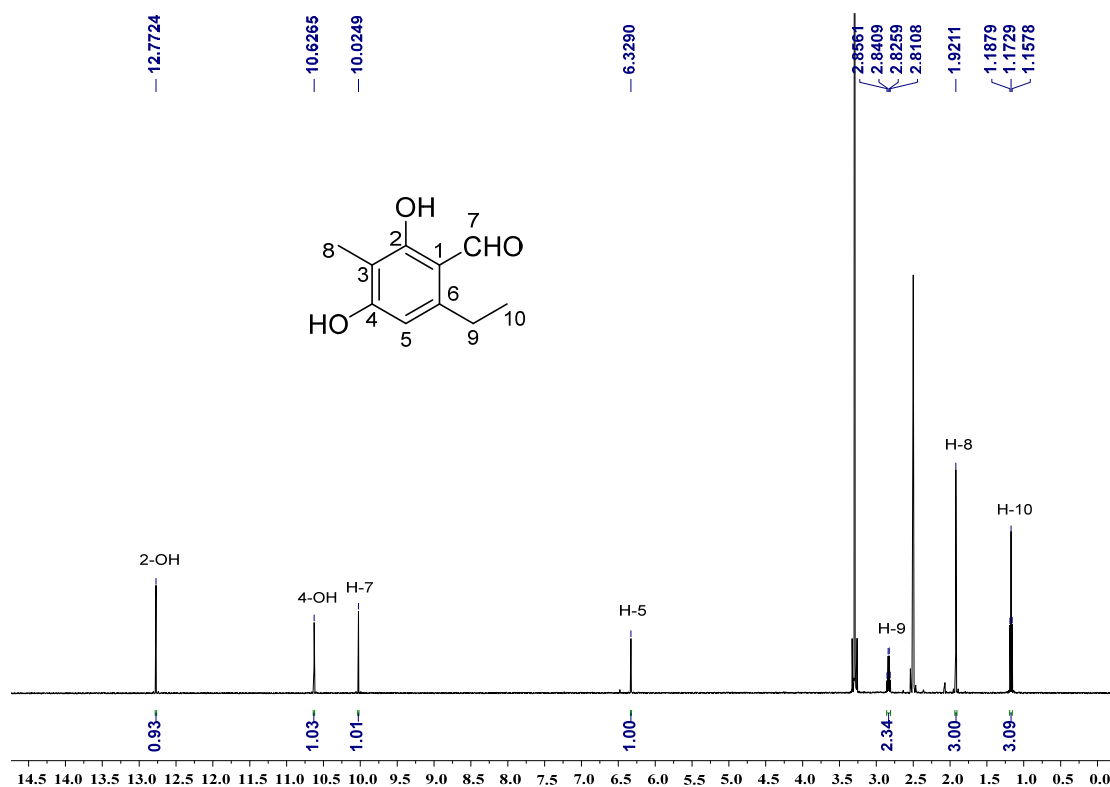


Figure S32. ¹H NMR spectrum of compound 6 in DMSO-*d*₆ (500 MHz)

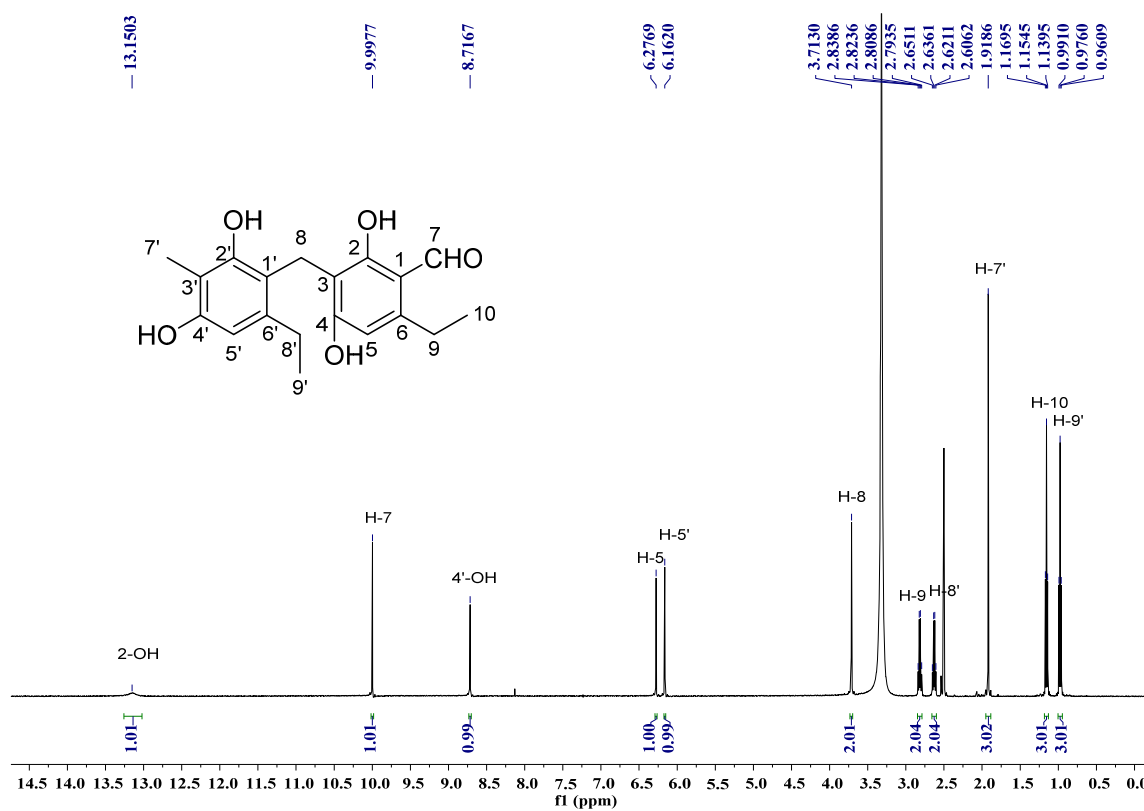
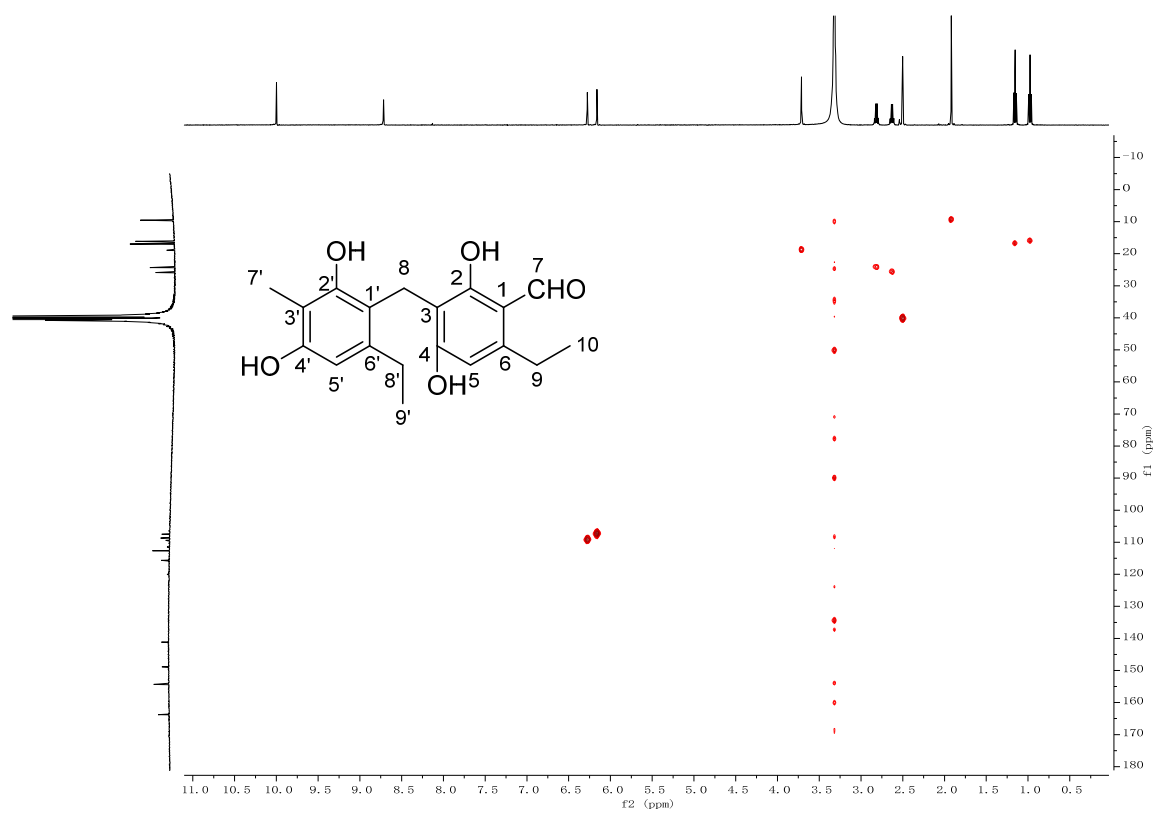
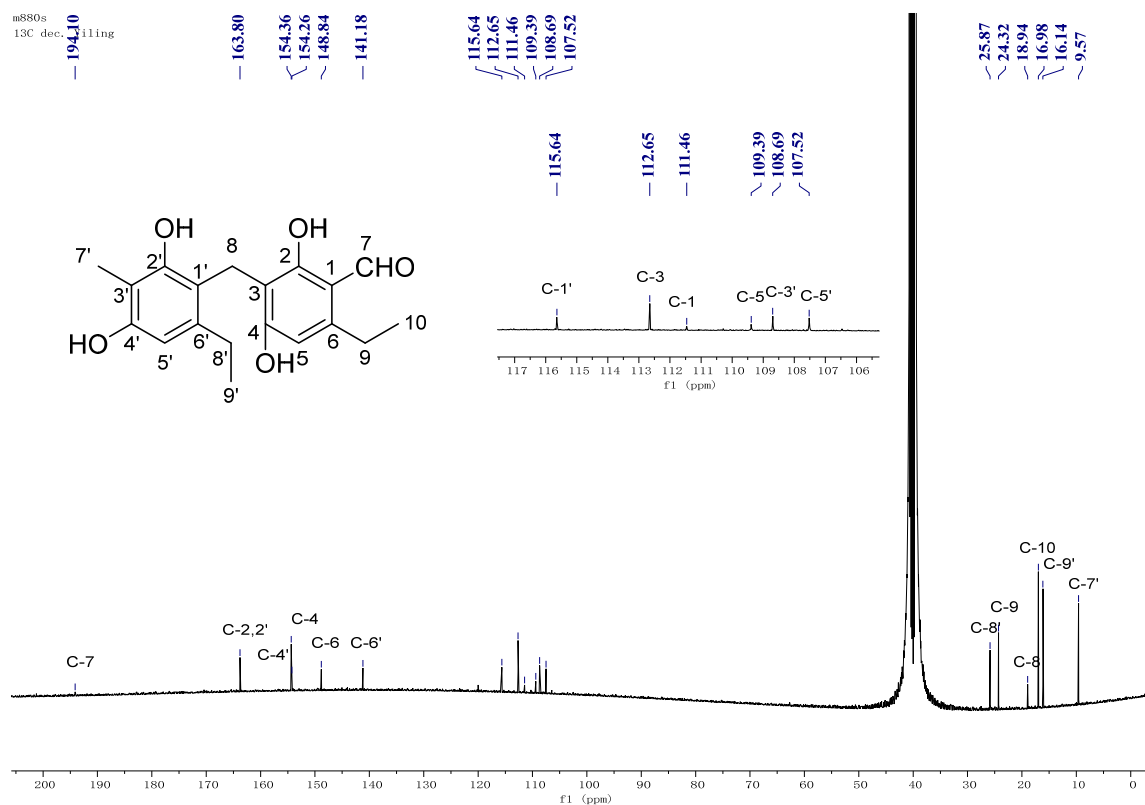


Figure S33. ¹H NMR spectrum of compound 7 in DMSO-*d*₆ (500 MHz)

SUPPORTING INFORMATION



SUPPORTING INFORMATION

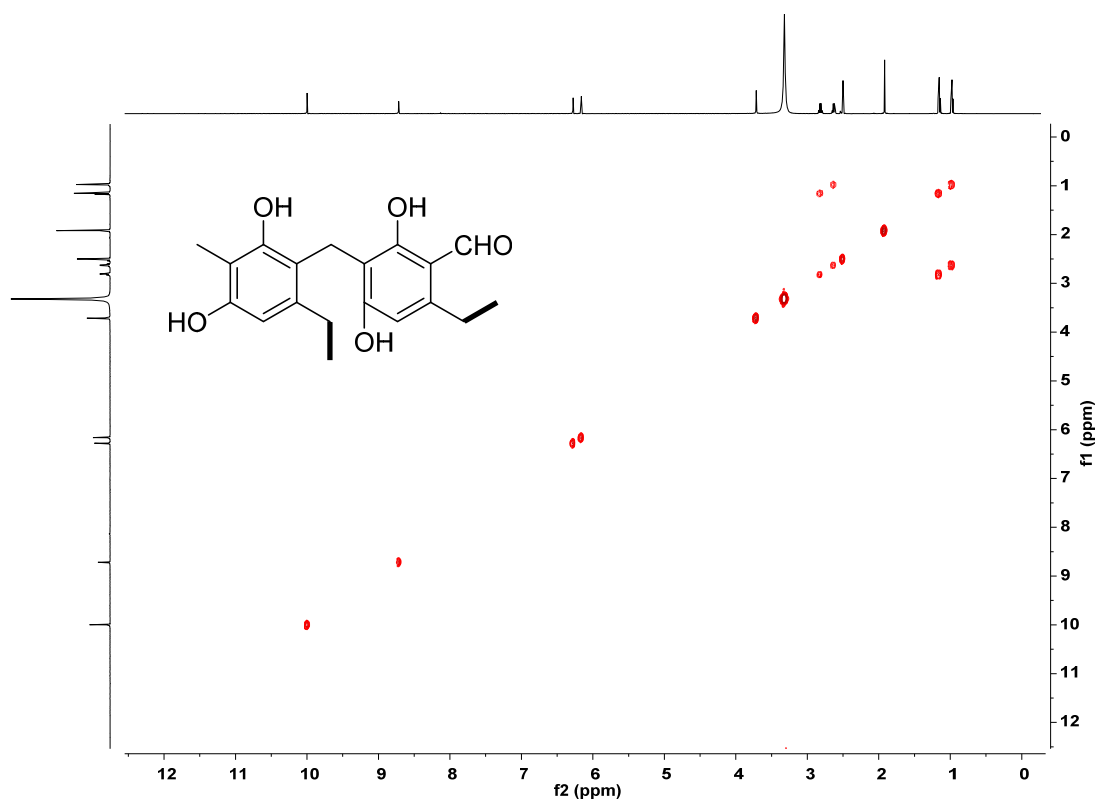


Figure S36. ^1H - ^1H COSY spectrum of compound **7** in $\text{DMSO}-d_6$

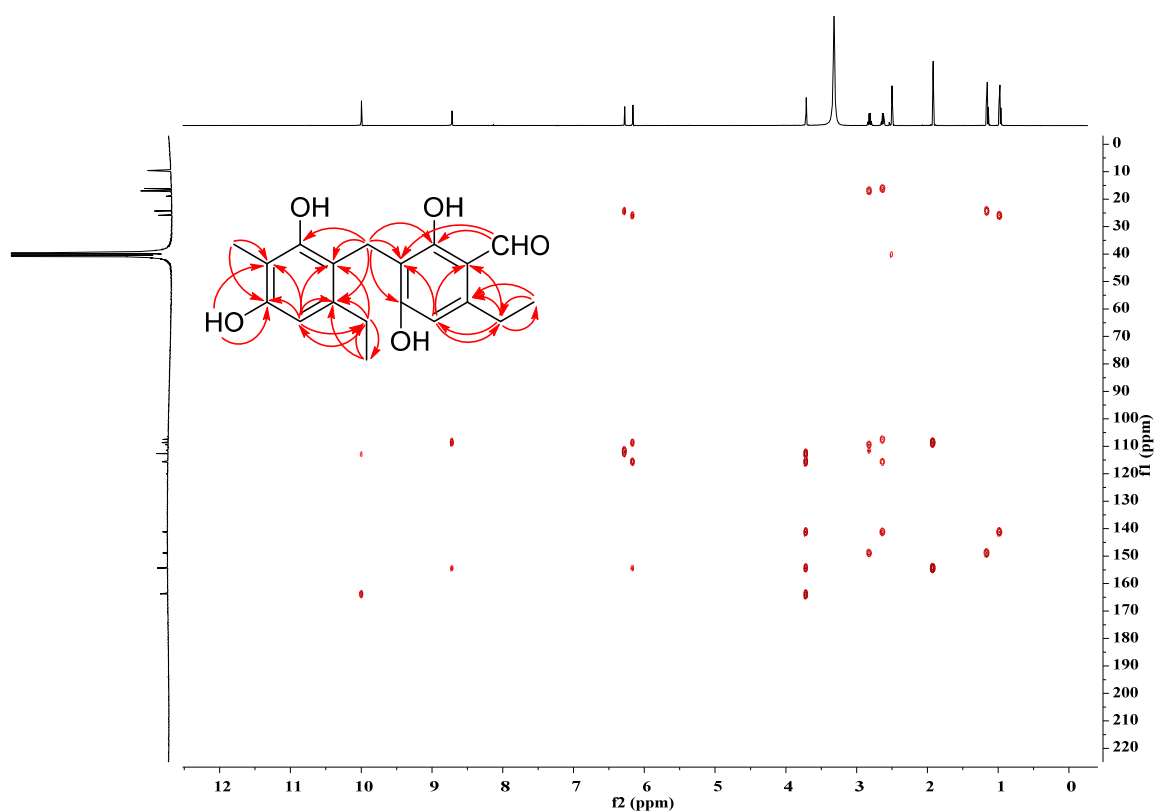
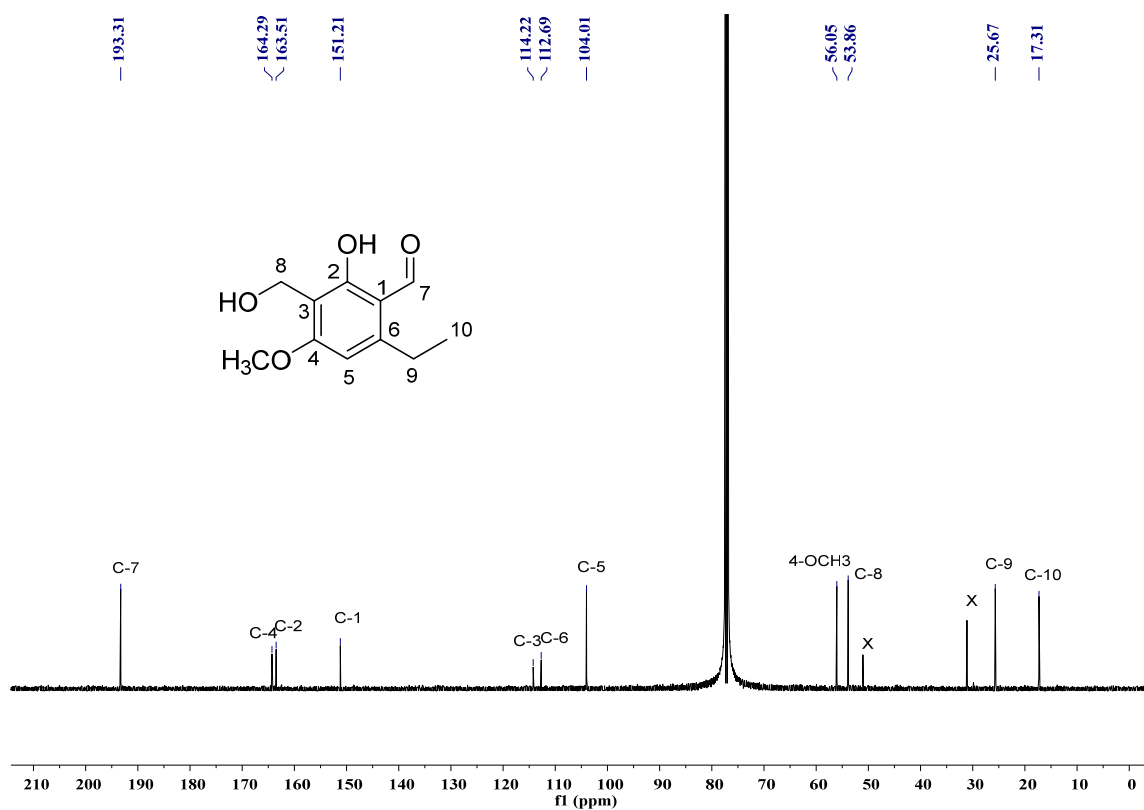
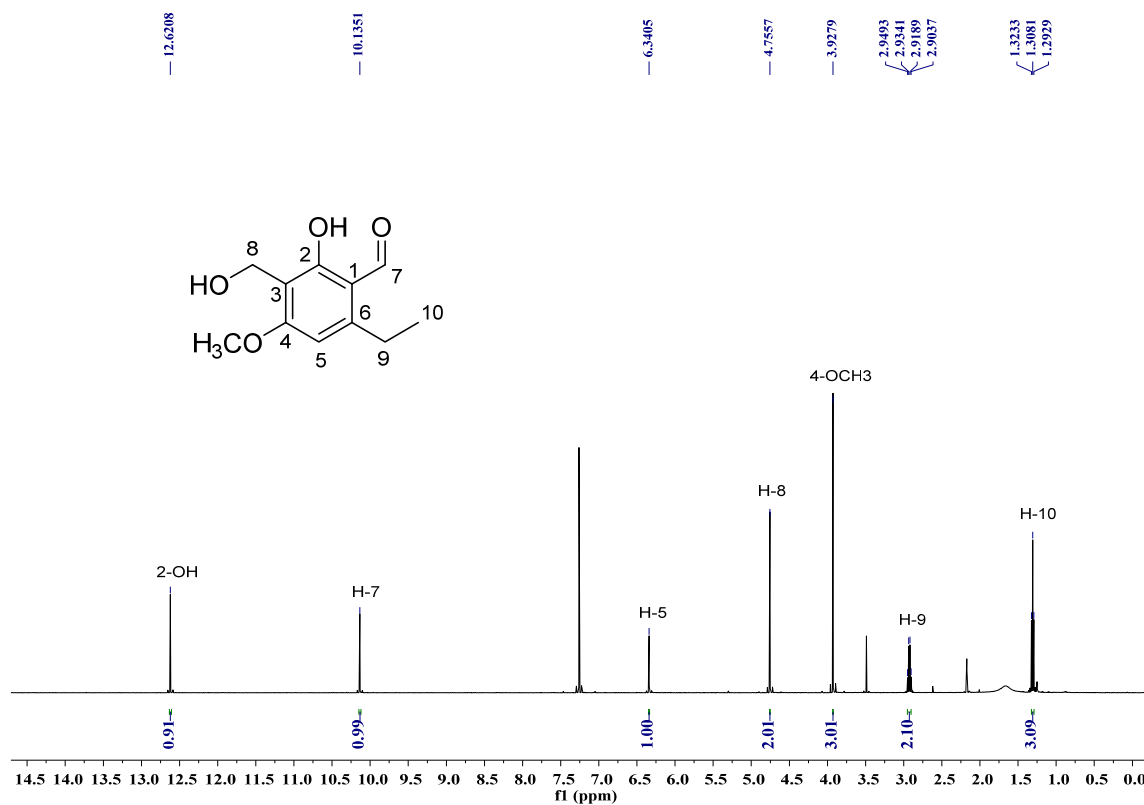


Figure S37. HMBC spectrum of compound **7** in $\text{DMSO}-d_6$

SUPPORTING INFORMATION



SUPPORTING INFORMATION

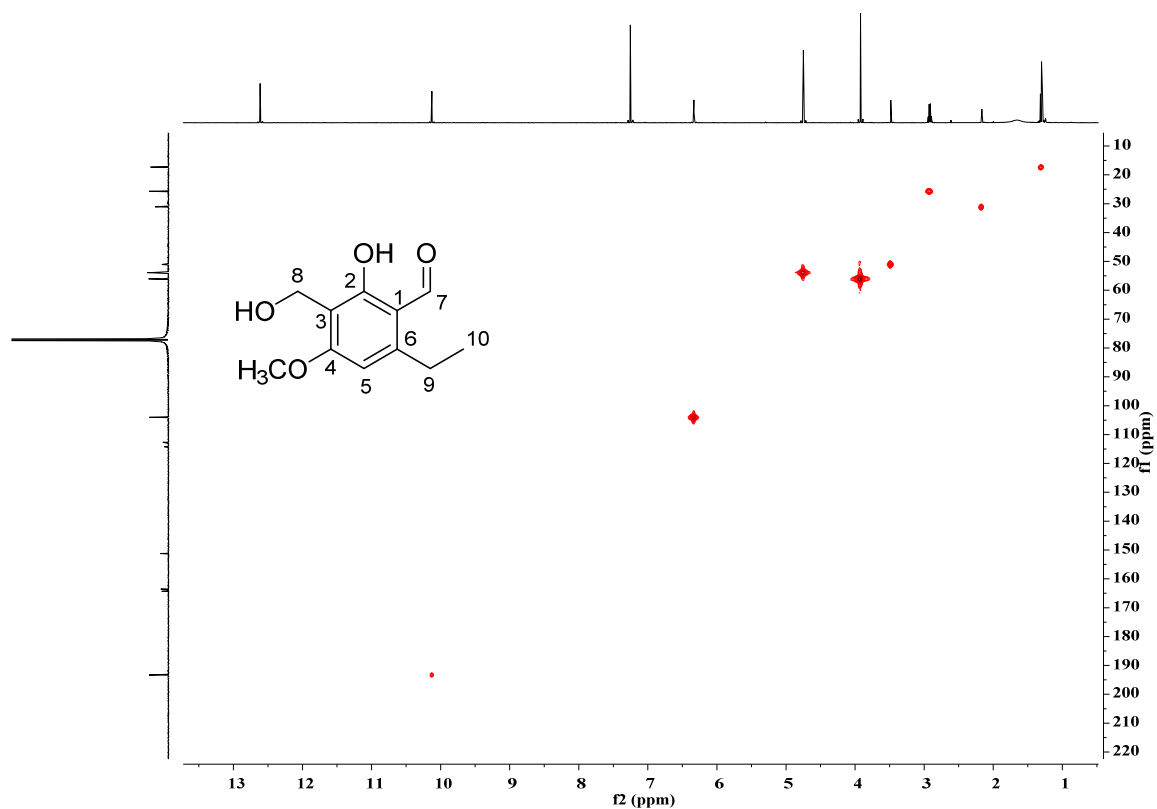


Figure S40. HSQC spectrum of compound **8** in CDCl₃

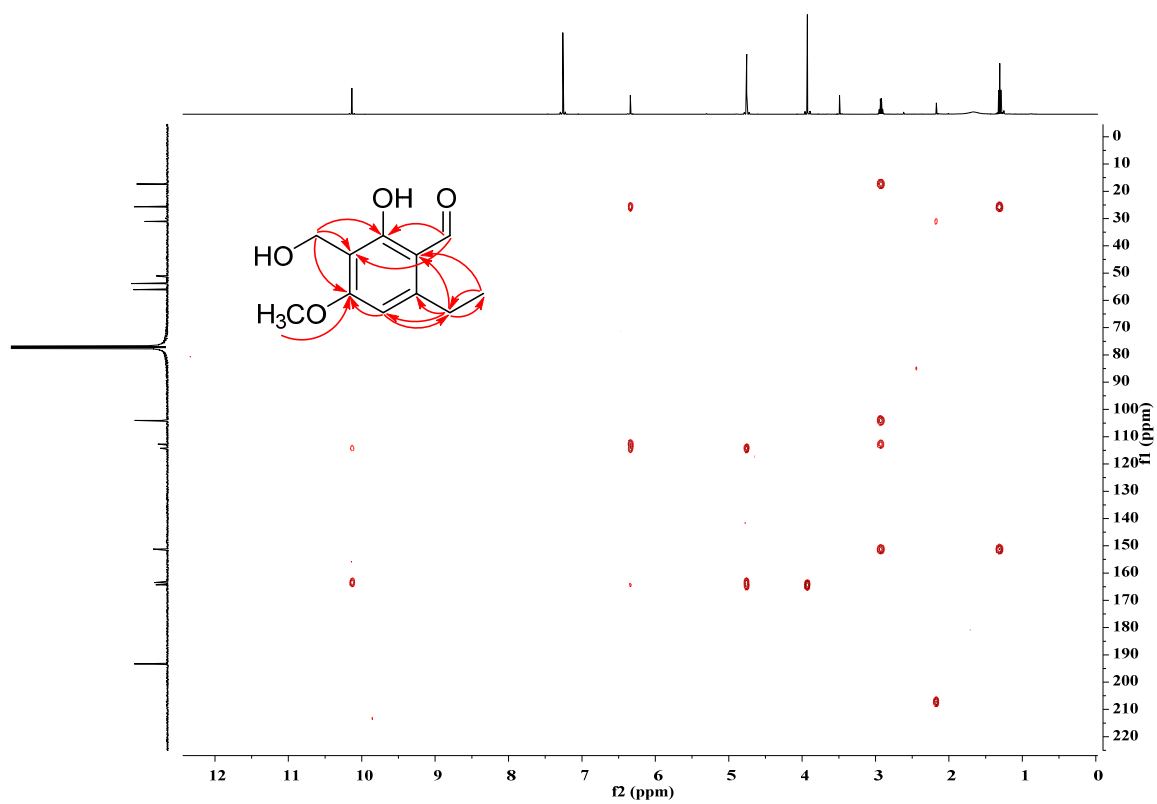
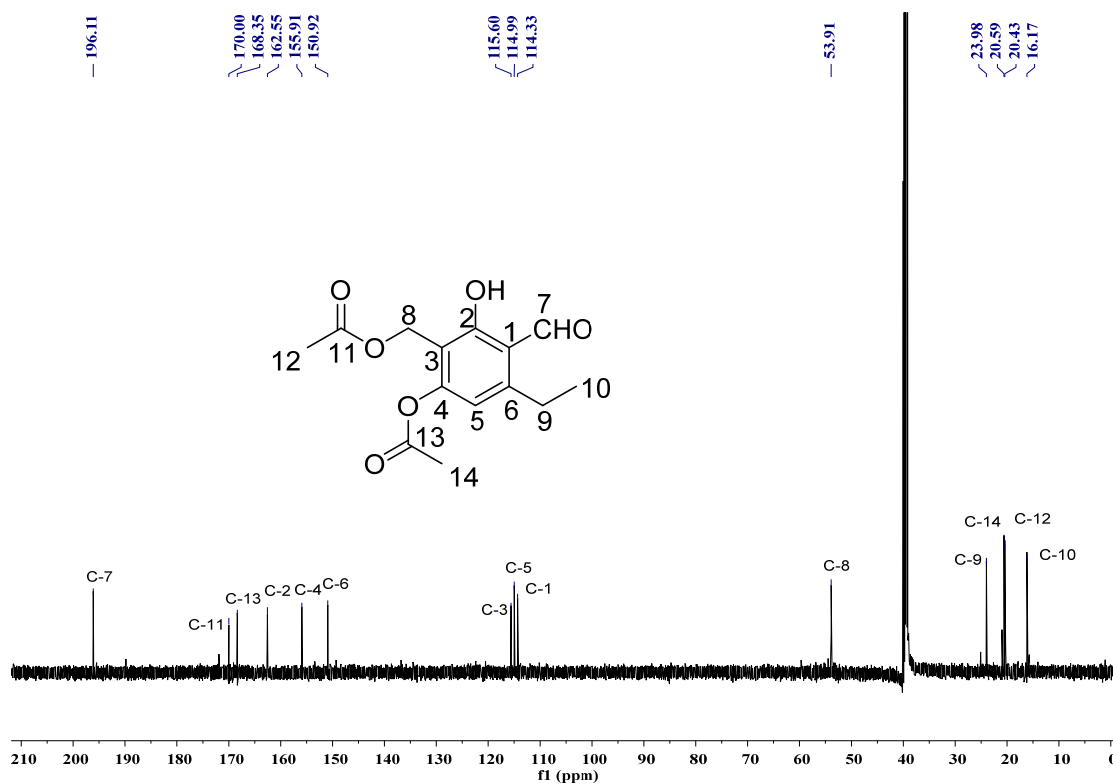
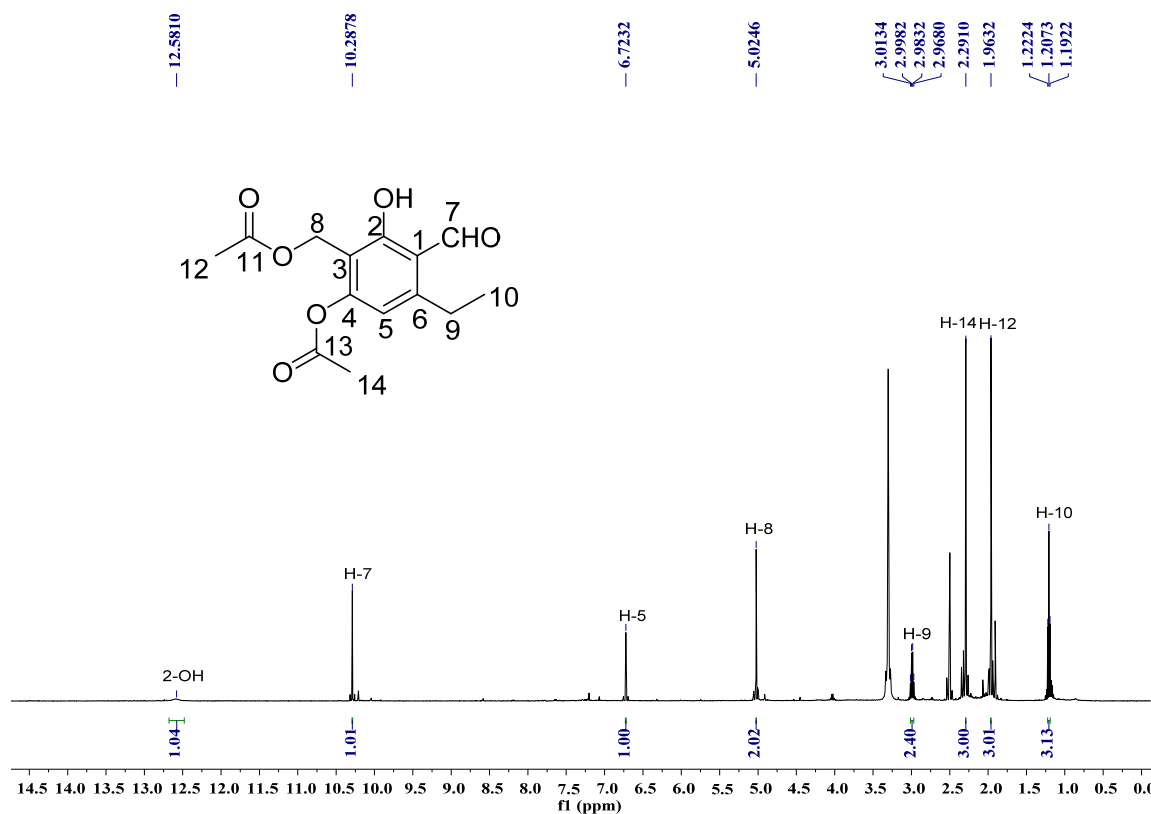


Figure S41. HMBC spectrum of compound **8** in CDCl₃

SUPPORTING INFORMATION



SUPPORTING INFORMATION

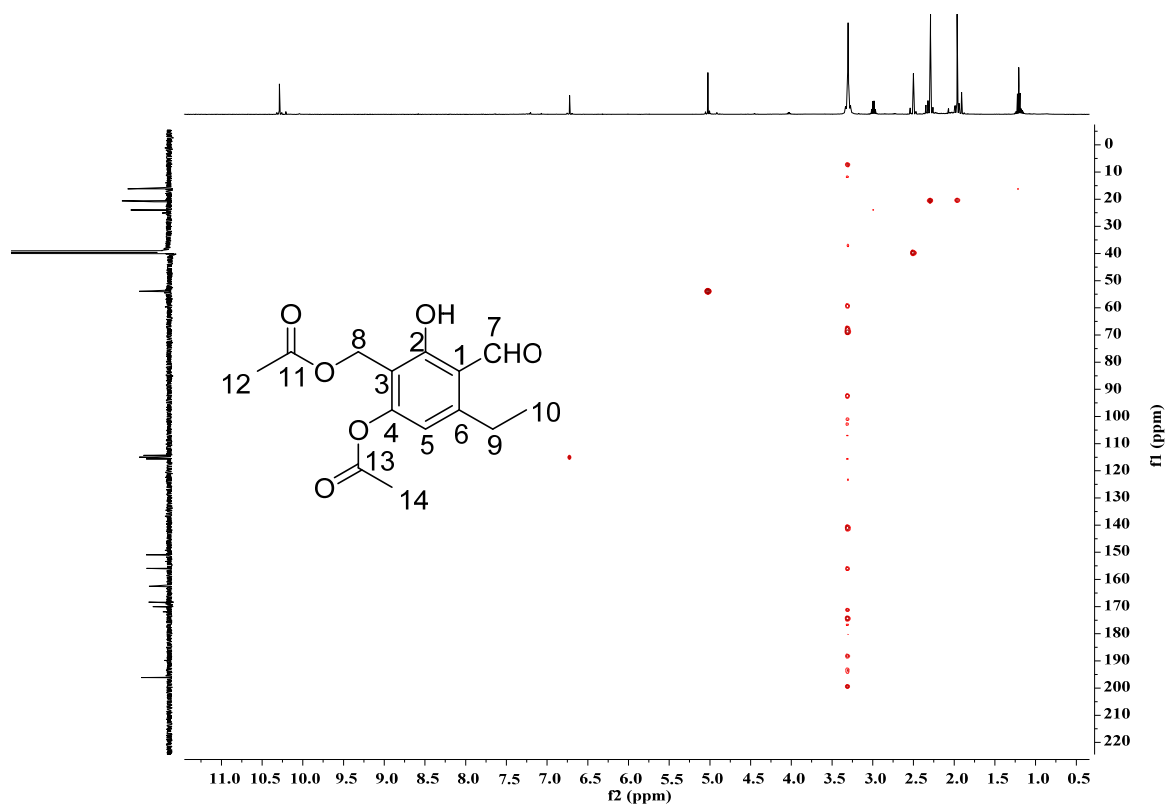


Figure S44. HSQC spectrum of compound **10** in DMSO- d_6

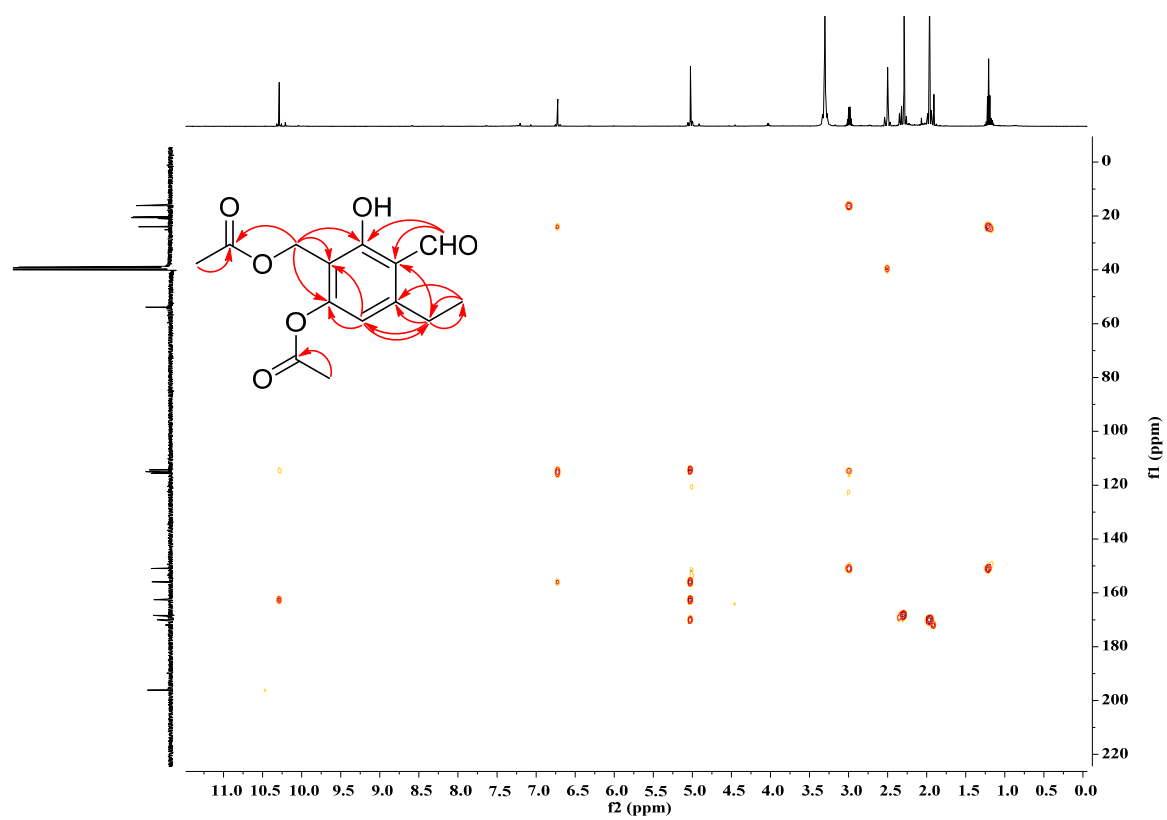


Figure S45. HMBC spectrum of compound **10** in DMSO- d_6

References

- (1) Weber, T.; Charusanti, P.; Musiol-Kroll, E. M.; Jiang, X.; Tong, Y.; Kim, H. U.; Lee, S. Y. Metabolic engineering of antibiotic factories: new tools for antibiotic production in actinomycetes. *Trends Biotechnol.* **2015**, *33*, 15.
- (2) Waterhouse, A.; Bertoni, M.; Bienert, S.; Studer, G.; Tauriello, G.; Gumienny, R.; Heer, F. T.; de Beer, T. A. P.; Rempfer, C.; Bordoli, L.; Lepore, R.; Schwede, T. SWISS-MODEL: homology modelling of protein structures and complexes. *Nucleic Acids Res.* **2018**, *46*, W296.
- (3) Emsley, P.; Lohkamp, B.; Scott, W. G.; Cowtan, K. Features and development of Coot. *Acta Crystallogr. D. Biol. Crystallogr.* **2010**, *66*, 486.
- (4) Chiang, Y. M.; Ahuja, M.; Oakley, C. E.; Entwistle, R.; Asokan, A.; Zutz, C.; Wang, C. C.; Oakley, B. R. Development of genetic dereplication strains in *Aspergillus nidulans* results in the discovery of aspercryptin. *Angew. Chem. Int. Ed. Engl.* **2016**, *55*, 1662.
- (5) Fan, J.; Liao, G.; Kindinger, F.; Ludwig-Radtke, L.; Yin, W.-B.; Li, S.-M. Peniphenone and penilactone formation in *Penicillium crustosum* via 1,4-Michael additions of *ortho*-quinone methide from hydroxyclovatol to g-butyrolactones from crustosic acid. *J. Am. Chem. Soc.* **2019**, *141*, 4225.
- (6) Mojtahedi, M. M. and Samadian, S. Efficient and rapid solvent-free acetylation of alcohols, phenols, and thiols using catalytic amounts of sodium acetate trihydrate. *J. Chem.* **2013**, *2013*, Article ID 642479.
- (7) Durrani, A. A. and Tyman, J. H. P. Long-chain phenols. Part 16. A novel synthesis of homologous orsellinic acids and their methyl ethers. *J. Chem. Soc. , Perkin Trans. 1* **1980**, 1658.
- (8) Culberson, C. F. and Culberson, W. L. β -Orcinol derivatives in lichens: Biogenetic evidence from *Oropogon loxensis*. *Experim. Mycol.* **1978**, *2*, 245.
- (9) Shao, C.; Wang, C.; Wei, M.; Jia, Z.; She, Z.; Lin, Y. Two new benzaldehyde derivatives from mangrove endophytic fungus (No. ZZF 32). *Chem. Nat. Compd.* **2009**, *45*, 779.
- (10) He, Y. and Cox, R. J. The molecular steps of citrinin biosynthesis in fungi. *Chem. Sci.* **2016**, *7*, 2119.
- (11) Hagel, J. M. and Facchini, P. J. Expanding the roles for 2-oxoglutarate-dependent oxygenases in plant metabolism. *Nat. Prod. Rep.* **2018**, *35*, 721.

4.2 Benzoyl ester formation in *Aspergillus ustus* by hijacking the polyketide acyl intermediates with alcohols.



Benzoyl ester formation in *Aspergillus ustus* by hijacking the polyketide acyl intermediates with alcohols

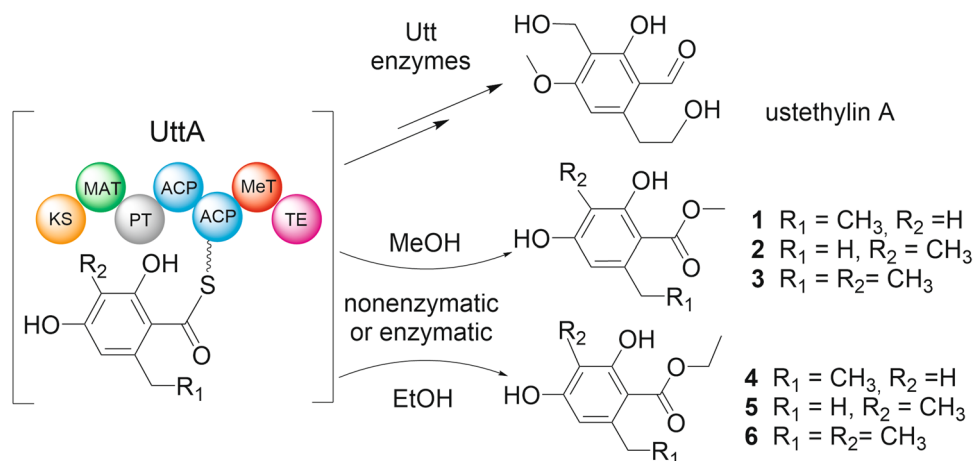
Liujuan Zheng¹ · Shu-Ming Li¹

Received: 2 December 2020 / Revised: 21 December 2020 / Accepted: 4 January 2021
© The Author(s) 2021

Abstract

Accumulation of two benzoyl esters in *Aspergillus ustus* after feeding with alcohols was reported 30 years ago. To the best of our knowledge, the biosynthesis for these esters has not been elucidated prior to this study. Here, we demonstrate that these compounds are artificial products of the phenethyl polyketide ustethylin A biosynthetic pathway. In addition, four additional benzoyl esters with different methylation levels were also isolated and identified as shunt products. Feeding experiments provided evidence that the enzyme-bound polyketide acyl intermediates are hijacked by externally fed MeOH or EtOH, leading to the formation of the benzoyl esters.

Graphic abstract



Keywords Benzoyl esters · Biosynthesis · *Aspergillus ustus* · Alcohols feeding · Polyketides

Communicated by Erko Stackebrandt.

Supplementary Information The online version contains supplementary material available at <https://doi.org/10.1007/s00203-021-02182-0>.

✉ Shu-Ming Li
shuming.li@staff.uni-marburg.de

¹ Institut für Pharmazeutische Biologie und Biotechnologie, Fachbereich Pharmazie, Philipps-Universität Marburg, Robert-Koch Straße 4, 35037 Marburg, Germany

Introduction

Secondary metabolites play an important role in ecological fitness of microorganisms, such as for protection from UV damage, toxic natural products and other microorganisms (Keller 2019). Polyketides with diverse biological and pharmacological activities are the most abundant fungal natural products (Keller et al. 2005; Ran and Li 2020). These compounds are biosynthesized by the well-studied multidomain proteins—polyketide synthases (PKSs). Based on the reduction status of their products, fungal PKSs can basically be

divided into three class: nonreducing, partially reducing and highly reducing PKSs (Cox 2007). The typical nonreducing PKSs contain starter unit ACP transacylase (SAT), ketosynthase (KS), malonyl-CoA-ACP transacylase (MAT), product template (PT), acyl-carrier protein (ACP) and thioesterase (TE) domains (Crawford and Townsend 2010).

A study in 1987 reported the accumulation of 2,4-dihydroxy-3-methyl-6-ethyl benzoyl methyl and ethyl ester after feeding an *Aspergillus ustus* culture with MeOH and EtOH, respectively. Isotope incorporation was observed for both methyl groups of the aryl acid after feeding with [methyl- ^{13}C]-L-methionine, indicating their origin from methylation. Isotope labeling experiments also proved that other carbons are derived from acetate (De Jesus et al. 1987). However, no further biosynthetic studies have been reported for these compounds.

Phenethyl-containing compounds are common microbial metabolites. In fungi, the ethyl groups in phenethyl residue are derived from *S*-adenosyl L-methionine and usually catalyzed by the methyltransferase domain of polyketide synthase (Zheng et al. 2020). Recently, we elucidated the first biosynthetic pathway of fungal phenethyl derivatives, i.e., that of ustethylin A in *A. ustus* 3.3904 (Zheng et al. 2020), a rare human pathogen fungus (Pi et al. 2015). In this pathway, the nonreducing PKS UttA is responsible for the formation of the key intermediate phenethyl benzoic acid. After reduction of the aryl carboxyl group to aldehyde by the NRPS-like enzyme UttJ, the methyl and ethyl groups are oxidized by the nonheme Fe^{II} /2-oxoglutarate-dependent oxygenase UttH and the

cytochrome P_{450} enzyme UttC, respectively. Phenolic methylation is catalyzed by the methyltransferase UttF (Scheme 1). The final pathway product ustethylin A was detected as the predominantly accumulated metabolite (Fig. 1a).

Materials and methods

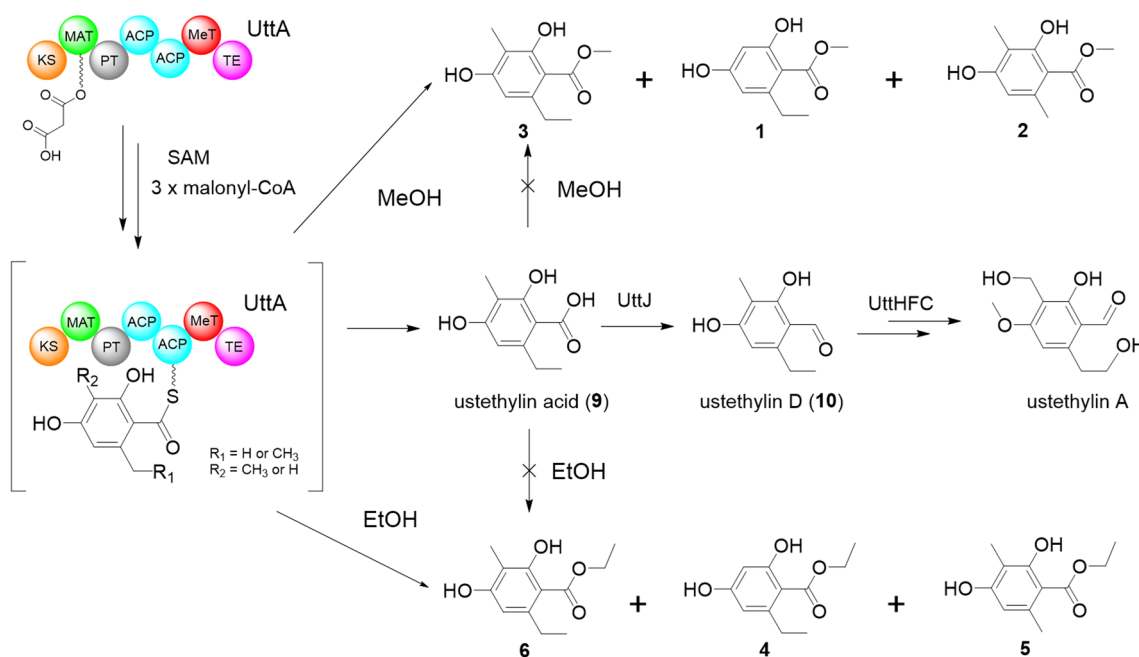
Strains, media and growth conditions

Aspergillus ustus 3.3904 was purchased from China General Microbiological Culture Collection Center (Beijing, China) and cultivated in PDB (potato dextrose broth, Sigma) medium at 230 rpm and 30 °C for secondary metabolite production. Construction of the *A. ustus* ΔuttA mutant has been reported previously (Zheng et al. 2020).

Alcoholic feeding experiments

1.5 mL (3%, v/v) of MeOH, EtOH or CD_3OD were added into the three day-old *A. ustus* cultures in 250 mL flask containing 50 mL PDB medium, which were further maintained at 230 rpm and 30 °C for five days. 1 mL culture was extracted with EtOAc for LC-MS analysis.

For large-scale fermentation, 15 mL of MeOH or EtOH were added to 500 mL PDB medium in 2 L flask and cultivated under the same condition as mentioned above.



Scheme 1. Simplified biosynthetic pathway of ustethylin A with 1–6 as shunt products after alcoholic feeding

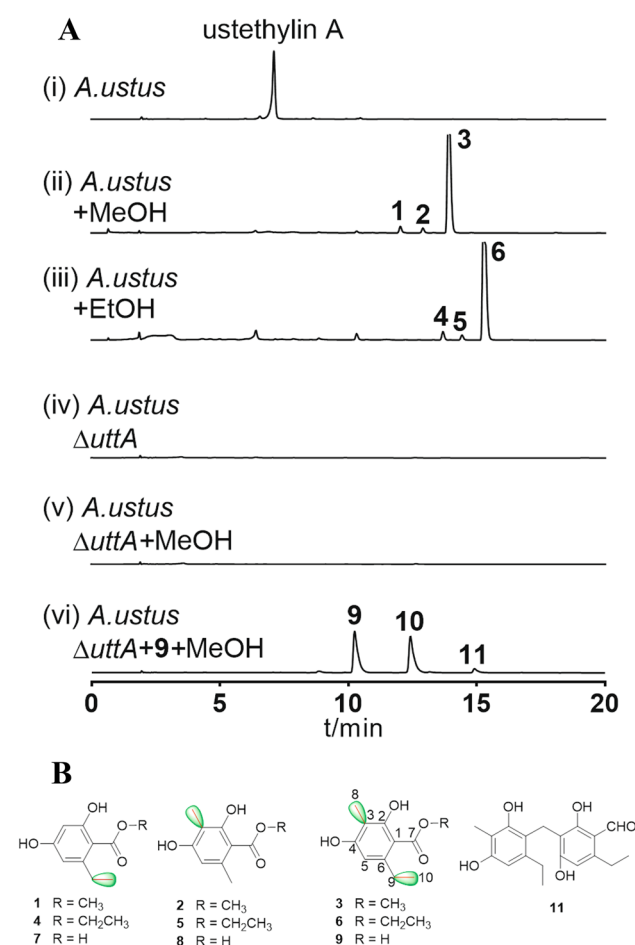


Fig. 1 **a** HPLC analysis of the *A. ustus* extracts. UV detection was carried on a photodiode array detector and absorptions at 254 nm are illustrated. **b** Structures of 1–9 and 11

Precursor feeding in Δ uttA mutant

Compound 9 was dissolved in MeOH at a concentration of 18 mg/mL. 277 μ L (5 mg) of this solution were added into the culture of the *A. ustus* Δ uttA mutant in 250 mL flask containing 50 mL PDB medium after fermentation at 230 rpm and 30 °C for three days. Two days later, 1 mL culture was extracted with EtOAc for LC–MS analysis.

HPLC analysis and isolation

Extracts were analyzed on an Agilent HPLC series 1200 (Agilent Technologies) equipped with an Agilent Eclipse XDB-C18 column (5 μ m, 4.6 \times 150 mm). A linear gradient from 10 to 90% ACN in H₂O in 20 min was used. The column was then washed with 100% ACN for 5 min and equilibrated with 10% ACN in H₂O for another 5 min. Detection was carried out on a photodiode array detector and absorptions at 254 nm are illustrated in this study.

A semi-preparative Multospher 120 RP-18 column (5 μ m, 10 \times 250 mm) was used for isolation of the products for structural elucidation on the same HPLC system with the same solvents at a flow rate of 2 mL/min. Separation was done by isocratic elution with 25–70% ACN for 10–20 min.

Large-scale fermentation, extraction and isolation of secondary metabolites

For isolation of compounds 1–3, large-scale fermentation of *A. ustus* 3.3904 with MeOH was carried out as described above. The supernatant was separated from mycelia by filtration and extracted with equal volume of EtOAc for three times. The mycelia were extracted with acetone and concentrated under reduced pressure to afford an aqueous solution and then extracted with EtOAc for three times. Both EtOAc extracts were evaporated under reduced pressure to afford the crude extracts for further purification. The crude extract was separated on a silica gel column with CHCl₃/MeOH (100:0–0:100) as elution solvents to give 8 fractions. Fraction 2 was purified on a semi-preparative HPLC (ACN/H₂O), leading to 8.0 mg of 1, 8.0 mg of 2 and 60.0 mg of 3. Similar procedure was used for product isolation after EtOH feeding. 6.5 mg of 4, 5.2 mg of 5 and 30.0 mg of 6 were obtained in high purity.

LC–MS and MS analysis

Extracts were also analyzed on an Agilent HPLC 1260 series system equipped with a Bruker microTOF QIII mass spectrometer using an Agilent Eclipse XDB C18 column (5 μ m, 4.6 \times 150 mm). Separation was performed at a flow rate of 0.5 mL/min with a 40 min linear gradient from 5 to 100% ACN in H₂O, both containing 0.1% (v/v) HCOOH. The column was then washed with 100% ACN for 5 min and equilibrated for 5 min with 5% ACN in H₂O. The parameters of the spectrometer were set as the following: electrospray positive ion mode for ionization, capillary voltage with 4.5 kV, collision energy with 8.0 eV. Sodium formate was used in each run for mass calibration. The masses were scanned in the range of m/z 100–1500. Data were evaluated with the Compass DataAnalysis 4.2 software (Bruker Daltonik, Bremen, Germany).

NMR analysis

NMR spectra of the isolated products were recorded at room temperature on a JEOL ECA-500 (JEOL, Akishima, Tokyo, Japan). The samples were dissolved in CDCl₃ or CD₃OD. All spectra were processed with MestReNov.9.0.0 (Mestrelab Research, Santiago de Compostella, Spain).

Physiochemical properties of the compounds described in this study

1: white needle crystal; ^1H NMR data see Table S1; HRMS (ESI) m/z : $[\text{M} + \text{H}]^+$ calcd. for $\text{C}_{10}\text{H}_{13}\text{O}_4$ 197.0808; found 197.0756.

2: white needle crystal; ^1H NMR data see Table S1; HRMS (ESI) m/z : $[\text{M} + \text{H}]^+$ calcd. for $\text{C}_{10}\text{H}_{13}\text{O}_4$ 197.0808; found 197.0755.

3: white bulk crystal; ^1H NMR data see Table S1, ^{13}C NMR data see Table S2; HRMS (ESI) m/z : $[\text{M} + \text{H}]^+$ calcd. for $\text{C}_{11}\text{H}_{15}\text{O}_4$ 211.0965; found 211.0916.

4: white needle crystal; ^1H NMR data see Table S1; HRMS (ESI) m/z : $[\text{M} + \text{H}]^+$ calcd. for $\text{C}_{11}\text{H}_{15}\text{O}_4$ 211.0965; found 211.0964.

5: white needle crystal; ^1H NMR data see Table S1; HRMS (ESI) m/z : $[\text{M} + \text{H}]^+$ calcd. for $\text{C}_{11}\text{H}_{15}\text{O}_4$ 211.0965; found 211.0960.

6: white bulk crystal; ^1H NMR data see Table S1; HRMS (ESI) m/z : $[\text{M} + \text{H}]^+$ calcd. for $\text{C}_{12}\text{H}_{17}\text{O}_4$ 225.1121; found 225.1119.

Structural elucidation

The structures of the isolated products were elucidated by interpretation of their MS and NMR spectra (Figures S1–S9) and by comparison of these data with those described in the literature. **1** (Sher and Langer 2008), **2** (Schleich et al. 2006)

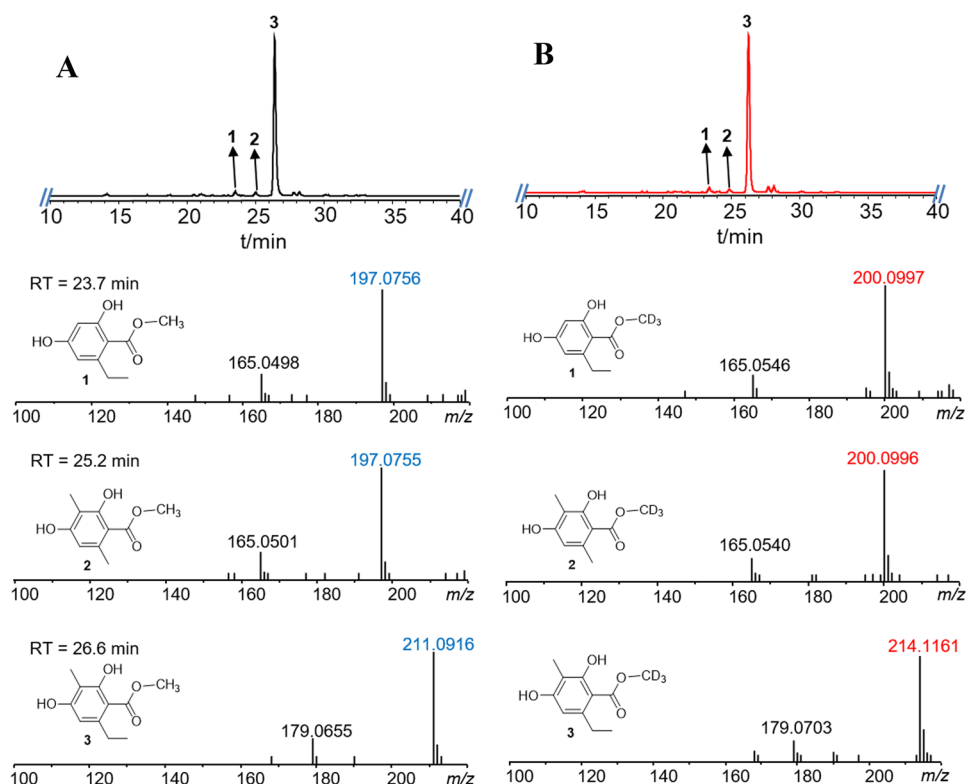
3 (De Jesus et al. 1987), **4** (Schleich et al. 2006), **5** (Sher and Langer 2008) and **6** (De Jesus et al. 1987) were identified as known compounds.

Results and discussion

The aryl acids involved in the biosynthesis of ustethylins are the acyl components of the previously identified esters (De Jesus et al. 1987) (Fig. 1b). We speculated therefore that they are also derived from the ustethylin pathway. To prove our hypothesis, we repeated the feeding experiments with alcohols using three day-old cultures of *A. ustus* 3.3904 wild-type and an *uttA* deficient mutant in PDB medium. As shown in Fig. 1a, HPLC analysis of the EtOAc extract of the wild-type revealed the presence of ustethylin A as the predominant metabolite (Fig. 1a), as reported previously (Zheng et al. 2020). In the extract of the culture with externally fed MeOH and EtOH, three metabolites each **1–3** and **4–6** were detected, respectively. **3** as a major peak was accompanied by two minor ones **1** and **2** in the culture with MeOH. LC–MS analysis revealed that **3** has an additional methyl group than **1** and **2** (Fig. 2a). It is noteworthy that compounds **1**, **2**, **4** and **5** were not reported in the previous study (De Jesus et al. 1987).

For structural elucidation, **1–3** were isolated from a 2 L *A. ustus* culture after feeding with 60 mL MeOH. Comparison of the NMR data of the isolated products (Tables

Fig. 2 LC–MS results (positive mode) of *A. ustus* extracts after feeding with MeOH (**a**) and CD_3OD (**b**). UV absorptions at 254 nm are illustrated



S1 and S2, Figures S1–S6) with those described in the literature confirmed **3** to be 2,4-dihydroxy-3-methyl-6-ethyl benzoyl methyl ester (De Jesus et al. 1987). NMR analysis also proved that **1** and **2** are two congeners of **3** lacking the C3-methyl group and replacing the C6-ethyl by a methyl group, respectively (Fig. 1b) (De Jesus et al. 1987; Schleich et al. 2006; Sher and Langer 2008). In analogy, the major peak **6** and the two minor ones **4** and **5** were also isolated from the culture fed with EtOH and identified as ethyl esters of the corresponding aryl acids (De Jesus et al. 1987; Schleich et al. 2006; Sher and Langer 2008) (Fig. 1b, Table S1, Figures S7–S9).

The isotopic feeding experiments in the previous study proved that the *O*-methyl group in compound **3** is not derived from methionine (De Jesus et al. 1987). The *O*-methyl groups in **1–3** originate likely from MeOH. To confirm this, CD₃OD was fed into the *Aspergillus ustus* culture and the EtOAc extract was analyzed via HPLC–MS. Detection of [M + H]⁺ ion of **3** at *m/z* 214.1161 after feeding with CD₃OD, 3 Daltons larger than that after feeding with MeOH at *m/z* 211.0916 (Fig. 2), proved the incorporation of the CD₃ group into the structure of **3**. Similar MS pattern changes were also observed for compounds **1** and **2** (Fig. 2).

As reported previously (Zheng et al. 2020), the PKS UttA from the ustethylin biosynthetic pathway is responsible for the formation of the aryl acids **7–9** (Fig. 1b), the acyl moieties of **1–3** and **4–6**. To prove its function, *uttA* was replaced with a hygromycin B resistance cassette in our former study (Zheng et al. 2020). HPLC analysis of the culture extract of the Δ *uttA* mutant revealed the abolishment of ustethylin A production. Feeding this Δ *uttA* mutant with MeOH did not lead to an accumulation of **1–3** (Fig. 1a). Similar results were also observed after feeding the Δ *uttA* mutant with EtOH (data not shown). This proved unequivocally the involvement of UttA in the formation of **1–6**.

To figure out whether the ester formation is from free acids in *A. ustus*, **9** in MeOH was fed to the culture of Δ *uttA* mutant. As shown in Fig. 1a, no trace of **3** was detected. Instead, **9** was converted to the corresponding benzaldehyde **10** (ustethylin D) and a dimeric metabolite **11**, as described previously (Zheng et al. 2020). In addition, **3** was not detected after incubation of **9** with MeOH at 37 °C for 16 h (data not shown). These results indicated that the ester formation in **1–6** requires activation of the acidic precursors.

In the previous study, we proposed that the PKS UttA utilizes malonyl-CoA as both starter and extension unit. Two methylation steps, at C-3 of the benzene ring and the C6-methyl group, are involved in the formation of the aryl acyl-ACP molecules (Scheme 1), which are then released as free aryl acids and modified by tailoring enzymes. Our results in this study provide evidence that after the phenyl ring formation catalyzed by UttA, the acyl-ACP molecules can be hijacked by alcohols for ester formation, as depicted

in Scheme 1. The formation of the minor products **1** and **2** after feeding with MeOH as well as **4** and **5** after feeding with EtOH confirmed the incomplete methylation steps by UttA, as observed in the previous study (Zheng et al. 2020). In vivo assays in our aforementioned study verified that reduction of the acid **9** to the benzaldehyde **10** by the NRPS-like enzyme UttJ is a prerequisite for further modification (Zheng et al. 2020). Therefore, the esters **1–6** cannot be further metabolized by the tailoring enzymes of the Utt pathway and were accumulated as artificial products.

Feeding *n*-PrOH to the culture of *A. ustus* wild-type led to the detection of trace amount of the corresponding ester by HPLC–MS analysis, which could not be isolated in substantial amount for structural identification. No ester formation was observed after feeding with *i*-PrOH or *n*-BuOH (data not shown). These results indicated that the ester formation is preferred for small alcohols. Ester bonds are commonly present in natural products and are usually formed during chain release in the polyketide (Wang et al. 2009) or nonribosomal peptide biosynthesis and by Baeyer–Villiger monooxygenases (Tsakos et al. 2015). However, spontaneous ester formation has also been described for carboxylic acids by incubation in alcoholic solvents at room temperature (Fan et al. 2020). Therefore, it cannot be concluded whether the formation of **1–6** is an enzymatic or nonenzymatic event (Scheme 1).

Conclusions

In conclusion, we demonstrated in this study that the aryl acyl esters from *A. ustus* 3.3904 are shunt products of the ustethylin biosynthetic pathway as response for the externally fed alcohols. It will be interesting to investigate the physiological relevance of this response.

Acknowledgements We thank Rixa Kraut, Lena Ludwig-Radtke and Stefan Newel for taking MS and NMR spectra. This project was financially funded in part by the Deutsche Forschungsgemeinschaft (DFG, INST 160/620-1). Liujuan Zheng (201604910536) is scholarship recipient from the China Scholarship Council.

Funding Open Access funding enabled and organized by Projekt DEAL.

Compliance with ethical standards

Conflict of interest There are no conflicts to declare.

Open Access This article is licensed under a Creative Commons Attribution 4.0 International License, which permits use, sharing, adaptation, distribution and reproduction in any medium or format, as long as you give appropriate credit to the original author(s) and the source, provide a link to the Creative Commons licence, and indicate if changes were made. The images or other third party material in this article are

included in the article's Creative Commons licence, unless indicated otherwise in a credit line to the material. If material is not included in the article's Creative Commons licence and your intended use is not permitted by statutory regulation or exceeds the permitted use, you will need to obtain permission directly from the copyright holder. To view a copy of this licence, visit <http://creativecommons.org/licenses/by/4.0/>.

References

- Cox RJ (2007) Polyketides, proteins and genes in fungi: programmed nano-machines begin to reveal their secrets. *Org Biomol Chem* 5:2010–2026
- Crawford JM, Townsend CA (2010) New insights into the formation of fungal aromatic polyketides. *Nat Rev Microbiol* 8:879–889
- De Jesus AE, Horak RM, Steyn PS, Vleggaar R (1987) Metabolites of *Aspergillus ustus*. Part 4. Stable-isotope labelling studies on the biosynthesis of the austalides. *J Chem Soc, Perkin Trans* 12253–2257
- Fan J, Liao G, Ludwig-Radtke L, Yin W-B, Li S-M (2020) Formation of terrestrial acid in *Penicillium crustosum* requires redox-assisted decarboxylation and stereoisomerization. *Org Lett* 22:88–92
- Keller NP (2019) Fungal secondary metabolism: regulation, function and drug discovery. *Nat Rev Microbiol* 17:167–180
- Keller NP, Turner G, Bennett JW (2005) Fungal secondary metabolism—from biochemistry to genomics. *Nat Rev Microbiol* 3:937–947
- Pi B, Yu D, Dai F, Song X, Zhu C, Li H, Yu Y (2015) A genomics based discovery of secondary metabolite biosynthetic gene clusters in *Aspergillus ustus*. *PLoS ONE* 10:e0116089
- Ran H, Li S-M (2021) Fungal benzene carbaldehydes: occurrence, structural diversity, activities and biosynthesis. *Nat Prod Rep*. <https://doi.org/10.1039/D0NP00026D>
- Schleich S, Papaioannou M, Baniahmad A, Matusch R (2006) Activity-guided isolation of an antiandrogenic compound of *Pygeum africanum*. *Planta Med* 72:547–551
- Sher M, Langer P (2008) Regioselective synthesis of functionalized resorcinols by cyclization of 1,3-bis(trimethylsilyloxy)-1,3-butadienes with 3,3-dimethoxypentanoyl chloride. *Synlett* 1050–1052
- Tsakos M, Schaffert ES, Clement LL, Villadsen NL, Poulsen TB (2015) Ester coupling reactions—an enduring challenge in the chemical synthesis of bioactive natural products. *Nat Prod Rep* 32:605–632
- Wang M, Zhou H, Wirz M, Tang Y, Boddy CN (2009) A thioesterase from an iterative fungal polyketide synthase shows macrocyclization and cross coupling activity and may play a role in controlling iterative cycling through product offloading. *Biochemistry* 48:6288–6290
- Zheng L, Yang Y, Wang H, Fan A, Zhang L, Li S-M (2020) Ustethylin biosynthesis implies phenethyl derivative formation in *Aspergillus ustus*. *Org Lett* 22:7837–7841

Publisher's Note Springer Nature remains neutral with regard to jurisdictional claims in published maps and institutional affiliations.

Supporting Information

Benzoyl ester formation in *Aspergillus ustus* by hijacking the polyketide acyl intermediates with alcohols

Liujuan Zheng¹ and Shu-Ming Li^{1*}

Corresponding Author: Shu-Ming Li, E-Mail: shuming.li@staff.uni-marburg.de

1. Institut für Pharmazeutische Biologie und Biotechnologie, Fachbereich Pharmazie, Philipps-Universität Marburg, Robert-Koch Straße 4, 35037 Marburg (Germany)

Table of Contents

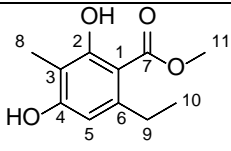
Table S1. ^1H NMR data of compounds 1 – 6 (500 MHz)	3
Table S2. ^{13}C NMR data of 3 (125 MHz in CDCl_3).....	4
Figure S1. ^1H NMR spectrum of compound 1 in CD_3OD (500 MHz).....	5
Figure S2. ^1H NMR spectrum of compound 2 in CDCl_3 (500 MHz).....	5
Figure S3. ^1H NMR spectrum of compound 3 in CDCl_3 (500 MHz).....	6
Figure S4. $^{13}\text{C}\{^1\text{H}\}$ NMR spectrum of compound 3 in CDCl_3 (125 MHz)	6
Figure S5. HSQC spectrum of compound 3 in CDCl_3	7
Figure S6. HMBC spectrum of compound 3 in CDCl_3	7
Figure S7. ^1H NMR spectrum of compound 4 in CDCl_3 (500 MHz).....	8
Figure S8. ^1H NMR spectrum of compound 5 in CDCl_3 (500 MHz).....	8
Figure S9. ^1H NMR spectrum of compound 6 in CDCl_3 (500 MHz).....	9

Table S1. ^1H NMR data of compounds **1** – **6** (500 MHz)

Compounds						
Position	δ_{H} (multi., J in Hz)	δ_{H} (multi., J in Hz)	δ_{H} (multi., J in Hz)	δ_{H} (multi., J in Hz)	δ_{H} (multi., J in Hz)	δ_{H} (multi., J in Hz)
3	6.14 (d, 2.5)	–	–	6.25 (d, 2.5)	–	–
5	6.20 (d, 2.5)	6.21 (s)	6.23 (s)	6.29 (d, 2.5)	6.20 (s)	6.22 (s)
8	2.81 (q, 7.4)	2.10 (s)	2.11 (s)	2.90 (q, 7.4)	2.10 (s)	2.10 (s)
9	1.13 (t, 7.4)	2.46 (s)	2.83 (q, 7.4)	1.19 (t, 7.4)	2.47 (s)	2.84 (q, 7.4)
10	3.87 (s)	3.92 (s)	1.15 (t, 7.4)	4.40 (q, 7.1)	4.39 (q, 7.1)	1.16 (t, 7.4)
11	–	–	3.93 (s)	1.42 (t, 7.1)	1.41 (t, 7.1)	4.40 (q, 7.1)
12	–	–	–	–	–	1.41 (t, 7.1)
2-OH	–	12.04 (s)	12.05 (s)	11.83 (s)	12.13 (s)	12.14 (s)
4-OH	–	5.15 (brs)	5.75 (brs)	5.96 (brs)	5.21 (brs)	5.73 (brs)

These data correspond well to those described in the literature: **1** (Sher and Langer 2008), **2** (Schleich et al. 2006), **3** (De Jesus et al. 1987), **4** (Schleich et al. 2006), **5** (Sher and Langer 2008) and **6** (De Jesus et al. 1987).

Table S2. ^{13}C NMR data of **3** (125 MHz in CDCl_3)

Compound	 3	
	Positions	δ_c in ppm
	1	104.6
	2	163.0
	3	108.9
	4	158.6
	5	109.3
	6	146.6
	7	172.6
	8	7.9
	9	29.7
	10	15.9
	11	52.1

These data correspond well to those reported previously (De Jesus et al. 1987).

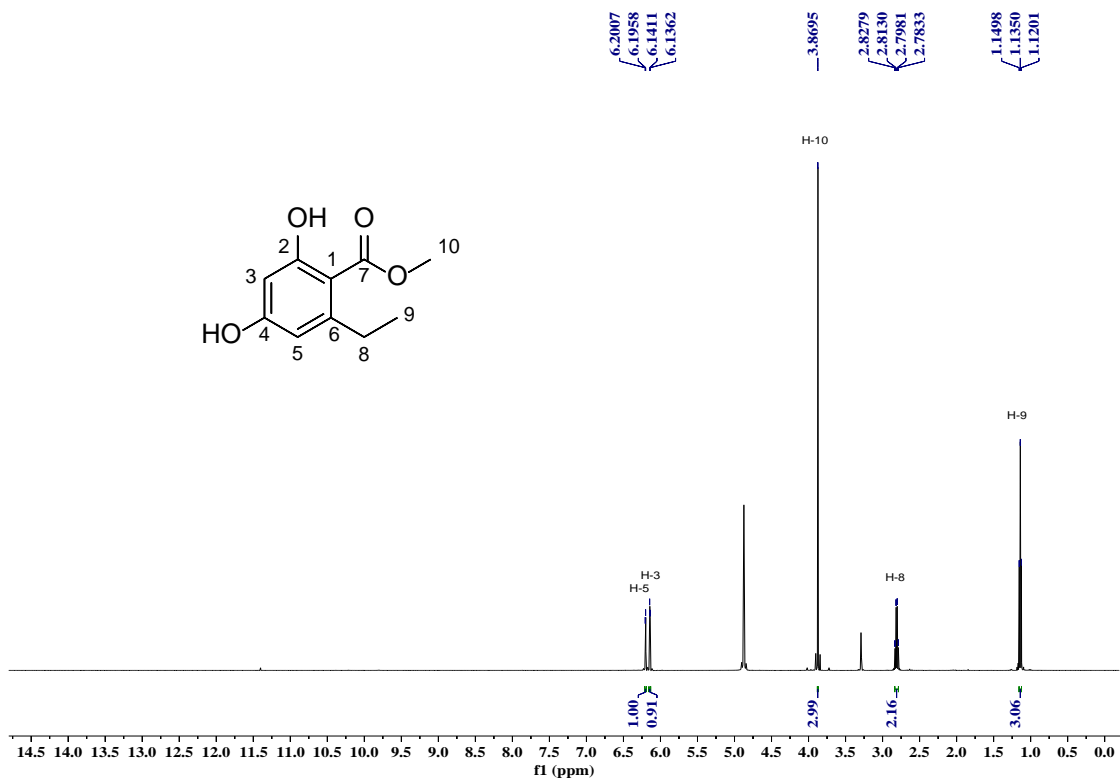


Figure S1. ¹H NMR spectrum of compound **1** in CD₃OD (500 MHz)

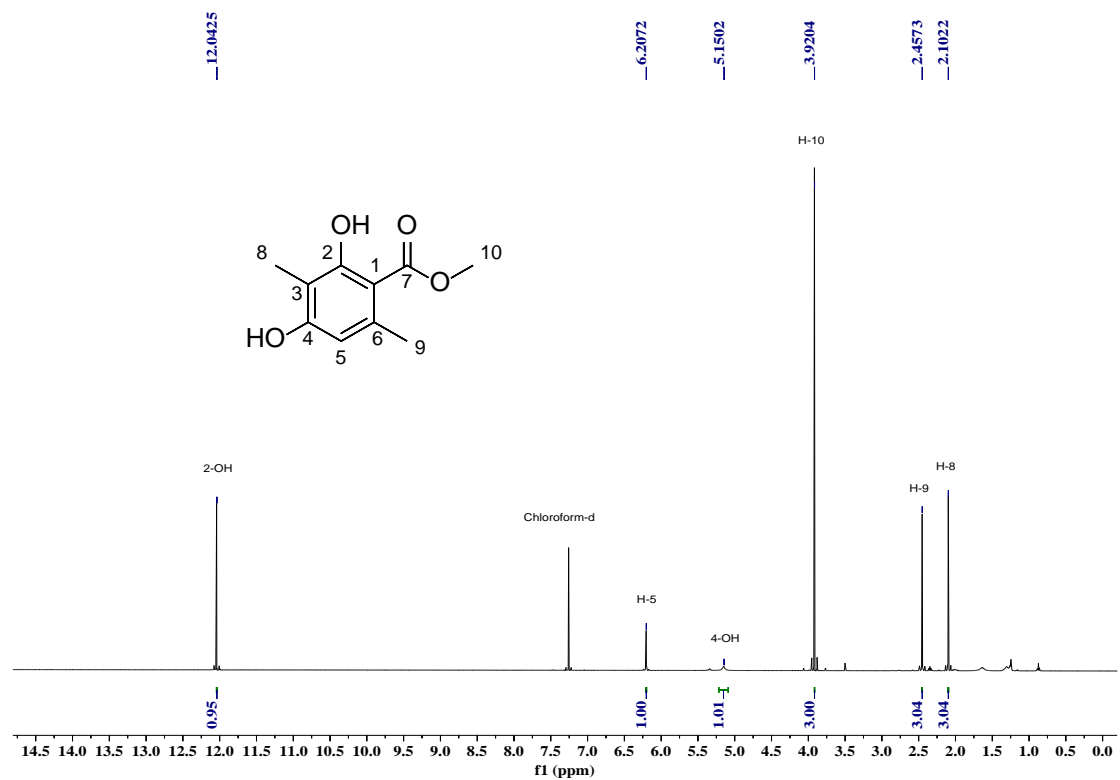


Figure S2. ¹H NMR spectrum of compound **2** in CDCl₃ (500 MHz)

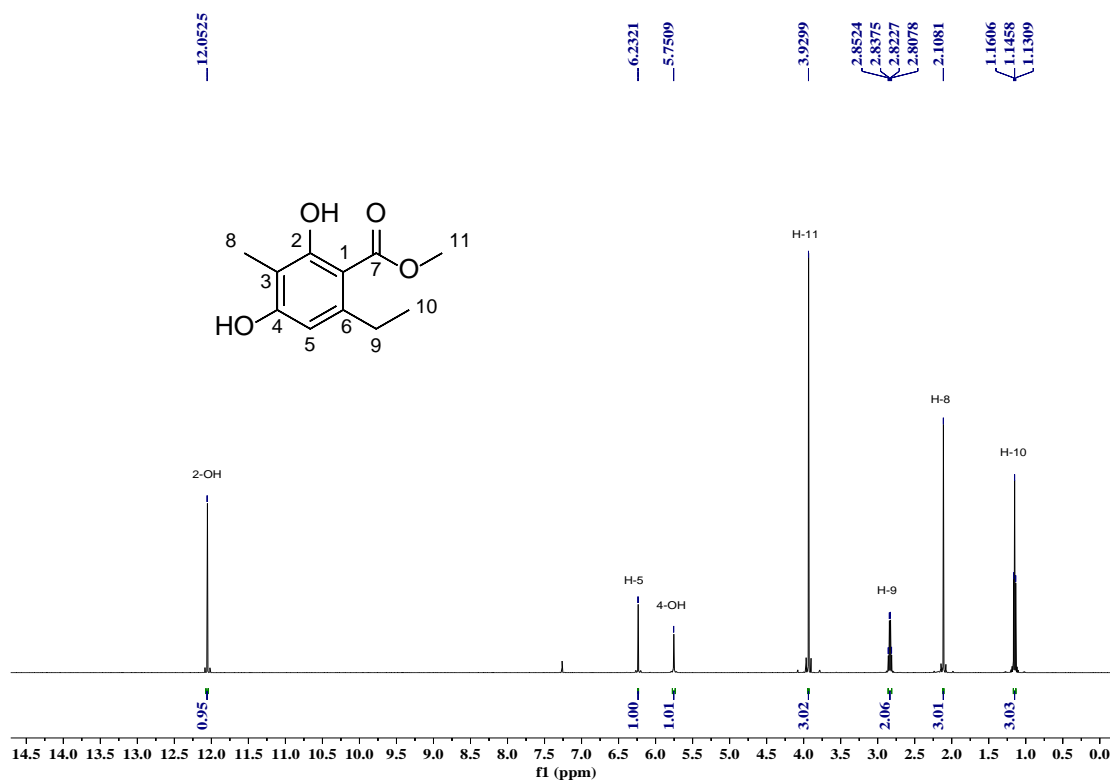


Figure S3. ¹H NMR spectrum of compound **3** in CDCl₃ (500 MHz)

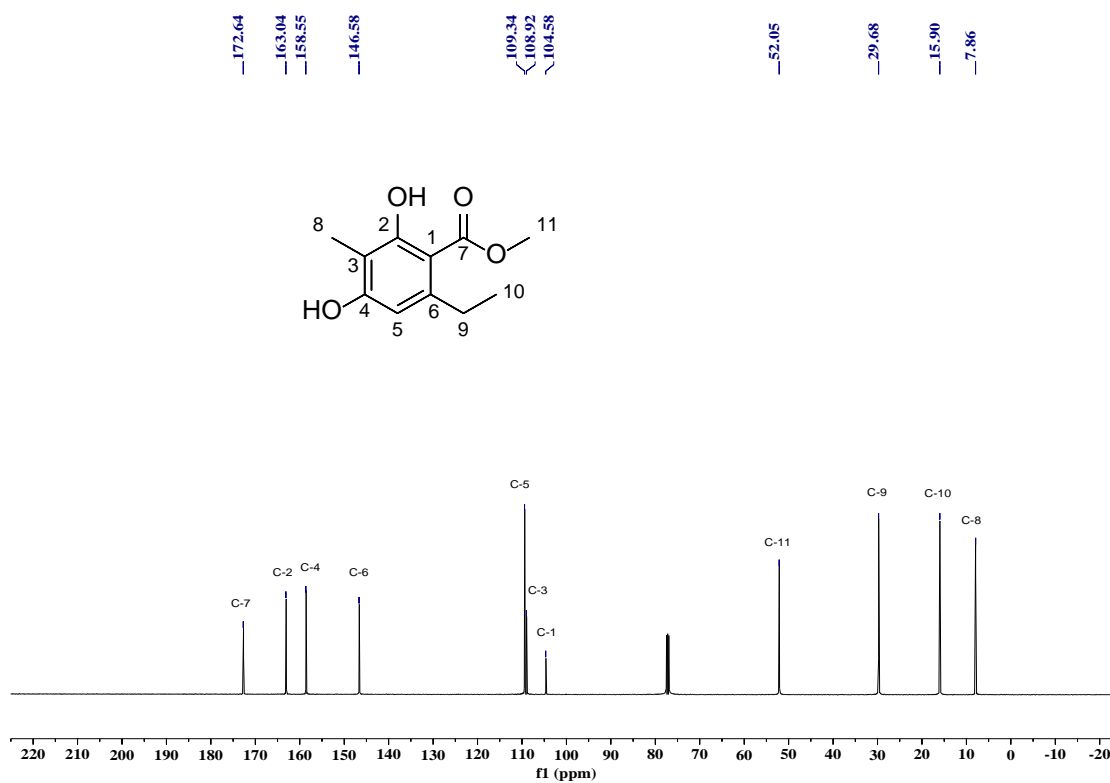


Figure S4. ¹³C{¹H} NMR spectrum of compound **3** in CDCl₃ (125 MHz)

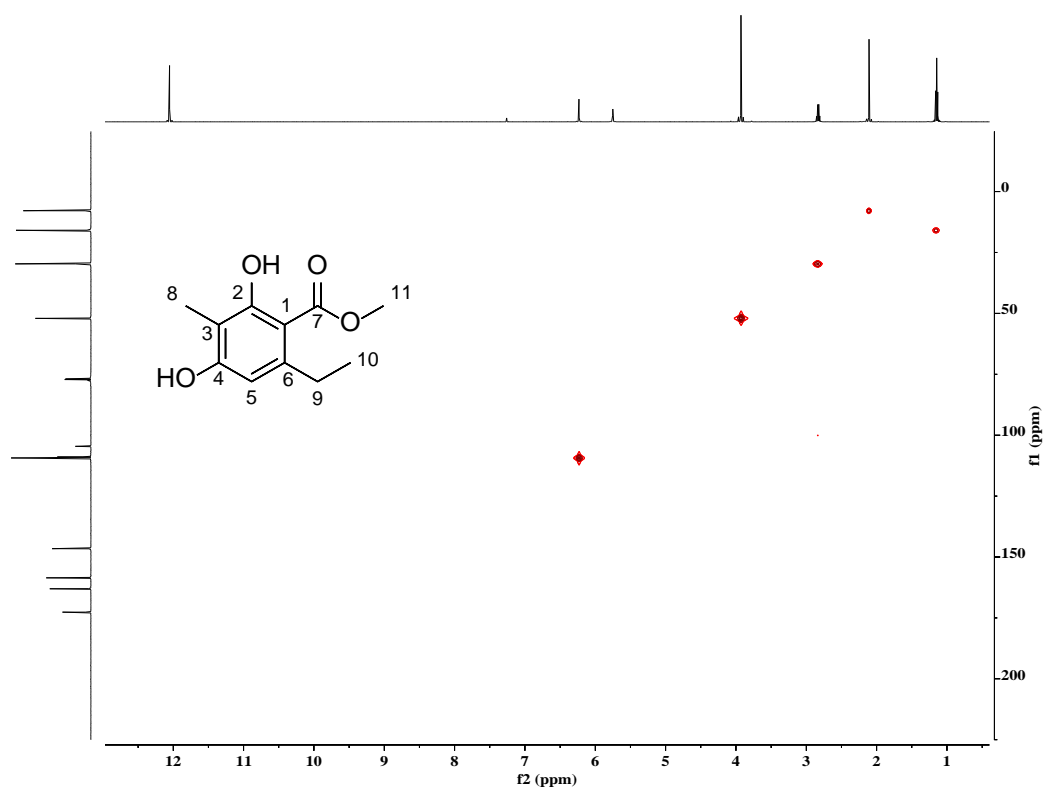


Figure S5. HSQC spectrum of compound **3** in CDCl_3

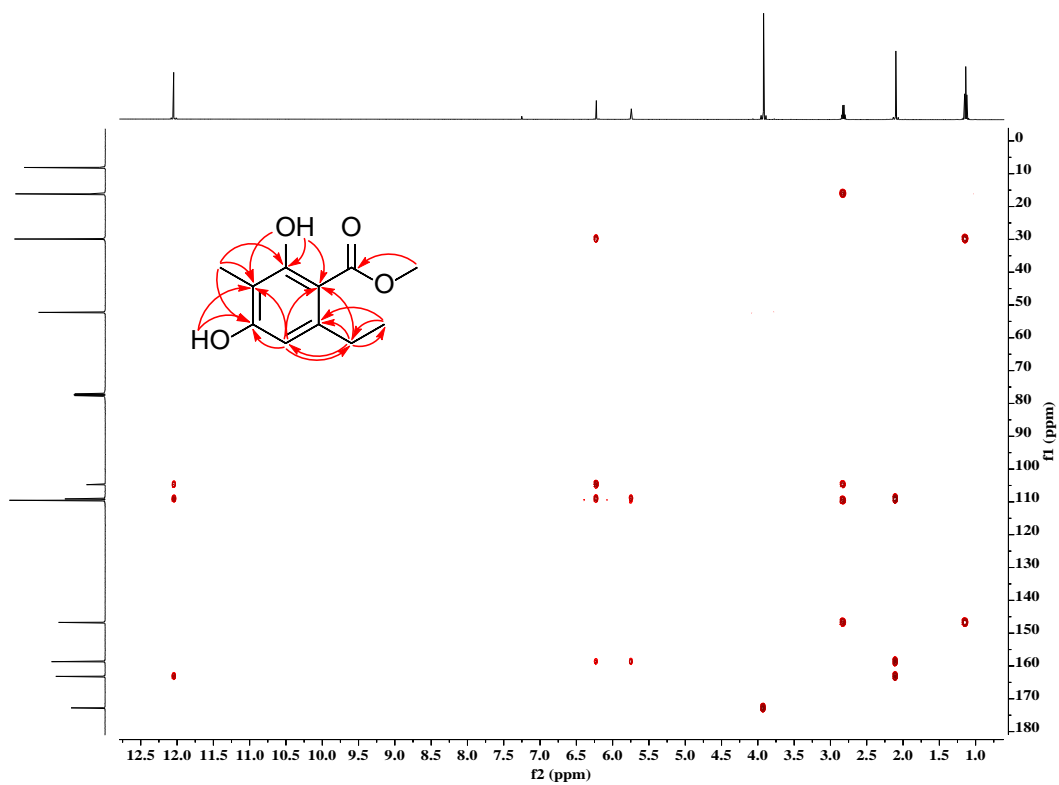


Figure S6. HMBC spectrum of compound **3** in CDCl_3

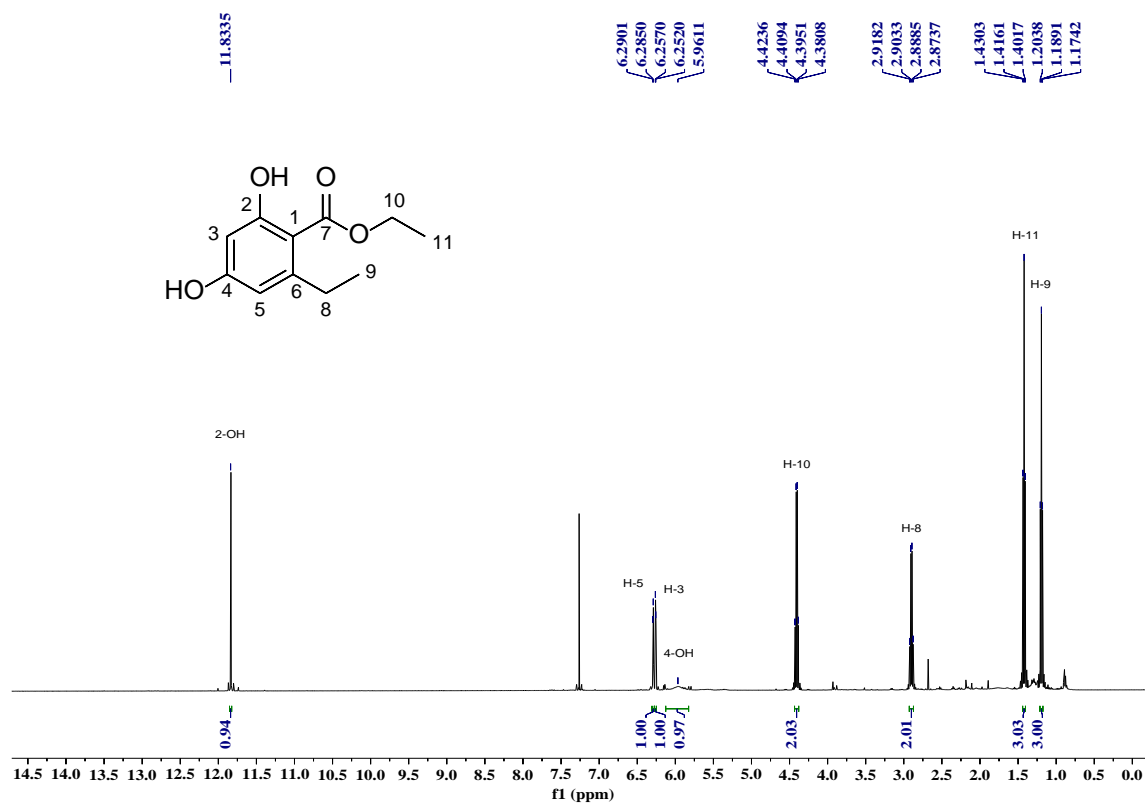


Figure S7. ^1H NMR spectrum of compound **4** in CDCl_3 (500 MHz)

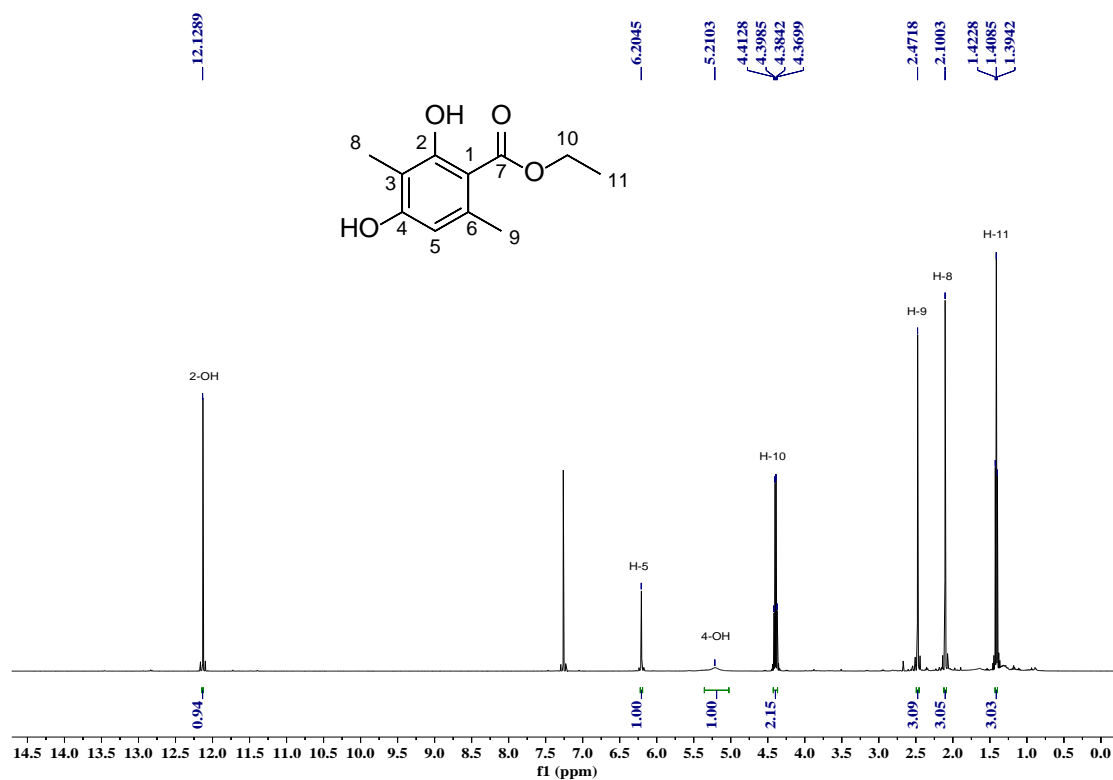


Figure S8. ^1H NMR spectrum of compound **5** in CDCl_3 (500 MHz)

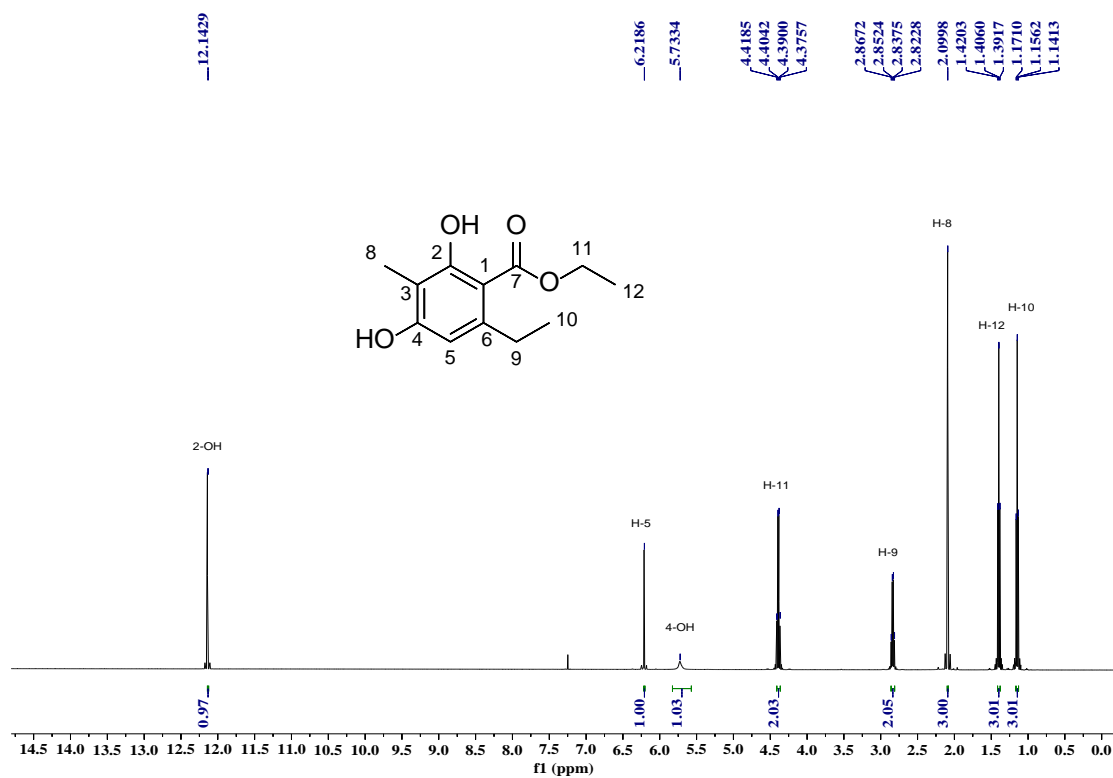


Figure S9. ¹H NMR spectrum of compound **6** in CDCl₃ (500 MHz)

References

1. De Jesus AE, Horak RM, Steyn PS, Vleggaar R (1987) Metabolites of *Aspergillus ustus*. Part 4. Stable-isotope labelling studies on the biosynthesis of the austalides. J Chem Soc , Perkin Trans 1:2253-2257.
2. Schleich S, Papaioannou M, Baniahmad A, Matusch R (2006) Activity-guided isolation of an antiandrogenic compound of *Pygeum africanum*. Planta Med 72:547-551.
3. Sher M, Langer P (2008) Regioselective synthesis of functionalized resorcins by cyclization of 1,3-bis(trimethylsilyloxy)-1,3-butadienes with 3,3-dimethoxypentanoyl chloride. Synlett:1050-1052.

4.3 Oxepinamide F biosynthesis involves enzymatic d-aminoacyl epimerization, 3*H*-oxepin formation, and hydroxylation induced double bond migration.



ARTICLE



<https://doi.org/10.1038/s41467-020-18713-0>

OPEN

Oxepinamide F biosynthesis involves enzymatic D-aminoacyl epimerization, 3H-oxepin formation, and hydroxylation induced double bond migration

Liujuan Zheng^{1,3}, Haowen Wang^{1,3}, Aili Fan²  & Shu-Ming Li¹  [✉]

Oxepinamides are derivatives of anthranilyl-containing tripeptides and share an oxepin ring and a fused pyrimidinone moiety. To the best of our knowledge, no studies have been reported on the elucidation of an oxepinamide biosynthetic pathway and conversion of a quinazolinone to a pyrimidinone-fused 1H-oxepin framework by a cytochrome P450 enzyme in fungal natural product biosynthesis. Here we report the isolation of oxepinamide F from *Aspergillus ustus* and identification of its biosynthetic pathway by gene deletion, heterologous expression, feeding experiments, and enzyme assays. The nonribosomal peptide synthase (NRPS) OpaA assembles the quinazolinone core with D-Phe incorporation. The cytochrome P450 enzyme OpaB catalyzes alone the oxepin ring formation. The flavoenzyme OpaC installs subsequently one hydroxyl group at the oxepin ring, accompanied by double bond migration. The epimerase OpaE changes the D-Phe residue back to L-form, which is essential for the final methylation by OpaF.

¹Institut für Pharmazeutische Biologie und Biotechnologie, Fachbereich Pharmazie, Philipps-Universität Marburg, Robert-Koch Straße 4, 35037 Marburg, Germany. ²College of Life Science and Technology, Beijing University of Chemical Technology, North Third Ring Road 15, Chaoyang District, 100029 Beijing, People's Republic of China. ³These authors contributed equally: Liujuan Zheng, Haowen Wang. ✉email: shuming.li@staff.uni-marburg.de

Oxepinamides are a class of oxepins with a fused pyrimidinone ring and were mainly found in fungi. For example, oxepinamides F, G, and H were isolated from *Aspergillus puniceus*^{1,2}, varioloid A and varioxepine A from *Paecilomyces variotii*^{3,4}, dihydrocinereain from *Aspergillus carneus*⁵, circumdatin A/B from *Aspergillus ochraceus*⁶, and versicoloid A/B from *Aspergillus versicolor*⁷ (Fig. 1a). Some oxepinamides show high affinity to liver X receptors (LXRs) and are potential agents for the treatment of Alzheimer's disease, atherosclerosis, diabetes, and inflammation^{1,2}. Oxepinamides are usually derived from quinazolinones with an anthranilyl (Ant) residue in common. They differ from each other by incorporation of two other varying amino acids and additional modifications. Until now, four trimodular non-ribosomal peptide synthetases (NRPSs) for assembling quinazolinones containing Trp, Ala, and Gly have been functionally characterized (Fig. 1b). In comparison to AldpA⁸ and CtqA⁹, TqaA⁹ and FmqA¹⁰ have an additional epimerization (E) domain in the Trp module, which is responsible for the conversion of L- to D- tryptophan in fumiquinazoline (FQF). As shown in Fig. 1a, phenylalanine, valine, leucine, and isoleucine residues are often found in the oxepinamide structures. To the best of our knowledge, genes responsible for quinazolinones with these amino acids have not been reported prior to this study.

In comparison to 1H-oxepins with three C=C in the oxepin ring, varioxepine A, varioloid A, oxepinamide F and G feature a 3H-oxepin structure with two C=C in the ring and one *exo* C=N

bond (Fig. 1a). To the best of our knowledge, despite the intriguing structural features and biological activities, studies on the biosynthesis of oxepinamides, especially the formation of the 3H-oxepin ring, have not been reported yet.

We identify in this study an oxepinamide (*opa*) biosynthetic gene cluster (BGC) in *Aspergillus ustus* by bioinformatic analysis. Gene deletion, heterologous expression, feeding experiments, and in vitro assays with purified enzymes prove the biosynthetic steps and the 3H-oxepin formation by consecutive ring expansion and regio- and stereospecific hydroxylation. Furthermore, the D-phenylalanyl epimerase OpaE converts the D-Phe residue back to L-form for the last methylation step to form oxepinamide F.

Results

Identification of the *opa* BGC. Oxepinamide F (1) was isolated, together with its nonmethylated congener oxepinamide E (2) from a rice culture of *A. ustus* 3.3904. Their structures were confirmed by mass spectrometry (MS), nuclear magnetic resonance (NMR), optical rotation, and circular dichroism (CD) analyses (NMR data are listed in Supplementary Tables 5–8 and spectra in Supplementary Figs 7–30. CD spectra are given in Supplementary Fig. 3)¹. Typical NMR signals for 3H-oxepins were observed at δ_H 6.7 (d, 7.3 Hz), δ_H 5.5 (t, 7.1 Hz), δ_H 6.2 (dd, 10.0, 7.0 Hz), and δ_H 5.8 ppm (d, 10.1 Hz), as well as δ_C 144, 104, 130, and 128 ppm in their spectra.

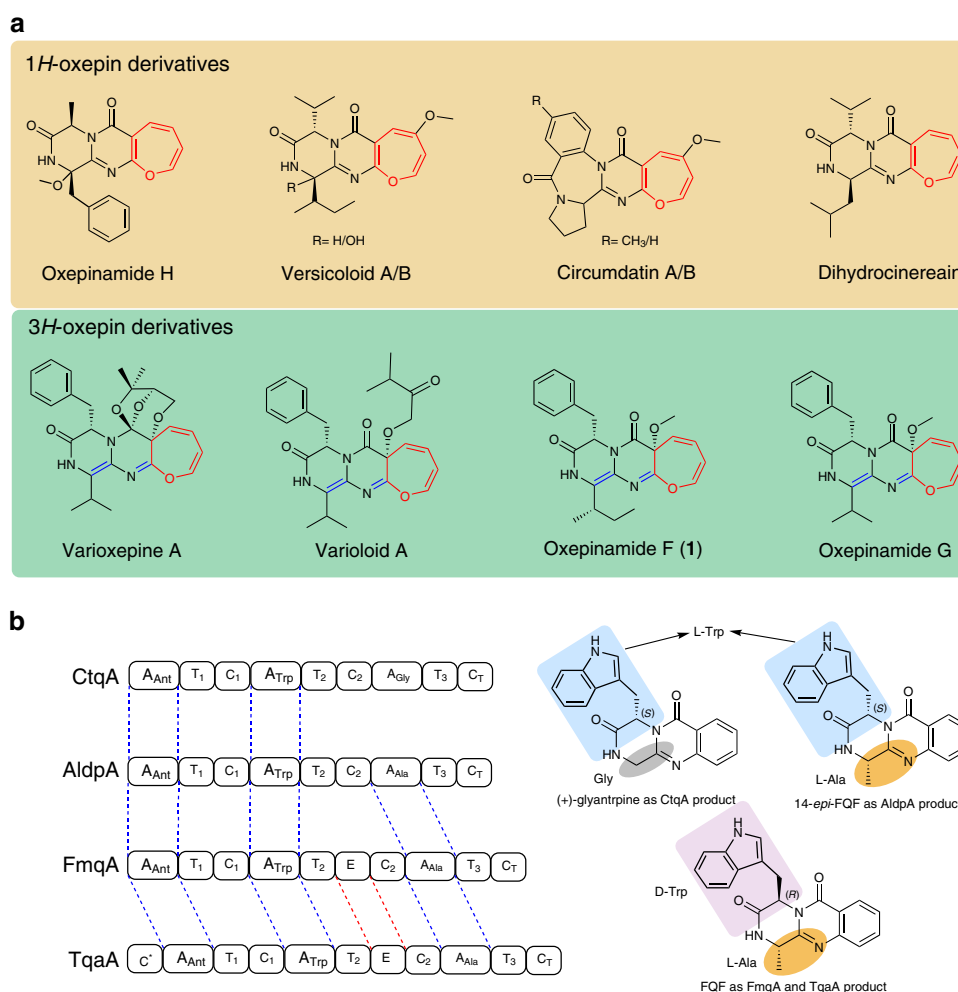


Fig. 1 Oxepinamides and backbone enzymes. **a** Examples of fungal oxepinamides including 1H-oxepins and 3H-oxepins. **b** Known NRPSs for quinazolinone assembling.

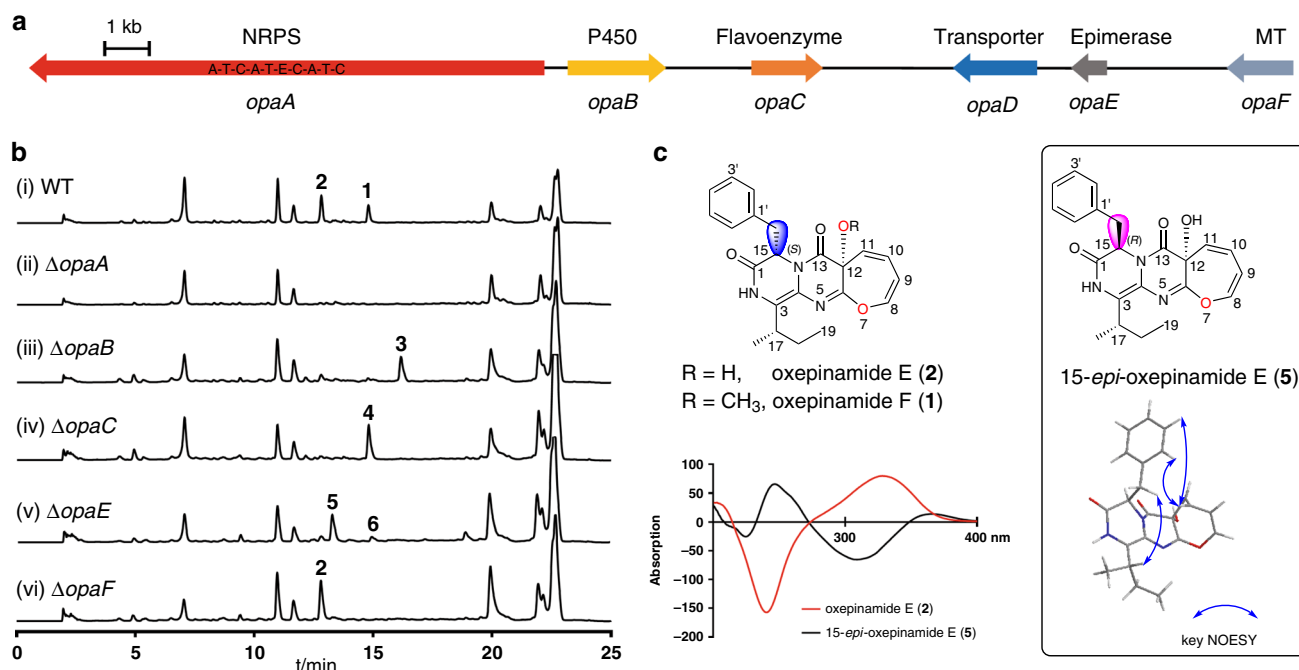


Fig. 2 Biosynthetic genes of oxepinamide F and intermediates. **a** The oxepinamide biosynthetic gene cluster (*opa*) from *A. ustus* 3.3904. **b** HPLC analysis at 254 nm of the extracts after 7 day cultivation. **c** Structures of oxepinamide F (1), E (2), and 15-*epi*-oxepinamide E (5), as well as the CD spectra of 2 and 5 (200–400 nm). Blue double-headed arrows represent NOESY interactions.

To find the biosynthetic genes of 1, we sequenced the *A. ustus* 3.3904 genome, carried out prediction for putative BGCs by using AntiSMASH¹¹, and compared them with the published data¹². The core structure of 1 is proposed to be assembled from Ant, Phe, and Ile by a NRPS containing at least three A-T-C (A: adenylation, T: thiolation, C: condensation) modules¹³. 1 differs from 2 merely in the methyl group at OH-12, implying that an O-methyltransferase (O-MeT) should be involved in its biosynthesis. Comprehensive sequence analysis revealed the presence of at least 11 genes for putative NRPSs. Two of them, KIA75458 and KIA75688, contain three A-T-C modules. Furthermore, a gene coding for a putative O-MeT (KIA75453) was only found neighboring to the gene for KIA75458. Thus, the KIA75458-related BGC was the best candidate for the 1 and 2 biosynthesis.

Inspection of the genomic neighborhood of these candidate genes in *A. ustus* revealed the presence of a putative BGC containing six genes *opaA*–*opaF*, coding for the putative proteins KIA75458–KIA75453 in the database (Fig. 2a). Sequence analysis and comparison suggested their functions as putative cytochrome P450 enzyme (OpaB, KIA75457), FAD-dependent oxygenase (OpaC, KIA75456), transporter (OpaD, KIA75455), epimerase (OpaE, KIA75454), and O-MeT (OpaF, KIA75453) (Supplementary Table 1).

Further sequence analysis revealed that KIA75458, named OpaA in this study, has a domain architecture of A-T-C-A-T-E-C-A-T-C (Fig. 2a). To prove its function, *opaA* in *A. ustus* was replaced with a hygromycin B resistance cassette by using a split marker gene replacement protocol¹⁴. The generated mutants were verified by PCR (Supplementary Fig. 1) and cultivated in rice media. High-performance liquid chromatography (HPLC) analysis of the culture extract of the $\Delta opaA$ mutant revealed the abolishment of both 1 and 2 production (Fig. 2b), proving its involvement in their biosynthesis. Deletion of *opaF* abolished 1, but not 2 production, indicating that OpaF acts as a methyltransferase for the conversion of 2 to 1 (Fig. 2b). Based on above results, the *opa* gene cluster is indeed responsible for biosynthesis of 1 and 2.

The oxepin ring in 1 and 2 was proposed to be formed by oxidative benzene ring expansion^{1,15}. However, it is unknown whether the P450 enzyme OpaB, the oxidase OpaC or both are responsible for this conversion. To figure out their functions, we firstly deleted *opaB* from *A. ustus* genome. Deletion of *opaB* led to the abolishment of 1 and 2, together with the accumulation of a new peak 3 at 16.2 min with a $[M + H]^+$ ion at *m/z* 362.189 (Fig. 2b). Typical signals for oxepins were not observed in the NMR spectra of 3. Extensive interpretation of the spectroscopic data including NMR and CD spectra and comparison with known compounds¹⁶ proved 3 to be protuboxepin K, a quinazolinone derivative of Ant, D-Phe, and L-Ile (Fig. 3)¹⁷.

Bioinformatic analysis and comparison with known proteins revealed that OpaA consists of a deduced A_{Ant}-T₁-C₁-A_{Phe}-T₂-E-C₂-A_{Ile}-T₃-C_T domain structures, similar to CtqA, AldpA, FmqA, and TqaA. OpaA has the same A_{Ant} domain for anthranilic acid activation (Fig. 1b). As aforementioned, the E domain in FmqA and TqaA is responsible for incorporation of a D-Trp residue in FQF. In analogy, the presence of an E domain in the second module of OpaA and the D-Phe residue in 3 imply that the second A domain is for activating of L-Phe, which is then converted to D-form by the E domain. The third A domain is responsible for L-Ile activation and the terminal C_T domain for cyclization and releasing the NRPS product. Thus, OpaA is a quinazolinone synthase using different amino acids from those listed in Fig. 1b, which expands clearly quinazolinone structure diversity.

OpaB functions as an oxepinase. The results from deletion experiments provide unambiguous evidence that OpaB is responsible for the expansion of the benzene to the oxepin ring. For further understanding of its function, *opaB* was amplified from genomic DNA and cloned into pYH-*gpdA*-*affyrg*¹⁸ via homologous recombination in yeast¹⁹ for heterologous expression in *Aspergillus nidulans*. The obtained plasmid pLZ61 was linearized by *Swa*I and integrated into the genome of *A. nidulans* LO8030²⁰ (Supplementary Fig. 2). Feeding 3 in the obtained overexpression

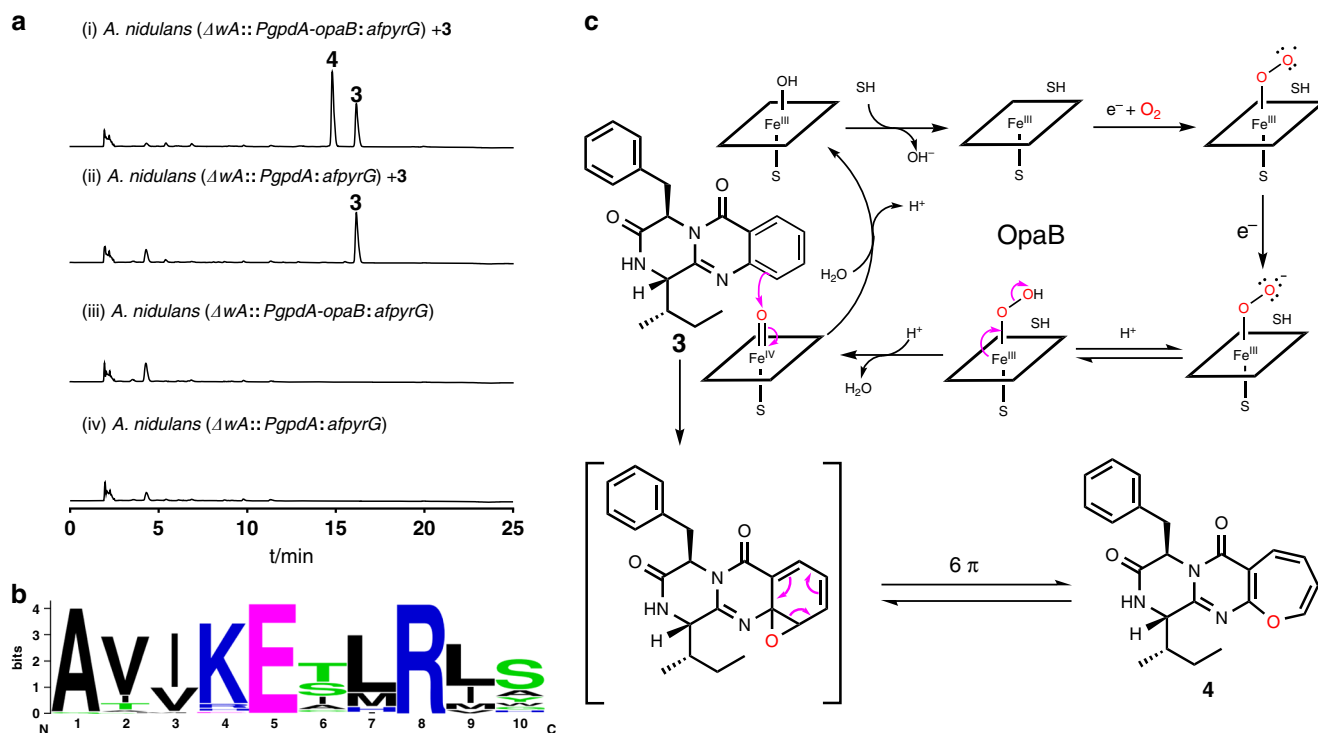


Fig. 3 Functional verification of the oxepinase OpaB. **a** HPLC analysis of the conversion of **3** to **4** in the *opaB* expression strain of *A. nidulans* at 254 nm. **b** A sequence logo for the conserved EXXR motif in OpaB using sequences of 96 P450 enzymes (Supplementary Table 9). **c** Proposed mechanism for oxepin formation catalyzed by OpaB (SH: substrate).

strain *A. nidulans* LZ61 led to the detection of compound **4**, which was not observed in a negative control. **4** was confirmed to be protuboxepin A by NMR analysis and by comparison of its optical rotation value with that reported in literature²¹. This confirmed that OpaB alone is responsible for the oxepin ring formation (Fig. 3a). Sequence alignment indicated that the conserved P450 motif ExxR is present as ETMR in OpaB (Fig. 3b and Supplementary Table 9)^{22–24}. In analogy to other P450 catalyzed alkane hydroxylations and alkene epoxidations^{25,26}, we postulated the electrophilic oxoferryliron ($\text{Fe}^{\text{IV}}=\text{O}$) as the active oxygen intermediate in the OpaB reaction. Attacking of the oxoferryliron species by the nucleophilic benzene double bond in **3** would result in the formation of an arene oxide, which is in rapid spontaneous equilibrium with the oxepin **4** through 6π electrocyclic ring opening (Fig. 3c)^{15,27}. The oxepin form is expected to be more stable at room temperature than its arene oxide^{27,28}. Only the 1*H*-oxepin **4** was detected as OpaB product in this study, which differs from an oxepin intermediate important for both phenylacetate degradation and tropone biosynthesis. In those cases, the isomerase PaaG forms a stable 3*H*-oxepin from a labile 1*H*-oxepin²⁹. On the other hand, both 1*H*- and 3*H*-oxepin derivatives listed in Fig. 1 were isolated as stable fungal metabolites. Phylogenetic analysis of OpaB with 51 known P450 enzymes from bacteria and fungi indicates clearly the presence of different clades (Supplementary Fig. 4). The bacterial P450 enzymes catalyzing diverse reactions, including the two hydroxylases P450cin and P450cam with trace oxepin formation activity²⁸, build a distinct clade from fungal enzymes. The majority of the fungal P450s in the phylogenetic tree catalyzes hydroxylations of diverse substrates. OpaB is located near to the epoxidase AtaY, but far away from the oxepinase AtaF, both involved in the biosynthesis of acetylarnotin in *Aspergillus terreus*³⁰.

OpaC catalyzes hydroxylation accompanied by double bond migration. Comparing the planar structures, **2** differs from **4** in

the OH-12 and two different double bonds. Sequence analysis suggested OpaC to be a FAD-containing monooxygenase and could be a good candidate for a consecutive hydroxylation at C12 of the oxepin ring. The double bonds could be shifted during the hydroxylation reaction. To verify its function biochemically, *opaC* was amplified from complementary DNA (cDNA) and cloned into pET28a (+) for overexpression in *Escherichia coli*. The recombinant *N*-terminally His₆-tagged protein was purified to near homogeneity with a yield of 3.5 mg per liter culture (Fig. 4b). To our surprise, one product peak **5** at 13.3 min, instead of **2** at 12.8 min, was detected in the incubation mixture of **4** with the purified OpaC in the presence of NADPH (Fig. 4a). **5** shares the same UV visible light absorption and mass spectral features with **2**. NMR data and CD data supported that **5** and **2** are diastereomers and differ from each other merely in the configuration at C15. **5** was, therefore, named 15-*epi*-oxepinamide E (Fig. 2c). Deletion of *opaC* from the *A. ustus* genome led indeed to the accumulation of **5** (Fig. 2b). Biochemical characterization revealed that OpaC also used NADH as a cofactor, but with a significantly reduced activity (Fig. 4a). No substrate consumption was observed in the incubation mixture of **3** and OpaC (Supplementary Fig. 5), proving the prerequisite of the oxepin ring for an acceptance by OpaC. The kinetic data of the OpaC reaction with **4** in the presence of NADPH fit well to a typical velocity equation with substrate inhibition^{31,32}. An apparent K_M value at 0.43 ± 0.04 mM, a turnover number (k_{cat}) at 0.16 ± 0.01 s⁻¹, the catalytic efficiency (k_{cat}/K_M) at 0.37 mM⁻¹ s⁻¹ and a substrate inhibition constant (K_i) at 0.39 ± 0.03 mM (Fig. 4c) were calculated by using the software GraphPad Prism 6.0.

Based on these results, a mechanism with a C4a-hydroperoxyflavin intermediate³³ was postulated for the OpaC reaction (Fig. 4d). The oxidized flavin Fl_{ox} is converted to its reduced form Fl_{red} by external electron donor NADPH. Subsequent reaction of Fl_{red} with O_2 produces the electrophilic reagent C4a-hydroperoxyflavin. The elimination of the proton at

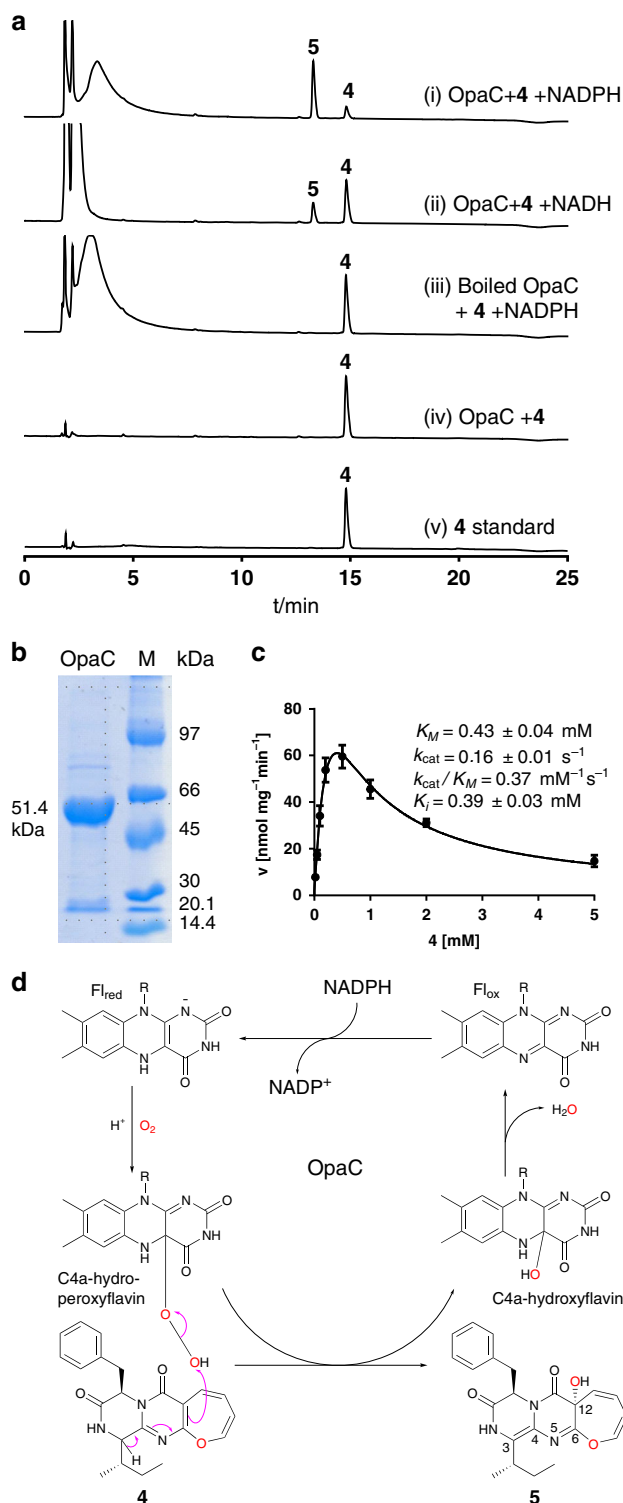


Fig. 4 Proof of the OpaC function. **a** HPLC analysis of in vitro assays of **4** with OpaC at 254 nm. **b** SDS-PAGE analysis of the purified OpaC. The experiments were repeated twice. **c** Determination of the kinetic parameters of the OpaC reaction. The error bars represent standard errors of velocity and the standard errors of mean (SEMs) are given as \pm values ($n =$ six independent experiments). **d** Proposed mechanism for the OpaC reaction with a C4a-peroxyflavin as a key intermediate.

C3 in **4** results in the double bond migration and attack on the C4a-hydroperoxyflavin, leading to the formation of **5** and C4a-hydroxyflavin. The latter one is then regenerated to Fl_{ox} by removal of one water molecule for the next reaction cycle.

Sequence analysis and biochemical investigation revealed that OpaC belongs to the well-studied class A flavin-dependent monooxygenases³⁴. Phylogenetic analysis of representatives from this group (Supplementary Fig. 6) indicates the presence of at least three clades. OpaC is located closely together with AspB in the biosynthesis of asperlicins and PhqK in that of paraherquimides. AspB catalyzes the hydroxylation at C3 of an indole moiety, resulting in the formation of a hexahydropyrrolo[2, 3-b] indole framework³⁵. PhqK converts an indole ring to a 2-keto indoline ring via a postulated arene oxide intermediate³⁶. In both cases, the C4a-hydroperoxyflavin species was proposed to serve as oxygen transferring agent, consistent with other class A flavin monooxygenases and our mechanistic proposal.

D-Phenylalanyl epimerization catalyzed by OpaE. As aforementioned, **2** differs from **5** only in the configuration at C15. The *S*-configuration at this position in **2** corresponds to that of L-Phe, which was epimerized to *R*-configuration by the E domain of OpaA in **3**. Conversion of **5** to **2** would need an epimerase like OpaE. Deletion of *opaE* led indeed to the abolishment of **1** and **2** production and main accumulation of **5** with a trace amount of a methylated product **6** (15-*epi*-oxepinamide F, Fig. 2b). To prove OpaE function in vitro and to understand the epimerization mechanism, the coding region of *opaE* was cloned and over-expressed as described for OpaC. HPLC analysis of the reaction mixture of **5** with the recombinant OpaE revealed **2** as the mere product peak (Fig. 5), proving unequivocally its function as an epimerase. Configuration change at C15 is a prerequisite for further methylation to the final product **1**, because only trace amounts of **5** were converted to its methylated product **6** in $\Delta opaE$ mutant (Fig. 2b). Determination of the kinetic parameters of the OpaE reaction with **5** via Michaelis-Menten equation gave a K_M value of 1.41 ± 0.05 mM, a turnover number (k_{cat}) of 0.28 ± 0.01 s⁻¹ and the catalytic efficiency (k_{cat}/K_M) at 0.20 mM⁻¹ s⁻¹ (Fig. 5c).

Incubation of **5** and OpaE in Tris-HCl buffer containing D₂O/H₂O (9:1) and subsequent analysis on liquid chromatography-mass spectrometry (LC-MS) led to detection of the shifted $[M+H]^+$ isotopic pattern of **2** ($[M+H]^+$ 395.184), which is 1 Da larger than that in H₂O ($[M+H]^+$ 394.177) (Fig. 5d). Incubation of **2** in Tris-HCl buffer containing D₂O/H₂O (9:1) did not change the isotopic pattern. These results proved the involvement of an enol intermediate in the OpaE-catalyzed epimerization, as proposed in Fig. 5e³⁷.

Discussion

Taken together, we identified the *opa* cluster for the oxepinamide F biosynthesis. OpaA was proven to activate Ant, L-Ile, and L-Phe, change the configuration of L-Phe to D-Phe by an epimerase domain, and assemble the quinazolinone **3**. The benzene ring in the Ant residue of **3** was expanded to an oxepin ring in **4** by the P450 enzyme OpaB alone. The regio- and stereospecific hydroxylation of **4** catalyzed by OpaC was accompanied by double bond migration from C4-N5 and C6-C12 in **4** to C3-C4 and N5-C6 in **5**, leading to the conversion of 1*H*-oxepin to 3*H*-oxepin system. The *R*-configuration in **5** was changed to *S*-configuration by the single epimerase OpaE for the final methylation of the OH-12 by the *O*-methyltransferase OpaF, to the end product **1** (Fig. 6).

Oxepin rings also play important roles in the bacterial degradation of phenylacetic acid and the biosynthesis of tropone

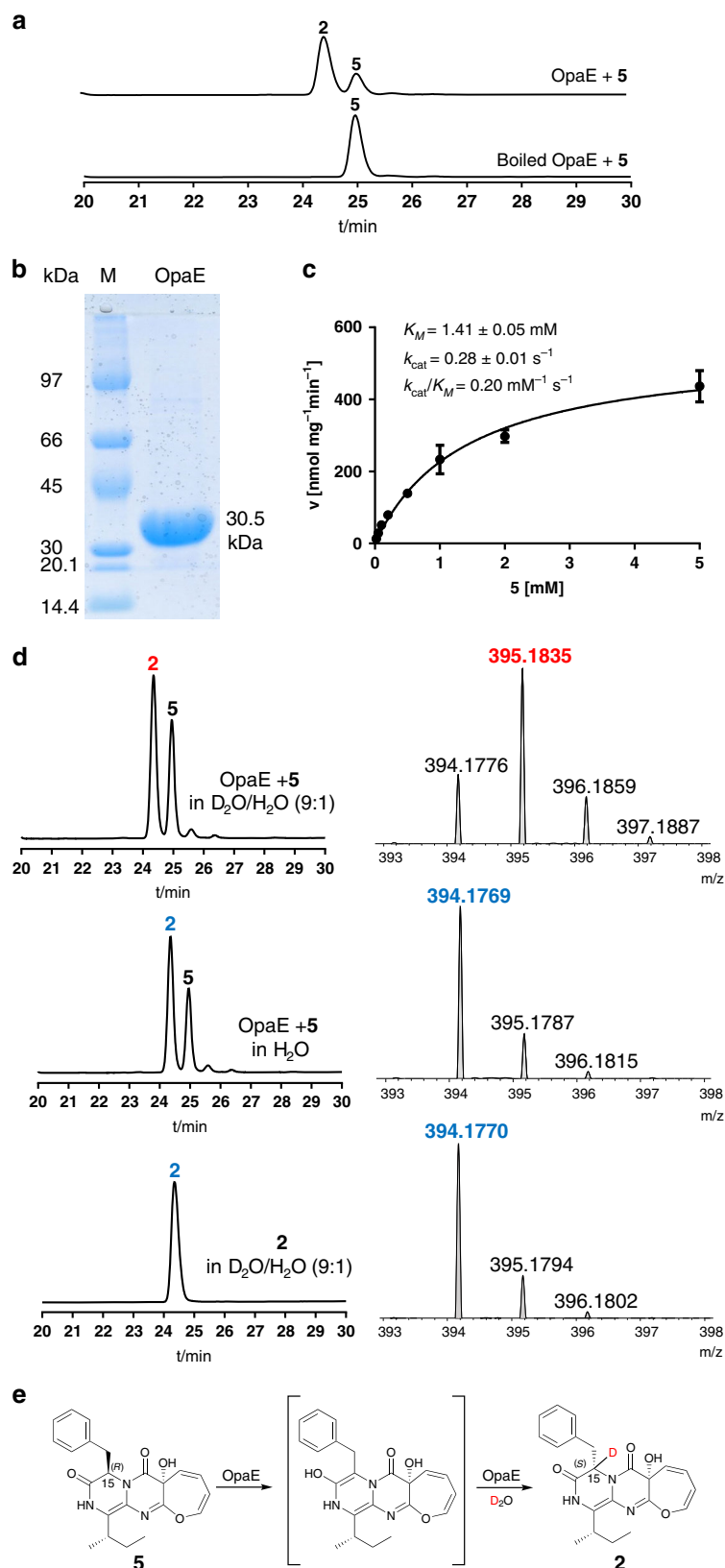


Fig. 5 In vitro verification of OpaE as a d-phenylalanyl epimerase. a HPLC analysis of in vitro assays with OpaE at 254 nm. **b** SDS-PAGE analysis of the purified OpaE. The experiments were repeated twice. **c** Determination of the kinetic parameters for OpaE with **5**. The error bars represent standard errors of velocity and SEMs are given as \pm values ($n =$ six independent experiments). **d** LC-MS monitoring of the OpaE reactions in D₂O/H₂O and negative controls. **e** Proposed mechanism for the OpaE reaction.

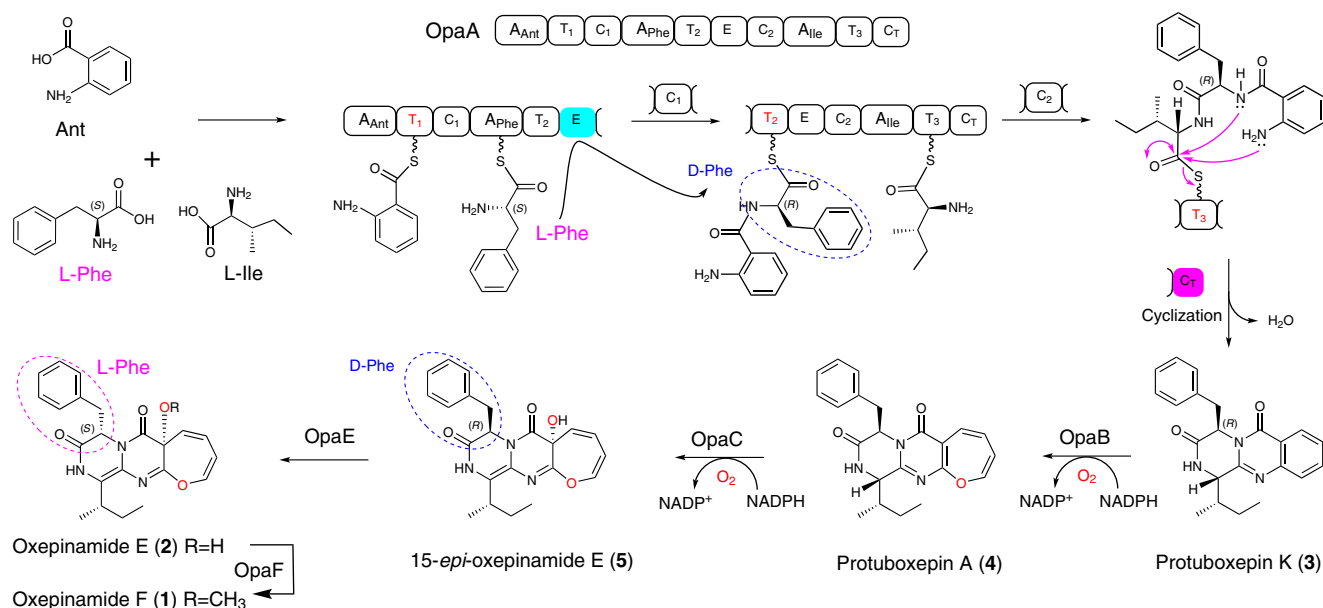


Fig. 6 Proposed biosynthetic pathway for oxpinamide F in *Aspergillus ustus*. Ant, L-Phe and L-Ile are assembled to protuboxepin K (**3**) by the NRPS OpaA with epimerization at the phenylalanyl residue. The oxepinase OpaB catalyzes the oxepin ring formation in protuboxepin A (**4**). The regio- and stereospecific hydroxylation of **4** by OpaC is accompanied by a double bond migration, leading to the conversion of a 1*H*-oxepin to a 3*H*-oxepin system in **5**. The D-Phe configuration in **5** is changed to L-Phe in **2** by the single epimerase OpaE. The O-methyltransferase OpaF catalyzes the conversion of **2** to the end product **1** by methylation of the hydroxyl group at C-12.

natural products that both depend on the multicomponent epoxidase PaaABCE and oxepin isomerase PaaG^{29,38}. Stok et al.²⁸ observed the formation of a simple oxepin derivative as a minor side product in the hydroxylation of *tert*-butyl benzene by two bacterial P450 enzymes, which usually use the monoterpenes camphor and 1, 8-cineole as natural substrates, respectively. Wang and coworkers reported the formation of a dihydrooxepin ring in the biosynthesis of an epipolythiodioxopiperazine by three enzymes, the epoxidase AtaF, the acetyltransferase AtaH, and the cytochrome P450 enzyme AtaY³⁰. The oxepin ring was formed from an acetoxylated cyclohexan-diene structure.

In peptide biosynthesis, conversion of L- to D-form amino acids during the peptide biosynthesis is usually catalyzed by epimerase domains of NRPSs or by radical S-adenosylmethionine-dependent enzymes in microorganisms^{39,40}. No single enzyme was reported to catalyze the conversion of D- to L-form of an amino acid residue. To the best of our knowledge, an oxepinamide biosynthetic gene cluster that includes the characterization of involved biosynthetic enzymes and reactions steps has not been reported before. Furthermore, conversion of an amino acid residue from L- to D-configuration and then back to the L-configuration by two different epimerases for structural modification has not been described in literature.

Methods

Genome sequencing and sequence analysis. The genome of *A. ustus* 3.3904 was sequenced by Genewiz (Suzhou, China) using Nova-seq6000/X-ten (Illumina). Initial prediction and analysis of biosynthetic gene clusters were carried out by using AntiSMASH⁴¹. Prediction of the enzyme function was performed with the online BLAST programmer (<http://blast.ncbi.nlm.nih.gov>). The genomic DNA sequence of the *opa* cluster (Supplementary Table 1) reported in this study corresponds well to that depicted at GenBank under accession number: JOMC01000153.1.

The phylogenetic trees were created by MEGA version 7.0 (<http://www.megasoftware.net>). Protein sequence alignments were performed with the program ClustalW (<https://www.genome.jp/tools-bin/clustalw>) to identify strictly conserved amino acid residues.

Strains, media, and growth conditions. *Escherichia coli* DH5 α and BL21(DE3) cells were grown in LB medium (1% NaCl, 1% tryptone, and 0.5% yeast extract) at 37 °C. In all, 50 μ g mL⁻¹ ampicillin or 50 μ g mL⁻¹ kanamycin were supplemented for cultivation of recombinant strains.

Saccharomyces cerevisiae HOD114-2B cells were grown in YPD medium (1% yeast extract, 2% peptone and 2% glucose, 1.5% agarose was used for plate). The SC-uracil medium (6.7 g L⁻¹ yeast nitrogen base with ammonium sulfate, 650 mg L⁻¹ CSM-His-Leu-Ura (MP Biomedicals), 20 mg L⁻¹ His and 60 mg L⁻¹ Leu, pH 6.2 – 6.3, 1.5% agarose was used for plate) with 2.0% glucose was used for selection.

Fungal strains used in this study are listed in Supplementary Table 2. *Aspergillus ustus* 3.3904 was purchased from China General Microbiological Culture Collection Center (Beijing, China) and cultivated in rice medium (20 g Alnatura long-grain rice with 30 mL H₂O in 250 mL flask) at 25 °C for of secondary metabolite production.

Aspergillus nidulans LO8030 and derivatives were grown at 37 °C on GMM medium (1.0% glucose, 50 mL L⁻¹ salt solution, 1 mL L⁻¹ trace element solution, and 1.6% agar) for sporulation and transformation with appropriate nutrition as required. The salt solution comprises (w/v) 12% NaNO₃, 1.04% KCl, 1.04% MgSO₄ · 7H₂O, and 3.04% KH₂PO₄. The trace element solution contains (w/v) 2.2% ZnSO₄ · 7H₂O, 1.1% H₃BO₃, 0.5% MnCl₂ · 4H₂O, 0.16% FeSO₄ · 7H₂O, 0.16% CoCl₂ · 5H₂O, 0.16% CuSO₄ · 5H₂O, 0.11% (NH₄)₆Mo₇O₂₄ · 4H₂O, and 5% Na₄EDTA.

Genomic DNA isolation. The *A. ustus* 3.3904 and *A. nidulans* mycelia were dried on filter paper and transferred into 2 mL Eppendorf tubes. After addition of 400 μ L LETS buffer (10 mM Tris-HCl pH 8.0, 20 mM EDTA pH 8.0, 0.5% SDS, and 0.1 M LiCl) and four glass beads (2.85 mm in diameter), the tubes were vigorously mixed for 4 min. After addition of another 300 μ L LETS buffer, the mixtures were treated with 700 μ L phenol: chloroform: isoamyl alcohol (25: 24: 1). The genomic DNA in the aqueous phase was precipitated by addition of 900 μ L absolute EtOH, followed by centrifugation at 17,000 \times g for 30 min and washing with 70% EtOH. The obtained DNA as pellet was dried at 55 °C for 15 min and dissolved in 50–100 μ L distilled H₂O.

RNA isolation from *A. ustus* 3.3904 and cDNA synthesis. For this purpose, *A. ustus* 3.3904 was cultivated in rice medium at 25 °C for 7 days. The mycelia were collected by washing with 50 mL H₂O and subsequent centrifugation. Fungal RNA Mini kit (VWR OMEGA bio-tek E.Z.N.A.) was used for RNA extraction following the standard protocol provided by the manufacturer. For cDNA synthesis, the ProtoScript II First Strand cDNA Synthesis kit (BioLabs) was used with Oligo-dT as primers.

The deduced polypeptide from the coding region of *opaC* obtained from cDNA comprises 457 amino acids, lacking the five residues from 248 to 252 in [KIA75456](#):

PCR amplification, gene cloning, and plasmid construction. Primers and plasmids used in this study are listed in Supplementary Tables 3 and 4, respectively. SeqLab GmbH (Göttingen, Germany) synthesized the PCR primers. Phusion® High-Fidelity DNA polymerase from New England Biolabs (NEB) were used for PCR amplification, which was carried out on a T100™ Thermal cycler from Bio-Rad by following the manufacturer's suggestion for temperature profiles.

Genetic manipulation in *A. ustus* 3.3904 and cultivation of deletion mutants.

To get germlings for protoplast preparation, fresh spores of *A. ustus* 3.3904 were inoculated in a 250 mL flask containing 50 mL LMM medium and incubated at 230 rpm and 30 °C. After 11 h, the germlings were harvested by centrifugation at 2280 x g in 4 °C for 15 min and washed with distilled H₂O. The pellets were suspended in 10 mL osmotic buffer (1.2 M MgSO₄ in 10 mM sodium phosphate, pH 5.8) containing 40 mg lysing enzyme from *Trichoderma harzianum* (Sigma) and 30 mg yatalase from *Corynebacterium* sp. OZ-21 (OZEKI Co., Ltd.) and incubated at 100 rpm and 30 °C for 10 h. The formation of protoplasts was monitored by controlling under microscope. The mixture was then transferred into a 50 mL falcon tube and overlaid gently with 10 mL of trapping buffer (0.6 M sorbitol in 0.1 M Tris-HCl, pH 7.0). The protoplasts appeared as an interface between the two buffer systems after centrifugation at 2280 x g and 4 °C for 15 min. This interface was transferred carefully into a 15 mL falcon tube. The protoplasts in this phase were collected by centrifugation at 2280 x g, and resuspended in 100 µL of STC buffer (1.2 M sorbitol, 10 mM CaCl₂ in 10 mM Tris-HCl, pH 7.5).

For transformation, the obtained protoplasts were incubated with DNA samples (2–3 µg in 8–10 µL) on ice for 50 min. 1.25 mL of PEG solution (60% PEG 4000, 50 mM CaCl₂, 50 mM Tris-HCl, pH 7.5) was then added, gently mixed and incubated at room temperature for 30 min. In all, 5 mL STC buffer were added into the mixture and spread on plates with SMM bottom medium (1.0% glucose, 50 mL L⁻¹ salt solution, 1 mL L⁻¹ trace element solution, 1.2 M sorbitol and 1.6% agar) containing 100 µg mL⁻¹ hygromycin B. The plates were overlaid softly by SMM top medium (1.0% glucose, 50 mL L⁻¹ salt solution, 1 mL L⁻¹ trace element solution, 1.2 M sorbitol, and 0.8% agar) containing 50 µg mL⁻¹ hygromycin B. After culturing at 30 °C for 3–4 days, the fungal colonies were transferred on fresh PDA plates (PD medium with 3% agar) containing 100 µg mL⁻¹ hygromycin B for selection. The potential transformants were verified via PCR amplification (Supplementary Fig. 1), cultivated in rice medium at 25 °C for 7 days and extracted with EtOAc. After evaporation, the extracts were dissolved in dimethyl sulfoxide (DMSO) and subjected to LC–MS for analysis.

Heterologous expression in *A. nidulans*. In this study, we used *A. nidulans* LO8030⁴² as expression host. The protoplast preparation procedure was similar to that for *A. ustus* 3.3904 as mentioned above. The germlings were shaken with 40 mg lysing enzyme from *Trichoderma harzianum* (Sigma) and 20 mg yatalase from *Corynebacterium* sp. OZ-21 (OZEKI Co., Ltd.) at 100 rpm and 37 °C for 3 h. pLZ61 containing the cytochrome P450 gene *opaB* was transformed into *A. nidulans* LO8030 to create the expression strain LZ61. The transformants were verified by PCR (Supplementary Fig. 2) and cultivated for biotransformation with protuboxepin K (3).

Overproduction and purification of OpaC and OpaE. The *opaC* and *opaE* expression plasmids pLZ62 and pLZ63 were transferred separately into *E. coli* BL21 (DE3). Terrific Broth (TB) medium (2.4% yeast extract, 2.0% tryptone, 0.4% glycerol, 0.1 M phosphate buffer, pH 7.4) was used for cultivation. OpaC overproduction was induced with 0.5 mM IPTG at 16 °C for 16 h, and OpaE with 1 mM IPTG at 20 °C for 20 h. The recombinant His₆-tagged proteins were purified by Ni-NTA affinity chromatography (Qiagen, Hilden). The protein concentration was determined on a Nanodrop 2000c spectrophotometer (Thermo Scientific, Braunschweig, Germany) and analyzed by sodium dodecyl sulfate-polyacrylamide gel electrophoresis (SDS-PAGE) (Figs. 4b and 5b). Protein yields of 3.5 and 20 mg per liter bacterial culture were calculated for OpaC and OpaE, respectively.

In vitro assays of OpaC and OpaE. To test the enzyme activity of OpaC, the reaction mixtures (50 µL) containing 50 mM Tris-HCl (pH 7.5), 5 mM NADPH, 1 mM protuboxepin A (4), 10 µg (3.9 µM) of the purified recombinant OpaC were incubated at 30 °C for 30 min. The reactions were terminated by addition of 50 µL methanol.

For OpaE, the reaction mixtures (50 µL) containing 50 mM Tris-HCl (pH 7.5), 1 mM 15-*epi*-oxepinamide E (5), 5 µg (3.2 µM) of the purified recombinant OpaE were incubated at 37 °C for 30 min. The reactions were terminated by addition of 50 µL methanol.

For deuterium labeling experiment with OpaE, the stock solutions of the assay components in H₂O were diluted with D₂O to a final D₂O/H₂O ratio of 9:1 in 50 mM Tris-HCl. The reaction mixtures were incubated and analyzed on LC–MS as described for standard assays.

Determination of kinetic parameters. Enzyme assays for determination of the kinetic parameters for OpaC (50 µL) contained 50 mM Tris-HCl (pH 7.5), 5 mM NADPH, 4 µg (1.6 µM) of the purified recombinant OpaC and protuboxepin A (4) at final concentrations from 0.025 to 2.5 mM. The incubations were carried out at 30 °C for 30 min. After extraction of the reaction mixtures with EtOAc and evaporation of the solvent to dryness, the residues were dissolved in DMSO and analyzed on HPLC.

For OpaE, 50 µL reaction mixtures contained 50 mM Tris-HCl (pH 7.5), 2 µg (1.3 µM) of the purified recombinant OpaE and compound 15-*epi*-oxepinamide E (5) at final concentrations from 0.02 to 2 mM. The incubations were carried out at 37 °C for 30 min. After addition of MeOH and centrifugation, the supernatants were analyzed on HPLC. The data presented in Figs. 4c and 5c were obtained from six independent experiments. SEMs are given as ± values (*n* = six independent experiments).

Kinetic parameters were determined by nonlinear regression using the software GraphPad Prism 6.0 via substrate inhibition velocity equation for OpaC and Michaelis–Menten equation for OpaE.

Large-scale fermentation, extraction, and isolation of secondary metabolites.

The strains were cultivated in 0.75 kg rice (1.75 L) for isolation. The rice culture was extracted with equal volume of EtOAc for three times. The EtOAc extracts were concentrated under reduced pressure to afford the crude extracts for further purification.

To isolate oxepinamide F (1) and E (2), the crude extract of *A. ustus* wildtype was subjected to silica gel (230–400 mesh) column chromatography, by using a gradient of CH₂Cl₂/CH₃OH (100:0–0:100) to give eight fractions (Fr.1–Fr.8). Fr.4 was purified on a semi-preparative HPLC (ACN/H₂O), leading to 38.42 mg of oxepinamide F (1), 57.24 mg of oxepinamide E (2). Similarly, 77.68 mg protuboxepin K (3) was obtained from a culture of the Δ OpaB mutant, 79.24 mg protuboxepin A (4) from a culture of the Δ OpaC mutant, 23.88 mg 15-*epi*-oxepinamide E (5) 16.88 mg 15-*epi*-oxepinamide F (6) from a culture of the Δ OpaE mutant and 15.78 mg oxepinamide E (2) from a culture of the Δ OpaF mutant.

Feeding experiments in the *opaB* expression strain *A. nidulans* LZ61. To figure out the function of the cytochrome P450 enzyme OpaB, *opaB* was overexpressed in *A. nidulans* with the *gpdA* promoter from *A. fumigatus*¹⁸. Ten milliliter PDB with 75 µL 0.5 mg mL⁻¹ riboflavin and 10 µL 0.5 mg mL⁻¹ pyridoxine in a 25 mL erlenmeyer flask were inoculated at 230 rpm and 30 °C. One milligram of protuboxepin K (3) (8 mg mL⁻¹ DMSO) was added into 3 days old culture of the transformant *A. nidulans* LZ61. 16 h later, 1 mL culture was extracted with 1 mL EtOAc. The extracts were dried and dissolved in 100 µL DMSO for LC–MS analysis. Strain LZ61 without feeding protuboxepin K (3) and *A. nidulans* assembled empty vector with or without feeding protuboxepin K (3) were used as negative controls.

HPLC analysis and metabolite isolation. Fungal extracts were analyzed on an Agilent HPLC series 1200 (Agilent Technologies) by using an Eclipse XDB-C18 column (Agilent Technologies, 5 µm, 4.6 × 150 mm) and ACN/H₂O as elution solvents. A linear gradient from 10 to 90% ACN in H₂O containing 0.1% (v/v) HCOOH in 20 min was used. After washing with 100% ACN for 5 min, the column was equilibrated with 10% ACN for another 5 min. A photodiode array detector was used for detection and the absorptions at 254 nm are illustrated in this study.

For product isolation, a Multospher 120 RP-18 column (5 µm, 10 × 250 mm) was used on the same HPLC system, with the same elution solvents at a flow rate of 2 mL min⁻¹. Separation was performed by isocratic elution with 45–70% ACN in H₂O containing 0.1% (v/v) HCOOH for 10–20 min, and.

LC–MS and MS analysis. Extracts were also analyzed on an Agilent HPLC 1260 series system equipped with a Bruker microTOF QIII mass spectrometer by using a Multospher 120 RP-18-5µ column (5 µm, 250 × 2 mm). Separation was accomplished in a 40 min linear gradient from 5 to 100% ACN in H₂O, both containing 0.1% (v/v) HCOOH at a flow rate of 0.25 mL min⁻¹. The column was then washed with 100% ACN for 5 min followed by equilibration with 5 % ACN for 10 min. Positive ions were scanned in the range of *m/z* 100–1500 under the following conditions: capillary voltage with 4.5 kV, collision energy with 8.0 eV and electrospray ionization. Mass calibration was achieved by using sodium formate in each run. Data collection and analysis were carried out with the Compass DataAnalysis 4.2 software (Bruker Daltonik, Bremen, Germany).

NMR analysis. Samples in high purity were dissolved in DMSO-*d*₆ or CDCl₃ and subjected to JEOL ECA-500 or ECA-400 (JEOL, Akishima, Tokyo, Japan) for taking NMR spectra. MestReNov.9.0.0 (Mestrelab Research, Santiago de Compostella, Spain) was used for spectral processing.

CD spectroscopic analysis. The samples were dissolved in CH₃OH and measured in the range of 200–400 nm by using a 1 mm path length quartz cuvette (Hellma Analytics, Mühlheim, Germany) on a J-815 CD spectrometer (Jasco Deutschland GmbH, Pfungstadt, Germany). The CD spectra are shown in Supplementary Fig. 3.

Measurement of optical rotations. Jasco DIP-370 at 25 °C equipped with the D-line of the sodium lamp at $\lambda = 589.3$ nm was utilized to measure the optical rotations of the isolated compounds in CHCl_3 or CH_3OH . The polarimeter was calibrated with the respective solvent before the measurement.

Reporting summary. Further information on research design is available in the Nature Research Reporting Summary linked to this article.

Data availability

The information of *opa* gene cluster can be obtained from JOMC01000153.1 in the NCBI database. The authors declare that all relevant data supporting the finding of this study are available within the paper and its Supplementary Information files. All data are available from the corresponding author on reasonable request. Source data are provided with this paper.

Received: 10 June 2020; Accepted: 4 September 2020;

Published online: 01 October 2020

References

- Lu, X. et al. Oxepinamides: Novel liver X receptor agonists from *Aspergillus puniceus*. *Eur. J. Org. Chem.* **2011**, 802–807 (2011).
- Liang, X. et al. Diketopiperazine-type alkaloids from a deep-sea-derived *Aspergillus puniceus* fungus and their effects on liver X receptor α . *J. Nat. Prod.* **82**, 1558–1564 (2019).
- Zhang, P., Li, X., Wang, J. & Wang, B. Oxepine-containing diketopiperazine alkaloids from the algal-derived endophytic fungus *Paecilomyces variotii* EN-291. *Helv. Chim. Acta* **98**, 800–804 (2015).
- Zhang, P. et al. Variopexine A, a 3H-oxepine-containing alkaloid with a new oxa-cage from the marine algal-derived endophytic fungus *Paecilomyces variotii*. *Org. Lett.* **16**, 4834–4837 (2014).
- Zhuravleva, O. I. et al. New metabolites from the algal associated marine-derived fungus *Aspergillus carneus*. *Nat. Prod. Commun.* **8**, 1071–1074 (2013).
- González-Jartín, J. M., Alfonso, A., Sainz, M. J., Vieytes, M. R. & Botana, L. M. Identification of circumdatins produced by *Aspergillus ochraceus*. *J. Agr. Food Chem.* **65**, 4843–4852 (2017).
- Wang, J. et al. Antifungal new oxepine-containing alkaloids and xanthenes from the deep-sea-derived fungus *Aspergillus versicolor* SCSIO 05879. *J. Agric. Food Chem.* **64**, 2910–2916 (2016).
- Yan, D. et al. Complexity and diversity generation in the biosynthesis of fumiquinazoline-related peptidyl alkaloids. *Org. Lett.* **21**, 1475–1479 (2019).
- Gao, X. et al. Cyclization of fungal nonribosomal peptides by a terminal condensation-like domain. *Nat. Chem. Biol.* **8**, 823–830 (2012).
- Wang, P. M. et al. TrpE feedback mutants reveal roadblocks and conduits toward increasing secondary metabolism in *Aspergillus fumigatus*. *Fungal Genet. Biol.* **89**, 102–113 (2016).
- Blin, K. et al. antiSMASH 5.0: updates to the secondary metabolite genome mining pipeline. *Nucleic Acids Res.* **47**, W81–W87 (2019).
- Pi, B. et al. A genomics based discovery of secondary metabolite biosynthetic gene clusters in *Aspergillus ustus*. *PLoS ONE* **10**, e0116089 (2015).
- Walsh, C. T., Haynes, S. W., Ames, B. D., Gao, X. & Tang, Y. Short pathways to complexity generation: fungal peptidyl alkaloid multicyclic scaffolds from anthranilate building blocks. *ACS Chem. Biol.* **8**, 1366–1382 (2013).
- Fan, J. et al. Peniphenone and penilactone formation in *Penicillium crustosum* via 1,4-Michael additions of *ortho*-quinone methide from hydroxyclovatol to γ -butyrolactones from crustosic acid. *J. Am. Chem. Soc.* **141**, 4225–4229 (2019).
- Beaudry, C. M., Malerich, J. P. & Trauner, D. Biosynthetic and biomimetic electrocyclizations. *Chem. Rev.* **105**, 4757–4778 (2005).
- Fan, Y. et al. Alkaloids with cardiovascular effects from the marine-derived fungus *Penicillium expansum* Y32. *Mar. Drugs* **13**, 6849–6504 (2015).
- Ohte, S. et al. A new diketopiperazine-like inhibitor of bone morphogenetic protein-induced osteoblastic differentiation produced by marine-derived *Aspergillus* sp. BFM-0085. *J. Antibiot.* **73**, 554–558 (2020).
- Yin, W. B. et al. Discovery of cryptic polyketide metabolites from dermatophytes using heterologous expression in *Aspergillus nidulans*. *ACS Synth. Biol.* **2**, 629–634 (2013).
- van Leeuwen, J., Andrews, B., Boone, C. & Tan, G. Rapid and efficient plasmid construction by homologous recombination in yeast. *Cold Spring Harb. Protoc.* **2015**, 853–861 (2015).
- Chiang, Y. M. et al. An efficient system for heterologous expression of secondary metabolite genes in *Aspergillus nidulans*. *J. Am. Chem. Soc.* **135**, 7720–7731 (2013).
- Lee, S. U. et al. Protuboxepins A and B and protubonines A and B from the marine-derived fungus *Aspergillus* sp. SF-5044. *J. Nat. Prod.* **74**, 1284–1287 (2011).
- Syed, K. & Mashele, S. S. Comparative analysis of P450 signature motifs EXXR and CXG in the large and diverse kingdom of fungi: identification of evolutionarily conserved amino acid patterns characteristic of P450 family. *PLoS ONE* **9**, e95616–1–e95616–14 (2014).
- Schneider, T. D. & Stephens, R. M. Sequence logos: a new way to display consensus sequences. *Nucleic Acids Res.* **18**, 6097–6100 (1990).
- Crooks, G. E., Hon, G., Chandonia, J. M. & Brenner, S. E. WebLogo: a sequence logo generator. *Genome Res.* **14**, 1188–1190 (2004).
- Jin, S., Bryson, T. A. & Dawson, J. H. Hydroperoxoferric heme intermediate as a second electrophilic oxidant in cytochrome P450-catalyzed reactions. *J. Biol. Inorg. Chem.* **9**, 644–653 (2004).
- Sono, M., Roach, M. P., Coulter, E. D. & Dawson, J. H. Heme-containing oxygenases. *Chem. Rev.* **96**, 2841–2888 (1996).
- Vogel, E. & Günther, H. Benzene oxide-oxepin valence tautomerism. *Angew. Chem. Intern. Ed.* **6**, 385–401 (1967).
- Stok, J. E. et al. Direct observation of an oxepin from a bacterial cytochrome P450-catalyzed oxidation. *Chem. Eur. J.* **22**, 4408–4412 (2016).
- Spieker, M., Saleem-Batcha, R. & Teufel, R. Structural and mechanistic basis of an oxepin-CoA forming isomerase in bacterial primary and secondary Metabolism. *ACS Chem. Biol.* **14**, 2876–2886 (2019).
- Guo, C. J. et al. Biosynthetic pathway for the epipolythiodioxopiperazine acetylarnotin in *Aspergillus terreus* revealed by genome-based deletion analysis. *J. Am. Chem. Soc.* **135**, 7205–7213 (2013).
- Valentino, H. et al. Structure and function of a flavin-dependent S-monooxygenase from garlic (*Allium sativum*). *J. Biol. Chem.* **295**, 11042–11055 (2020).
- Copeland, R. A. *Enzymes: A Practical Introduction to Structure, Mechanism, and Data Analysis*. (Wiley, New York, 2000).
- Teufel, R. Flavin-catalyzed redox tailoring reactions in natural product biosynthesis. *Arch. Biochem. Biophys.* **632**, 20–27 (2017).
- Huijbers, M. M. E., Montersino, S., Westphal, A. H., Tischler, D. & van Berkel, W. J. Flavin dependent monooxygenases. *Arch. Biochem. Biophys.* **544**, 2–17 (2014).
- Haynes, S. W., Gao, X., Tang, Y. & Walsh, C. T. Assembly of asperlicin peptidyl alkaloids from anthranilate and tryptophan: a two-enzyme pathway generates heptacyclic scaffold complexity in asperlicin E. *J. Am. Chem. Soc.* **134**, 17444–17447 (2012).
- Fraley, A. et al. Molecular basis for spirocycle formation in the paraherquamide biosynthetic pathway. *J. Am. Chem. Soc.* **142**, 2244–2252 (2020).
- Wiese, A., Pietzsch, M., Syltack, C., Mattes, R. & Altenbuchner, J. Hydantoin racemase from *Arthrobacter aureus* DSM 3747: heterologous expression, purification and characterization. *J. Biotechnol.* **80**, 217–230 (2000).
- Duan, Y., Petzold, M., Saleem-Batcha, R. & Teufel, R. Bacterial tropone natural products and derivatives: Overview of their biosynthesis, bioactivities, ecological role and biotechnological potential. *Chembiochem* **21**, 2384–2407 (2020).
- Hur, G. H., Vickery, C. R. & Burkart, M. D. Explorations of catalytic domains in non-ribosomal peptide synthetase enzymology. *Nat. Prod. Rep.* **29**, 1074–1098 (2012).
- Ogasawara, Y. & Dai, T. Peptide epimerization machineries found in microorganisms. *Front. Microbiol.* **9**, 1–8 (2018).
- Weber, T. et al. Metabolic engineering of antibiotic factories: new tools for antibiotic production in actinomycetes. *Trends Biotechnol.* **33**, 15–26 (2015).
- Chiang, Y. M. et al. Development of genetic dereplication strains in *Aspergillus nidulans* results in the discovery of aspercryptin. *Angew. Chem. Int. Ed. Engl.* **55**, 1662–1665 (2016).

Acknowledgements

We thank Rixa Kraut, Lena Ludwig-Radtke, and Stefan Newel for taking MS and NMR spectra, Lena Ludwig-Radtke and Yiling Yang for technical assistance. This project was funded in part by the Deutsche Forschungsgemeinschaft (DFG, INST 160/620-1). Lijuan Zheng (201604910536) is a scholarship recipient from the China Scholarship Council. The CD spectrometer was provided by the core facility for protein biochemistry and spectroscopy in the Institute of Cytobiology.

Author contributions

S.-M.L. directed the research. L.Z. conducted genetic manipulation and biochemical studies. H.W. performed compound isolation and structure elucidation. L.Z., H.W., A.F., and S.-M.L. designed the experiments, analyzed the data, and wrote the manuscript. L.Z. and H.W. contributed equally to this work.

Funding

Open Access funding enabled and organized by Projekt DEAL.

Competing interests

The authors declare no competing interests.

Additional information

Supplementary information is available for this paper at <https://doi.org/10.1038/s41467-020-18713-0>.

Correspondence and requests for materials should be addressed to S.-M.L.

Peer review information *Nature Communications* thanks the anonymous reviewers for their contribution to the peer review of this work. Peer review reports are available.

Reprints and permission information is available at <http://www.nature.com/reprints>

Publisher's note Springer Nature remains neutral with regard to jurisdictional claims in published maps and institutional affiliations.



Open Access This article is licensed under a Creative Commons Attribution 4.0 International License, which permits use, sharing, adaptation, distribution and reproduction in any medium or format, as long as you give appropriate credit to the original author(s) and the source, provide a link to the Creative Commons license, and indicate if changes were made. The images or other third party material in this article are included in the article's Creative Commons license, unless indicated otherwise in a credit line to the material. If material is not included in the article's Creative Commons license and your intended use is not permitted by statutory regulation or exceeds the permitted use, you will need to obtain permission directly from the copyright holder. To view a copy of this license, visit <http://creativecommons.org/licenses/by/4.0/>.

© The Author(s) 2020

Supporting Information

Oxepinamide F biosynthesis involves enzymatic D-aminoacyl epimerization, 3*H*-oxepin formation, and hydroxylation induced double bond migration

Zheng et al.

This PDF file contains:

- Supplementary Tables
- Supplementary Figures
- Supplementary Note 1
- Supplementary References

Supplementary Tables

Supplementary Table 1. Putative functions of the genes from opa gene cluster

Protein	No.	Size (aa)	coverage/identity, homologous protein, organism	Putative function
OpA	KIA75458	3901	95/39 nonribosomal peptide synthetase FmqA, Q4WLW5.1, <i>Aspergillus fumigatus</i> Af293	quinazolinone formation
OpB	KIA75457	575	84/30, Cytochrome P450 PenB, ANY57880.1, <i>Penicillium thymicola</i>	P450, Oxepin formation
OpC	KIA75456	462	93/40, FAD-dependent monooxygenase NodY2, A0A2I6PIZ8.1, <i>Hyphoxylon pulicicidium</i>	C-12 hydroxylation
OpD	KIA75455	587	98/51, efflux pump RoqT, KAF3399802.1, <i>Penicillium rolfsii</i>	transport
OpE	KIA75454	274	79/28 hydantoin racemase, Q9F466.1, <i>Paenarthrobacter aureus</i>	C-15 epimerization
OpF	KIA75453	420	86/39, O-methyltransferase KntB, A2QK65.1 (XP_001402308.1), <i>Aspergillus niger</i> CBS 513.88	O-methylation

Supplementary Table 2. Strains used in this study

Strains	Genotype
Wild type	<i>A. ustus</i> 3.3904
$\Delta opaA$	$\Delta opaA::hph$ in <i>A. ustus</i> 3.3904
$\Delta opaB$	$\Delta opaB::hph$ in <i>A. ustus</i> 3.3904
$\Delta opaC$	$\Delta opaC::hph$ in <i>A. ustus</i> 3.3904
$\Delta opaE$	$\Delta opaE::hph$ in <i>A. ustus</i> 3.3904
$\Delta opaF$	$\Delta opaF::hph$ in <i>A. ustus</i> 3.3904
<i>A. nidulans</i> LO8030	<i>pyroA4</i> , <i>riboB2</i> , <i>pyrG89</i> , <i>nkuA::argB</i> sterigmatocystin cluster (<i>AN7804-AN7825</i>) Δ , emerlicellamide cluster (<i>AN2545-AN2549</i>) Δ , asperfuranone cluster (<i>AN1039-AN1029</i>) Δ , monodictyphenone cluster (<i>AN10023-AN10021</i>) Δ , terrequinone cluster (<i>AN8512-AN8520</i>) Δ , austinol cluster part 1 (<i>AN8379-AN8384</i>) Δ , austinol cluster part 2 (<i>AN9246-AN9259</i>) Δ , F9775 cluster (<i>AN7906-AN7915</i>) Δ , asperthecin cluster (<i>AN6000-AN6002</i>) Δ
LZ61	<i>gpdA::opaB::Afp_{pyrG}</i> in <i>A. nidulans</i> LO8030

Supplementary Table 3. Plasmids constructed and used in this study

Plasmids	Description
p5HY	Two-third of the hph resistance gene at the 5'-end, originated from the pUChph and inserted into pESC-URA. For gene replacement using hph as selection marker.
p3YG	Two-third of the <i>hph</i> resistance gene at the 3'-end, originated from the pUChph and inserted into pESC-URA. For gene replacement using <i>hph</i> as selection marker.
PLZ131 (p5HY- <i>opaA</i>)	a 1453 bp US PCR fragment of <i>opaA</i> from genomic DNA of <i>A. ustus</i> 3.3904 inserted in p5HY.
PLZ132 (p3YG- <i>opaA</i>)	a 1427 bp DS PCR fragment of <i>opaA</i> from genomic DNA of <i>A. ustus</i> 3.3904 inserted in p3YG.
PLZ133 (p5HY- <i>opaB</i>)	a 1252 bp US PCR fragment of <i>opaB</i> from genomic DNA of <i>A. ustus</i> 3.3904 inserted in p5HY.
PLZ134 (p3YG- <i>opaB</i>)	a 1285 bp DS PCR fragment of <i>opaB</i> from genomic DNA of <i>A. ustus</i> 3.3904 inserted in p3YG.
PLZ135 (p5HY- <i>opacC</i>)	a 1303 bp US PCR fragment of <i>opacC</i> from genomic DNA of <i>A. ustus</i> 3.3904 inserted in p5HY.
PLZ136 (p3YG- <i>opacC</i>)	a 1247 bp DS PCR fragment of <i>opacC</i> from genomic DNA of <i>A. ustus</i> 3.3904 inserted in p3YG.
PLZ137 (p5HY- <i>opaeE</i>)	a 1391 bp US PCR fragment of <i>opaeE</i> from genomic DNA of <i>A. ustus</i> 3.3904 inserted in p5HY.
PLZ138 (p3YG- <i>opaeE</i>)	a 1231 bp DS PCR fragment of <i>opaeE</i> from genomic DNA of <i>A. ustus</i> 3.3904 inserted in p3YG.
PLZ139 (p5HY- <i>opafF</i>)	a 1277 bp US PCR fragment of <i>opafF</i> from genomic DNA of <i>A. ustus</i> 3.3904 inserted in p5HY.
PLZ140 (p3YG- <i>opafF</i>)	a 1253 bp DS PCR fragment of <i>opafF</i> from genomic DNA of <i>A. ustus</i> 3.3904 inserted in p3YG.
PLZ61	<i>pYH-gpda-opaB-pyrG</i> ; a 2957 bp fragment of <i>opaB</i> with its terminator from genomic DNA of <i>A. ustus</i> 3.3904 inserted in <i>pYH-gpda-pyrG</i>
PLZ62	PET-28a(+)- <i>opacC</i> ; a 1595 bp fragment of <i>opacC</i> from cDNA of <i>A. ustus</i> 3.3904 with BamHI and EcoRI inserted in PET28a(+)
PLZ63	PET-28a(+)- <i>opaeE</i> ; a 825 bp fragment of <i>opaeE</i> from cDNA of <i>A. ustus</i> 3.3904 with BamHI and EcoRI inserted in PET28a(+)

US: upstream; DS: downstream

Supplementary Table 4. Primers used in this study

Primers	Sequence 5'-3'	Targeted amplification
P5HY	CAAGACCAATGCCGAGCATATAC	2/3 of the <i>hph</i> resistance gene at the 5'-end from pUChp to construct p5HY
P3YG	GAATTGATTCCGGAAGTGCTTGAC	2/3 of the <i>hph</i> resistance gene at the 3'-end from pUChp to construct p3YG
p5HY-R	GCTGAAGTCGATTTGAGTCAC	US of <i>hph</i> to verify 5F of <i>A. ustus</i> 3.3904 mutant
p3YG-F	GCATTAAATGCATTGGACCTCGC	DS of <i>hph</i> to verify 3F of <i>A. ustus</i> 3.3904 mutant
opaA-U-F	ACCCCTCACTAAAGGCGCGCCGCACTAGGTCCTTTGTAGCGGGAGTTGTC	1453bp US fragment of <i>opaA</i> to construct pLZ131
opaA-U-R	AAGAATTGTTAATTAAAGAGCTCAGATCCACCTTCATGCATCGCACCTACA	
opaA-D-F	ACTCACTATAGGGCCCGGCGCTCGAAGCTCCACACAAGGATGACTGT	
opaA-D-R	TAGCCGCGGTACCAAGCTTACTCGAACAATCTCCTAGCGTACATACGG	1427 bp DS fragment of <i>opaA</i> to construct pLZ132
opaA-F	ATCCAGAGGCCCATTCAGATGG	
opaA-R	CCCGTGATCCTGACGTAAT	1556 bp partial fragment of <i>opaA</i>
opaA-5F-F	CGGGCATGATTGCTTCACA	US of <i>hph</i> to verify Δ <i>opaA</i> mutant
opaA-3F-R	AGCCATGGATGTTGGCAGTC	DS of <i>hph</i> to verify Δ <i>opaA</i> mutant
opab-U-F	AAGAATTGTTAATTAAAGAGCTCAGATCGGTACCTTACAATGTGGGGT	
opab-U-R	ACCCCTCACTAAAGGCGCGCCGCACTAGAGTGTCTGTACTCCTGTTG	1252 bp US fragment of <i>opab</i> to construct pLZ133
opab-D-F	ACTCACTATAGGGCCCGGCGCTCGACACGGGTCAAGGTTGTTCAAT	
opab-D-R	TAGCCGCGGTACCAAGCTTACTCGAATCTCCCGTTGTATCGGAGAG	1285 bp DS fragment of <i>opab</i> to construct pLZ134
opab-F	CCCGCGAGATCATGATATCAT	
opab-R	GCACGTATCCTGGTGAACATG	1542 bp partial fragment of <i>opab</i>
opab-5F-F	CCTCAGTCTCGAATGGCAATG	US of <i>hph</i> to verify Δ <i>opab</i> mutant

Supplementary Table 4. (continued)

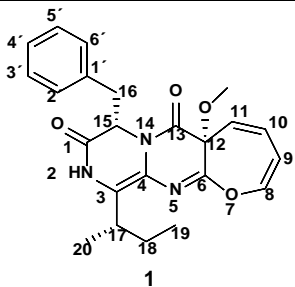
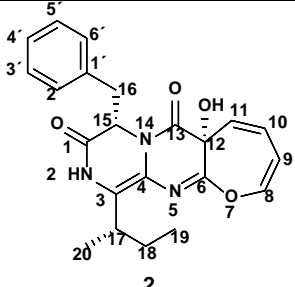
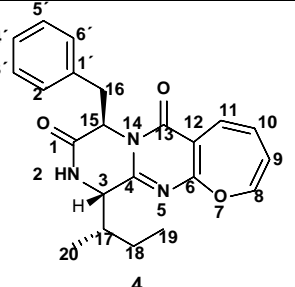
opaB-3F-R	TCGCTTCATCCAACTCCCTGGT	DS of <i>hph</i> to verify Δ <i>opaB</i> mutant
opac-U-F	AAGAATTGTTAATTAAAGAGCTCAGATCAAGGATGGAAGCTGCGAGAT	
opac-U-R	ACCCCTACTAAAGGGCGCGCCGCACTAGGCTGTGTACGAGCATTTGGAATT	1303 bp US fragment of <i>opac</i> to construct pLZ135
opac-D-F	ACTCAGTATAGGGCCCGGGCGTCGATTTGGTGAGAATGGGGACAGG	
opac-D-R	TAGCCGCGGTACCAAGCTTACTCGACTGGAATCAGTCAAGGGGGAT	1247 bp DS fragment of <i>opac</i> to construct pLZ136
opac-F	TTTTCGCCGTGCTTACTGAGGC	
opac-R	AGCTTGAGAACCTCGAACCAT	1486 bp partial fragment of <i>opac</i>
opac-5F-F	TCTATTGCGGATCCATTCTGCG	US of <i>hph</i> to verify Δ <i>opac</i> mutant
opac-3F-R	CCCGCACAAAGAGAAATAACC	DS of <i>hph</i> to verify Δ <i>opac</i> mutant
opae-U-F	AAGAATTGTTAATTAAAGAGCTCAGATCGTTACTCTATCCTAGCAACGCC	
opae-U-R	ACCCCTACTAAAGGGCGCGCCGCACTAGCTTTTGCAAGGTTGTGCGC	1391 bp US fragment of <i>opae</i> to construct pLZ137
opae-D-F	ACTCAGTATAGGGCCCGGGCGTCGAGGAGTGATGTTAGGACTTC	
opae-D-R	TAGCCGCGGTACCAAGCTTACTCGACGAGCATGTAGGCACTGACATA	1231 bp DS fragment of <i>opae</i> to construct pLZ138
opae-F	CCGCAAGCTTGTGACGGAGCTCGAATTCCTAGATTTCAATCCTCCAC	
opae-R	TGGTGACAGCAAAATGGGTCGCGGATCCATGGGTCCTCCTCGTGTTTT C	825 bp partial fragment of <i>opae</i>
opae-5F-F	GTGTGCTGCTGCCCTTTGCTA	US of <i>hph</i> to verify Δ <i>opae</i> mutant
opae-3F-R	TGTTCCAGAAATTGCTCGTCCG	DS of <i>hph</i> to verify Δ <i>opae</i> mutant
opaf-U-F	AAGAATTGTTAATTAAAGAGCTCAGATCGACACGTGCTCTTACAGTGC	
opaf-U-R	ACCCCTACTAAAGGGCGCGCCGCACTAGCTATAAAGGTCGGAAGCGGAG	1277 bp US fragment of <i>opaf</i> to construct pLZ139
opaf-D-F	ACTCAGTATAGGGCCCGGGCGTCGAGAAGACTCGTACAGTGTGCCCT	
opaf-D-R	TAGCCGCGGTACCAAGCTTACTCGAAAGGAAGTATCCAGCTGCAG	1253 bp DS fragment of <i>opaf</i> to construct pLZ140

Supplementary Table 4. (continued)

opaF-F	TCTCTACGCGGAATCCAGCT	1448 bp partial fragment of opaF
opaF-R	CTCAGACGCGAAAGGTGTCATGA	
opaF-5F-F	CCCCATGGGTTGACCAATTAGG	US of <i>hph</i> to verify Δ opaF mutant
opaF-3F-R	AGTCTCCCCCATGGCTTAAAG	DS of <i>hph</i> to verify Δ opaF mutant
HE-opaB-F	CATCTTCCCATCCAAGAACCCTTAATCATGGCGGTTGCCCAATGTCT	2957 bp partial fragment of opaB from <i>A. ustus</i>
HE-opaB-R	TCGTACAGACAGAAATACTCTCGCTAGTTGCCATTAGGCGTCTGGCT	3.3904 to construct pLZ61
PET-opaC-F	GCAAGCTTGTGACGGAAGCTCGAATTCCTAATTTTTTCTTTCTCGTCG	1375 bp fragment of opaC <i>A. ustus</i> 3.3904 cDNA
PET-opaC-R	GGTGACACAGCAAAATGGGTCGCGGATCCATGACTGTCCCCCAATACATC G	with was fused into pET28a(+) to construct pLZ62
PET-opaE-F	CCGCAAGCTTGTGACGGAAGCTCGAATTCCTAGATTTCATTCCTTCCAC	825 bp fragment of opaE from <i>A. ustus</i> 3.3904
PET-opaE-R	TGGTGACACAGCAAAATGGGTCGCGGATCCATGGGTCCTCTCCGTGTTTT C	cDNA was fused into pET28a(+) to construct pLZ63

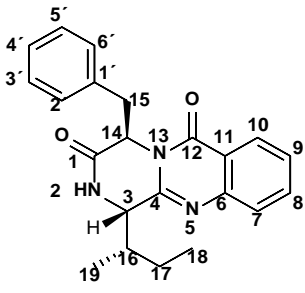
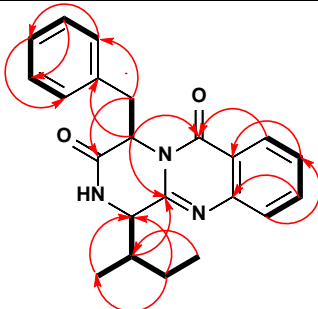
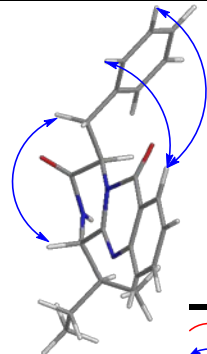
US: upstream; DS: downstream

Supplementary Table 5. The ^1H and ^{13}C NMR spectroscopic data of oxepinamide F (1), E (2), and protuboxepin A (4)

<div style="display: flex; justify-content: space-around; align-items: center;"> <div style="text-align: center;">  <p>1</p> </div> <div style="text-align: center;">  <p>2</p> </div> <div style="text-align: center;">  <p>4</p> </div> </div>						
solvents	DMSO- d_6		DMSO- d_6		CDCl_3	
Position	δ_{H} (multi., J)	δ_{C}	δ_{H} (multi., J)	δ_{C}	δ_{H} (multi., J)	δ_{C}
1		165.3		165.0		167.9
2	9.89, s		9.73, s		7.08, s	
3		123.4		122.1	2.64, d, 2.8	58.6
4		115.1		115.7		156.3
6		151.8		153.3		163.1
8	6.74, d, 7.3	144.4	6.72, d, 7.3	144.2	6.04, d, 5.8	143.3
9	5.48, t, 7.1	104.0	5.49, t, 7.1	104.1	5.64, t, 5.8	117.3
10	6.24, dd, 10.0, 7.0	130.8	6.18, dd, 10.2, 7.0	129.6	6.17, dd, 11.2, 5.8	128.1
11	5.77, d, 10.0	127.0	5.89, d, 10.2	130.0	6.78, d, 11.2	125.6
12		76.3		70.0		110.3
12-OCH ₃ / 12-OH	2.77, s	52.3	6.34, s			
13		163.4		166.2		161.0
15	5.18, dd, 7.9, 5.7	55.8	5.03, dd, 6.9, 5.5	56.3	5.45, t, 4.7	57.0
16	2.88, m	36.4	2.96, dd, 13.7, 5.5	36.3	3.39 – 3.40, m	36.7
	3.12, dd, 13.7, 5.6		3.05, dd, 13.7, 6.9		3.39 – 3.40, m	
17	2.91, m	32.1	2.82, m	31.9	2.27, m	37.1
18	1.31, m	25.6	1.18, m	25.5	0.99 – 1.04, m	23.2
19	0.73, t, 7.4	12.1	0.62, t, 7.6	11.9	0.74, t, 7.5	12.0
20	0.95, d, 7.2	17.8	0.90, d, 7.3	17.5	0.85, d, 7.3	15.8
1'		135.1		135.4		134.4
2', 6'	7.08, d, 6.9	129.6	7.06, dd, 8.2	129.3	6.94, dd, 8.4, 1.5	129.8
3', 5'	7.24, t, 7.3	128.3	7.24, tt, 7.0, 1.6	128.2	7.24, tt, 7.0, 1.5	129.0
4'	7.18, d, 7.3	126.8	7.20, d, 7.1	126.7	7.30, t, 7.0	128.2

The NMR data of **1**, **2**, and **4** correspond well to those of oxepinamide F,¹ oxepinamide E,¹ and protuboxepin A,² respectively

Supplementary Table 6. The ^1H and ^{13}C NMR spectroscopic data with key HMBC, COSY, and NOESY correlations of protuboxepin K (3)

— COSY

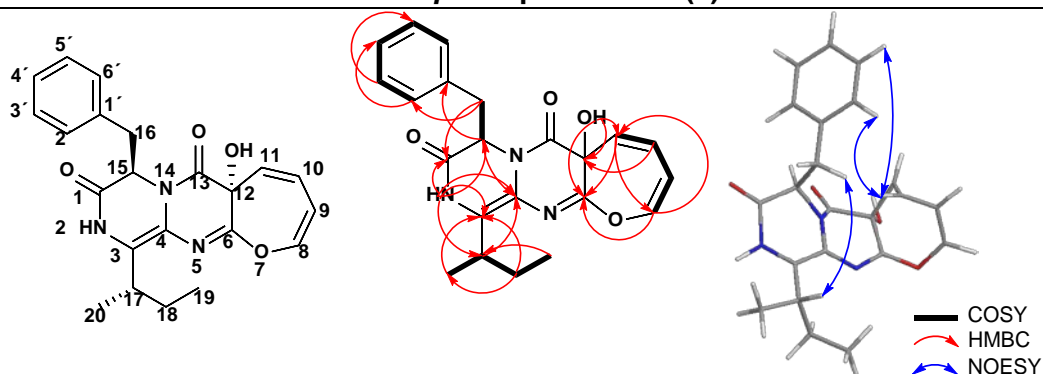
— HMBC

— NOESY

solvent		CDCl_3		
Position	δ_{H} (multi., J)	δ_{C}	HMBC	NOESY
1		168.8		
3	2.76, d, 2.2	58.4	C-4, C-16, C-17, C-19	H-15, H-16, H-19
4		150.3		
6		147.1		
7	7.62, br d, 8.3	127.5	C-6, C-8, C-9, C-11	H-8, H-9, H-10
8	7.78, ddd, 8.3, 7.2, 1.2	134.8	C-6, C-10, C-11	H-7, H-9, H-10
9	7.52, ddd, 8.0, 7.2, 1.2	127.2	C-6, C-7, C-8, C-11	H-7, H-8, H-10
10	8.34, dd, 8.0, 1.2	126.9	C-6, C-7, C-8, C-12	H-8, H-9, H-2',6', H-3',5'
11		120.1		
12		160.9		
14	5.64, br t, 4.7	57.1	C-1, C-4, C-1', C-15, C-12	H-15, H-2',6'
15	3.47, dd, 13.8, 5.5 3.44, dd, 13.8, 4.0	37.3	C-1, C-1', C-14, C-2',6'	H-3, H-14, H-2',6'
16	2.47, m	36.5	C-4, C-17, C-18, C-19	H-3, H-17, H-18, H-19
17	1.19, m	23.3	C-3, C-16, C-18, C-19	H-16, H-18, H-19
	1.04, m			H-16, H-18, H-19
18	0.77, t, 7.4	12.3	C-16, C-17	H-16, H-17, H-19
19	0.91, d, 7.3	15.8	C-3, C-16, C-17	H-3, H-16, H-17, H-18
1'		135.1		
2',6'	6.92, dd, 8.2, 1.4	129.9	C-1, C-4, C-1', C-4', C-2',6', C-14, C-15	H-10, H-14, H-15, H-3',4',5'
3',5'	7.18, t, 7.5	128.8	C-1', C-3',5'	H-10, H-2',4',6'
4'	7.27, t, 7.5	128.0	C-1', C-2',6'	H-2',6', H-3',5'

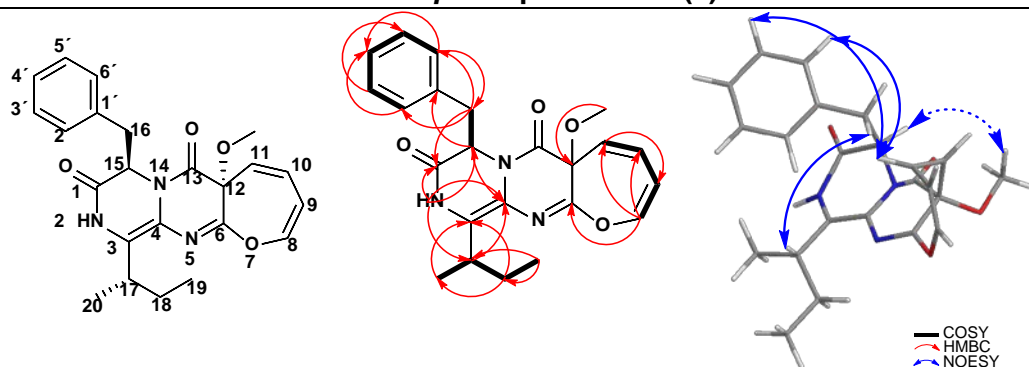
The NMR data of **3** correspond well to those of protuboxepin K, published recently by Ohte *et al.*³

Supplementary Table 7. The ^1H and ^{13}C NMR spectroscopic data with key HMBC, COSY, and NOESY correlations of 15-*epi*-oxepinamide E (5)

































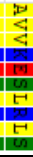


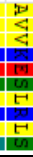





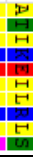





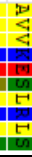























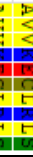


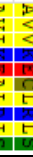


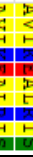




















solvent		DMSO- d_6		
Positio	$\delta_{\text{H}}(\text{multi.}, J)$	δ_{C}	HMBC	NOESY
n				
1		164.9		
2	9.64, s		C-1, C-3, C-4, C-15, C-17	H-20, H-3',4',5'
3		120.7		
4		116.2		
6		153.5		
8	6.64, d, 7.2	144.0	C-6, C-10, C-9, C-11	H-9, H-10, H-11, H-2',6', H-3',5'
9	5.49, t, 7.2	105.3	C-8, C-11	H-8, H-10, H-11, H-2',6', H-3',5'
10	6.12, dd, 10.4, 6.8	128.6	C-8, C-12	H-8, H-9, H-2',6', H-3',5'
11	5.70, d, 10.4	131.5	C-6, C-8, C-9, C-12, C-13	H-8, H-9, H-15
12-		69.6	C-6, C-11, C-12	
(OH)	6.52, s			
13		165.5		
15	5.19, t, 5.1	55.7	C-1, C-1', C-4, C-16	H-11
16	3.01, dd, 13.7, 5.3	36.5	C-1, C-1', C-2',6', C-15	H-17
	3.13, dd, 13.7, 5.0			H-17
17	2.82, m	31.5	C-3, C-4, C-18, C-19, C-20	H-16, H-18, H-19, H-20
18	1.40, m	25.7	C-3, C-17, C-19, C-20	H-17, H-18b, H-19, H-20
	1.30, m			H-17, H-18a, H-19, H-20
19	0.67, t, 7.4	11.9	C-17, C-18	H-17, H-18, H-20
20	0.63, d, 7.1	17.0	C-3, C-17, C-18	HN-2, H-17, H-18, H-19
1'		135.0		
2', 6'	7.00, dd, 7.0, 2.9	129.6	C-4', C-2',6', C-16	H-8, H-9, H-10, H-3',4',5'
3', 5'	7.20, m	128.1	C-1', C-3',5', C-2',6'	HN-2, H-8, H-9, H-10, H-2',6'
4'	7.20, m	126.8	C-1', C-2',6'	HN-2, H-10, H-2',6',H-3',5'

Supplementary Table 8. The ^1H and ^{13}C NMR spectroscopic data with key HMBC, COSY, and NOESY correlations of 15-*epi*-oxepinamide F (6)

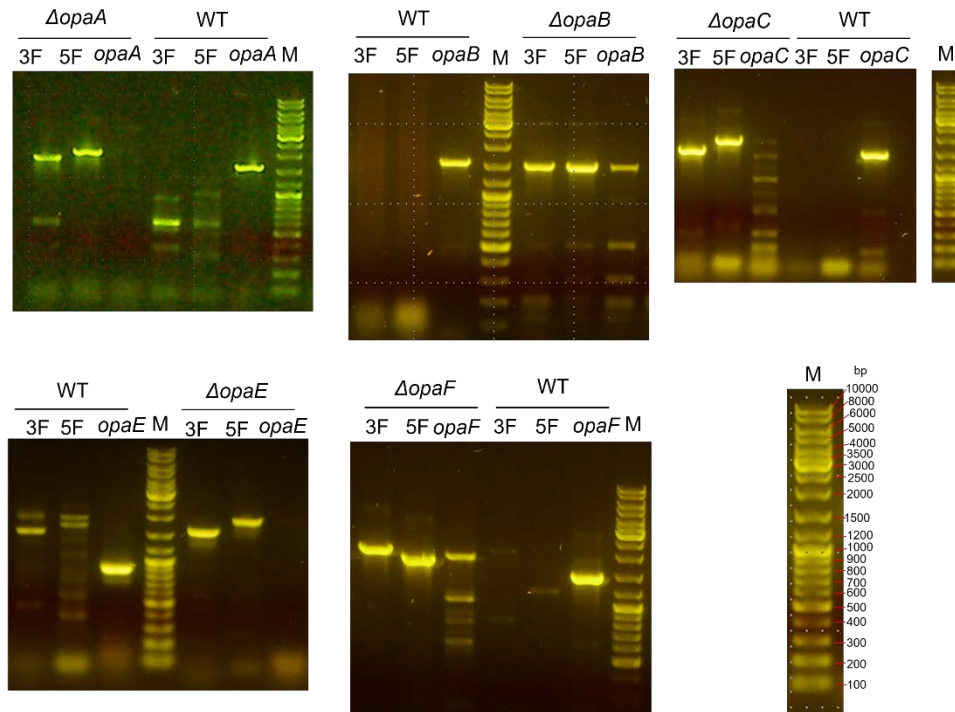


solvent		DMSO- d_6		
Positio	$\delta_{\text{H}}(\text{multi.}, \text{J})$	δ_{C}	HMBC	NOESY
n				
1		165.0		
2	9.75, s		C-1, C-3, C-4, C-15, C-17	H-18, H-20, H-3', 5', H-2', 6', H-4'
3		122.0		
4		115.9		
6		151.3		
8	6.67, d, 7.2	144.3	C-6, C-10, C-9, C-11	H-9, H-10, H-11, H-2', 6'
9	5.50, t, 7.2	105.4	C-8, C-10, C-11	H-8, H-10, H-11, OCH ₃ -12, H-15
10	6.21, dd, 10.4, 6.8	128.7	C-8, C-12	H-8, H-9, H-11, H-2', 6', H-3', 5'
11	5.64, d, 10.4	130.0	C-6, C-8, C-9, C-12, C-13	H-8, H-9, H-10, H-15
12		76.1		
12-OCH ₃	3.11, s	52.8	C-12	H-9, H-15
13		163.0		
15	5.24, t, 5.2	55.9	C-1, C-1', C-4, C-13, C-16	H-9, H-11, OCH ₃ -12, H-16a
16	3.01, dd, 14.1, 5.3 3.14, dd, 14.1, 5.1	36.4	C-1, C-1', C-2', 6', C-15	H-15, H-16b, H-17 H-16a, H-17
17	2.84, m	31.6	C-3, C-18, C-20	H-16a, H-16b, H-18a, H-20
18	1.41, m 1.30, m	25.8	C-17, C-19 C-3, C-17, C-19, C-20	HN-2, H-17, H-18b, H-19, H-20 HN-2, H-18a, H-19, H-20
19	0.66, t, 7.4	11.7	C-3, C-17, C-18	H-18, H-20
20	0.66, d, 7.0	16.9	C-3, C-17, C-18	HN-2, H-17, H-18, H-19
1'		134.9		
2', 6'	6.99, dd, 7.0, 3.0	129.6	C-4', C-2', 6', C-16	HN-2, H-8, H-10, H-3', 5', H-4'
3', 5'	7.20, m	128.2	C-1', C-3', 5', C-2', 6'	HN-2, H-10, H-2', 6', H-4'
4'	7.20, m	126.8	C-1', C-2', 6'	HN-2, H-10, H-2', 6', H-3', 5'

Supplementary Table 9. Conserved motifs in P450 enzymes used in Weblogo analysis for Opab

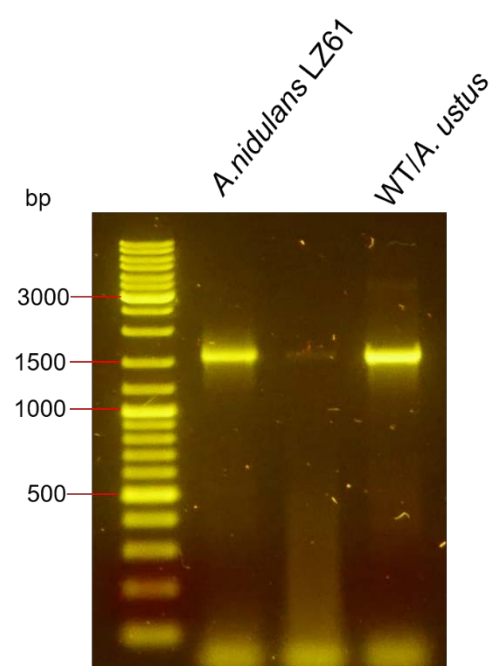
Entries	Conserved sequence	Entries	Conserved sequence	Entries	Conserved sequence
1. ACM47223.1_8-506	AVI 	33. KAF3893027.1_16-495	AVV 	65. RYP76854.1_33-503	AVM 
2. ADY18333.1_21-506	AVI 	34. KAF477391.1_24-504	AVI 	66. SCV45835.1_49-420	AVI 
3. AET10042.1_8-506	AVI 	35. KIA75457.1_1-575	AVI 	67. TEY57352.1_27-515	AAV 
4. AEV21239.1_8-506	AVI 	36. KIA75687.1_41-518	AI 	68. TGJ85573.1_7-412	A 
5. AGA37280.1_48-520	AVL 	37. KLP01168.1_49-420	AVI 	69. TGO15980.1_44-505	AVV 
6. AGN89898.1_8-506	AVI 	38. KPA41271.1_49-423	AVI 	70. TGO83795.1_21-421	AVV 
7. AGS31995.1_8-506	AVI 	39. KXG49075.1_25-413	GVI 	71. THC90386.1_21-501	AVV 
8. ANY57880.1_1-438	AVV 	40. KXH34948.1_24-504	AVI 	72. THV46788.1_67-578	AVV 
9. CEL05736.1_45-421	AVI 	41. KXH37991.1_15-507	AVI 	73. TRX96397.1_25-409	AAI 
10. CEO59279.1_38-411	AI 	42. KXH39310.1_24-504	AVI 	74. XP_001267636.1_26-411	AVI 
11. EGD97062.1_33-512	AVV 	43. KZL82384.1_37-422	A 	75. XP_015409727.1_24-402	AVI 
12. EGE01905.1_33-512	AVV 	44. OJI99626.1_8-543	AVI 	76. XP_016598809.1_33-416	AVI 
13. EYR81817.1_1-438	AVV 	45. OJU05850.1_14-509	AVV 	77. XP_018060973.1_14-510	AVV 
14. EQB44036.1_2-504	A 	46. OJU57312.1_40-512	AVV 	78. XP_020056257.1_2-494	AVI 
15. EXF79469.1_15-402	AVI 	47. OOO90409.1_38-411	AI 	79. XP_022388567.1_14-504	AVI 
16. EZF29424.1_16-495	AVV 	48. OOO91747.1_19-514	A 	80. XP_022470328.1_15-505	AVI 
17. GAO81247.1_31-521	AVV 	49. OOD98286.1_24-412	AVI 	81. XP_023426771.1_49-420	AVI 
18. GAO87325.1_29-521	AVI 	50. OQE41206.1_33-522	AVI 	82. XP_024548999.1_26-516	AVV 
19. GAO88330.1_104-491	AVI 	51. OQE41255.1_24-412	GVI 	83. XP_024678521.1_46-521	AVV 
20. GAM23203.1_12-418	A 	52. OTA60878.1_17-500	AVV 	84. XP_025429720.1_6-502	AVI 
21. GBF60059.1_16-495	AVV 	53. OTA61602.1_19-501	AVI 	85. XP_025434452.1_47-509	AVI 
22. GEF33539.1_29-518	AVI 	54. OTAB1174.1_25-500	AVV 	86. XP_025447741.1_31-508	AI 
23. GEF48416.1_46-521	AVV 	55. OTA98483.1_29-501	AVI 	87. XP_025487304.1_10-453	AVI 
24. GEF51631.1_31-523	AVV 	56. OTB14165.1_14-489	AVI 	88. XP_025502623.1_31-508	AI 
25. GEF92884.1_46-521	AVV 	57. FOS72677.1_32-504	A 	89. XP_026601988.1_19-498	AVV 
26. KAB8069486.1_31-399	AVI 	58. RAK81184.1_20-508	AI 	90. XP_026602854.1_14-530	AVI 
27. KAB8073414.1_5-387	AVI 	59. RHZ55947.1_35-408	AVI 	91. XP_026613670.1_71-448	AI 
28. KAE8351816.1_19-501	AVV 	60. RLL97463.1_15-497	AVI 	92. XP_026617163.1_53-522	AVV 
29. KAF0324645.1_2-504	A 	61. RMA13246.1_12-418	A 	93. XP_031881851.1_2-504	A 
30. KAF2971667.1_65-440	A 	62. RYC50098.1_7-408	AAV 	94. XP_033423998.1_21-503	AVV 
31. KAF3761239.1_6-482	AVI 	63. RYP2796.1_5-406	AVM 	95. XP_664089.1_6-392	AI 
32. KAF3809983.1_2-513	A 	64. RYP6740.1_19-400	AVI 	96. XP_682494.1_48-464	AI 

Supplementary Figures



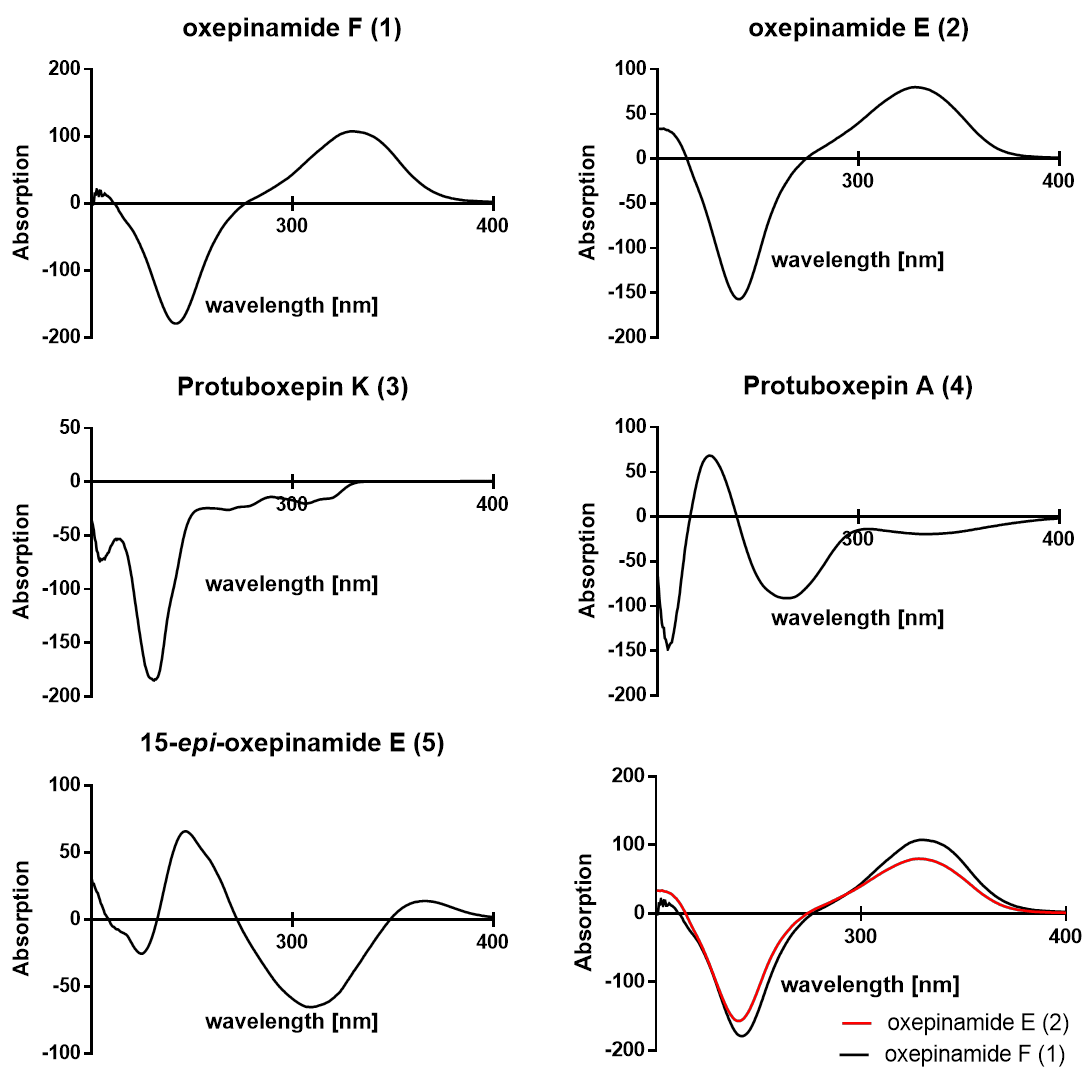
Supplementary Figure 1. PCR verification of deletion mutants of *A. ustus* 3.3904.

PCR amplification for three different fragments from genomic DNA of WT and deletion mutants was used to prove the presence/absence of the target gene and the integration site of the selection marker with up- and downstream regions. The PCR primers are given in Table S4. All the experiments were repeated twice.

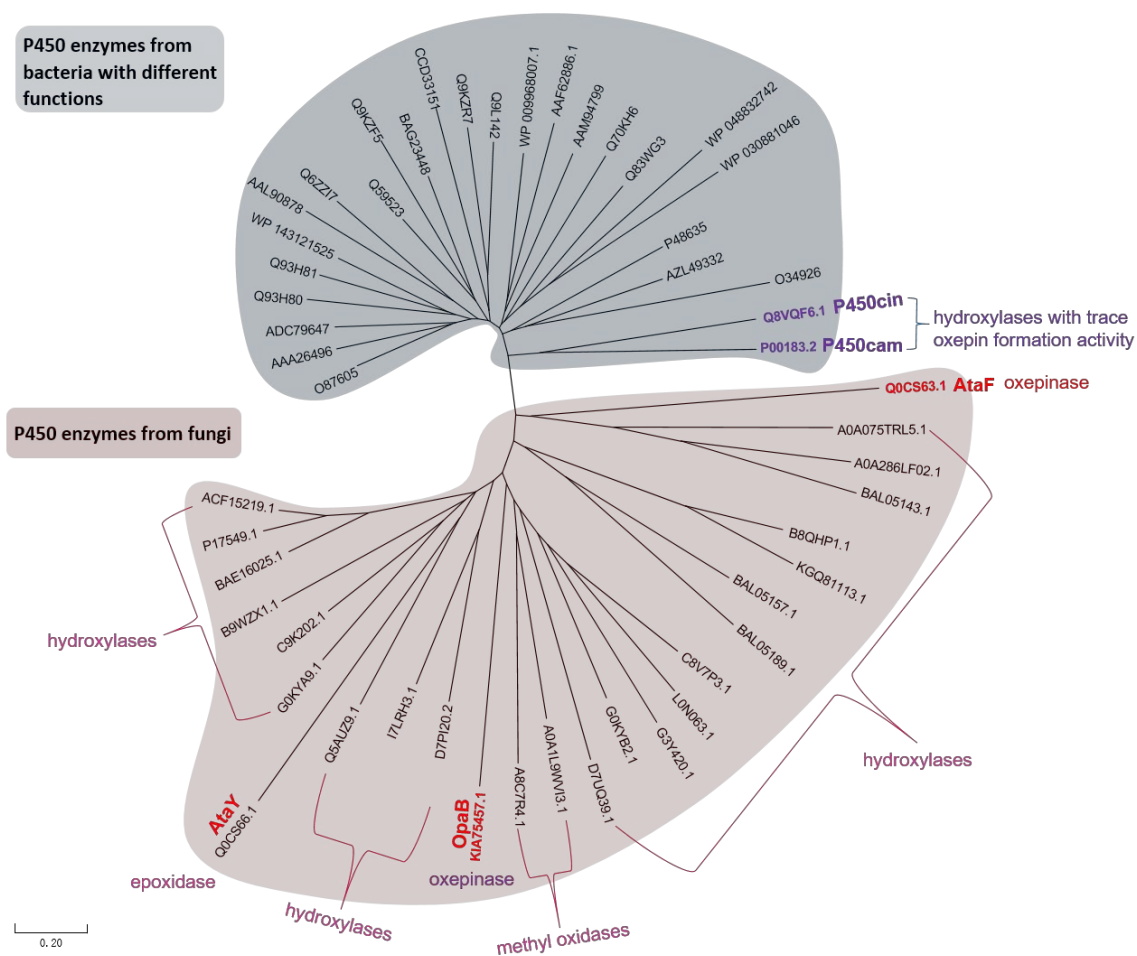


Supplementary Figure 2. PCR verification of *opaB* heterologous expression transformant

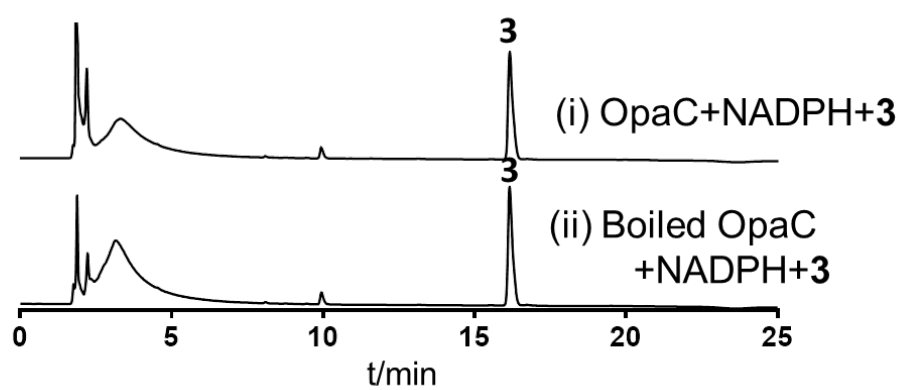
A. nidulans-pYH-*gpdA-opaB-pyrG* (HE-*opaB*). A fragment of 1.5 kb within the target gene was amplified from the primers listed in Table S4. The experiments were repeated twice.



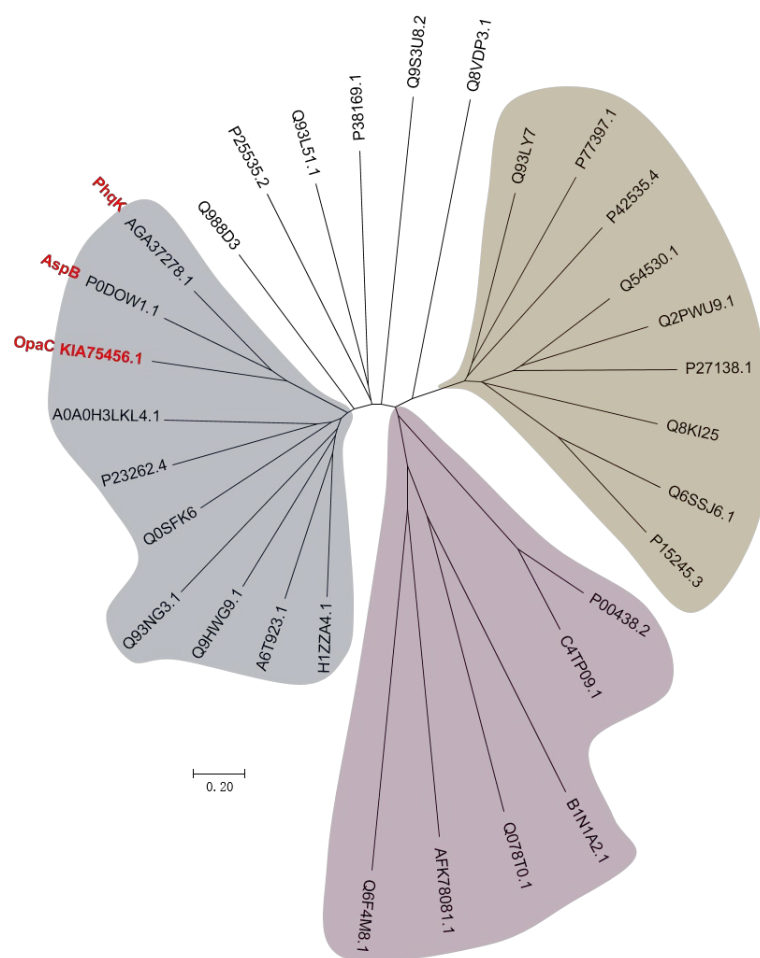
Supplementary Figure 3. CD spectra of compounds 1 – 5 in CH₃OH (200 – 400 nm)



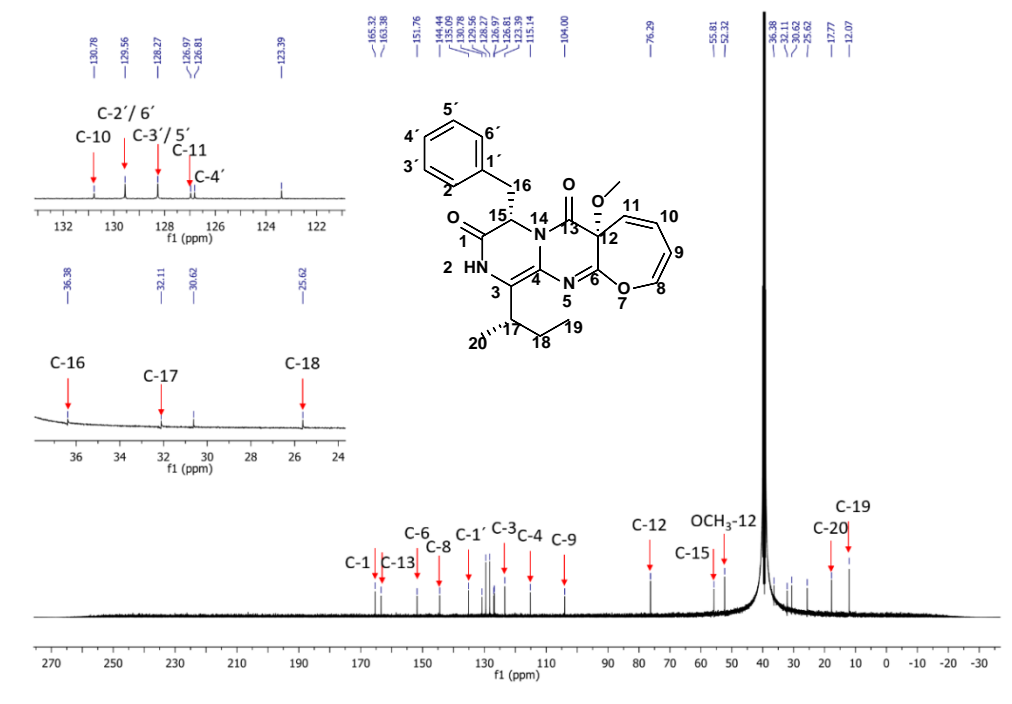
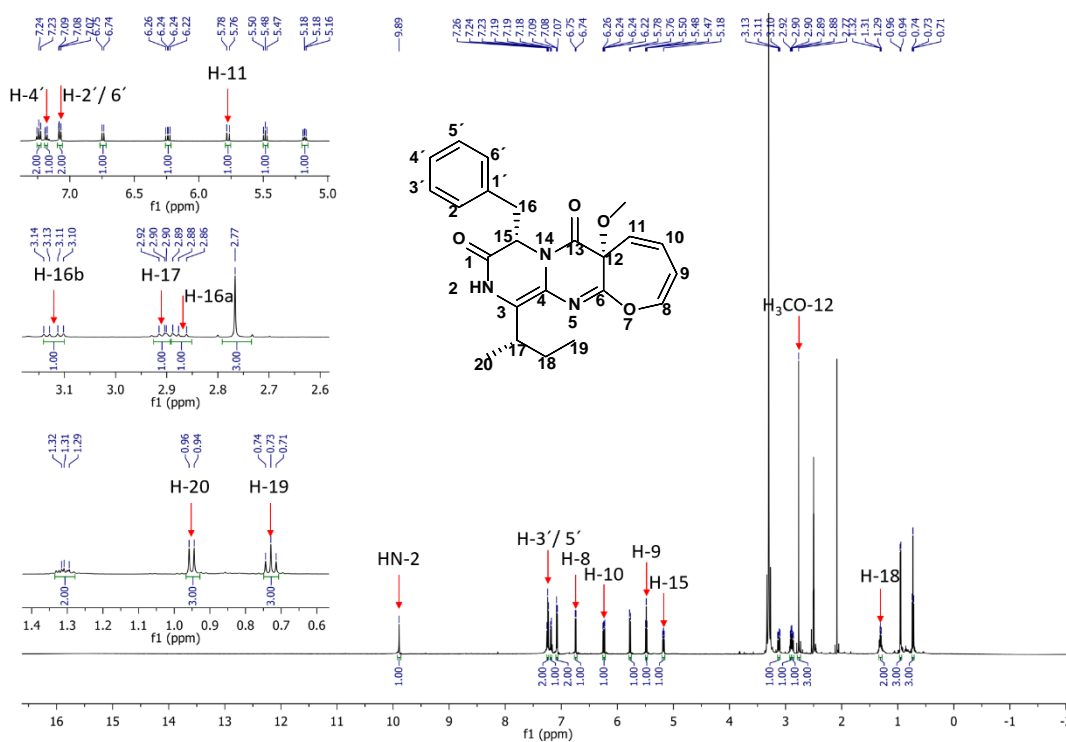
Supplementary Figure 4. Phylogenetic analysis of OpaB and functionally characterized P450s from bacteria and fungi. The protein sequences were downloaded from NCBI database.

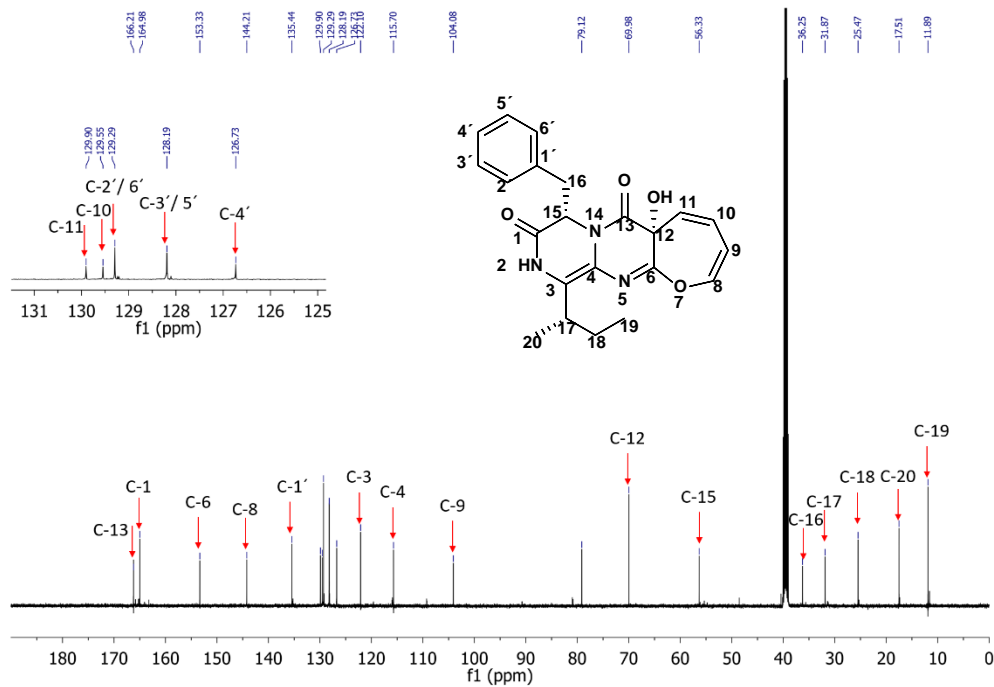
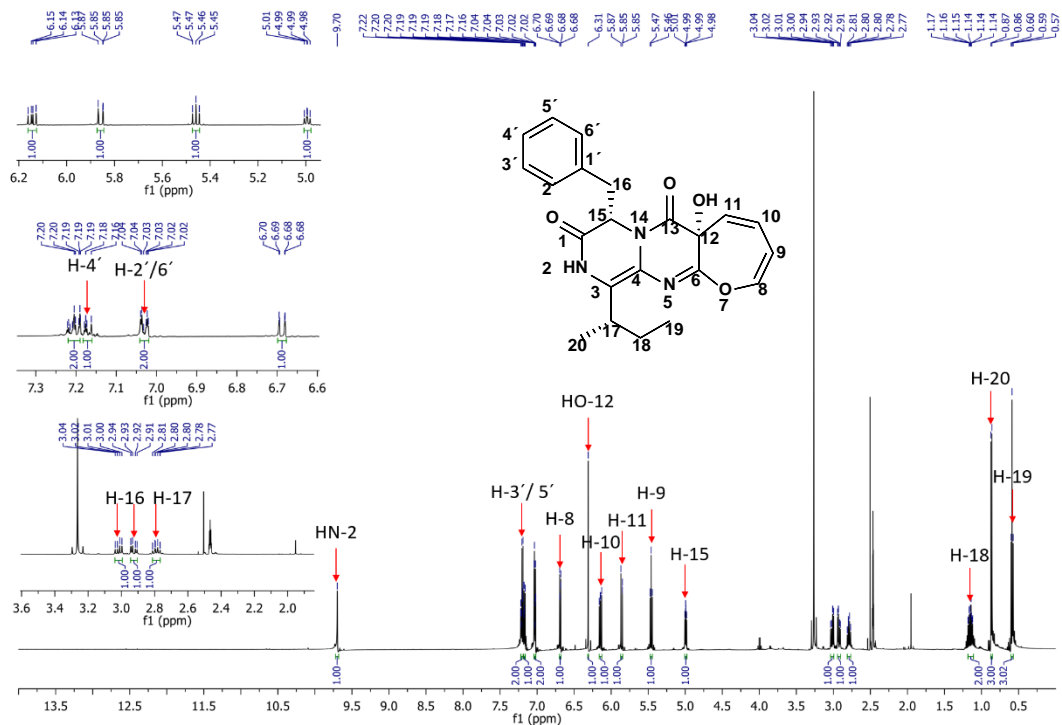


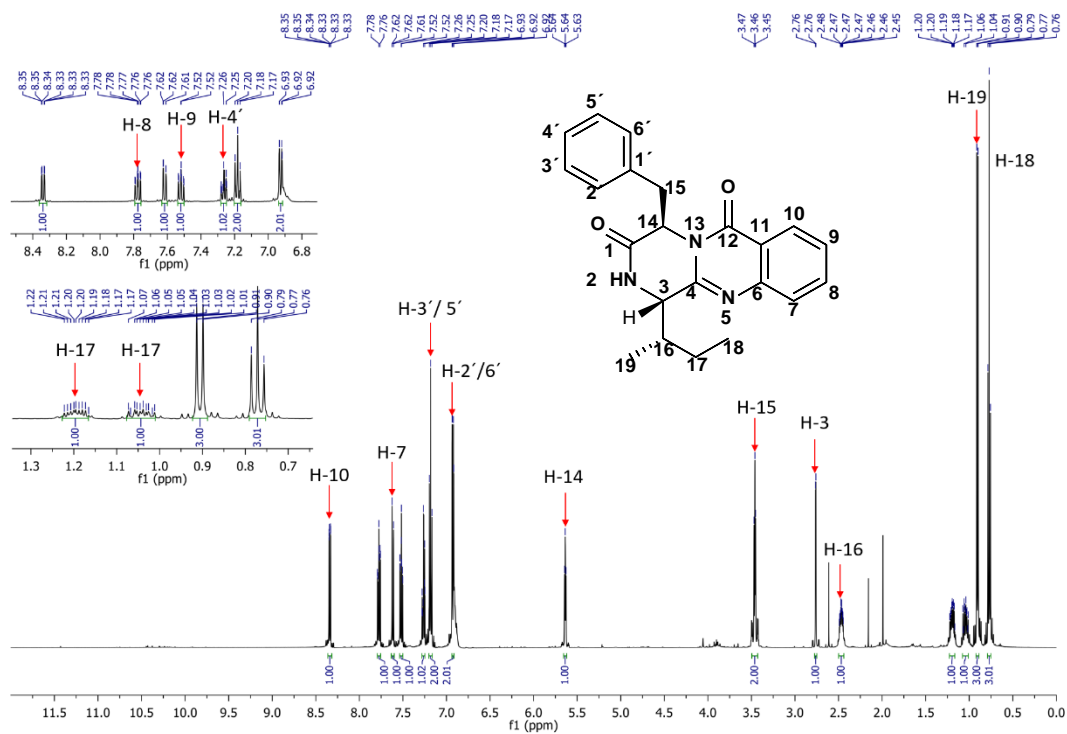
Supplementary Figure 5. HPLC analysis of the incubation mixtures of OpaC with protuboxepin K (3)



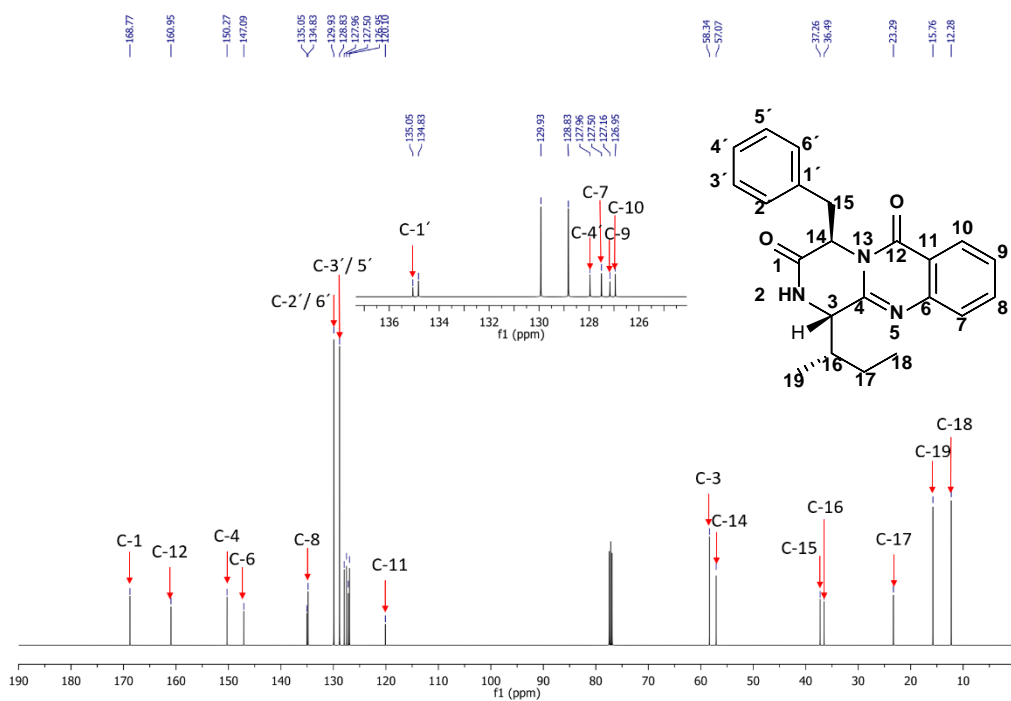
Supplementary Figure 6. Phylogenetic analysis of class A flavin monooxygenases. OpaC, AspB and PhqK are highlighted in red. The protein sequences were downloaded from NCBI database.



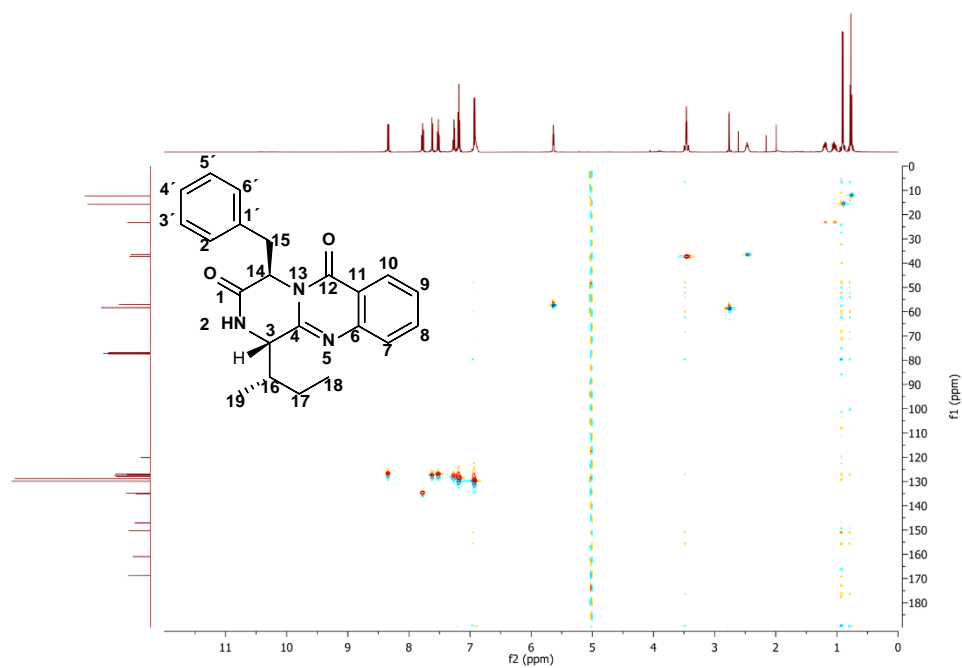




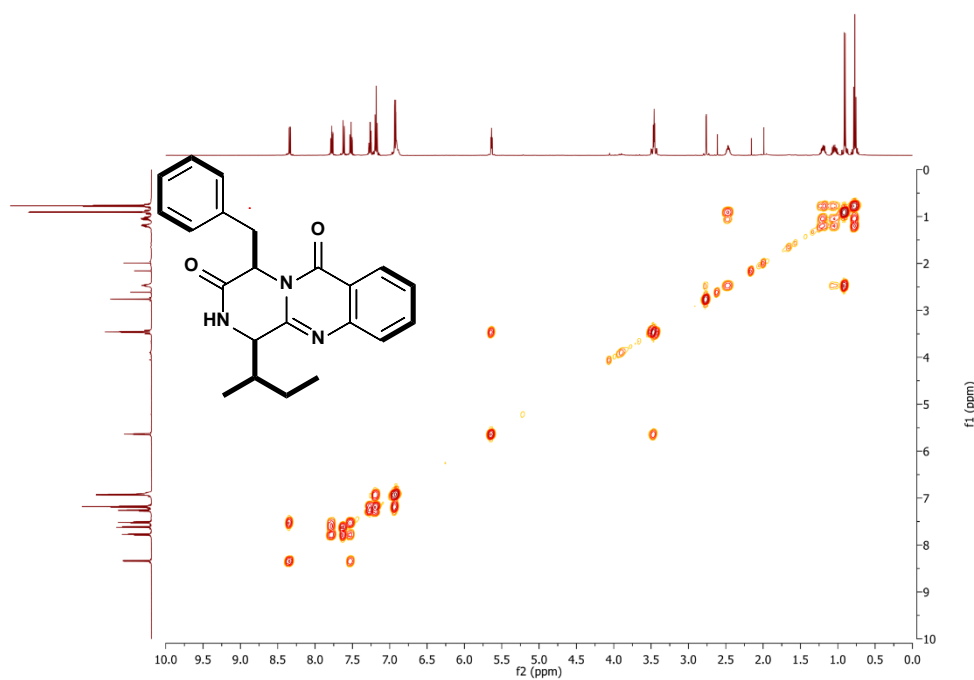
Supplementary Figure 11. ¹H NMR spectrum of protuboxepin K (3) in CDCl₃ (500 MHz)



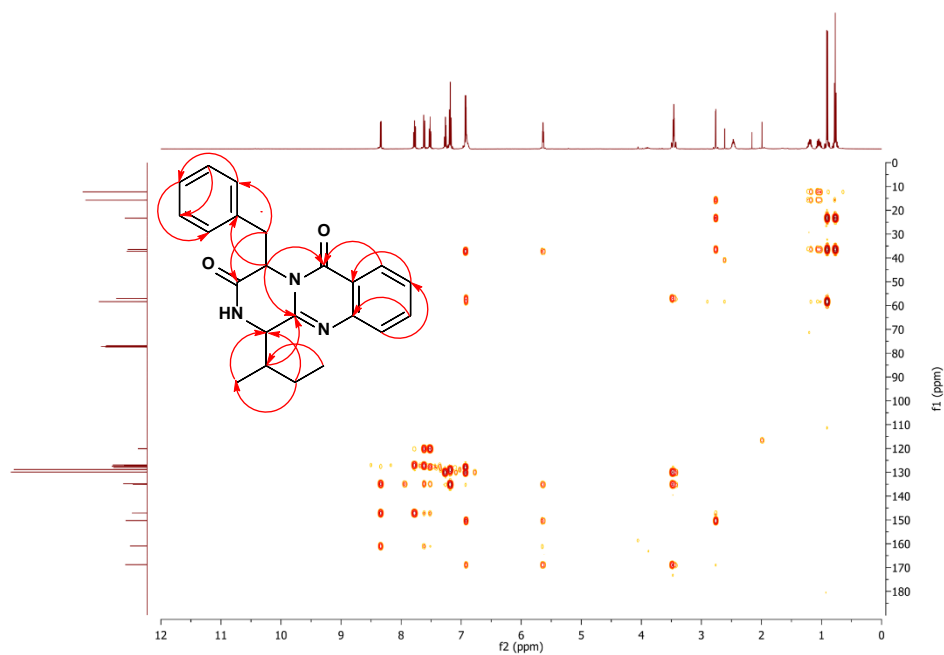
Supplementary Figure 12. ¹³C{¹H} NMR spectrum of protuboxepin K (3) in CDCl₃ (125 MHz)



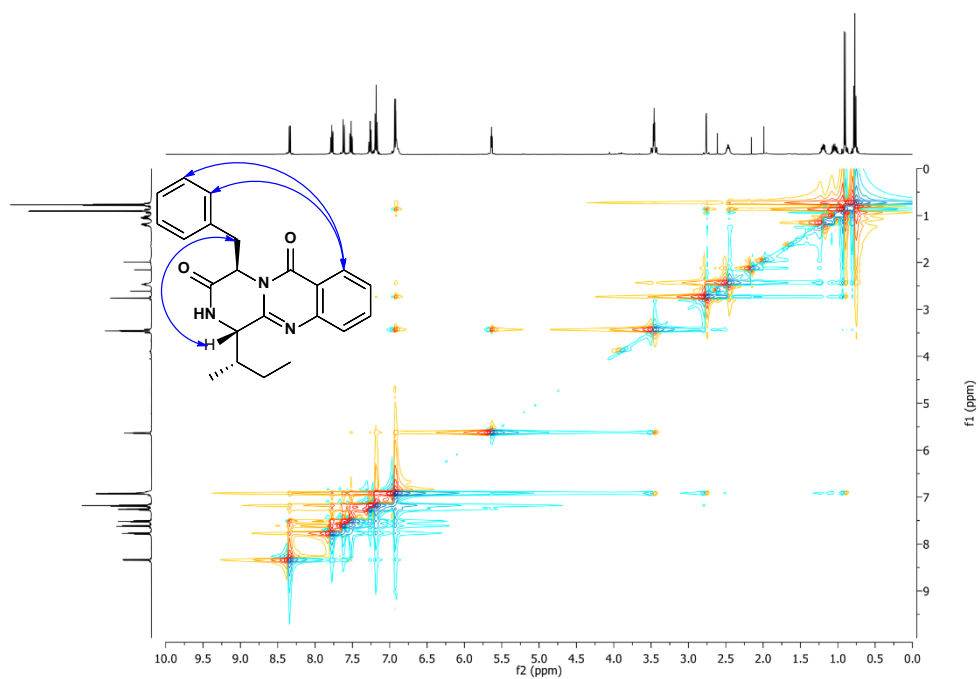
Supplementary Figure 13. HSQC spectrum of protuboxepin K (3) in CDCl_3



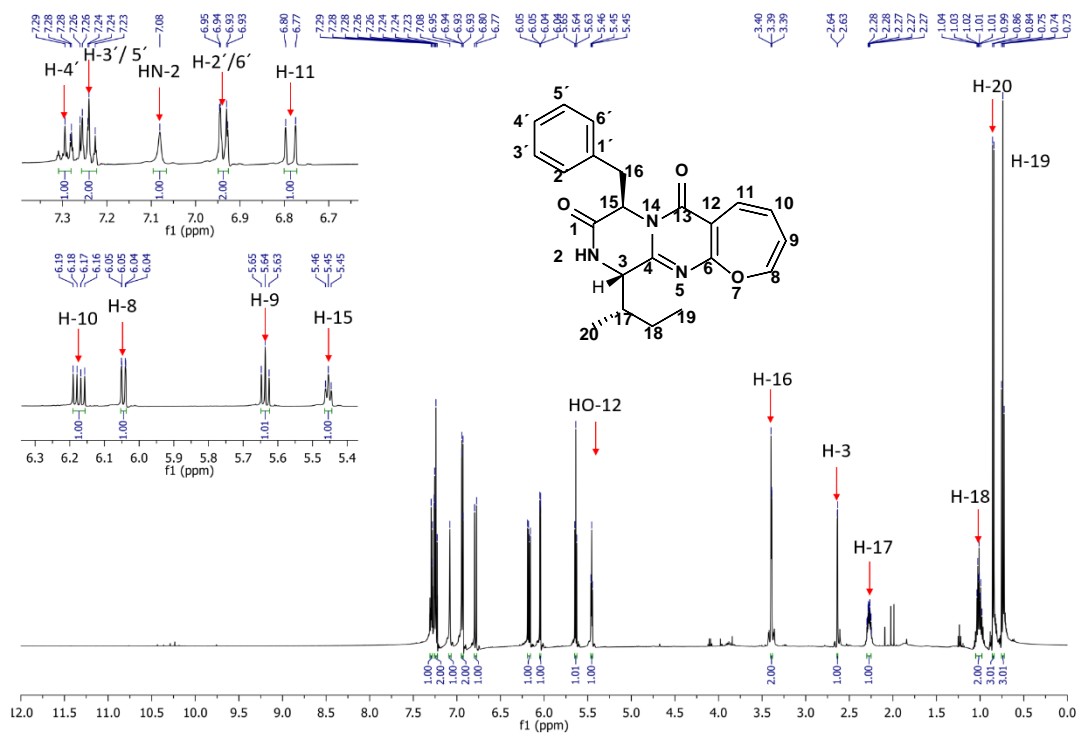
Supplementary Figure 14. COSY spectrum of protuboxepin K (3) in CDCl_3



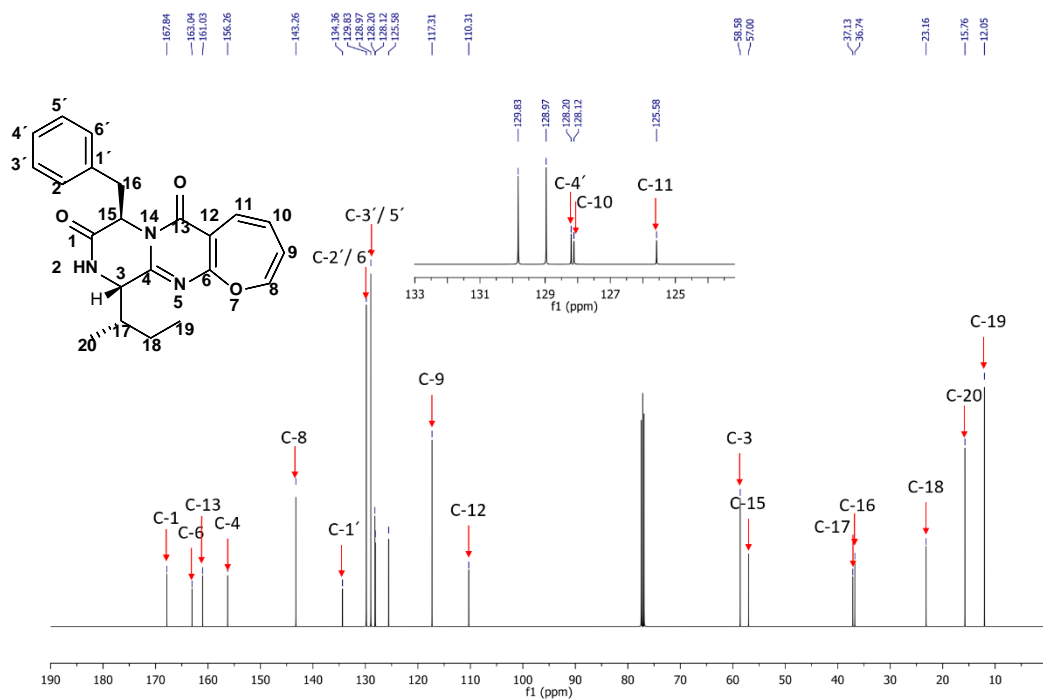
Supplementary Figure 15. HMBC spectrum of protuboxepin K (3) in CDCl_3



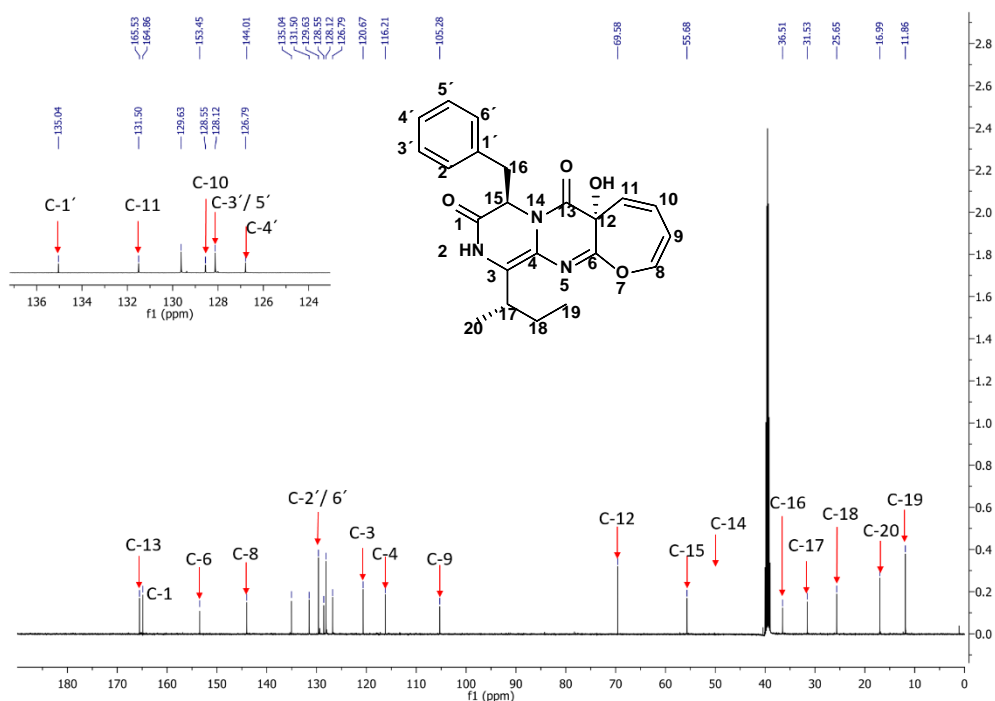
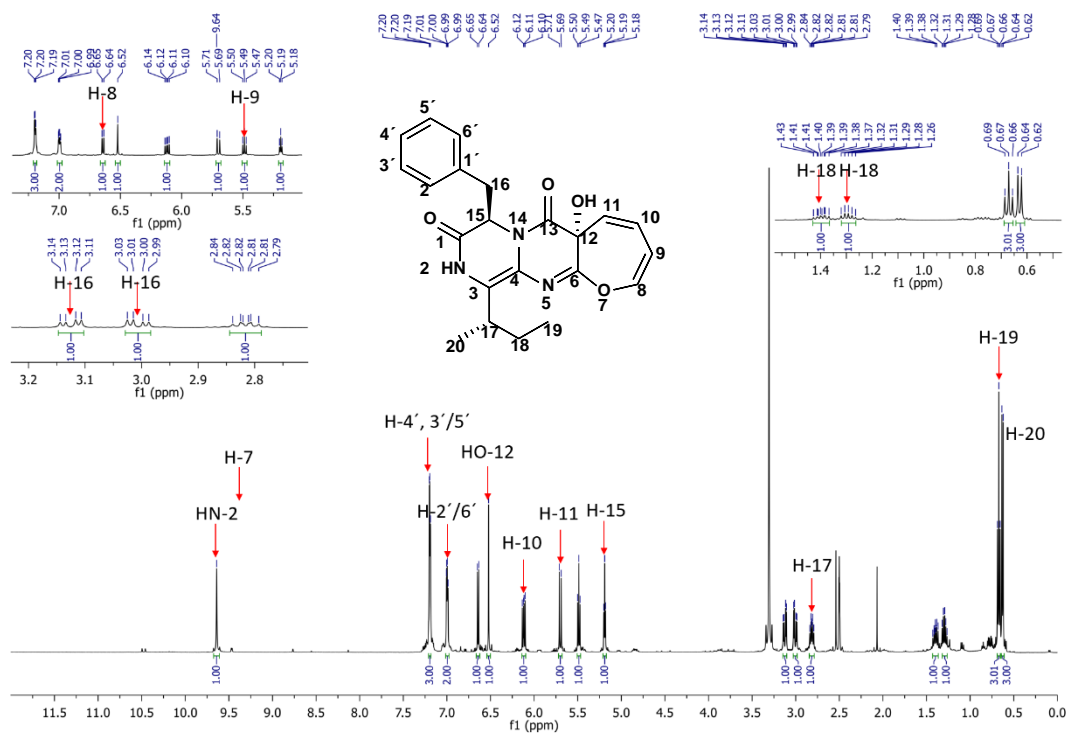
Supplementary Figure 16. NOESY spectrum of protuboxepin K (3) in CDCl_3

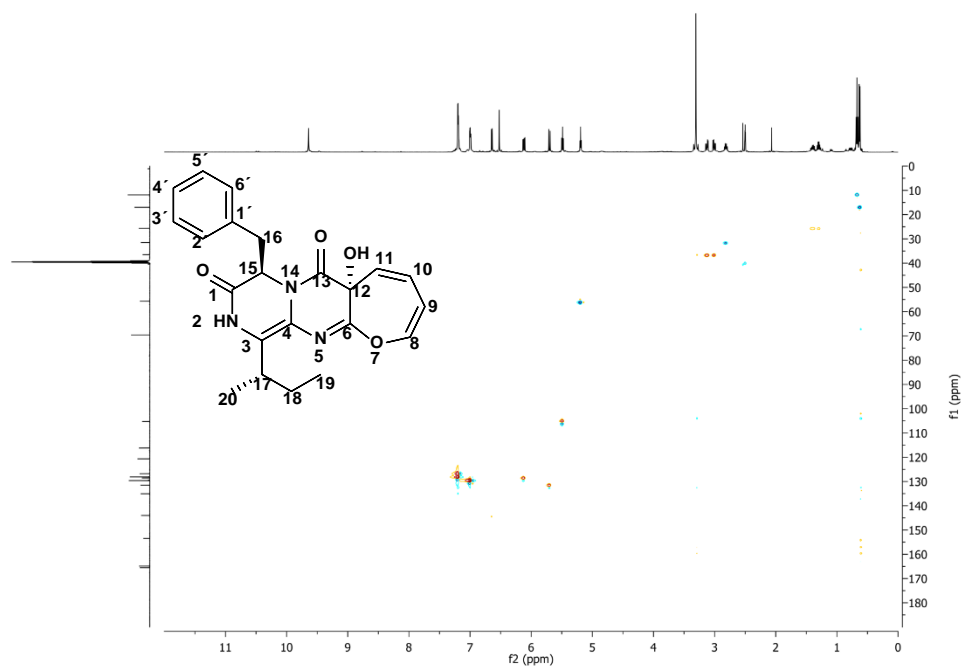


Supplementary Figure 17. ¹H NMR spectrum of protuboxepin A (4) in CDCl₃ (500 MHz)

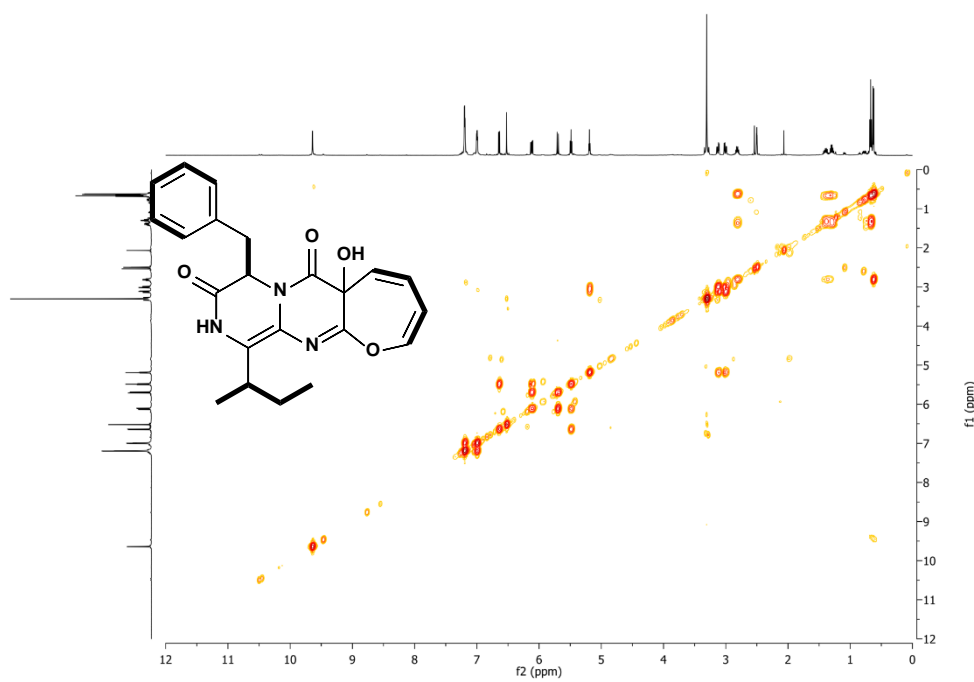


Supplementary Figure 18. ¹³C{¹H} NMR spectrum of protuboxepin A (4) in CDCl₃ (125 MHz)

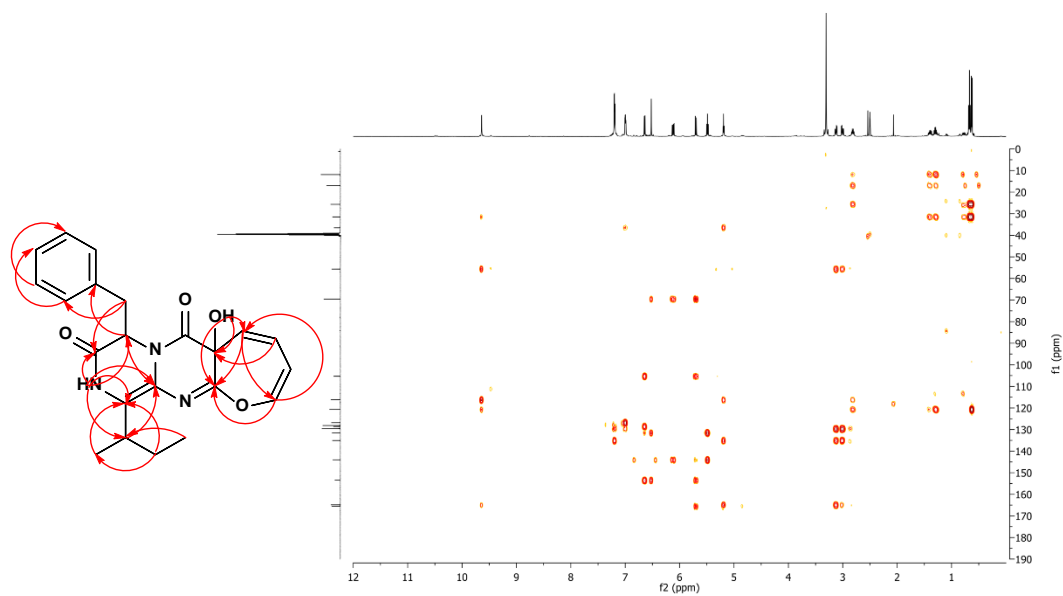




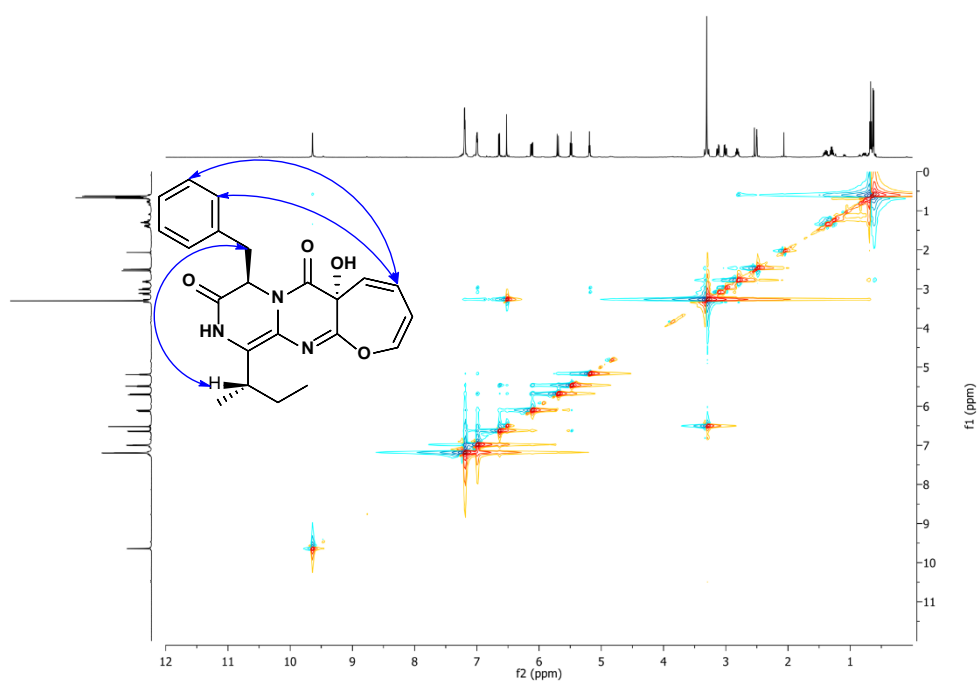
Supplementary Figure 21. HSQC spectrum of 15-*epi*-oxepinamide E (5) in DMSO- d_6



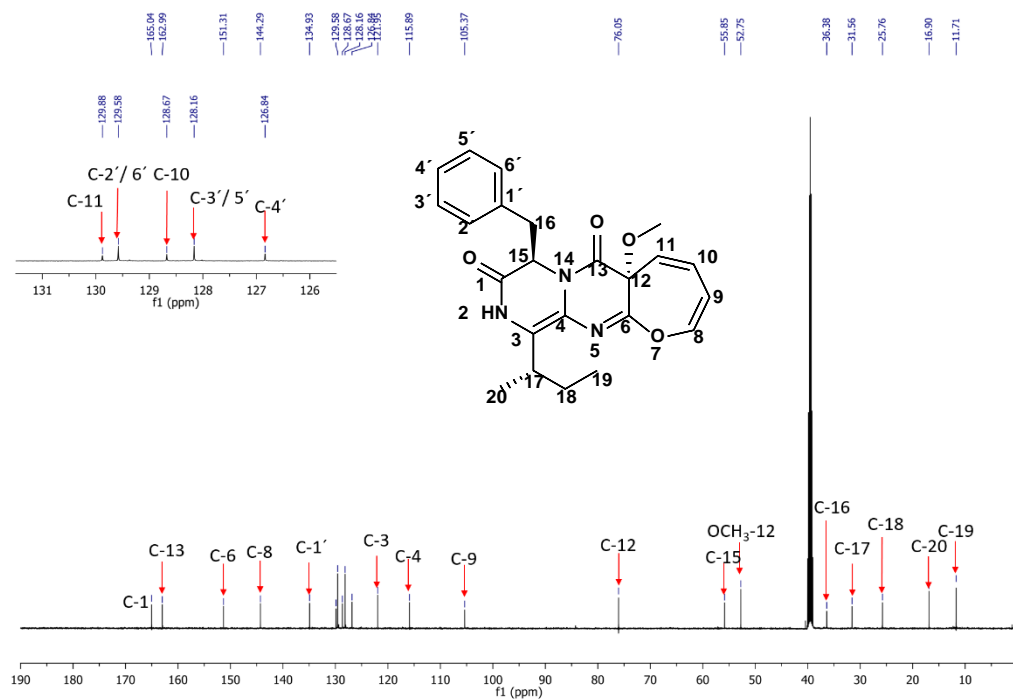
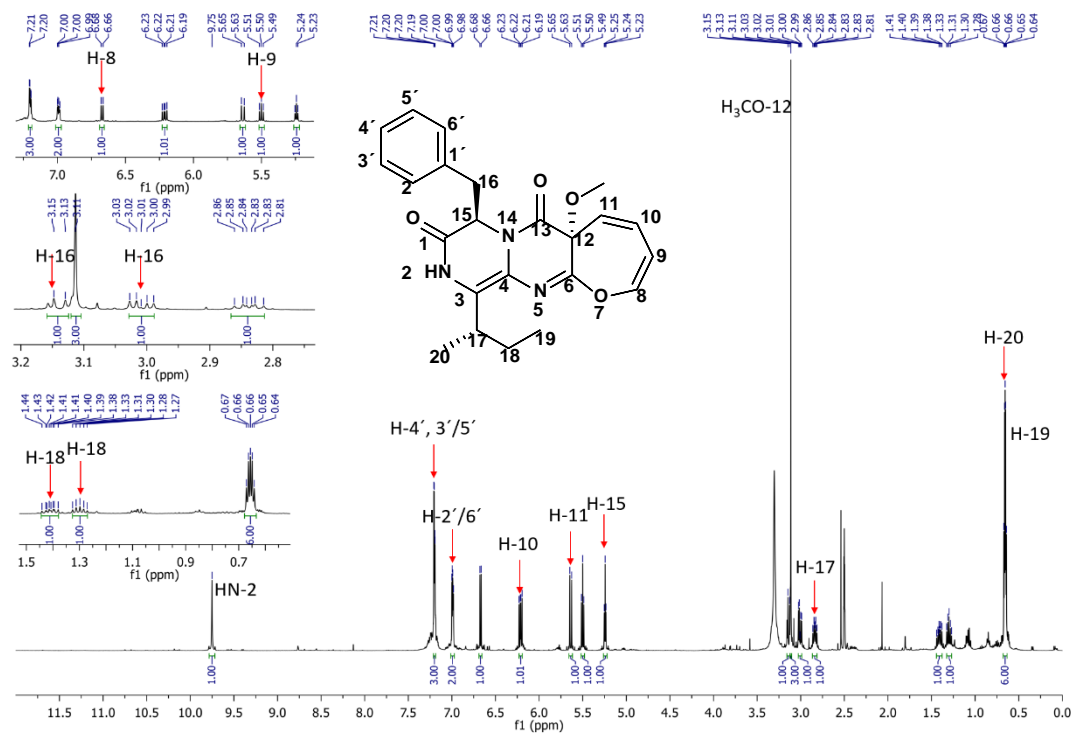
Supplementary Figure 22. COSY spectrum of 15-*epi*-oxepinamide E (5) in DMSO- d_6

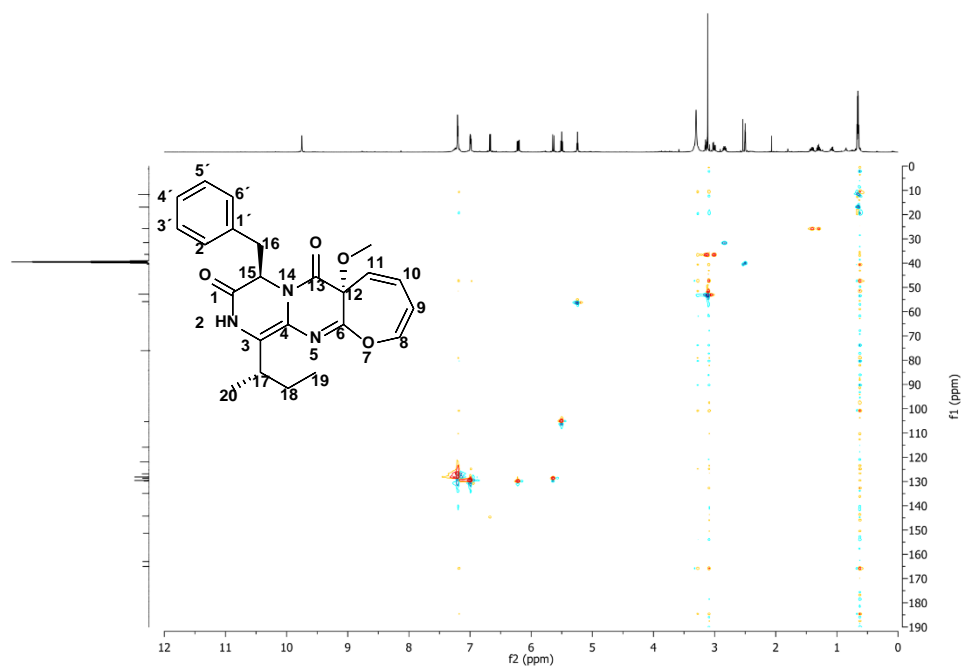


Supplementary Figure 23. HMBC spectrum of 15-*epi*-oxepinamide E (5) in DMSO- d_6

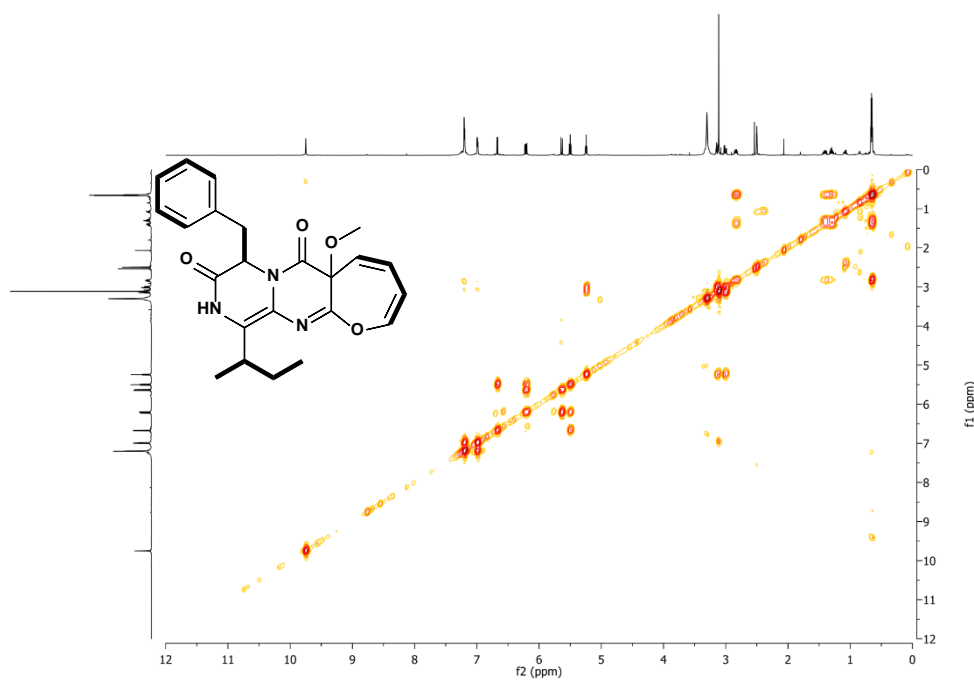


Supplementary Figure 24. NOESY spectrum of 15-*epi*-oxepinamide E (5) in DMSO- d_6

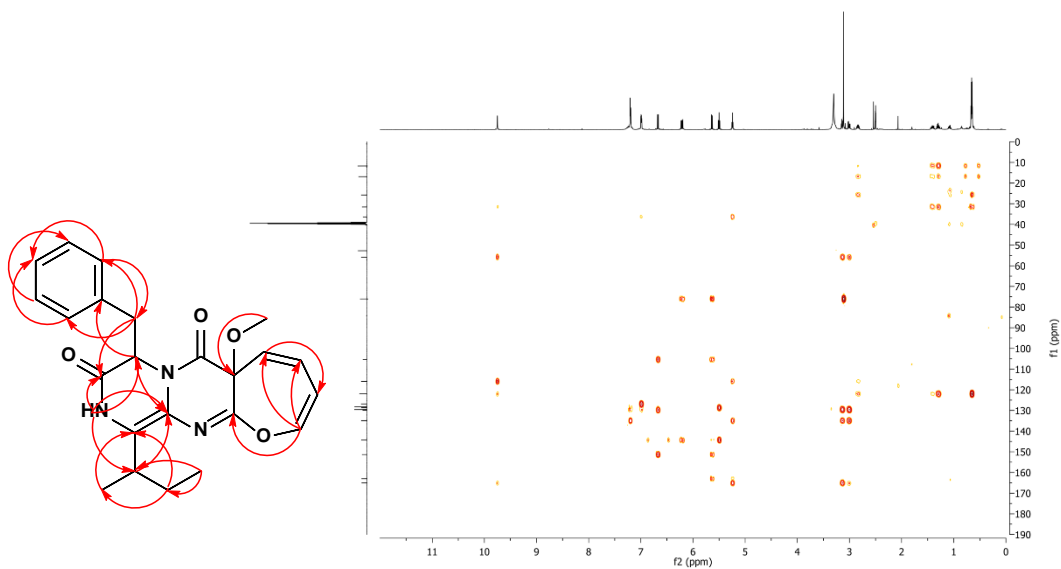




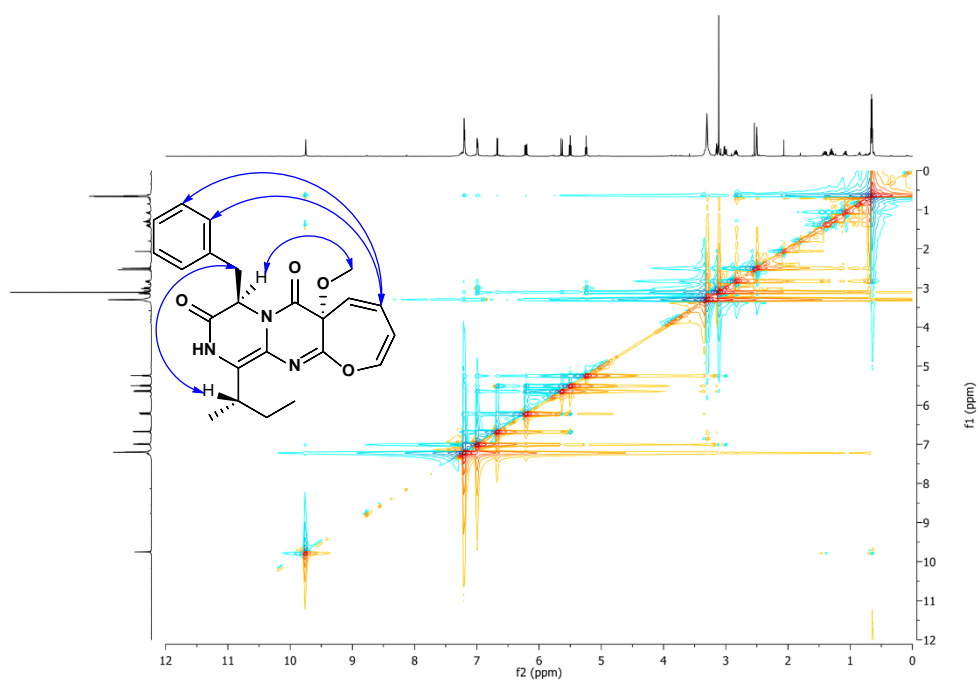
Supplementary Figure 27. HSQC spectrum of 15-*epi*-oxepinamide F (6) in DMSO- d_6



Supplementary Figure 28. COSY spectrum of 15-*epi*-oxepinamide F (6) in DMSO- d_6



Supplementary Figure 29. HMBC spectrum of 15-*epi*-oxepinamide F (6) in DMSO- d_6



Supplementary Figure 30. NOESY spectrum of 15-*epi*-oxepinamide F (6) in DMSO- d_6

Supplementary Note 1

Physiochemical properties of the compounds described in this study.

Oxepinamide F (**1**): orange oil; $[\alpha]_D^{25} +480$ (c 0.25 , CHCl_3) ; ^1H and ^{13}C NMR data see Supplementary Table 5; HRMS (ESI) m/z $[\text{M} + \text{H}]^+$ calcd. for $\text{C}_{23}\text{H}_{25}\text{N}_3\text{O}_4$ 408.192; found 408.192 .

Oxepinamide E (**2**): red brown power; $[\alpha]_D^{25} +517$ (c 0.25 , CHCl_3) ; ^1H and ^{13}C NMR data see Supplementary Table 5; HRMS (ESI) m/z $[\text{M} + \text{H}]^+$ calcd. for $\text{C}_{22}\text{H}_{23}\text{N}_3\text{O}_4$ 394.176; found 394.177.

Protuboxepin K (**3**): yellow oil; $[\alpha]_D^{25} -236$ (c 0.1 , CHCl_3) ; ^1H , ^{13}C NMR, HMBC, and NOESY data see Supplementary Table 6; HRMS (ESI) m/z $[\text{M} + \text{H}]^+$ calcd. for $\text{C}_{22}\text{H}_{23}\text{N}_3\text{O}_2$ 362.186; found 362.189.

Protuboxepin A (**4**): orange oil; $[\alpha]_D^{25} -362$ (c 0.35 , MeOH) ; ^1H and ^{13}C NMR data see Supplementary Table 5; HRMS (ESI) m/z $[\text{M} + \text{H}]^+$ calcd. for $\text{C}_{22}\text{H}_{23}\text{N}_3\text{O}_3$ 378.181; found 378.182.

15-*epi*-oxepinamide E (**5**): red brown power; $[\alpha]_D^{25} +10$ (c 0.23 , CHCl_3) ; ^1H , ^{13}C NMR, HMBC, and NOESY data see Supplementary Table 7; HRMS (ESI) m/z $[\text{M} + \text{H}]^+$ calcd. for $\text{C}_{22}\text{H}_{23}\text{N}_3\text{O}_4$ 394.176; found 394.176.

15-*epi*-oxepinamide F (**6**): red brown power; $[\alpha]_D^{25} +10$ (c 0.15 , CHCl_3) ; ^1H , ^{13}C NMR, HMBC, and NOESY data see Supplementary Table 8; HRMS (ESI) m/z $[\text{M} + \text{Na}]^+$ calcd. for $\text{C}_{23}\text{H}_{25}\text{N}_3\text{O}_4$ 408.192; found 408.192.

Structural elucidation.

The structures of oxepinamide F (**1**), E (**2**), protuboxepin K (**3**), and protuboxepin A (**4**) were elucidated by comprehensive interpretation of their MS, optical rotation, and NMR data (Supplementary Table 5, Supplementary Table 6, Supplementary Figures 7-18) and comparison with those reported in the literature.¹⁻³

15-*epi*-oxepinamide E (**5**) shares the same $[\text{M} + \text{H}]^+$ ion and similar NMR data with oxepinamide E (**2**) (Supplementary Table 7, Supplementary Figures 19-24), but exhibit different cotton effects in their CD spectra. Correlation of H-17 to H-16 in NOESY spectrum of **5** proved the 15S configuration.

15-*epi*-oxepinamide F (**6**) shares the same $[\text{M} + \text{H}]^+$ ion and similar NMR data with oxepinamide F (**1**). Correlation of H-17 to H-16 and 12-OCH₃ to H15 in NOESY spectrum of **6** confirmed the 15S configuration.

Supplementary References

1. Lu,X. *et al.* Oxepinamides: Novel liver X receptor agonists from *Aspergillus puniceus*. *Eur. J. Org. Chem.* **2011**, 802-807 (2011).
2. Lee,S.U. *et al.* Protuboxepins A and B and protubonines A and B from the marine-derived fungus *Aspergillus* sp. SF-5044. *J. Nat. Prod.* **74**, 1284-1287 (2011).
3. Ohte,S. *et al.* A new diketopiperazine-like inhibitor of bone morphogenetic protein-induced osteoblastic differentiation produced by marine-derived *Aspergillus* sp. BFM-0085. *J. Antibiot.* **73**, 554-558 (2020).

4.4 Oxepin formation in fungi implies specific and stereoselective ring expansion

Oxepin Formation in Fungi Implies Specific and Stereoselective Ring Expansion

Liujuan Zheng,[†] Haowen Wang,[†] Lena Ludwig-Radtke, and Shu-Ming Li*

Cite This: *Org. Lett.* 2021, 23, 2024–2028

Read Online

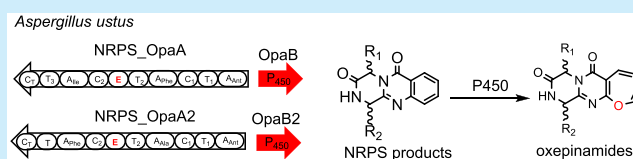
ACCESS |

Metrics & More

Article Recommendations

Supporting Information

ABSTRACT: Oxepinamides are fungal oxepine–pyrimidinone–ketopiperazine derivatives. In this study, we elucidated the biosynthetic pathway of oxepinamide D in *Aspergillus ustus* by gene deletion, heterologous expression, feeding experiments, and enzyme assays. We demonstrated that the cytochrome P450 enzymes catalyzed highly specific and stereoselective oxepin ring formation.



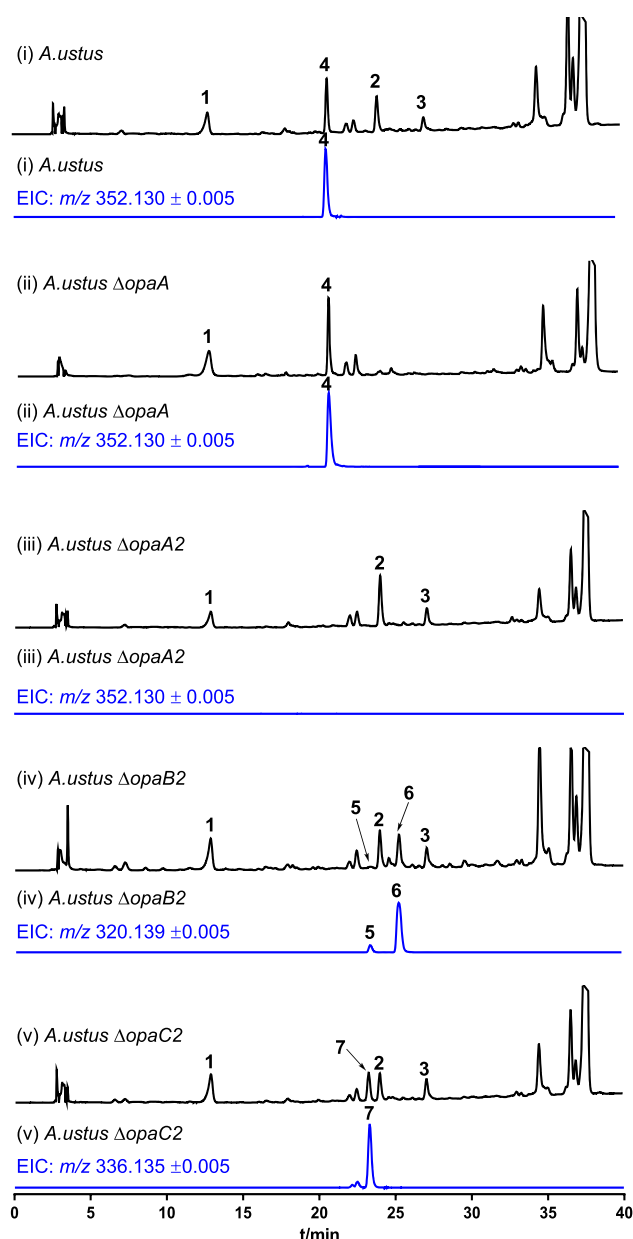


Figure 2. LC-MS analysis of the *A. ustus* extracts. UV absorptions at 254 nm in black and EICs in blue.

oxepinamide F are products of two similar BGCs. More importantly, the two cytochrome P450 enzymes for the oxepin ring formation, OpaB2 identified in this study and OpaB reported previously, show high substrate specificity and stereo selectivity.

4 was detected at 21.0 min in the HPLC chromatogram of a rice culture (Figure 2i) and has a $[M + H]^+$ ion at m/z 352.1301 with a deduced molecular formula of $C_{19}H_{17}N_3O_4$. Its UV spectrum is similar to those of oxepinamides E and F. The 1H and ^{13}C NMR spectra of 4 also show the typical oxepin signals (Table S5 and Figures S8 and S9). Together with CD spectrum, 4 was identified as oxepinamide D, isolated previously from *Aspergillus puniceus*.¹⁰ 4 belongs to type A of OPK, while 2 and 3 are members of type B (Figure 1A). Based on the structure, 4 can be speculated as a derivative of Ant, Ala, and Phe.

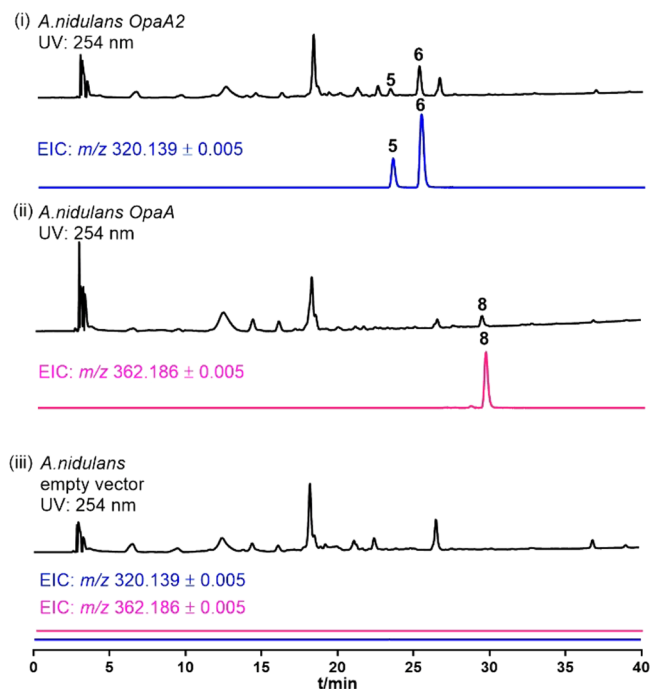


Figure 3. LC-MS analysis of *A. nidulans opaA2* and *opaA* strains with UV (254 nm, black) and EIC detection (blue and pink).

Deletion of *opaA* from *A. ustus* genome abolished the production of 2 and 3, but not that of 4 (Figure 2ii), proving the involvement of another biosynthetic pathway for 4. Genome mining in *A. ustus* and sequence analysis identified a gene encoding a trimodular NRPS KIA75688 (termed herewith OpaA2) with a domain architecture of A-T-C-A-T-E-C-A-T-C. OpaA2 shares a sequence identity of 48% with OpaA. Inspection of the genomic neighborhood of *opaA2* indicated the presence of a putative BGC containing three additional genes, *opaB2*–*opaD2* (Figure 1B and Table S1). Sequence analysis suggested their functions as a putative cytochrome P450 enzyme (OpaB2, KIA75687), a FAD-dependent oxygenase (OpaC2, KIA75686), and a transporter (OpaD2, KIA75689) (Table S1). To prove its function, *opaA2* was replaced with a hygromycin B resistance cassette by using a split marker gene replacement protocol.¹¹ The obtained $\Delta opaA2$ mutant was verified by PCR (Figure S1) and cultivated in rice media. LC-MS analysis of the culture extract confirmed the abolishment of the production of 4, but not that of 2 and 3 (Figure 2i,iii), proving its involvement only in the biosynthesis of 4.

To identify the NRPS product, *opaA2* was cloned into pYH-*gpdA-pyrG* via homologous recombination in yeast¹² for expression in *Aspergillus*.¹³ The obtained plasmid pLZ65 was linearized by *Sma*I and integrated into the *Aspergillus nidulans* genome (Figure S2). Compared with that of the negative control carrying the empty vector, two additional peaks, 5 and 6, with the same $[M + H]^+$ ions at m/z 320.139 \pm 0.005 were detected in the *opaA2* overexpression strain (Figure 3). The ratio of 5 and 6 was estimated to be 1:4. Typical signals for the oxepin ring were not observed in their NMR spectra (Tables S5 and S6 and Figures S10–S16). Detailed spectroscopic analysis led to the identification of 5 and 6 as diastereomeric quinazolinones derived from Ant, Ala, and Phe. They differ from each other just in the configuration at C-3.

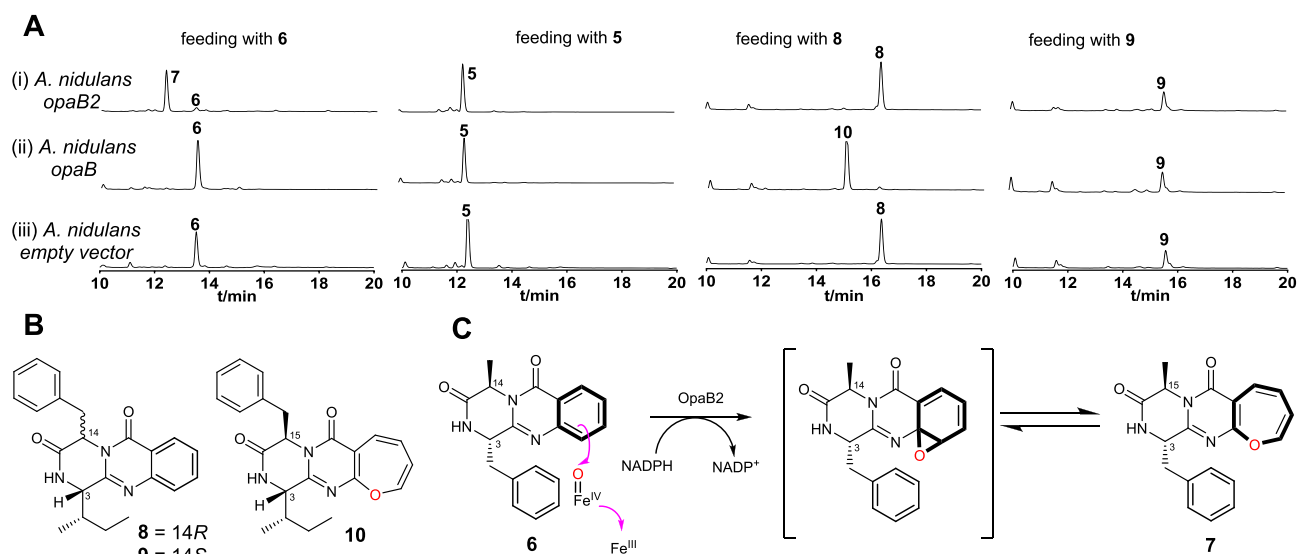


Figure 4. (A) HPLC results of feeding experiments in *opaB* and *opaB2* overexpression strains with detection at 254 nm. (B) Structures of compounds 8–10. (C) Mechanism of OPK formation catalyzed by OpaB2.

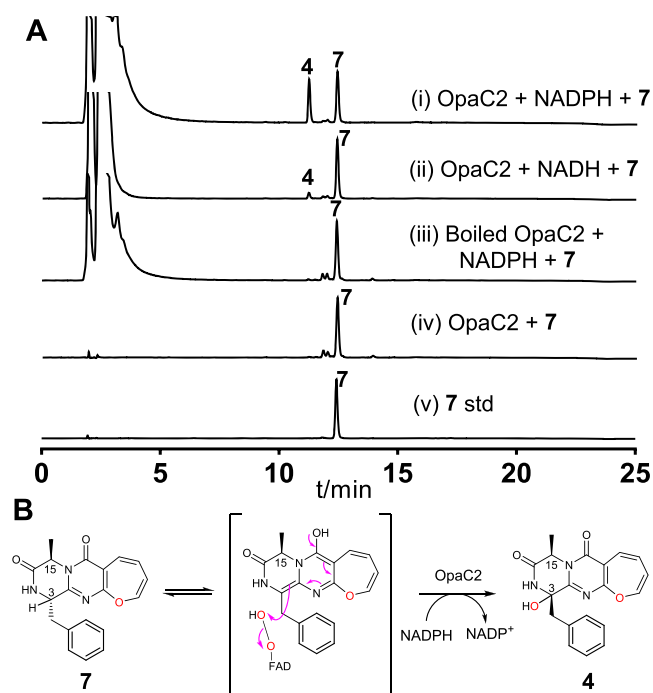


Figure 5. (A) HPLC analysis of *in vitro* assays of 7 with UV detection at 254 nm. (B) Proposed mechanism for OpaC2 reaction.

Plasmid pLZ64 containing *opaA* from the oxapinamide F BGC was constructed in a parallel fashion and expressed in *A. nidulans* following the same procedure for *opaA2*. As expected, protuboxepin K (8) with a D-Phe residue was detected by LC-MS (Figures 3 and 4B), proving the E domain in the second OpaA module for L-phenylalanine epimerization.

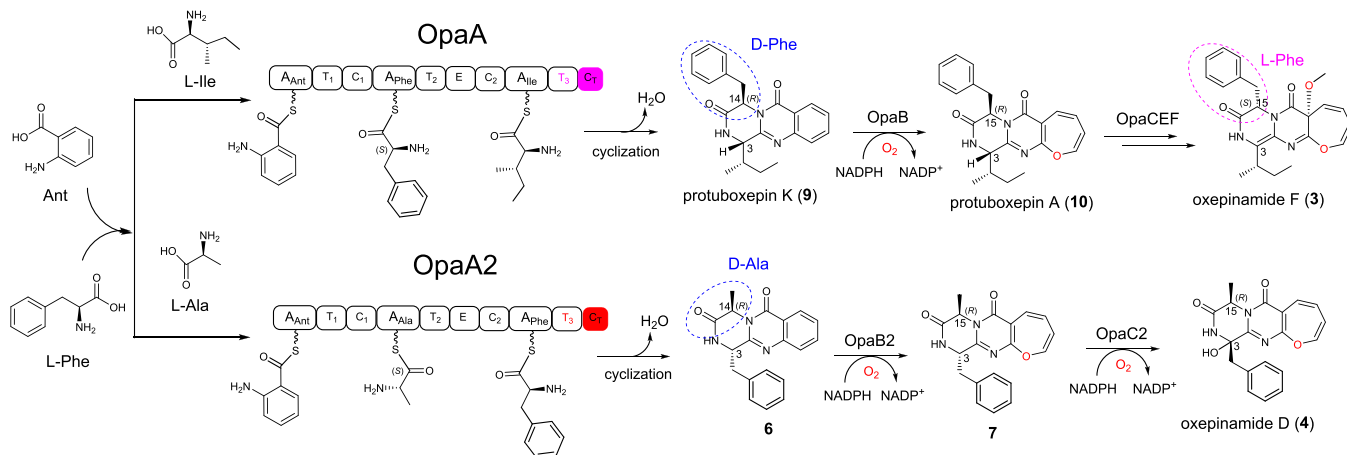
The presence of a D-Ala residue in 5 and 6 can be explained by the existence of the E domain in the second module in OpaA2, as in the case of OpaA. However, for the D-Phe residue in 5, no redundant epimerization domain in OpaA2 was predicted. To prove the possibility that 5 is a non-enzymatic product of 6, 5 and 6 were incubated at 37 °C and different pH values for 20 h (Figure S3A). HPLC analysis showed that both

5 and 6 were stable under acid conditions. In contrast, 6 was much more easily converted to 5 at pH 10. This is very likely via a keto–enol tautomeric event with the involvement of a two-double bond migration mechanism in the fused quinazolinone ring (Figure S3B).

As reported previously, OpaB from the oxapinamide F BGC catalyzed the formation of the oxepin ring in the OPK backbone.⁸ Although OpaB2 shares only a sequence identity of 30% with OpaB, it could still be responsible for oxepin ring formation in oxapinamide D. Deletion of *opaB2* from the *A. ustus* genome led indeed to the abolishment of 4 and the accumulation of two tripeptide derivatives, 5 and 6 (Figure 2iv), the same products after *opaA2* expression in *A. nidulans* (Figure 3i). Again, 6 was detected as the predominant product. The pH value of the culture was changed from 6.0 at the beginning to 8.2 at day 8. It seems that 6 was converted by non-enzymatic diastereomerization during the cultivation process.

To understand its catalytic role, *opaB2* was amplified from genomic DNA and expressed in *A. nidulans* following the same procedure for *opaA2* expression. The resulted transformants were verified by PCR (Figure S2). Feeding 6 in the *opaB2* overexpression strain led to the detection of compound 7, which was not observed in a negative control [Figure 4A(i)]. 7 shows an $[M + H]^+$ ion at m/z 336.1354, 16 Da larger than that of 6, indicating insertion of one oxygen atom into 6. Interpretation of NMR data (Table S7 and Figures S17–S22) led to the identification of 7 as a precursor of 4 without the hydroxyl group at C-3 (Figure 4B). Feeding 5 into the *A. nidulans opaB2* culture did not lead to any conversion (Figure 4A), indicating the absolute importance of the stereochemistry at the quinazolinone core for the OpaB2 reaction.

As mentioned above, the E domain of OpaA changes the configuration of the Phe residue from the L- to D-form during the formation of the quinazolinone derivative (14R) protuboxepin K (8), the substrate of another oxapinase OpaB. To determine whether this change in configuration is essential for the oxepin ring formation catalyzed by OpaB, (14S)-*epi*-protuboxepin K (9) was chemically synthesized according to the methods reported previously^{14,15} and fed into

Scheme 1. Comparative Illustration of the Biosynthetic Pathways for Oxepinamides D and F in *A. ustus*

the culture of an *A. nidulans opaB* transformant created in the previous study.⁸ As shown in Figure 4A, no product was detected by HPLC analysis. In contrast, almost complete conversion of the natural substrate protuboxepin K (8) to protuboxepin A (10) was observed after feeding into the *A. nidulans opaB* culture. This proves the stereoselective properties of the OpaB reaction and the necessity of the change in the configuration during the NRPS assembly line. Feeding 5 and 6 into the *A. nidulans opaB* transformant did not lead to any consumption. Similar results were also obtained after feeding of 8 and 9 into the *A. nidulans opaB2* transformant (Figure 4A). All of these results prove the high substrate specificity and stereoselectivity of the ring expansion reactions catalyzed by the two oxepinases, OpaB and OpaB2.

Epimerization in microbial peptides is usually catalyzed by the E domain in NRPSs¹⁶ and essential for the availability of the correct intermediates.¹⁷ In the tyrocidine biosynthesis in *Bacillus*, the C₅ domain utilizes only the E₄ domain product, D-Phe-L-Pro-L-Phe-D-Phe-PCP, as a substrate for condensation.¹⁸ In the biosynthesis of acetylazonalenin from the fungus *Neosartorya fischeri*, <1% of the cyclodipeptide Ant-D-Trp was detected after deletion of the E domain, in comparison to the amount of the cyclodipeptide Ant-D-Trp produced by the wild type. However, in the fumiquinazoline F biosynthesis in *Penicillium aethiopicum*, the C_T utilizes not only Ant-D-Trp-L-Ala-S-CoA but also Ant-L-Trp-L-Ala-S-CoA to form the cyclic tripeptide derivative.¹⁹ In the absence of the E domain, the truncated C_TqA and AldpA²⁰ still produce quinazolinone derivatives, indicating that the epimerization might not be essential for the tripeptide assembly lines. Bioinformatic analysis showed that both OpaA and OpaA2 contain an E domain in the second module. We proved here that the E domains in these NRPSs are responsible for the formation of products with correct stereochemistry for oxepin ring formation catalyzed by oxepinases.

4 differs from 7 just by an additional hydroxyl group at C-3. OpaC2 shares a sequence identity of 61% with OpaC. Deletion of *opaC2* from the *A. ustus* genome led indeed to the abolishment of the production of 4 and the accumulation of 7 (Figure 2v), proving the involvement of OpaC2 in the conversion of 7 to 4. To characterize OpaC2 biochemically, *opaC2* was amplified from *A. ustus* cDNA and cloned into pET28a(+) for overexpression in *Escherichia coli*. The recombinant N-terminally His₆-tagged protein was purified to near homogeneity with a yield of 1.6 mg/L of culture (Figure

S5). 4 was detected as the sole product in the incubation mixture of 7 with the purified OpaC2 in the presence of NADPH. Comparison of the CD spectra of 7 and 4 indicated that the orientation of the phenyl ring at C-3 has been changed (Figure S5B and Figure S4). These results provide unambiguous evidence that OpaC2 catalyzes the regio- and stereospecific C3 hydroxylation of 7 with retaining the 1H-oxepin system. In comparison, OpaC installs a hydroxyl group at C-12 with the change from the 1H- to 3H-oxepin system. Similar to OpaC, OpaC2 also utilized NADH as a cofactor, but with an obviously decreased activity (Figure 5A). Hydroxylations catalyzed by flavin-dependent monooxygenases usually take places at the sp² carbon.²¹ We propose therefore that the substrate of OpaC2 is the keto-enol intermediate with a C-3=C-4 bond (Figure 5B). The kinetic data of the reaction of OpaC2 with 7 in the presence of NADPH fit well to a Michaelis–Menten velocity equation. An apparent *K_m* value of 0.14 ± 0.01 mM, a turnover number (*k_{cat}*) of 0.085 ± 0.002 s⁻¹, and a catalytic efficiency (*k_{cat}*/*K_m*) of 607 M⁻¹ s⁻¹ (Figure S6) were calculated by using GraphPad Prism 6.0.

To test the substrate flexibility, 10 and 7 were incubated with OpaC2 and OpaC, respectively. No product formation was detected in either case (Figure S7), being in agreement with the *in vivo* results of the $\Delta opaC$ and $\Delta opaC2$ mutants and proving their high substrate specificity. Together with the aforementioned feeding results in the *opaB* and *opaB2* transformants, we can conclude that there is no crosstalk between the two BGCs.

In summary, we identified in this study the second oxepinamide BGC *opa2* in *A. ustus*, being responsible for the biosynthesis of the 1H-oxepin oxepinamide D carrying a C3-hydroxyl group. The 3H-oxepin oxepinamide F as the final product of the previously reported BGC *opa* has a methoxyl group at C-12. Both compounds also differ from each other in the third amino acid for backbone formation. However, both clusters share a NRPS (OpaA and OpaA2) for a quinazolinone skeleton and P450 (OpaB and OpaB2) for oxepin formation. The two flavin-dependent monooxygenases OpaC and OpaC2 install hydroxyl groups at different positions. Two additional enzymes complete afterward the oxepinamide F biosynthesis (Scheme 1). In addition, we demonstrated in this study that the E domains in OpaA and OpaA2 are responsible for the epimerization of phenylalanine and alanine, respectively, which is a prerequisite for the ring expansion catalyzed by oxepinases OpaB and OpaB2.

■ ASSOCIATED CONTENT

■ Supporting Information

The Supporting Information is available free of charge at <https://pubs.acs.org/doi/10.1021/acs.orglett.1c00166>.

Materials, experimental procedures, physicochemical properties, and spectroscopic data (PDF)

■ AUTHOR INFORMATION

Corresponding Author

Shu-Ming Li – Institut für Pharmazeutische Biologie und Biotechnologie, Fachbereich Pharmazie, Philipps-Universität Marburg, 35037 Marburg, Germany; orcid.org/0000-0003-4583-2655; Email: shuming.li@staff.uni-marburg.de

Authors

Liujuan Zheng – Institut für Pharmazeutische Biologie und Biotechnologie, Fachbereich Pharmazie, Philipps-Universität Marburg, 35037 Marburg, Germany

Haowen Wang – Institut für Pharmazeutische Biologie und Biotechnologie, Fachbereich Pharmazie, Philipps-Universität Marburg, 35037 Marburg, Germany

Lena Ludwig-Radtke – Institut für Pharmazeutische Biologie und Biotechnologie, Fachbereich Pharmazie, Philipps-Universität Marburg, 35037 Marburg, Germany

Complete contact information is available at: <https://pubs.acs.org/doi/10.1021/acs.orglett.1c00166>

Author Contributions

[†]L.Z. and H.W. contributed equally to this work.

Notes

The authors declare no competing financial interest.

■ ACKNOWLEDGMENTS

The authors thank Rixa Kraut and Stefan Newel from the Philipps-Universität Marburg for recording MS and NMR spectra, respectively. This project was funded in part by the Deutsche Forschungsgemeinschaft (DFG, INST 160/620-1). L.Z. (201604910536) received a scholarship from the China Scholarship Council. The CD spectrometer was a part of the core facility for protein biochemistry and spectroscopy in the Institute of Cytobiology, Philipps-Universität Marburg.

■ REFERENCES

- (1) Felnagle, E. A.; Jackson, E. E.; Chan, Y. A.; Podevels, A. M.; Berti, A. D.; McMahon, M. D.; Thomas, M. G. Nonribosomal peptide synthetases involved in the production of medically relevant natural products. *Mol. Pharmaceutics* **2008**, *5*, 191.
- (2) Le Govic, Y.; Papon, N.; Le Gal, S.; Bouchara, J.; Vandeputte, P. Vandeputte Non-ribosomal peptide synthetase gene clusters in the human pathogenic fungus *Scedosporium apiospermum*. *Front. Microbiol.* **2019**, *10*, 2062.
- (3) Walsh, C. T.; Chen, H.; Keating, T. A.; Hubbard, B. K.; Losey, H. C.; Luo, L.; Marshall, C. G.; Miller, D. A.; Patel, H. M. Tailoring enzymes that modify nonribosomal peptides during and after chain elongation on NRPS assembly lines. *Curr. Opin. Chem. Biol.* **2001**, *5*, 525.
- (4) Guo, Y.; Ghidinelli, S.; de la Cruz, M.; Mackenzie, T. A.; Ramos, M. C.; Sánchez, P.; Vicente, F.; Genilloud, O.; Larsen, T. O. Oxepinamides L and M, two new oxepine-pyrimidinone-ketopiperazine type nonribosomal peptides from *Aspergillus californicus*. *Nat. Prod. Res.* **2020**, *1*.
- (5) Guo, Y.; Frisvad, J. C.; Larsen, T. O. Review of oxepine-pyrimidinone-ketopiperazine type nonribosomal peptides. *Metabolites* **2020**, *10*, 246.
- (6) Fan, Y.; Li, P.; Chao, Y.; Chen, H.; Du, N.; He, Q.; Liu, K. Alkaloids with cardiovascular effects from the marine-derived fungus *Penicillium expansum* Y32. *Mar. Drugs* **2015**, *13*, 6849.
- (7) Lu, X.; Shi, Q.; Zheng, Z.; Ke, A.; Zhang, H.; Huo, C.; Ma, Y.; Ren, X.; Li, Y.; Lin, J.; Jiang, Q.; Gu, Y.; Kiyota, H. Oxepinamides: Novel liver X receptor agonists from *Aspergillus puniceus*. *Eur. J. Org. Chem.* **2011**, *2011*, 802.
- (8) Zheng, L.; Wang, H.; Fan, A.; Li, S.-M. Oxepinamide F biosynthesis involves enzymatic D-aminoacyl epimerization, 3H-oxepin formation, and hydroxylation induced double bond migration. *Nat. Commun.* **2020**, *11*, 4914.
- (9) Zheng, L.; Yang, Y.; Wang, H.; Fan, A.; Zhang, L.; Li, S.-M. Ustethylin biosynthesis implies phenethyl derivative formation in *Aspergillus ustus*. *Org. Lett.* **2020**, *22*, 7837.
- (10) Liang, X.; Zhang, X.; Lu, X.; Zheng, Z.; Ma, X.; Qi, S. Diketopiperazine-type alkaloids from a deep-sea-derived *Aspergillus puniceus* fungus and their effects on liver X receptor α . *J. Nat. Prod.* **2019**, *82*, 1558.
- (11) Goswami, R. S. Targeted gene replacement in fungi using a split-marker approach. *Methods Mol. Biol.* **2012**, *835*, 255.
- (12) Joska, T. M.; Mashruwala, A.; Boyd, J. M.; Belden, W. J. A universal cloning method based on yeast homologous recombination that is simple, efficient, and versatile. *J. Microbiol. Methods* **2014**, *100*, 46.
- (13) Zhang, P.; Wang, X.; Fan, A.; Zheng, Y.; Liu, X.; Wang, S.; Zou, H.; Oakley, B. R.; Keller, N. P.; Yin, W. B. A cryptic pigment biosynthetic pathway uncovered by heterologous expression is essential for conidial development in *Pestalotiopsis fici*. *Mol. Microbiol.* **2017**, *105*, 469.
- (14) Hernández, F.; Morales, V.; Buenadicha, F. L.; Söllhuber, M.; Avendaño, C. Influence of N(2)-substitution in the alkylation of (4S)-alkyl-2,4-dihydro-1H-pyrazino[2,1-b]quinazoline-3,6-diones. *Tetrahedron: Asymmetry* **2004**, *15*, 3045.
- (15) Haynes, S. W.; Gao, X.; Tang, Y.; Walsh, C. T. Complexity generation in fungal peptidyl alkaloid biosynthesis: A two-enzyme pathway to the hexacyclic MDR export pump inhibitor ardeemin. *ACS Chem. Biol.* **2013**, *8*, 741.
- (16) Ogasawara, Y.; Dairi, T. Peptide epimerization machineries found in microorganisms. *Front. Microbiol.* **2018**, *9*, 156.
- (17) Hur, G. H.; Vickery, C. R.; Burkart, M. D. Explorations of catalytic domains in non-ribosomal peptide synthetase enzymology. *Nat. Prod. Rep.* **2012**, *29*, 1074.
- (18) Luo, L.; Kohli, R. M.; Onishi, M.; Linne, U.; Marahiel, M. A.; Walsh, C. T. Timing of epimerization and condensation reactions in nonribosomal Peptide assembly lines: kinetic analysis of phenylalanine activating elongation modules of tyrocidine synthetase B. *Biochemistry* **2002**, *41*, 9184.
- (19) Gao, X.; Haynes, S. W.; Ames, B. D.; Wang, P.; Vien, L. P.; Walsh, C. T.; Tang, Y. Cyclization of fungal nonribosomal peptides by a terminal condensation-like domain. *Nat. Chem. Biol.* **2012**, *8*, 823.
- (20) Yan, D.; Chen, Q.; Gao, J.; Bai, J.; Liu, B.; Zhang, Y.; Zhang, L.; Zhang, C.; Zou, Y.; Hu, Y. Complexity and diversity generation in the biosynthesis of fumiquinazoline-related peptidyl alkaloids. *Org. Lett.* **2019**, *21*, 1475.
- (21) Huijbers, M. M. E.; Montersino, S.; Westphal, A. H.; Tischler, D.; van Berkel, W. J. Flavin dependent monooxygenases. *Arch. Biochem. Biophys.* **2014**, *544*, 2.

Supporting Information

Oxepin formation in fungi implies specific and stereoselective ring expansion

Liujuan Zheng,^{‡a} Haowen Wang,^{‡a} Lena Ludwig-Radtke^a and Shu-Ming Li ^{*a}

[‡] These authors contributed equally

a Institut für Pharmazeutische Biologie und Biotechnologie, Fachbereich Pharmazie, Philipps-Universität Marburg, Robert-Koch Straße 4, 35037 Marburg (Germany); E-mail: shuming.li@staff.uni-marburg.de

Table of contents

Experimental Procedures	4
1. Chemicals	4
2. Genome sequencing and sequence analysis	4
3. Strains, media and growth conditions	4
4. Genomic DNA isolation	4
5. RNA isolation and cDNA synthesis	5
6. PCR amplification, gene cloning and plasmid construction.....	5
7. Genetic manipulation in <i>A. ustus</i> 3.3904 and cultivation of deletion mutants.....	5
8. Heterologous expression in <i>A. nidulans</i>	6
9. Overproduction and purification of OpaC and OpaC2	6
10. <i>In vitro</i> assays of OpaC and OpaC2.....	6
11. Determination of kinetic parameters	6
12. Large-scale fermentation, extraction and isolation of secondary metabolites	6
13. Feeding experiments in the <i>opaB</i> and <i>opaB2</i> expression strains <i>A. nidulans</i> LZ61 and LZ66	7
14. HPLC analysis and metabolite isolation.....	7
15. LC-HRMS analysis	7
16. NMR analysis	8
17. Circular dichroism (CD) spectroscopic analysis	8
18. Measurement of optical rotations	8
19. Physiochemical properties of the compounds described in this study	8
20. Structural elucidation	8
Table S1. Putative functions of the genes from <i>opa2</i> gene cluster.....	10
Table S2. Strains used in this study	11
Table S3. Plasmids constructed and used in this study.....	12
Table S4. Primers used in this study.....	13
Table S5. The ¹ H and ¹³ C NMR spectroscopic data of oxepinamide D (4) in DMSO-d ₆ and compound 5 in CDCl ₃	16
Table S6. The ¹ H (400 MHz) and ¹³ C NMR (125 MHz) spectroscopic data of compound 6 in CDCl ₃ with key HMBC and COSY correlations	17
Table S7. The ¹ H (500 MHz) and ¹³ C NMR (125 MHz) spectroscopic data of compound 7 in DMSO-d ₆ with key HMBC, COSY and NOESY correlations.....	18
Figure S1. PCR verification of deletion mutants of <i>A. ustus</i> 3.3904.	19
Figure S2. PCR verification of heterologous expression transformants	20

Figure S3. The non-enzymatic conversion between compounds 5 and 6 .	21
Figure S4. The CD spectra of compounds 4 and 7 in CH ₃ OH	22
Figure S5. SDS-PAGE analysis of the purified OpaC2.	23
Figure S6. Determination of the kinetic parameters of OpaC2 toward compound 7 in presence of NADPH.	24
Figure S7. Enzyme assays to prove the crosstalk between OpaC and OpaC2.	25
Figure S8. ¹ H NMR spectrum of oxepinamide D (4) in DMSO-d ₆ (500 MHz)	26
Figure S9. ¹³ C NMR spectrum of oxepinamide D (4) in DMSO-d ₆ (125 MHz)	26
Figure S10. ¹ H NMR spectrum of compound (5) in CDCl ₃ (500 MHz)	27
Figure S11. ¹³ C NMR spectrum of compound 5 in CDCl ₃ (125 MHz)	27
Figure S12. ¹ H NMR spectrum of compound 6 in CDCl ₃ (500 MHz)	28
Figure S13. ¹³ C{ ¹ H} NMR spectrum of compound 6 in CDCl ₃ (125 MHz)	28
Figure S14. HSQC spectrum of compound 6 in CDCl ₃	29
Figure S15. COSY spectrum of compound 6 in CDCl ₃	29
Figure S16. HMBC spectrum of compound 6 in CDCl ₃	30
Figure S17. ¹ H NMR spectrum of compound 7 in DMSO-d ₆ (500 MHz)	30
Figure S18. ¹³ C{ ¹ H} NMR spectrum of compound 7 in DMSO-d ₆ (125 MHz)	31
Figure S19. HSQC spectrum of compound 7 in DMSO-d ₆	31
Figure S20. COSY spectrum of compound 7 in DMSO-d ₆	32
Figure S21. HMBC spectrum of compound 7 in DMSO-d ₆	32
Figure S22. NOESY spectrum of compound 7 in DMSO-d ₆	33
References	34

Experimental Procedures

1. Chemicals

The reagents used in this study were purchased from Fischer Scientific, Roth, VWR or Sigma-Aldrich. (14*S*)-*epi*-protuboxepin K (**9**) was synthesized by using anthranilic acid, Boc-L-Ileu, and triphenylphosphite as reactants following the previously described methods.^{1,2}

2. Genome sequencing and sequence analysis

The genome of *Aspergillus ustus* 3.3904 was sequenced by Genewiz (Suzhou, China) using Nova-seq6000/X-ten (Illumina). Initial prediction and analysis for biosynthetic gene clusters were carried out by using AntiSMASH.³ Prediction of the enzyme function was performed with the online BLAST program (<http://blast.ncbi.nlm.nih.gov>). The genomic DNA sequence of the *opa2* cluster (Table S1) reported in this study corresponds to that depicted at GenBank under accession number: JOMC01000058.1.

3. Strains, media and growth conditions

Fungal strains used in this study are listed in Table S2. *A. ustus* 3.3904 was purchased from China General Microbiological Culture Collection Center (Beijing, China) and cultivated in rice medium (20 g Alnatura long-grain rice with 30 mL H₂O in 250 mL flask) at 25°C and 7 days for secondary metabolite production.

Aspergillus nidulans LO8030 and derivatives were grown at 37°C on GMM medium (1.0% glucose, 50 mL/L salt solution, 1 mL/L trace element solution, and 1.6% agar) for sporulation and transformation with appropriate nutrition as required. The salt solution comprises (w/v) 12% NaNO₃, 1.04% KCl, 1.04% MgSO₄·7H₂O, and 3.04% KH₂PO₄. The trace element solution contains (w/v) 2.2% ZnSO₄·7H₂O, 1.1% H₃BO₃, 0.5% MnCl₂·4H₂O, 0.16% FeSO₄·7H₂O, 0.16% CoCl₂·5H₂O, 0.16% CuSO₄·5H₂O, 0.11% (NH₄)₆Mo₇O₂₄·4H₂O, and 5% Na₄EDTA.

Escherichia coli DH5α and BL21(DE3) cells were grown in LB medium (1% NaCl, 1% tryptone, and 0.5% yeast extract) at 37°C. 50 μg/mL ampicillin or 50 μg/mL kanamycin were supplemented for cultivation of recombinant strains.

Saccharomyces cerevisiae HOD114-2B cells were grown in YPD medium (1% yeast extract, 2% peptone and 2% glucose. 1.5% agarose were used for plates. The SC-uracil medium (6.7 g/L yeast nitrogen base with ammonium sulfate, 650 mg/L CSM-His-Leu-Ura (MP Biomedicals), 20 mg/L His, and 60 mg/L Leu, pH 6.2-6.3) with 2.0% galactose was used for selection. 1.5% agarose were used for plates.

4. Genomic DNA isolation

The mycelia of *A. ustus* 3.3904 and *A. nidulans* were handled with filter paper to remove the media and collected in 2 mL Eppendorf tubes. Four glass beads (2.85 mm in diameter) and 400 μL of LETS buffer

(10 mM Tris-HCl pH 8.0, 20 mM EDTA pH 8.0, 0.5% SDS, and 0.1 M LiCl) were added to the tubes. After vigorous mixing for 4 min, 300 μ L LETS buffer were added. The solution was then treated with 700 μ L phenol: chloroform: isoamyl alcohol (25: 24: 1). Genomic DNA was precipitated by addition of 900 μ L absolute EtOH. After centrifugation at 13,000 rpm for 30 min and washing with 70% EtOH, the obtained DNA was dissolved in 50 – 100 μ L distilled H₂O.

5. RNA isolation and cDNA synthesis

A. ustus 3.3904 was cultivated in rice medium at 25°C for 7 days and the cells were collected by adding 50 mL H₂O and centrifugation. RNA extraction was performed by using Fungal RNA Mini kit (VWR OMEGA bio-tek E.Z.N.A) according to the standard manufacturer's instruction. The ProtoScript II First Strand cDNA Synthesis kit (BioLabs) was used for cDNA synthesis with Oligo-dT primers.

6. PCR amplification, gene cloning and plasmid construction

Plasmids and primers used in this study are listed in Tables S3 and S4, respectively. Primers were synthesized by SeqLab GmbH (Göttingen, Germany). PCR amplification was carried out by using Phusion® High-Fidelity DNA polymerase from New England Biolabs (NEB) on a T100™ Thermal cycler from Bio-Rad. PCR reaction mixtures and thermal profiles were set as recommended by the manufacturer's instruction.

To construct the plasmids for gene deletion, a 1.2 – 1.5 kbp PCR fragment containing downstream sequence of the target gene was amplified from the genomic DNA of *A. ustus*. The vector p3YG (Table S3) was linearized by the restriction enzymes Sall and Sfal. Both DNA fragments were then transferred into *E.coli* DH5 α for homologous recombination.⁴ In analogy, the vector p5HY was linearized by NotI and BglII and used for homologous recombination with the upstream sequence of the target gene.

The vector pYH-*gpda-pyrG* with flanking sequences of the *A. nidulans* *wA* gene (Table S3) was used for heterologous expression of *opaA*, *opaA2*, and *opaB2* in *A. nidulans*. The target genes were PCR amplified from the genomic DNA of *A. ustus* and cloned via homologous recombination in yeast⁵ into the vector, which had been linearized by SmaI or SwaI.

To construct the plasmid for overproduction of OpaC2 in *E.coli*, the coding region of OpaC2 was amplified by PCR from cDNA of *A. ustus* with the primers in Table S4. The vector pET-28a(+) was linearized by BamHI and EcoRI and used for homologous recombination with *opaC2*,⁴ yielding the expression plasmid pLZ67.

7. Genetic manipulation in *A. ustus* 3.3904 and cultivation of deletion mutants

Protoplast preparation and transformation of *A. ustus* 3.3904 for deletion were carried out as described previously.⁶ The obtained transformants were cultivated in PD medium for isolation of genomic DNA to

verify the integrity via PCR amplification (Figure S1). After cultivation in rice medium at 25°C for 7 days, the cultures were extracted with EtOAc, dissolved in DMSO, and subjected to HPLC and HPLC-MS analyzes.

8. Heterologous expression in *A. nidulans*

A. nidulans LO8030⁷ was used as the expression host. Protoplast preparation and transformation were performed as described previously.⁸ pLZ64 – 66 containing the NRPS genes *opaA* and *opaA2* as well as the cytochrome P450 gene *opaB2*, were transformed into *A. nidulans* LO8030 to create expression strains. The transformants were verified by PCR (Figure S2) and were cultivated in rice media for metabolite production.

9. Overproduction and purification of OpaC and OpaC2

OpaC was overproduced and purified as described previously.⁶ The *opaC2* expression plasmid pLZ67 was transferred into *E. coli* BL21(DE3). The recombinant strain was cultivated in Terrific Broth (TB) medium (2.4% yeast extract, 2.0% tryptone, 0.4% glycerol, 0.1 M phosphate buffer, pH 7.4). OpaC2 overproduction was induced with 0.5 mM IPTG at 16°C for 16 h. The recombinant His₆-tagged protein was purified by Ni-NTA affinity chromatography (Qiagen, Hilden) and analyzed by sodium dodecyl sulfate-polyacrylamide gel electrophoresis (SDS-PAGE, Figure S5). The protein concentration was determined on a Nanodrop 2000c spectrophotometer (Thermo Scientific, Braunschweig, Germany). Protein yield of 1.6 mg per liter bacterial culture was calculated.

10. *In vitro* assays of OpaC and OpaC2

To test the enzyme activity of OpaC and OpaC2, the reaction mixtures (50 μ L) containing 50 mM Tris-HCl (pH 7.5), 5 mM NADPH or NADH, 1 mM **7** or **10**, 10 μ g of the purified recombinant OpaC or OpaC2 were incubated at 30 °C for 30 min. The reactions were terminated by addition of 50 μ L methanol. The HPLC results of the enzyme assays are given in Figures 5 and S7.

11. Determination of kinetic parameters

Enzyme assays for determination of the kinetic parameters for OpaC2 (50 μ L) contained 50 mM Tris-HCl (pH 7.5), 5 mM NADPH, 4 μ g of the purified recombinant OpaC2 and **7** at final concentrations from 0.025 to 2 mM. Incubations were carried out at 30 °C for 30 min. After addition of MeOH and centrifugation, the supernatants were analyzed on HPLC. The reaction product **4** was used as authentic standard for quantification.

12. Large-scale fermentation, extraction and isolation of secondary metabolites

The fungal strains were cultivated in 0.75 kg rice (1.75 L) for isolation. The rice culture was extracted with equal volume of EtOAc for 3 times. The EtOAc extracts were concentrated under reduced pressure to afford the crude extracts for further purification.

To isolate oxepinamide D (**4**), the crude extract of *A. ustus* wildtype was subjected to silica gel (230 – 400 mesh) column chromatography, by using a gradient of CH₂Cl₂/CH₃OH (100:0 – 0:100) to give nine fractions (Fr. 1 – Fr. 9). Fr. 7 was purified on a semi-preparative HPLC (ACN/H₂O), leading to 89.2 mg of oxepinamide D (**4**). Similarly, 6.9 mg of **5** and 5.1 mg of **6** were obtained from a culture of the $\Delta opaB2$ mutant, 21.91 mg of **7** from a culture of the $\Delta opaC2$ mutant.

13. Feeding experiments in the *opaB* and *opaB2* expression strains *A. nidulans* LZ61 and LZ66

To figure out the catalytic characters of the oxepinases OpaB and OpaB2. 10 mL PDB with 75 μ L 0.5 mg/mL riboflavin and 10 μ L 0.5 mg/ml pyridoxine in a 25 ml flask were cultivated at 230 rpm and 30°C. 0.5 mg of precursor was added into 3 days old culture of the transformant *A. nidulans* LZ61 (*opaB*) and *A. nidulans* LZ66 (*opaB2*). 16 h later, 1 mL culture was extracted with 1 mL EtOAc. The extracts were dried and dissolved in 100 μ L DMSO for LC-MS analysis. Strains without fed precursors and *A. nidulans* assembled empty vector with or without feeding of precursors were used as controls.

14. HPLC analysis and metabolite isolation

Extracts were analyzed on an Agilent HPLC series 1200 (Agilent Technologies) equipped with an Agilent Eclipse XDB-C18 column (5 μ m, 4.6 \times 150 mm). A linear gradient from 10 to 90 % ACN in H₂O, containing 0.1% (v/v) HCOOH, in 20 min was used. The column was then washed with 100% ACN for 5 min and equilibrated with 10 % ACN in H₂O for another 5 min. Detection was carried out on a photodiode array detector and absorptions at 254 nm were illustrated in this study.

A semi-preparative Multospher 120 RP-18 column (5 μ m, 10 \times 250 mm) was used for product isolation on the same HPLC system with the same solvents at a flow rate of 2 mL/min. Separation was done by isocratic elution with 45 – 70% ACN in H₂O containing 0.1% (v/v) HCOOH, for 10-20 min.

15. LC-HRMS analysis

Extracts were also analyzed on an Agilent HPLC 1260 series system equipped with a quadrupole mass spectrometer microTOF QIII (Bruker Daltonics, Bremen, Germany) by using a Multospher 120 RP18-5 μ column (5 μ m, 250 \times 2 mm). Separation was performed at a flow rate of 0.25 mL/min with a 40 min linear gradient from 5 to 100% ACN in H₂O, both containing 0.1% (v/v) HCOOH. The column was then washed with 100% ACN for 5 min and equilibrated for 10 min. The parameters of the mass spectrometer were set as following: electrospray positive ion mode for ionization, capillary voltage with 4.5 kV, collision energy with 8.0 eV. Sodium formate was used in each run for mass calibration. The masses were

scanned in the range of m/z 100 – 1500. The data were analyzed by using the DataAnalysis 4.2 software (Bruker Daltonik, Bremen, Germany).

16. NMR analysis

NMR spectra of the isolated products were recorded at room temperature on a JEOL ECA-500 or ECX-400S spectrometer (JEOL, Akishima, Tokyo, Japan). The samples were dissolved in DMSO- d_6 or $CDCl_3$. All spectra were processed with MestReNov.9.0.0 (Mestrelab Research, Santiago de Compostella, Spain).

17. Circular dichroism (CD) spectroscopic analysis

CD spectra were measured on a J-815 CD spectrometer (Jasco Deutschland GmbH, Pfungstadt, Germany). The samples were dissolved in methanol and measured in the range of 200 – 400 nm by using a 1 mm path length quartz cuvette (Hellma Analytics, Müllheim, Germany). The CD spectra are given in Figure S4.

18. Measurement of optical rotations

The optical rotation was measured on the polarimeter Jasco DIP-370 at 25°C using the D-line of the sodium lamp at $\lambda = 589.3$ nm. Prior to the measurement, the polarimeter was calibrated with CH_3Cl or CH_3OH as solvents.

19. Physiochemical properties of the compounds described in this study

Oxepinamide D (**4**): orange oil; see Table S5 for 1H and ^{13}C NMR data; HRMS (ESI) m/z : $[M + H]^+$ calcd. for $C_{19}H_{17}N_3O_4$ 352.1291; found 352.1301 .

Compound (**5**): yellow oil; $[\alpha]_D^{25} -53.33$ (c 0.15 , $CHCl_3$); see Table S5 for 1H and ^{13}C NMR data; HRMS (ESI) m/z : $[M + H]^+$ calcd. for $C_{19}H_{17}N_3O_2$ 320.1393; found 320.1399.

Compound (**6**): orange oil; $[\alpha]_D^{25} -42.58$ (c 0.14 , $CHCl_3$); see Table S6 for 1H , ^{13}C NMR, HMBC, and NOESY data; HRMS (ESI) m/z : $[M + H]^+$ calcd. for $C_{19}H_{17}N_3O_2$ 320.1393; found 320.1392.

Compound (**7**): aureate solid; see Table S7 for 1H and ^{13}C NMR data; HRMS (ESI) m/z : $[M + H]^+$ calcd. for $C_{19}H_{17}N_3O_3$ 336.1342; found 336.1354.

20. Structural elucidation

The structures of oxepinamide D (**4**) and compound **5** were elucidated by comprehensive interpretation of their MS, optical rotation, and NMR data (Table S5, Figures S8 – S11) and comparison with those reported in the literature.⁹⁻¹¹ The typical oxepin signals were clearly observed in the 1H and ^{13}C NMR spectra of **4** at δ_H 6.59 (d, 11.1 Hz), δ_H 5.81 (t, 5.6 Hz), δ_H 6.21 (dd, 11.1, 5.6 Hz), and δ_H 6.29 ppm (d, 5.6 Hz) as well as δ_C 125.1, 117.3, 128.3, and 143.6 ppm (Table S5, Figures S8 and S9).

Compound **6** shares the same $[M + H]^+$ ion with compound **5**, but different NMR data (Table S6, Figures S12 – S16). The chiral center of compound **6** was determined by comparison with that of compound **7**. Correlation of H-3 to H-16 in NOESY spectrum of **7** confirmed the 3*S* configuration.

Compound **7** has a $[M + H]^+$ ion at m/z 336.1354 and similar NMR data with compound **6** (Table S7, Figures S17 – S22). Intensive interpretation of its NMR spectra including 1H , ^{13}C , HMQC, and HMBC revealed the presence of typical oxepin signals at δ_H 6.59 (d, 11.1 Hz), δ_H 5.78 (t, 5.6 Hz), δ_H 6.23 (d, 5.6 Hz), and δ_H 6.19 ppm (dd, 11.1, 5.6 Hz) as well as δ_C 125.2, 117.2, 143.2, and 127.9 ppm, which confirmed its structure as a precursor of **4** without the hydroxyl group at C-3.

Table S1. Putative functions of the genes from *opa2* gene cluster

Protein	No.	Size (aa)	cover/identity, homologous protein, <i>A. ustus</i> 3.3904	Putative function
OpaA2	KIA75688	3905	99/48, Nonribosomal peptide synthetase, OpaA (KIA75458)	Nonribosomal peptide synthetase
OpaB2	KIA75687	522	91/32, Oxepinase OpaB (KIA75457)	P450, Oxepin formation
OpaC2	KIA75686	462	91/61, Flavin-dependent monooxygenase, OpaC (KIA75456)	hydroxylase
OpaD2	KIA75689	587	98/63, MFS toxin efflux pump, OpaD (KIA75455)	Transporter

Table S2. Strains used in this study

Strains	Genotype
Wild type	<i>A. ustus</i> 3.3904
$\Delta opaA2$	$\Delta opaA2::hph$ in <i>A. ustus</i> 3.3904
$\Delta opaB2$	$\Delta opaB2::hph$ in <i>A. ustus</i> 3.3904
$\Delta opaC2$	$\Delta opaC2::hph$ in <i>A. ustus</i> 3.3904
<i>A. nidulans</i> LO8030	<i>pyroA4</i> , <i>riboB2</i> , <i>pyrG89</i> , <i>nkuA::argB</i> sterigmatocystin cluster (<i>AN7804-AN7825</i>) Δ , emerellamide cluster (<i>AN2545-AN2549</i>) Δ , asperfuranone cluster (<i>AN1039-AN1029</i>) Δ , monodictyphenone cluster (<i>AN10023-AN10021</i>) Δ , terrequinone cluster (<i>AN8512-AN8520</i>) Δ , austinol cluster part 1 (<i>AN8379-AN8384</i>) Δ , austinol cluster part 2 (<i>AN9246-AN9259</i>) Δ , F9775 cluster (<i>AN7906-AN7915</i>) Δ , asperthecin cluster (<i>AN6000-AN6002</i>) Δ
LZ61	<i>gpdA::opaB::Afp_{pyrG}</i> in <i>A. nidulans</i> LO8030
LZ64	<i>gpdA::opaA::Afp_{pyrG}</i> in <i>A. nidulans</i> LO8030
LZ65	<i>gpdA::opaA2::Afp_{pyrG}</i> in <i>A. nidulans</i> LO8030
LZ66	<i>gpdA::opaB2::Afp_{pyrG}</i> in <i>A. nidulans</i> LO8030

Table S3. Plasmids constructed and used in this study

Plasmids	Description
p5HY	Two-third of the hph resistance gene at the 5'-end, originated from the pUChph and inserted into pESC-URA. For gene replacement using hph as selection marker.
p3YG	Two-third of the <i>hph</i> resistance gene at the 3'-end, originated from the pUChph and inserted into pESC-URA. For gene replacement using <i>hph</i> as selection marker.
pYH-wA-pyrG	URA3, wA flanking, AfpyrG, Amp
PET28a(+)	vector with T7 promoter, 6xHis tag, T7 terminator, kanamycin resistance.
PLZ141 (p5HY- <i>opaA2</i>)	a 1326 bp US PCR fragment of <i>opaA2</i> from genomic DNA of <i>A. ustus</i> 3.3904 inserted in p5HY.
PLZ142 (p3YG- <i>opaA2</i>)	a 1281 bp DS PCR fragment of <i>opaA2</i> from genomic DNA of <i>A. ustus</i> 3.3904 inserted in p3YG.
PLZ143 (p5HY- <i>opaB2</i>)	a 1234 bp US PCR fragment of <i>opaB2</i> from genomic DNA of <i>A. ustus</i> 3.3904 inserted in p5HY.
PLZ144 (p3YG- <i>opaB2</i>)	a 1300 bp DS PCR fragment of <i>opaB2</i> from genomic DNA of <i>A. ustus</i> 3.3904 inserted in p3YG.
PLZ145 (p5HY- <i>opaC2</i>)	a 1323 bp US PCR fragment of <i>opaC2</i> from genomic DNA of <i>A. ustus</i> 3.3904 inserted in p5HY.
PLZ146 (p3YG- <i>opaC2</i>)	a 1255 bp DS PCR fragment of <i>opaC2</i> from genomic DNA of <i>A. ustus</i> 3.3904 inserted in p3YG.
PLZ64	<i>pYH-gpddA-opaA-pyrG</i> ; a 12537 bp fragment of <i>opaB</i> with its terminator from genomic DNA of <i>A. ustus</i> 3.3904 inserted in <i>pYH-gpddA-pyrG</i>
PLZ65	<i>pYH-gpddA-opaA2-pyrG</i> ; a 12536 bp fragment of <i>opaA2</i> with its terminator from genomic DNA of <i>A. ustus</i> 3.3904 inserted in <i>pYH-gpddA-pyrG</i>
PLZ66	<i>pYH-gpddA-opaB2-pyrG</i> ; a 2721 bp fragment of <i>opaB2</i> with its terminator from genomic DNA of <i>A. ustus</i> 3.3904 inserted in <i>pYH-gpddA-pyrG</i>
PLZ67	PET-28a(+)- <i>opaC2</i> ; a 1214 bp fragment of <i>opaC2</i> from cDNA of <i>A. ustus</i> 3.3904 with BamHI and EcoRI inserted in PET28a(+)

US: upstream; DS: downstream

Table S4. Primers used in this study

Primers	Sequence 5'-3'	Targeted amplification
P5HY	CAAGACCAATGCGGAGCATATAC	2/3 of the <i>hph</i> resistance gene at the 5'-end from pUC <i>hph</i> to construct p5HY
P3YG	GAATTGATTCCGGAAGTGCTTGAC	2/3 of the <i>hph</i> resistance gene at the 3'-end from pUC <i>hph</i> to construct p3YG
p5HY-R	GCTGAAGTCGATTTGAGTCCAC	US of <i>hph</i> to verify 5F of <i>A. ustus</i> 3.3904 mutant
p3YG-F	GCATTAAATGCATTGGACCTCGC	DS of <i>hph</i> to verify 3F of <i>A. ustus</i> 3.3904 mutant
opaA2-U-F	AAGAATTGTTAATTAAGAGCTCAGATCGGCGTAACACTACATTGGAGCGA	1323bp US fragment of <i>opaA2</i> to construct pLZ141
opaA2-U-R	ACCCTCACTAAAGGGCGCGCCGCACTAGCAGATAGACGGCCGGATTGTA	
opaA2-D-F	ACTCAGTATAGGGCGCCGGCGTCGACCCCAAGACATAGCACACG	1281 bp DS fragment of <i>opaA2</i> to construct pLZ142
opaA2-D-R	TAGCCGCGGTACCAAGCTTACTGACGGCATACATCATGCGCG	
opaA2-F	TCAAACAGCCTTGCCCATACC	
opaA2-R	TTCTCCGCGTAATCCCACTGAA	1541 bp partial fragment of <i>opaA2</i>
opaA2-5F-F	TCGAGTCCGACAATGCAAGGT	US of <i>hph</i> to verify Δ <i>opaA2</i> mutant
opaA2-3F-R	GATCCTCAGCGGGGAGAGAATA	DS of <i>hph</i> to verify Δ <i>opaA2</i> mutant
opab2-U-F	AAGAATTGTTAATTAAGAGCTCAGATCCTTATCAACACCCCTTGTTTC	1234 bp US fragment of <i>opab2</i> to construct pLZ143
opab2-U-R	ACCCTCACTAAAGGGCGCGCCGCACTAGTTGAGCTTGATGAAAAAGGGGG	
opab2-D-F	ACTCACTATAGGGCGCGCGGCTCGAGGACGGCACCAATCGGATACAA	1300 bp DS fragment of <i>opab2</i> to construct pLZ144
opab2-D-R	TAGCCGCGGTACCAAGCTTACTGATTATGGGTAGTCCCGCCATAC	
opab2-F	TCCAACGCTTGACCTTCTTCAC	
opab2-R	CTAACGAGGTCACGTTGAATG	1465 bp partial fragment of <i>opab2</i>

opaC2-U-F	AAGAATTGTTAATTAGAGCTCAGATCCCAAGTGACATAGCCAGCTAGA	1323 bp US fragment of opaC2 to construct PLZ145
opaC2-U-R	ACCCCTACTAAAGGGCGCGCCGCACTAGGGATATGTCGGCAGAGAAC	
opaC2-D-F	ACTCACTATAGGGCCCGGGCGCTCGAGAGGCCAAATCGGGCAGCAAAA	1255 bp DS fragment of opaC2 to construct PLZ146
opaC2-D-R	TAGCCGCGGTACCAAGCTTACTCGAGACGGCCATAATCAAGGAGTC	
opaC2-F	ACAGTGATAATCGTCGGTCTGG	
opaC2-R	CGGGAAGATTGCTTGGGTGA	1433 bp partial fragment of opaC2
opaC2-5F-F	GCGAGGACACATGATCCGATA	US of hph to verify ΔopaC2 mutant
opaC2-3F-R	GTATCTGCATTGGTCGACGAG	DS of hph to verify ΔopaC2 mutant
HE-opaA-P1-F	TTCATCTTCCCATCCAAAGAACCTTTAATCATGCTATCGGAAACGATGA	4494 bp partial fragment of opaA
HE-opaA-P1-R	CCCGTGATCCTGACGTAAT	
HE-opaA-P2-F	GGGTCTGCTATTGTGCTTTGG	
HE-opaA-P2-R	GATAGTTTCGTGGATAGGTGCC	4353 bp partial fragment of opaA
HE-opaA-P3-F	CCGGTCGAGTATGCAATTGC	
HE-opaA-P3-R	CGTCAGACACAGAATACTCTCGCTAGGGACAGTTCTGCGACTAGCATA	4208 bp partial fragment of opaA
opaA-F	ATCCAGAGGCCATTGAGATGG	
opaA-R	CCCGTGATCCTGACGTAAT	1556 bp partial fragment of opaA
HE-opaA2-P1-F	ATTGATCTTCCCATCCAAAGAACCTTTAATCATGCGCATTTGAAGACGCCG	
HE-opaA2-P1-R	TGCCCTGTGCTCCAAGGATT	4518 bp partial fragment of opaA2
HE-opaA2-P2-F	GTTTGATCTCGGGGCTATAGGC	
HE-opaA2-P2-R	TCTGGAAAGATGAAACGCCCTC	4302 bp partial fragment of opaA2

Table S4. (continued)

HE- <i>opaA2</i> -P3-F	GCGAGGGGAACCGTTCCAATT	4246 bp partial fragment of <i>opaA2</i>
HE- <i>opaA2</i> -P3-R	TCGTCAGACACAGAATAACTCTCGCTAGGGTCACCCCATGCAAGGTATT	
HE- <i>opAB2</i> -F	CATCTTCCCATCCAAGAACCCTTTAATCATGTGGTCATGGAGTCCCTACT	a 2721 bp fragment of <i>opAB2</i> with its terminator from <i>A.ustus</i> 3.3904 gDNA to construct pLZ66
HE- <i>opAB2</i> -R	CGTCAGACACAGAATAACTCTCGCTAGCGAGGCAAAATCGGGCAGCAAAAA	
PET- <i>opAC2</i> -F	CCGCAAGCTTGTGACGCGAGCTCGAATTCTAGAAAAGGAAGCCCATGCC	1214 bp fragment of <i>opAC2</i> from <i>A.ustus</i> 3.3904 cDNA with was fused into pET28a(+) to construct pLZ67
PET- <i>opAC2</i> -R	CTGGTGACAGCAAAATGGGTCGCGGATCCATGCTGGACCCCTCGAATTGCT	
<i>opAB2</i> -5F-F	TCGAGTCCGACAATGCAAGGT	US of <i>hph</i> to verify Δ <i>opAB2</i> mutant
<i>opAB2</i> -3F-R	TCACCATGCATTTCGATGTCC	DS of <i>hph</i> to verify Δ <i>opAB2</i> mutant

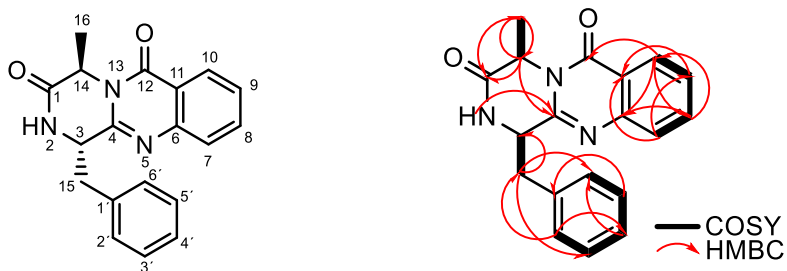
US: upstream; DS: downstream

Table S5. The ^1H and ^{13}C NMR spectroscopic data of oxepinamide D (**4**) in DMSO-d_6 and compound **5** in CDCl_3

	Oxepinamide D (4)		Compound 5	
	500 MHz	125 MHz	400 MHz	100 MHz
Position	δ_{H} (multi., J)	δ_{C}	δ_{H} (multi., J)	δ_{C}
1		165.0		168.7
2	9.19, s		6.40, t, 4.9	
3/3-OH	7.09, s		4.81, dt, 9.9, 3.8	
4		157.7		147.3
6		162.3		149.8
7			7.71, dd, 8.3, 1.5	127.3
8	6.29, d, 5.6	143.6	7.81, ddd, 8.3, 7.1, 1.5	135.0
9	5.81, t, 5.6	117.3	7.52, ddd, 8.1, 7.1, 1.2	127.9
10	6.21, dd, 11.1, 5.6	128.3	8.30, dd, 8.1, 1.2	127.0
11	6.59, d, 11.1	125.1		120.3
12		109.8		160.6
13		159.6		
14			5.24, q, 2.1	58.2
15	4.45, q, 6.9	51.5	1.51, d, 7.1	19.0
16	0.38, d, 6.9	17.7	3.48, dd, 13.5, 3.8	44.4
			3.16, dd, 13.5, 9.9	
17	3.08, d, 12.9	46.4		
	3.54, d, 12.9			
1'		134.5		135.3
2', 6'	7.08, m	130.6	7.24, m	129.3
3', 5'	7.25, t, 7.3	128.4	7.36, m	129.8
4'	7.19, t, 7.3	127.3	7.30, m	127.0

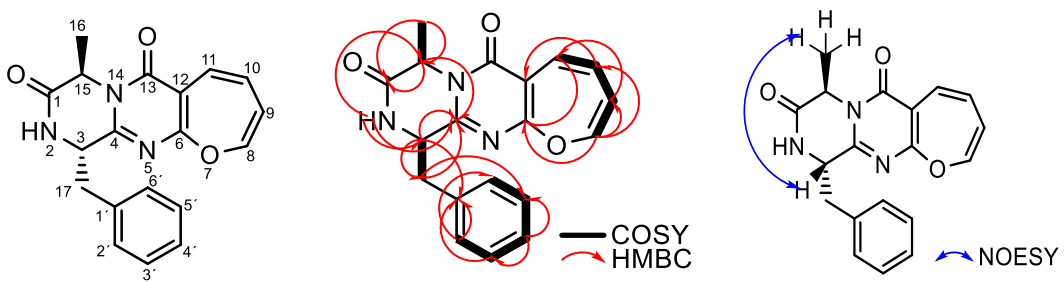
The NMR data of **4** and **5** correspond well to those of oxepinamide D,⁹ and (+)-(1S,4S)-1-Benzyl-4-methyl-2,4-dihydro-1H-pyrazino[2,1-b]quinazolino-3,6-dione,⁹ respectively

Table S6. The ^1H (400 MHz) and ^{13}C NMR (125 MHz) spectroscopic data of compound **6** in CDCl_3 with key HMBC and COSY correlations



Position	δ_{H} (multi., J)	δ_{C}	HMBC
1		169.2	
2	5.82, s		C-4
3	4.82, dd, 10.6, 3.6	54.1	
4		149.7	
6		147.0	
7	7.74, dd, 8.2, 1.5	127.6	C-9, C-11
8	7.81, ddd, 8.2, 7.1, 1.5	134.9	C-6, C-10
9	7.54, ddd, 8.1, 7.1, 1.2	127.6	C-7, C-11
10	8.31, dd, 8.1, 1.2	127.0	C-6, C-8, C-12
11		120.7	
12		160.5	
14	5.46, dd, 7.2, 0.8	52.3	C-1, C-4, C-16
15a	2.98, dd, 14.4, 3.6	38.2	C-3, C-2',6', C-3',5'
15b	4.15, dd, 14.4, 10.6	38.2	
16	1.62, d, 7.2	17.1	C-1, C-14
1'		135.5	
2', 6'	7.32, d, 7.5	129.4	C-4', C-15
3', 5'	7.42, br. t, 7.5	129.7	C-1', C-3',5'
4'	7.36, dd, 7.3, 1.4	128.1	C-2',6'

Table S7. The ^1H (500 MHz) and ^{13}C NMR (125 MHz) spectroscopic data of compound **7** in DMSO-d_6 with key HMBC, COSY and NOESY correlations



Position	δ_{H} (multi., J)	δ_{C}	HMBC	NOESY
1		167.2		
2	8.53, s		C-3, C-4, C-15	H-3
3	5.15, t, 4.7	53.6	C-1', C-4, C-17	H-2, H-16, H-17
4		156.1		
6		161.7		
8	6.23, d, 5.6	143.2	C-6, C-9, C-10	H-9, H-10
9	5.78, t, 5.6	117.2	C-8, C-11	H-8, H-10
10	6.19, dd, 11.1, 5.6	127.9	C-8, C-12	H-8, H-9, H-11
11	6.59, d, 11.1	125.2	C-6, C-9	H-9, H-10
12		109.3		
13		159.9		
15	4.63, q, 7.1	51.8	C-1, C-4, C-16	H-16
16	1.44, d, 7.1	16.8	C-1, C-15	H-3, H-15
17	Overlapping with H_2O signal	36.4	C-1', C-3', 5', C-3, C-4	H-3, H-2', 6'
1'		135.8		
2', 6'	7.25-7.24, m	129.9	C-1', C-2', 6', C-3', 5'	H-3', 4', 5'
3', 5'	7.25-7.24, m	127.9	C-1', C-2', 6', C-3', 5'	H-2', 4', 6'
4'	7.22-7.19, m	126.6	C-3', 5'	H-2', 6', H-3', 5'

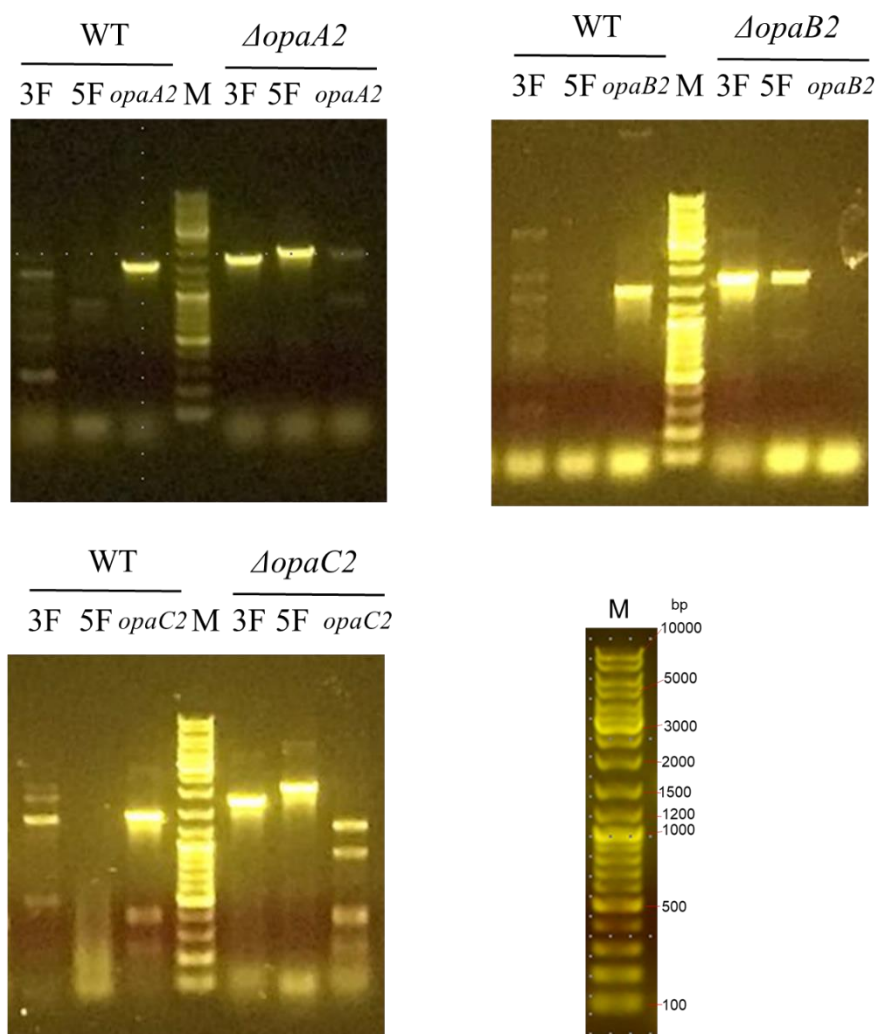


Figure S1. PCR verification of deletion mutants of *A. ustus* 3.3904
 PCR amplification for three different fragments from genomic DNA of WT and deletion mutants was used to prove the presence/absence of the target gene and the integration site of the selection marker with up- and downstream regions. The PCR primers are given in Table S4.

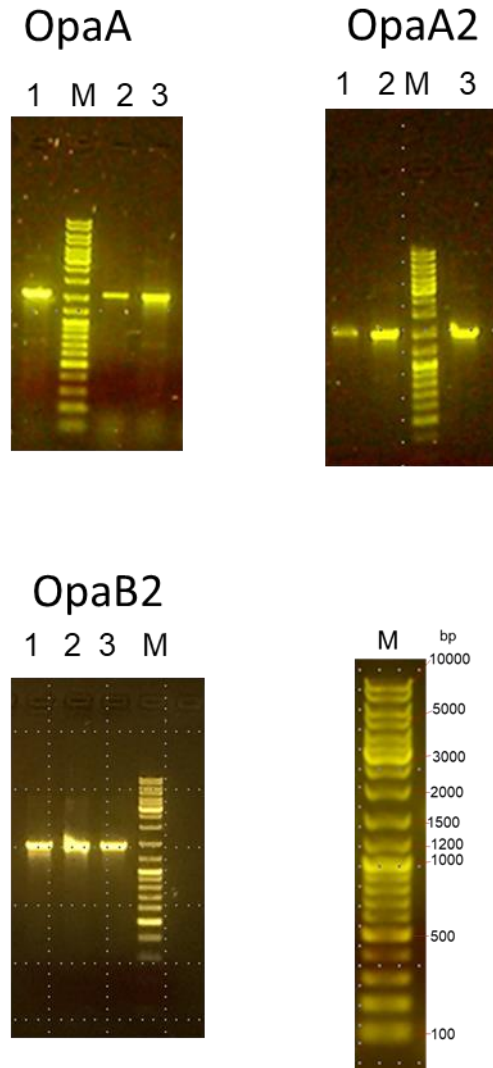


Figure S2. PCR verification of heterologous expression transformants
 For *A. nidulans*-pYH-*gpdA-opaA-pyrG* (HE-*opaA*), *A. nidulans*-pYH-*gpdA-opaA2-pyrG* (HE-*opaA2*), and *A. nidulans*-pYH-*gpdA-opaA-pyrG* (HE-*opaB2*), fragments of 1556 bp, 1541 bp, and 1465 bp within the target genes were amplified from genomic DNA by using the primers listed in Table S4, respectively.

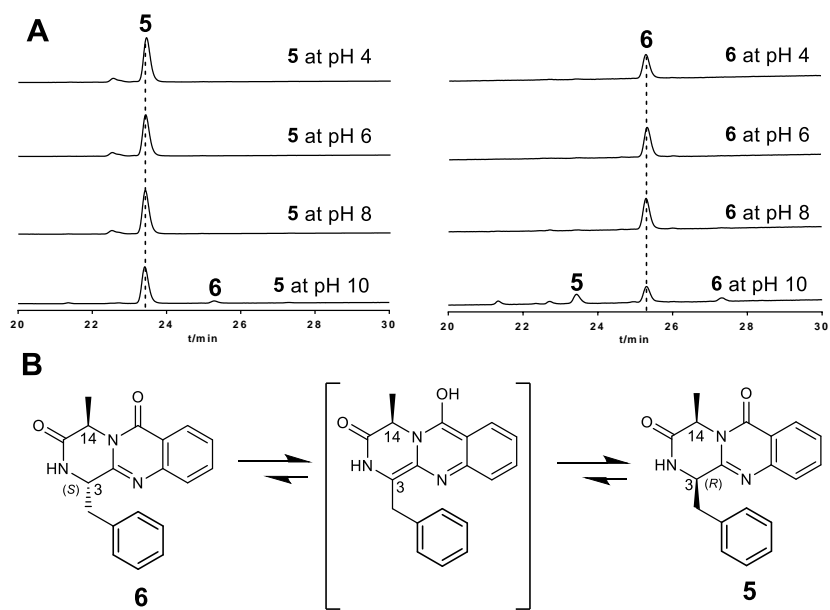


Figure S3. The non-enzymatic conversion between compounds **5** and **6**

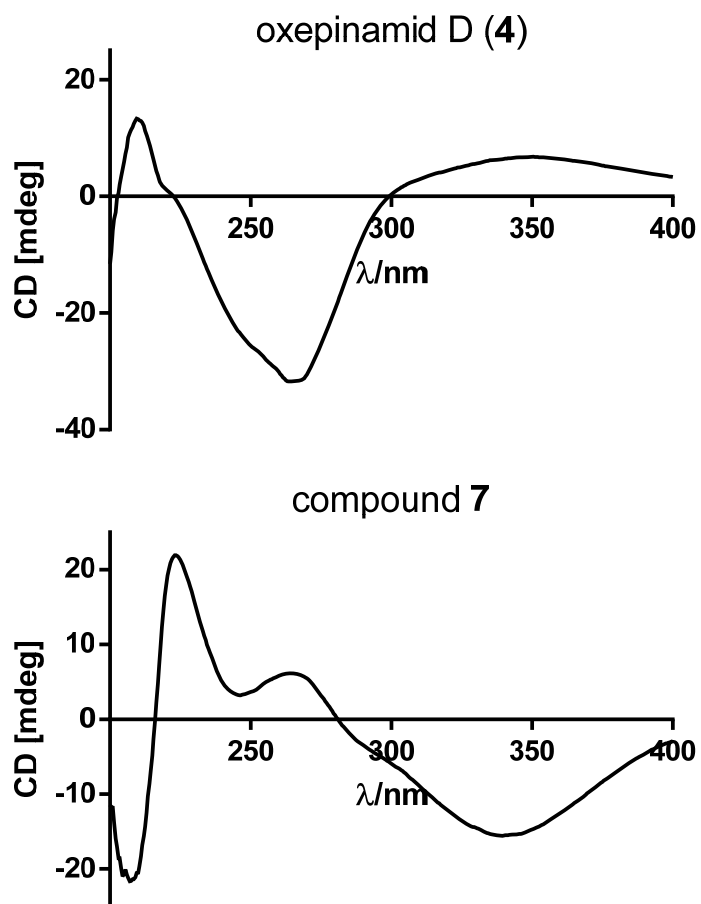


Figure S4. The CD spectra of compounds **4** and **7** in CH₃OH

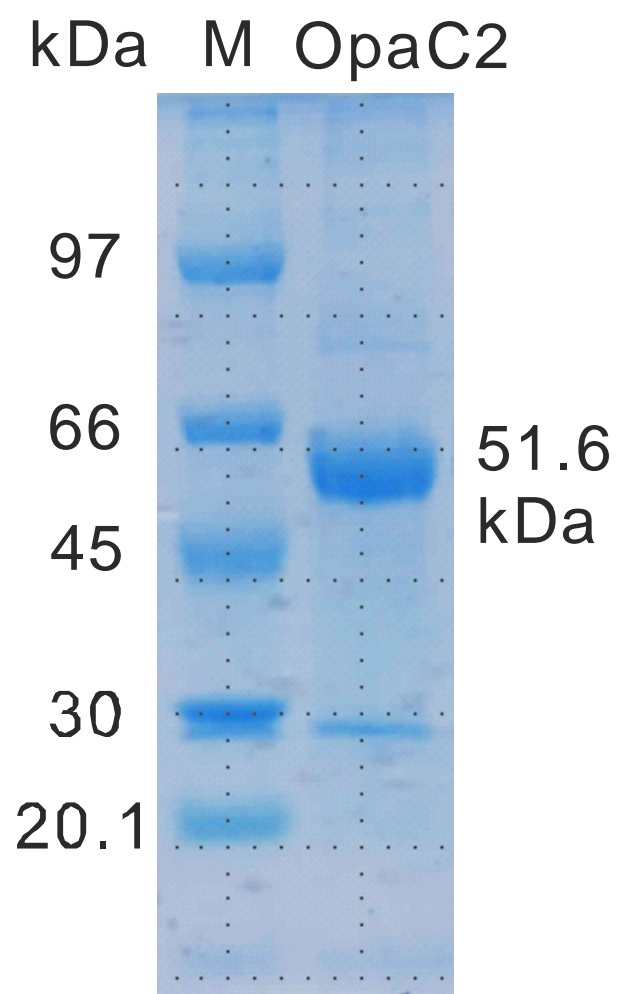


Figure S5. SDS-PAGE analysis of the purified OpaC2

The proteins were separated on a 12% polyacrylamide gel and stained with Coomassie brilliant blue R-250.

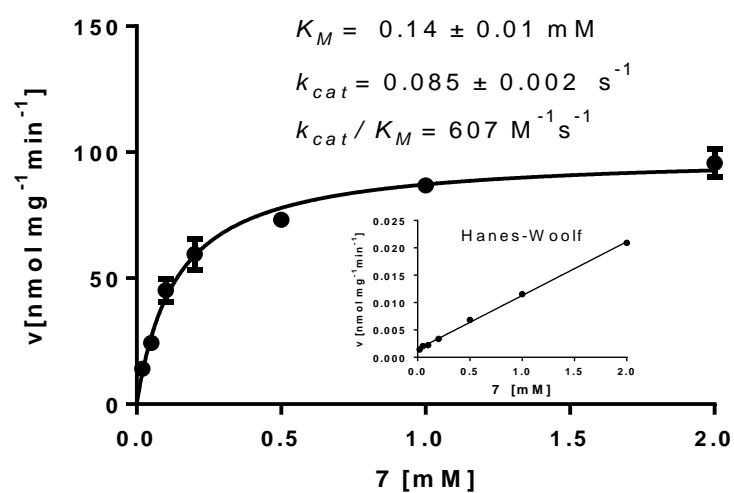


Figure S6. Determination of the kinetic parameters of OpaC2 toward compound **7** in presence of NADPH

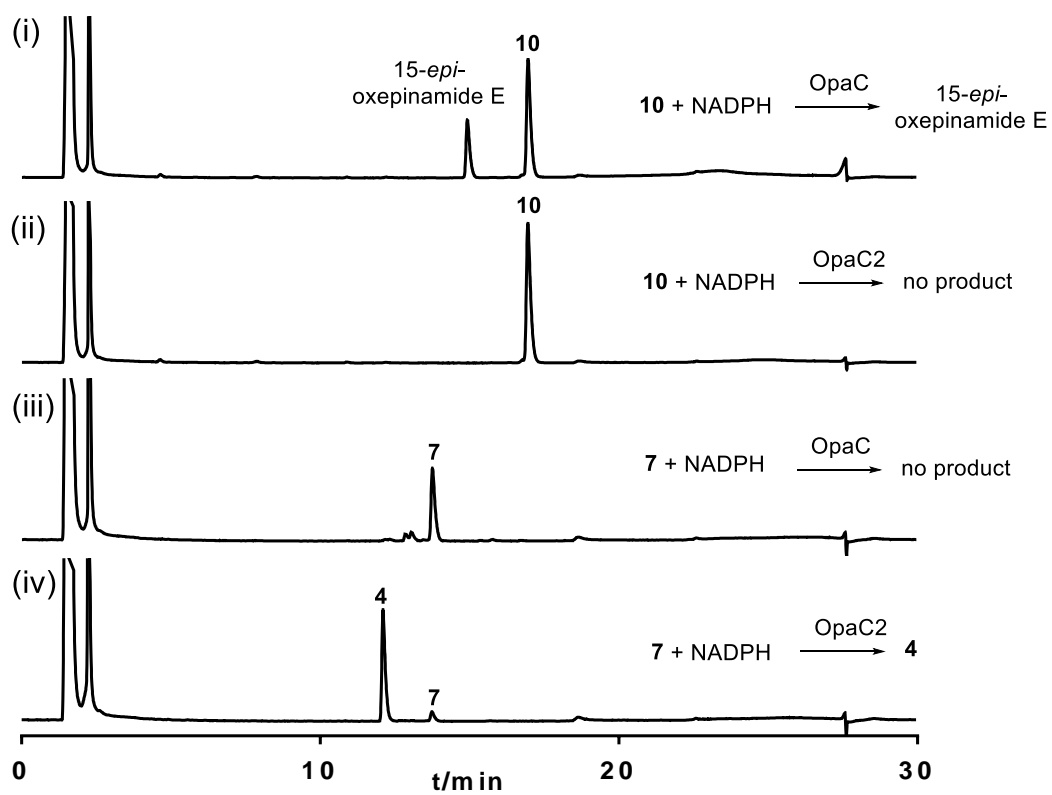


Figure S7. Enzyme assays to prove the crosstalk between OpaC and OpaC2

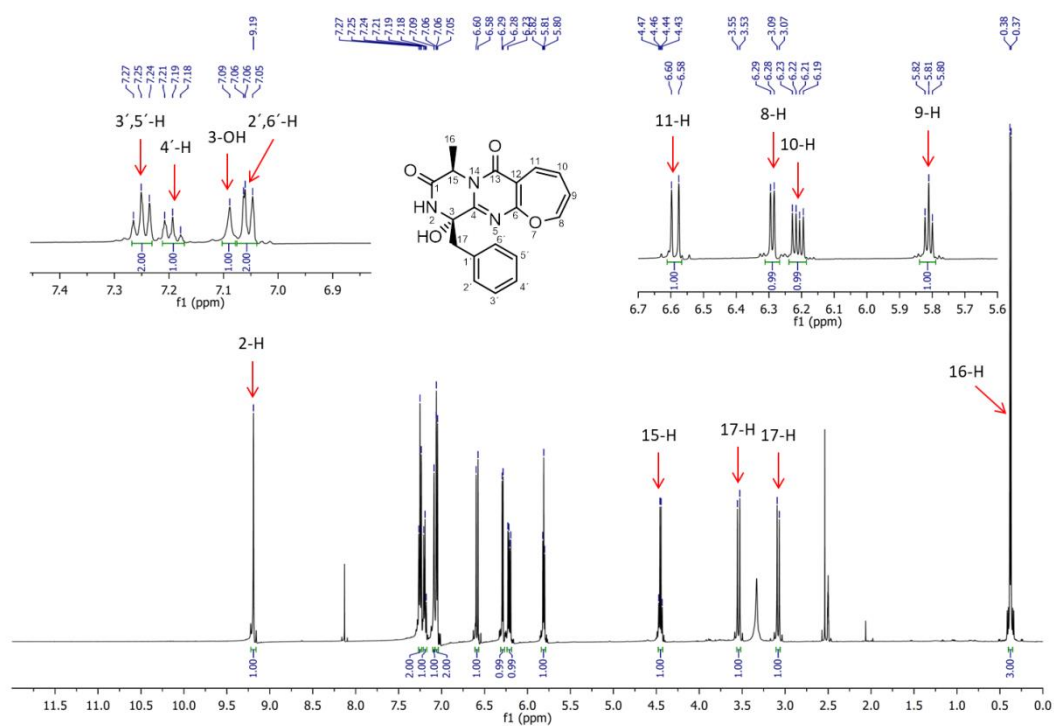


Figure S8. ^1H NMR spectrum of oxepinamide D (**4**) in DMSO-d_6 (500 MHz)

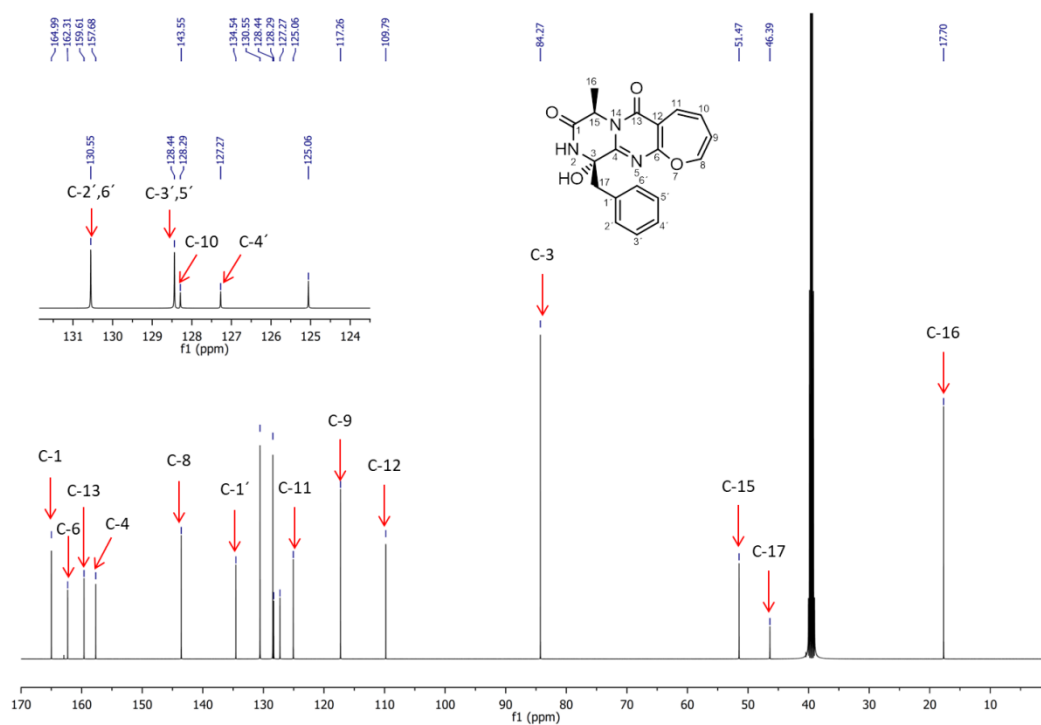


Figure S9. ^{13}C NMR spectrum of oxepinamide D (**4**) in DMSO-d_6 (125 MHz)

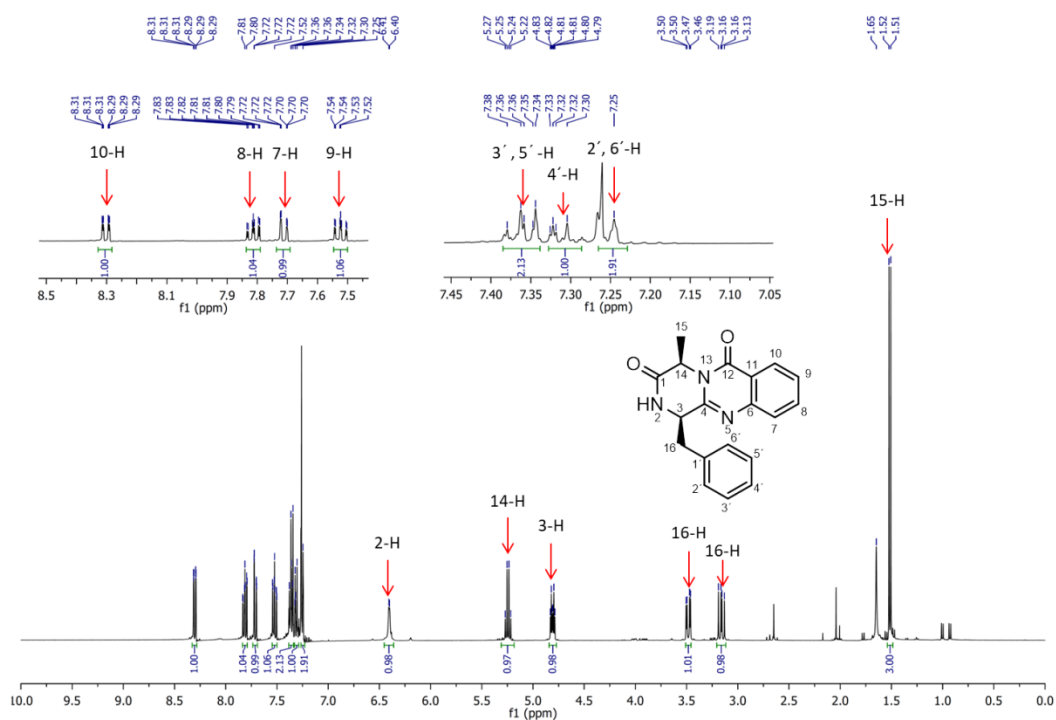


Figure S10. ^1H NMR spectrum of compound (5) in CDCl_3 (500 MHz)

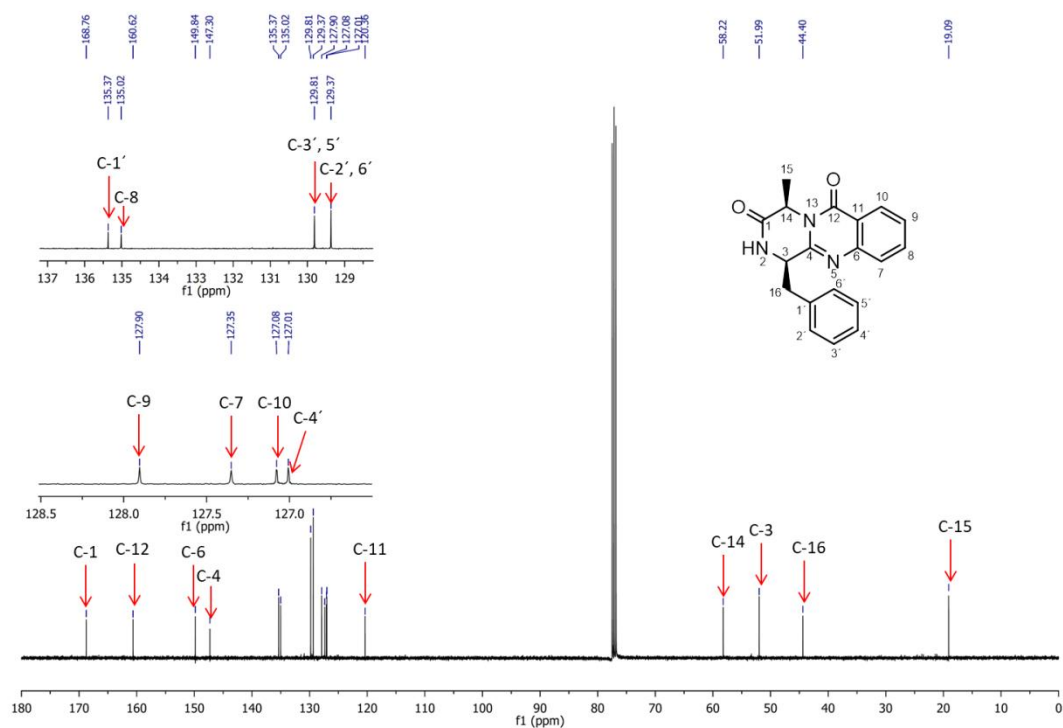


Figure S11. ^{13}C NMR spectrum of compound 5 in CDCl_3 (125 MHz)

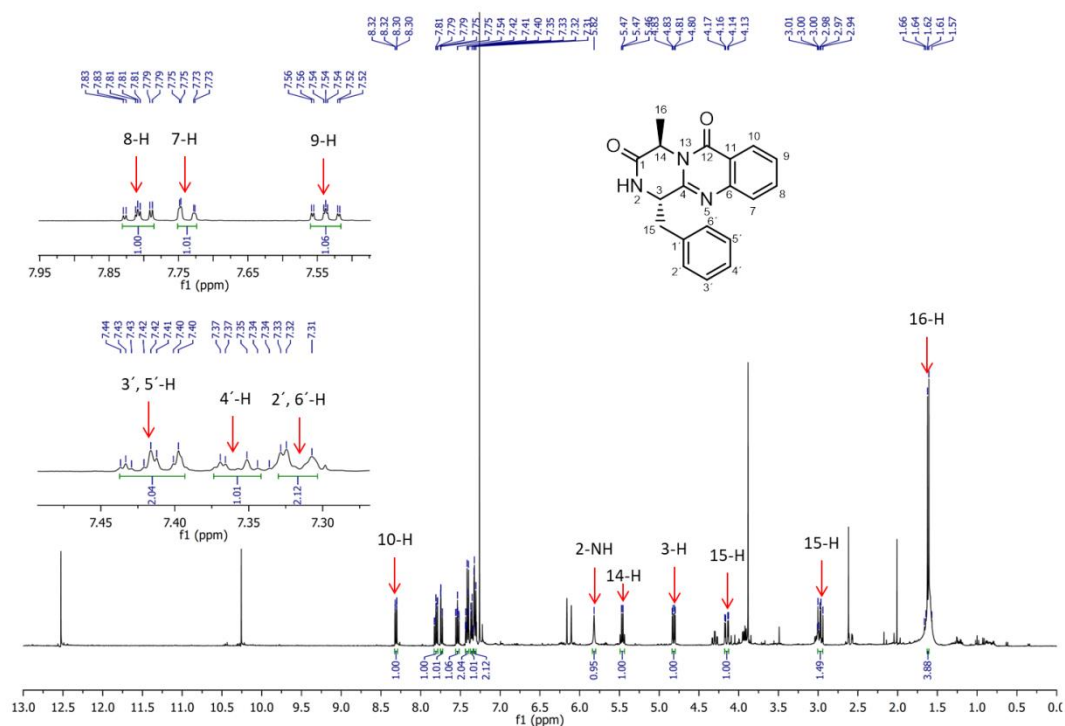


Figure S12. ^1H NMR spectrum of compound **6** in CDCl_3 (500 MHz)

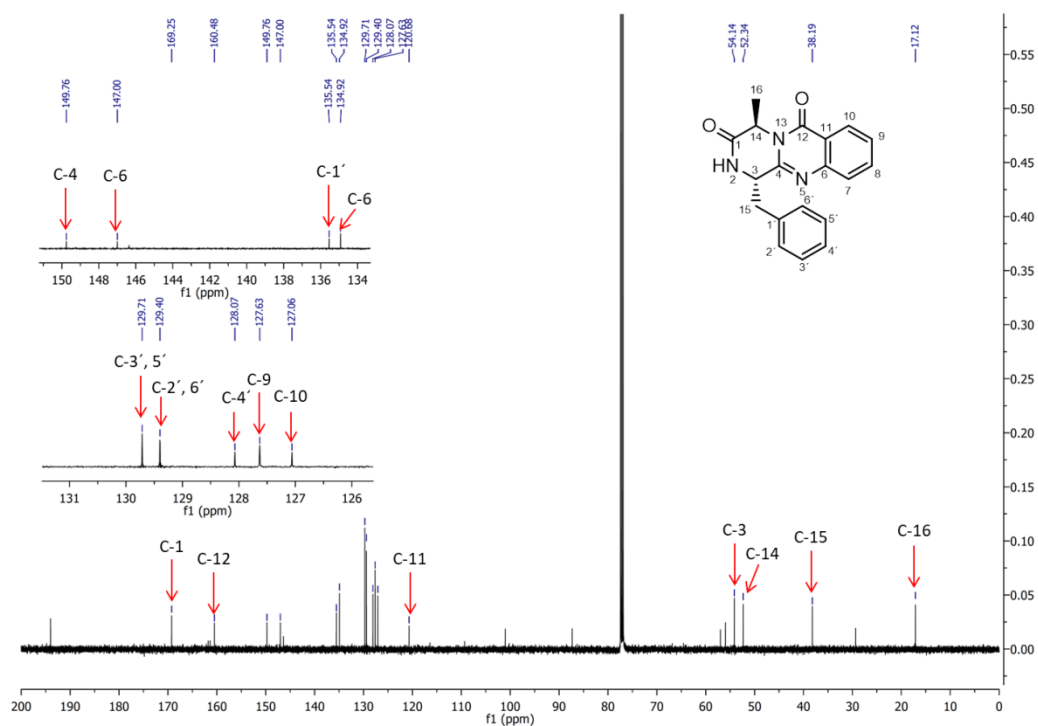


Figure S13. $^{13}\text{C}\{^1\text{H}\}$ NMR spectrum of compound **6** in CDCl_3 (125 MHz)

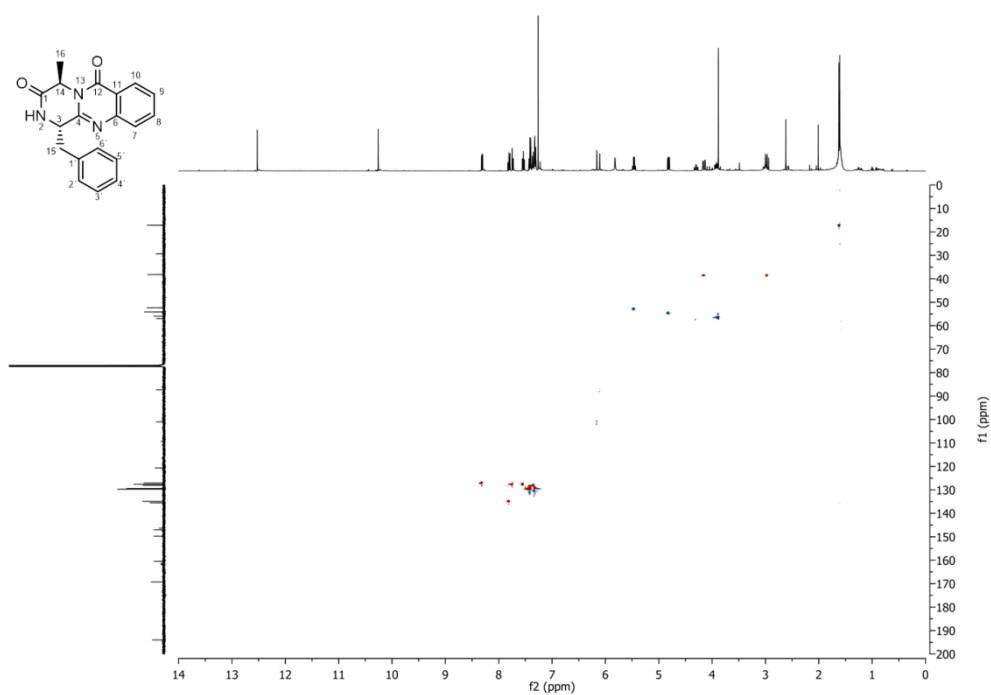


Figure S14. HSQC spectrum of compound **6** in CDCl₃

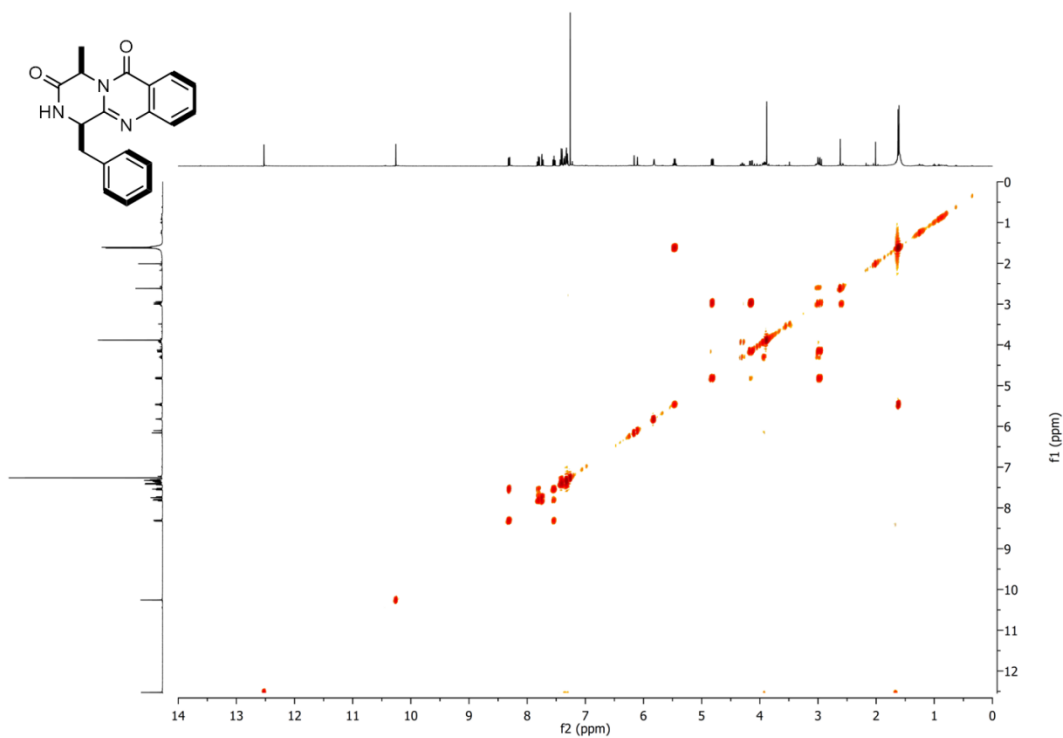


Figure S15. COSY spectrum of compound **6** in CDCl₃

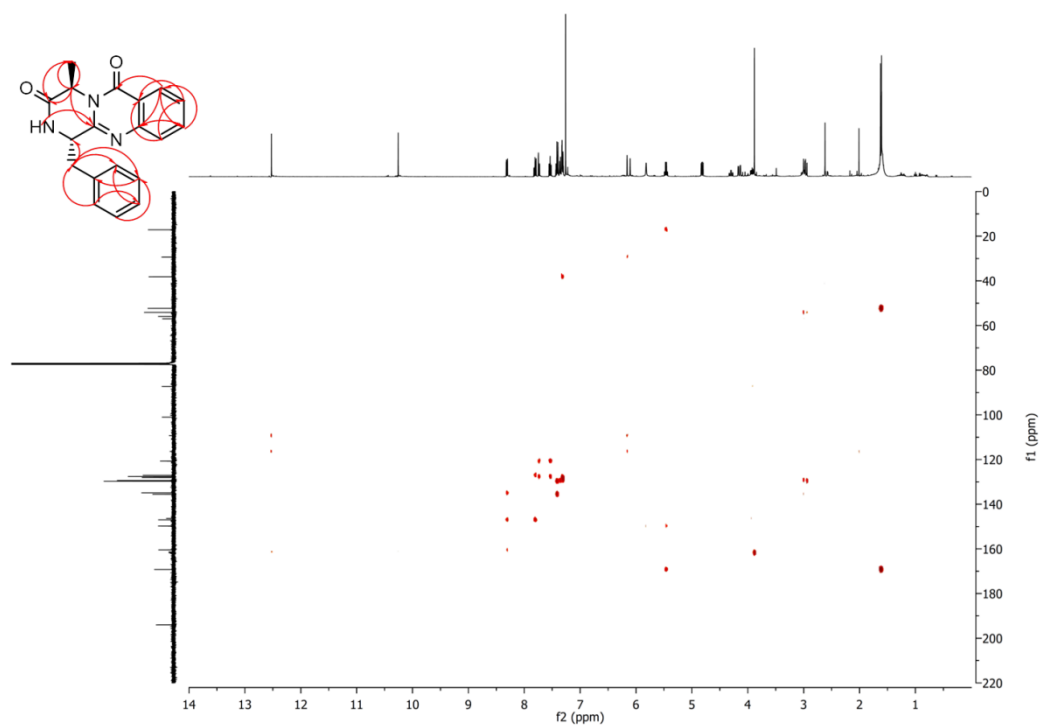


Figure S16. HMBC spectrum of compound **6** in CDCl_3

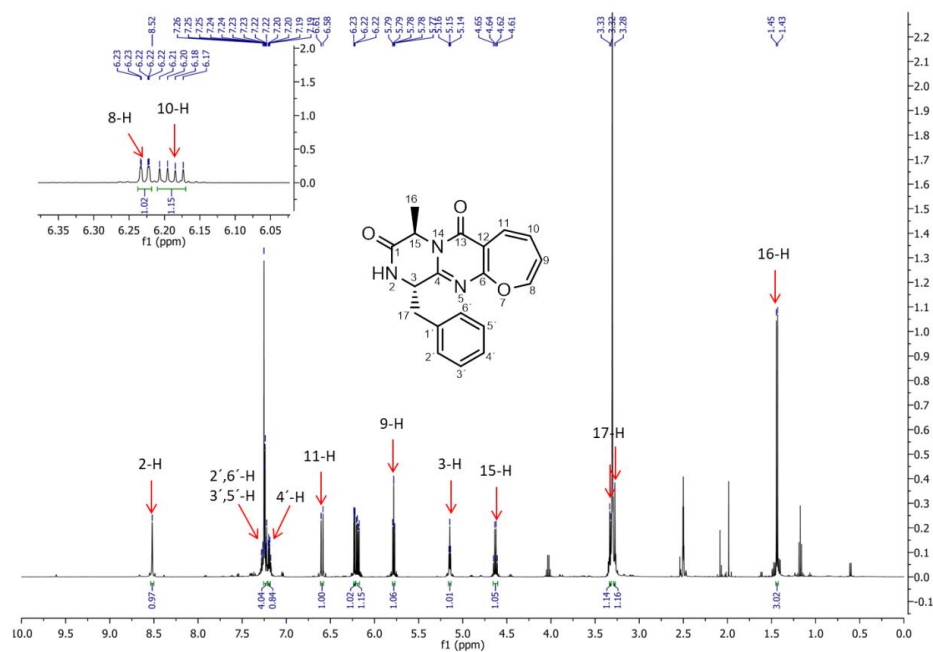


Figure S17. ^1H NMR spectrum of compound **7** in DMSO-d_6 (500 MHz)

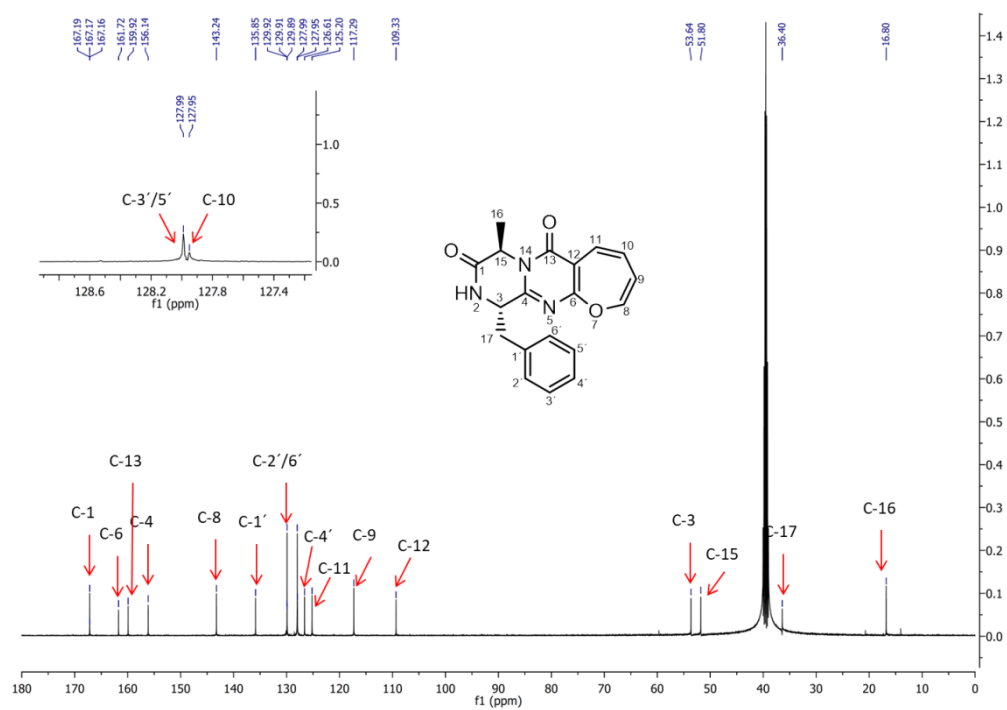


Figure S18. $^{13}\text{C}\{^1\text{H}\}$ NMR spectrum of compound **7** in DMSO-d_6 (125 MHz)

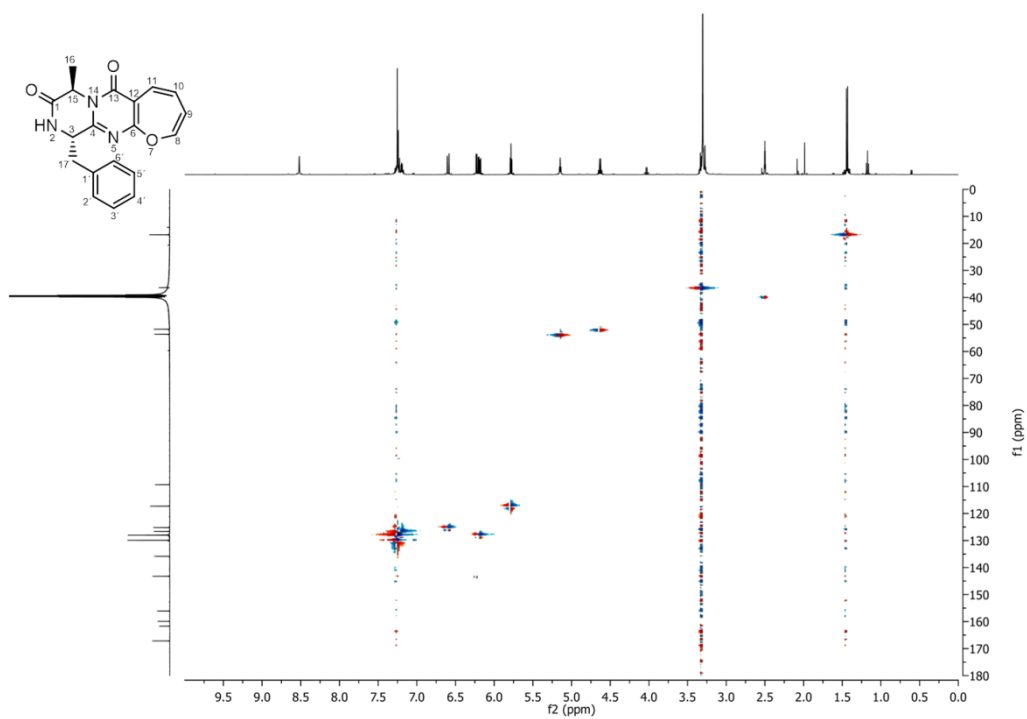


Figure S19. HSQC spectrum of compound **7** in DMSO-d_6

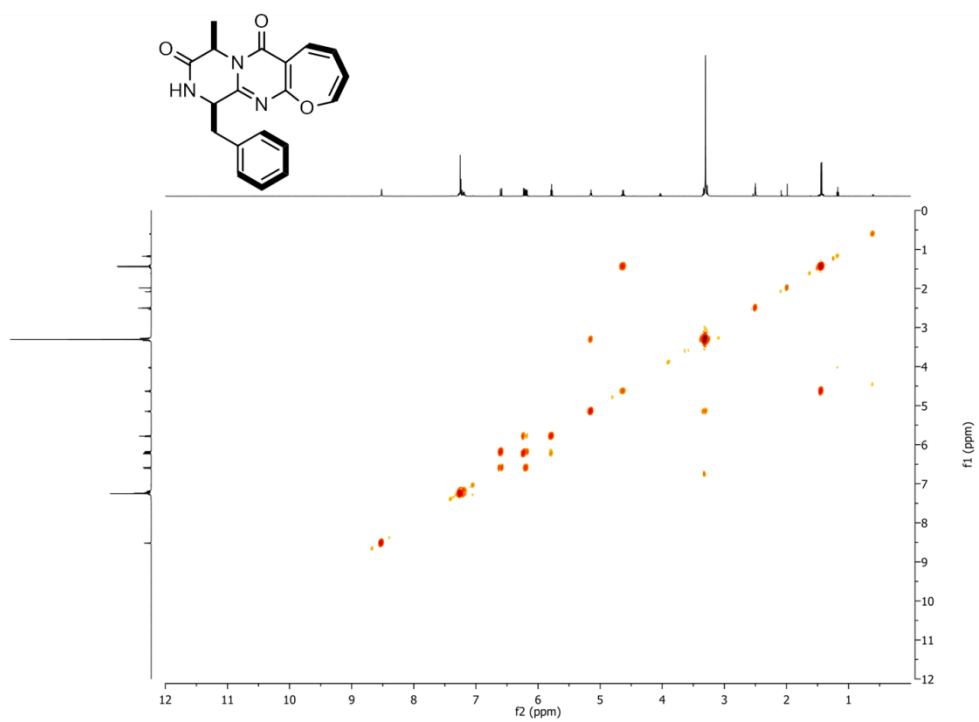


Figure S20. COSY spectrum of compound **7** in DMSO- d_6

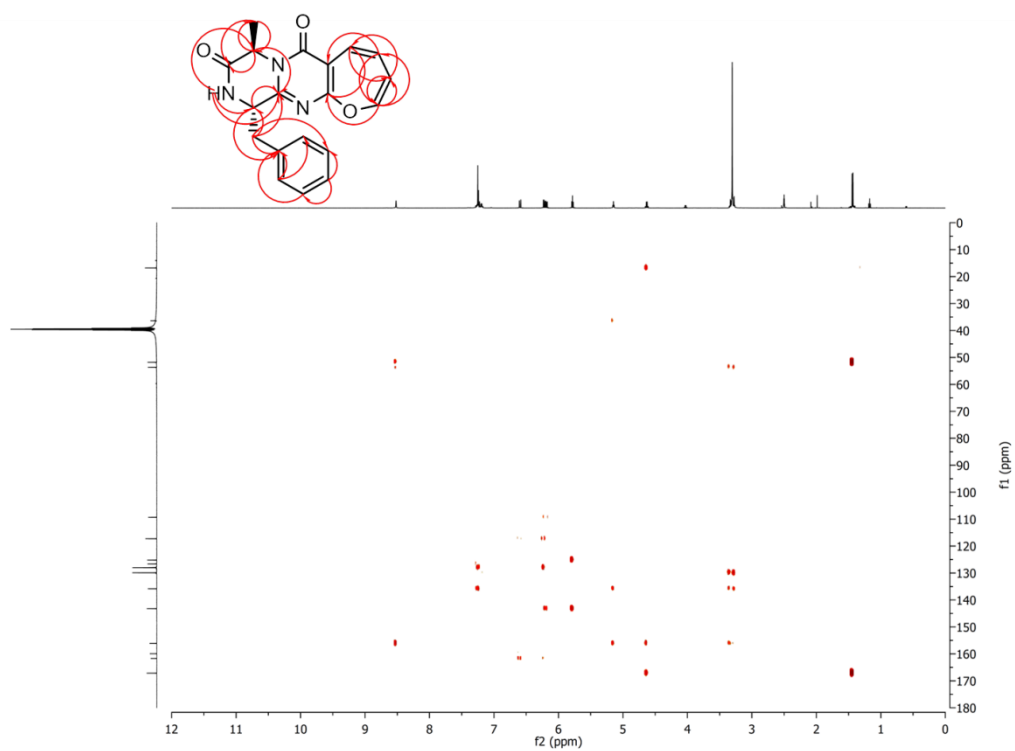


Figure S21. HMBC spectrum of compound **7** in DMSO- d_6

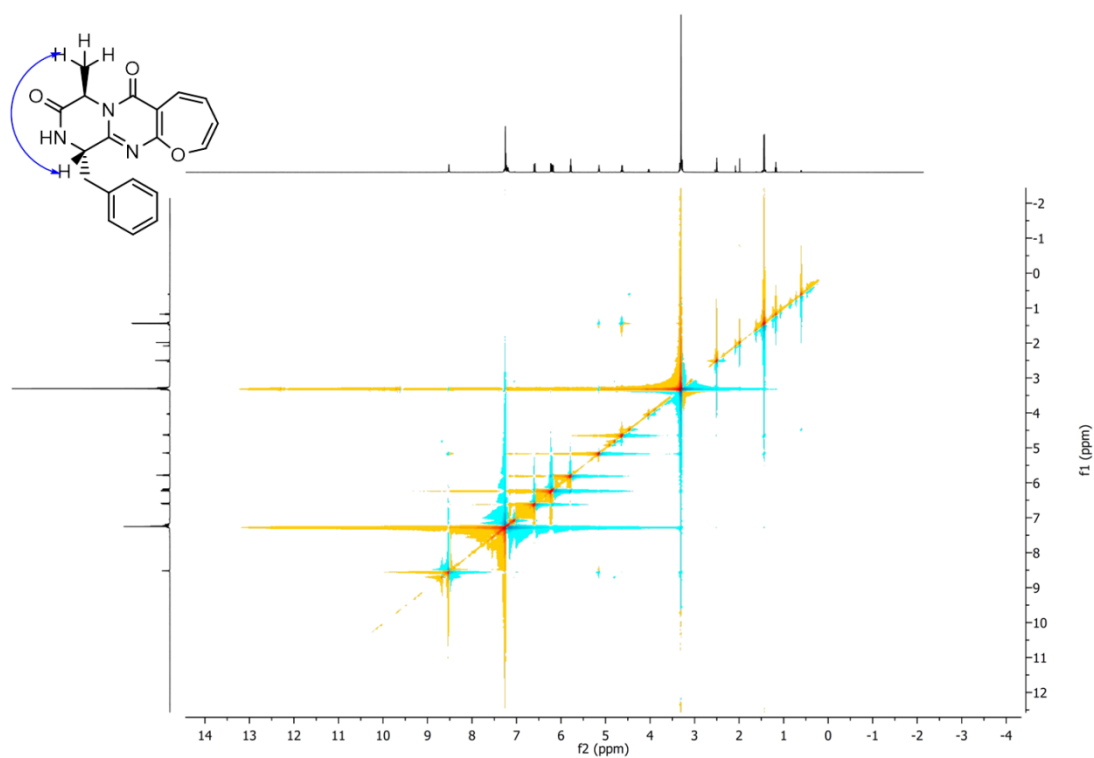


Figure S22. NOESY spectrum of compound **7** in DMSO-d₆

References

- (1) Haynes, S. W.; Gao, X.; Tang, Y.; Walsh, C. T. Complexity generation in fungal peptidyl alkaloid biosynthesis: A two-enzyme pathway to the hexacyclic MDR export pump inhibitor ardeemin. *ACS Chem. Biol.* **2013**, *8*, 741.
- (2) Hernández, F.; Morales, V.; Buenadicha, F. L.; Söllhuber, M.; Avendaño, C. Influence of *N*(2)-substitution in the alkylation of (4*S*)-alkyl-2,4-dihydro-1*H*-pyrazino[2,1-*b*]quinazoline-3,6-diones. *Tetrahedron: Asymmetry* **2004**, *15*, 3045.
- (3) Weber, T.; Charusanti, P.; Musiol-Kroll, E. M.; Jiang, X.; Tong, Y.; Kim, H. U.; Lee, S. Y. Metabolic engineering of antibiotic factories: new tools for antibiotic production in actinomycetes. *Trends Biotechnol.* **2015**, *33*, 15.
- (4) Jacobus, A. P. and Gross, J. Optimal cloning of PCR fragments by homologous recombination in *Escherichia coli*. *PLoS. One.* **2015**, *10*, e0119221.
- (5) Joska, T. M.; Mashruwala, A.; Boyd, J. M.; Belden, W. J. A universal cloning method based on yeast homologous recombination that is simple, efficient, and versatile. *J. Microbiol. Methods* **2014**, *100*, 46.
- (6) Zheng, L.; Wang, H.; Fan, A.; Li, S.-M. Oxepinamide F biosynthesis involves enzymatic D-aminoacyl epimerization, 3*H*-oxepin formation, and hydroxylation induced double bond migration. *Nat. Commun.* **2020**, *11*, 4914.
- (7) Chiang, Y. M.; Ahuja, M.; Oakley, C. E.; Entwistle, R.; Asokan, A.; Zutz, C.; Wang, C. C.; Oakley, B. R. Development of genetic dereplication strains in *Aspergillus nidulans* results in the discovery of aspercryptin. *Angew. Chem. Int. Ed. Engl.* **2016**, *55*, 1662.
- (8) Fan, J.; Liao, G.; Kindinger, F.; Ludwig-Radtke, L.; Yin, W.-B.; Li, S.-M. Peniphenone and penilactone formation in *Penicillium crustosum* via 1,4-Michael additions of *ortho*-quinone methide from hydroxyclovatol to γ -butyrolactones from crustosic acid. *J. Am. Chem. Soc.* **2019**, *141*, 4225.
- (9) Lu, X.; Shi, Q.; Zheng, Z.; Ke, A.; Zhang, H.; Huo, C.; Ma, Y.; Ren, X.; Li, Y.; Lin, J.; Jiang, Q.; Gu, Y.; Kiyota, H. Oxepinamides: Novel liver X receptor agonists from *Aspergillus puniceus*. *Eur. J. Org. Chem.* **2011**, *2011*, 802.
- (10) Lee, S. U.; Asami, Y.; Lee, D.; Jang, J. H.; Ahn, J. S.; Oh, H. Protuboxepins A and B and protubonines A and B from the marine-derived fungus *Aspergillus* sp. SF-5044. *J. Nat. Prod.* **2011**, *74*, 1284.
- (11) Ohte, S.; Shiokawa, T.; Koyama, N.; Katagiri, T.; Imada, C.; Tomoda, H. A new diketopiperazine-like inhibitor of bone morphogenetic protein-induced osteoblastic differentiation produced by marine-derived *Aspergillus* sp. BFM-0085. *J. Antibiot.* **2020**, *73*, 554.

4.5 Switching a regular tryptophan C4-prenyltransferase to a reverse tryptophan-containing cyclic dipeptide C3-prenyltransferase by sequential site-directed mutagenesis.



Cite this: *Org. Biomol. Chem.*, 2018, **16**, 6688

Switching a regular tryptophan C4-prenyltransferase to a reverse tryptophan-containing cyclic dipeptide C3-prenyltransferase by sequential site-directed mutagenesis†

Liujuan Zheng,‡ Peter Mai,‡ Aili Fan§ and Shu-Ming Li *

FgaPT2 from *Aspergillus fumigatus* catalyzes a regular C4- and its mutant K174A a reverse C3-prenylation of L-tryptophan in the presence of dimethylallyl diphosphate. FgaPT2 also uses tryptophan-containing cyclic dipeptides for C4-prenylation, while FgaPT2_K174A showed almost no activity toward these substrates. In contrast, Arg244 mutants of FgaPT2 accept very well cyclic dipeptides for regular C4-prenylation. In this study, we demonstrate that FgaPT2_K174F, which catalyzes a regular C3-prenylation on tyrosine, can also use *cyclo*-L-Trp-L-Ala, *cyclo*-L-Trp-L-Trp, *cyclo*-L-Trp-Gly, *cyclo*-L-Trp-L-Phe, *cyclo*-L-Trp-L-Pro, and *cyclo*-L-Trp-L-Tyr as substrates, but only with low activity. Combinational mutation on Lys174 and Arg244 increases significantly the acceptance of these cyclic dipeptides. With the exception of *cyclo*-L-Trp-L-Trp, the tested dipeptides were much better accepted by FgaPT2_K174F_R244X (X = L, N, Q, Y) than FgaPT2, with an increase of two- to six-fold activity. In comparison to FgaPT2_K174F, even two- to ten-fold conversion yields were calculated for the double mutants. Isolation and structural elucidation of the enzyme products revealed stereospecific reverse C3-prenylation on the indole ring, resulting in the formation of *syn*-*cis* configured hexahydropyrroloindole derivatives. The results presented in this study highlight the convenience of site-directed mutagenesis for creating new biocatalysts.

Received 19th July 2018,
Accepted 28th August 2018

DOI: 10.1039/c8ob01735b

rsc.li/obc

Introduction

Cyclic dipeptides (CDPs) and derivatives are widely distributed in microorganisms and exhibit diverse biological and pharmacological activities.^{1–3} In nature, these dipeptides are biosynthesized by bimodular non-ribosomal peptide synthetases or cyclodipeptide synthases.^{4–6} Due to the various modification possibilities on the indole ring, tryptophan-containing CDPs are the richest precursors of natural products with pharmaceutical interest.^{2,3} These dipeptides are frequently modified by methylation, hydroxylation, prenylation, dimerization, and further cyclization.^{2,3,7,8} Chart 1 lists several examples of CDP derivatives such as the antitumor active rugulosuvine A from

Penicillium species,⁹ the sterol O-acyltransferase inhibitor amauromine from *Nocardiosis* sp.,^{10,11} and the two mycotoxins roquefortine C and acetylaszonalenin from different fungal strains.^{3,12,13} They are modification products of CDPs obtained by tailoring enzymes including prenyltransferases (PTs).^{3,14}

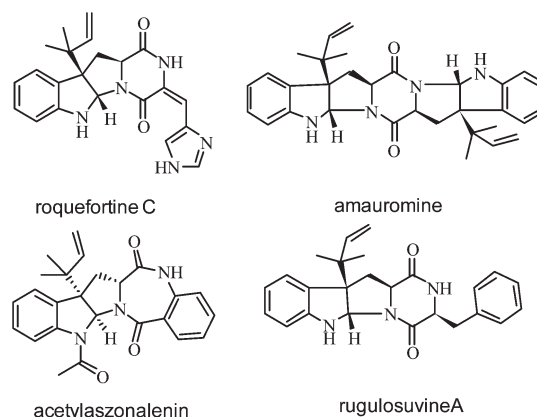


Chart 1 Examples of CDP derivatives.

Institut für Pharmazeutische Biologie und Biotechnologie, Philipps-Universität Marburg, Robert-Koch-Straße 4, 35037 Marburg, Germany.

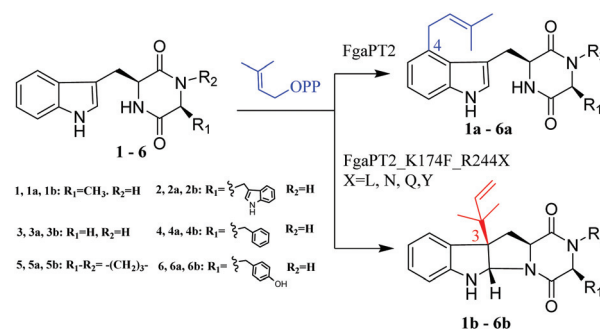
E-mail: shuming.li@staff.uni-marburg.de

† Electronic supplementary information (ESI) available: Primers and constructs, NMR data and spectra as well as determination of kinetic parameters. See DOI: 10.1039/c8ob01735b

‡ These authors contributed equally to this work.

§ Present address: Beijing Advanced Innovation Center for Soft Matter Science and Engineering, Beijing Key Laboratory of Bioprocess, Beijing University of Chemical Technology, Beijing, 100029, People's Republic of China.

Mutation of Lys174 to Phe switches FgaPT2 to a tyrosine C3-prenyltransferase FgaPT2_K174F.²⁸ Arg244 mutants enhance significantly the catalytic ability of FgaPT2 toward tryptophan-containing CDPs and keep the prenylation position at C-4.²⁹ Luk *et al.*³⁰ demonstrated that FgaPT2_K174A can prenylate L-tryptophan at both C-3 and C-4 positions and proposed the C4-prenylated derivative to be the result of the Cope rearrangement of a C3-prenylated derivative. Acceptance of tryptophan-containing CDPs by FgaPT2_K174A has not been tested before, while FgaPT2 was also demonstrated to prenylate these compounds at C-4, *i.e.* the same position as for the natural substrate L-tryptophan (Scheme 1). All these results proved FgaPT2 as an excellent model for enzyme design by site-directed mutagenesis. In this study, we describe the creation of a reverse C3-prenyltransferase for tryptophan-containing CDPs by two step-mutations on Lys174 and Arg244.



Scheme 1 Prenylation of cyclic dipeptides by FgaPT2 and its mutants.

Acceptance of tryptophan-containing cyclic dipeptides by FgaPT2 K174F

To prove the acceptance toward tryptophan-containing CDPs, we constructed the plasmid pLZ1 for overproduction of FgaPT2_K174A (Table S1†). One predominant protein band with the expected size was detected using SDS-PAGE analysis for the purified FgaPT2_K174A (Fig. S1†), which was used for incubation with L-tryptophan and DMAPP. LC-MS analysis of the reaction mixture revealed the presence of two product peaks at 7.3 and 8.0 min. The peak at 8.0 min was identified as the C4-prenylated derivative by comparison of its retention time, UV (λ_{max} 278 nm), and MS data with those of the FgaPT2 product (Fig. S2†). The peak at 7.3 min showed the same $[\text{M} + \text{H}]^+$ ion, but a clearly different UV spectrum (λ_{max} at 240 and 294 nm) as the peak at 8.0 min. These data would correspond to those of the C3-prenylated L-tryptophan reported for FgaPT2_K174A.³⁰ After proof of its functionality, the overproduced FgaPT2_K174A was incubated with six L-tryptophan-containing cyclic dipeptides, *i.e.* *cyclo*-L-Trp-L-Ala (1), *cyclo*-L-Trp-L-Trp (2), *cyclo*-L-Trp-Gly (3), *cyclo*-L-Trp-L-Phe (4), *cyclo*-L-Trp-L-Pro (5), and *cyclo*-L-Trp-L-Tyr (6) in the presence of DMAPP at 37 °C for 3 h. HPLC analysis of the incubation mixtures indicated no product formation in all enzyme assays under the tested conditions (Fig. 1). LC-MS analysis with EIC detection for the $[\text{M} + \text{H}]^+$ ion of monoprenylated products showed product peaks with very low intensity (Fig. S3†).

In contrast, the cyclic dipeptides **1–6** were accepted by the wildtype FgaPT2 with product yields in the range from 6.6 to 29.5% (Fig. 1). With the exception for **2**, one product peak each (**1a** or **3a–6a**) was observed. These products showed a typical UV λ_{max} peak at 278 nm for the indole system and have $[\text{M} + \text{H}]^+$ ions, which are 68 Daltons larger than the respective substrate (Fig. S3†), indicating the presence of an indole chromophore and corresponding to the *C4*-prenylation of cyclic dipeptides by FgaPT2 (Scheme 1).³¹ In the case of **2**, two products **2a** and **2a*** were detected, with $[\text{M} + \text{H}]^+$ ions, which are 68 and 136 Daltons larger than that of **2**, indicating a mono- and diprenylation, respectively (Fig. S3†).

In a previous study, we demonstrated that Lys174 also plays an important role in aromatic substrate selection.

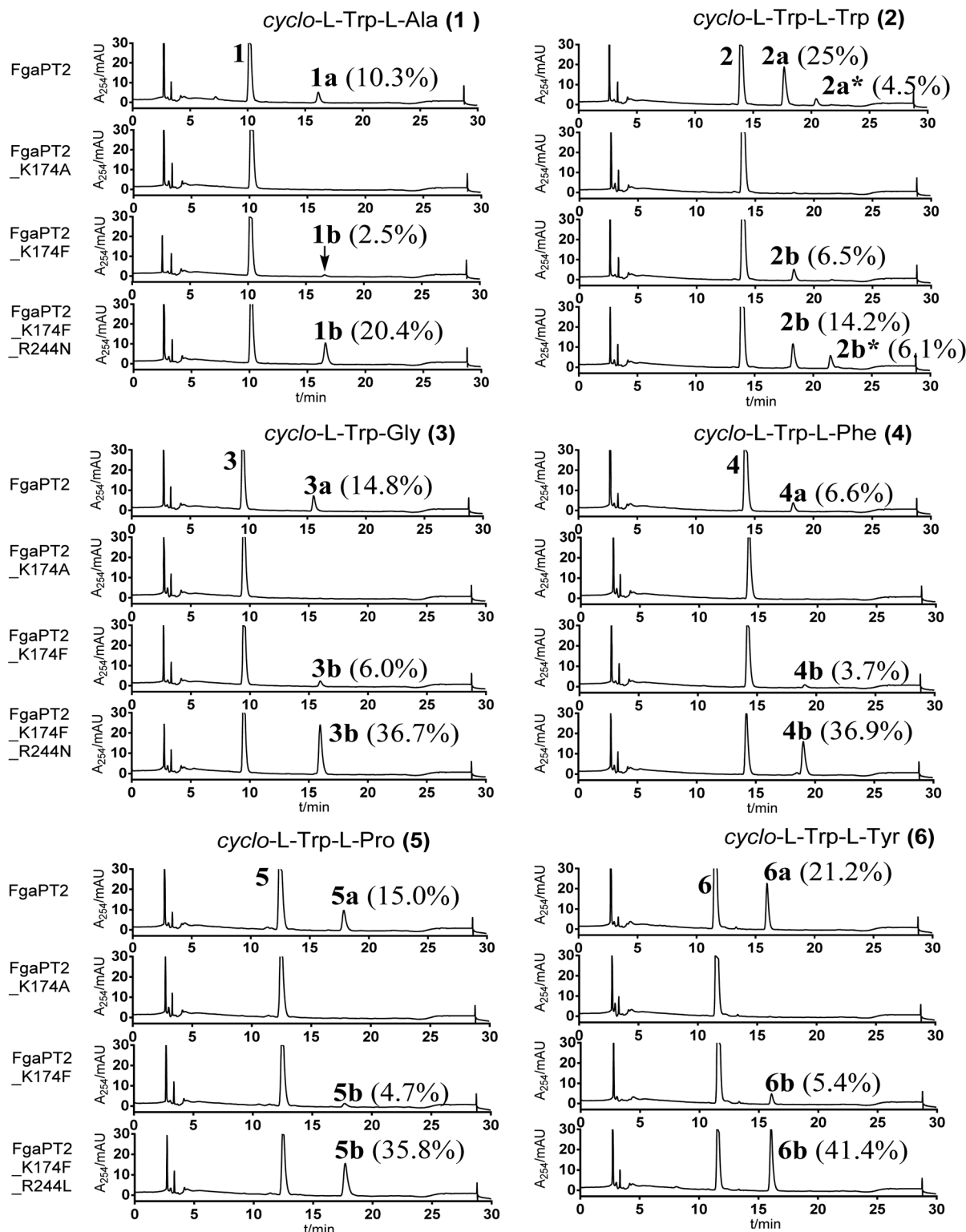


Fig. 1 HPLC analysis of incubation mixtures of FgaPT2 and its mutants with cyclic dipeptides.

FgaPT2_K174F accepts L-tryptophan only with a 240-fold decreased activity compared to FgaPT2, while its catalytic ability for L-tyrosine increased 28-fold.²⁸ We proved therefore its behavior toward cyclic dipeptides 1–6 under the same con-

ditions used for FgaPT2_K174A. As shown in Fig. 1, all six substrates were accepted by FgaPT2_K174F with product yields of 2.5 to 6.5%. Detailed inspection of the HPLC chromatograms revealed the presence of one product each (1b–6b) with slightly

delayed retention times and clear different UV spectra compared to **1a–6a**.

The UV absorption maxima of **1b–6b** at 240 and 294 nm indicated the disruption of the indole and the presence of a hexahydropyrroloindole system by C3-prenylation. LC-ESI-HRMS analysis of the incubation mixtures of FgaPT2_K174F with **1–6** confirmed the monoprenylation in **1b–6b** by detection of $[M + H]^+$ ions, which are 68 Daltons larger than those of the respective substrates (Fig. S3†). We speculated that **1–6** were converted to C3-prenylated derivatives by FgaPT2_K174F. However, the conversion yields are too low to be used as convenient biocatalyst for CDP prenylation.^{10,30} In the case of **2**, a diprenylated product was also detected using LC-MS analysis (Fig. S3†).

Enhancing the conversion of tryptophan-containing cyclic dipeptides by combinational mutation on Lys174 and Arg244

We demonstrated previously that Arg244 mutants, especially R244N, R244Q, R244Y, and R244L, showed strongly increased activities toward tryptophan-containing cyclic dipeptides, while L-tryptophan was less accepted by these mutants than the wildtype FgaPT2.²⁹ The prenylation position remained at C-4 of the indole ring. To increase the conversion yields of cyclic dipeptides for potential C3-prenylation, we created double mutants by site-directed mutagenesis of Lys174 to Phe and Arg244 to Leu, Asn, Gln, and Tyr, resulting in the four double mutants FgaPT2_K174F_R244L, FgaPT2_K174F_R244N, FgaPT2_K174F_R244Q, and FgaPT2_K174F_R244Y (Table S1†). The overproduced proteins with yields of 1.2–2.3 mg per liter culture were purified to apparent homogeneity (Fig. S1†) and exploited to enzyme assays with **1–6** under the conditions used for FgaPT2_K174F.

HPLC analysis of the reaction mixtures delivered remarkable results (Fig. 1 and 2). (i) Product formation was detected in all the enzyme assays (Fig. 1, for simplification, only the result of the best mutant for a given substrate is illustrated). (ii) All double mutants exhibited increased activities toward all the tested substrates (Fig. 2). Total product yields of 20.3 to 41.4% were calculated for the best mutant with a given substrate, *i.e.* FgaPT2_K174F_R244N for **1–4** and FgaPT2_K174F_R244L for **5** and **6**. This means an activity increase of two- to ten-fold, in comparison with those with FgaPT2_K174F. (iii) The products have the same retention times and UV spectra as those of the FgaPT2_K174F for a given substrate (**1b–6b**). (iv) The corresponding products also have almost the same $[M + H]^+$ ions from LC-MS analysis (Fig. S3†). In the case of **2**, the additional peak **2b*** with a $[M + H]^+$ ion for a diprenylated derivative was detected. All these data underline successful mutational combinations for acceptance of tryptophan-containing CDPs.

Structure elucidation of the enzyme products with FgaPT2_K174F_R244X

To elucidate the structures, the enzyme products of **1–4** were isolated from incubation mixtures with FgaPT2_K174F_R244N and those of **5** and **6** with FgaPT2_K174F_R244L. HRMS data

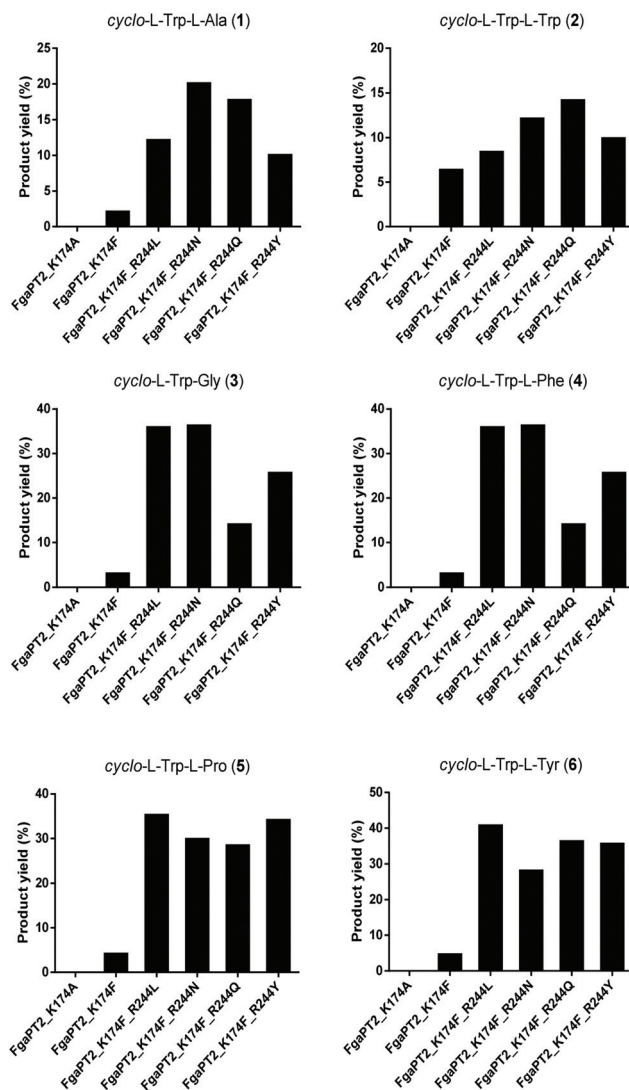


Fig. 2 Yields of **1b–6b** with Lys174 and Arg244 mutants. The components and incubation conditions are identical to those of Fig. 1.

Table 1 ESI-HRMS data of the enzyme products

Compound	Formula	$[M + H]^+$		
		Measured	Calculated	Deviation (ppm)
1b	C ₁₉ H ₂₄ N ₃ O ₂	326.1858	326.1863	1.5
2b	C ₂₇ H ₂₉ N ₄ O ₂	441.2292	441.2285	−1.6
2b*	C ₃₂ H ₃₆ N ₄ O ₂	509.2927	509.2911	−3.1
3b	C ₁₈ H ₂₂ N ₃ O ₂	312.1719	312.1707	−3.8
4b	C ₂₅ H ₂₈ N ₃ O ₂	402.2187	402.2176	−2.7
5b	C ₂₁ H ₂₆ N ₃ O ₂	352.2029	352.2020	−2.6
6b	C ₂₅ H ₂₈ N ₃ O ₃	418.2138	418.2125	−3.1

(Table 1) confirmed the monoprenylation in **1b–6b** and diprenylation in **2b***. Inspection of the ¹H NMR spectra of **1b–6b** (Fig. S4–S9†) revealed the presence of signals for a reverse prenyl moiety each at δ_{H} 4.97–5.13 (dd, 1H), 5.05–5.09 (dd, 1H), 5.76–5.98 (dd, 1H), 0.93–1.11 (s, 3H), and 0.79–1.01 (s, 3H)

ppm (Table S2†). The signals of H-2 at the original indole rings are significantly up-field shifted to 5.32–5.55 ppm, indicating the disruption of the indole and formation of a hexahydropyrroloindole system caused by a C3-prenylation.^{10,23} The signals of H-11 appear as double doublets of doublets with coupling constants of approximately 11, 6.0, and 2.0 Hz, proving the 3 β -prenylation of the L-configured tryptophanyl moiety, *i.e.* *syn-cis* configuration (2S, 3R, 11S).¹⁰ A literature search confirmed the structures **1b–6b** (Scheme 1) as reported previously.^{10,23} They were obtained as enzyme products of the prenyltransferase CdpC3PT from *Neosartorya fischeri*.^{10,23} In the case of **2b***, the structure cannot be confirmed using NMR analysis, due to the low quantity. We speculated here C3-prenylation at both the indole rings, as observed for other C3-prenyltransferases with *cyclo*-L-Trp-L-Trp.¹⁴

To get detailed insights into the reaction mechanism, we carried out molecular docking using the program AutoDock Vina.³² The models of FgaPT2_K174A, FgaPT2_K174F, and FgaPT2_K174F_R244L were created from the FgaPT2 structure (PDB code: 3I4X) using SWISS-MODEL. The tested cyclic dipeptides and DMAPP were docked *in silico* into the models of FgaPT2 and its mutants. Unfortunately, the observed enzyme activities and prenylation positions can be explained neither by the distances of C-1/C-3 of DMAPP to C-3/C-4 of the indole ring of the cyclic dipeptides, nor by π - π or van der Waals force interaction (data not shown). Therefore, crystal structures of the mutants are needed for understanding the observed results presented in this study, which should be explored in the near future.

Determination of kinetic parameters

Kinetic parameters including Michaelis Menten constants (K_M) and turnover numbers (k_{cat}) were determined at pH 7.5 for the two best mutants in the presence of DMAPP, *i.e.* FgaPT2_K174F_R244N with **1–4** as well as FgaPT2_K174F_R244L with **5** and **6**. The reactions catalyzed by both mutants apparently followed the Michaelis Menten kinetics (Fig. S10–S15†). With the exception of **3**, K_M values in the range of 0.15 to 0.79 mM were determined (Table 2). The high catalytic efficiencies of FgaPT2_K174F_R244N for **4** and FgaPT2_K174F_R244L for **5** and **6** confirmed their high conversions illustrated in Fig. 1.

Table 2 Kinetic parameters of FgaPT2_K174F_R244N and FgaPT2_K174F_R244L

S	FgaPT2_K174F_R244N			FgaPT2_K174F_R244L		
	K_M [mM]	k_{cat} [s ⁻¹]	k_{cat}/K_M [s ⁻¹ M ⁻¹]	K_M [mM]	k_{cat} [s ⁻¹]	k_{cat}/K_M [s ⁻¹ M ⁻¹]
1	0.36	0.012	33.3	—	—	—
2	0.79	0.13	164.6	—	—	—
3	3.10	0.19	61.3	—	—	—
4	0.15	0.03	200.0	—	—	—
5	—	—	—	0.41	0.15	365.9
6	—	—	—	0.62	0.25	403.2

S: substrate.

Experimental

Chemicals

DMAPP was synthesized according to the method described for geranyl diphosphate reported previously.³³ Substrates used for the enzyme assays were purchased from Bachem (Bubendorf, Switzerland) or synthesized as described previously.³⁴

Bacterial strains, plasmids, and culture conditions

E. coli BL21 (DE3) pLysS (Invitrogen, Karlsruhe, Germany) and SoluBL21 (Novagen, Darmstadt, Germany) were used for expression experiments. pIU18 was used as a DNA template for the creation of FgaPT2_K174A. pES26 containing the mutation for FgaPT2_K174F²⁸ was used as a template for the construction of the double mutants FgaPT2_K174F_R244L, FgaPT2_K174F_R244N, FgaPT2_K174F_R244Q, and FgaPT2_K174F_R244Y. *E. coli* cells harboring plasmids were grown in liquid Lysogeny Broth (LB) or Terrific Broth (TB) medium and on solid LB medium with 2% (w/v) agar at 37 °C. Kanamycin (50 μ g mL⁻¹) was used for the selection of recombinant *E. coli* strains.

Site-directed mutagenesis, overproduction and purification of the recombinant proteins

The Expand™ Long Template PCR system (Roche Diagnostic, Mannheim, Germany) was used for the construction of plasmids listed in Table S1.† The primers are given in Table S1.† The obtained plasmids were sequenced by Seqlab Sequence Laboratories (Göttingen, Germany) to confirm the desired mutations in the respective constructs. FgaPT2 and its mutated derivatives were overproduced and purified as described previously.^{28,35}

Enzyme assays with purified recombinant proteins

To test the enzyme activity, the reaction mixtures (50 μ L) containing 50 mM Tris-HCl (pH 7.5), 10 mM CaCl₂, 0.5 mM cyclic dipeptide, 1 mM DMAPP, and 10 μ g of the purified recombinant protein were incubated at 37 °C for 3 h. The reactions were terminated by the addition of 50 μ L methanol. After removal of the precipitated protein by centrifugation at 13 000g for 30 min, 20 μ L supernatant was subjected to HPLC or LC-HRMS analysis.

Enzyme assays for the determination of kinetic parameters (50 μ L) contained 1 mM DMAPP, 5–10 μ g FgaPT2_K174F_R244N or FgaPT2_K174F_R244L and the aromatic substrates at final concentrations from 0.025 to 5 mM. The incubations were carried out at 37 °C for 30 min. After addition of MeOH and centrifugation, the supernatants were analyzed on a HPLC system.

HPLC analysis of enzyme assays

Enzyme assays were analyzed on an Agilent HPLC series 1200 system (Agilent Technologies) equipped with an Agilent Eclipse XDB-C18 column (5 μ m, 4.6 \times 150 mm). A linear gradient from 10 to 90% CH₃CN in H₂O in 20 min was used. The

column was then washed with 100% CH₃CN for 5 min and equilibrated with 10% CH₃CN in H₂O for another 5 min. Detection was carried out with a photodiode array detector and absorptions at 254 nm were illustrated in this study.

Isolation of the enzyme products

For isolation of the enzyme products, the assays (10 mL) contained 50 mM Tris-HCl (pH 7.5), 5 mM CaCl₂, 1 mM cyclic dipeptide, 1 mM DMAPP, and 0.2–0.5 mg mL⁻¹ recombinant protein. After incubation at 37 °C for 24 h, the reaction mixtures were extracted with equal volume of EtOAc for three times. The extracts were concentrated on a rotating vacuum evaporator at 30 °C and the residues are dissolved in 1 mL MeOH for isolation on a HPLC system. A semipreparative Multospher 120 RP-18 column (5 µm, 10 × 250 mm) was used for isolation of the enzyme products on the same HPLC system mentioned above with the same solvents at a flow rate of 2.5 mL min⁻¹. Separation was done by isocratic elution with 40–70% CH₃CN for 10–20 min. The fractions of interest were collected, combined, and concentrated to dryness on a rotating vacuum evaporator at 30 °C. The isolated enzyme products were then subjected to NMR and MS analyses.

LC-MS and MS analysis

Enzyme products were also analyzed on an Agilent HPLC 1260 series system equipped with a Bruker microTOF QIII mass spectrometer using the Multospher 120 RP-18 column (5 µm, 2 × 250 mm). Separation was performed at a flow rate of 0.5 mL min⁻¹ with a 10 min linear gradient from 5 to 100% CH₃CN in H₂O, both containing 0.1% (v/v) formic acid. The column was then washed with 100% CH₃CN for 5 min and equilibrated for 5 min. The parameters of the spectrometer were set as the following: electrospray positive ion mode for ionization, capillary voltage with 4.5 kV, collision energy with 8.0 eV.

NMR analysis

NMR spectra of the isolated enzyme products were recorded at room temperature on a JEOL ECA-500 system (JEOL, Akishima, Tokyo, Japan). The samples were dissolved in DMSO-*d*₆ or CDCl₃. All spectra were processed with MestReNov.6.1.0 (Mestrelab Research, Santiago de Compostella, Spain).

Conclusions

In summary, we demonstrated that FgaPT2_K174F catalyzes a reverse C3-prenylation of cyclic dipeptides, instead of C4-prenylation by the non-mutated enzyme, but only with low activity. Significant increase of the reaction velocity was achieved by additional mutation on Arg244. Our results provide an excellent example of protein engineering by site-directed mutagenesis on the basis of structural information.

Funding information

The Bruker microTOF QIII mass spectrometer was financially supported in part by a grant from the Deutsche Forschungsgemeinschaft (INST 160/620-1 to S.-M. L.). Liujuan Zheng is a scholarship recipient of the China Scholarship Council (201604910536).

Conflicts of interest

The authors declare no competing financial interest.

Acknowledgements

We thank R. Kraut from the Philipps-Universität Marburg for the synthesis of substrates and taking mass spectra, S. Newel for taking NMR spectra, and Liping Zhang from the South China Sea Institute of Oceanology, CAS, for discussion on homology modeling and molecular docking.

Notes and references

- 1 L. Liu, L. Wang, L. Bao, J. Ren, B. Bahadur, R. Liu, L. He, J. Han, W. B. Yin and H. Liu, *Org. Lett.*, 2017, **19**, 942–945.
- 2 A. D. Borthwick, *Chem. Rev.*, 2012, **112**, 3641–3716.
- 3 S.-M. Li, *Nat. Prod. Rep.*, 2010, **27**, 57–78.
- 4 T. W. Giessen and M. A. Marahiel, *Int. J. Mol. Sci.*, 2014, **15**, 14610–14631.
- 5 P. Belin, M. Moutiez, S. Lautru, J. Seguin, J. L. Pernodet and M. Gondry, *Nat. Prod. Rep.*, 2012, **29**, 961–979.
- 6 A. K. Mishra, J. Choi, S. J. Choi and K. H. Baek, *Molecules*, 2017, **22**, E1796.
- 7 T. W. Giessen, A. M. von Tesmar and M. A. Marahiel, *Biochemistry*, 2013, **52**, 4274–4283.
- 8 W. Xu, D. J. Gavia and Y. Tang, *Nat. Prod. Rep.*, 2014, **31**, 1474–1487.
- 9 A. G. Kozlovsky, V. M. Adanin, H. M. Dahse and U. Gräfe, *Appl. Biochem. Microbiol.*, 2001, **37**, 253–256.
- 10 X. Yu, G. Zocher, X. Xie, M. Liebhold, S. Schütz, T. Stehle and S.-M. Li, *Chem. Biol.*, 2013, **20**, 1492–1501.
- 11 K. Kobayashi, T. Fukuda, T. Terahara, E. Harunari, C. Imada and H. Tomoda, *J. Antibiot.*, 2015, **68**, 638–641.
- 12 W.-B. Yin, A. Grundmann, J. Cheng and S.-M. Li, *J. Biol. Chem.*, 2009, **284**, 100–109.
- 13 C. Finoli, A. Vecchio, A. Galli and I. Dragoni, *J. Food Prot.*, 2001, **64**, 246–251.
- 14 J. Winkelblech, A. Fan and S.-M. Li, *Appl. Microbiol. Biotechnol.*, 2015, **99**, 7379–7397.
- 15 H. F. Tsai, H. Wang, J. C. Gebler, C. D. Poulter and C. L. Schardl, *Biochem. Biophys. Res. Commun.*, 1995, **216**, 119–125.
- 16 S.-M. Li, *Phytochemistry*, 2009, **70**, 1746–1757.
- 17 M. Shibuya, H. M. Chou, M. Fountoulakis, S. Hassam, S. U. Kim, K. Kobayashi, H. Otsuka, E. Rogalska,

- J. M. Cassady and H. G. Floss, *J. Am. Chem. Soc.*, 1990, **112**, 297–304.
- 18 L. Y. P. Luk and M. E. Tanner, *J. Am. Chem. Soc.*, 2009, **131**, 13932–13933.
- 19 U. Metzger, C. Schall, G. Zocher, I. Unsöld, E. Stec, S.-M. Li, L. Heide and T. Stehle, *Proc. Natl. Acad. Sci. U. S. A.*, 2009, **106**, 14309–14314.
- 20 S. Yin, X. Yu, Q. Wang, X. Q. Liu and S.-M. Li, *Appl. Microbiol. Biotechnol.*, 2013, **97**, 1649–1660.
- 21 Y. Ding, J. R. Wet, J. Cavalcoli, S. Li, T. J. Greshock, K. A. Miller, J. M. Finefield, J. D. Sunderhaus, T. J. McAfoos, S. Tsukamoto, R. M. Williams and D. H. Sherman, *J. Am. Chem. Soc.*, 2010, **132**, 12733–12740.
- 22 V. Wohlgemuth, F. Kindinger and S.-M. Li, *Appl. Microbiol. Biotechnol.*, 2018, **102**, 2671–2681.
- 23 W.-B. Yin, X. Yu, X.-L. Xie and S.-M. Li, *Org. Biomol. Chem.*, 2010, **8**, 2430–2438.
- 24 I. A. Unsöld and S.-M. Li, *Microbiology*, 2005, **151**, 1499–1505.
- 25 X. Yu, Y. Liu, X. Xie, X.-D. Zheng and S.-M. Li, *J. Biol. Chem.*, 2012, **287**, 1371–1380.
- 26 J. Winkelblech and S.-M. Li, *ChemBioChem*, 2014, **15**, 1030–1039.
- 27 A. Kremer, L. Westrich and S.-M. Li, *Microbiology*, 2007, **153**, 3409–3416.
- 28 A. Fan, G. Zocher, E. Stec, T. Stehle and S.-M. Li, *J. Biol. Chem.*, 2015, **290**, 1364–1373.
- 29 A. Fan and S.-M. Li, *Appl. Microbiol. Biotechnol.*, 2016, **100**, 5389–5399.
- 30 L. Y. Luk, Q. Qian and M. E. Tanner, *J. Am. Chem. Soc.*, 2011, **133**, 12342–12345.
- 31 N. Steffan and S.-M. Li, *Arch. Microbiol.*, 2009, **191**, 461–466.
- 32 O. Trott and A. J. Olson, *J. Comput. Chem.*, 2010, **31**, 455–461.
- 33 A. B. Woodside, Z. Huang and C. D. Poulter, *Org. Synth.*, 1988, **66**, 211–215.
- 34 B. Wollinsky, L. Ludwig, A. Hamacher, X. Yu, M. U. Kassack and S. M. Li, *Bioorg. Med. Chem. Lett.*, 2012, **22**, 3866–3869.
- 35 N. Steffan, I. A. Unsöld and S.-M. Li, *ChemBioChem*, 2007, **8**, 1298–1307.

Electronic Supplementary Information (ESI)

Switching a Regular Tryptophan *C4*-Prenyltransferase to a Reverse Tryptophan-containing Cyclic Dipeptide *C3*-Prenyltransferase by Sequential Site-directed Mutagenesis

Liujuan Zheng,^{‡a} Peter Mai,^{‡a} Aili Fan,^{a,b} and Shu-Ming Li,^{*a}

^a Institut für Pharmazeutische Biologie und Biotechnologie, Philipps-Universität Marburg, Robert-Koch-Straße 4, 35037 Marburg, Germany

^b Present address: Beijing Advanced Innovation Center for Soft Matter Science and Engineering, Beijing Key Laboratory of Bioprocess, Beijing University of Chemical Technology, Beijing, 100029, People's Republic of China

*Corresponding authors:

Shu-Ming Li, Tel/Fax: + 49-6421-28-22461/25365.

Email: shuming.li@staff.uni-marburg.de.

Author Contributions

[‡] Liujuan Zheng and Peter Mai contributed equally to this work.

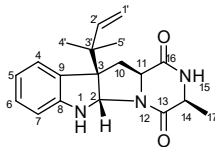
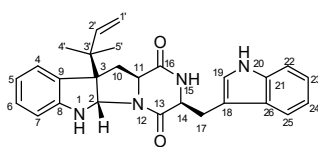
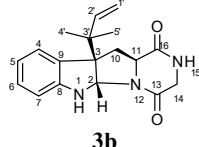
TableS1 Construction of expression plasmids.....	3
Table S2 ¹ H NMR (500 MHz) Data for 1b-5b in CDCl ₃ and 6b in DMSO- <i>d</i> ₆	4
Fig. S1 SDS-PAGE analysis of the purified proteins.....	5
Fig. S2 The LC-HRMS results of FgaPT2 and FgaPT2_K174A reactions with L-tryptophan.....	6
Fig. S3 LC-MS analysis of the incubation mixtures with FgaPT2 and mutants	7
Fig. S4 ¹ H NMR spectrum of 1b (500 MHz, CDCl ₃).....	8
Fig. S5 ¹ H NMR spectrum of 2b (500 MHz, CDCl ₃).....	9
Fig. S6 ¹ H NMR spectrum of 3b (500 MHz, CDCl ₃).....	10
Fig. S7 ¹ H NMR spectrum of 4b (500 MHz, CDCl ₃).....	11
Fig. S8. ¹ H NMR spectrum of 5b (500 MHz, CDCl ₃).....	12
Fig. S9 ¹ H NMR spectrum of 6b (500 MHz, DMSO- <i>d</i> ₆)	13
Fig. S10 Determination of the kinetic parameters of the FgaPT2_K174F_R244N reaction toward 1 in the presence of DMAPP	14
Fig. S11 Determination of the kinetic parameters of the FgaPT2_K174F_R244N reaction toward 2 in the presence of DMAPP.	14
Fig. S12 Determination of the kinetic parameters of the FgaPT2_K174F_R244N reaction toward 3 in the presence of DMAPP.	15
Fig. S13 Determination of the kinetic parameters of the FgaPT2_K174F_R244N reaction toward 4 in the presence of DMAPP.	15
Fig. S14 Determination of the kinetic parameters of the FgaPT2_K174F_R244L reaction toward 5 in the presence of DMAPP.	16
Fig. S15 Determination of the kinetic parameters of the FgaPT2_K174F_R244L reaction toward 6 in the presence of DMAPP.	16
References and Notes.	17

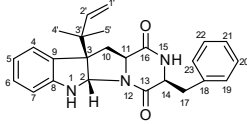
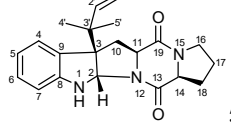
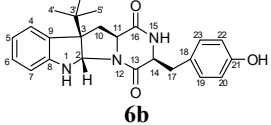
Table S1 Construction of expression plasmids

Mutants	Primer name	Primer sequence for PCR amplification (5'-3')	Plasmid name	Protein yield (mg/L culture)
FgaPT2_K174A	FgaPT2_K174A_f FgaPT2_K174A_r	CAGAACGCACCTCGCGCTCGATCTGAAGGATGGCCGCTTGC GAGCGCGAGTGCCTTCTGCGTGCCTGATAGTGCCGCCCA	pLZ1	1.2
FgaPT2_K174F_R244Q	FgaPT2_R244Q_f FgaPT2_R244Q_r	GCCAGTCCCCAACTAGTGTCTGTGAT GGACACTAGTTGGGGACTGGCAAGTGCT	pALF56	2.3
FgaPT2_K174F_R244N	FgaPT2_R244N_f FgaPT2_R244N_r	GCCAGTCCC(A/G)ATCTAGTGTCTGTGAT GGACACTAGATYGGGACTGGCAAGTGCT	pALF55	1.5
FgaPT2_K174F_R244Y	FgaPT2_R244Y_f FgaPT2_R244Y_r	CAGAACTTTCTCGCGCTCGATCTGAAGGATGGCCGCTTGC GAGCGCGAGAAAGTTCTGCGTGCCTGATAGTGCCGCCCA	pPM72	2.0
FgaPT2_K174F_R244L	FgaPT2_R244L_f FgaPT2_R244L_r	CAGAACTTTCTCGCGCTCGATCTGAAGGATGGCCGCTTGC GAGCGCGAGAAAGTTCTGCGTGCCTGATAGTGCCGCCCA	pPM71	2.2

pIU18¹ was used as template for creation of FgaPT2_K174A and pES26 containing the K174F mutation² for creation of double mutants

Table S2 ^1H NMR (500 MHz) Data for **1b–5b** in CDCl_3 and **6b** in $\text{DMSO}-d_6$

<div style="display: flex; justify-content: space-around; align-items: center;"> <div style="text-align: center;">  <p>1b</p> </div> <div style="text-align: center;">  <p>2b</p> </div> <div style="text-align: center;">  <p>3b</p> </div> </div>			
no	δ_{H} , mult., (J in Hz)	δ_{H} , mult., (J in Hz)	δ_{H} , mult., (J in Hz)
2	5.50, s	5.55, s	5.55, s
4	7.16, dd (7.5, 0.7)	7.14 ^a	7.16, ddd (7.5, 1.2, 0.5)
5	6.77, td (7.5, 1.0)	6.75, td (7.5, 1.0)	6.77, td (7.5, 1.0)
6	7.11, td (7.5, 1.0)	7.11 ^a	7.11, td (7.6, 1.0)
7	6.58, d (7.8)	6.61, d (7.8)	6.59, ddd (7.6, 1.0, 0.5)
10	2.47, dd (12.7, 11.0)	2.42, dd (12.5, 11.2)	2.45, dd (12.7, 11.2)
	2.55, dd (12.8, 6.5)	2.52, dd (12.5, 6.2)	2.56, dd (12.7, 6.2)
11	3.96, ddd (10.9, 6.4, 1.7)	3.92, ddd (10.9, 6.3, 1.7)	3.95, ddd (11.2, 6.2, 1.6)
14	4.05, qd (6.9, 1.6)	4.31, ddd (10.9, 3.6, 1.8)	4.04, dd (17.0, 2.0)
	-	-	3.87, dd (17.0, 4.1)
15	-	5.65, s	-
17	1.46, d (6.9)	3.75, ddd (15.2, 3.7, 0.9)	-
	-	2.97, dd (15.1, 11.0)	-
19	-	7.11 ^a	-
20	-	8.13, s	-
22	-	7.39, dt (8.3, 0.9)	-
23	-	7.23, td (7.7, 0.9)	-
24	-	7.13 ^a	-
25	-	7.55, d (7.9)	-
1'	5.13, dd (10.8, 1.1)	5.13, dd (10.8, 1.1)	5.13, dd (10.8, 1.1)
	5.08, dd (17.4, 1.1)	5.08, dd (17.4, 1.1)	5.09, dd (17.4, 1.1)
2'	5.98, dd (17.4, 10.8)	5.97, dd (17.4, 10.8)	5.98, dd (17.4, 10.8)
4'	1.12, s	1.11, s	1.12, s
5'	1.01, s	1.01, s	1.01, s

<div style="display: flex; justify-content: space-around; align-items: center;"> <div style="text-align: center;">  <p>4b</p> </div> <div style="text-align: center;">  <p>5b</p> </div> <div style="text-align: center;">  <p>6b</p> </div> </div>			
no.	δ_{H} , mult., (J in Hz)	δ_{H} , mult., (J in Hz)	δ_{H} , mult., (J in Hz)
2	5.54, s	5.46, s	5.32, d (1.1)
4	7.14, d (7.5)	7.16, dd, (7.5, 1.0)	7.09, d (7.0)
5	6.76, d (7.5)	6.77, td, (7.5, 1.0)	6.59, t (7.4)
6	7.11, t (7.7)	7.11, td (7.5, 1.0)	6.98, t (7.4)
7	6.59, d (7.7)	6.59, d (7.5)	6.49, d (7.0)
10	2.40, t (1.9)	2.49, dd (12.9, 10.8)	2.50 ^b
	2.52, dd (12.8, 6.2)	2.54, dd (12.9, 6.7)	
11	3.93, ddd (11.3, 6.2, 1.8)	3.98, dd (10.8, 6.7)	3.67, ddd (11.6, 5.7, 1.8)
14	4.21, ddd (10.8, 3.6, 1.8)	4.05, t (8.3)	4.07, m
15	5.50, s		-
	-	2.12, m	-
16	-	3.56, m	-
	-	3.50, m	-
17	3.60, dd (14.4, 3.6)	2.04, m	3.06, dd (14.0, 3.8)
	2.78, dd (14.4, 10.8)	1.89, m	2.84, dd (14.0, 5.0)
18		2.32, dtd (9.1, 6.7, 2.5)	
19	7.19, d (7.1)	-	7.01, d (8.4)
20	7.34, t (7.3)	-	6.66, m (8.4)
21	7.29, t (7.4)	-	9.17, s (OH)
22	7.34, t (7.3)	-	6.66, m (8.4)
23	7.19, d (7.1)	-	7.01, d (8.4)
1'	5.13, dd (10.8, 1.0)	5.07, dd (17.4, 1.1)	4.97, dd (17.3, 1.4)
	5.08, dd (17.4, 10)	5.05, dd (10.8, 1.1)	5.05, dd (10.8, 1.4)
2'	5.96, dd (17.3, 10.8)	5.99, dd (17.4, 10.8)	5.76, dd (17.3, 10.8)
4'	1.11, s	1.11, s	0.93, s
5'	1.01, s	1.00, s	0.79, s

^a Signals overlapping with each other. ^b signals overlapping with those of solvent. The data of **1b** – **6b** correspond well to those of published previously.^{3,4}

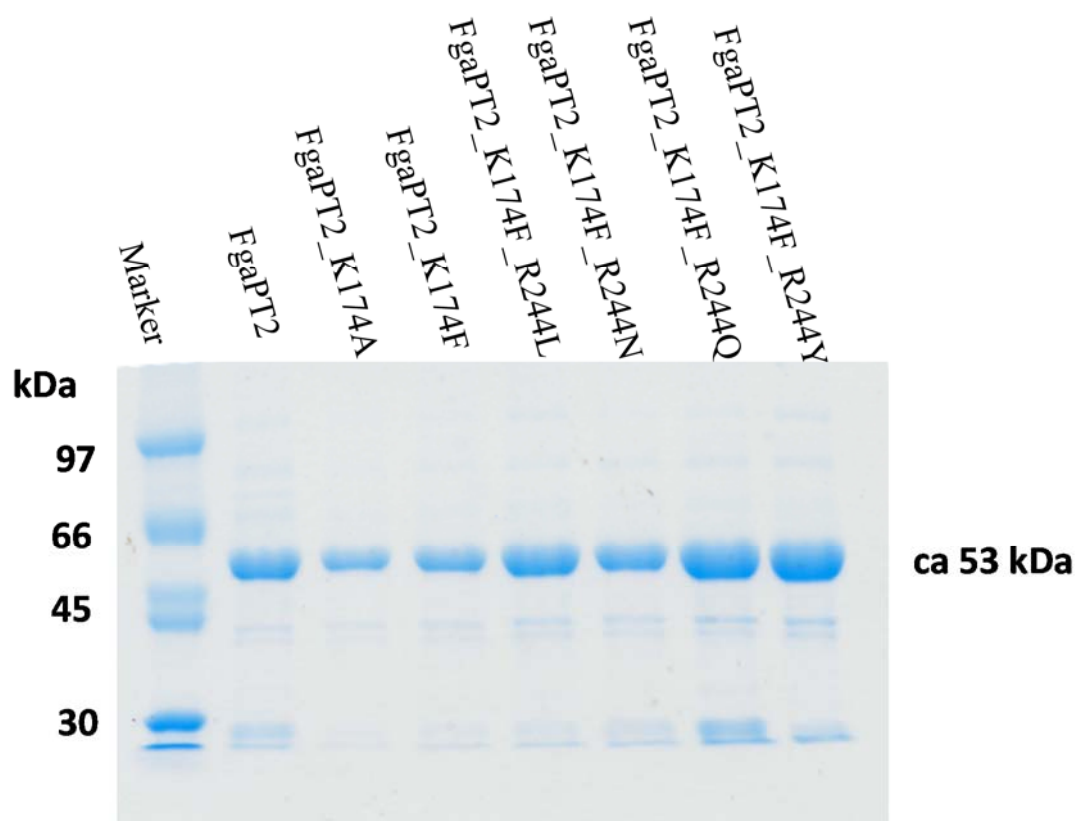


Fig. S1 SDS-PAGE analysis of the purified proteins.

The proteins were separated on a 12% polyacrylamide gel and stained with Coomassie brilliant blue R-250

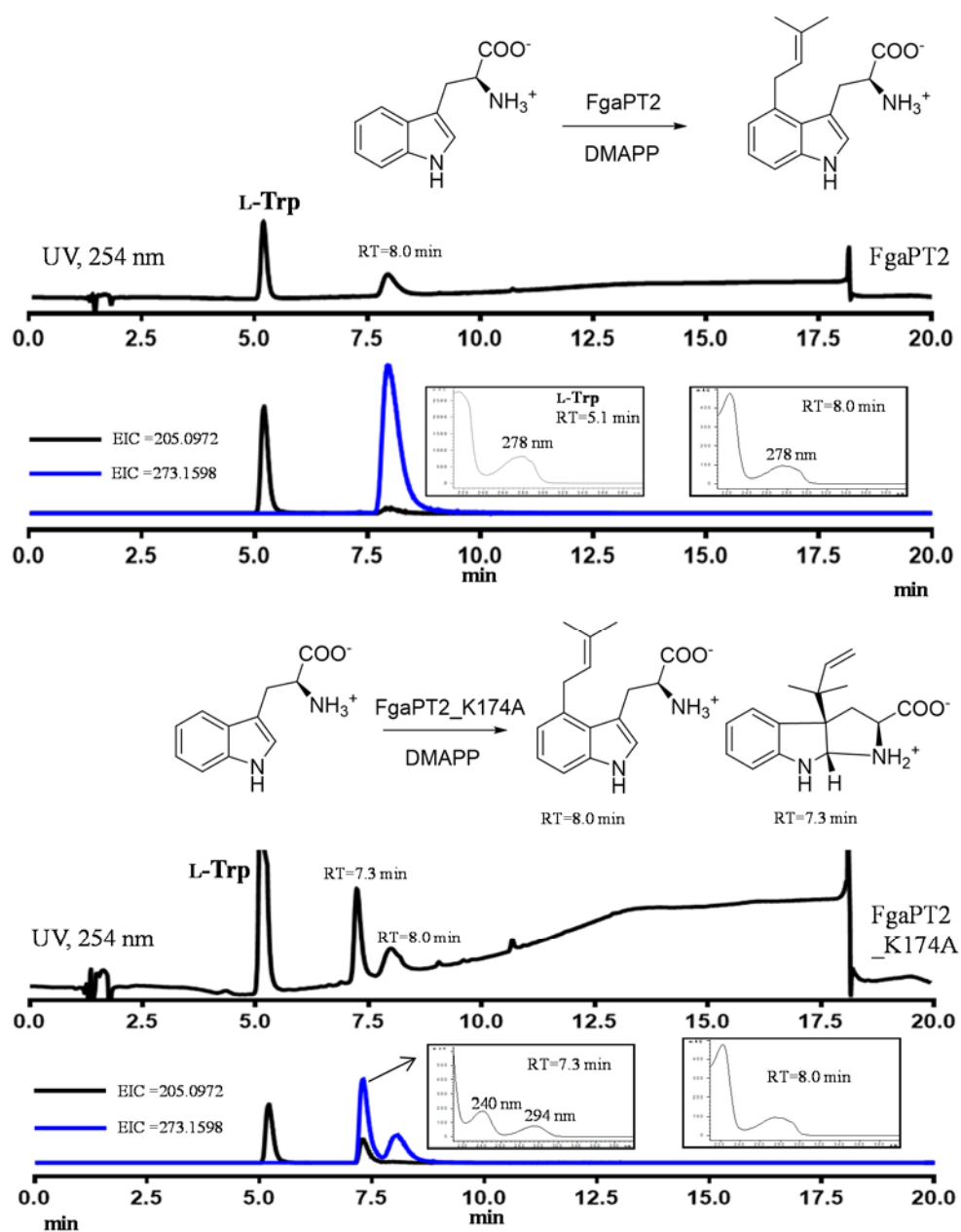


Fig. S2 LC-HRMS analysis of FgaPT2 and FgaPT2_K174A reactions with L-tryptophan in the presence of DMAPP.

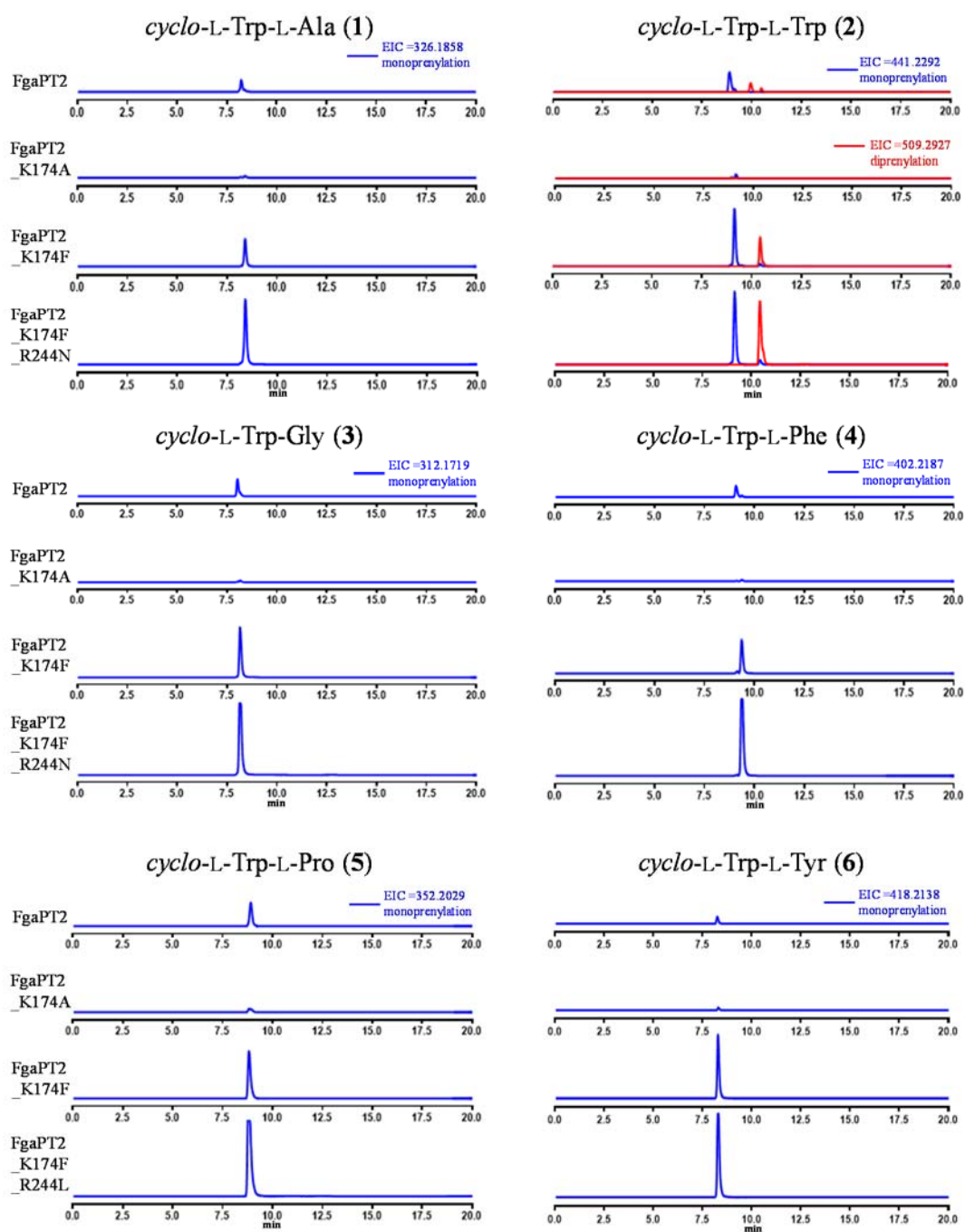


Fig. S3 LC-MS analysis of the incubation mixtures of cyclic dipeptides with FgaPT2 and its mutants

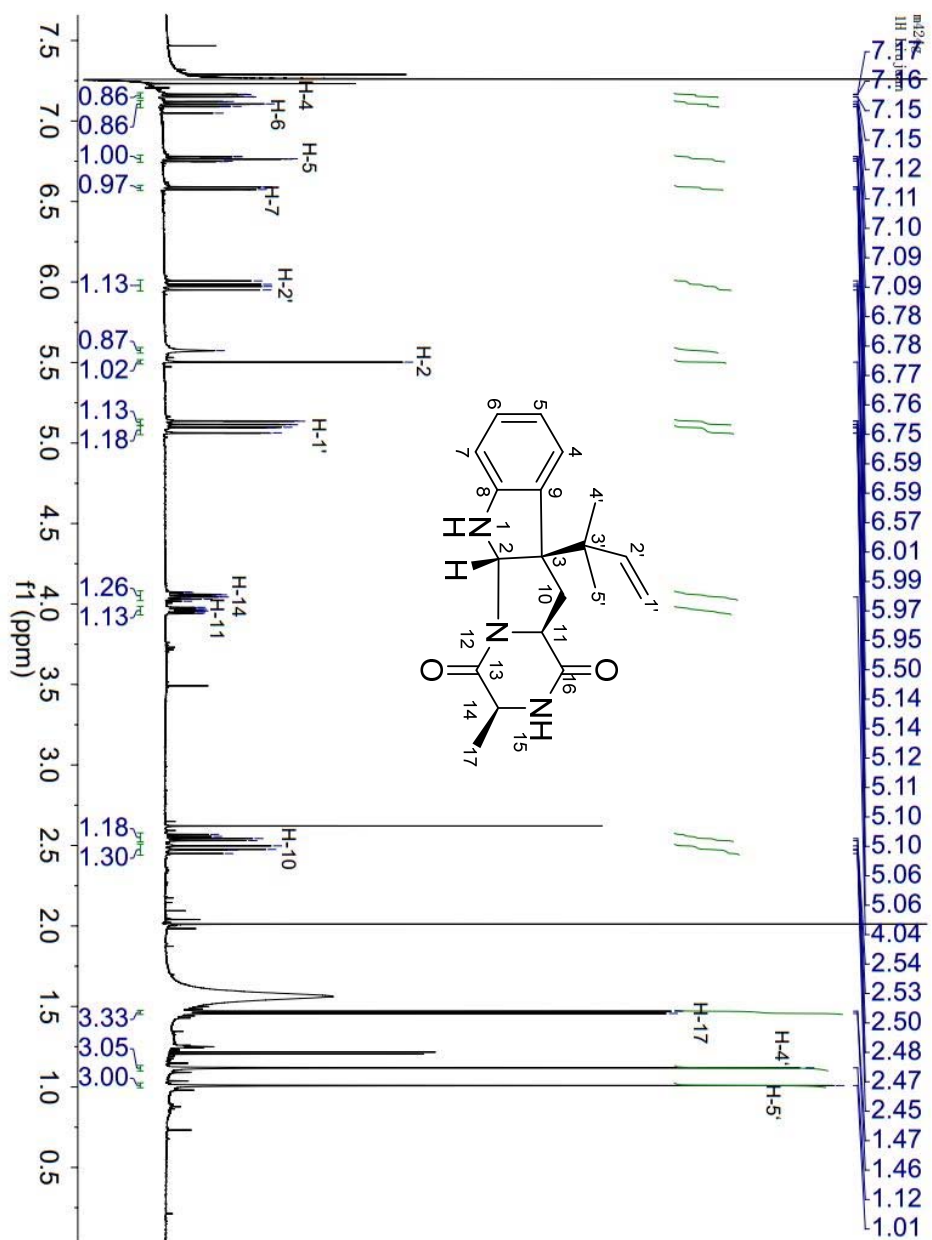


Fig. S4 ^1H NMR (500 MHz) spectrum of **1b** in CDCl_3

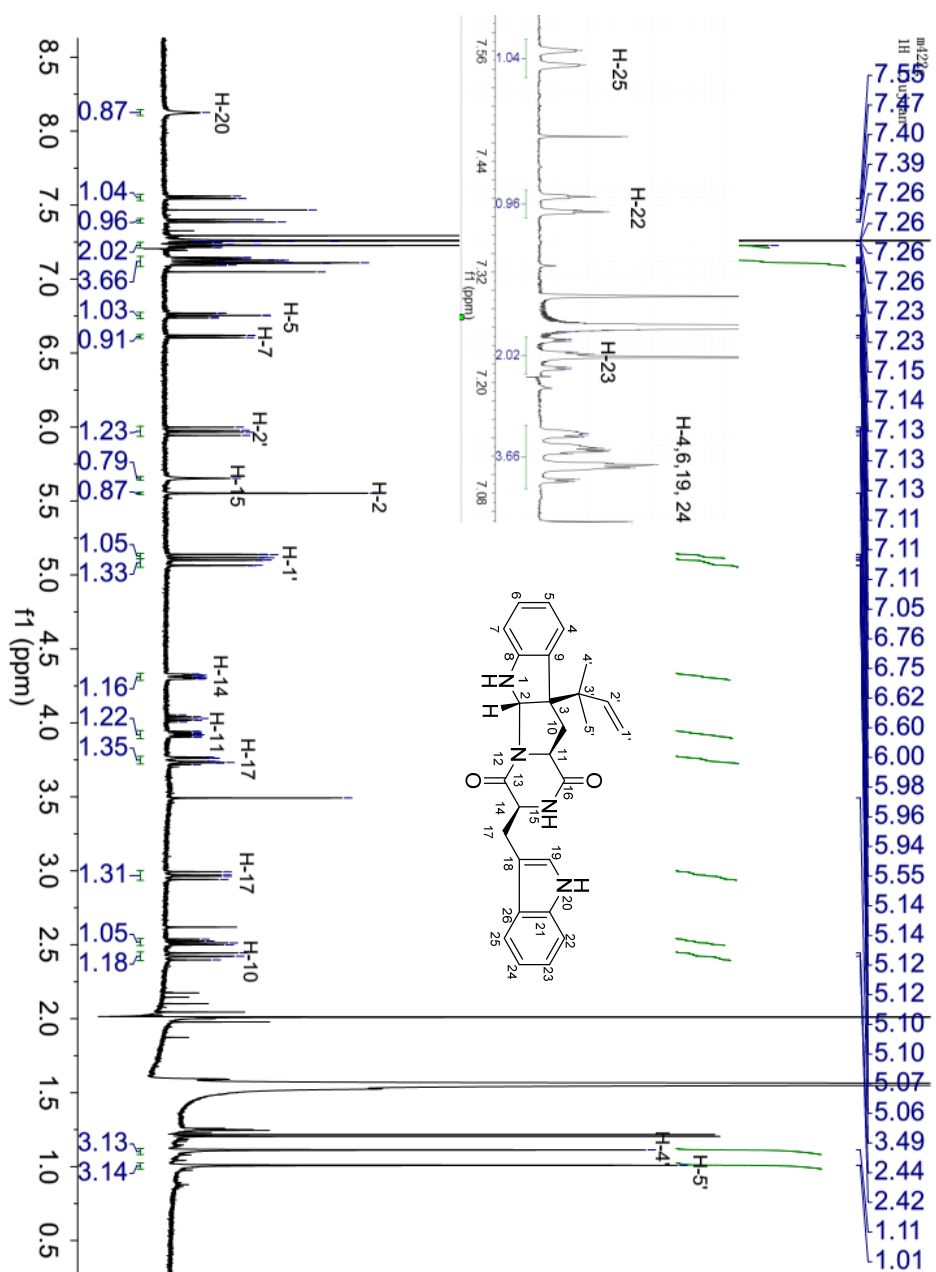


Fig. S5 ¹H NMR (500 MHz) spectrum of **2b** in CDCl₃

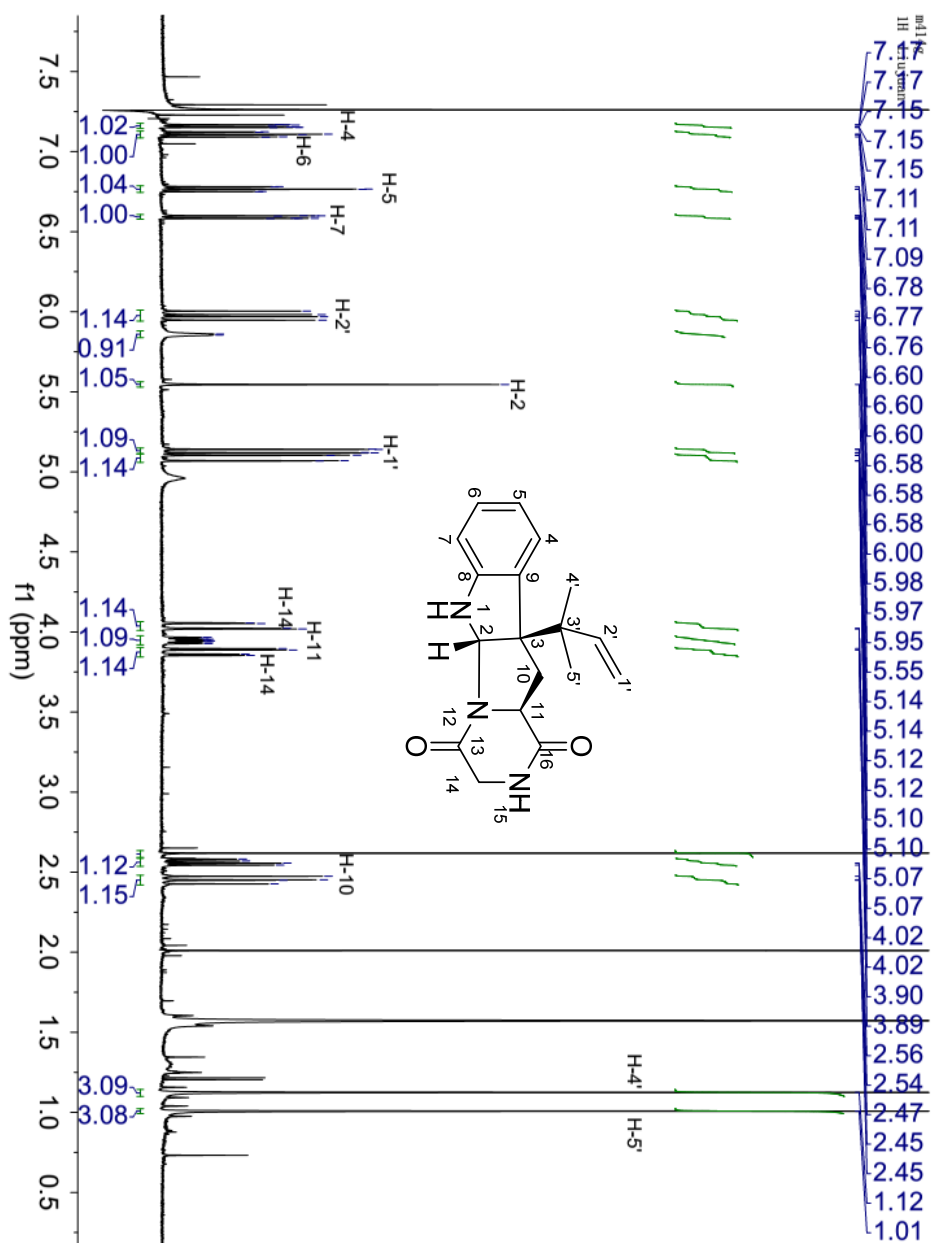


Fig. S6 ^1H NMR (500 MHz) spectrum of **3b** in CDCl_3

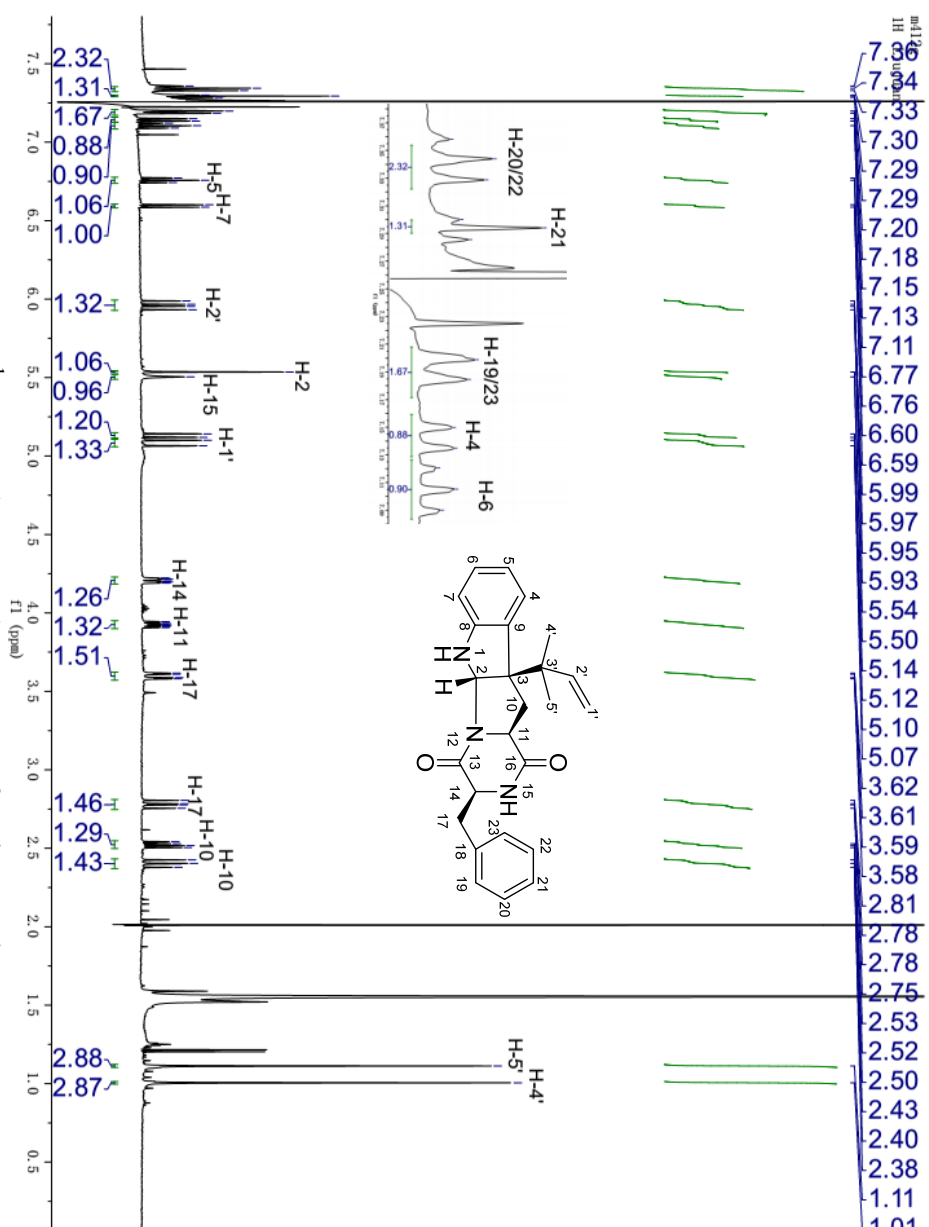


Fig. S7 ¹H NMR (500 MHz) spectrum of **4b** in CDCl₃

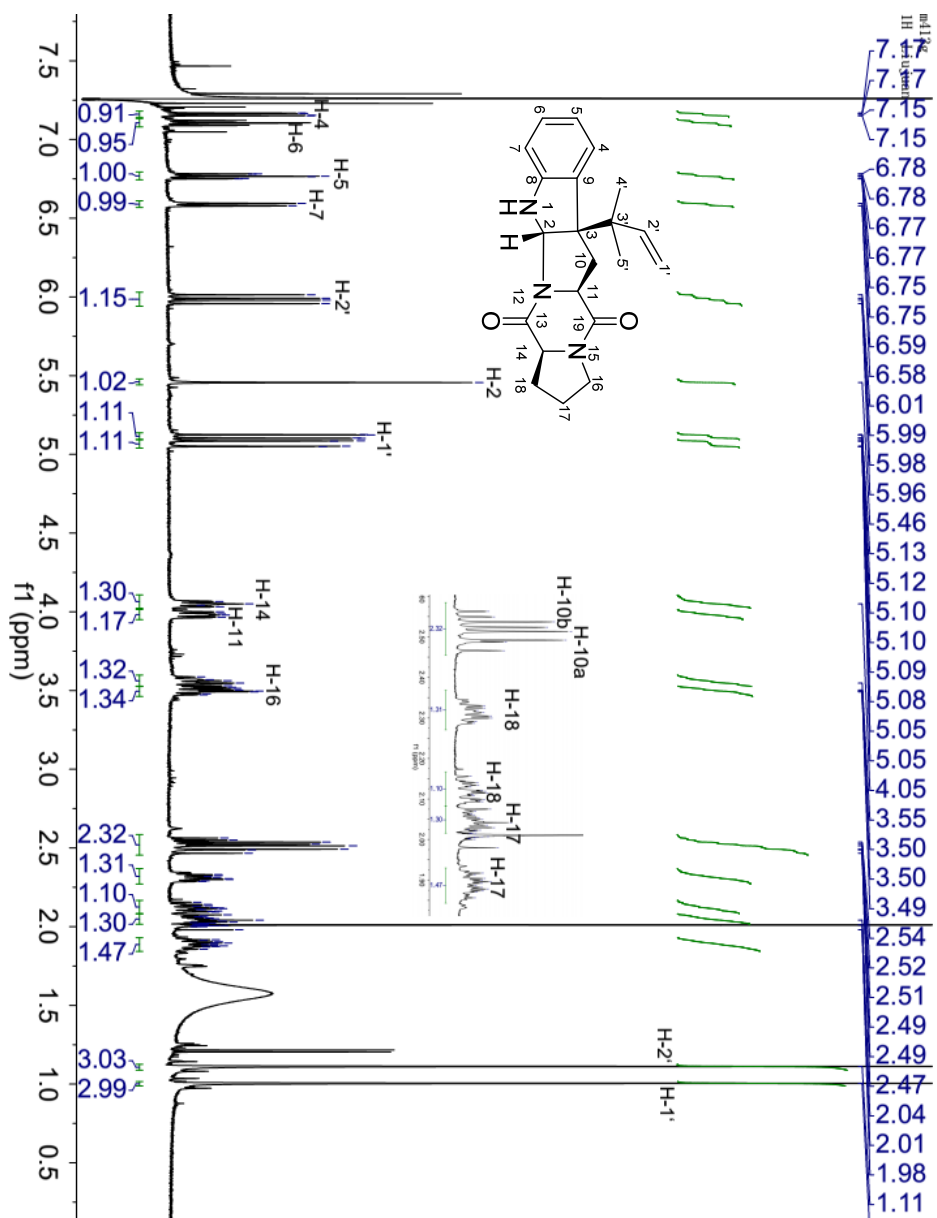


Fig. S8 ¹H NMR (500 MHz) spectrum of **5b** in CDCl₃

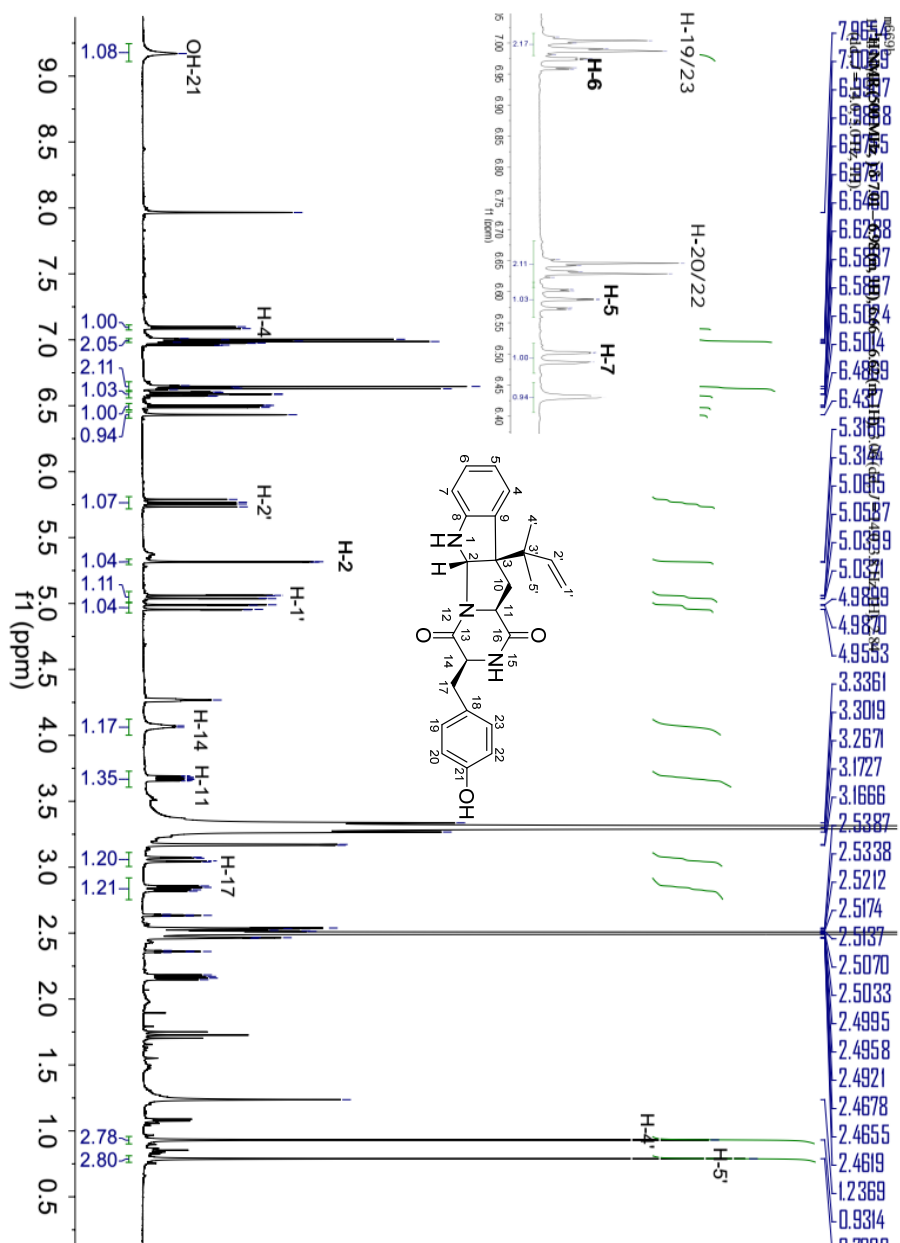


Fig. S9 ^1H NMR(500 MHz) spectrum of compound **6b** in $\text{DMSO-}d_6$

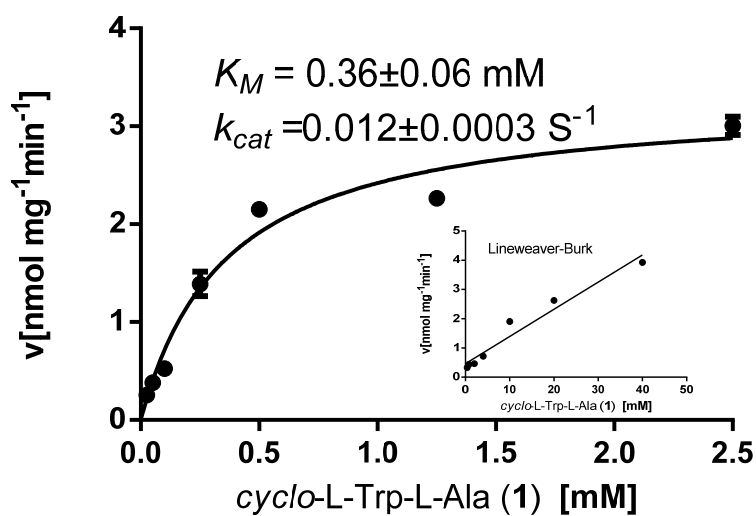


Fig. S10 Determination of the kinetic parameters of the FgaPT2_K174F_R244N reaction toward **1** in the presence of DMAPP.

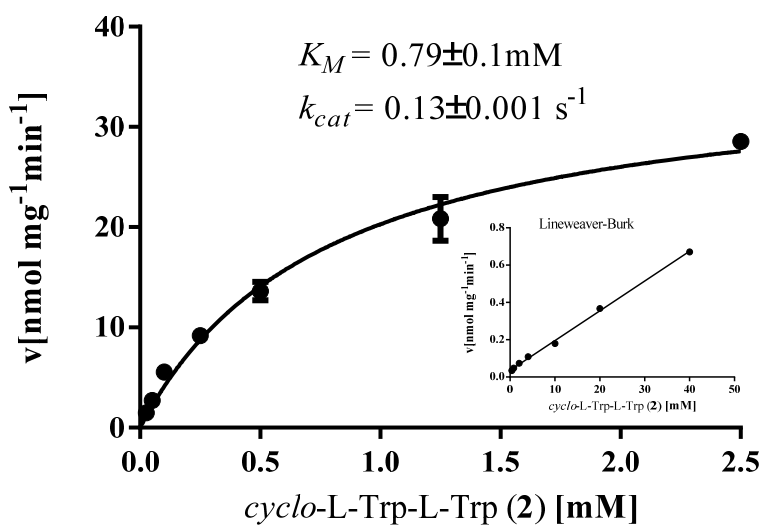


Fig. S11 Determination of the kinetic parameters of the FgaPT2_K174F_R244N reaction toward **2** in the presence of DMAPP.

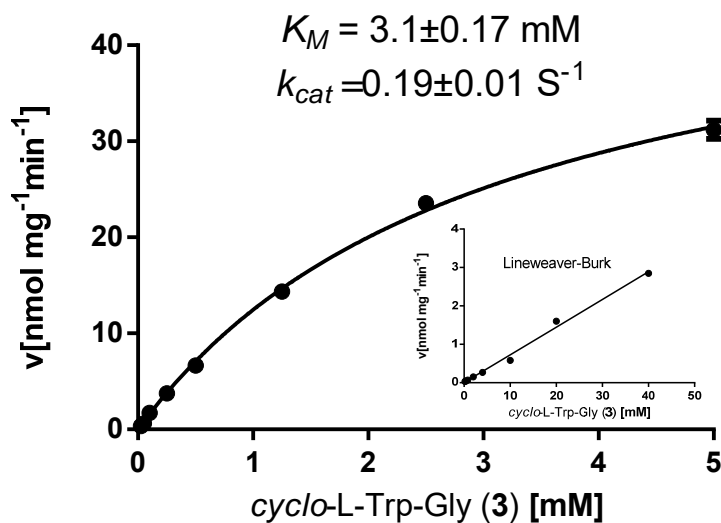


Fig. S12 Determination of the kinetic parameters of the FgaPT2_K174F_R244N reaction toward 3 in the presence of DMAPP.

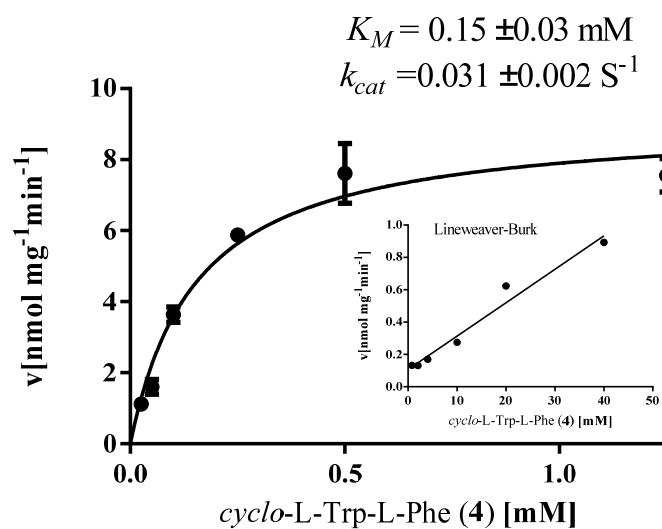


Fig. S13 Determination of the kinetic parameters of the FgaPT2_K174F_R244N reaction toward 4 in the presence of DMAPP.

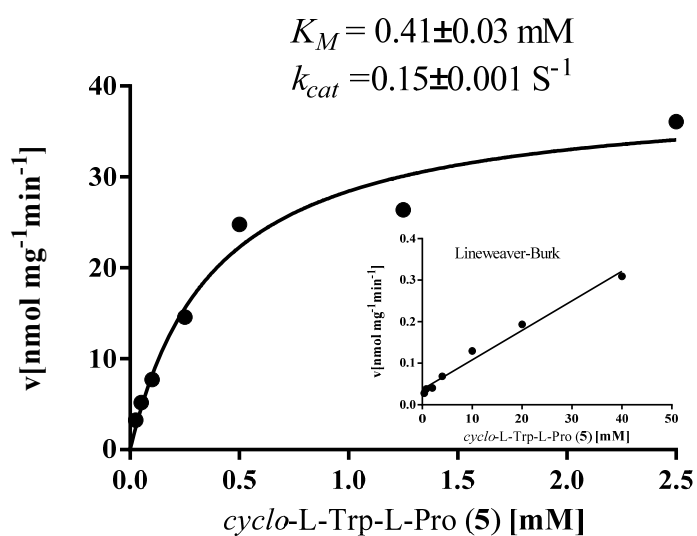


Fig. S14 Determination of the kinetic parameters of the FgaPT2_K174F_R244L reaction toward **5** in the presence of DMAPP.

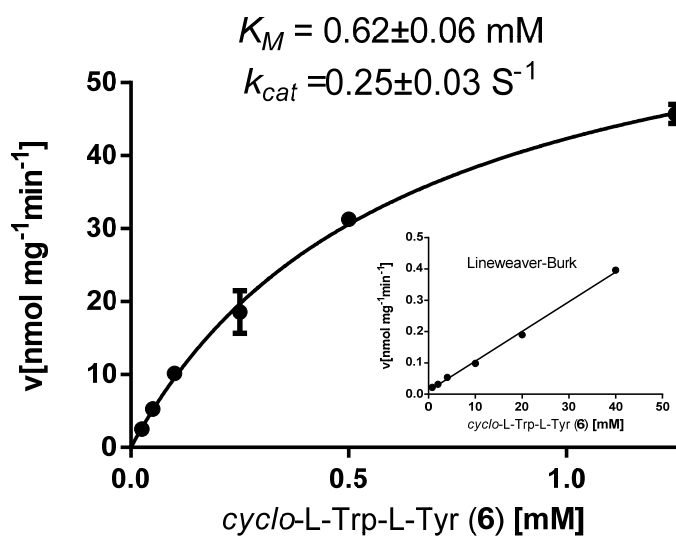


Fig. S15 Determination of the kinetic parameters of the FgaPT2_K174F_R244L reaction toward **6** in the presence of DMAPP.

References and Notes

- (1) Steffan, N.; Unsöld, I. A.; Li, S.-M. *Chembiochem* **2007**, 8, 1298-1307.
- (2) Fan, A.; Zocher, G.; Stec, E.; Stehle, T.; Li, S.-M. *J. Biol. Chem.* **2015**, 290, 1364-1373.
- (3) Yin, W.-B.; Yu, X.; Xie, X.-L.; Li, S.-M. *Org. Biomol. Chem.* **2010**, 8, 2430-2438.
- (4) Yu, X.; Zocher, G.; Xie, X.; Liebhold, M.; Schütz, S.; Stehle, T.; Li, S.-M. *Chem. Biol.* **2013**, 20, 1492-1501.

5. Conclusions and future prospects

In this thesis, BGCs for secondary metabolites from *A. ustus* have been investigated via multiple approaches. The identified PKS-containing *utt* BGC and two similar NRPS-containing *opa* and *opa2* BGCs from the same fungus *A. ustus* demonstrated clearly the large fungal potential for natural product production and new enzyme discovery. In addition, site-directed mutagenesis for a fungal PT led to the functional switching with enhanced conversion yields, indicating that site-directed mutagenesis is an effective tool to increase the structural diversity of natural products.

In the biosynthesis of ustethylin A, isotopic feeding and heterologous expression experiments confirmed that the PKS UttA is responsible for assembling the phenethyl core structure with methylation as key reactions. The *in vivo* results proved that the NRPS-like enzyme UttJ catalyzes reduction of the aryl acid to aldehyde and the nonheme Fe^{II}/2-oxoglutarate dependent oxygenase UttH performs the subsequent hydroxylation at the benzyl group. After methylation by the O-MeT UttF, the cytochrome P450 enzyme UttC catalyzes the hydroxylation of the phenethyl residue to form the product ustethylin A. Deletion of *uttD* coding for a regulator completely abolished product formation, proving its role in regulating the expression of *utt* BGC. The feeding experiments of MeOH and EtOH to *A. ustus* and the mutants revealed that the pathway for ustethylin A can be shunted in the stage of enzyme-bound polyketide acyl intermediates, leading to the production of benzoyl ester derivatives.

For the biosynthesis of oxepinamide F, the heterologous expression results proved that the NRPS OpaA assembles the quinazolinone backbone. The *in vivo* experiments revealed that the cytochrome P450 enzyme OpaB alone catalyzes the ring expansion in quinazolinone to form the OPK backbone. The *in vitro* assays proved that the flavin-dependent enzyme OpaC is responsible for the regio- and stereospecific hydroxylation, which is accompanied by a double bond migration leading to the conversion of a 1*H*-oxepin to a 3*H*-oxepin system. Subsequently, the epimerase OpaE converts the configuration of Phe residue from *R*- to *S*- configuration, which is essential for the final methylation of the OH-12 by the O-Met OpaF to form oxepinamide F. In analogy, an additional NRPS containing BGC is involved in the biosynthesis of oxepinamide D. Gene deletion, heterologous expression as well as *in vitro* assays proved that the NRPS OpaA2 assembles the quinazolinone skeleton, the cytochrome P450 enzyme OpaB2 is responsible for the conversion of quinazolinone to OPK backbone, and the flavin-dependent monooxygenase OpaC2 performs the last hydroxylation in the OPK backbone to form the oxepinamide D. Feeding experiments in the *opaB* and *opaB2* transformants as well as the results of the enzyme assays with OpaC and OpaC2 demonstrated that there is very likely no crosstalk between the *opa* and *opa2* BGCs

5. CONCLUSIONS AND FUTURE PROSPECTS

Mutation of the key residues Lys174 and Arg244 in the fungal PT FgaPT2 was also performed in this thesis. The combined mutations of these two sites *i.e.* FgaPT2_K174F_R244X (X=L, N, Q, Y) show much better acceptance for *cyclo*-L-Trp- L-Ala, *cyclo*- L-Trp- L-Trp, *cyclo*- L-Trp-Gly, *cyclo*- L-Trp- L-Phe, *cyclo*- L-Trp- L-Pro, and *cyclo*- L-Trp- L-Tyr as substrates for reverse C3-prenylation. These results demonstrated that site-directed mutagenesis is a powerful tool to increase the structural diversity of natural products.

For future prospects, the following works can be performed:

- Investigation of the functions of the unknown enzymes UttB, UttE, and UttI in the *utt* BGC *via in vivo* and *in vitro* experiments.
- prove if ustethylin A can be further metabolized by other enzymes, e.g. UttB, UttE, and UttI.
- Based on the *opa* and *opa2* BGC, mining more similar BGCs with NRPS bearing a domain structure of A-T-C-A-T-E-C-A-T-C_T and a P450 enzyme next to the NRPS in other fungi.
- Site-directed mutagenesis with OpaC and OpaC2 to understand the molecular basis of the hydroxylation of the OPK backbone.

6. References

1. Newman, D. J.; Cragg, G. M. Natural products as sources of new drugs over the nearly four decades from 01/1981 to 09/2019. *J. Nat. Prod.* **2020**, *83*, 770-803.
2. Zhang, Z.; Pan, H. X.; Tang, G. L. New insights into bacterial type II polyketide biosynthesis. *F1000 Research* **2017**, *6* (172), 1-12.
3. Sapadin, A. N.; Fleischmajer, R. Tetracyclines: Nonantibiotic properties and their clinical implications. *J. Am. Acad. Dermatol.* **2006**, *54* (2), 258-265.
4. Bills, G. F.; Gloer, J. B. Biologically active secondary metabolites from the fungi. *Microbiol Spectr.* **2016**, *4* (6), 1-32.
5. Shepherd, M. D.; Kharel, M. K.; Zhu, L. L.; Van Lanen, S. G.; Rohr, J. A. Delineating the earliest steps of gilvocarcin biosynthesis: role of GilP and GilQ in starter unit specificity. *Org. Biomol. Chem.* **2010**, *8* (17), 3851-3856.
6. Yu, Z.; Zhang, H.; Yuan, C.; Zhang, Q.; Khan, I.; Zhu, Y.; Zhang, C. Characterizing two cytochrome P450s in tiacumicin biosynthesis reveals reaction timing for tailoring modifications. *Org. Lett.* **2019**, *21* (18), 7679-7683.
7. Better, J.; Gatenbeck, S. Intermediates in the barnol biosynthesis in *Penicillium baarnense*. *Acta Chem. Scand. B* **1977**, *31*, 391-394.
8. El Maddah, F.; Eguereva, E.; Kehraus, S.; König, G. M. Biosynthetic studies of novel polyketides from the marine sponge-derived fungus *Stachylidium* sp. 293K04. *Org. Biomol. Chem.* **2019**, *17* (10), 2747-2752.
9. Yeh, H. H.; Chang, S. L.; Chiang, Y. M.; Bruno, K. S.; Oakley, B. R.; Wu, T. K.; Wang, C. C. Engineering fungal nonreducing polyketide synthase by heterologous expression and domain swapping. *Org. Lett.* **2013**, *15* (4), 756-759.
10. McIntyre, C. R.; Simpson, T. J.; Trimble, L. A.; Vederas, J. C. Biosynthesis of LL-D253a in *Phoma pigmentivora*. Incorporation of ^{13}C , ^2H , and ^{18}O enriched precursors. *J. Chem. Soc. Chem. Comm.* **1984**, (11), 706-709.
11. Simpson, T. J.; Stenzel, D. J. ^{13}C and ^2H n.m.r. studies on the biosynthesis of O-methylasparvenone, a hexaketide metabolite of *Aspergillus parvulus*. *J. Chem. Soc. Chem. Comm.* **1981**, (5), 239-240.
12. De Jesus, A. E.; Horak, R. M.; Steyn, P. S.; Vleggaar, R. Metabolites of *Aspergillus ustus*. Part 4. Stable-isotope labelling studies on the biosynthesis of the australides. *J. Chem. Soc., Perkin Trans. 1* **1987**, 2253-2257.
13. Süssmuth, R. D.; Mainz, A. Nonribosomal peptide synthesis - Principles and prospects. *Angew. Chem. Int. Ed. Engl.* **2017**, *56* (14), 3770-3821.
14. Guo, Y.; Ghidinelli, S.; de la Cruz, M.; Mackenzie, T. A.; Ramos, M. C.; Sánchez, P.; Vicente, F.; Genilloud, O.; Larsen, T. O. Oxepinamides L and M, two new oxepine-pyrimidinone-ketopiperazine type nonribosomal peptides from *Aspergillus californicus*. *Nat. Prod. Res.* **2020**, doi: 10.1080/14786419.2020.1844699.
15. Guo, Y.; Frisvad, J. C.; Larsen, T. O. Review of oxepine-pyrimidinone-ketopiperazine type nonribosomal peptides. *Metabolites* **2020**, *10* (6), 246.
16. Lu, X.; Shi, Q.; Zheng, Z.; Ke, A.; Zhang, H.; Huo, C.; Ma, Y.; Ren, X.; Li, Y.; Lin, J.; Jiang, Q.; Gu, Y.; Kiyota, H. Oxepinamides: Novel liver X receptor agonists from *Aspergillus puniceus*. *Eur. J. Org. Chem.* **2011**, *2011* (4), 802-807.
17. Liang, X.; Zhang, X.; Lu, X.; Zheng, Z.; Ma, X.; Qi, S. Diketopiperazine-type alkaloids from a deep-sea-derived *Aspergillus puniceus* fungus and their effects on liver X receptor α . *J. Nat. Prod.* **2019**, *82* (6), 1558-1564.
18. Zhang, P.; Li, X.; Wang, J.; Wang, B. Oxepine-containing diketopiperazine alkaloids from the algal-derived endophytic fungus *Paecilomyces variotii* EN-291. *Helv. Chim. Acta* **2015**, *98* (6), 800-804.

6. REFERENCES

19. Zhang, P.; Mándi, A.; Li, X.; Du, F.; Wang, J.; Li, X.; Kurtán, T.; Wang, B. Varioxepine A, a 3H-oxepine-containing alkaloid with a new oxa-cage from the marine algal-derived endophytic fungus *Paecilomyces variotii*. *Org. Lett.* **2014**, *16* (18), 4834-4837.
20. Zhuravleva, O. I.; Afiyatullo, S. S.; Yurchenko, E. A.; Denisenko, V. A.; Kirichuk, N. N.; Dmitrenok, P. S. New metabolites from the algal associated marine-derived fungus *Aspergillus carneus*. *Nat. Prod. Commun.* **2013**, *8* (8), 1071-1074.
21. González-Jartín, J. M.; Alfonso, A.; Sainz, M. J.; Vieytes, M. R.; Botana, L. M. Identification of circumdatins produced by *Aspergillus ochraceus*. *J. Agr. Food Chem.* **2017**, *65* (23), 4843-4852.
22. Wang, J.; He, W.; Huang, X.; Tian, X.; Liao, S.; Yang, B.; Wang, F.; Zhou, X.; Liu, Y. Antifungal new oxepine-containing alkaloids and xanthenes from the deep-sea-derived fungus *Aspergillus versicolor* SCSIO 05879. *J. Agric. Food Chem.* **2016**, *64* (14), 2910-2916.
23. Sprogø, K.; Manniche, S.; Larsen, T. O.; Christophersen, C. Janoxepin and brevicompanine B: antiplasmodial metabolites from the fungus *Aspergillus janus*. *Tetrahedron* **2005**, *61* (36), 8718-8721.
24. Blackwell, M. The Fungi: 1, 2, 3... 5.1 million species? *Am. J. Bot.* **2011**, *98* (3), 426-438.
25. Keller, N. P. Fungal secondary metabolism: regulation, function and drug discovery. *Nat. Rev. Microbiol.* **2019**, *17*, 167-180.
26. Zhang, P.; Wang, X.; Fan, A.; Zheng, Y.; Liu, X.; Wang, S.; Zou, H.; Oakley, B. R.; Keller, N. P.; Yin, W. B. A cryptic pigment biosynthetic pathway uncovered by heterologous expression is essential for conidial development in *Pestalotiopsis fici*. *Mol. Microbiol.* **2017**, *105* (3), 469-483.
27. Zhao, L.; Kim, J. C.; Paik, M. J.; Lee, W.; Hur, J.-S. A multifunctional and possible skin UV protectant, (3R)-5-hydroxymellein, produced by an endolichenic fungus isolated from *Parmotrema austrosinense*. *Molecules* **2017**, *22* (1).
28. Zheng, H.; Kim, J.; Liew, M.; Yan, J.; Herrera, O.; Bok, J. W.; Kelleher, N.; Keller, N.; Wan Redox metabolites signal polymicrobial biofilm development via the NapA oxidative stress cascade in *Aspergillus*. *Curr. Biol.* **2015**, *25* (1), 29-37.
29. Lyu, H. N.; Liu, H. W.; Keller, N. P.; Yin, W. B. Harnessing diverse transcriptional regulators for natural product discovery in fungi. *Nat. Prod. Rep.* **2020**, *37*, 6-16.
30. Samson, R. A.; Hoekstra, E. S.; Frisvad, J. C. *Introduction to food-and airborne fungi*; Centraalbureau voor Schimmelcultures (CBS): 2004; Vol. Ed. 7.
31. Houbraken, J.; Due, M.; Varga, J.; Meijer, M.; Frisvad, J. C.; Samson, R. A. Polyphasic taxonomy of *Aspergillus* section Usti. *Stud. Mycol.* **2007**, *59*, 107-128.
32. Chexal, K. K.; Springer, J. P.; Clardy, J.; Cole, R. J.; Kirksey, J. W.; Dorner, J. W.; Cutler, H. G.; Strawter, B. J. Austin, a novel polyisoprenoid mycotoxin from *Aspergillus ustus*. *J. Am. Chem. Soc.* **1976**, *98* (21), 6748-6750.
33. Steyn, P. S. Structure of five dioxopiperazines from *Aspergillus ustus*. *Tetrahedron* **1973**, *29* (1), 107-120.
34. Vleggaar, R.; Steyn, P. S.; Nagel, D. W. Constitution and absolute configuration of austdiol, the main toxic metabolite from *Aspergillus ustus*. *J. Chem. Soc. Perkin Trans. I* **1974**, (0), 45-49.
35. Pi, B.; Yu, D.; Dai, F.; Song, X.; Zhu, C.; Li, H.; Yu, Y. A genomics based discovery of secondary metabolite biosynthetic gene clusters in *Aspergillus ustus*. *PLoS One* **2015**, *10* (2), e0116089.
36. Cox, R. J.; Skellam, E.; Williams, K. Biosynthesis of fungal polyketides. *Physiology and Genetics* **2018**, 385-412.
37. Omura, S.; Crump, A. The life and times of ivermectin - a success story. *Nat. Rev. Microbiol.* **2004**, *2* (12), 984-989.
38. Khosla, C.; Tang, Y.; Chen, A. Y.; Schnarr, N. A.; Cane, D. E. Structure and mechanism of the 6-deoxyerythronolide B synthase. *Annu. Rev. Biochem.* **2007**, *76* (1), 195-221.
39. Chooi, Y. H.; Tang, Y. Navigating the fungal polyketide chemical space: from genes to molecules. *J. Org. Chem.* **2012**, *77* (22), 9933-9953.
40. Crawford, J. M.; Townsend, C. A. New insights into the formation of fungal aromatic polyketides. *Nat. Rev. Microbiol.* **2010**, *8* (12), 879-889.

6. REFERENCES

41. Watanabe, C. M. H.; Townsend, C. A. Initial characterization of a type I fatty acid synthase and polyketide synthase multienzyme complex NorS in the biosynthesis of aflatoxin B1. *Chem. Biol.* **2002**, *9* (9), 981-988.
42. Bailey, A. M.; Cox, R. J.; Harley, K.; Lazarus, C. M.; Simpson, T. J.; Skellam, E. Characterisation of 3-methylorcinolaldehyde synthase (MOS) in *Acremonium strictum*: first observation of a reductive release mechanism during polyketide biosynthesis. *Chem. Comm.* **2007**, (39), 4053-4055.
43. Fisch, K. M.; Skellam, E.; Iverson, D.; Cox, R. J.; Bailey, A. M.; Lazarus, C. M.; Simpson, T. J. Catalytic role of the C-terminal domains of a fungal non-reducing polyketide synthase. *Chem. Commun. (Camb.)* **2010**, *46* (29), 5331-5333.
44. Skellam, E. J.; Hurley, D.; Davison, J.; Lazarus, C. M.; Simpson, T. J.; Cox, R. J. Mutation of key residues in the C-methyltransferase domain of a fungal highly reducing polyketide synthase. *Mol. Biosyst* **2010**, *6* (4), 680-682.
45. Storm, P. A.; Herbst, D. A.; Maier, T.; Townsend, C. A. Functional and structural analysis of programmed C-methylation in the biosynthesis of the fungal polyketide citrinin. *Cell Chem. Biol.* **2017**, *24* (3), 316-325.
46. Pickens, L. B.; Tang, Y. Decoding and engineering tetracycline biosynthesis. *Metab. Eng.* **2009**, *11* (2), 69-75.
47. Zhang, W.; Watanabe, K.; Cai, X.; Jung, M. E.; Tang, Y.; Zhan, J. Identifying the minimal enzymes required for anhydrotetracycline biosynthesis. *J. Am. Chem. Soc.* **2008**, *130* (19), 6068-6069.
48. Jaremko, M. J.; Davis, T. D.; Corpuz, J. C.; Burkart, M. D. Type II non-ribosomal peptide synthetase proteins: structure, mechanism, and protein-protein interactions. *Nat. Prod. Rep.* **2020**, *37*, 355-379.
49. Brown, A. S.; Calcott, M. J.; Owen, J. G.; Ackerley, D. F. Structural, functional and evolutionary perspectives on effective re-engineering of non-ribosomal peptide synthetase assembly lines. *Nat. Prod. Rep.* **2018**, *35* (11), 1210-1228.
50. Hur, G. H.; Vickery, C. R.; Burkart, M. D. Explorations of catalytic domains in non-ribosomal peptide synthetase enzymology. *Nat. Prod. Rep.* **2012**, *29* (10), 1074-1098.
51. Hoyer, K. M.; Mahlert, C.; Marahiel, M. A. The iterative gramicidin S thioesterase catalyzes peptide ligation and cyclization. *Chem. Biol.* **2007**, *14* (1), 13-22.
52. Kopp, F.; Marahiel, M. A. Where chemistry meets biology: the chemoenzymatic synthesis of nonribosomal peptides and polyketides. *Curr. Opin. Biotechnol.* **2007**, *18* (6), 513-520.
53. Conti, P.; Tamborini, L.; Pinto, A.; Blondel, A.; Minoprio, P.; Mozzarelli, A.; De Micheli, C. Drug discovery targeting amino acid racemases. *Chem. Rev.* **2011**, *111* (11), 6919-6946.
54. Luo, L.; Kohli, R. M.; Onishi, M.; Linne, U.; Marahiel, M. A.; Walsh, C. T. Timing of epimerization and condensation reactions in nonribosomal Peptide assembly lines: kinetic analysis of phenylalanine activating elongation modules of tyrocidine synthetase B. *Biochemistry* **2002**, *41* (29), 9184-9196.
55. Samel, S. A.; Czodrowski, P.; Essen, L. O. Structure of the epimerization domain of tyrocidine synthetase A. *Acta Crystallographica Section D: Biological Crystallography* **2014**, *70* (5), 1442-1452.
56. Chhabra, A.; Haque, A. S.; Pal, R. K.; Goyal, A.; Rai, R.; Joshi, S.; Panjikar, S.; Pasha, S.; Sankaranarayanan, R.; Gokhale, R. S. Nonprocessive [2+2] e^- off-loading reductase domains from mycobacterial nonribosomal peptide synthetases. *Proc. Natl. Acad. Sci. U. S. A.* **2012**, *109* (15), 5681.
57. Xu, W.; Gavia, D. J.; Tang, Y. Biosynthesis of fungal indole alkaloids. *Nat. Prod. Rep.* **2014**, *31* (10), 1474-1487.
58. Gao, X.; Haynes, S. W.; Ames, B. D.; Wang, P.; Vien, L. P.; Walsh, C. T.; Tang, Y. Cyclization of fungal nonribosomal peptides by a terminal condensation-like domain. *Nat. Chem. Biol.* **2012**, *8*, 823-830.

6. REFERENCES

59. Ames, B. D.; Liu, X.; Walsh, C. T. Enzymatic processing of fumiquinazoline F: A tandem oxidative-acylation strategy for the generation of multicyclic scaffolds in fungal indole alkaloid biosynthesis. *Biochemistry* **2010**.
60. Zhang, J.; Liu, N.; Cacho, R. A.; Gong, Z.; Liu, Z.; Qin, W.; Tang, C.; Tang, Y.; Zhou, J. Structural basis of nonribosomal peptide macrocyclization in fungi. *Nat. Chem Biol.* **2016**, *12* (12), 1001-1003.
61. Wang, P. M.; Choera, T.; Wiemann, P.; Pisithkul, T.; Amador-N, D.; Keller, N. P. TrpE feedback mutants reveal roadblocks and conduits toward increasing secondary metabolism in *Aspergillus fumigatus*. *Fungal. Genet. Biol.* **2016**, *89*, 102-113.
62. Gao, X.; Chooi, Y. H.; Ames, B. D.; Wang, P.; Walsh, C. T.; Tang, Y. Fungal indole alkaloid biosynthesis: Genetic and biochemical investigation of the tryptoqualanine pathway in *Penicillium aethiopicum*. *J Am. Chem Soc.* **2011**.
63. Yan, D.; Chen, Q.; Gao, J.; Bai, J.; Liu, B.; Zhang, Y.; Zhang, L.; Zhang, C.; Zou, Y.; Hu, Y. Complexity and diversity generation in the biosynthesis of fumiquinazoline-related peptidyl alkaloids. *Org Lett.* **2019**, *21* (5), 1475-1479.
64. Haynes, S. W.; Gao, X.; Tang, Y.; Walsh, C. T. Assembly of asperlicin peptidyl alkaloids from anthranilate and tryptophan: A two-enzyme pathway generates heptacyclic scaffold complexity in asperlicin E. *J. Am. Chem. Soc.* **2012**, *134* (42), 17444-17447.
65. Walsh, C. T.; Chen, H.; Keating, T. A.; Hubbard, B. K.; Losey, H. C.; Luo, L.; Marshall, C. G.; Miller, D. A.; Patel, H. M. Tailoring enzymes that modify nonribosomal peptides during and after chain elongation on NRPS assembly lines. *Curr. Opin. Chem. Biol.* **2001**, *5* (5), 525-534.
66. Olano, C.; Mendez, C.; Salas, J. A. Post-PKS tailoring steps in natural product-producing actinomycetes from the perspective of combinatorial biosynthesis. *Nat. Prod. Rep.* **2010**, *27* (4), 571-616.
67. Zhang, X.; Li, S. Expansion of chemical space for natural products by uncommon P450 reactions. *Nat. Prod. Rep.* **2017**, *34* (9), 1061-1089.
68. Chen, C.-C.; Min, J.; Zhang, L.; Yang, Y.; Yu, X.; Guo, R.-T. Advanced understanding of electron transfer pathway of cytochrome P450s. *Chembiochem* **2021**, doi: 10.1002/cbic.202000705.
69. van den Brink, H.; van Gorcom, R. F. M.; van den Hondel, C. A. M. J.; Punt, P. J. Cytochrome P450 enzyme systems in fungi. *Fungal Genet. Biol.* **1998**, *23* (1), 1-17.
70. Durairaj, P.; Hur, J. S.; Yun, H. Versatile biocatalysis of fungal cytochrome P450 monooxygenases. *Microb. Cell Fact.* **2016**, *15* (1), 125.
71. Stok, J. E.; Chow, S.; Krenske, E. H.; Soto, C. F.; Matyas, C.; Poirier, R. A.; Williams, C. M.; De Voss, J. J. Direct observation of an oxepin from a bacterial cytochrome P450-catalyzed oxidation. *Chem. Eur. J.* **2016**, *22* (13), 4408-4412.
72. Agarwal, V.; El Gamal, A. A.; Yamanaka, K.; Poth, D.; Kersten, R. D.; Schorn, M.; Allen, E. E.; Moore, B. S. Biosynthesis of polybrominated aromatic organic compounds by marine bacteria. *Nat. Chem. Biol.* **2014**, *10* (8), 640-647.
73. Mantovani, S. M.; Moore, B. S. Flavin-linked oxidase catalyzes pyrrolizine formation of dichloropyrrole-containing polyketide extender unit in chlorizidine A. *J. Am. Chem. Soc.* **2013**, *135* (48), 18032-18035.
74. Zhang, Q.; Li, H.; Yu, L.; Sun, Y.; Zhu, Y.; Zhu, H.; Zhang, L.; Li, S.-M.; Shen, Y.; Tian, C.; Li, A.; Liu, H.; Zhang, C. Characterization of the flavoenzyme XiaK as an N-hydroxylase and implications in indolosesquiterpene diversification. *Chem. Sci.* **2017**, *8* (7), 5067-5077.
75. Teufel, R. Flavin-catalyzed redox tailoring reactions in natural product biosynthesis. *Arch. Biochem. Biophys.* **2017**, *632*, 20-27.
76. Teufel, R.; Agarwal, V.; Moore, B. S. Unusual flavoenzyme catalysis in marine bacteria. *Curr. Opin. Chem. Biol.* **2016**, *31*, 31-39.
77. Huijbers, M. M. E.; Montersino, S.; Westphal, A. H.; Tischler, D.; van Berkel, W. J. Flavin dependent monooxygenases. *Arch. Biochem. Biophys.* **2014**, *544*, 2-17.

6. REFERENCES

78. Leys, D.; Scrutton, N. S. Flavin does't put all oxygens in one basket. *Nat. Chem. Biol.* **2020**, *16* (5), 485-486.
79. Fraley, A. E.; Caddell, H. K.; Ye, Y.; Kelly, S. P.; Newmister, S. A.; Yu, F.; Williams, R. M.; Smith, J. L.; Houk, K. N.; Sherman, D. H. Molecular basis for spirocycle formation in the paraherquamide biosynthetic pathway. *J. Am. Chem. Soc.* **2020**, *142* (5), 2244-2252.
80. Xiang, L.; Kalaitzis, J. A.; Moore, B. S. EncM, a versatile enterocin biosynthetic enzyme involved in Favorskii oxidative rearrangement, aldol condensation, and heterocycle-forming reactions. *Proc. Natl. Acad. Sci. U. S. A* **2004**, *101* (44), 15609.
81. Zheng, L.; Jiang, X.; Zhang, Q.; Zhu, Y.; Zhang, H.; Zhang, W.; Saurav, K.; Liu, J.; Zhang, C. Discovery and biosynthesis of neoenterocins indicate a skeleton rearrangement of enterocin. *Org. Lett.* **2019**, *21* (22), 9066-9070.
82. Teufel, R.; Miyanaga, A.; Michaudel, Q.; Stull, F.; Louie, G.; Noel, J. P.; Baran, P. S.; Palfey, B.; Moore, B. S. Flavin-mediated dual oxidation controls an enzymatic Favorskii-type rearrangement. *Nature* **2013**, *503* (7477), 552-556.
83. Fan, J. Biosynthesis of penilactones and peniphenones in *Penicillium crustosum*. *Thesis* **2020**.
84. Nakamura, H.; Matsuda, Y.; Abe, I. Unique chemistry of non-heme iron enzymes in fungal biosynthetic pathways. *Nat. Prod. Rep.* **2018**, *35*, 633-645.
85. Perry, C.; De Los Santos, E. L.; Alkhalaf, L. M.; Challis, G. L. Rieske non-heme iron-dependent oxygenases catalyse diverse reactions in natural product biosynthesis. *Nat. Prod. Rep.* **2018**, *35* (7), 622-632.
86. Ran, H.; Wohlgemuth, V.; Xie, X.; Li, S.-M. A non-heme FeII/2-oxoglutarate-dependent oxygenase catalyzes a double bond migration within a dimethylallyl moiety accompanied by hydroxylation. *ACS Chem. Biol.* **2018**, *13*, 2949-2955.
87. Fan, J.; Liao, G.; Kindinger, F.; Ludwig-Radtke, L.; Yin, W.-B.; Li, S.-M. Peniphenone and penilactone formation in *Penicillium crustosum* via 1,4-Michael additions of *ortho*-quinone methide from hydroxyclovatol to γ -butyrolactones from crustosic acid. *J. Am. Chem. Soc.* **2019**, *141*, 4225-4229.
88. Winkelblech, J.; Fan, A.; Li, S.-M. Prenyltransferases as key enzymes in primary and secondary metabolism. *Appl. Microbiol. Biotechnol.* **2015**, *99* (18), 7379-7397.
89. Tsai, H. F.; Wang, H.; Gebler, J. C.; Poulter, C. D.; Schardl, C. L. The *Claviceps purpurea* gene encoding dimethylallyltryptophan synthase, the committed step for ergot alkaloid biosynthesis. *Biochem. Biophys. Res. Commun.* **1995**, *216* (1), 119-125.
90. Li, S.-M. Evolution of aromatic prenyltransferases in the biosynthesis of indole derivatives. *Phytochemistry* **2009**, *70*, 1746-1757.
91. Shibuya, M.; Chou, H. M.; Fountoulakis, M.; Hassam, S.; Kim, S. U.; Kobayashi, K.; Otsuka, H.; Rogalska, E.; Cassady, J. M.; Floss, H. G. Stereochemistry of the isoprenylation of tryptophan catalyzed by 4-(g,g-dimethylallyl)tryptophan synthase from *Claviceps*, the first pathway-specific enzyme in ergot alkaloid biosynthesis. *J. Am. Chem. Soc.* **1990**, *112* (1), 297-304.
92. Luk, L. Y. P.; Tanner, M. E. Mechanism of dimethylallyltryptophan synthase: evidence for a dimethylallyl cation intermediate in an aromatic prenyltransferase reaction. *J. Am. Chem. Soc.* **2009**, *131* (39), 13932-13933.
93. Metzger, U.; Schall, C.; Zocher, G.; Unsöld, I.; Stec, E.; Li, S.-M.; Heide, L.; Stehle, T. The structure of dimethylallyl tryptophan synthase reveals a common architecture of aromatic prenyltransferases in fungi and bacteria. *Proc. Natl. Acad. Sci. U. S. A* **2009**, *106* (34), 14309-14314.
94. Yin, S.; Yu, X.; Wang, Q.; Liu, X. Q.; Li, S.-M. Identification of a brevianamide F reverse prenyltransferase BrePT from *Aspergillus versicolor* with a broad substrate specificity towards tryptophan-containing cyclic dipeptides. *Appl. Microbiol. Biotechnol.* **2013**, *97*, 1649-1660.
95. Ding, Y.; Wet, J. R.; Cavalcoli, J.; Li, S.; Greshock, T. J.; Miller, K. A.; Finefield, J. M.; Sunderhaus, J. D.; McAfoos, T. J.; Tsukamoto, S.; Williams, R. M.; Sherman, D. H. Genome-based characterization of two prenylation steps in the assembly of the stephacidin and notoamide

6. REFERENCES

- anticancer agents in a marine-derived *Aspergillus* sp. *J. Am. Chem. Soc.* **2010**, 132 (36), 12733-12740.
96. Wohlgemuth, V.; Kindinger, F.; Li, S.-M. Convenient synthetic approach for tri- and tetraprenylated cyclodipeptides by consecutive enzymatic prenylations. *Appl. Microbiol. Biotechnol.* **2018**, 102 (6), 2671-2681.
97. Yin, W.-B.; Grundmann, A.; Cheng, J.; Li, S.-M. Acetylaszonalenin biosynthesis in *Neosartorya fischeri*: Identification of the biosynthetic gene cluster by genomic mining and functional proof of the genes by biochemical investigation. *J. Biol. Chem.* **2009**, 284 (1), 100-109.
98. Yin, W.-B.; Yu, X.; Xie, X.-L.; Li, S.-M. Preparation of pyrrolo[2,3-*b*]indoles carrying a β -configured reverse C3-dimethylallyl moiety by using a recombinant prenyltransferase CdpC3PT. *Org. Biomol. Chem.* **2010**, 8, 2430-2438.
99. Unsöld, I. A.; Li, S.-M. Overproduction, purification and characterization of FgaPT2, a dimethylallyltryptophan synthase from *Aspergillus fumigatus*. *Microbiology* **2005**, 151 (Pt 5), 1499-1505.
100. Yu, X.; Liu, Y.; Xie, X.; Zheng, X.-D.; Li, S.-M. Biochemical characterization of indole prenyltransferases: Filling the last gap of prenylation positions by a 5-dimethylallyltryptophan synthase from *Aspergillus clavatus*. *J. Biol. Chem.* **2012**, 287 (2), 1371-1380.
101. Winkelblech, J.; Li, S.-M. Biochemical investigations of two 6-DMATS enzymes from *Streptomyces* revealing novel features of L-tryptophan prenyltransferases. *Chembiochem.* **2014**, 15, 1030-1039.
102. Kremer, A.; Westrich, L.; Li, S.-M. A 7-dimethylallyltryptophan synthase from *Aspergillus fumigatus*: overproduction, purification and biochemical characterization. *Microbiology* **2007**, 153 (Pt 10), 3409-3416.
103. Fan, A.; Zocher, G.; Stec, E.; Stehle, T.; Li, S.-M. Site-directed mutagenesis switching a dimethylallyl tryptophan synthase to a specific tyrosine C3-prenylating enzyme. *J. Biol. Chem.* **2015**, 290, 1364-1373.
104. Fan, A.; Li, S.-M. Saturation mutagenesis on Arg244 of the tryptophan C4-prenyltransferase FgaPT2 leads to enhanced catalytic ability and different preferences for tryptophan-containing cyclic dipeptides. *Appl. Microbiol. Biotechnol.* **2016**, 100, 5389-5399.
105. Luk, L. Y.; Qian, Q.; Tanner, M. E. A cope rearrangement in the reaction catalyzed by dimethylallyltryptophan synthase? *J. Am. Chem. Soc.* **2011**, 133 (32), 12342-12345.
106. Mojtahedi, M. M.; Samadian, S. Efficient and rapid solvent-free acetylation of alcohols, phenols, and thiols using catalytic amounts of sodium acetate trihydrate. *J. Chem.* **2013**, 2013, Article ID 642479.
107. Brock, M.; Fischer, R.; Linder, D.; Buckel, W. Methylcitrate synthase from *Aspergillus nidulans*: implications for propionate as an antifungal agent. *Mol. Microbiol.* **2000**, 35 (5), 961-973.
108. Cox, R. J. Polyketides, proteins and genes in fungi: programmed nano-machines begin to reveal their secrets. *Org. Biomol. Chem.* **2007**, 5 (13), 2010-2026.
109. Chiang, Y. M.; Ahuja, M.; Oakley, C. E.; Entwistle, R.; Asokan, A.; Zutz, C.; Wang, C. C.; Oakley, B. R. Development of genetic dereplication strains in *Aspergillus nidulans* results in the discovery of aspercryptin. *Angew. Chem. Int. Ed. Engl.* **2016**, 55 (5), 1662-1665.
110. Wang, M.; Zhou, H.; Wirz, M.; Tang, Y.; Boddy, C. N. A thioesterase from an iterative fungal polyketide synthase shows macrocyclization and cross coupling activity and may play a role in controlling iterative cycling through product offloading. *Biochemistry* **2009**, 48 (27), 6288-6290.
111. Tsakos, M.; Schaffert, E. S.; Clement, L. L.; Villadsen, N. L.; Poulsen, T. B. Ester coupling reactions - an enduring challenge in the chemical synthesis of bioactive natural products. *Nat. Prod. Rep.* **2015**, 32 (4), 605-632.
112. Fan, J.; Liao, G.; Ludwig-Radtke, L.; Yin, W.-B.; Li, S.-M. Formation of terrestric acid in *Penicillium crustosum* requires redox-assisted decarboxylation and stereoisomerization. *Org. Lett.* **2020**, 22 (1), 88-92.

6. REFERENCES

113. Blin, K.; Shaw, S.; Steinke, K.; Villebro, R.; Ziemert, N.; Lee, S. Y.; Medema, M. H.; Weber, T. antiSMASH 5.0: updates to the secondary metabolite genome mining pipeline. *Nucleic Acids Res.* **2019**, *47* (W1), W81-W87.
114. Walsh, C. T.; Haynes, S. W.; Ames, B. D.; Gao, X.; Tang, Y. Short pathways to complexity generation: Fungal peptidyl alkaloid multicyclic scaffolds from anthranilate building blocks. *ACS Chem. Biol.* **2013**, *8*, 1366-1382.
115. Chiang, Y. M.; Oakley, C. E.; Ahuja, M.; Entwistle, R.; Schultz, A.; Chang, S. L.; Sung, C. T.; Wang, C. C.; Oakley, B. R. An efficient system for heterologous expression of secondary metabolite genes in *Aspergillus nidulans*. *J. Am. Chem. Soc.* **2013**, *135* (20), 7720-7731.
116. Yin, W. B.; Chooi, Y. H.; Smith, A. R.; Cacho, R. A.; Hu, Y.; White, T. C.; Tang, Y. Discovery of cryptic polyketide metabolites from dermatophytes using heterologous expression in *Aspergillus nidulans*. *ACS Synth. Biol.* **2013**, *2* (11), 629-634.
117. van Leeuwen, J.; Andrews, B.; Boone, C.; Tan, G. Rapid and efficient plasmid construction by homologous recombination in yeast. *Cold Spring Harb. Protoc.* **2015**, *2015* (9), 853-861.
118. Fan, Y.; Li, P.; Chao, Y.; Chen, H.; Du, N.; He, Q.; Liu, K. Alkaloids with cardiovascular effects from the marine-derived fungus *Penicillium expansum* Y32. *Mar. Drugs* **2015**, *13* (10), 6849-6504.
119. Ohte, S.; Shiokawa, T.; Koyama, N.; Katagiri, T.; Imada, C.; Tomoda, H. A new diketopiperazine-like inhibitor of bone morphogenetic protein-induced osteoblastic differentiation produced by marine-derived *Aspergillus* sp. BFM-0085. *J. Antibiot.* **2020**, *73*, 554-558.
120. Lee, S. U.; Asami, Y.; Lee, D.; Jang, J. H.; Ahn, J. S.; Oh, H. Protuboxepins A and B and protubonines A and B from the marine-derived fungus *Aspergillus* sp. SF-5044. *J. Nat. Prod.* **2011**, *74* (5), 1284-1287.
121. Guo, C. J.; Yeh, H. H.; Chiang, Y. M.; Sanchez, J. F.; Chang, S. L.; Bruno, K. S.; Wang, C. C. C. Biosynthetic pathway for the epipolythiodioxopiperazine acetylaranotin in *Aspergillus terreus* revealed by genome-based deletion analysis. *J. Am. Chem. Soc.* **2013**, *135* (19), 7205-7213.
122. Syed, K.; Mashele, S. S. Comparative analysis of P450 signature motifs EXXR and CXG in the large and diverse kingdom of fungi: identification of evolutionarily conserved amino acid patterns characteristic of P450 family. *PLoS One* **2014**, *9* (4), e95616-1-e95616-14.
123. Schneider, T. D.; Stephens, R. M. Sequence logos: a new way to display consensus sequences. *Nucleic. Acids. Res.* **1990**, *18* (20), 6097-6100.
124. Crooks, G. E.; Hon, G.; Chandonia, J. M.; Brenner, S. E. WebLogo: A sequence logo generator. *Genome. Res.* **2004**, *14* (6), 1188-1190.
125. Jin, S.; Bryson, T. A.; Dawson, J. H. Hydroperoxoferric heme intermediate as a second electrophilic oxidant in cytochrome P450-catalyzed reactions. *J. Biol. Inorg. Chem.* **2004**, *9* (6), 644-653.
126. Sono, M.; Roach, M. P.; Coulter, E. D.; Dawson, J. H. Heme-containing oxygenases. *Chem. Rev.* **1996**, *96* (7), 2841-2888.
127. Beaudry, C. M.; Malerich, J. P.; Trauner, D. Biosynthetic and biomimetic electrocyclizations. *Chem. Rev.* **2005**, *105* (12), 4757-4778.
128. Vogel, E.; Günther, H. Benzene oxide-oxepin valence tautomerism. *Angew. Chem. Intern. Ed.* **1967**, *6* (5), 385-401.
129. Wiese, A.; Pietzsch, M.; Syltatk, C.; Mattes, R.; Altenbuchner, J. Hydantoin racemase from *Arthrobacter aurescens* DSM 3747: heterologous expression, purification and characterization. *J. Biotechnol.* **2000**, *80* (3), 217-230.
130. Hernández, F.; Morales, V.; Buenadicha, F. L.; Söllhuber, M.; Avendaño, C. Influence of *N*(2)-substitution in the alkylation of (4*S*)-alkyl-2,4-dihydro-1*H*-pyrazino[2,1-*b*]quinazoline-3,6-diones. *Tetrahedron: Asymmetry* **2004**, *15* (19), 3045-3058.
131. Haynes, S. W.; Gao, X.; Tang, Y.; Walsh, C. T. Complexity generation in fungal peptidyl alkaloid biosynthesis: A two-enzyme pathway to the hexacyclic MDR export pump inhibitor ardeemin. *ACS Chem. Biol.* **2013**, *8*, 741-748.

6. REFERENCES

132. Li, S.-M. Prenylated indole derivatives from fungi: structure diversity, biological activities, biosynthesis and chemoenzymatic synthesis. *Nat. Prod. Rep.* **2010**, 27 (1), 57-78.
133. Giessen, T. W.; von Tesmar, A. M.; Marahiel, M. A. A tRNA-dependent two-enzyme pathway for the generation of singly and doubly methylated ditryptophan 2,5-diketopiperazines. *Biochemistry* **2013**, 52 (24), 4274-4283.
134. Borthwick, A. D. 2,5-diketopiperazines: synthesis, reactions, medicinal chemistry, and bioactive natural products. *Chem. Rev.* **2012**, 112 (7), 3641-3716.
135. Steffan, N.; Li, S.-M. Increasing structure diversity of prenylated diketopiperazine derivatives by using a 4-dimethylallyltryptophan synthase. *Arch. Microbiol.* **2009**, 191 (5), 461-466.
136. Yu, X.; Zocher, G.; Xie, X.; Liebhold, M.; Schütz, S.; Stehle, T.; Li, S.-M. Catalytic mechanism of stereospecific formation of *cis*-configured prenylated pyrroloindoline diketopiperazines by indole prenyltransferases. *Chem. Biol.* **2013**, 20 (12), 1492-1501.

STATUTORY DECLARATION

Statutory Declaration

Ich, Liujuan Zheng, versichere, dass ich meine Dissertation

„Investigations on the biosynthesis of secondary metabolites and biosynthetic enzymes from *Aspergillus* species “

selbständig ohne unerlaubte Hilfe angefertigt und mich dabei keiner anderen als der von mir ausdrücklich bezeichneten Quellen bedient habe. Alle vollständig oder sinngemäß übernommenen Zitate sind als solche gekennzeichnet.

Die Dissertation wurde in der jetzigen oder einer ähnlichen Form noch bei keiner anderen Hochschule eingereicht und hat noch keinen sonstigen Prüfungszwecken gedient.

Marburg, den.....

.....

Liujuan Zheng

Acknowledgements

Finally, it is time to say goodbye to my PhD study, not only an amazing academic trip in lab, but also an incredible tour in Germany to know the people and culture.

I would like to show my sincere thanks to Prof. Dr. Shu-Ming Li for bringing me to Germany and guiding me in the research. I can still clearly remember the situation of the first time for me listening his presentation in SCSIO. When I have huge difficulties in my projects, Professor Li can always give me a lot of constructive suggestions. In these years, he teach me about not only how to do good research work, but also the personality of a good scientist. These will benefit me in the rest of my life.

Sincere thanks to Prof. Dr. Michael Keusgen for kindly being my second referee and examiner.

I show my sincere and special thanks to my fiancée Haowen. She is my best partner both in research and life. Her love and accompany largely help me go through those difficult times.

Thanks to Yiling for the nice cooperation in the ustethylin story and Peter in the PT story. Thank you very much to Aili, Lena L, Liping for help in the projects. Thanks to Elena and Dr. Zocher for the nice story of 5- and 6-DMATSS. Thanks to Jie, Jing, and Jonas for their helps in molecular biology technics. Thanks to Rixa for taking mass spectra, and Dr. Regina Ortmann and Stefan Newel for taking NMR spectra. Special gratitude to Sina and Lauritz for proof reading this dissertation.

Many thanks to the colleagues in AG Li. Florian, Bastian, Jonas, Linus, Johana, Kristin, Lena M, and Lindsay for the wonderful beer time and parties. Katja, Huili, Kang, Alexander, Viola, Kirsten, Ge, Huomiao, Elisabeth, Pan, Wen, Zhengxi, Zhanghai, Jenny, Yu, Marlies, Danniell J, Danniell O, Andreas, Nina G, Torben, Dr. Kreusch, Sabine, Sonja as well as Keyan, Jinglin, Wei Li, Huan Liu, Shuang Zhou, Yuan Zhou, Xiao Wu, Changxing and other short-term communication professors and students in our institute for the great and wonderful time.

I also thanks to my friends, e.g. Gaoyuan, Shuzhuang, Haisen, Xiaowei and the basketball teammates.

I thank the China Scholarship Council (CSC) for financial supports.

I deeply thank my family for their encouragement and support over the past years.

